



**Technische Universität München**

**Lehrstuhl für Maschinen- und Apparatekunde**

# **Continuous dynamic mixing of cohesive powders**

**Dipl.-Ing. Volker Kehlenbeck**

Vollständiger Abdruck der von der Fakultät Wissenschaftszentrum Weihenstephan für Ernährung, Landnutzung und Umwelt der Technischen Universität München zur Erlangung des akademischen Grades eines

**Doktor-Ingenieurs  
(Dr.-Ing.)**

genehmigten Dissertation.

Vorsitzender: Univ.-Prof. Dr. rer. nat. habil. Rudi F. Vogel

Prüfer der Dissertation:

1. Univ.-Prof. Dr.-Ing. Karl Sommer
2. Univ.-Prof. Dr.-Ing. Jörg Schwedes,  
Technische Universität Braunschweig
3. Prof. Dr.-Ing. John A. Dodds,  
Ecole des Mines d'Albi, Frankreich  
(schriftliche Beurteilung)

Die Dissertation wurde am 09.01.2006 bei der Technischen Universität München eingereicht und durch die Fakultät Wissenschaftszentrum Weihenstephan für Ernährung, Landnutzung und Umwelt am 16.02.2006 angenommen.

Dieser Titel ist auch im Shaker Verlag unter der ISBN 3-8322-5726-8 erschienen.

To my parents

*Ingrid and Reinhard Kehlenbeck*

for everything they have done for me!

## Acknowledgements

This thesis is the result of my work as scientific employee at the *Lehrstuhl für Maschinen- und Apparatekunde* of the *Technische Universität München – Weihenstephan* (February 1998 until November 2003).

My most special thanks go to my doctoral advisor Univ.-Prof. Dr.-Ing. Karl Sommer who inspired my fascination in powder technology, in particular in powder mixing. He shared with me his universal knowledge during many engrossing discussions and the fascinating lectures of our annual seminars. In addition, he gave me great freedom in realizing own ideas and in my subsequent personal development. I also want to express my gratitude to Univ.-Prof. Dr.-Ing. Jörg Schwedes who was one of my lecturers during my studies of Mechanical Engineering at the *Technische Universität Braunschweig*. He is the one who initially stirred my interest in powder technology and encouraged me to start a PhD. Prof. Dr.-Ing. John A. Dodds also supervised a PhD thesis on continuous dynamic mixing at the *Ecole des Mines d'Albi-Carmaux* (France). Therefore, I was very happy that he agreed to advise my work, too. I also wish to express gratitude to Univ.-Prof. Dr. rer. nat. habil. Rudi F. Vogel for taking over the chair of the PhD examination.

All former colleagues I want to thank very much for the terrific atmosphere at our institute. My particular thanks go to my colleagues and close friends Dr.-Ing. Heinz Dauth, Dr.-Ing. Sven Fischer, Markus Hartmann, Dr.-Ing. Jan Herrmann, Jürgen Hofmann, Dr.-Ing. Susanne Kuschel, Dr.-Ing. Heidi Lankes and Dr.-Ing. Stefan Palzer. The time we spent together at the *Lehrstuhl für Maschinen- und Apparatekunde* as well as during spare time activities and journeys I will never forget! I am indebted to them that the expression friendship has taken on a new meaning for me.

Without the fantastic help and support of the workshop members, especially Peter Rauscher, Anton Fischer, Alfons Seitzl, Christian Stanglmaier and Hans Wagner, the build-up of the complex experimental rigs would not have been possible. I also want to give many thanks to my neighbor Wolfgang Schmidt who assisted me greatly during the planning of the electronic installation of the main experimental rig.

All the students who helped me solving problems connected with the project deserve my gratitude. Especially I want to mention Sofia Tempfli, who aided me very much with her semester and following diploma thesis. She improved the in-line concentration measurement by means of near-infrared spectroscopy and the calibration of the spectrometer. Bettina Weinzierl also provided important assistance with her semester and following diploma thesis. She tested and assessed dosing tube ends and dosing tube attachments, which were developed during the project to improve the short-term dosing constancy of the volumetric feeders used. After their diploma theses, Ms. Tempfli and Ms. Weinzierl worked for me as temporary scientific assistants and ensured that the experimental examinations did not stop during my scientific stay at the *Particle Engineering Research Center* at the *University of Florida* (USA). I also want to mention Andreas Fischer, who developed the software to control the experimental rig during his diploma thesis, and Jan-Dirk Prigge, who examined different possibilities to improve the sample preparation necessary for the calibration of the near-infrared spectrometer used during his semester thesis.



Mr. Daniel Dopfer, Dr. tech. Ralf Kehlenbeck, Dr. Lucy Kunz, Dr.-Ing. Heidi Lankes, Dr. Andreas Niemöller, Dr.-Ing. Stefan Palzer and Dr. Ralf Weinekötter spent many hours of their spare time reading and discussing my work.

The thesis was financially supported by the *Deutsche Forschungsgemeinschaft (DFG)* and the *International Fine Particles Research Institute (IFPRI)*. Besides gathering manifold experiences and the scientific development, the financial support of the *DFG* offered me the opportunity of a two-month stay at the *Particle Engineering Research Center* at the *University of Florida (USA)* and to present the research results at different international conferences. The annual *DFG* colloquia and our annual meetings of the PhD students I will miss in the future. Besides many contacts with professors and their co-workers, also some true friendships formed. In this context, I want to mention especially Dr. rer. nat. Ursula Dowe and Dr.-Ing. Günther Huber.

Without the sponsoring of more than one hundred companies, the build-up of the experimental rigs would not have been possible. I want to mention and deeply thank the main sponsors of the project and the main contact persons I owe the support:

The company *Bruker Optik GmbH* (Ettlingen, Germany) put the FT-NIR spectrometer *VECTOR 22/N* at our disposal. Despite initial doubts, Mr. J. Gast, Dr. H. Weiler and Dr. J.-P. Conzen believed in my vision of controlling the mixing process in a continuous mixer by near-infrared spectroscopy. During the realization of the in-line adaptation and the necessary calibration of the near-infrared spectrometer, Dr. A. Niemöller helped me very much. The companies *Gericke AG* (Regensdorf, Switzerland) and *Gericke GmbH* (Rielasingen, Germany) sponsored the continuous dynamic mixer *GCM 500* and two volumetric feeders of the type *GAC 132*. Dr. R. Weinekötter, Dr.-Ing. M. Kruse and Mr. E. Leeger I want to thank for the discussions about powder mixing and powder dosing. The companies *Sartorius AG* (Göttingen, Germany) and *Global Weighing Technologies GmbH* (Hamburg, Germany) made the whole weighing equipment available. Mr. K. Thornagel, Mr. T. Konow and Mr. M. Stoppert enabled me to realize many of my ideas during the project. Mr. J. Dittrich supported me in programming the weighing controller used. The sponsoring of two suction conveyors by Mr. T. Volkmann and Mr. T. Ramme from the company *VOLKMANN GmbH* (Soest, Germany) made the handling of the huge amounts of powder necessary for continuous mixing experiments much easier. An optimum operation of the suction conveyors was possible by the sponsoring of two bins from the company *Dietrich Reimelt GmbH & Co. KG* (Rödermark, Germany). Mr. P.-G. Dellmann made the sponsoring possible. Mr. W. Heldenberger and Mr. E. Pretsch from the company *Rudolf Loh GmbH & Co. KG* (Herborn, Germany) made several *Rittal* switch cupboards and housings available to protect the control computers and other sensitive equipment against dust. The switch cupboards and housings contributed essentially to the attractive appearance of the experimental rig.

All individuals and companies not specifically mentioned above but who also helped and supported me during my work on my PhD I wish to thank as well.

## List of symbols

### Latin symbols

$\overline{\Delta x_1}$	Average displacement of species 1 in $x$ -direction	[m]
$\overline{\Delta x_1^2}$	Mean square deviation of the displacement of species 1 in $x$ -direction	[m]
$\Delta x_{1,i}$	Single displacement of species 1 in $x$ -direction	[m]
$\dot{m}, \Delta m/\Delta t, dm/dt$	Mass flow	[kg/s]
$\bar{m}$	Average mass flow	[kg/s]
$A$	Cross section area	[m <sup>2</sup> ]
$AU$	Absorbance unit	[-]
$c$	Chamber concentration (mass per chamber volume)	[kg/m <sup>3</sup> ]
$CD$	Normalized dispersion coefficient $D$ multiplied with $\Delta\tau / \Delta\lambda^2$	[-]
$CU$	Normalized transport coefficient $U$ multiplied with $\Delta\tau / 2 \cdot \Delta\lambda$	[-]
$D$	Normalized dispersion coefficient of the Fokker-Planck-Equation	[-]
$D^*$	Dispersion coefficient of the Fokker-Planck-Equation	[m <sup>2</sup> /s]
$dx$	Width of a cut-off in $x$ -direction	[m]
$dy$	Width of a cut-off in $y$ -direction	[m]
$dz$	Width of a cut-off in $z$ -direction	[m]
$f(\alpha, \xi, t)$	Local probability density that a particle with the origin position $\alpha$ is located at the position $\xi$ at the time $t$	[-]
$f(t)$	Function depending on the time $t$	
$f(n, \Delta m/\Delta t, T, \phi)$	Function depending on the rotational speed $n$ , the mass flow $\Delta m/\Delta t$ , the period length $T$ , the filling degree $\phi$	
$FR$	Fluctuation ratio	[-]
$i$	Counting number	[-]
$I$	Abbreviation for an integral	[-]
$j$	Counting number	[-]
$k$	Degree of freedom $k = n - 1$	[-]
$l$	Distance between mirror and beam splitter	[m]
$L$	Length of the mixer	[m]
$L_s$	Length of the mixer, over which the entering powders are spread	[m]
$M$	Normalized overall mass hold-up in the mixer	[-]
$m$	Mass	[kg]
$m_{hold}$	Mass hold-up taking part in the mixing process	[kg]
$m_{hold}'$	Mass hold-up remaining in the mixer after pressing the emergency bottom	[kg]
$m_{hold}''$	Mass hold-up sticking on the mixer shell and not taking part in the mixing process	[kg]
$n$	Revolution number of the mixing device	[1/s]

$n$	Number of truncation chambers	[-]
$n_s$	Number of truncation chambers, over which the entering powders are spread	[-]
$nt$	Number of truncation steps in time	[-]
$p$	Set mass concentration	[kg/kg]
$Q_3$	Cumulative volume distribution	[-]
$R_3$	Residue volume distribution	[-]
$RMSECV$	Root Mean Square Error of Cross Validation	[kg/kg]
$Rt$	Dimensionless running time (multiple of the period length)	[-]
$s$	Empirical standard deviation of the concentration	[kg/kg]
$s^2$	Empirical variance of the concentration	[(kg/kg) <sup>2</sup> ]
$s(t)$	Function describing a square wave mass flow fluctuation	[kg/s]
$SF$	Spreading factor	[-]
$T$	Period length of the entering sinusoidal mass flow fluctuations	[s]
$t$	Time	[s]
$t_R^*$	Average residence time of the particles in the mixer	[s]
$t_R$	Normalized average residence time of the particles in the mixer	[-]
$U$	Normalized transport coefficient of the Fokker-Planck-Equation	[-]
$U^*$	Transport coefficient of the Fokker-Planck-Equation	[m/s]
$u(x,y,z,t)$	Local probability density that a particle is located at the position $(x,y,z)$ at the time $t$	[-]
$V$	Volume	[m <sup>3</sup> ]
$VRR$	Variance reduction ratio	[-]
$x$	Position in $x$ -direction	[m]
$y$	Position in $y$ -direction	[m]
$z$	Position in $z$ -direction	[m]

## Greek symbols

$\alpha$	Initial position in $x$ -direction	[m]
$\eta$	Displacement in $x$ -direction during the time $\theta$	[m]
$\Theta$	Characteristic time	[s]
$\theta$	Time	[s]
$\lambda$	Wavelength	[m]
$\lambda$	Normalized length in $x$ -direction	[-]
$\Delta\lambda$	Normalized truncation step in space	[-]
$\dot{\mu}$	Normalized mass flow	[1/s]
$\nu(x,t)$	Local probability density that a particle is located in the plane $x = \text{constant}$ at the time $t$	[-]
$\xi$	Position in $x$ -direction	[m]
$\rho_{bulk}$	Bulk density	[kg/m <sup>3</sup> ]

$\sigma$	Standard deviation of the displacements	[m]
$\sigma$	Standard deviation of the concentration	[kg/kg]
$\sigma^2$	Variance of the concentration	[(kg/kg) <sup>2</sup> ]
$\sigma_1$	Consolidation stress	[Pa]
$\sigma_c$	Unconfined yield stress	[Pa]
$\tau$	Normalized time	[-]
$\Delta\tau$	Normalized truncation step in time	[-]
$\tilde{\tau}$	Normalized time according to WEINEKÖTTER	[-]
$\Phi$	Probability density function of the displacements	[m]
$\phi^*$	Filling degree	[m <sup>3</sup> /m <sup>3</sup> ]
$\phi$	Normalized filling degree	[-]
$\varphi_1(\Delta x_1)$	Distribution function of the displacements $\Delta x_{1,i}$	[-]
$\varphi_2(\Delta x_2)$	Distribution function of the displacements $\Delta x_{2,i}$	[-]
$\chi^2$	Chi-square value	[-]
$\psi_1(x)$	Average velocity at the position $x$	[m/s]
$\psi_2(x)$	Second moment of the probability density of the particle movement during the time $\theta$ at the position $x$ (with $\theta \rightarrow 0$ )	[m <sup>2</sup> /s]
$\Omega$	Normalized angular velocity	[-]
$\omega$	Angular velocity	[1/s]

## Indices

<i>1</i>	Component 1
<i>2</i>	Component 2
<i>A</i>	Amplitude of sinusoidal mass flow fluctuation
<i>chamber</i>	Truncation chamber
<i>i</i>	Running index
<i>j</i>	Running index
<i>s</i>	Running index for the truncation in space
<i>t</i>	Running index for the truncation in time
<i>in</i>	Inlet of the mixer
<i>max</i>	Maximum
<i>O</i>	Offset of the sinusoidal mass flow fluctuation
<i>out</i>	Outlet of the mixer
<i>w</i>	Weir
<i>l</i>	Lower
<i>u</i>	Upper
<i>sys</i>	Systematic
<i>rel</i>	Relative

## Abbreviations

<i>BMG</i>	Bruised maize grain
<i>Bo</i>	Bodenstein number
<i>CPU</i>	Central processing unit
<i>DEM</i>	Discrete element method
<i>DFG</i>	Deutsche Forschungsgemeinschaft
<i>FDA</i>	United States Food and Drug Administration
<i>FFT</i>	Fast Fourier transformation
<i>FT</i>	Fourier transformation
<i>IFPRI</i>	International Fine Particles Research Institute
<i>NIR</i>	Near-infrared
<i>PAT</i>	Process analytical technology
<i>PCR</i>	Principal component regression
<i>Pe</i>	Peclet number
<i>PEPT</i>	Positron emission particle tracking
<i>PG</i>	Plastic granulate
<i>PLS</i>	Partial least squares
<i>s</i>	Second
<i>SPC</i>	Stored Program Control
<i>SPS</i>	Speicherprogrammierbare Steuerung

# List of contents

<b>1 Introduction .....</b>	<b>1</b>
<b>2 State of the art .....</b>	<b>5</b>
<b>3 Modeling the mixing process in a continuous dynamic powder mixer.....</b>	<b>14</b>
3.1 Derivation of the Fokker-Planck-Equation.....	15
3.2 Normalization of the Fokker-Planck-Equation and the boundary conditions.....	21
3.3 Coupling of two Fokker-Planck-Equations for a two-component system .....	26
3.4 Numerical solving of the partial differential equation system .....	27
3.4.1 Truncation of the entering mass flows .....	29
3.4.2 Truncation of the mixer inlet (truncation chamber 1) .....	30
3.4.3 Truncation of the chambers in the middle of the mixer (truncation chamber 2 ... n-1).....	31
3.4.4 Truncation of the mixer outlet (truncation chamber n) .....	32
3.4.5 Determination of the mixing quality in the outlet of the mixer .....	35
3.4.6 Calculation of the normalized average residence time of the powder in the mixer .....	36
3.5 Results of the performed simulation experiments .....	37
3.5.1 Influence of the transport and dispersion coefficient on the fluctuation ratio (mixing quality).....	40
3.5.2 Influence of the transport and dispersion coefficient on the normalized average residence time .....	43
3.5.3 Influence of the normalized average residence time on the fluctuation ratio (mixing quality).....	45
3.5.4 Estimation of the necessary running time .....	48
3.5.5 Influence of the number of truncation chambers and the number of time steps on the calculated results.....	50
3.5.6 Influence of the mass $m_w$ on the calculated mixing results .....	50
3.5.7 Influence of the mass flow on the calculated mixing results .....	51
3.5.8 Influence of the normalized transport and dispersion coefficient on the normalized filling degree .....	52
3.5.8.1 Influence of the normalized transport coefficient .....	52
3.5.8.2 Influence of the normalized dispersion coefficient .....	55
3.5.9 Influence of the spreading factor of the entering mass flow on the mixing results .....	57
<b>4 Experimental validation of the mixing model .....</b>	<b>59</b>
4.1 Experimental rig .....	59

4.2 Powders used for the mixing experiments .....	62
4.2.1 Calcium carbonate .....	63
4.2.2 Maize starch .....	65
4.2.3 Compilation of the main bulk characteristics.....	67
4.3 Generation of defined mass flow fluctuations .....	68
4.3.1 Possibilities to improve the short-term dosing constancy of volumetric feeders .....	70
4.3.1.1 State of the art .....	72
4.3.1.2 Own developments and examinations.....	75
4.3.1.2.1 Dosing examinations using calcium carbonate.....	79
4.3.1.2.2 Dosing examinations using maize starch.....	97
4.3.2 Powder dosing in the continuous dynamic mixer.....	99
4.3.3 Hardware and software used for the generation of defined mass flow fluctuations.....	100
4.3.4 Comparison between the generated mass flow fluctuations and the measured ones .....	104
4.4 In-line determination of the concentration in the outlet of the continuous mixer .....	106
4.4.1 Radiometric analysis techniques .....	107
4.4.2 Image analysis techniques .....	107
4.4.3 Capacitance analysis techniques.....	108
4.4.4 Photometric reflection analysis techniques.....	108
4.4.5 In-line concentration determination by Fourier Transformation Near- Infrared (FT-NIR) spectroscopy .....	108
4.4.5.1 Existing applications for the in-line concentration determination of powder mixtures .....	119
4.4.5.2 Adaptation of the FT-NIR spectrometer VECTOR 22/N to the in- line concentration determination in the outlet of the continuous mixer GCM 500.....	124
4.4.5.3 Calibration of the FT-NIR spectrometer VECTROR 22/N.....	127
4.4.5.4 Analysis of calibration mixtures .....	127
4.4.5.5 Preparation of calibration mixtures .....	131
4.4.5.6 Development and validation of a calibration model .....	143
4.4.5.7 Estimation of the sample size .....	147
4.5 Mixing experiments .....	151
4.5.1 Determination of the average residence time .....	155
4.5.1.1 Determination of the average residence time using the “hold-up method” .....	155
4.5.1.2 Determination of the average residence time using of the “step method” .....	156
4.5.1.3 Comparison of the experimental results obtained by using the “hold-up method” and the “step method” .....	158

4.5.2	Mixing experiments for the validation of the mixing model .....	159
4.5.2.1	Influence of the average overall mass flow on the mixing result (half-closed weir) .....	163
4.5.2.2	Influence of the rotational speed of the mixing device on the mixing result (half-closed weir) .....	167
4.5.2.3	Influence of the period length on the mixing result (half-closed weir) .....	171
4.5.2.4	Compilation of the mixing results (half-closed weir).....	175
4.5.2.5	Influence of the average overall mass flow on the mixing result (closed weir) .....	176
4.5.2.6	Influence of the rotational speed of the mixing device on the mixing result (closed weir) .....	180
4.5.2.7	Influence of the period length on the mixing result (closed weir).....	184
4.5.2.8	Compilation of the mixing results (closed weir).....	188
4.5.3	Comparison of the mixing results calculated with the experimental mixing results.....	189
4.5.4	Comparison of the calculated mixing results and the experimental mixing results with literature data.....	191
<b>5</b>	<b>Outlook.....</b>	<b>195</b>
5.1	Ideas for future work in the field of in-line concentration determination by near-infrared spectroscopy .....	195
5.1.1	Improvement of the attachment used for cleaning the probe of the NIR spectrometer with compressed air .....	195
5.1.2	Adaptation of the FT-NIR spectrometer to the examination of powder mixtures with larger particles .....	198
5.1.3	In-line control of the mixing process in continuous mixers without any calibration .....	198
5.2	Ideas for future work in the field of continuous dynamic powder mixing .....	200
5.2.1	Validation of the mixing model using higher mass flows.....	200
5.2.2	Validation of the mixing model using powders with different characteristics .....	201
5.2.3	Validation of the mixing model using different mixing devices and mixers .....	202
5.2.4	Validation of the mixing model using two sinusoidally fluctuating mass flows .....	205
5.2.5	Comparison between the mixing results obtained by using a square wave oscillation and the mixing results obtained by using a superposition of sinusoidal oscillations.....	206
5.2.6	Calculation of the residence time distribution .....	207
5.2.7	Validation of the calculated inclination of the filling degree in the continuous mixer.....	207
<b>6</b>	<b>Summary.....</b>	<b>208</b>
<b>7</b>	<b>Zusammenfassung .....</b>	<b>211</b>



<b>8 References</b> .....	<b>215</b>
<b>9 Appendix</b> .....	<b>226</b>
9.1 Tabular literature survey .....	226
9.2 Published transport and dispersion coefficients.....	229
9.2.1 Experiments by Merz .....	229
9.2.2 Experiments by Merz and Lücke.....	231
9.2.3 Experiments by Holzmüller .....	232
9.3 Mathcad algorithm for the calculation of the fluctuation ratio and the normalized average residence time .....	235
9.4 Tabular compilation of the experimental mixing results .....	242
9.4.1 Mass hold-ups as well as standard deviations of the concentration fluctuations in the inlet and the outlet of the mixer (half-closed weir) .....	242
9.4.2 Mass hold-ups as well as standard deviations of the concentration fluctuations in the inlet and the outlet of the mixer (closed weir) .....	244

## 1 Introduction

The mixing of powders is one of the oldest unit operations. The first mixing vessels were mortars, which were used for the production of natural earth pigments such as ochre and manganese oxide in the Stone Age. Despite the long application history of more than 40 000 years, comparatively little is known about the mixing mechanisms. The mixing of powders is still more an art than a science [1, 2]. The first scientific approaches in examining powder mixing started in the middle of the last century and were concentrated on batchwise working mixers.

Traditionally, the mixing of powders is performed in batchwise working mixers with large volumes. The main time necessary for producing mixtures is the set-up time for the weighing of the powders, the filling and the subsequent emptying of the mixer. The increasing costs and competitive pressure force the companies to automate their production processes. Reduced personnel costs as well as a better documentation of recipes and production parameters are the consequence. The continuous mixing of powders is gaining an increasing share of the market. This tendency is supported by the technical transformation of scientific experiences in the field of continuous powder mixing and the availability of feeders with a high dosing constancy. [3]

The answer to the question if a continuous or a discontinuous mixer is the right choice depends on manifold process parameters, constructive constraints of the factory and economical considerations. Parameters influencing the decision-making are, for example, the complexity of the recipes and the process control, the loading and unloading, the geometrical dimensions, the dosing of additives, the storage of single ingredients and pre-mixes, the throughput, the contamination of the product, the quality control, the heating-up of the product, the mixing time as well as cleaning aspects. Examples of a continuous dynamic powder mixer and a continuous mixing installation as well as a discontinuous mixer and a discontinuous mixing installation are shown in *Fig. 1-1* and *Fig. 1-2* respectively.



*Fig. 1-1: Continuous mixer GCM 500 with a mixing chamber volume of 15 l from the company Gericke (left) and continuous mixing installation (right) [Courtesy of Gericke AG]*



*Fig. 1-2: Discontinuous mixer GMS 5 000 with a mixing chamber volume of 5 000 l from the company Gericke (left) and discontinuous mixing installation (right) [Courtesy of Gericke AG]*

The advantages and disadvantages of continuous mixers in comparison to batch mixers are discussed below. Because of the high automation level of continuous mixing plants the labor costs for filling, emptying and cleaning a continuous mixer are comparatively low. The available space for the installation is often limited. Continuous mixers are comparatively small even though high throughputs can be obtained. This results in shorter mixing distances and less energy consumption because smaller amounts of powder have to be agitated. If hazardous powders are mixed or the danger of dust explosions exists, continuous mixers have a smaller potential risk because less powder is accumulated in the mixer. In the process of mixing, segregation is often a problem, which arises if the size, density and/or shape of the particles to be mixed differ significantly. Segregation problems often do not occur during the mixing process itself but during the following discharging, transportation or storage of the mixtures. Because of the compactness, continuous mixers can often be positioned right before the next process step. Therefore, the best possible quality of the mixture is available and the risk of segregation is reduced. The integration of continuous mixers can often render silos and other intermediate storage facilities superfluous. Continuous mixers can reduce mass flow fluctuations and resulting concentration fluctuations. However, continuous mixers have also some disadvantages. Feeding the powders with a high constancy into the continuous mixers is required. Often several expensive loss in weight feeders are necessary. Using a continuous mixer, a certain time is necessary to reach the steady state. During this time, which is about three times the residence time of the bulk material in the mixer, only a mixture with a diminished quality can be produced. If a high number of components has to be mixed or a flexible adjustment to material and recipe changes is necessary, continuous mixers are not the right

choice. For some industries batch tracing is regulated by law. Using continuous mixers, a batch tracing is difficult and a batch can often be defined only by means of the production time. [4]

Continuous powder mixers are normally used to mix entering components radially. If fluctuations of entering mass flows occur, continuous mixers have to reduce concentration differences in axial direction, too. Mass flow fluctuations can mainly be the result of pulsating powder flows coming out of feeders or other upstream process units. KEUTER [5, 6] described two examples of industrial production processes where the mass flow of at least one entering powder is fluctuating approximately in a periodic manner. The first example describes the mixing process of calcium carbonate and polystyrene at a building material factory. The second example is a process of the company *BAYER AG*. The process is shown in *Fig. 1-3*. A powder coming out of a dryer and a filter cake coming from a continuous rotor filter have to be mixed. The mass flow of the filter cake is fluctuating. Within a period of up to one minute, no filter cake falls into the continuous mixer. The mass flow of the dried powder is almost constant. Based on experience, it is known that the powder mixture sticks to the feeding devices of a down-stream feeder if the humidity is too high. If the humidity is too low, problems due to dust development occur. Therefore, the goal of the mixing process is to homogenize the two powders and to reduce the concentration fluctuations in order to keep the humidity of the mixture within defined limits.

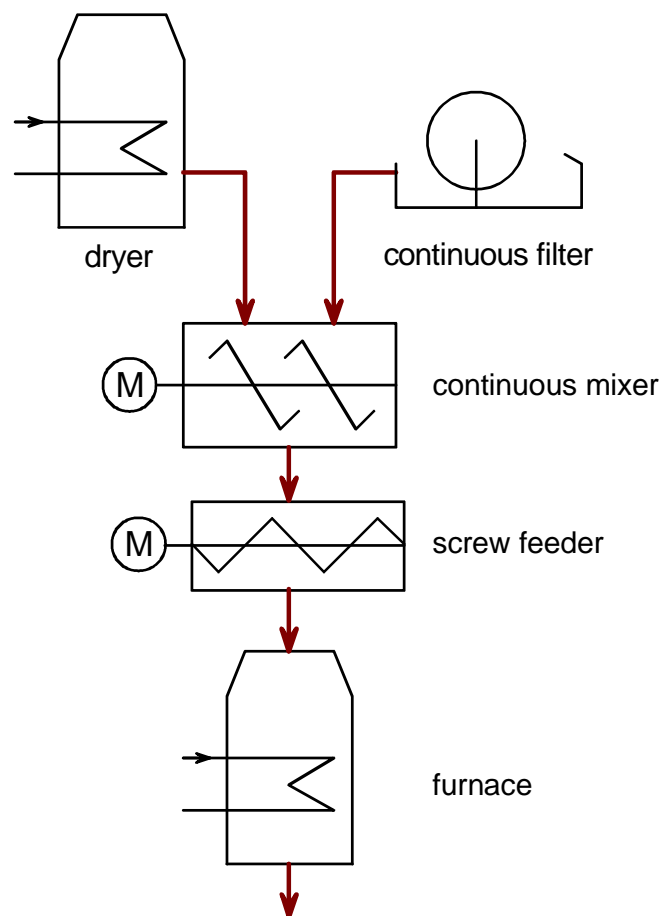


*Fig. 1-3: Example of a process where periodical concentration fluctuations are smoothed by a continuous dynamic mixer [6]*

In the past, different models were developed to calculate the reduction of periodic concentration fluctuations entering a continuous powder mixer. However, the models have the restriction that the amount of the tracer component has to be negligible compared to the amount of the main ingredient. In 1994, SOMMER [7] presented a new model, which is valid for any concentration composition of the mixture. The model is independent of the mixer dimensions and the type of the mixing devices used. Only a few experimental results were published which could have been used to validate the developed model. The objective of this thesis was the experimental validation and the improvement of SOMMER's model.

The validation of the model is only possible if defined mass fluctuations entering the continuous mixer can be generated and the reduction of the resulting concentration fluctuations can be determined in the outlet of the continuous mixer. In this context, a great amount of research work was necessary to improve the short-term dosing constancy of the volumetric feeders used as well as to find and adapt an analyzing technique that allows the in-line concentration determination of the tracer component in the mixture. A promising technique seemed to be the near-infrared spectroscopy, which has already been used for the in-line concentration determination in batchwise working mixers. The analytical results obtained by using a near-infrared spectrometer can only be as exact as the previous calibration. Therefore, much effort was applied improving the calibration procedure. This research work contained an improvement of the calibration sample preparation as well as the later presentation of the samples for calibration.

The research project was integrated in the *Priority Research Program 1062 (Schwerpunktprogramm 1062)* of the *German Research Foundation (Deutsche Forschungsgemeinschaft, DFG)*. Within the framework of the program, which started in 1998 and ended in 2004, more than 35 research teams from different German universities examined the handling of highly dispersed powders, e.g. forming, suspending, mixing, sintering, conveying and storing of ultra fine powders [8]. Pre-condition for the participation in the program was the examination of powders with a median diameter of less than  $10\ \mu\text{m}$ . That is the reason why only cohesive powders, which roughly fulfill this condition, were used for the experimental validation of the developed model.

The results of this thesis can be used to construct an optimum continuous powder mixer as well as to improve the control and monitoring of existing continuous mixing processes. Consequently, the amount of waste can be reduced and the quality of the produced mixtures can be increased.



## 2 State of the art

The scientific knowledge about powder mixing processes is quite scant compared with the long application history. This is especially valid for the continuous mixing of powders. During the last 50 years, only a few articles summarizing the state of the art in the field of powder mixing have been published: In 1958, WEIDENBAUM [9] reviewed the state of the art. The time between 1958 and 1969 was surveyed by FAN et al. [10]. A literature survey about powder mixing was published in 1976 by COOKE et al. [11]. In 1991, POUX et al. [12] reviewed and updated the available data on powder mixing in vessels. An extensive overview about the manifold areas of powder mixing can be found in SOMMER's contribution to Ullmann's Encyclopedia of Industrial Chemistry [13] and in the books of WEINEKÖTTER [14, 15] and KAYE [16].

In *Fig. 2-1*, the subdivision of powder mixers with a special interest in continuous mixers is shown. In general, powder mixers can be grouped in discontinuous (batchwise working) mixers and continuous mixers. The continuous powder mixers can be subdivided in gravity, non-dynamic and dynamic mixers. Continuous mills are also assigned to the group of continuous mixers because a mixing of entering bulk material occurs besides the grinding [17, 18, 19]. The driving force in gravity mixers is gravitation. Static mixers can mix entering powders mainly in radial direction [20, 21, 22]. Therefore, a high short-term dosing constancy of the feeding equipment used is necessary. In silo mixers, gravitation is also used to homogenize the bulk material. Often several circulations are necessary to obtain the set mixing quality [23, 24]. Rotating drums belong to the group of non-dynamic mixers [25, 26]. In contrast to continuous dynamic mixers, they have no rotating mixing devices. Depending on the orientation of the mixing device, dynamic mixers can be subdivided in vertical and horizontal dynamic mixers. Besides the mixing device, gravitation is the driving force in vertical dynamic mixers [27, 28]. In this work, the attention is turned to horizontal dynamic mixers with rotating mixing devices, which can be blades, paddles, plowshares or ribbons.

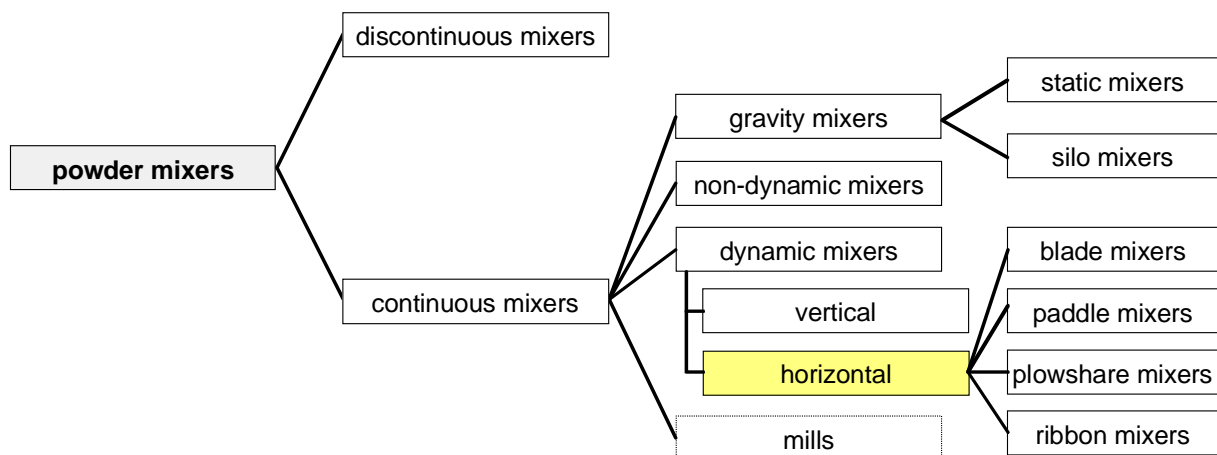


*Fig. 2-1: Subdivision of powder mixers with special interest in continuous mixers*

The main tasks of continuous dynamic powder mixers are summarized in *Fig. 2-2*. Besides the radial mixing of bulk materials, continuous mixers have often to fulfill a smoothing of concentration fluctuations, which is called axial mixing (compare *Fig. 2-3*). The radial mixing is much faster and more efficient than the axial mixing.

Cohesive powders tend to stick together and to build up lumps. The energy induced by the mixing devices is often not high enough to destroy lumps and to disperse the powder in primary particles. This problem can be overcome by using a rotating star attachment for the dosing tube of the volumetric feeders [29, 30, 31] or by inserting choppers in the continuous mixer. In addition to the radial and axial mixing, special tasks such as wetting, coating, agglomerating, heating and cooling of the bulk material can be necessary.

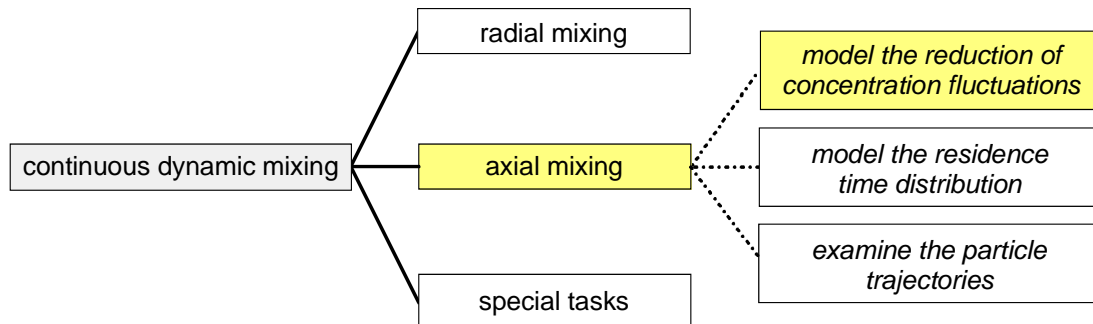


**Fig. 2-2:** Tasks of continuous dynamic mixers

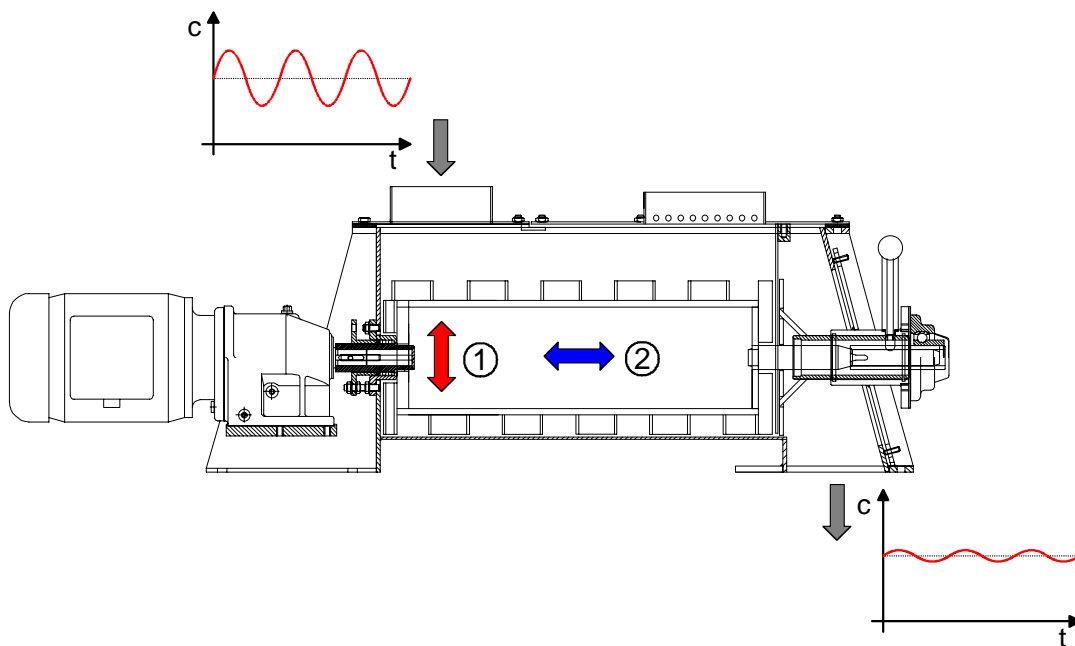


**Fig. 2-3:** Illustration of the radial and axial mixing in a continuous dynamic powder mixer (① radial mixing, ② axial mixing) [32]

The main interest of this work is the axial mixing, in particular modeling the reduction of concentration fluctuations entering the continuous mixer. The modeling is only possible if the particle movement in the mixer can be described mathematically. Modeling the reduction of concentration fluctuations is closely connected with the modeling of the residence time distribution of particles in the mixer.

The following literature survey concentrates on scientific publications about continuous powder mixing in horizontal dynamic mixers. The main research topics and results are described. In *Table 9-1* of the appendix (see p. 226), the mentioned publications are tabulated chronologically. The dates, the names of the authors and the titles of the publications are listed.

Many models for calculating the reduction of concentration fluctuations by continuous powder mixers have their roots in the considerations of DANCKWERTS and SELLER, published in 1951 [33]. They had the job to design a gas holder which can reduce caloric value fluctuations of town gas. For the assumption of an ideally stirred gas holder, they developed a model to calculate the reduction of composition fluctuations in the gas stream depending on the size of the holder. The variance reduction ratio, which is defined as the variance of the fluctuations in the inlet divided by the variance of the fluctuations in the outlet, was introduced. In 1953, DANCKWERTS enlarged the model for non-ideal mixers [34]. Based on the autocorrelation coefficient of the fluctuations in the feed and the residence time distribution in the mixer, DANCKWERTS derived an equation to calculate the variance reduction ratio.

The first experimental results about the continuous mixing of solids were published by RAOUF in 1963 [35]. Free-flowing glass and sand particles with a median diameter between  $0.4$  and  $0.6$  mm were continuously mixed in an U-shaped trough. The mixing element consisted of an inner screw conveyor of small diameter surrounded by a helical ribbon which transported the bulk material opposing to the screw. Two types of mixing elements, differing in the pitch lengths, were used. Additionally, mixing experiments with a plain rotating cylinder were performed. RAOUF investigated the influence of the rotational speed and the mixing element type on the mixing degree as well as the influence of the rotational speed, the mixer length and the mixing element type on the residence time distribution. At different distances from the mixer inlet, samples were taken with a sampling device. The resulting mixing degree was determined. RAOUF stated that increasing the rotational speed of the mixing elements as well as increasing the pitches of the screw and the ribbon used cause a better mixing performance. Because of missing confidence intervals and a high spreading of the measured concentration values, the results are not statistically proofed. For the examination of the residence time distribution, the inlet stream was changed from red sand to blue sand. To determine concentrating changes, small metal containers were moved through the bulk material flowing out of the mixer. The examinations of the residence time distribution showed a substantial amount of axial mixing which is influenced by the mixer length as well as the rotational speed and the type of the mixing elements. The obtained residence time distributions were described by a cascade of perfect mixers, a method developed for continuous fluid flow systems.

In 1965, POOLE et al. [36] published experimental data of their mixing trials using a continuous ribbon-blender. For copper/nickel and uranium oxide/nickel mixtures with mean particle diameters between  $10$  and  $55$   $\mu\text{m}$ , the influence of the mixture ratio on the final mixing quality and the influence of the mixing time on the mixing quality were examined. It was stated that the mixing degree increases if the relative amount of the second component increases. However, the statement has to be questioned because of the minimal differences between the measured values and the missing confidence intervals. For copper/nickel and uranium oxide/thorium oxide mixtures, the influence of the flow rate, the rotational speed and the mixer length on the average residence time and the spreading of the residence distribution was determined. For uranium



oxide and thorium oxide, the influence of the frequency of an intermittent feeding on the fluctuation reduction in the mixer was examined. High frequency fluctuations were reduced more effectively than low frequency fluctuations.

Theoretical considerations about the axial mixing during the transport of bulk materials through continuously working apparatus were published by MOLERUS [37] in 1966. For the calculation of residence time distributions, he derived a convection diffusion model based on stochastic considerations. The model is founded on the so-called Fokker-Planck-Equation, which is named for the scientists FOKKER and PLANCK, who introduced the convection diffusion equation for the first time in stochastic physics. MOLERUS established a correlation between the average value as well as the spreading of the residence time distribution, characterized by the first and second momentum of the residence time distribution, and the convective as well as the diffusive transport parameter of the Fokker-Planck-Equation. His considerations were mainly dedicated to processes taking place in continuously working ball mills, but they can also be applied to continuously working dynamic mixers.

In 1971/1972, WILLIAMS and RAHMAN predicted theoretically the performance of continuous mixers for particulate solids [38] and validated the developed model experimentally [39]. The results of residence time distribution tests were used to predict the variance reduction ratio. The variance reduction ratio is the ratio of the variance of concentration fluctuations entering the continuous mixer to the variance of concentration fluctuations leaving the mixer. The idea of the developed model was to split up the entering concentration fluctuations in a sequence of impulses. By stimulus response tests, the effect of each impulse on the output stream is known. Superimposing the effect of the single impulses, the fluctuations leaving the continuous mixer can be calculated. A numerical and an analytical method for the calculation of the variance reduction were presented. Both methods showed a good agreement. The developed model was validated with a drum mixer. For the mixing experiments, the sieve fractions between 355 and 420  $\mu\text{m}$  of sand and salt particles were used. For random fluctuations as well as for periodic input fluctuations, a very good agreement between the predicted and the measured output fluctuations was found using tracer concentrations smaller than 10 %.

In 1973, MERZ [26] adapted scintillation detectors to the in-line concentration determination of radioactive tracers along a rotating drum as well as in the outlet of a rotating drum. The analyzing technique allows the determination of temporal concentration distributions at different positions inside the continuous drum mixer. For the experiments, different sieve fractions between 150 and 1000  $\mu\text{m}$  of quartz sand were used. MERZ applied the momentum method, introduced by MOLERUS [37], to determine the transport and dispersion coefficient by means of stimulus response experiments. The experimental results showed an influence of the particle size on the transport and dispersion coefficient. The influence of the drum length on the transport and dispersion coefficient was also examined. The transport coefficient was independent of the drum length. The dispersion coefficient decreased with increasing drum length. The influence of the rotational speed on the transport and the dispersion coefficient was not explicitly determined. But the influence of the rotational speed on the average residence time and the spreading of the residence time distribution were examined. The influence of the rotational speed on the average residence time is not significant. The spreading of the

residence time distributions, which corresponds to a higher dispersion, increased with higher rotational speeds.

In 1973, ENNS [40] took up the reflections from WILLIAMS and RAHMAN [38, 39] on the prediction of the variance reduction ratio by means of impulse response tests. He reported on an alternative numerical solution of the derived integral equation by using the Laplace transformation. This can be interesting because input impulse response measurements are often not possible or allowed for process reasons. Additionally, the measurement of the impulse response nearby the maximum is difficult because of the limited resolution of analyzing devices. The proposed Laplace transformation allows the usage of any measurable inlet fluctuation and the calculation of the overall response of different devices connected serially if the single response is known.

HARWOOD et al. [41] compared the performance of seven different continuous powder mixers in 1975. They used sand and sugar particles with a mixing ratio of 20 : 1. By using sieving fractions of different mesh sizes, the mixing of cohesive/cohesive, cohesive/free-flowing and free-flowing/free-flowing powder pairs could have been examined. Based on the standard deviations of concentrations measured in taken samples, the authors made recommendations for the use of different mixers.

In 1975, SCHOFIELD's [42] PhD thesis on "The continuous mixing of particulate solids" was published. He examined the continuous mixing of free-flowing silicate sand (median diameter about  $250 \mu\text{m}$ ) and cohesive calcium carbonate (median diameter about  $35 \mu\text{m}$ ) in a ribbon blade mixer. SCHOFIELD developed a reflectivity device for in-line concentration measurements. The analyzing device was used for the experimental determination of the smoothing of periodic impulses as well as the experimental determination of residence time distribution curves resulting from stimulus response experiments. It was shown that the residence time distributions and the smoothing of periodic composition fluctuations can be calculated with a model based on a cascade of ideally stirred vessels.

In 1976, COOKE, STEPHENS and BRIDGWATER [11] published a comprehensive list of 650 references to the topic of powder mixing in general. The list is classified in different topics and contains among other things 15 references to continuous mixing and 44 references to PhD theses about solid mixing.

In 1976, WILLIAMS [43] reviewed the state of the art of continuous solid mixing. He discussed the advantages and disadvantages of continuous mixing and presented approaches to calculate the variance reduction ratio for ideal and non-ideal mixers. Ten years later, WILLIAMS [44] published a quite similar article. However, he did not mention publications about continuous solid mixing published in the meantime in German.

In 1977, LÜCKE and MERZ [45, 46] determined the performance of a continuous *Lödige* plowshare mixer with a capacity of  $150 \text{ l}$ . They used an in-line analysis technique, which MERZ [26] developed to examine the mixing process in continuous drum mixers. Five scintillation detectors were installed in the *Lödige* mixer, and five above a conveyor belt, which was positioned under the outlet of the mixer. The temporal concentration changes of radio-activated bruised maize grain in not activated maize grain resulting from impulse response tests were determined by using scintillation detectors. The average particle diameter of the maize grain

was  $0.37\text{ mm}$ . The influence of the mass flow on the average residence time as well as the standard deviation of the residence time distribution was examined. By mathematical superposition of measured residence time distribution curves, they simulated an intermitted dosing in the continuous mixer. For different mass flows and rotational speeds, the influence of the period length of entering concentration fluctuations normalized by the average residence time on the mixing quality was examined. The mixing quality was defined as the maximum concentration deviation related to the average concentration. LÜCKE and MERZ [46, 47] found out that the mixing qualities obtained experimentally are better than the calculated results for an ideal mixing vessel. The experimental results showed that concentration deviations from the average concentration decrease for smaller ratios of the period length and the average residence time. Parts of the results were published again by LÜCKE [47] in 1978.

In 1977, SOMMER [1] described the mixing process by displacements of particles located in the cutout of a continuous mixer. The stochastic displacements can be described by a displacement distribution, characterized by the mean displacement of the particles and the standard deviation of the displacement distribution. SOMMER established a correlation between the concentration and the local probability density used by MOLERUS [37]. Additionally, a correlation between the average displacement of the particles and the transport coefficient of the Fokker-Planck-Equation as well as the standard deviation of the displacement distribution and the dispersion coefficient of the Fokker-Planck-Equation was given. The English version of the work was published in 1979 [2].

In 1978, MERZ and LÜCKE [48] examined the influence of the rotational speed, the mixing device type (plowshares or blades) as well as the throughput on the transport and dispersion coefficient. The coefficients were determined by the algorithm introduced by MOLERUS [37]. Free-flowing bruised maize grain with a median diameter of  $370\ \mu\text{m}$  was used for the mixing experiments. Because of missing confidence intervals, the results are more useful to estimate the order of the transport coefficient and the dispersion coefficient than to derive tendencies. For the maximum throughput, the transport coefficient was higher than for the minimum throughput. The use of plowshares in combination with higher rotational speeds caused higher transport coefficients than the use of blades. Higher rotational speeds caused higher dispersion coefficients. The dispersion coefficient stayed approximately constant in the case the mixing device and the throughput are changed.

In 1984, HOLZMÜLLER published his PhD thesis on examinations of bulk material movement during continuous solid mixing [4]. For the experiments he used bruised maize grain with a median diameter of  $340\ \mu\text{m}$  and plastic granulate with a median diameter of  $2700\ \mu\text{m}$ . Each granulate was mixed separately. The temporal concentration changes of radio-activated fractions in not activated bulk material as a result of impulse response tests were determined. For the mixing experiments, HOLZMÜLLER used the same experimental set-up as LÜCKE and MERZ [45, 46, 47]. However, the *Lödige* mixer without a weir was replaced by a *Lödige* mixer with an inlaying weir. The flow of the bulk material is described with the dispersion model. The momentum method was used for the interpretation of the mixing results. The influence of the mass flow ( $1\text{ kg/min}$  and  $4\text{ kg/min}$ ), the radial positioning of the plowshares (one setting supporting the mass flow and one acting against) and the rotational speed ( $Fr = 0.43, 1.73, 3.9, 6.93$ ) on the average residence time as well as the transport and dispersion coefficient was

examined. HOLZMÜLLER found out that the bulk material can be better mixed in a fluidized state than in a non-fluidized state. The mass flow, the radial positioning of the plowshares and the rotational speed had a strong influence. The results of the residence time distribution examinations were published in [32], too.

In 1986, WANG [49] gave a brief overview about residence time distribution models for continuous solid mixers. Additionally, he described the features of eleven different continuous mixers.

In 1993, WEINEKÖTTER [50] finished his PhD thesis on the continuous mixing of small particles. He developed a laser optical in-line measuring system to examine the mixing process of binary powder systems, consisting of silicon carbide or Irgalite in aluminum hydroxide. The tracer components, silicon carbide (median diameter of  $24 \mu\text{m}$ ) or Irgalite (median diameter of  $0.22 \mu\text{m}$ ), differed in color from the major component aluminum hydroxide (median diameters between  $27$  and  $72 \mu\text{m}$ ). For the mixing experiments, WEINEKÖTTER used a two-shaft *Gericke* mixer with two different settings of the mixing device and a prototype one-shaft *Gericke* mixer. He found out that feed concentration fluctuations with high frequencies were much more reduced in the mixers than fluctuations with low frequencies. For the case that the period length of the entering concentration fluctuations was three times higher than the average residence time of the powder in the mixer, no reduction of the fluctuations was detected. A significant reduction was observed for the case that the period lengths of the entering concentration fluctuations were in the same order as the average residence time of the powder in the mixer or smaller. For the calculation of the variance reduction ratio, WEINEKÖTTER used DANCKWERTS' approach [34]. DANCKWERTS developed his model for fluids, which can be ideally mixed. For particles, the random mixture is the best reachable mixing quality. WEINEKÖTTER took the limitation of the reachable homogeneity of particulate mixtures into account. For the calculation of residence time distributions, he developed an axial dispersion model. Parts of WEINEKÖTTER's PhD thesis were also published in [51, 52, 53].

In 1994 and 1996, SOMMER [7, 54] reported about a new model for calculating the reduction of concentration fluctuations entering a continuous mixer. The model is based on the Fokker-Planck-Equation, which describes the particle transport by convection and dispersion. SOMMER pointed out that in most previous publications the transport by convection was considered identically with the average mass flow through the mixer. This assumption is only valid if the amount of the tracer component is much smaller than the amount of the main component and no significant dispersion occurs. For powder mixing, this assumption is not valid. Therefore, SOMMER used a separate Fokker-Planck-Equation for each component. The equations are coupled by the transactions at the weir located at the end of the mixer. For batch mixing, it is well known that higher dispersion coefficients induce a faster mixing. The same is expected for continuous mixing. SOMMER's simulations with his new model have shown that this is not valid in general. For higher transport coefficients, the expectation is correct. For smaller transport coefficients, the mixing quality decreases with an increase of the dispersion coefficient. Additional simulations revealed that the average residence time related to the period length of the entering concentration fluctuation is the main parameter influencing the reduction of concentration fluctuations.

In 1995, KEUTER and PAHL [5] published a survey about the continuous mixing of powders. They mainly described two known mixing models. The model based on a cascade of ideally stirred vessels was used to calculate the residence time distribution for different vessel numbers as well as to calculate the amplitude reduction of entering concentration fluctuations. WEINEKÖTTER's convection and dispersion model [50] was used to calculate the variance reduction of entering concentration fluctuations. For a mixture of 95 mass-% calcium carbonate and 5 mass-% polystyrene not expended, KEUTER and PAHL determined the cumulative residence time distribution and calculated the corresponding number of ideally stirred vessels. By means of the vessel number, it was checked if a preset amplitude reduction of 93 % can be obtained. Together with NOTHELLE and SEYFFERT, KEUTER [6] used the cascade model of ideally stirred vessels to examine a mixing process at the company BAYER AG, where a periodically fluctuating filter cake was mixed with dried powder. For a set period length and varying average residence times as well as varying vessel numbers, the remaining mass flow fluctuations and the dry content fluctuations in the mixer outlet were calculated.

LAURENT, BRIDGWATER and REISEMANN [55] used the Positron Emission Particle Tracking (PEPT) technique to examine the flow regime in a continuous dynamic powder mixer with two inlaying and rotating weirs. The movement of a single radioactive particle, emitting positrons, was observed. Because of collisions between the positrons and neighboring electrons, collinear gamma rays are transmitted. Using the gamma rays, the location of the radioactive particle was determined 20 times per second. The determined positions were used to plot the axial movement of the particle, the probability of presence of the particle in the longitudinal section of the mixer and the particle velocity in the radial section of the mixer. The PEPT technique was already used to study the particle movement in batchwise working mixers [56, 57, 58, 59, 60, 61, 62].

In 2000, WALCH's [63] PhD thesis on transport mechanisms of bulk materials and pastes in a paddle reactor was published. WALCH examined the residence time behavior of rice (median diameter 278  $\mu\text{m}$ ), semolina coarse (median diameter 1540  $\mu\text{m}$ ), semolina fine (median diameter 744  $\mu\text{m}$ ) and flour particles (median diameter 124  $\mu\text{m}$ ) in a rotary-paddle reactor. The influence of the rotational speed and the paddle configuration of the mixing device, the flowability of the products as well as the flow rate on the residence time distribution were determined. Based on the Fokker-Planck-Equation, WALCH developed a model, which allows the calculation of tracer concentration changes in the outlet of the paddle reactor for a given periodic tracer concentration fluctuation in the inlet. The required transport and dispersion coefficients were determined by fitting the developed model to the measured residence time distributions.

In 2001, KEHLENBECK and SOMMER [64] reported of a new project to validate and improve SOMMER's model [7, 54], which can be used to calculate the reduction of concentration fluctuations entering continuous dynamic mixers. Publications about the model and its experimental validation followed [65, 66, 67, 68].

Since 1997, GHADERI has dealt with the continuous mixing of particulate materials in scope of his PhD thesis. For the mixing experiments, he used a self-made continuous paddle mixer with two shafts. Until now, only theoretical considerations to describe the mixer efficiency were published [69, 70]. For the description of the mixer efficiency, GHADERI used DANCKWERTS' approach [34] for calculating the variance reduction ratio. As WEINEKÖTTER [50], he added an

additional term, which denotes the variance of the outlet fluctuations in the case of a constant feeding.

In 2004, MARIKH [71] finished her PhD thesis about continuous mixing of powders. She modeled the residence time distribution resulting from a stimulus response and the variance reduction of entering sinusoidal mass flow fluctuations by using the theory of Markov chains. For the experimental validation, couscous (particle size between 1 and 2 mm) and semolina (particle size between 200 and 500  $\mu\text{m}$ ) were mixed in a continuous dynamic *Gericke* mixer. Parts of the thesis had already been published [72].

In 2005, HABERMANN [73] finished his PhD thesis on the correlation between residence time distribution and mixing quality. Calcium carbonate (median diameter 6  $\mu\text{m}$ ), calcium carbonate colored with toner carbon black (median diameter 5.8  $\mu\text{m}$ ) and polystyrene granulate not expanded (median diameter 832  $\mu\text{m}$ ) were mixed in a continuous *Lödige* plowshare mixer with a capacity of 150 l. HABERMANN examined the influence of the tooling Froude number, the mass flow and the filling degree of the mixer on the residence time distribution, the mixing quality (defined as variation coefficient) and the variance reduction of entering sinusoidal mass flow fluctuations. For the determination of the residence time distribution, the tracer concentration (colored calcium carbonate) was changed in a stepwise manner. The concentration response in the mixer outlet was determined in-line with a self-developed analyzer. The analyzer consists of an illumination device and a CCD camera. The significance of the residence time experiments concerning the influence of the Froude number, the mass flow and the filling degree is limited because the trials were not repeated and the difference between the plotted curves is not large in most cases. Selected residence time distributions were compared with the residence time distribution calculated with the dispersion model, the tank in series model, a transfer function based on second order delay element, a Weibull distribution and double Weibull distribution. The performed mixing experiments showed no significant influence of the Froude number, the mass flow and the filling degree on the mixing quality and the variation coefficient respectively. For the examination of the variance reduction, a sinusoidally fluctuating polystyrene granulate mass flow was mixed with a constant calcium carbonate mass flow. The remaining concentration fluctuations in the outlet of the continuous mixer were determined by manual sampling. The concentration of polystyrene in the samples was determined by sieving. The average residence time of the particles in the mixer was at least two times higher than the period length of the generated fluctuations. Therefore, no significant difference between the measured results was found. HABERMANN also calculated the variance reduction using WEINEKÖTTER's model [50]. Because of the large confidence intervals and the fact that the experimental results do not cover ratios of the average residence time to the period length smaller than 2, the validation of WEINEKÖTTER's model is not possible. Parts of the thesis were already published in [74].

### 3 Modeling the mixing process in a continuous dynamic powder mixer

Although computer performance has increased tremendously during the last decades, the simulation of particle displacements in a particle collective by means of Discrete Element Methods (DEM) is still limited. In 2000, KANEKO et al. [75] used DEM to simulate the particle mixing in a single helical ribbon agitator. To reduce the computational load of their personal computer, they had to reduce the particle number to  $10^5$  and increase the particle diameter up to  $8\text{ mm}$ . Approximately  $8\text{ h}$  were necessary to calculate the particle displacements during  $1\text{ s}$ . In 2001, STEWART et al. [76] compared the measured flow of granules in a bladed mixer with DEM simulations. The simulations were limited to  $16 \cdot 10^4$  glass beads with a diameter of  $5\text{ mm}$ . In 2002, CLEARY et al. [77] reported that DEM simulations with up to  $5 \cdot 10^6$  particles are possible in reasonable times on current single processor workstations. They used a DEM code to predict the flow patterns and mixing rates in a plowshare mixer ( $450\text{ mm}$  long,  $250\text{ mm}$  inner diameter) with a single blade and in a plowshare mixer ( $1\text{ m}$  long,  $250\text{ mm}$  inner diameter) with four blades. About  $103 \cdot 10^3$  spherical particles were used for the single blade mixer and about  $250 \cdot 10^3$  spherical particles for the mixer with four blades. For the simulations, particles with a diameter between  $2.5$  and  $5\text{ mm}$  were considered. In 2005, BERTRAND et al. [78] gave an actual overview about different DEM-based models to simulate the mixing process of granular materials as well as the time necessary to simulate one impeller revolution depending on the number of particles and the used computer system (see *Table 3-1*). Even with a “supercomputer” (64-processor Beowulf cluster), the expected CPU time to simulate the impeller revolution for  $10^6$  particles is about half a week.

**Table 3-1:** CPU time necessary to simulate the flow of spherical particles in a tumbling mill using a DEM-based model [78]

Number of particles	CPU time per impeller revolution		
	serial computer	32 processors	64 processors
$10^3$	3 hours	10 minutes	5 minutes
$10^4$	1.25 days	2 hours	1 hour
$10^6$	4 months	1 week	3.5 days

Using cohesive powders with a particle diameter of about  $10\text{ }\mu\text{m}$ , the real particle number in the mixer exceeds the limit of the particle number, which can be simulated with DEM codes and available computers, in order of magnitudes. This is even valid for small mixers with a low filling degree. In addition to the missing computer performance,

- the consideration of different particle shapes,
- the exact mathematical description of the particle-particle-interactions and
- the description of the interactions between the single particles and the mixing device as well as the walls of the mixing chamber

are difficult. Therefore, stochastic approaches to describe the particle displacements were mainly used to model mixing processes.

Within the scope of this thesis, SOMMER's model [7, 54] for calculating the reduction of concentration fluctuations entering a continuous mixer was applied and improved. Basis of the model is the Fokker-Planck-Equation, also known as the Convection-Diffusion-Equation (see *Eq. 3-1*). The Fokker-Planck-Equation describes the temporal concentration alteration at a specific position  $x$  inside the continuous mixer. The concentration is defined as mass per chamber concentration. Parameters of the Fokker-Planck-Equation are the transport coefficient  $U^*$  and the dispersion coefficient  $D^*$ .

$$\frac{\partial c(x,t)}{\partial t} = -U^* \cdot \frac{\partial c(x,t)}{\partial x} + D^* \cdot \frac{\partial^2 c(x,t)}{\partial x^2} \quad \text{Eq. 3-1}$$

At the beginning of this chapter, the Fokker-Planck-Equation used is derived under the stochastic point of view. Afterwards, the necessary normalization and coupling of the used Fokker-Planck-Equations are explained. Finally, the numerical solution of the differential equation system is discussed.

### 3.1 Derivation of the Fokker-Planck-Equation

A derivation of the Fokker-Planck-Equation, based on probability reflections, was performed by MOLERUS [37]. He derived the equation for the description of axial mixing processes in continuously operating apparatuses. A schematic continuously operating apparatus is shown in *Fig. 3-1*. The entry and exit of the mass flow only takes place at the faces. The position of a particle inside the apparatus can be described by the Cartesian coordinates  $x, y, z$ . The  $x$ -coordinate is directed to the outlet.

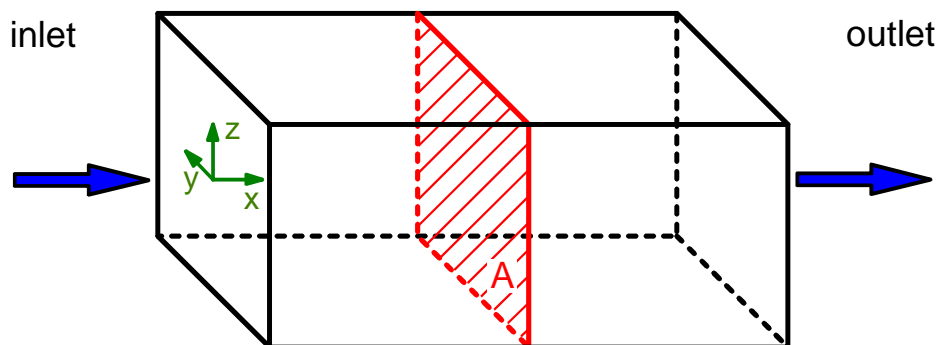


*Fig. 3-1: Schematic continuous apparatus with mass inlet and outlet at the face sides [37]*

The probability that a particle with the position  $(x,y,z)$  is located inside the volume  $dx \cdot dy \cdot dz$  at the time  $t$  describes the term  $u(x,y,z,t) \cdot dx \cdot dy \cdot dz$ . The term  $u(x,y,z,t)$  is the local probability density that a particle is located at the position  $(x,y,z)$  at the time  $t$ .

For simplification, an ideal mixing in planes transverse to the  $x$ -axis is assumed (no gradient in  $y$ - and  $z$ -direction). Therefore, the processes in the apparatus can be described by a one-dimensional equation. Integrating over the cross section area  $A$  of the apparatus ( $y$ - $z$ -plane), the probability density  $v(x,t)$  in the cross-section is derived:



$$v(x, t) = \iint_A u(x, y, z) \cdot dy \cdot dz \quad \text{Eq. 3-2}$$

The term  $v(x, t)$  is the local probability density that a particle is located in the plane  $A$  at the position  $x$  and the time  $t$ .

The assumption is made that a particle is placed at the position  $x = \alpha$  at the time  $t = 0$ . For every other position ( $x \neq \alpha$ ) inside the apparatus, the probability density is  $v(x, t) = 0$  for  $t = 0$ . Corresponding to the definition of  $v(x, t)$ ,

$$\int_{-\infty}^{+\infty} v(x, t) \cdot dx = 1 \quad \text{Eq. 3-3}$$

results for every time.

For the case that the probability density  $v$  depends on the initial position  $\alpha$  of the particle, the probability density has to be defined as a function of the initial position  $\alpha$  as well as the position  $x$  and the time  $t$ :

$$v = f(\alpha, x, t) \quad \text{Eq. 3-4}$$

The probability density  $f(\alpha, x, t + \theta)$  for every following time  $t + \theta$  can be calculated as follows:

After a certain time  $t$ , the local probability density for the existence of a particle at the position  $\xi$  is  $f(\alpha, \xi, t)$ . The resulting probability that the particle is located in the interval between  $\xi$  and  $\xi + d\xi$  is given by  $f(\alpha, \xi, t) \cdot d\xi$ . During the time  $\theta$ , the particle moves from the interval between  $\xi$  and  $\xi + d\xi$  to the position  $x$ . As the transport process does not change, the probability density for the movement is  $f(\alpha, \xi, t) \cdot d\xi \cdot f(\xi, x, \theta)$ . The probability density that a particle has moved from the initial position  $x = \alpha$  to the new position  $x$  during the time  $t + \theta$  can be calculated by superposition of all explained steps for  $-\infty < \xi < +\infty$ . The superposition is described by the Chapman-Kolmogorov-Equation [79, 80]:

$$f(\alpha, x, t + \theta) = \int_{-\infty}^{+\infty} f(\alpha, \xi, t) \cdot f(\xi, x, \theta) \cdot d\xi \quad \text{Eq. 3-5}$$

For the starting position  $x = \alpha$  at the time  $t = 0$  and specific boundary conditions, the solution of the integral equation describes the stochastic movement of a particle during the time  $t + \theta$ .

In a powder mixer, the events happening at the time  $t$  only depend on the conditions at this moment and not on the initial conditions:

$$v = f(x, t) \Rightarrow v(x, t) \quad \text{Eq. 3-6}$$

Such processes are called Markov processes. The probability density  $v(x, t)$  that a particle is located at the position  $x$  at the time  $t$  is known. The probability density  $v(x, t + \theta)$  for every following time  $t + \theta$  can be derived according to *Eq. 3-5*:

$$v(x, t + \theta) = \int_{-\infty}^{+\infty} v(\xi, t) \cdot f(\xi, x, \theta) \cdot d\xi \quad \text{Eq. 3-7}$$

For solving the integral equation **Eq. 3-7**, the variable  $\xi$  is substituted with  $\eta = x - \xi$ , which is the displacement during the time  $\theta$ .

$$v(x, t + \theta) = \int_{-\infty}^{+\infty} v(x - \eta, t) \cdot f(x - \eta, x, \theta) \cdot d\eta \quad \text{Eq. 3-8}$$

Because of the formal context  $f(x - \eta, x, \theta) = f(x - \eta, (x - \eta) + \eta, \theta) \equiv w(x - \eta, \eta, \theta)$  the following equation arises:

$$v(x, t + \theta) = \int_{-\infty}^{+\infty} v(x - \eta, t) \cdot w(x - \eta, \eta, \theta) \cdot d\eta \quad \text{Eq. 3-9}$$

To solve **Eq. 3-9**, an expansion of both sides in a Taylor series is necessary. In general an expansion of a function  $f(z)$  in a Taylor series about the point  $z_0$  can be written according to **Eq. 3-10** [81].  $f^{(j)}(z_0)$  is the  $j^{\text{th}}$  deviation of the function  $f(z_0)$  to  $z$ .

$$f(z) = \sum_{j=0}^{\infty} \frac{f^{(j)}(z_0)}{j!} \cdot (z - z_0)^j = f^{(0)}(z_0) + f^{(1)}(z_0) \cdot (z - z_0) + \frac{f^{(2)}(z_0)}{2} \cdot (z - z_0)^2 + \dots \quad \text{Eq. 3-10}$$

It is assumed that  $\theta$  is a short period. The left side of the integral equation **Eq. 3-9** is expanded in the Taylor series about  $\theta$ . The expansion is aborted after the second term.

$$v(x, t + \theta) = v(x, t) + \frac{\partial v(x, t)}{\partial t} \cdot \theta \quad \text{Eq. 3-11}$$

The function  $v(x - \eta, t) \cdot w(x - \eta, \eta, \theta)$  under the integral on the right side of **Eq. 3-9** is expanded in the Taylor series about the displacement  $\eta$  during the time  $\theta$ . The expansion is aborted after the third term.

$$v(x - \eta, t) \cdot w(x - \eta, \eta, \theta) = v(x, t) \cdot w(x, \eta, \theta) + \frac{\partial(v(x, t) \cdot w(x, \eta, \theta))}{\partial x} \cdot (-\eta) + \frac{1}{2} \cdot \frac{\partial^2(v(x, t) \cdot w(x, \eta, \theta))}{\partial x^2} \cdot (-\eta)^2 \quad \text{Eq. 3-12}$$

Incorporating **Eq. 3-12**, the right side of **Eq. 3-9** can be written as **Eq. 3-13** and **Eq. 3-14** respectively.

$$\int_{-\infty}^{+\infty} v(x-\eta, t) \cdot w(x-\eta, \eta, \theta) \cdot d\eta = \int_{-\infty}^{+\infty} \left( v(x, t) \cdot w(x, \eta, \theta) - \frac{\partial(v(x, t) \cdot w(x, \eta, \theta))}{\partial x} \cdot \eta + \frac{1}{2} \cdot \frac{\partial^2(v(x, t) \cdot w(x, \eta, \theta))}{\partial x^2} \cdot \eta^2 \right) \cdot d\eta \quad \text{Eq. 3-13}$$

$$\int_{-\infty}^{+\infty} v(x-\eta, t) \cdot w(x-\eta, \eta, \theta) \cdot d\eta = v(x, t) \cdot \int_{-\infty}^{+\infty} w(x, \eta, \theta) \cdot d\eta - \frac{\partial \left( v(x, t) \cdot \int_{-\infty}^{+\infty} \eta \cdot w(x, \eta, \theta) \cdot d\eta \right)}{\partial x} + \frac{1}{2} \cdot \frac{\partial^2 \left( v(x, t) \cdot \int_{-\infty}^{+\infty} \eta^2 \cdot w(x, \eta, \theta) \cdot d\eta \right)}{\partial x^2} \quad \text{Eq. 3-14}$$

Using the following simplification

$$\int_{-\infty}^{+\infty} \eta^n \cdot w(x, \eta, \theta) \cdot d\eta = I_n(x, \theta) \quad \text{with } n = 0, 1, 2 \quad \text{Eq. 3-15}$$

**Eq. 3-9** can be written as

$$v(x, t) + \frac{\partial v(x, t)}{\partial t} \cdot \theta = v(x, t) \cdot I_0 - \frac{\partial(v(x, t) \cdot I_1(x, \theta))}{\partial x} + \frac{1}{2} \cdot \frac{\partial^2(v(x, t) \cdot I_2(x, \theta))}{\partial x^2} \quad \text{Eq. 3-16}$$

Based on the definition of the probability density  $w(x, \eta, \tau)$ , the integral  $I_0$  becomes one. If the limit

$$\psi_n(x) = \lim_{\theta \rightarrow 0} \frac{I_n(x, \theta)}{\theta} \quad \text{with } n = 0, 1, 2 \quad \text{Eq. 3-17}$$

exists, the differential equation **Eq. 3-18** arises.

$$\frac{\partial v(x, t)}{\partial t} = - \frac{\partial(v(x, t) \cdot \psi_1(x))}{\partial x} + \frac{1}{2} \cdot \frac{\partial^2(v(x, t) \cdot \psi_2(x))}{\partial x^2} \quad \text{Eq. 3-18}$$

Related to FOKKER and PLANCK, who introduced **Eq. 3-18** for the first time in stochastical physics, the equation is often called Fokker-Planck-Equation [37]. For a particle that is influenced by stochastical transport and distribution respectively, the equation describes the temporal change of the probability density  $v(x, t)$  of a particle at a position  $x$  at the time  $t$ . Prerequisites are:

- The basic transport mechanisms remain the same for every time step.
- The events at the time  $t$  depend only on the conditions of the system at that time and are independent of the previous time steps (Markov process).

MOLERUS [37] interpreted the Fokker-Planck-Equation regarding axial mixing processes in continuously operating apparatuses. With **Eq. 3-15** and **Eq. 3-17** follows **Eq. 3-19**.

$$\psi_1(x) = \lim_{\theta \rightarrow 0} \int_{-\infty}^{+\infty} \frac{\eta}{\theta} \cdot w(x, \eta, \theta) \cdot d\eta \quad \text{Eq. 3-19}$$

As  $\eta$  is the movement of a particle during the time  $\theta$ ,  $\psi_1(x)$  describes the average velocity at the position  $x$ . For  $\psi_1(x) = \text{constant}$ , which corresponds to a constant average axial transport velocity of the particles,  $\psi_1(x)$  can be replaced by a transport coefficient  $U^*$ .

For  $\psi_2(x)$  follows with **Eq. 3-15** and **Eq. 3-17**:

$$\psi_2(x) = \lim_{\theta \rightarrow 0} \int_{-\infty}^{+\infty} \frac{\eta^2}{\theta} \cdot w(x, \eta, \theta) \cdot d\eta \quad \text{Eq. 3-20}$$

$\psi_2(x)$  is the second moment of the probability density of the particle movement during the time  $\theta$  (with  $\theta \rightarrow 0$ ) at the position  $x$ . In statistics, the second moment characterizes the spreading of the particle position. Therefore, the term  $\psi_2(x)$  is a measure for the deviation of the particle position in comparison to an ordered transport. In the diffusion theory  $\psi_2(x)$  is set equal to  $2 \cdot D^*$  and the description of the molecule movement caused by the Brownian motion arises:

$$D^* = \lim_{\theta \rightarrow 0} \frac{1}{2 \cdot \theta} \cdot \int_{-\infty}^{+\infty} \eta^2 \cdot w(x, \eta, \theta) \cdot d\eta \quad \text{Eq. 3-21}$$

For the axial mixing processes in a continuously operating apparatus, MOLERUS also used  $D^* = \psi_2(x)/2 = \text{constant}$  to describe the spreading.

Substituting  $\psi_1(x)$  and  $\psi_2(x)$  in **Eq. 3-18**, results in **Eq. 3-22**.

$$\frac{\partial v(x, t)}{\partial t} = -U^* \cdot \frac{\partial v(x, t)}{\partial x} + D^* \cdot \frac{\partial^2 v(x, t)}{\partial x^2} \quad \text{Eq. 3-22}$$

An illustration of the axial mixing processes in a continuously operating apparatus by means of the Fokker-Planck-Equation is given by SOMMER [1, 2]. He used the well-known stochastic expressions average value and variance.

The stylized continuously working apparatus in **Fig. 3-1** is filled with spherical particles of two different species. The diameter of the red particles of species 1 is smaller than the diameter of the blue particles of species 2. Each particle of one species has the same particle size and density. The upper illustration of **Fig. 3-2** shows a cutout of the apparatus with the width  $dx$  at the position  $x$ . The mixing in radial direction exceeds the mixing in axial direction in order of magnitudes. Therefore, an ideal mixing in radial direction can be assumed and concentration changes are only considered in  $x$ -direction. At a certain time  $t$ , the chamber concentration of species 1 (mass of species 1 per chamber volume) is  $c_1(x, t)$  in the cutout. Induced by the rotation of the mixing device, the particles in the cutout are in motion and exposed to random impulses. During the time  $\theta$ , the particles change their position several times in different directions. As a result, the chamber concentration  $c_1(x, t)$  changes to  $c_1(x, t + \theta)$ . The overall displacement of particle  $i$  of species 1 is  $\Delta x_{1,i}(\theta)$  and can be derived from the sum of the single displacements  $\Delta x_{1,i}(\Delta t_1)$ ,  $\Delta x_{1,i}(\Delta t_2)$  and  $\Delta x_{1,i}(\Delta t_3)$  in  $x$ -direction. Every particle of species 1 has a different displacement  $\Delta x_{1,i}(\theta)$ , which is stochastically distributed. For species 1, the

displacement distribution can be described with the distribution function  $\varphi_1(\Delta x_1)$  (see **Fig. 3-2**). The largest displacement  $\Delta x_{1,max}$  during the time  $\theta$  has to be in order of magnitudes smaller than the length of the apparatus. The average displacement of the particles is  $\overline{\Delta x_1}$  and describes the average convection. In addition to the convective movement, a stochastic spreading of the particles occurs which can be characterized by the average square deviation  $\overline{\Delta x_1^2}$  (see **Eq. 3-23**).  $\sigma^2(\Delta x_1)$  is the variance of the probability density function  $\varphi_1(\Delta x_1)$ .

$$\overline{\Delta x_1^2} = \sigma^2(\Delta x_1) + \overline{\Delta x_1}^2 \tag{Eq. 3-23}$$

In the same way, the particle displacements of species 2 can be described. The displacement distribution  $\varphi_2(\Delta x_2)$  of species 2 will be different to the distribution of species 1 because the particles of species 2 have a different mobility than the particles of species 1.

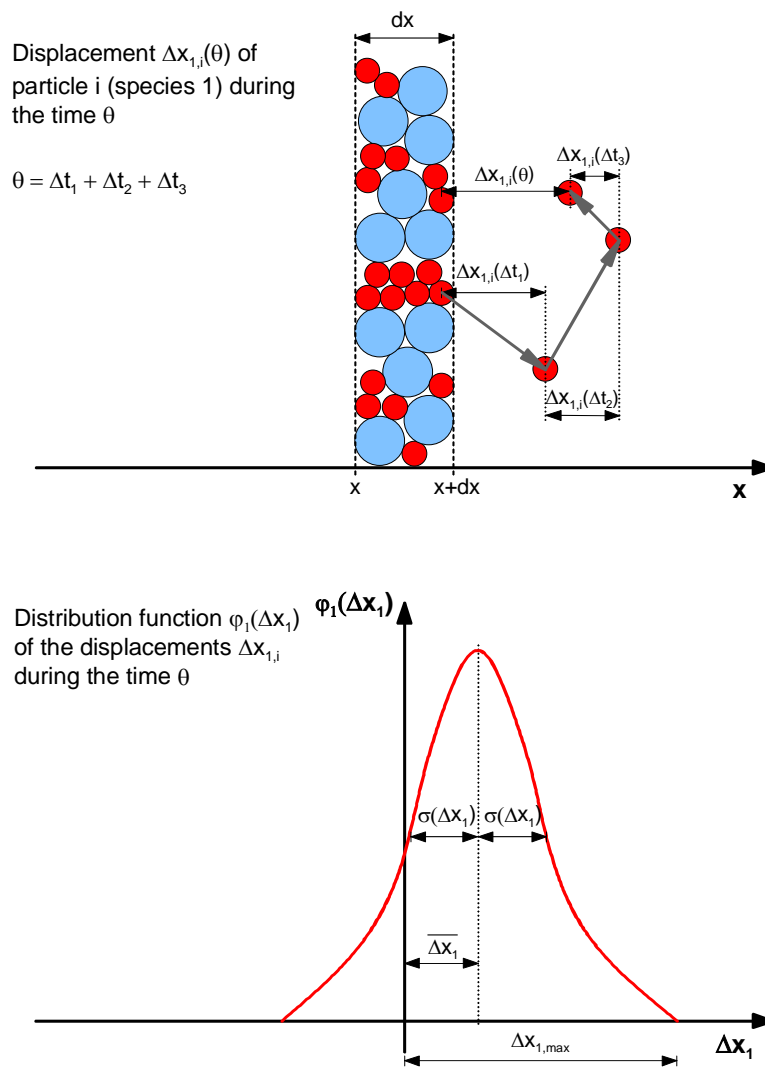


**Fig. 3-2:** Illustration of the axial particle displacement in a continuously operating apparatus [1, 2]

Instead of the probability density  $v(x,t)$  for the existence of a particle at the position  $x$  at the time  $t$  SOMMER [1, 2] used the chamber concentration  $c(x,t)$ . According to the interpretation of **Eq. 3-19** and **Eq. 3-20**, **Eq. 3-18** can be written as **Eq. 3-24** by using the average displacement of the particles  $\overline{\Delta x}$  and the average square deviation  $\overline{\Delta x^2}$  :

$$\frac{\partial c(x,t)}{\partial t} = -\frac{\partial \left( c(x,t) \cdot \lim_{\theta \rightarrow 0} \frac{\Delta x}{\theta} \right)}{\partial x} + \frac{\partial^2 \left( c(x,t) \cdot \lim_{\theta \rightarrow 0} \frac{\Delta x^2}{2 \cdot \theta} \right)}{\partial x^2} \quad \text{Eq. 3-24}$$

According to the previous considerations, *Eq. 3-24* can be transformed into *Eq. 3-25*.

$$\frac{\partial c(x,t)}{\partial t} = -\frac{\partial (c(x,t) \cdot U^*(x,t))}{\partial x} + \frac{\partial^2 (c(x,t) \cdot D^*(x,t))}{\partial x^2} \quad \text{Eq. 3-25}$$

For a constant transport coefficient  $U^*(x,t)$  and a constant dispersion coefficient  $D^*(x,t)$ , *Eq. 3-26* is derived. *Eq. 3-26* is known as Fokker-Planck-Equation and describes the temporal concentration changes at the position  $x$  inside the continuously operating apparatus.

$$\frac{\partial c(x,t)}{\partial t} = -U^* \cdot \frac{\partial c(x,t)}{\partial x} + D^* \cdot \frac{\partial^2 c(x,t)}{\partial x^2} \quad \text{Eq. 3-26}$$

This form of the Fokker-Planck-Equation is the basis of the mixing model, presented in this thesis, to describe the mixing process in a continuous dynamic powder mixer.

### 3.2 Normalization of the Fokker-Planck-Equation and the boundary conditions

For a general description of the mixing process, independent of the working conditions as well as the design and type of the continuous dynamic mixer, a normalization of the Fokker-Planck-Equation is necessary.

#### Normalization of the Fokker-Planck-Equation used by Weinekötter

WEINEKÖTTER [50] normalized the Fokker-Planck-Equation by using a characteristic time  $\Theta$ , a normalized time  $\tilde{\tau}$ , a normalized length  $\lambda$  and the mixer length  $L$ :

$$\text{Characteristic time:} \quad \Theta = \frac{L}{U^*} \quad \text{Eq. 3-27}$$

$$\text{Normalized time:} \quad \tilde{\tau} = \frac{t}{\Theta} = t \cdot \frac{U^*}{L} \Leftrightarrow t = \tilde{\tau} \cdot \frac{L}{U^*} \quad \text{Eq. 3-28}$$

$$\text{Normalized length:} \quad \lambda = \frac{x}{L} \Leftrightarrow x = \lambda \cdot L \quad \text{Eq. 3-29}$$

Inserting *Eq. 3-27*, *Eq. 3-28* and *Eq. 3-29* in *Eq. 3-26* results in:

$$\frac{U^*}{L} \cdot \frac{\partial c(\lambda, \tilde{\tau})}{\partial \tilde{\tau}} = -\frac{U^*}{L} \cdot \frac{\partial c(\lambda, \tilde{\tau})}{\partial \lambda} + \frac{D^*}{L^2} \cdot \frac{\partial^2 c(\lambda, \tilde{\tau})}{\partial \lambda^2} \quad \text{Eq. 3-30}$$

$\Downarrow$

$$\frac{\partial c(\lambda, \tilde{\tau})}{\partial \tilde{\tau}} = -\frac{\partial c(\lambda, \tilde{\tau})}{\partial \lambda} + \frac{D^*}{U^* \cdot L} \cdot \frac{\partial^2 c(\lambda, \tilde{\tau})}{\partial \lambda^2} \quad \text{Eq. 3-31}$$

The term in front of the second deviation of the concentration (see *Eq. 3-31*) is well known as the inverse of the Bodenstein number  $Bo$  and the Peclet number  $Pe$  respectively:

$$Bo = Pe = \frac{U^* \cdot L}{D^*} \quad \text{Eq. 3-32}$$

Inserting *Eq. 3-32* in *Eq. 3-31* results in:

$$\frac{\partial c(\lambda, \tilde{\tau})}{\partial \tilde{\tau}} = -\frac{\partial c(\lambda, \tilde{\tau})}{\partial \lambda} + \frac{1}{Bo} \cdot \frac{\partial^2 c(\lambda, \tilde{\tau})}{\partial \lambda^2} \quad \text{Eq. 3-33}$$

The solutions of the normalized differential equation *Eq. 3-33* only depend on the Bodenstein number. This seems to be advantageous because the roots of the differential equation are reduced. In addition,  $U^*$  and  $L$  are easier to vary than  $D^*$ . However, SOMMER [7] pointed out that this kind of normalization has two disadvantages:

1. The equation is not defined for  $Bo = 0$ , which is a possible case.
2. The equation cannot be used for time-varying boundary conditions because a changing of  $L$  and  $U^*$  influences the boundary conditions, too. Consequently, the solutions of the differential equation are not comparable! This statement will be explained below.

In addition to the radial mixing, continuous dynamic mixers are often used to reduce concentration fluctuations, which result from mass flow fluctuations entering the mixer. Assuming sinusoidal mass flow fluctuations of component 1, *Eq. 3-34* describes the temporal changes of the mass flow.  $\dot{m}_{O,1}$  is the off-set of the fluctuations,  $\dot{m}_{A,1}$  the amplitude and  $\omega_1$  the angular velocity.

$$\dot{m}_1(t) = \dot{m}_{O,1} + \dot{m}_{A,1} \cdot \sin(\omega_1 \cdot t) \quad \text{Eq. 3-34}$$

Inserting *Eq. 3-28* in *Eq. 3-34* and substituting the angular velocity  $\omega_1$  by the normalized angular velocity  $\tilde{\Omega}_1$

$$\tilde{\Omega}_1 = \frac{\omega_1 \cdot L}{U^*} \quad \text{Eq. 3-35}$$

results in *Eq. 3-36*.

$$\dot{m}_1(\tilde{\tau}) = \dot{m}_{O,1} + \dot{m}_{A,1} \cdot \sin\left(\frac{\omega_1 \cdot L}{U^*} \cdot \tilde{\tau}\right) = \dot{m}_{O,1} + \dot{m}_{A,1} \cdot \sin(\tilde{\Omega}_1 \cdot \tilde{\tau}) \quad \text{Eq. 3-36}$$

The solution of *Eq. 3-33* is the same for bisecting  $D^*$  or doubling  $U^*$ . The changing of  $D^*$  does not influence the boundary condition (see *Eq. 3-36*) but a doubling of  $U^*$  causes a bisecting of  $\tilde{\Omega}_1$ . The same problem occurs for a constant Bodenstein number. If  $U^*$  and  $D^*$  are doubled, the Bodenstein number is still the same but the boundary condition changes. That is the reason why for time-varying boundary conditions a new normalized time  $\tau$  has to be defined.

### Normalization of the Fokker-Planck-Equation used in this thesis

In this thesis, the period length  $T$  of the entering mass flow fluctuations was used to normalize the time  $t$  and to define a new normalized time  $\tau$ :

$$\tau = \frac{1}{T} \cdot t \quad \text{Eq. 3-37}$$

Using *Eq. 3-29* and *Eq. 3-37*, *Eq. 3-26* changes as follows:

$$\frac{1}{T} \cdot \frac{\partial c(\lambda, \tau)}{\partial \tau} = -\frac{U^*}{L} \cdot \frac{\partial c(\lambda, \tau)}{\partial \lambda} + \frac{D^*}{L^2} \cdot \frac{\partial^2 c(\lambda, \tau)}{\partial \lambda^2} \quad \text{Eq. 3-38}$$

$$\frac{\partial c(\lambda, \tau)}{\partial \tau} = -\frac{U^* \cdot T}{L} \cdot \frac{\partial c(\lambda, \tau)}{\partial \lambda} + \frac{D^* \cdot T}{L^2} \cdot \frac{\partial^2 c(\lambda, \tau)}{\partial \lambda^2} \quad \text{Eq. 3-39}$$

The factors of the differentials are dimensionless and can be substituted by a normalized transport coefficient  $U$  and a normalized dispersion coefficient  $D$ :

$$U = \frac{U^* \cdot T}{L} \quad \text{Eq. 3-40}$$

$$D = \frac{D^* \cdot T}{L^2} \quad \text{Eq. 3-41}$$

$$\Rightarrow \frac{\partial c(\lambda, \tau)}{\partial \tau} = -U \cdot \frac{\partial c(\lambda, \tau)}{\partial \lambda} + D \cdot \frac{\partial^2 c(\lambda, \tau)}{\partial \lambda^2} \quad \text{Eq. 3-42}$$

For the later described coupling of two Fokker-Planck-Equations (one for component 1 and one for component 2), a transformation of the concentration  $c(\lambda, \tau)$  in a filling degree  $\phi_1^*(\lambda, \tau)$  is necessary. The filling degree  $\phi_1^*(\lambda, \tau)$  is defined as the ratio of the bulk volume  $V_{\text{bulk},1}(\lambda, \tau)$  of component 1 in the truncation chamber to the volume  $V_{\text{chamber}}$  of the truncation chamber (see *Eq. 3-43* and *Fig. 3-3*).

$$\phi_1^*(\lambda, \tau) = \frac{V_{\text{bulk},1}(\lambda, \tau)}{V_{\text{chamber}}} \Leftrightarrow V_{\text{chamber}} = \frac{V_{\text{bulk},1}(\lambda, \tau)}{\phi_1^*(\lambda, \tau)} \quad \text{Eq. 3-43}$$

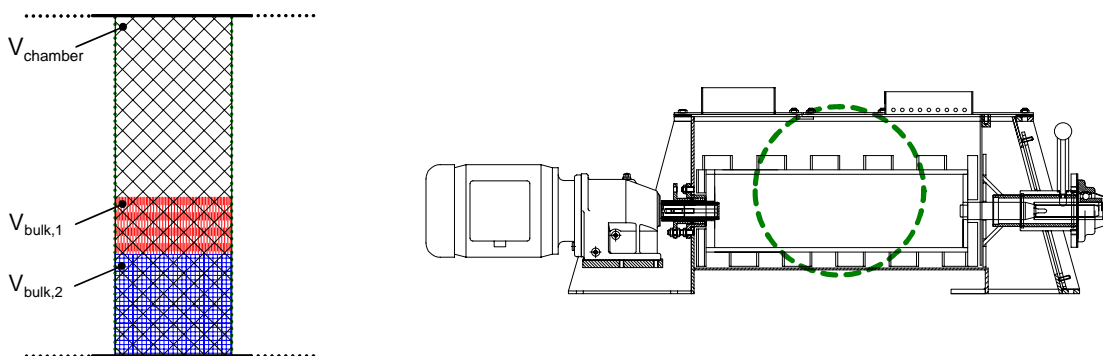


**Fig. 3-3:** Cutout of the continuous dynamic powder mixer to illustrate the definition of the filling degree (compare *Eq. 3-43*)



The chamber concentration  $c_1(\lambda, \tau)$  is defined as the ratio of the bulk mass  $m_{bulk,1}(\lambda, \tau)$  of component 1 in the truncation chamber to the volume  $V_{chamber}$  of the truncation chamber:

$$c_1(\lambda, \tau) = \frac{m_{bulk,1}(\lambda, \tau)}{V_{chamber}} \quad \text{Eq. 3-44}$$

$$\rho_{bulk,1} = \frac{m_{bulk,1}(\lambda, \tau)}{V_{bulk,1}(\lambda, \tau)} \Leftrightarrow m_{bulk,1}(\lambda, \tau) = \rho_{bulk,1} \cdot V_{bulk,1}(\lambda, \tau) \quad \text{Eq. 3-45}$$

Using *Eq. 3-43*, *Eq. 3-44* and *Eq. 3-45* the following correlation between concentration  $c_1(\lambda, \tau)$  and filling degree  $\phi_1^*(\lambda, \tau)$  can be derived:

$$c_1(\lambda, \tau) = \phi_1^*(\lambda, \tau) \cdot \rho_{bulk,1} \quad \text{Eq. 3-46}$$

At the end of the continuous dynamic mixer used, a weir is located. The weir is used to vary the filling degree in the mixer. Reaching steady state in the mixer, the last truncation chamber  $n$  is filled up to the height of the weir (see *Fig. 3-4*).

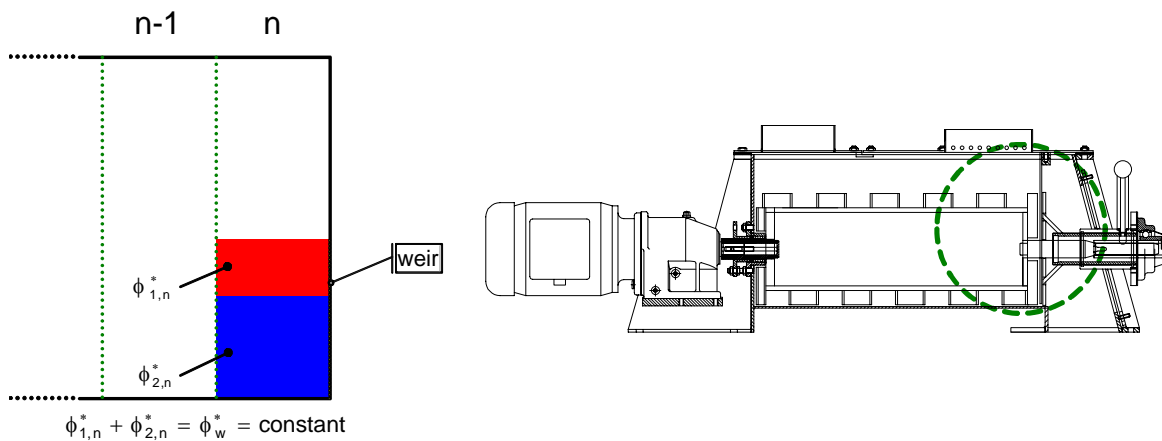


*Fig. 3-4: Cutout of the continuous dynamic powder mixer used to illustrate the coupling of the two Fokker-Planck-Equations*

The sum  $\phi_w^*$  of the filling degree  $\phi_{1,n}^*$  of component 1 and the filling degree  $\phi_{2,n}^*$  of component 2 is constant for all following time steps.

$$\phi_w^* = \phi_{1,n}^* + \phi_{2,n}^* = \text{constant} \quad \text{Eq. 3-47}$$

The overall filling degree  $\phi_w^*$  in the last truncation chamber is used to normalize the filling degree  $\phi_1^*(\lambda, \tau)$ :

$$\phi_1(\lambda, \tau) = \frac{\phi_1^*(\lambda, \tau)}{\phi_w^*} \quad \text{Eq. 3-48}$$

Finally, the following normalized Fokker-Planck-Equation arises for component 1:

$$\frac{\partial \phi_1(\lambda, \tau)}{\partial \tau} = -U_1 \cdot \frac{\partial \phi_1(\lambda, \tau)}{\partial \lambda} + D_1 \cdot \frac{\partial^2 \phi_1(\lambda, \tau)}{\partial \lambda^2} \quad \text{Eq. 3-49}$$

For component 2, the Fokker-Planck-Equation is normalized in the same way:

$$\frac{\partial \phi_2(\lambda, \tau)}{\partial \tau} = -U_2 \cdot \frac{\partial \phi_2(\lambda, \tau)}{\partial \lambda} + D_2 \cdot \frac{\partial^2 \phi_2(\lambda, \tau)}{\partial \lambda^2} \quad \text{Eq. 3-50}$$

### Normalization of the boundary conditions

Substituting the time  $t$  in *Eq. 3-34* by the normalized time  $\tau$  (compare *Eq. 3-37*) results in *Eq. 3-51*, which describes the mass flow fluctuations of component 1. The product of the period length  $T$  and the angular velocity  $\omega_1$  is dimensionless and can be replaced by the normalized angular velocity  $\Omega_1$ .

$$\dot{m}_1(\tau) = \dot{m}_{O,1} + \dot{m}_{A,1} \cdot \sin(\omega_1 \cdot T \cdot \tau) \quad \text{Eq. 3-51}$$

$$\Omega_1 = \omega_1 \cdot T \quad \text{Eq. 3-52}$$

$$\dot{m}_1(\tau) = \dot{m}_{O,1} + \dot{m}_{A,1} \cdot \sin(\Omega_1 \cdot \tau) \quad \text{Eq. 3-53}$$

To normalize the mass flow  $\dot{m}_1(\tau)$ ,  $\dot{m}_1(\tau)$  is divided by the mass  $m_w$  (compare *Eq. 3-54*).  $m_w$  corresponds to the mass in the mixer which could be measured in the case that the filling degree in every truncation chamber is equal to the filling degree  $\phi_w^*$  in the last truncation chamber.

$$\frac{\dot{m}_1(\tau)}{m_w} = \frac{\dot{m}_{O,1}}{m_w} + \frac{\dot{m}_{A,1}}{m_w} \cdot \sin(\Omega_1 \cdot \tau) \quad \text{Eq. 3-54}$$

*Eq. 3-55* describes the normalized mass flow fluctuations  $\dot{\mu}_1(\tau)$  of component 1 entering the continuous mixer.  $\dot{\mu}_{O,1}$  is the normalized offset of the fluctuations and  $\dot{\mu}_{A,1}$  is the normalized amplitude of the fluctuations.

$$\dot{\mu}_1(\tau) = \dot{\mu}_{O,1} + \dot{\mu}_{A,1} \cdot \sin(\Omega_1 \cdot \tau) \quad \text{Eq. 3-55}$$

$$\text{with } \dot{\mu}_1(\tau) = \frac{\dot{m}_1(\tau)}{m_w}; \quad \dot{\mu}_{O,1} = \frac{\dot{m}_{O,1}}{m_w}; \quad \dot{\mu}_{A,1} = \frac{\dot{m}_{A,1}}{m_w}$$

*Eq. 3-56* describes the normalized mass flow fluctuations  $\dot{\mu}_2(\tau)$  of component 2 entering the continuous mixer.

$$\dot{\mu}_2(\tau) = \dot{\mu}_{O,2} + \dot{\mu}_{A,2} \cdot \sin(\Omega_2 \cdot \tau) \quad \text{Eq. 3-56}$$

$$\text{with } \dot{\mu}_2(\tau) = \frac{\dot{m}_2(\tau)}{m_w}; \quad \dot{\mu}_{O,2} = \frac{\dot{m}_{O,2}}{m_w}; \quad \dot{\mu}_{A,2} = \frac{\dot{m}_{A,2}}{m_w}$$

### 3.3 Coupling of two Fokker-Planck-Equations for a two-component system

WEINEKÖTTER's mixing model [50] has the disadvantage that the concentration of the tracer component has to be neglected. To overcome this restriction, SOMMER [7] used a Fokker-Planck-Equation for each component to be mixed and introduced a new boundary condition for coupling the differential equations. For the new boundary condition, the correlation between the composition of the mass leaving the mixer and the composition of the mass in front of the mixer weir is considered.

The coupling of the Fokker-Planck-Equations will be illustrated for a two-component mixture but the model can be extended to as many components as wanted. Only the experimental validation would become more complicated. The two Fokker-Planck-Equations *Eq. 3-49* and *Eq. 3-50* are coupled. For simplification, the two transport coefficients  $U_1$  and  $U_2$  as well as the two dispersion coefficients  $D_1$  and  $D_2$  are set equal.

$$U_1 = U_2 = U \quad \text{Eq. 3-57}$$

$$D_1 = D_2 = D \quad \text{Eq. 3-58}$$

This is possible because the particles of the two powders used for the experimental validation of the derived mixing model had approximately the same density, size and shape.

$$\frac{\partial \phi_1(\lambda, \tau)}{\partial \tau} = -U \cdot \frac{\partial \phi_1(\lambda, \tau)}{\partial \lambda} + D \cdot \frac{\partial^2 \phi_1(\lambda, \tau)}{\partial \lambda^2} \quad \text{Eq. 3-59}$$

$$\frac{\partial \phi_2(\lambda, \tau)}{\partial \tau} = -U \cdot \frac{\partial \phi_2(\lambda, \tau)}{\partial \lambda} + D \cdot \frac{\partial^2 \phi_2(\lambda, \tau)}{\partial \lambda^2} \quad \text{Eq. 3-60}$$

The coupling of the two Fokker-Planck-Equations is shown in *Fig. 3-5*. The last two truncation chambers  $n-1$  and  $n$  are shown at a certain time. The weir is located at the end of the last chamber  $n$ . Reaching the steady state, the last truncation chamber  $n$  is filled up to the height of the weir and the sum of the filling degree  $\phi_{1,n}^*$  of component 1 and the filling degree  $\phi_{2,n}^*$  of component 2 is constant for all following time steps (see ① in *Fig. 3-5*). If the transport by dispersion and/or convection causes the filling degree at the end of the mixer, a rising above the given height of the weir will cause an immediate discharging of the overflow over the weir. Based on the conservation of mass, the sum of the mass flows  $\dot{m}_{1,n-1}$  and  $\dot{m}_{2,n-1}$ , entering the last truncation chamber, is the same as the sum of the mass flows  $\dot{m}_{1,n}$  and  $\dot{m}_{2,n}$ , discharged over the weir (see ② in *Fig. 3-5*). However, the amount of the entering mass flows  $\dot{m}_{1,n-1}$  and  $\dot{m}_{2,n-1}$  of each component is different from the amount of the mass flows  $\dot{m}_{1,n}$  and  $\dot{m}_{2,n}$  discharged from the last truncation chamber. The amount of the discharged mass flows is calculated with *Eq. 3-61* and *Eq. 3-62* (see ③ in *Fig. 3-5*).

$$\dot{m}_{1,n} = (\dot{m}_{1,n-1} + \dot{m}_{2,n-1}) \cdot \frac{\phi_{1,n}^*}{\phi_{1,n}^* + \phi_{2,n}^*} = (\dot{m}_{1,n-1} + \dot{m}_{2,n-1}) \cdot \frac{\phi_{1,n}}{\phi_{1,n} + \phi_{2,n}} \quad \text{Eq. 3-61}$$

$$\dot{m}_{2,n} = (\dot{m}_{1,n-1} + \dot{m}_{2,n-1}) \cdot \frac{\phi_{2,n}^*}{\phi_{1,n}^* + \phi_{2,n}^*} = (\dot{m}_{1,n-1} + \dot{m}_{2,n-1}) \cdot \frac{\phi_{2,n}}{\phi_{1,n} + \phi_{2,n}} \quad \text{Eq. 3-62}$$

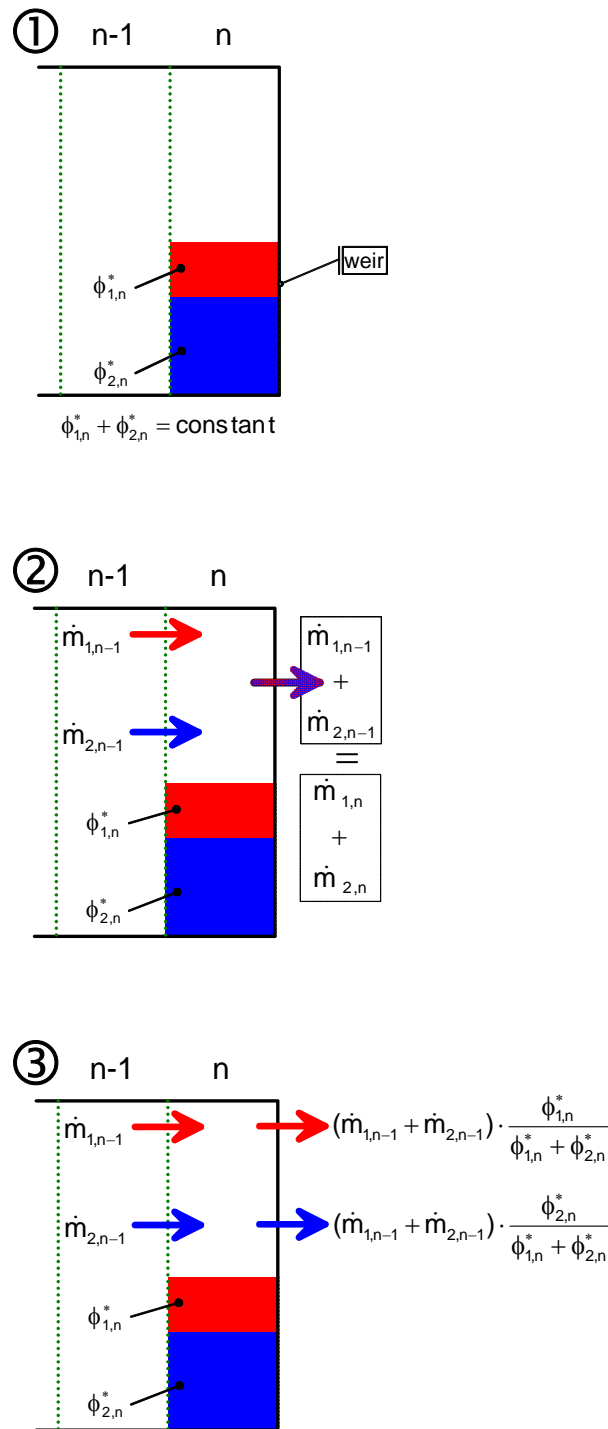


*Fig. 3-5: Illustration for the coupling of two Fokker-Planck-Equations*

### 3.4 Numerical solving of the partial differential equation system

The presented mixing model for calculating the reduction of periodical concentration fluctuations entering a continuous mixer is based on two partial differential equations. The two Fokker-Planck-Equations are coupled by means of the interactions at the weir located at the end of the mixer. A numerical algorithm for solving the differential equation system had to be developed because an analytical solving is not possible. The numerical algorithm used is based on the

“forward time and centered space” truncation algorithm, which SCHÖNERT [19] applied in his postdoctoral thesis to solve a differential equation system describing the grinding process in continuous mills.

A truncation in time and space has to be carried out for a numerical solving of the differential equation system. For the truncation in space, the mixing chamber of the continuous mixer is divided in  $n$  truncation chambers (see *Fig. 3-6*). The changing of the conditions in each truncation chamber is calculated for  $nt$  truncation steps in time. The running index for the truncation in space is  $s$ .  $t$  is the running index used for the truncation in time:

$$s = 1, 2, 3, \dots, n \quad \text{Eq. 3-63}$$

$$t = 1, 2, 3, \dots, nt \quad \text{Eq. 3-64}$$

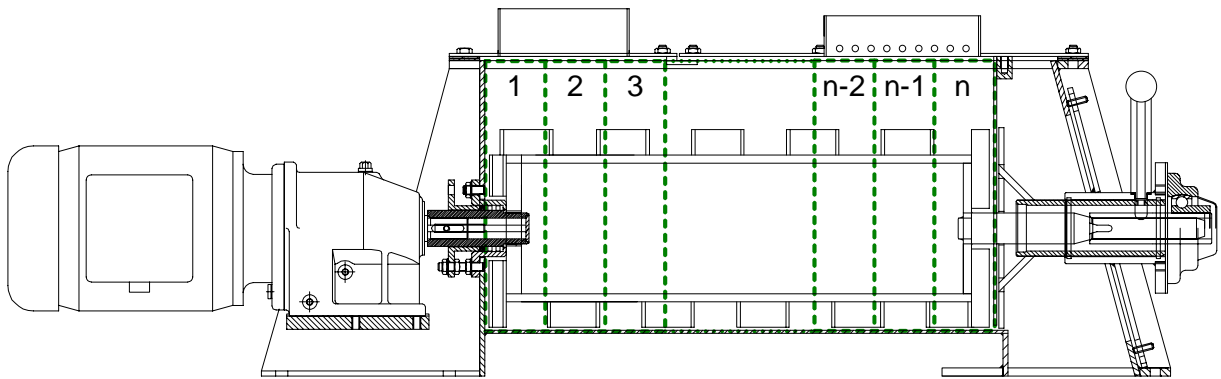


*Fig. 3-6: Truncation of the mixing chamber of the continuous mixer*

The mathematical truncation is shown for the normalized general Fokker-Planck-Equation (*Eq. 3-65*).

$$\frac{\partial \phi(\lambda, \tau)}{\partial \tau} = -U \cdot \frac{\partial \phi(\lambda, \tau)}{\partial \lambda} + D \cdot \frac{\partial^2 \phi(\lambda, \tau)}{\partial \lambda^2} \quad \text{Eq. 3-65}$$

At every truncated place  $s$  in the mixer, the differential coefficients are replaced approximately by difference coefficients:

$$\frac{\partial \phi(\lambda, \tau)}{\partial \tau} \approx \frac{\phi_{s,t+1} - \phi_{s,t}}{\Delta \tau} \quad \text{Eq. 3-66}$$

$$\frac{\partial \phi(\lambda, \tau)}{\partial \lambda} \approx \frac{\phi_{s,t} - \phi_{s-1,t}}{\Delta \lambda} \quad \text{Eq. 3-67}$$

$$\frac{\partial^2 \phi(\lambda, \tau)}{\partial \lambda^2} \approx \frac{\phi_{s+1,t} - 2 \cdot \phi_{s,t} + \phi_{s-1,t}}{\Delta \lambda^2} \quad \text{Eq. 3-68}$$

Inserting *Eq. 3-66*, *Eq. 3-67* and *Eq. 3-68* into *Eq. 3-65*, results in:

$$\frac{\phi_{s,t+1} - \phi_{s,t}}{\Delta\tau} = -U \cdot \frac{\phi_{s,t} - \phi_{s-1,t}}{\Delta\lambda} + D \cdot \frac{\phi_{s+1,t} - 2 \cdot \phi_{s,t} + \phi_{s-1,t}}{\Delta\lambda^2} \quad \text{Eq. 3-69}$$

Solving *Eq. 3-69* to  $\phi_{s,t+1}$ , the normalized filling degree in the truncation chamber  $s$  at the time  $t+1$ , after a time step with the width  $\Delta\tau$  can be calculated:

$$\begin{aligned} \phi_{s,t+1} &= \phi_{s,t} - U \cdot \frac{\phi_{s,t} - \phi_{s-1,t}}{\Delta\lambda} \cdot \Delta\tau + D \cdot \frac{\phi_{s+1,t} - 2 \cdot \phi_{s,t} + \phi_{s-1,t}}{\Delta\lambda^2} \cdot \Delta\tau \\ \Leftrightarrow \phi_{s,t+1} &= \phi_{s,t} - \frac{U \cdot \Delta\tau}{\Delta\lambda} \cdot (\phi_{s,t} - \phi_{s-1,t}) + \frac{D \cdot \Delta\tau}{\Delta\lambda^2} (\phi_{s+1,t} - 2 \cdot \phi_{s,t} + \phi_{s-1,t}) \end{aligned} \quad \text{Eq. 3-70}$$

The differential  $\Delta\tau$  and  $\Delta\lambda$  as well as the normalized transport coefficient  $U$  and the normalized dispersion coefficient  $D$  are constant. To get a more concise equation, the following terms are introduced:

$$CU = \frac{U \cdot \Delta\tau}{\Delta\lambda} \quad \text{Eq. 3-71}$$

$$CD = \frac{D \cdot \Delta\tau}{\Delta\lambda^2} \quad \text{Eq. 3-72}$$

$$\Rightarrow \phi_{s,t+1} = \phi_{s,t} - CU \cdot (\phi_{s,t} - \phi_{s-1,t}) + CD \cdot (\phi_{s+1,t} - 2 \cdot \phi_{s,t} + \phi_{s-1,t}) \quad \text{Eq. 3-73}$$

### 3.4.1 Truncation of the entering mass flows

The normalized mass flow  $\dot{\mu}(\tau)$ , which enters the continuous mixer, describes *Eq. 3-74*.  $\dot{\mu}_0$  is the normalized offset of the fluctuations and  $\dot{\mu}_A$  the normalized amplitude.

$$\dot{\mu}(\tau) = \dot{\mu}_0 + \dot{\mu}_A \cdot \sin(\Omega \cdot \tau) \quad \text{Eq. 3-74}$$

If the entering bulk material flows completely into the first truncation chamber, the normalized mass flow  $\dot{\mu}(\tau)$  is equivalent to

- the difference coefficient of the normalized filling degree  $\Delta\phi(\tau)/\Delta\tau$  divided by the number  $n$  of the truncation chambers and
- the difference coefficient of the normalized filling degree  $\Delta\phi(\tau)/\Delta\tau$  multiplied with the width  $\Delta\lambda$  of the truncation steps in space:

$$\dot{\mu}(\tau) = \frac{\Delta\mu(\tau)}{\Delta\tau} = \frac{\dot{m}(\tau)}{m_w} = \frac{\Delta m(\tau)}{m_w \Delta\tau} \quad \text{Eq. 3-75}$$

$$\frac{\frac{\Delta m(\tau)}{\Delta \tau}}{m_w} = \frac{\rho_{bulk} \cdot \frac{\Delta V_{bulk}(\tau)}{\Delta \tau}}{\rho_{bulk} \cdot V_{bulk,w}} = \frac{\frac{\Delta V_{bulk}(\tau)}{\Delta \tau}}{\frac{V_{chamber}}{V_{bulk,w}}} = \frac{\frac{\Delta \phi^*(\tau)}{\Delta \tau}}{n \cdot \phi_w^*} = \frac{\Delta \phi(\tau)}{\Delta \tau} \cdot \frac{1}{n} = \frac{\Delta \phi(\tau)}{\Delta \tau} \cdot \Delta \lambda \quad Eq. 3-76$$

$\Delta V_{bulk}(\tau)$  is the amount of the bulk material entering the continuous mixer during the time  $\Delta \tau$ .  $V_{chamber}$  is the volume of one truncation chamber.  $m_w$  corresponds to the mass in the mixer which could be measured if the filling degree in every truncation chamber is equal to the filling degree  $\phi_w^*$  in the last truncation chamber.  $V_{bulk,w}$  is the volume of the mass  $m_w$ .

Combining *Eq. 3-75* and *Eq. 3-76*, results in *Eq. 3-77*.

$$\frac{\Delta \mu(\tau)}{\Delta \tau} = \frac{\Delta \phi(\tau)}{\Delta \tau} \cdot \Delta \lambda \Leftrightarrow \Delta \phi(\tau) = \frac{\Delta \mu(\tau)}{\Delta \lambda} \quad Eq. 3-77$$

The mass of the powder entering the first truncation chamber during a time step can be calculated with the following equations. It is assumed that the mass flow of component 1 is fluctuating in a sinusoidal manner and the mass flow of component 2 is constant.

$$\Delta \mu_1(\tau) = \dot{\mu}_1(\tau) \cdot \Delta \tau = (\dot{\mu}_{O,1} + \dot{\mu}_{A,1} \cdot \sin(\Omega \cdot \tau)) \cdot \Delta \tau \quad Eq. 3-78$$

$$\Delta \mu_2(\tau) = \dot{\mu}_2(\tau) \cdot \Delta \tau = \dot{\mu}_{O,2} \cdot \Delta \tau \quad Eq. 3-79$$

The resulting change of the normalized filling degree in the first truncation chamber is described by *Eq. 3-80* and *Eq. 3-81*.

$$\Delta \phi 1(\tau) = (\dot{\mu}_{O,1} + \dot{\mu}_{A,1} \cdot \sin(\Omega \cdot \tau)) \cdot \frac{\Delta \tau}{\Delta \lambda} \quad Eq. 3-80$$

$$\Delta \phi 2(\tau) = \dot{\mu}_{O,2} \cdot \frac{\Delta \tau}{\Delta \lambda} \quad Eq. 3-81$$

### 3.4.2 Truncation of the mixer inlet (truncation chamber 1)

The processes in the first truncation chamber are shown in *Fig. 3-7*. During a time step  $\Delta \tau$ , the normalized filling degree of each component ( $\phi 1_{1,t}$  and  $\phi 2_{1,t}$ ) in the first truncation chamber will change due to

- feeding in the first truncation chamber ( $\Delta \phi 1(t \cdot \Delta \tau)$  and  $\Delta \phi 2(t \cdot \Delta \tau)$ ),
- a convective transport of powder from the first to the second truncation chamber ( $CU \cdot \phi 1_{1,t}$  and  $CU \cdot \phi 2_{1,t}$ ),
- a dispersive transport from the first to the second truncation chamber ( $CD \cdot \phi 1_{1,t}$  and  $CD \cdot \phi 2_{1,t}$ ) and
- a dispersive transport from the second to the first truncation chamber ( $CD \cdot \phi 1_{2,t}$  and  $CD \cdot \phi 2_{2,t}$ ).

The processes in the first truncation chamber are described mathematically by *Eq. 3-82* and *Eq. 3-83*.

$$\phi_{1,t+1} = (1 - CU - CD) \cdot \phi_{1,t} + CD \cdot \phi_{2,t} + \Delta\phi_1(t \cdot \Delta\tau) \quad \text{Eq. 3-82}$$

$$\phi_{2,t+1} = (1 - CU - CD) \cdot \phi_{2,t} + CD \cdot \phi_{1,t} + \Delta\phi_2(t \cdot \Delta\tau) \quad \text{Eq. 3-83}$$

The first index of the normalized filling degree is the number of the truncation chamber. The second index is the number of the time step.

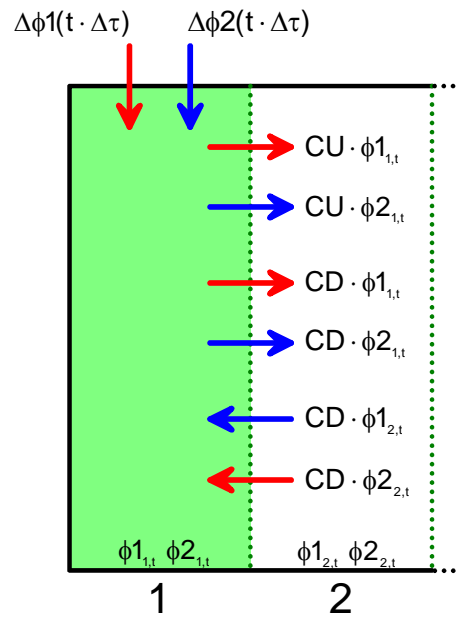


*Fig. 3-7: Illustration of the processes in the first truncation chamber*

### 3.4.3 Truncation of the chambers in the middle of the mixer (truncation chamber 2 ... n-1)

The processes in the truncation chamber  $s$ , which is located somewhere between the first and the last truncation chamber, is shown in *Fig. 3-8*. During a time step  $\Delta\tau$ , the normalized filling degree of each component ( $\phi_{1,s,t}$  and  $\phi_{2,s,t}$ ) in the truncation chamber  $s$  will change due to

- a convective transport ( $CU \cdot \phi_{1,s-1,t}$  and  $CU \cdot \phi_{2,s-1,t}$ ) from the truncation chamber  $s-1$  to the truncation chamber  $s$ ,
- a convective transport ( $CU \cdot \phi_{1,s,t}$  and  $CU \cdot \phi_{2,s,t}$ ) from the truncation chamber  $s$  to the truncation chamber  $s+1$ ,
- a dispersive transport ( $CD \cdot \phi_{1,s-1,t}$  and  $CD \cdot \phi_{2,s-1,t}$ ) from the truncation chamber  $s-1$  to the truncation chamber  $s$ ,
- a dispersive transport ( $CD \cdot \phi_{1,s,t}$  and  $CD \cdot \phi_{2,s,t}$ ) from the truncation chamber  $s$  to the truncation chamber  $s+1$ ,
- a dispersive transport ( $CD \cdot \phi_{1,s,t}$  and  $CD \cdot \phi_{2,s,t}$ ) from the truncation chamber  $s$  to the truncation chamber  $s-1$  and
- a dispersive transport ( $CD \cdot \phi_{1,s+1,t}$  and  $CD \cdot \phi_{2,s+1,t}$ ) from the truncation chamber  $s+1$  to the truncation chamber  $s$ .



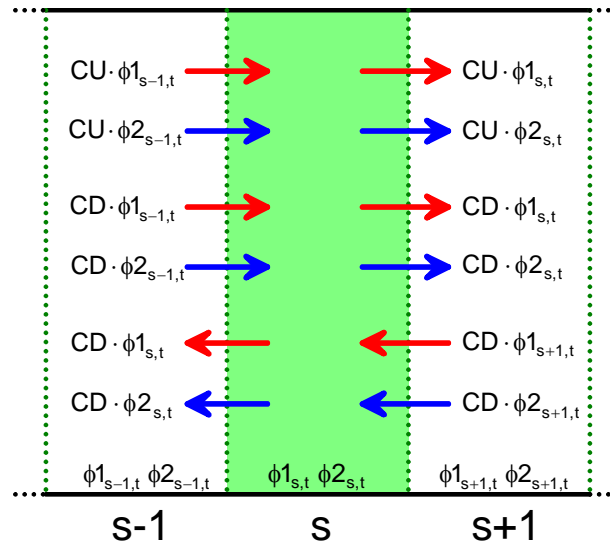


**Fig. 3-8:** Illustration of the processes in the truncation chambers  $s = 2 \dots n-1$

The processes in the truncation chambers  $s = 2 \dots n-1$  are described mathematically by **Eq. 3-84** and **Eq. 3-85**.

$$\phi 1_{s,t+1} = (CU + CD) \cdot \phi 1_{s-1,t} + (1 - CU - 2 \cdot CD) \cdot \phi 1_{s,t} + CD \cdot \phi 1_{s+1,t} \quad \text{Eq. 3-84}$$

$$\phi 2_{s,t+1} = (CU + CD) \cdot \phi 2_{s-1,t} + (1 - CU - 2 \cdot CD) \cdot \phi 2_{s,t} + CD \cdot \phi 2_{s+1,t} \quad \text{Eq. 3-85}$$

### 3.4.4 Truncation of the mixer outlet (truncation chamber n)

The processes in the last truncation chamber  $n$  are described in two steps. In the first part, only the processes at the interface between the last and the previous truncation chamber are considered (see **Fig. 3-9**). During a time step  $\Delta\tau$ , the normalized filling degree of each component ( $\phi 1_{n,t}$  and  $\phi 2_{n,t}$ ) in the last truncation chamber  $n$  will change due to

- a convective transport ( $CU \cdot \phi 1_{n-1,t}$  and  $CU \cdot \phi 2_{n-1,t}$ ) from the truncation chamber  $n-1$  to the truncation chamber  $n$ ,
- a dispersive transport ( $CD \cdot \phi 1_{n-1,t}$  and  $CD \cdot \phi 2_{n-1,t}$ ) from the truncation chamber  $n-1$  to the truncation chamber  $n$  and
- a dispersive transport ( $CD \cdot \phi 1_{n,t}$  and  $CD \cdot \phi 2_{n,t}$ ) from the truncation chamber  $n$  to the truncation chamber  $n-1$ .

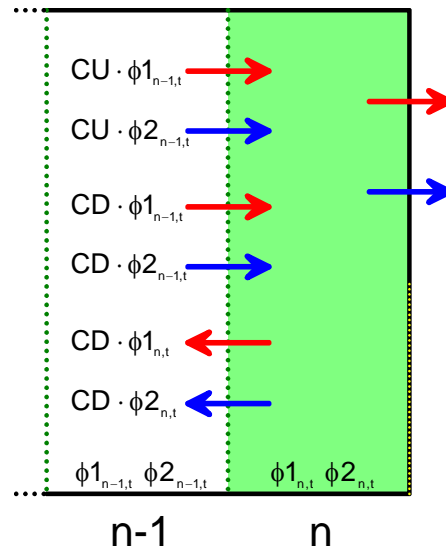


**Fig. 3-9:** Illustration of the processes at the interface between the last and the previous truncation chamber

The processes at the interface between the last and the previous truncation chamber are described mathematically by *Eq. 3-86* and *Eq. 3-87*.

$$si\phi_{1_{n,t}} = (CU + CD) \cdot \phi_{1_{n-1,t}} - CD \cdot \phi_{1_{n,t}} \quad \text{Eq. 3-86}$$

$$si\phi_{2_{n,t}} = (CU + CD) \cdot \phi_{2_{n-1,t}} - CD \cdot \phi_{2_{n,t}} \quad \text{Eq. 3-87}$$

$si\phi_{1_{n,t}}$  and  $si\phi_{2_{n,t}}$  characterize the changes of the normalized filling degrees  $\phi_{1_{n,t}}$  and  $\phi_{2_{n,t}}$  in the last truncation chamber  $n$  due to processes at the interface between the last and the previous truncation chamber (see *Fig. 3-10*).

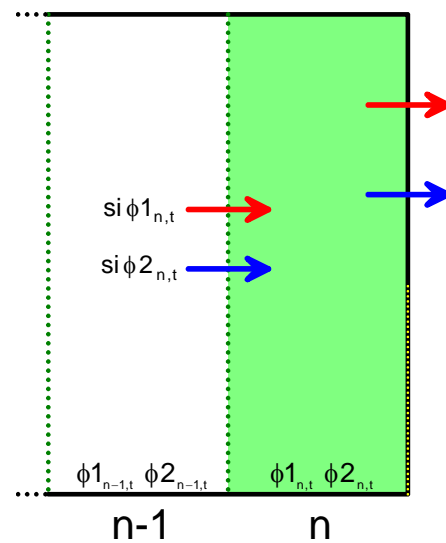


**Fig. 3-10:** Illustration of the processes at the interface between the last and the previous truncation chamber

Until now, only the changes of the normalized filling degree of each component ( $\phi_{1,n,t}$  and  $\phi_{2,n,t}$ ) in the last truncation chamber  $n$  due to the processes at the interface between the last and the previous truncation chamber were considered. The transport of the powder by dispersion and/or convection inside the mixer causes an immediate discharging of the overflow over the weir, if the filling degree rises above the given height of the weir. The mathematical description of the overflow was already introduced in *Chapter 3.3*. Based on the conservation of mass the sum of the mass flows of powder 1 and powder 2 entering the last chamber from the previous is the same as the sum of the mass flows of powder 1 and powder 2 discharged over the weir. However, the amount of the entering mass flow of component 1 and component 2 differs from the amount of the mass flow of component 1 and component 2 discharged from the last chamber. As a result, the changes of the filling degree ( $so\phi_{1,n,t}$  and  $so\phi_{2,n,t}$ ) in the last truncation chamber due to the powder overflow over the weir can be described by *Eq. 3-88* and *Eq. 3-89*.

$$so\phi_{1,n,t} = (si\phi_{1,n,t} + si\phi_{2,n,t}) \cdot \frac{\phi_{1,n,t}}{\phi_{1,n,t} + \phi_{2,n,t}} \quad \text{Eq. 3-88}$$

$$so\phi_{2,n,t} = (si\phi_{1,n,t} + si\phi_{2,n,t}) \cdot \frac{\phi_{2,n,t}}{\phi_{1,n,t} + \phi_{2,n,t}} \quad \text{Eq. 3-89}$$

During a time step  $\Delta\tau$ , the normalized filling degree of each component ( $\phi_{1,n,t}$  and  $\phi_{2,n,t}$ ) in the last truncation chamber  $n$  will change due to

- the processes at the interface between the last and the previous truncation chamber ( $si\phi_{1,n,t}$  and  $si\phi_{2,n,t}$ ) as well as
- the discharging over the weir ( $so\phi_{1,n,t}$  and  $so\phi_{2,n,t}$ ).

These processes are shown in *Fig. 3-11* and described mathematically by *Eq. 3-90* and *Eq. 3-91*.

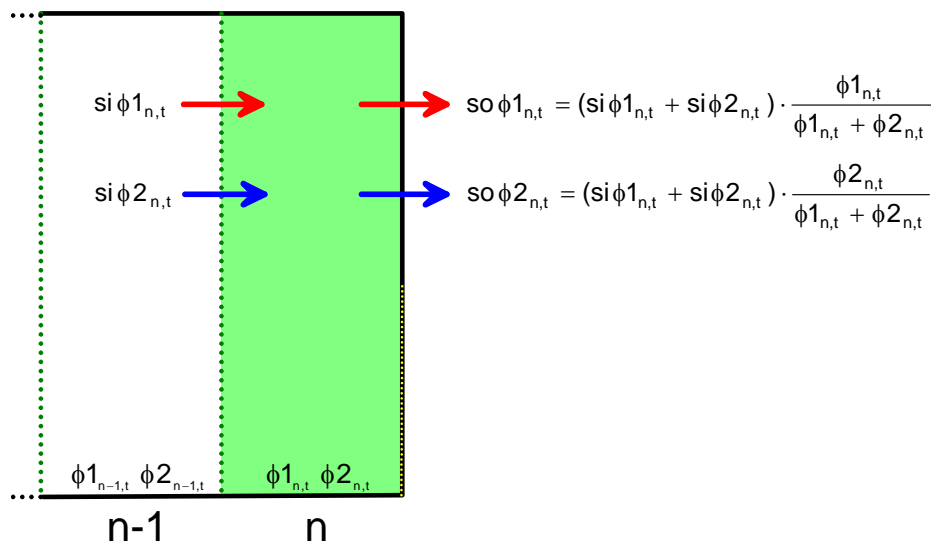


*Fig. 3-11: Illustration of the processes in the last truncation chamber  $s = n$*

$$\phi 1_{n,t+1} = \phi 1_{n,t} + si \phi 1_{n,t} - so \phi 1_{n,t} \quad Eq. 3-90$$

$$\phi 2_{n,t+1} = \phi 2_{n,t} + si \phi 2_{n,t} - so \phi 2_{n,t} \quad Eq. 3-91$$

### 3.4.5 Determination of the mixing quality in the outlet of the mixer

For the characterization of the achieved mixing quality, the fluctuation ratio (*FR*) is introduced. The fluctuation ratio is defined as the standard deviation  $\sigma_{out}$  of the concentration fluctuations leaving the continuous mixer to the standard deviation  $\sigma_{in}$  of the concentration fluctuations entering the continuous mixer:

$$FR = \frac{\sigma_{out}}{\sigma_{in}} \quad Eq. 3-92$$

Commonly, the variance reduction ratio (*VRR*) is used to characterize the reduction of concentration fluctuations entering a continuous mixer [e.g. 50]:

$$VRR = \frac{\sigma_{in}^2}{\sigma_{out}^2} \quad Eq. 3-93$$

$\sigma_{in}^2$  is the variance of the concentration fluctuations entering the continuous mixer and  $\sigma_{out}^2$  the variance of the concentration fluctuations leaving the continuous mixer.

Using the fluctuation ratio has the advantage that the values of *FR* trend to zero for a high reduction of entering fluctuations. In contrast, the Variance Reduction Ratio trends to infinity for high mixing qualities.

### Calculation of the standard deviation at the inlet of the continuous mixer

During the simulation experiments, the changes in each truncation chamber were calculated *nt* times (normally *nt* = 100 000). The standard deviation  $\sigma_{in}$  of the concentration fluctuations entering the continuous mixer was calculated for the last period (normally the last 5 000 time steps) using *Eq. 3-94*.

$$\sigma_{in} = \sqrt{\frac{1}{4999} \sum_{j=nt-5000}^{nt} (cI_{in,j} - \bar{cI}_{in})^2} \quad Eq. 3-94$$

The concentration  $cI_{in,j}$  of component 1 in the mixer inlet is defined as the ratio of the normalized mass flow  $\dot{\mu}_1(j \cdot \Delta\tau)$  of component 1 to the sum of the normalized mass flow  $\dot{\mu}_1(j \cdot \Delta\tau)$  of component 1 and the normalized mass flow  $\dot{\mu}_2(j \cdot \Delta\tau)$  of component 2 at the time step *j*:

$$cI_{in,j} = \frac{\dot{\mu}_1(j \cdot \Delta\tau)}{\dot{\mu}_1(j \cdot \Delta\tau) + \dot{\mu}_2(j \cdot \Delta\tau)} \quad Eq. 3-95$$

The average concentration  $\overline{cI}_{in}$  of component 1 in the mixer inlet was calculated for the last period of the concentration fluctuations entering the continuous mixer (normally the last 5000 time steps) using *Eq. 3-96*.

$$\overline{cI}_{in} = \frac{1}{5000} \cdot \sum_{j=nt-5000}^{nt} cI_{in,j} \quad \text{Eq. 3-96}$$

### Calculation of the standard deviation at the outlet of the continuous mixer

The standard deviation  $\sigma_{out}$  of the concentration fluctuations leaving the continuous mixer was calculated for the last period (normally the last 5000 time steps) using *Eq. 3-97*.

$$\sigma_{out} = \sqrt{\frac{1}{4999} \sum_{j=nt-5000}^{nt} (cI_{out,j} - \overline{cI}_{out})^2} \quad \text{Eq. 3-97}$$

The concentration  $cI_{out,j}$  of component 1 in the mixer outlet can be calculated with *Eq. 3-98*.  $so\phi 1_{n,j}$  and  $so\phi 2_{n,j}$  are the changes of the filling degree in the last truncation chamber during a time interval  $\Delta\tau$  at the time step  $j$ . The changes of the filling degree are due to the powder discharge over the weir (compare *Eq. 3-88* and *Eq. 3-89*).

$$cI_{out,j} = \frac{so\phi 1_{n,j}}{so\phi 1_{n,j} + so\phi 2_{n,j}} \quad \text{with } j = nt - 5000 \dots nt \quad \text{Eq. 3-98}$$

The average concentration  $\overline{cI}_{out}$  of component 1 in the mixer outlet was calculated for the last period of the concentration fluctuations leaving the continuous mixer (normally the last 5000 time steps) using *Eq. 3-99*.

$$\overline{cI}_{out} = \frac{1}{5000} \cdot \sum_{j=nt-5000}^{nt} cI_{out,j} \quad \text{Eq. 3-99}$$

### 3.4.6 Calculation of the normalized average residence time of the powder in the mixer

The average residence time  $t_R^*$  in the mixer is defined by the ratio of the active mass hold-up  $m_{hold}$  in the mixer and the average overall mass flow  $\overline{m}$  of the two components.

$$t_R^* = \frac{m_{hold}}{\overline{m}} \quad \text{Eq. 3-100}$$

For normalization, the average residence time is divided by the period length  $T$  of the entering mass flow fluctuations and the entering concentration fluctuations respectively.

$$t_R = \frac{t_R^*}{T} \quad \text{Eq. 3-101}$$

The normalized average overall mass flow  $\bar{\mu}$  is the sum of the normalized offset  $\bar{\mu}_{1,0}$  of the mass flow of component 1 and the normalized offset  $\bar{\mu}_{2,0}$  of the mass flow of component 2:

$$\bar{\mu} = \bar{\mu}_{0,1} + \bar{\mu}_{0,2} \quad \text{Eq. 3-102}$$

The normalized overall mass hold-up  $M$  in the mixer is calculated after the last time step  $nt$ .  $M$  is the sum of the normalized mass hold-up  $M1$  of component 1 and the normalized mass hold-up  $M2$  of component 2:

$$M = M1 + M2 \quad \text{Eq. 3-103}$$

The equation for calculating the normalized mass hold-up by means of the normalized filling degree is derived for component 1:

$$M1 = \sum_{s=1}^n \frac{mI_{s,nt}}{m_w} = \sum_{s=1}^n \frac{VI_{s,nt}}{V_{bulk,w}} = \sum_{s=1}^n \frac{V_{chamber}}{V_{bulk,w}} = \frac{1}{n} \sum_{s=1}^n \frac{\phi I_{s,nt}^*}{\phi_w^*} \quad \text{Eq. 3-104}$$

$$\Rightarrow M1 = \frac{1}{n} \sum_{s=1}^n \phi I_{s,nt}$$

$n$  is the number of truncation chambers,  $mI_{s,nt}$  is the mass of component 1 in the truncation chamber  $s$  after time step  $nt$  and  $VI_{s,nt}$  the corresponding volume.  $m_w$  corresponds to the mass in the mixer which can be measured for the case that the filling degree in every truncation chamber is equal to the filling degree  $\phi_w^*$  in the last truncation chamber.  $V_{bulk,w}$  is the volume of the mass  $m_w$  and  $V_{chamber}$  the volume of a truncation chamber.

$$M2 = \frac{1}{n} \sum_{s=1}^n \phi 2_{s,nt} \quad \text{Eq. 3-105}$$

The normalized average residence time  $t_R$  can be calculated with *Eq. 3-106*.

$$t_R = \frac{M}{\bar{\mu}} \cdot \frac{1}{T} \quad \text{Eq. 3-106}$$

### 3.5 Results of the performed simulation experiments

For the calculation of the fluctuation ratio  $FR$  and the normalized average residence time  $t_R$ , the algorithm shown in *Chapter 9.3* of the appendix was developed. The algorithm was programmed with *Mathcad 2000 Professional* from the company *MathSoft Inc.* (Cambridge, USA).

The following parameters have to be set for the simulations:

- The normalized transport coefficient  $U$ ,
- the normalized dispersion coefficient  $D$ ,
- the number of truncation chambers  $n$ ,
- the number of time steps  $nt$ ,
- the dimensionless running time  $Rt$  (multiple of the period length),
- the normalized offset  $\dot{\mu}_{0,1}$  as well as the normalized amplitude  $\dot{\mu}_{A,1}$  of the normalized mass flow  $\dot{\mu}_1(\tau)$  of component 1 (here calcium carbonate) and
- the normalized offset  $\dot{\mu}_{0,2}$  as well as the normalized amplitude  $\dot{\mu}_{A,2}$  of the normalized mass flow  $\dot{\mu}_2(\tau)$  of component 2 (here maize starch).

The normalized transport coefficient and the normalized dispersion coefficient are unknown and have to be estimated and varied respectively. In literature, only a few dispersion and transport coefficients were published for powdery components mixed in a continuous mixer. MERZ [26] determined dispersion and transport coefficients for the mixing process in a continuously mixing drum. MERZ and LÜCKE [48] as well as HOLZMÜLLER [4] determined dispersion and transport coefficients for the mixing process in continuous *Lödige* mixers equipped with blades and plowshares respectively. The determined coefficients as well as the corresponding coefficients normalized according to the model derived in this thesis are shown in **Chapter 9.2** of the appendix. The normalized transport coefficients vary approximately between  $U = 0.02$  and  $U = 1.0$ , the normalized dispersion coefficients approximately between  $D = 0.0001$  and  $D = 0.7$ .

The simulations were performed with 50 truncation chambers, 100 000 time steps and a running time which was twenty times higher than the period length. The normalized transport coefficient was varied between  $U = 0.001$  and  $U = 6$ . The normalized dispersion coefficient was varied between  $D = 0.1$  and  $D = 0.9$ . Using 50 truncation chambers and 100 000 time steps, the programmed algorithm was not able to handle normalized dispersion coefficients smaller than  $D = 0.1$ . In this case, the algorithm was unstable. Simulations with smaller dispersion coefficients and a higher number of time steps were foreseen only for the case that the results of the later experimental validation would have made such simulations necessary.

The normalized offsets and amplitudes of the entering mass flows were calculated according to **Eq. 3-55** and **Eq. 3-56** using the settings of the standard mixing experiment performed experimentally:

*Powder 1 (fluctuating mass flow, calcium carbonate):*

- $\dot{m}_{0,1} = 15 \text{ g/s} = 54.0 \text{ kg/h}$  (offset),
- $\dot{m}_{A,1} = 14 \text{ g/s} = 50.4 \text{ kg/h}$  (amplitude),
- $T = 40 \text{ s}$  (period length)

*Powder 2 (constant mass flow, maize starch):*

- $\dot{m}_{0,2} = 10 \text{ g/s} = 36.0 \text{ kg/h}$  (offset),
- $\dot{m}_{A,2} = 0 \text{ g/s}$  (amplitude)

In *Chapter 3.5.7* it will be shown that the mass  $m_w$ , which is necessary for the normalization, can be set equal to the active mass hold-up  $m_{hold} = 560$  g of the standard mixing experiment.

The following normalized offsets and amplitudes of the entering mass flows arise:

$$\dot{\mu}_{O,1} = \frac{\dot{m}_{O,1} \cdot T}{m_w} = \frac{15 \frac{\text{g}}{\text{s}} \cdot 40 \text{ s}}{560 \text{ g}} = 1.07 \quad \text{Eq. 3-107}$$

$$\dot{\mu}_{A,1} = \frac{\dot{m}_{A,1} \cdot T}{m_w} = \frac{14 \frac{\text{g}}{\text{s}} \cdot 40 \text{ s}}{560 \text{ g}} = 1.0 \quad \text{Eq. 3-108}$$

$$\dot{\mu}_{O,2} = \frac{\dot{m}_{O,2} \cdot T}{m_w} = \frac{10 \frac{\text{g}}{\text{s}} \cdot 40 \text{ s}}{560 \text{ g}} = 0.7 \quad \text{Eq. 3-109}$$

$$\dot{\mu}_{A,2} = \frac{\dot{m}_{A,2} \cdot T}{m_w} = \frac{0 \frac{\text{g}}{\text{s}} \cdot 40 \text{ s}}{560 \text{ g}} = 0 \quad \text{Eq. 3-110}$$

The settings used for the simulations are summarized in *Table 3-2*.

**Table 3-2:** Compilation of the general settings used for the simulations

parameter	description	setting
$U$	normalized transport coefficient	0.001 ... 6
$D$	normalized dispersion coefficient	0.1 ... 0.9
$n$	number of truncation chambers	50
$nt$	number of time steps	100 000
$Rt$	normalized running time (multiple of the period length)	20
$\dot{\mu}_{O,1}$	normalized offset component 1	1.07
$\dot{\mu}_{A,1}$	normalized amplitude component 1	1.00
$\dot{\mu}_{O,2}$	normalized offset component 2	0.70
$\dot{\mu}_{A,2}$	normalized amplitude component 2	0.00



### 3.5.1 Influence of the transport and dispersion coefficient on the fluctuation ratio (mixing quality)

The influence of the normalized transport coefficient  $U$  on the fluctuation ratio  $\sigma_{out}/\sigma_{in}$  is shown in *Fig. 3-12* for the standard settings. The different curves were calculated for different constant normalized dispersion coefficients and varying normalized transport coefficients.

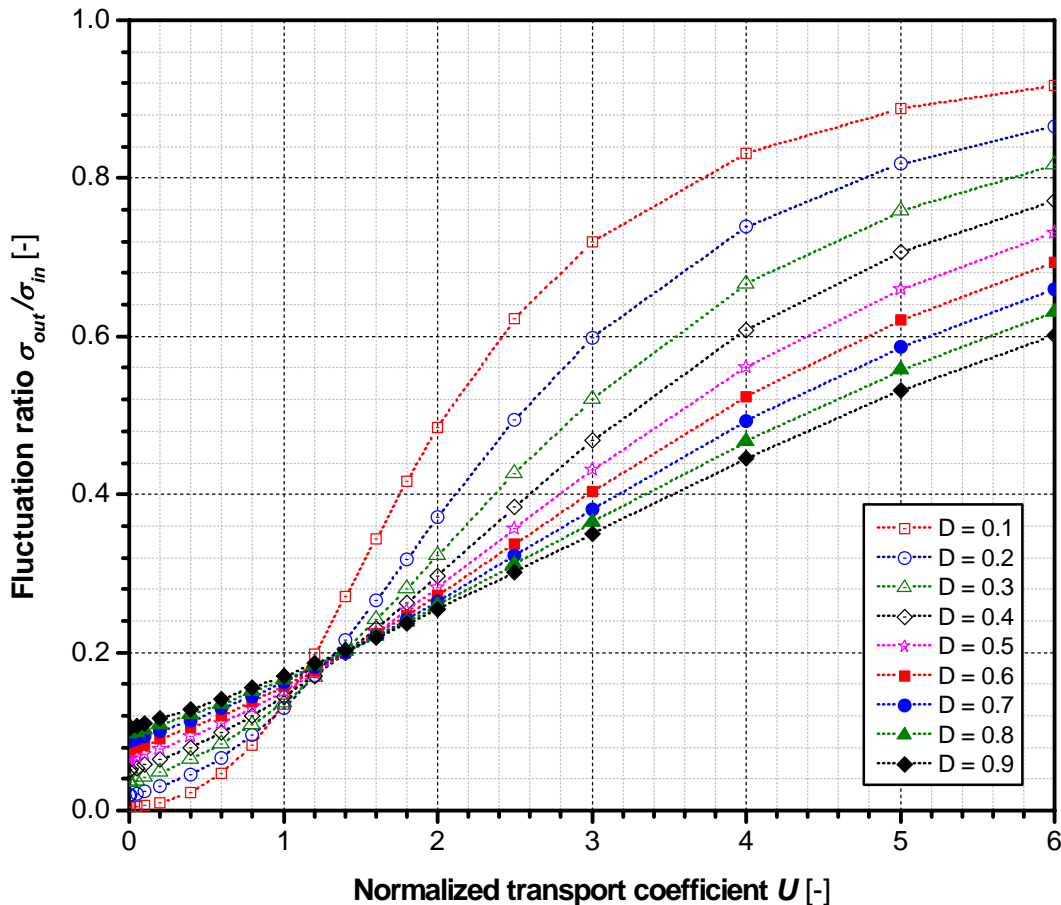


*Fig. 3-12: Influence of the normalized transport coefficient on the calculated fluctuation ratio ( $\dot{\mu}_{O,1} = 1.07$ ,  $\dot{\mu}_{A,1} = 1.0$ ,  $\dot{\mu}_{O,2} = 0.7$ ,  $\dot{\mu}_{A,2} = 0$ ,  $n = 50$ ,  $nt = 100\,000$ ,  $Rt = 20$ )*

With increasing normalized transport coefficients  $U$ , the fluctuation ratio  $\sigma_{out}/\sigma_{in}$  increases because of a higher convective transport, which causes a shorter average residence time of the particles in the continuous mixer. The dispersion coefficient  $D$  influences the shape of the curves. With increasing dispersion coefficients, the curves change from a S-shape to an almost linear shape. Up to a normalized transport coefficient of about  $U = 1.2$ , smaller normalized dispersion coefficients cause better mixing results than higher normalized dispersion coefficients. For normalized transport coefficients higher than  $U = 1.2$  the influence of the normalized dispersion coefficient is vice versa.

The corresponding influence of the normalized dispersion coefficient  $D$  on the fluctuation ratio  $\sigma_{out}/\sigma_{in}$  is shown in *Fig. 3-13* for the standard settings. The curves were calculated for different constant normalized transport coefficients and varying normalized dispersion coefficients.

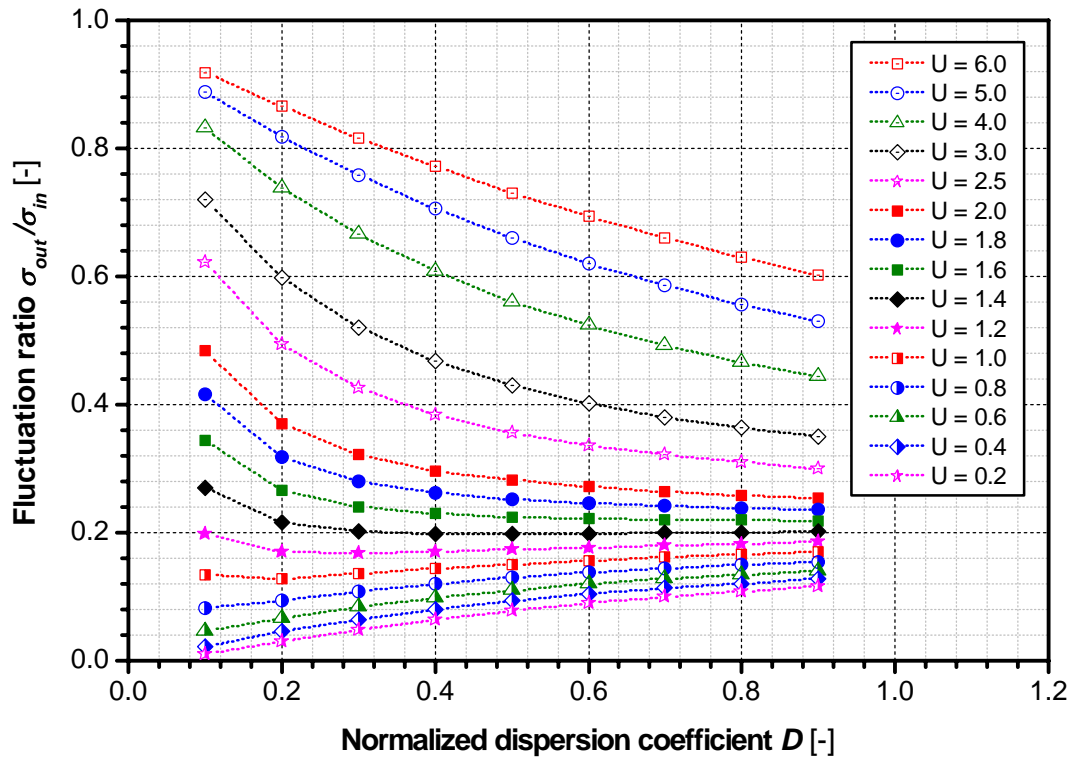


Fig. 3-13: Influence of the normalized dispersion coefficient on the calculated fluctuation ratio ( $\dot{\mu}_{O,1} = 1.07$ ,  $\dot{\mu}_{A,1} = 1.0$ ,  $\dot{\mu}_{O,2} = 0.7$ ,  $\dot{\mu}_{A,2} = 0$ ,  $n = 50$ ,  $nt = 100\,000$ ,  $Rt = 20$ )

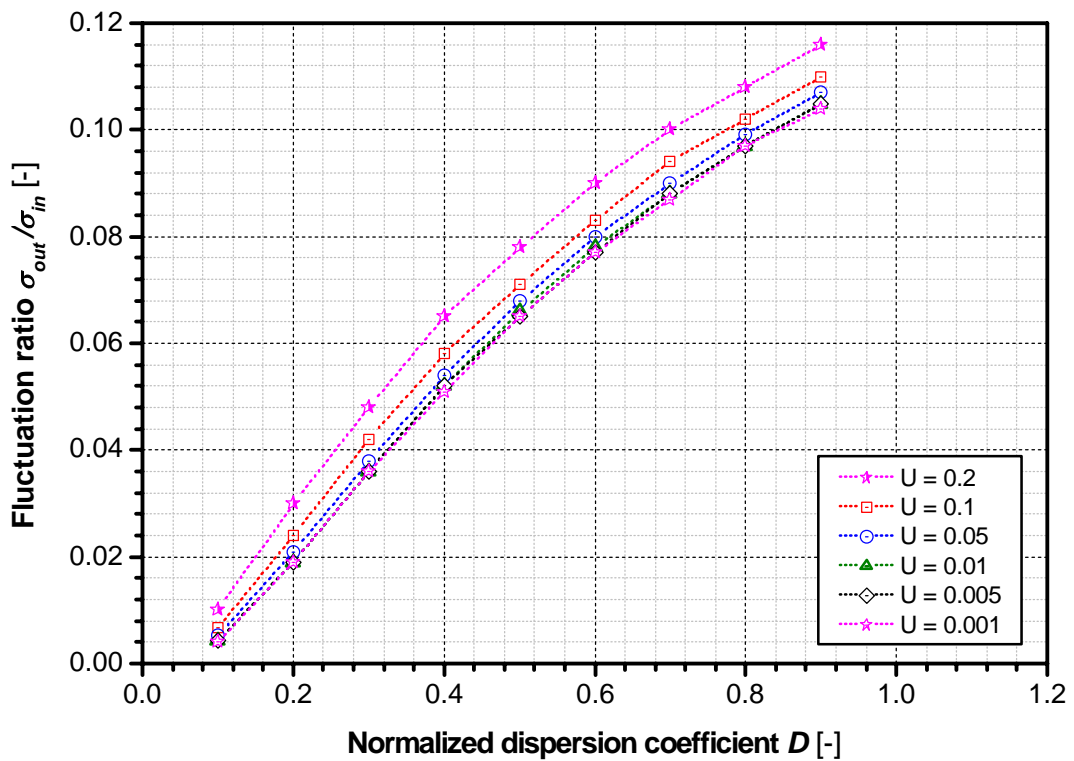
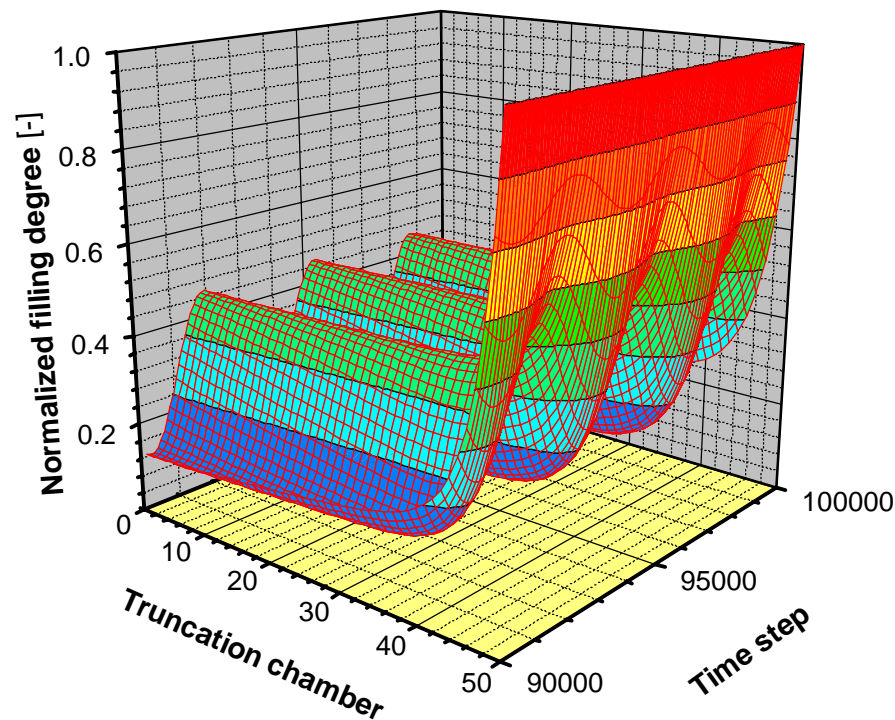


Fig. 3-14: Influence of the normalized dispersion coefficient on the calculated fluctuation ratio ( $\dot{\mu}_{O,1} = 1.07$ ,  $\dot{\mu}_{A,1} = 1.0$ ,  $\dot{\mu}_{O,2} = 0.7$ ,  $\dot{\mu}_{A,2} = 0$ ,  $n = 50$ ,  $nt = 100\,000$ ,  $Rt = 20$ )

For normalized transport coefficients between  $U = 1.4$  and  $U = 6.0$ , an increase of the normalized dispersion coefficient causes a decrease of the fluctuation ratio and an increase of the mixing quality respectively. For normalized transport coefficients between  $U = 1.0$  and  $U = 1.2$ , the fluctuation ratio decreases at first, passes through a low point and increases again. For normalized transport coefficients smaller than  $U = 1.0$ , the fluctuation ratio increases with increasing normalized dispersion coefficients.

SOMMER [54] already discussed the surprising influence of the dispersion coefficient on the fluctuation ratio and the mixing quality respectively. In batchwise working mixers, an increase of the dispersion coefficient results in a better mixing performance. In contrast to batch mixing, the influence of the dispersion coefficient on the mixing performance of a continuous mixer depends on the transport coefficient. SOMMER explains this phenomenon by the fact that the inclination of the filling degree in the mixer is much more influenced by the transport coefficient than by the dispersion coefficient. For high transport coefficients, which are equivalent to higher convective transport rates, the filling degree of the mixer increases from the mixer inlet to the outlet. This is shown in *Fig. 3-15*, where the normalized filling degree of the truncation chambers 1 to 50 is plotted for the last 10 000 time steps. In the case of high transport coefficients, high dispersion coefficients counteract the mass transport through the mixer and increase the hold-up mass in the mixer. An increased hold-up mass in the mixer causes a higher mixing performance because of the higher average residence time of the particles in the mixer (compare *Fig. 3-18*).



*Fig. 3-15: Local and temporal changing of the normalized filling degree in the continuous mixer for a normalized transport coefficient  $U = 6$  and a normalized dispersion coefficient  $D = 0.3$  ( $\dot{\mu}_{O,1} = 1.07$ ,  $\dot{\mu}_{A,1} = 1.0$ ,  $\dot{\mu}_{O,2} = 0.7$ ,  $\dot{\mu}_{A,2} = 0$ ,  $n = 50$ ,  $nt = 100\,000$ ,  $Rt = 20$ )*

For small transport coefficients, the filling degree of the mixer decreases from the mixer inlet to the outlet (see *Fig. 3-16*). In this case, higher dispersion coefficients support the mass transport through the mixer and the mixing performance decreases.

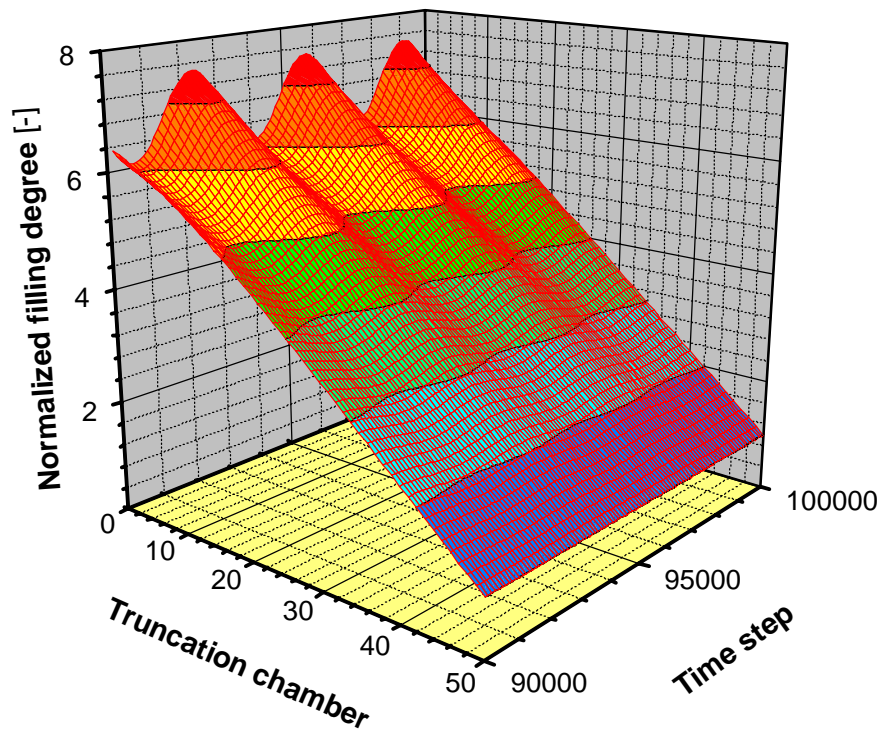


*Fig. 3-16: Local and temporal changing of the normalized filling degree in the continuous mixer for a normalized transport coefficient  $U = 0.001$  and a normalized dispersion coefficient  $D = 0.3$  ( $\dot{\mu}_{O,1} = 1.07$ ,  $\dot{\mu}_{A,1} = 1.0$ ,  $\dot{\mu}_{O,2} = 0.7$ ,  $\dot{\mu}_{A,2} = 0$ ,  $n = 50$ ,  $nt = 100\,000$ ,  $Rt = 20$ )*

### 3.5.2 Influence of the transport and dispersion coefficient on the normalized average residence time

The influence of the normalized transport coefficient  $U$  on the normalized average residence time  $t_R^*/T$  is shown in *Fig. 3-17* for the standard settings. The curves were calculated for different constant normalized dispersion coefficients and varying normalized transport coefficients.

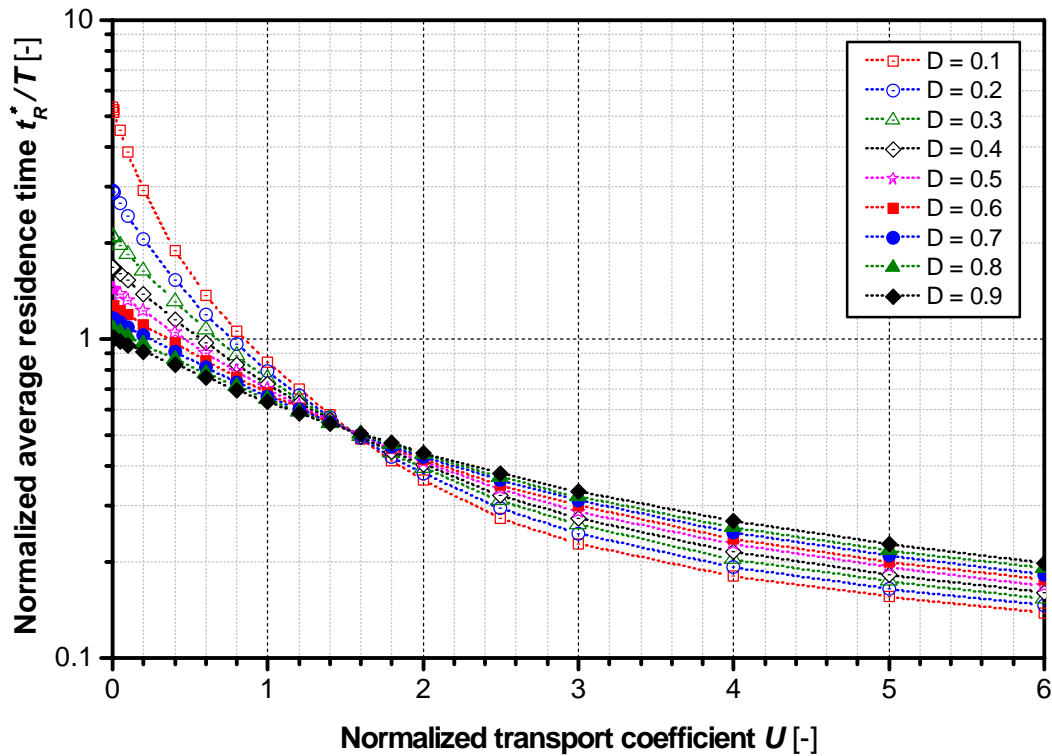


**Fig. 3-17:** Influence of the normalized transport coefficient on the calculated normalized average residence time ( $\dot{\mu}_{O,1} = 1.07$ ,  $\dot{\mu}_{A,1} = 1.0$ ,  $\dot{\mu}_{O,2} = 0.7$ ,  $\dot{\mu}_{A,2} = 0$ ,  $n = 50$ ,  $nt = 100\,000$ ,  $Rt = 20$ )

For increasing normalized transport coefficients (equivalent to an increasing of the convective transport), the normalized average residence time of the particles in the mixer decreases. Up to a normalized transport coefficient of about  $U = 1.5$ , smaller normalized dispersion coefficients cause higher normalized average residence times than smaller ones. For normalized transport coefficients higher than  $U = 1.5$ , the influence of the normalized dispersion coefficient is vice versa. As mentioned in the previous chapter, high transport coefficients cause a decrease of the mixer filling degree from the mixer inlet to the outlet (compare **Fig. 3-16**). In this case, higher dispersion coefficients support the mass transport through the mixer, which results in shorter average residence times. For high transport coefficients, the filling degree of the mixer increases from the mixer inlet to the outlet (compare **Fig. 3-15**). In this case, the influence of the dispersion coefficient is vice versa. High dispersion coefficients reduce the mixer throughput and the average residence time increases.

The corresponding influence of the normalized dispersion coefficient  $D$  on the normalized average residence time  $t_R^*/T$  is shown in **Fig. 3-18**. The curves were calculated for different constant normalized transport coefficients and varying normalized dispersion coefficients. For normalized transport coefficients between  $U = 6.0$  and  $U = 1.6$ , the normalized residence time increases with increasing normalized dispersion coefficients. For normalized transport coefficients smaller than  $U = 1.4$ , the normalized average residence time decreases with increasing normalized dispersion coefficients.



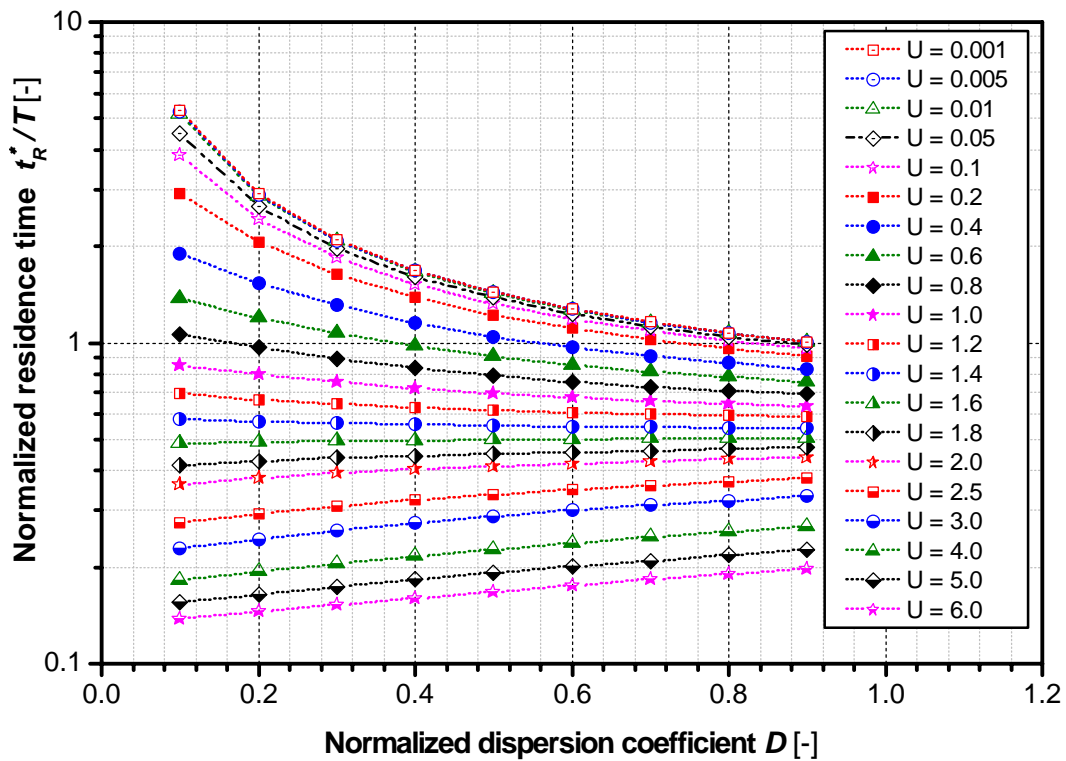


**Fig. 3-18:** Influence of the normalized dispersion coefficient on the calculated normalized average residence time ( $\dot{\mu}_{O,1} = 1.07$ ,  $\dot{\mu}_{A,1} = 1.0$ ,  $\dot{\mu}_{O,2} = \text{varied}$ ,  $\dot{\mu}_{A,2} = 0$ ,  $n = 50$ ,  $nt = 100\,000$ ,  $Rt = 20$ )

### 3.5.3 Influence of the normalized average residence time on the fluctuation ratio (mixing quality)

In the last two chapters, the fluctuation ratio and the normalized average residence time calculated for different combinations of the normalized transport and the normalized dispersion coefficients were presented. To every fluctuation ratio, a corresponding average residence time exists. The results shown in *Fig. 3-12* and *Fig. 3-17* are combined in *Fig. 3-19* and *Fig. 3-20* (different scale of the abscissa) respectively. The results shown in *Fig. 3-13* and *Fig. 3-18* are combined in *Fig. 3-21* and *Fig. 3-22* (different scale of the abscissa) respectively:

- In *Fig. 3-19* and *Fig. 3-20*, the influence of the normalized average residence time  $t_R^*/T$  on the fluctuation ratio  $\sigma_{out}/\sigma_{in}$  for constant normalized dispersion coefficients and varying normalized transport coefficients is shown.
- In *Fig. 3-21* and *Fig. 3-22*, the influence of the normalized average residence time  $t_R^*/T$  on the fluctuation ratio  $\sigma_{out}/\sigma_{in}$  for constant normalized transport coefficients and varying normalized dispersion coefficients is shown.

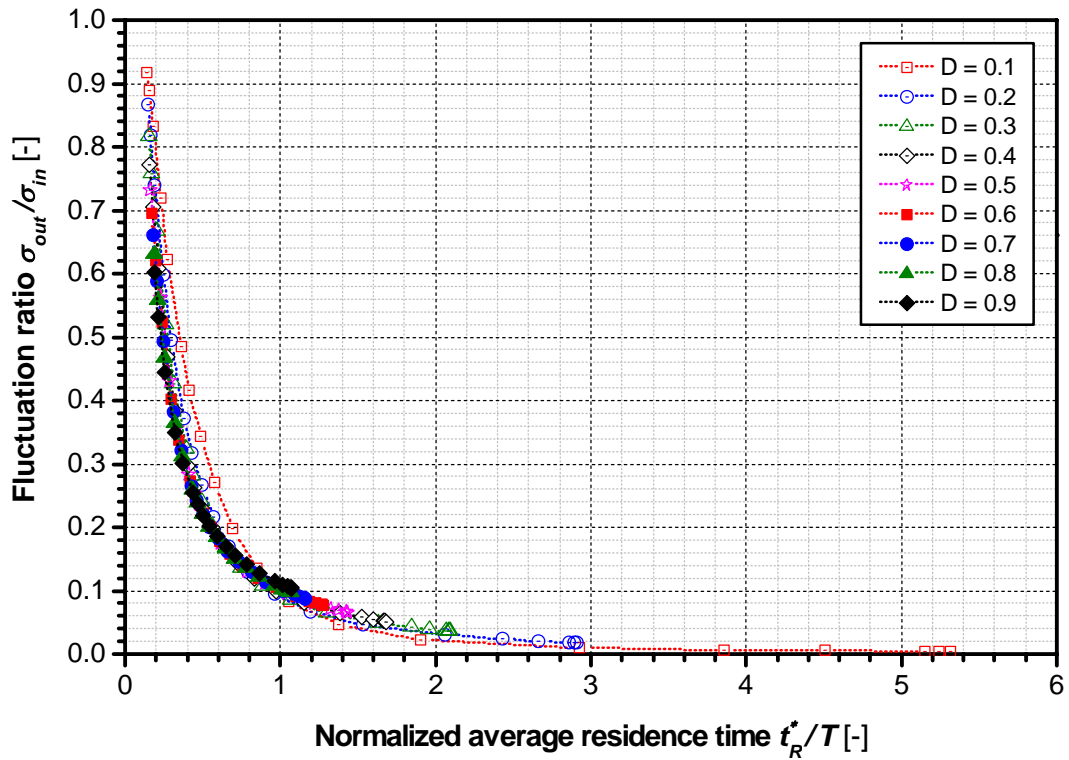


Fig. 3-19: Influence of the normalized average residence time on the fluctuation ratio ( $\dot{\mu}_{O,1} = 1.07$ ,  $\dot{\mu}_{A,1} = 1.0$ ,  $\dot{\mu}_{O,2} = 0.7$ ,  $\dot{\mu}_{A,2} = 0$ ,  $n = 50$ ,  $nt = 100\,000$ ,  $Rt = 20$ )

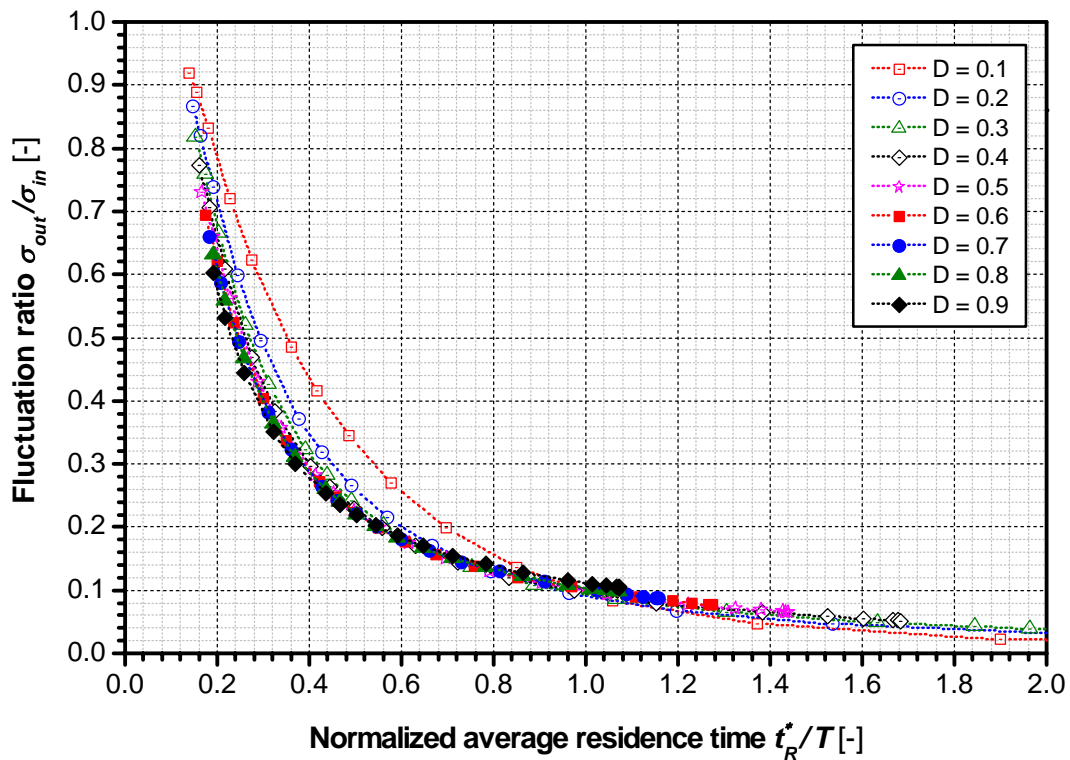


Fig. 3-20: Influence of the normalized average residence time on the fluctuation ratio ( $\dot{\mu}_{O,1} = 1.07$ ,  $\dot{\mu}_{A,1} = 1.0$ ,  $\dot{\mu}_{O,2} = 0.7$ ,  $\dot{\mu}_{A,2} = 0$ ,  $n = 50$ ,  $nt = 100\,000$ ,  $Rt = 20$ ); the scale of the abscissa differs in comparison to Fig. 3-19

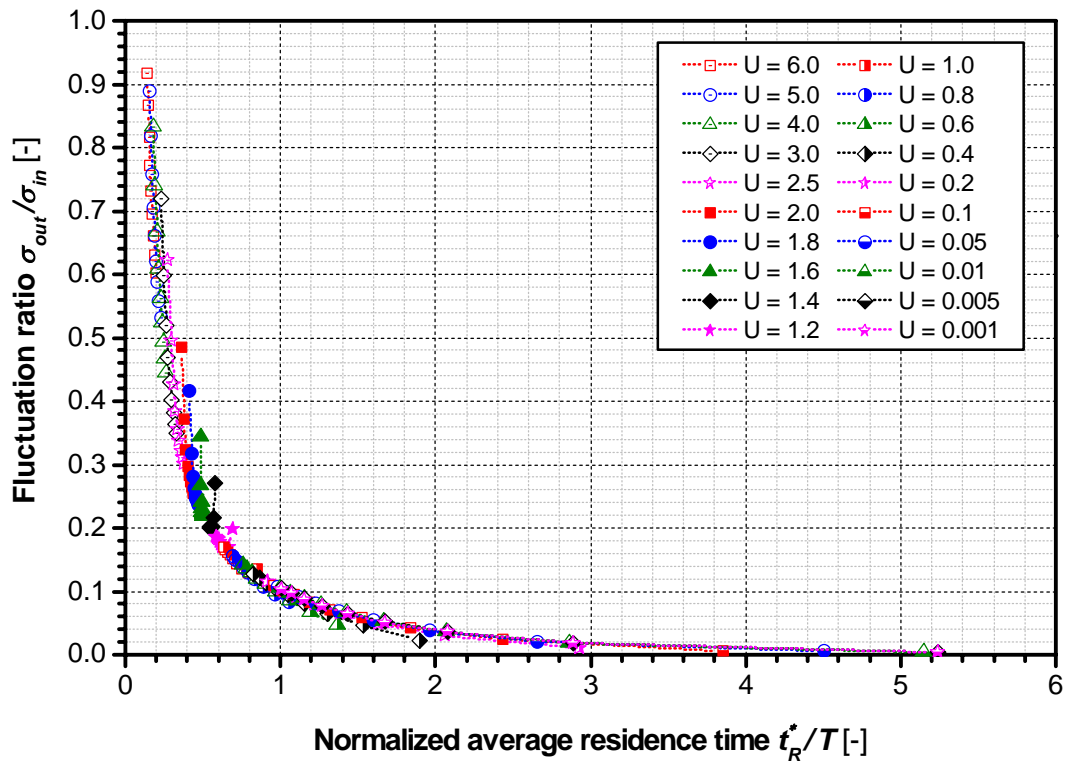


Fig. 3-21: Influence of the normalized average residence time on the fluctuation ratio ( $\dot{\mu}_{O,1} = 1.07$ ,  $\dot{\mu}_{A,1} = 1.0$ ,  $\dot{\mu}_{O,2} = 0.7$ ,  $\dot{\mu}_{A,2} = 0$ ,  $n = 50$ ,  $nt = 100\,000$ ,  $Rt = 20$ )

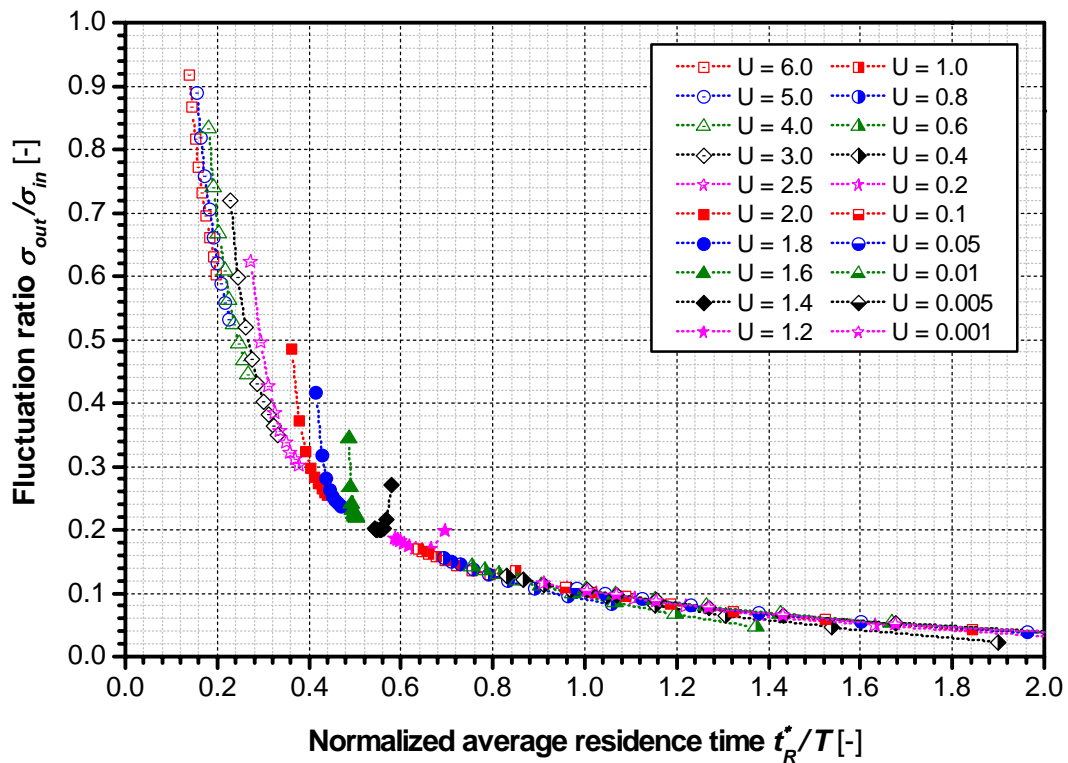


Fig. 3-22: Influence of the normalized average residence time on the fluctuation ratio ( $\dot{\mu}_{O,1} = 1.07$ ,  $\dot{\mu}_{A,1} = 1.0$ ,  $\dot{\mu}_{O,2} = 0.7$ ,  $\dot{\mu}_{A,2} = 0$ ,  $n = 50$ ,  $nt = 100\,000$ ,  $Rt = 20$ ); the scale of the abscissa differs in comparison to Fig. 3-21



All curves show a decrease of the fluctuation ratio with an increase of the normalized average residence time. The differences between the curves, especially for normalized dispersion coefficients higher than  $D = 0.2$ , are quite small. The normalized dispersion coefficients depend on the mobility of the single particle and the normalized transport coefficient corresponds to the convective transport in the mixer, which is influenced by the operating parameters of the mixer (rotational speed, filling degree). By the variation of the normalized transport coefficient and the normalized dispersion coefficient, different operation conditions and particle mobilities were simulated. Because all single curves can be approximated by a master curve, the following hypothesis can be proposed:

**The normalized average residence time is the main influencing parameter of the fluctuation ratio independent of the mixer type!**

#### 3.5.4 Estimation of the necessary running time

The steady state is obtained in the mixer simulated, when the concentration fluctuations calculated in the outlet of the mixer are constant. For a normalized dispersion coefficient of  $D = 0.3$  as well as for normalized transport coefficients of  $U = 0.001$  and  $U = 6.0$ , the temporal changes of the concentration in the outlet of the mixer were calculated. In *Fig. 3-23*, the temporal changes of the calcium carbonate concentration in the inlet and the outlet of the mixer are plotted against the dimensionless running time  $Rt$  for  $U = 0.001$ . In *Fig. 3-24*, the same is done for  $U = 6.0$ . The dimensionless running time  $Rt$  is defined as the multiple of the period length  $T$  of the entering mass flow fluctuations. For  $U = 0.001$ , the steady state is reached after a dimensionless running time of  $Rt = 6$ . For  $U = 6.0$ , the steady state is reached after a dimensionless running time of  $Rt = 1$  (visual comparison). To be on the safe side, a dimensionless running time of 20, which is twenty times the period length of the fluctuations, was chosen for the simulations.

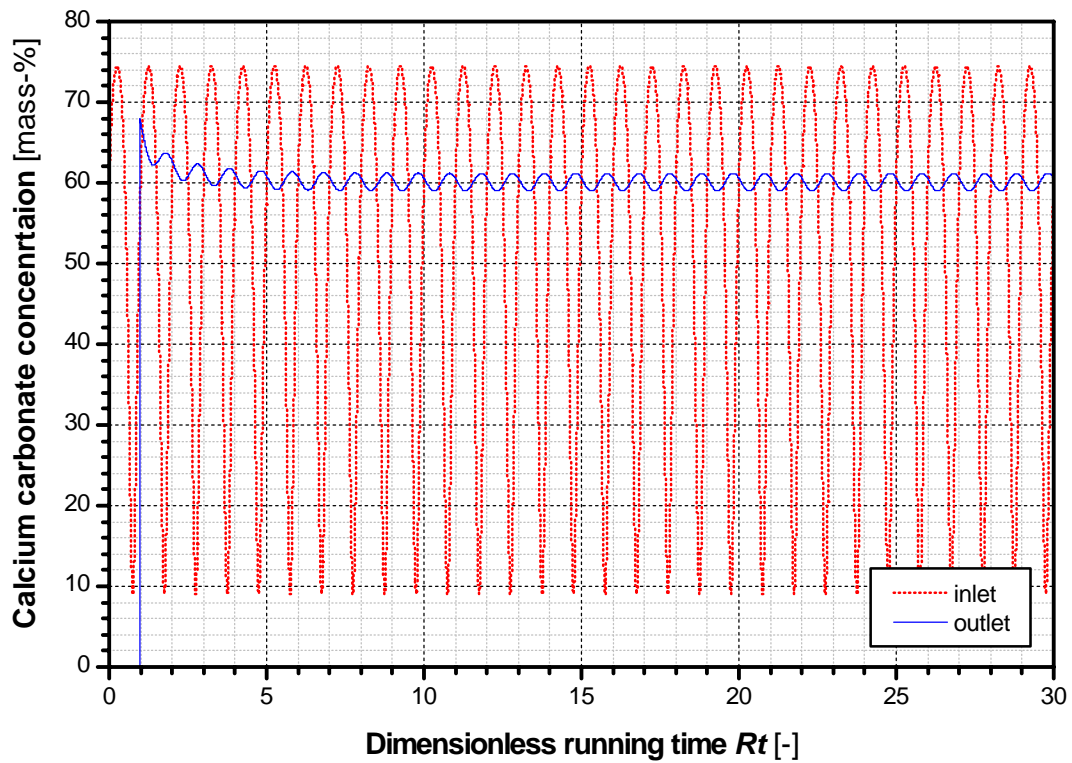


**Fig. 3-23:** Concentration fluctuations in the inlet and outlet of the mixer ( $U = 0.001$ ,  $D = 0.3$ ,  $\dot{\mu}_{O,1} = 1.07$ ,  $\dot{\mu}_{A,1} = 1.0$ ,  $\dot{\mu}_{O,2} = 0.7$ ,  $\dot{\mu}_{A,2} = 0$ ,  $n = 50$ ,  $nt = 100\,000$ )

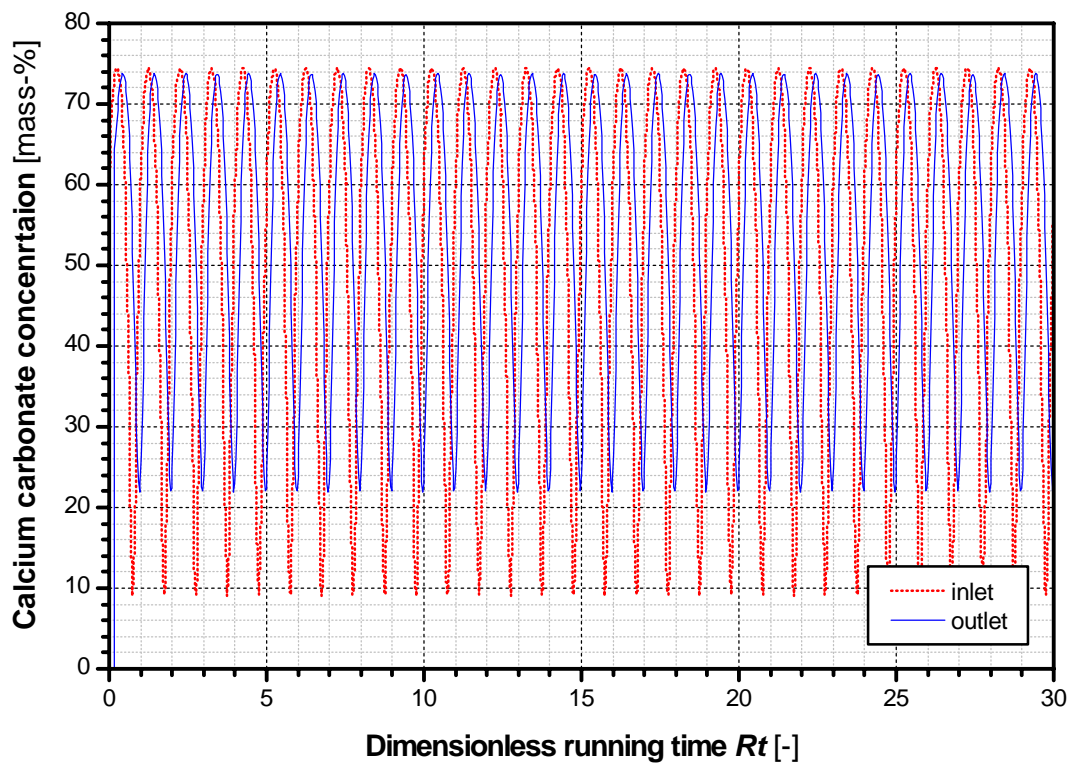


**Fig. 3-24:** Concentration fluctuations in the inlet and the outlet of the mixer ( $U = 6.0$ ,  $D = 0.3$ ,  $\dot{\mu}_{O,1} = 1.07$ ,  $\dot{\mu}_{A,1} = 1.0$ ,  $\dot{\mu}_{O,2} = 0.7$ ,  $\dot{\mu}_{A,2} = 0$ ,  $n = 50$ ,  $nt = 100\,000$ )

### 3.5.5 Influence of the number of truncation chambers and the number of time steps on the calculated results

To evaluate the stability of the truncation algorithm used, the influence of the normalized average residence time on the fluctuation ratio was calculated for 50 truncation chambers and 100 000 time steps as well as for 100 truncation chambers and 200 000 time steps. The results are shown in Fig. 3-25 for a normalized dispersion coefficient of  $D = 0.3$  and transport coefficients varied between  $U = 0.2$  and  $U = 2.0$ . The two curves are approximately identical. The result indicates that the used truncation algorithm is stable and simulations with 50 truncation chambers and 100 000 time steps are sufficient.

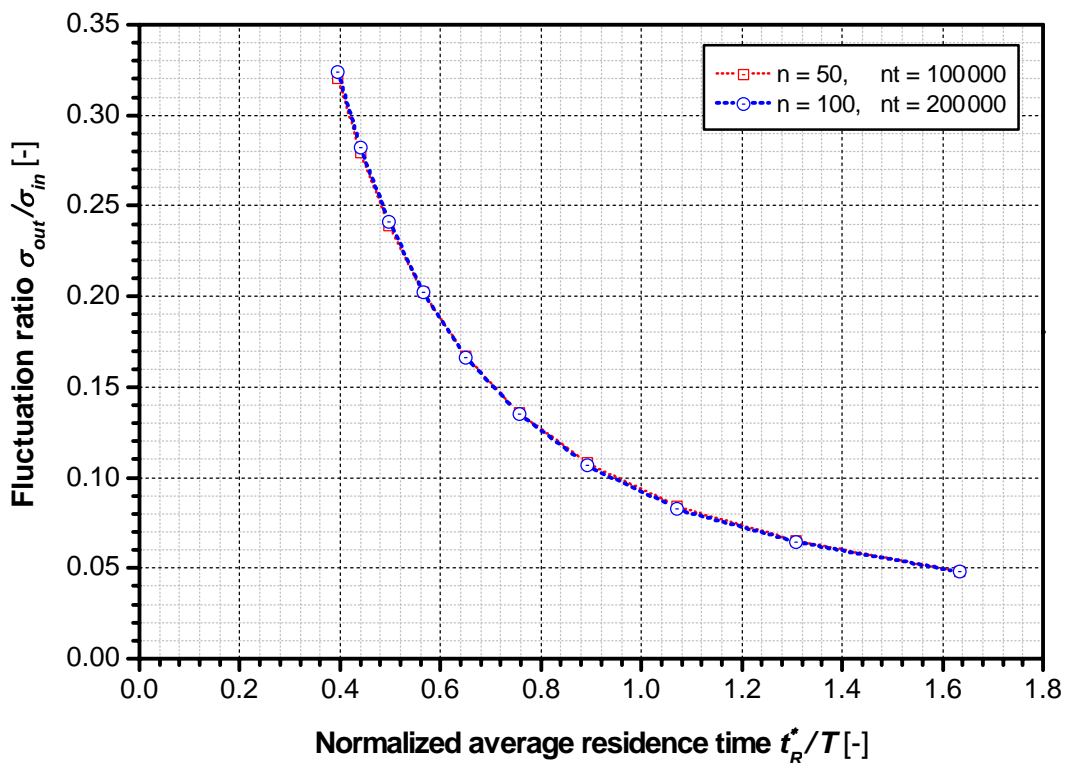
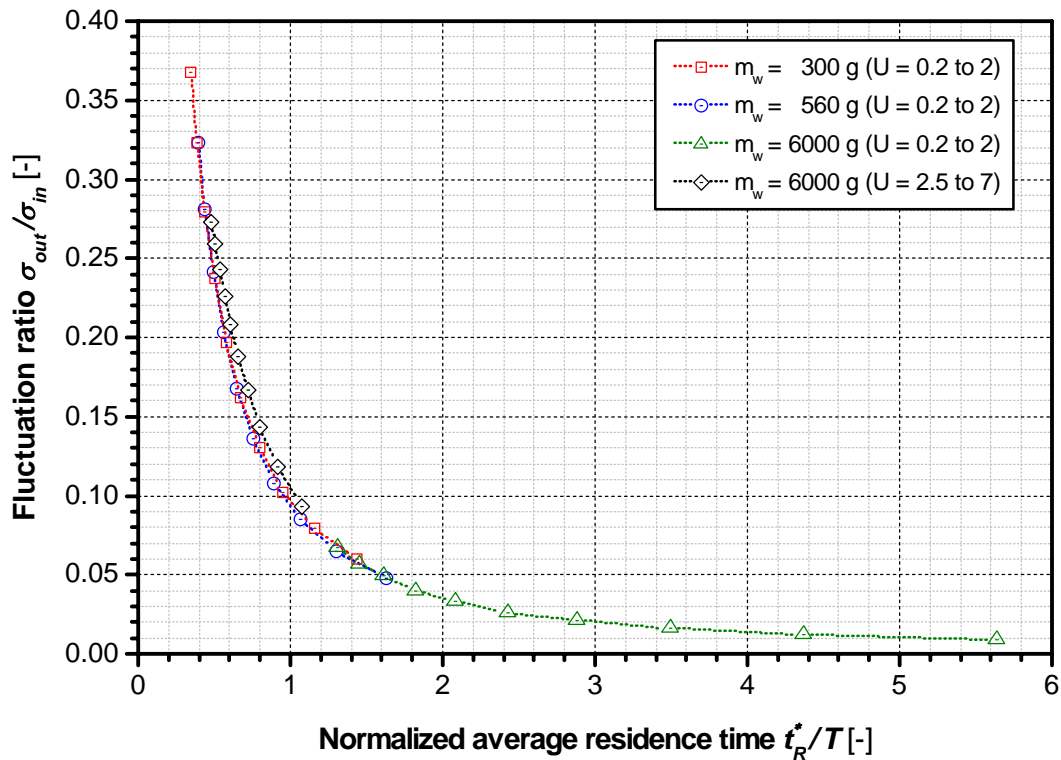


Fig. 3-25: Influence of the truncation chamber number and number of time steps on the calculated mixing results ( $U = \text{varied}$ ,  $D = 0.3$ ,  $\dot{\mu}_{O,1} = 1.07$ ,  $\dot{\mu}_{A,1} = 1.0$ ,  $\dot{\mu}_{O,2} = 0.7$ ,  $\dot{\mu}_{A,2} = 0$ ,  $Rt = 20$ )

### 3.5.6 Influence of the mass $m_w$ on the calculated mixing results

The mass  $m_w$  corresponds to the mass in the mixer which could be measured in the case that the filling degree in every truncation chamber is equal to the filling degree up to the height of the weir  $\phi_w^*$  in the last truncation chamber. The mass  $m_w$  is used to normalize the entering mass flows of component 1 and component 2 (compare Eq. 3-55 and Eq. 3-56, p. 25). The position of the weir, the mass flow of the entering powders as well as the rotational speed of the mixing device are the main parameters influencing  $m_w$ . The mass flow and the rotational speed will influence the porosity of the bulk material in the mixer and therefore the mass  $m_w$ . During the experimental validation of the model developed, it was not possible to determine the mass of the powder up to the height of the weir. Therefore, the mass was estimated by the measured active mass hold-ups. The measured active mass hold-ups varied between 0.3 and 6.0 kg.

The influence of the mass up to the height of the weir on the calculated mixing results is shown in **Fig. 3-26** for the lowest value ( $m_{weir} = 0.3 \text{ kg}$ ), the standard mixing experiment ( $m_{weir} = 0.56 \text{ kg}$ ) and the highest value ( $m_{weir} = 6 \text{ kg}$ ). The influence of the mass up to the height of the weir on the shape of the curve can be neglected. For higher masses  $m_w$ , the calculated values move along the master curve in the direction of smaller normalized average residence times.



**Fig. 3-26:** Influence of the mass up to the height of the weir on the calculated mixing results ( $U = \text{varied}$ ,  $D = 0.3$ ,  $\dot{\mu}_{O,1} = 1.07$ ,  $\dot{\mu}_{A,1} = 1.0$ ,  $\dot{\mu}_{O,2} = 0.7$ ,  $\dot{\mu}_{A,2} = 0$ ,  $n = 50$ ,  $nt = 100\,000$ ,  $Rt = 20$ )

### 3.5.7 Influence of the mass flow on the calculated mixing results

For the experimental validation of the developed model, an average maize starch mass flow  $\Delta m/\Delta t$  of 5, 10, 15 and 20 g/s was used. The influence of varying maize starch mass flows on the calculated fluctuation ratio is shown in **Fig. 3-27**. Keeping the normalized average residence time constant, the fluctuation ratios decrease with decreasing average maize starch mass flows.

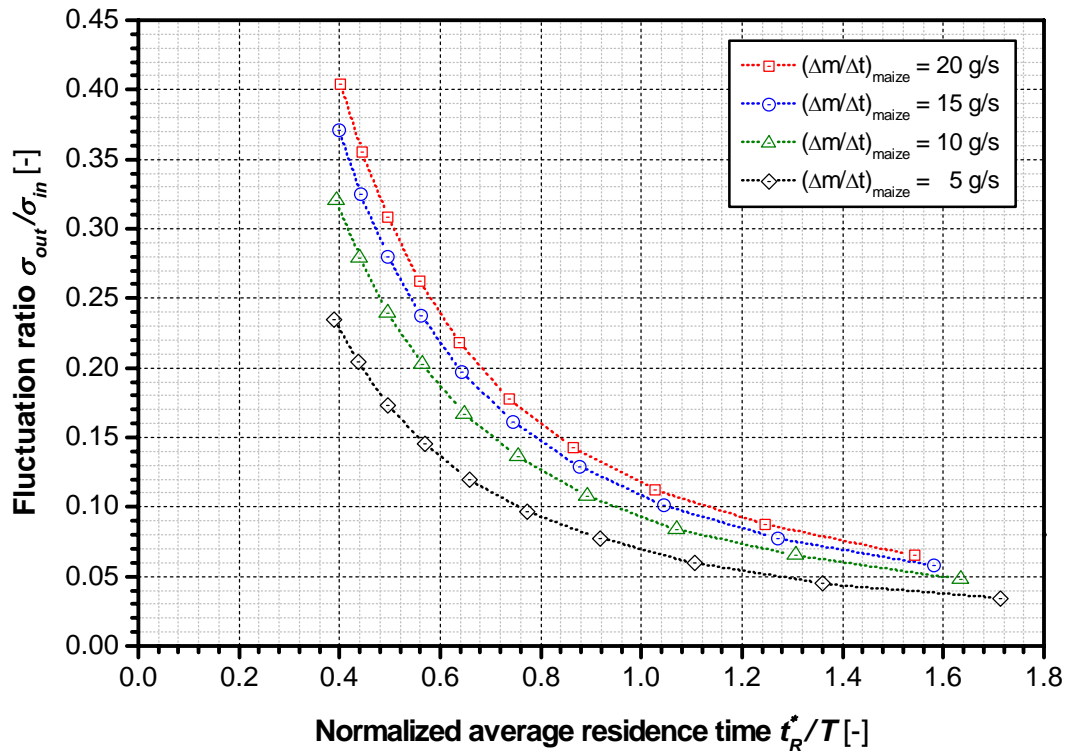


**Fig. 3-27:** Influence of the mass flow on the calculated mixing results ( $U = \text{varied}$ ,  $D = 0.3$ ,  $\dot{m}_{0,1} = 15$  g/s,  $\dot{m}_{A,1} = 14$  g/s,  $\dot{\mu}_{O,1} = 1.07$ ,  $\dot{\mu}_{A,1} = 1.0$ ,  $\dot{\mu}_{O,2} = \text{varied}$ ,  $\dot{\mu}_{A,2} = 0$ ,  $n = 50$ ,  $nt = 100\,000$ ,  $Rt = 20$ )

### 3.5.8 Influence of the normalized transport and dispersion coefficient on the normalized filling degree

Besides the calculation of the fluctuation ratio and the normalized average residence time, the model developed can be used to calculate the normalized filling degree in the truncation chambers of the continuous mixer.

In the following subchapters, the results of the simulations are shown in two separate figures for each simulation setting. In the first figure, the changing of the filling degree during the first 5000 time steps is shown. The second figure shows the changing for up to 40000 time steps. The continuous mixer is empty at the beginning of the simulation. The powder enters the mixer at the first truncation chamber and leaves the mixer over a weir, which is located at the end of the last truncation chamber. The filling degree at the height of the weir is 1 because of the normalization condition used for the filling degree.

#### 3.5.8.1 Influence of the normalized transport coefficient

In **Fig. 3-28** to **Fig. 3-32**, the influence of the normalized transport coefficient ( $U = 0.001, 0.01, 0.1, 1.0, 6.0$ ) on the normalized filling degree for a constant normalized dispersion coefficient ( $D = 0.3$ ) is shown. The time necessary to fill the last truncation chamber up to the height of the weir as well as the maximum height of the first truncation chamber decreases with increasing normalized transport coefficients, which corresponds to a higher convective transport. For normalized transport coefficients up to  $U = 1$ , the normalized filling degree decreases from the



inlet to the outlet of the mixer. For a normalized transport coefficients of  $U = 6$ , the normalized filling degree increases from the inlet to the outlet of the mixer.

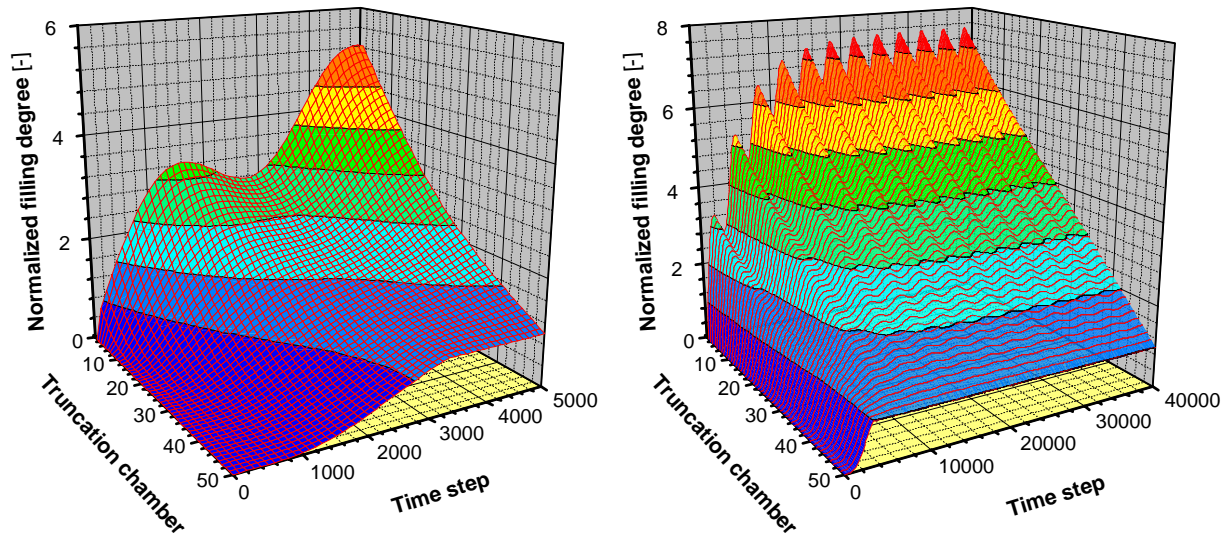


*Fig. 3-28: Temporal change of the normalized filling degree in the truncation chambers for a normalized transport coefficient of  $U = 0.001$  ( $D = 0.3$ ,  $\dot{\mu}_{O,1} = 1.07$ ,  $\dot{\mu}_{A,1} = 1.0$ ,  $\dot{\mu}_{O,2} = 0.7$ ,  $\dot{\mu}_{A,2} = 0$ ,  $n = 50$ ,  $nt = 100\,000$ ,  $Rt = 20$ )*

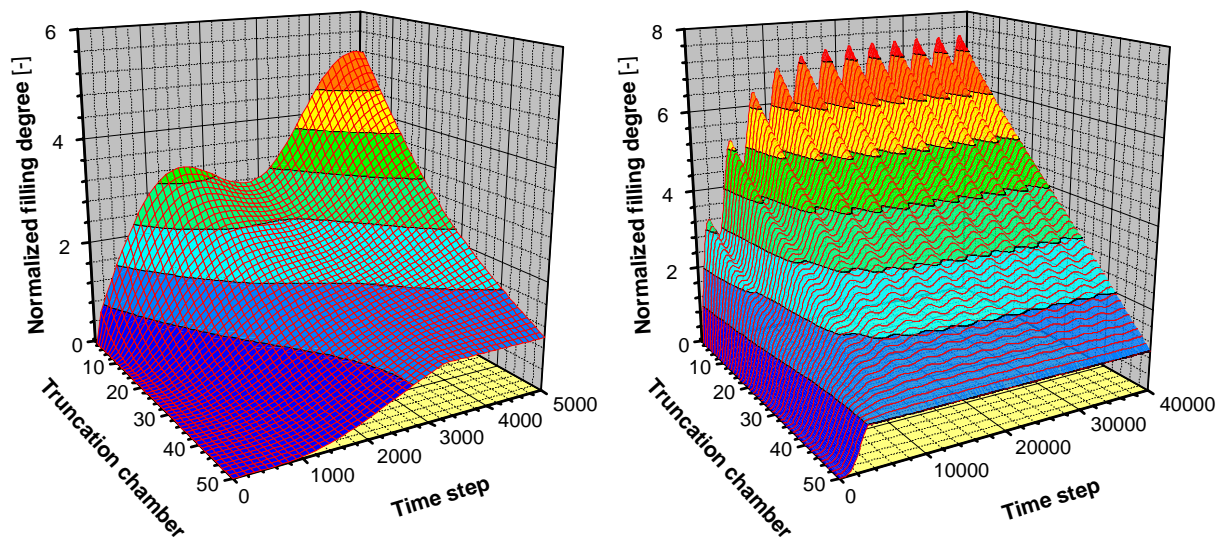


*Fig. 3-29: Temporal change of the normalized filling degree in the truncation chambers for a normalized transport coefficient of  $U = 0.01$  ( $D = 0.3$ ,  $\dot{\mu}_{O,1} = 1.07$ ,  $\dot{\mu}_{A,1} = 1.0$ ,  $\dot{\mu}_{O,2} = 0.7$ ,  $\dot{\mu}_{A,2} = 0$ ,  $n = 50$ ,  $nt = 100\,000$ ,  $Rt = 20$ )*

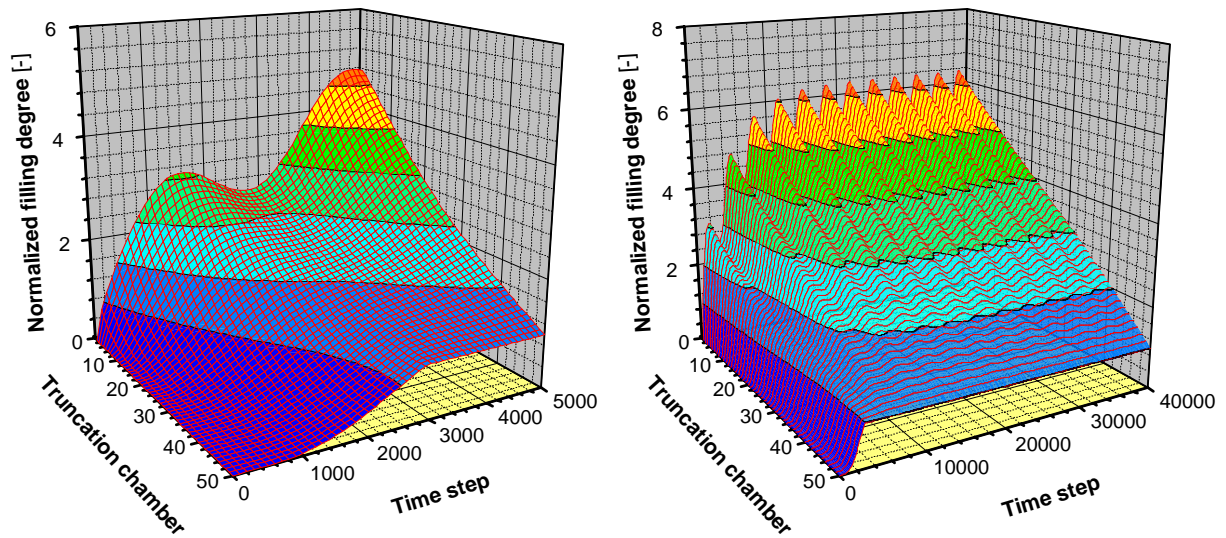


**Fig. 3-30:** Temporal change of the normalized filling degree in the truncation chambers for a normalized transport coefficient of  $U = 0.1$  ( $D = 0.3$ ,  $\dot{\mu}_{O,1} = 1.07$ ,  $\dot{\mu}_{A,1} = 1.0$ ,  $\dot{\mu}_{O,2} = 0.7$ ,  $\dot{\mu}_{A,2} = 0$ ,  $n = 50$ ,  $nt = 100\,000$ ,  $Rt = 20$ )

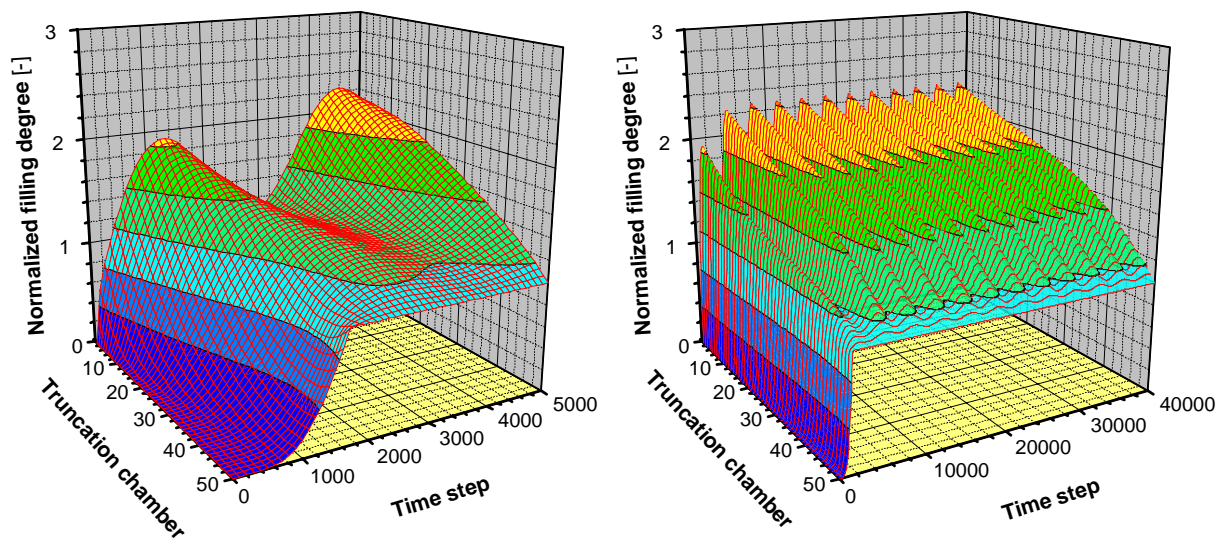


**Fig. 3-31:** Temporal change of the normalized filling degree in the truncation chambers for a normalized transport coefficient of  $U = 1.0$  ( $D = 0.3$ ,  $\dot{\mu}_{O,1} = 1.07$ ,  $\dot{\mu}_{A,1} = 1.0$ ,  $\dot{\mu}_{O,2} = 0.7$ ,  $\dot{\mu}_{A,2} = 0$ ,  $n = 50$ ,  $nt = 100\,000$ ,  $Rt = 20$ )



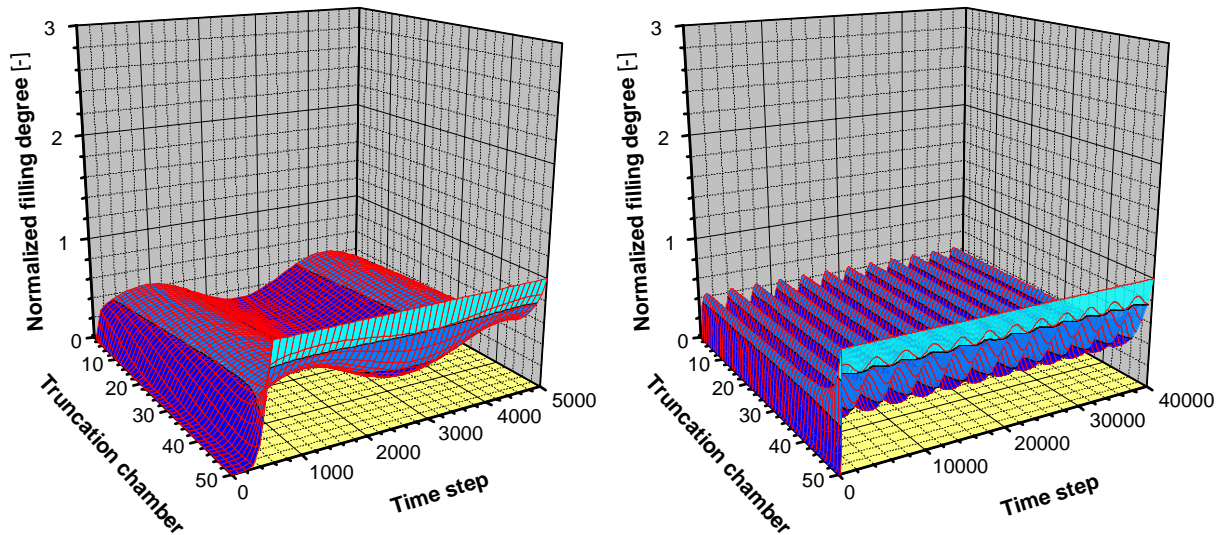


**Fig. 3-32:** Temporal change of the normalized filling degree in the truncation chambers for a normalized transport coefficient of  $U = 6.0$  ( $D = 0.3$ ,  $\dot{\mu}_{O,1} = 1.07$ ,  $\dot{\mu}_{A,1} = 1.0$ ,  $\dot{\mu}_{O,2} = 0.7$ ,  $\dot{\mu}_{A,2} = 0$ ,  $n = 50$ ,  $nt = 100\,000$ ,  $Rt = 20$ )

### 3.5.8.2 Influence of the normalized dispersion coefficient

In *Fig. 3-33* to *Fig. 3-35*, the influence of the normalized dispersion coefficient ( $D = 0.1, 0.45, 0.9$ ) on the normalized filling degree for a constant normalized transport coefficient ( $U = 1.2$ ) is shown. For a normalized transport coefficient of  $U = 1.2$ , the normalized dispersion coefficient has only a small influence on the number of time steps necessary to fill the last truncation chamber up to the height of the weir. The necessary number of time steps increases from  $D = 0.1$  to  $D = 0.45$  and decreases for  $D = 0.9$  again. The maximum filling degree decreases with increasing normalized dispersion coefficients.

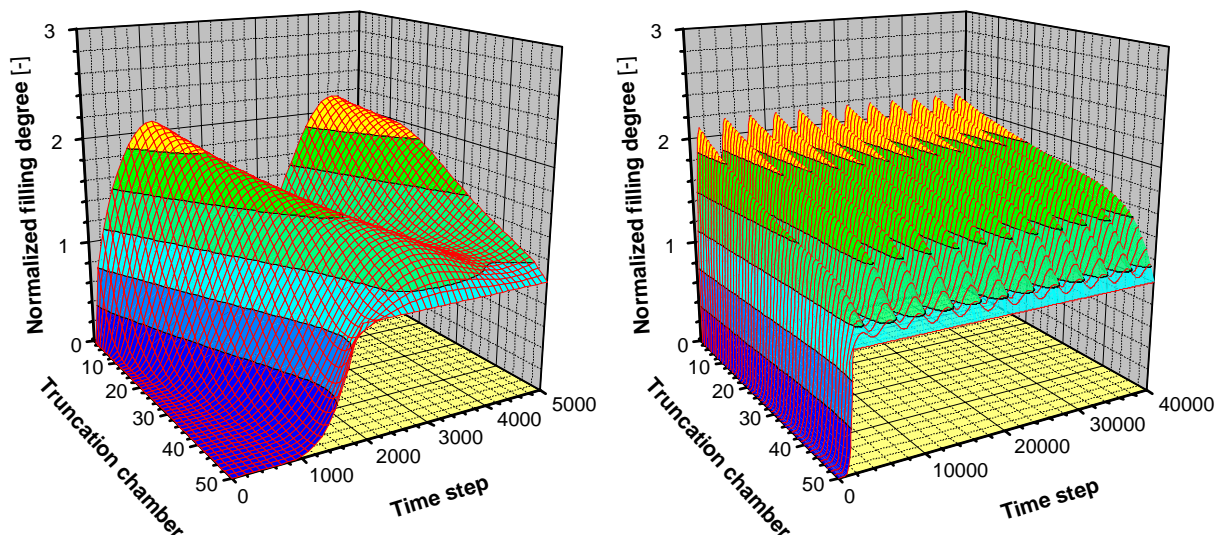


**Fig. 3-33:** Temporal change of the normalized filling degree in the truncation chambers for a normalized dispersion coefficient of  $D = 0.1$  ( $U = 1.2$ ,  $\dot{\mu}_{O,1} = 1.07$ ,  $\dot{\mu}_{A,1} = 1.0$ ,  $\dot{\mu}_{O,2} = 0.7$ ,  $\dot{\mu}_{A,2} = 0$ ,  $n = 50$ ,  $nt = 100\,000$ ,  $Rt = 20$ )



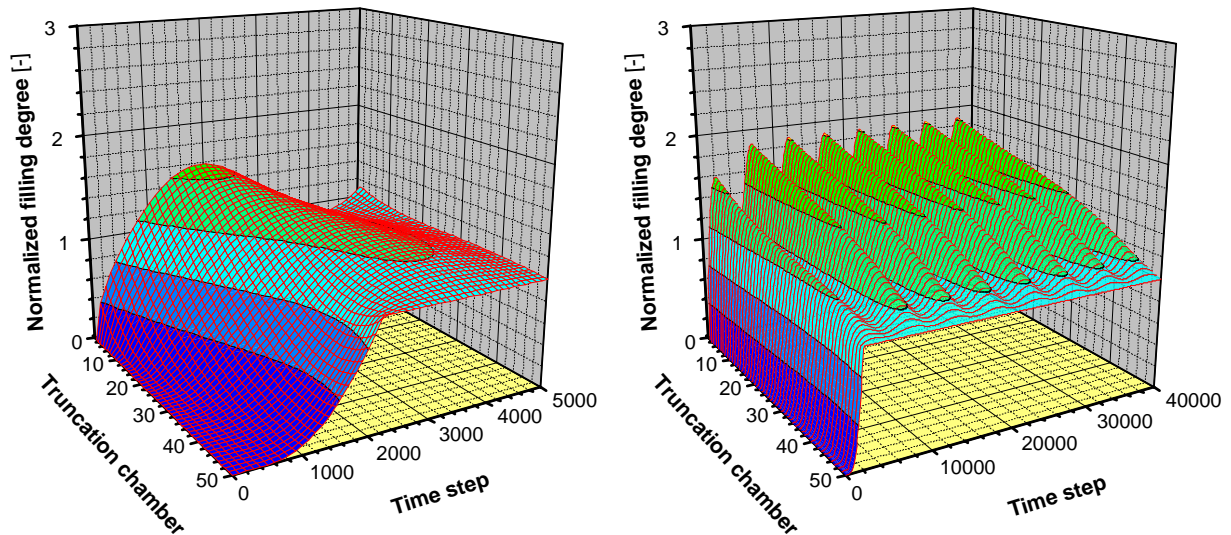


**Fig. 3-34:** Temporal change of the normalized filling degree in the truncation chambers for a normalized dispersion coefficient of  $D = 0.45$  ( $U = 1.2$ ,  $\dot{\mu}_{O,1} = 1.07$ ,  $\dot{\mu}_{A,1} = 1.0$ ,  $\dot{\mu}_{O,2} = 0.7$ ,  $\dot{\mu}_{A,2} = 0$ ,  $n = 50$ ,  $nt = 100\,000$ ,  $Rt = 20$ )

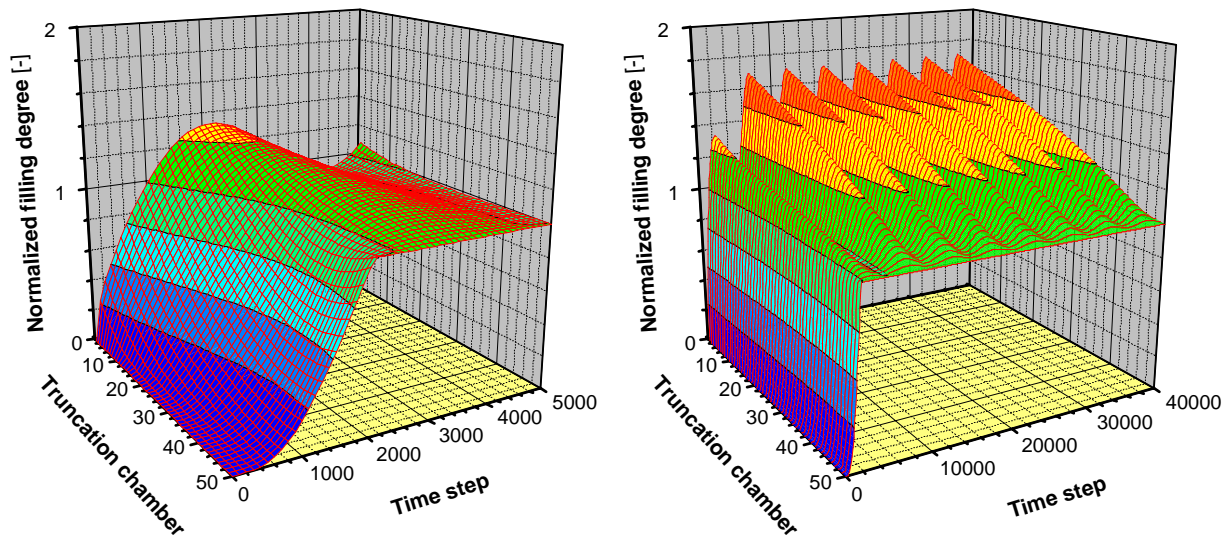


**Fig. 3-35:** Temporal change of the normalized filling degree in the truncation chambers for a normalized dispersion coefficient of  $D = 0.9$  ( $U = 1.2$ ,  $\dot{\mu}_{O,1} = 1.07$ ,  $\dot{\mu}_{A,1} = 1.0$ ,  $\dot{\mu}_{O,2} = 0.7$ ,  $\dot{\mu}_{A,2} = 0$ ,  $n = 50$ ,  $nt = 100\,000$ ,  $Rt = 20$ )

### 3.5.9 Influence of the spreading factor of the entering mass flow on the mixing results

During the mixing experiments, the outlets of the volumetric feeders used were in the same plane as the axis of the continuous mixer and the entering powder was spread over a certain length of the mixer. For the simulations, it was assumed that the whole powder flows only in the first truncation chamber. Following, the influence of spreading the entering powder over a certain number of truncation chambers is examined. The amount of spreading is characterized by the spreading factor  $SF$ . The spreading factor is defined as the ratio of the number  $n_s$  of truncation chambers, over which the entering powders are spread, to the number  $n$  of all truncation chambers. Transferred to the real mixer, the spreading factor is the ratio of the length  $L_s$  of the mixer, over which the entering powders are spread, to the length  $L$  of the mixer (see *Fig. 3-36* and *Eq. 3-19*). The spreading begins at the first truncation chamber and ends at any chamber, depending on the spreading factor. It is assumed that the same amount of powder is spread in each chamber.

$$SF = \frac{n_s}{n} = \frac{L_s}{L} \quad \text{Eq. 3-111}$$

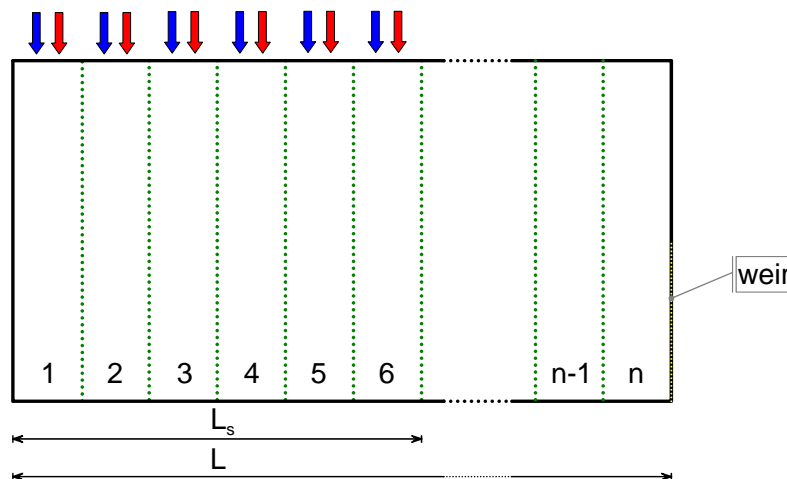


*Fig. 3-36: Illustration of the spreading factor*

Taking the spreading of the entering powder into consideration, the truncation of the mixer inlet and the following truncation chambers changes (compare *Eq. 3-82* to *Eq. 3-85*):

Chamber  $s = 1$ :

$$\phi_{1,t+1} = (1 - CU - CD) \cdot \phi_{1,t} + CD \cdot \phi_{2,t} + \frac{I}{SF \cdot n} \Delta\phi 1(t \cdot \Delta\tau) \quad \text{Eq. 3-112}$$

$$\phi_{2,t+1} = (1 - CU - CD) \cdot \phi_{2,t} + CD \cdot \phi_{3,t} + \frac{I}{SF \cdot n} \cdot \Delta\phi 2(t \cdot \Delta\tau) \quad \text{Eq. 3-113}$$

Chamber  $s = 2 \dots SF \cdot n$ :

$$\phi_{1,s,t+1} = (CU + CD) \cdot \phi_{1,s-1,t} + (1 - CU - 2 \cdot CD) \cdot \phi_{1,s,t} + CD \cdot \phi_{1,s+1,t} + \frac{1}{SF \cdot n} \Delta \phi I(t \cdot \Delta \tau) \quad \text{Eq. 3-114}$$

$$\phi_{2,s,t+1} = (CU + CD) \cdot \phi_{2,s-1,t} + (1 - CU - 2 \cdot CD) \cdot \phi_{2,s,t} + CD \cdot \phi_{2,s+1,t} + \frac{1}{SF \cdot n} \Delta \phi I(t \cdot \Delta \tau) \quad \text{Eq. 3-115}$$

Chamber  $s = SF \cdot n + 1 \dots n - 1$ :

$$\phi_{1,s,t+1} = (CU + CD) \cdot \phi_{1,s-1,t} + (1 - CU - 2 \cdot CD) \cdot \phi_{1,s,t} + CD \cdot \phi_{1,s+1,t} \quad \text{Eq. 3-116}$$

$$\phi_{2,s,t+1} = (CU + CD) \cdot \phi_{2,s-1,t} + (1 - CU - 2 \cdot CD) \cdot \phi_{2,s,t} + CD \cdot \phi_{2,s+1,t} \quad \text{Eq. 3-117}$$

For spreading factors varying between  $SF = 0.02$  and  $SF = 0.9$ , the influence of the spreading factor on the fluctuation ratio is shown in *Eq. 3-20*.

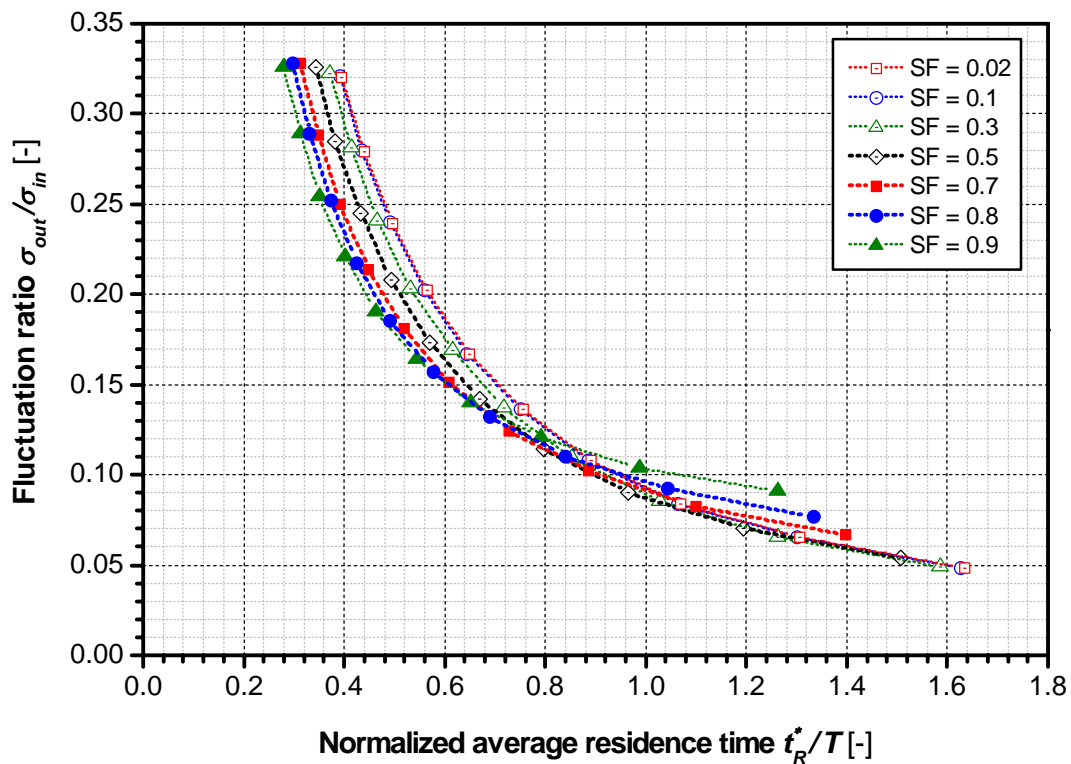


**Fig. 3-37:** Influence of the spreading factor of the entering mass flow on the fluctuation ratio ( $U = \text{varied}$ ,  $D = 0.3$ ,  $\dot{\mu}_{O,1} = 1.07$ ,  $\dot{\mu}_{A,1} = 1.0$ ,  $\dot{\mu}_{O,2} = 0.7$ ,  $\dot{\mu}_{A,2} = 0$ ,  $n = 50$ ,  $nt = 100\,000$ ,  $Rt = 20$ )

Up to a normalized average residence time of about  $t_R^*/T = 0.8$ , higher spreading factors cause smaller fluctuation ratios and better mixing results respectively. For higher normalized average residence times, a spreading with  $SF = 0.7$ ,  $0.8$  and  $0.9$  has a significant negative influence on the mixing result.



## 4 Experimental validation of the mixing model

Experimental data, which can be used for the validation of the mixing model, can hardly be found in literature. Only a few experimental results can be extracted from WEINEKÖTTER's PhD thesis [50]. Therefore, an experimental rig had to be planned, constructed and built up to determine

- the reduction of concentration fluctuations entering the continuous mixer as well as
- the corresponding average residence time of the particles in the continuous mixer for different operation parameters.

### 4.1 Experimental rig

*Fig. 4-1* shows the front view, *Fig. 4-2* the rear view and *Fig. 4-3* a flowchart of the experimental rig.



*Fig. 4-1:* Front view of the experimental rig: ① continuous mixer, ② volumetric feeders, ③ suction conveyors

For the mixing experiments, the continuous dynamic powder mixer *GCM 500* from the company *Gericke AG* (Regensdorf, Switzerland) was used. The continuous mixer is able to handle volume flow rates of up to  $2.8 \text{ m}^3/\text{h}$ . The mixing chamber is about  $500 \text{ mm}$  long,  $200 \text{ mm}$  broad and has a maximum height of  $185 \text{ mm}$ . Two volumetric feeders from the company *Gericke GmbH* (Rielasingen, Germany) feed the powders into the continuous mixer. The volumetric feeders *GAC 132* have a capacity of about  $200 \text{ l}$ . The feed rate can be varied between  $0.06$  and  $430 \text{ l/h}$ . The Fourier Transform Near-InfraRed (FT-NIR) spectrometer *VECTOR 22/N* from the company *Bruker Optik GmbH* (Ettlingen, Germany) was used to determine in-line the mixing quality of powders mixed. For an easy and fast refilling of the volumetric feeders, two suction conveyors from the company *VOLKMANN GmbH* (Soest, Germany) are available. The suction conveyors suck the powder out of two reservoir bins from the company *Dietrich Reimelt GmbH & Co. KG* (Rödermark, Germany) standing on the ground floor. The mixed powders coming out of the continuous mixer fall on a conveyor belt, which conveys the powder to a vertical pipe. The pipe ends in a big bag located on the ground floor. The volumetric feeders and the continuous mixer are positioned on weighing cells, which are connected with the weighing controller *PR 1730* from the company *GLOBAL Weighing Technologies GmbH* (Hamburg, Germany). The weighing controller displays the weight values of the connected weighing cells. The programmable logic controller, integrated in the weighing controller, controls the mass flow of the volumetric feeders, the rotational speed of the mixing device and the velocity of the conveyor belt.



*Fig. 4-2: Rear view of the experimental rig*

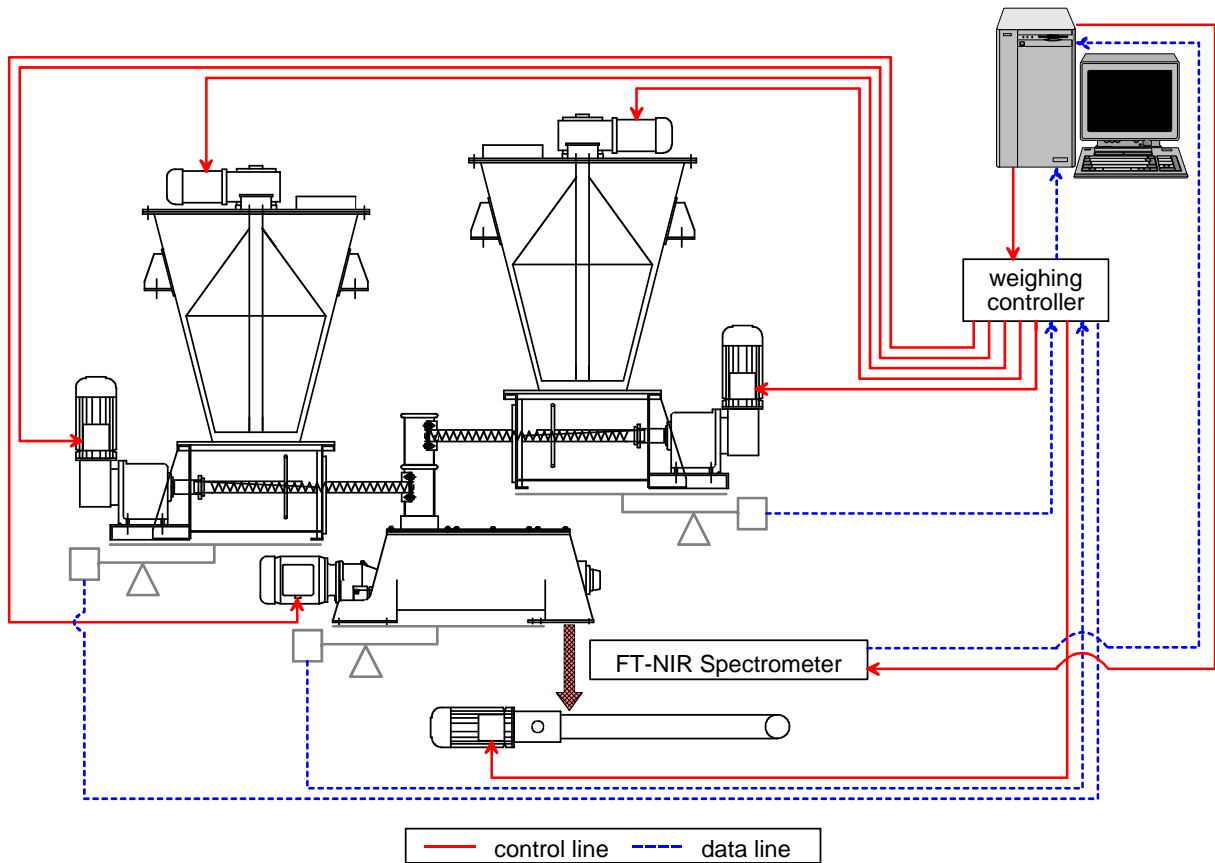


**Fig. 4-3:** Flowchart of the experimental rig

The visualization and control surface shown in *Fig. 4-4* was programmed with the programming tool *LabVIEW* from the company *National Instruments Germany GmbH* (München, Germany). The actual filling weight of the volumetric feeders and the continuous mixer as well as the approximated filling degree of the volumetric feeders and the mass flow coming out of the volumetric feeders are displayed. The proportioning devices and the agitator in the reservoirs of the volumetric feeders, the continuous mixer and the conveyor belt can be started and stopped. The rotational speed of the proportioning devices and the mixing device as well as the velocity of the conveyor belt can be set in percent of the maximum values. A modulation of the mass flow coming out of the volumetric feeders is possible. A sinusoidal or a rectangle fluctuation of the mass flow can be chosen. The offset, the amplitude and the period length of the fluctuation can be changed. The setting of a phase shift between the two mass flow fluctuations is also possible.



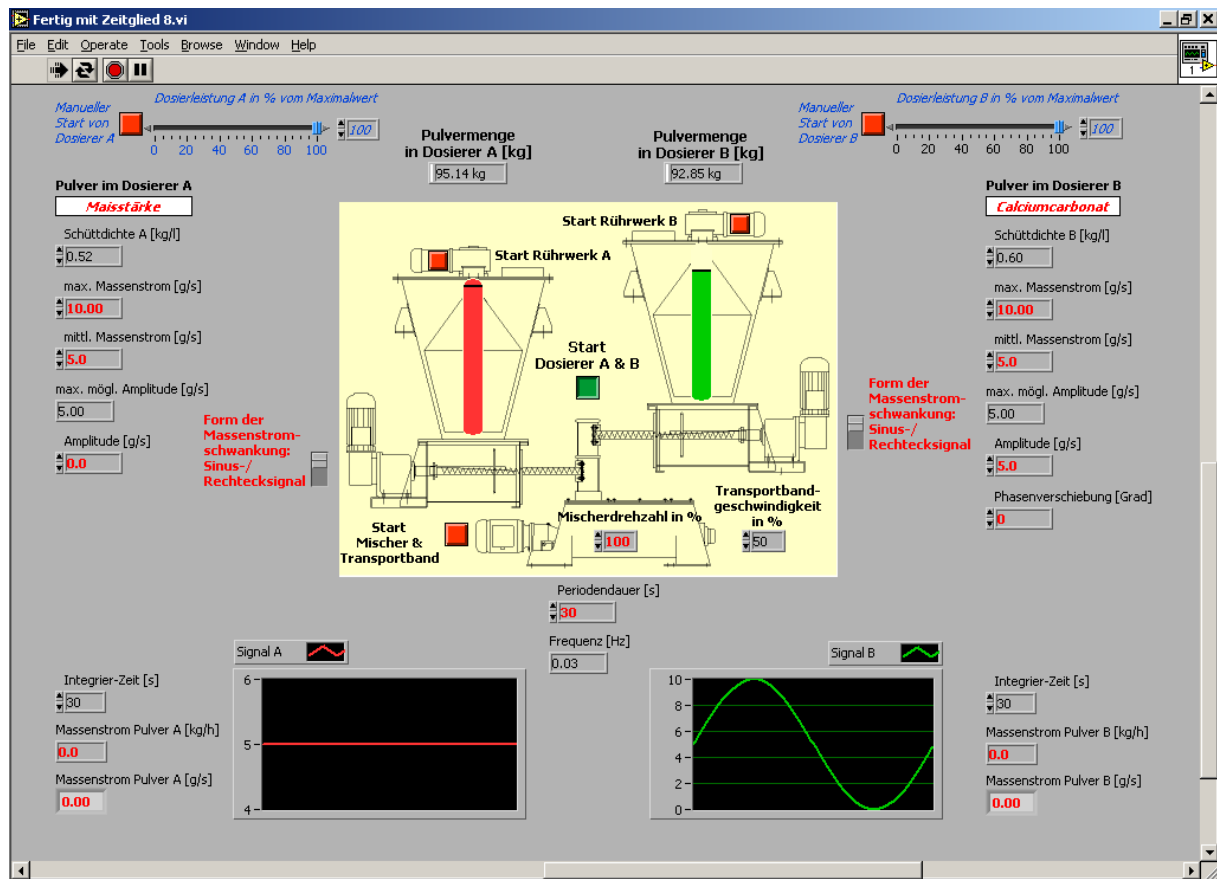


Fig. 4-4: Control and visualization surface for the experimental rig (programmed with LabVIEW)

## 4.2 Powders used for the mixing experiments

As mentioned in the introduction, this research project about the “Continuous dynamic mixing of cohesive powders” was integrated in the research program “Handhabung hochdisperser Pulver”, which was launched by the *Deutsche Forschungsgemeinschaft (DFG)*. Within the scope of the *DFG* research program, researchers from different German universities and from the company *Degussa AG* (Hanau, Germany) examined the generation, the storage and the mixing of high-cohesive powders. The prerequisite for a participation in the program was the examination of powders with a diameter of less than  $10 \mu\text{m}$ . Therefore, the powders used for the validation of the mixing model developed should have a median diameter of about  $10 \mu\text{m}$  or less. Furthermore, the powders must be not harmful, easy to recycle as well as available in big amounts (at least 3 tons) and cheap at the same time.

To simplify the validation of the mixing model, a two-component system was examined. For the in-line determination of the mixing quality using FT-NIR spectroscopy, it is advantageous to use an organic and an inorganic powder because the absorbance spectra differ significantly. NIR radiation is absorbed by C-H-, N-H- and O-H-groups, which are found in organic materials and only in small amounts in inorganic materials.

Calcium carbonate and maize starch fulfill the requirements set and were used for the performed mixing experiments.

### 4.2.1 Calcium carbonate

Calcium carbonate is a mineral, which is widely used in different industries. Examples for the industrial application of calcium carbonate are

- the use as filler for the paper, plastic and painting production,
- the use as cleaning agent,
- the use as coating pigment,
- the use as mineral fertilizer,
- the use as polish or
- the use as solidifying agent for the flue gas desulfurization [82, 83].

For the validation of the mixing model, the calcium carbonate *OMYACARB 2 SV* with a median diameter of  $2\ \mu\text{m}$  was used. For the later described examinations for improving the calibration procedure of the FT-NIR spectrometer, *OMYACARB 10 SV* with a median particle diameter of  $6\ \mu\text{m}$  was also used. The calcium carbonate was made available by the company *Omya GmbH* (Cologne, Germany). The particle size distributions of the two powders are shown in *Fig. 4-5*. They were determined with the *Sympatec* laser diffraction sensor *HELOS* in combination with the dispersion unit *RODOS*. Scanning electron microscope pictures of *OMYACARB 2 SV* are shown in *Fig. 4-6* and *Fig. 4-7*. The calcium carbonate particles are lamella-like and have an irregular shape.

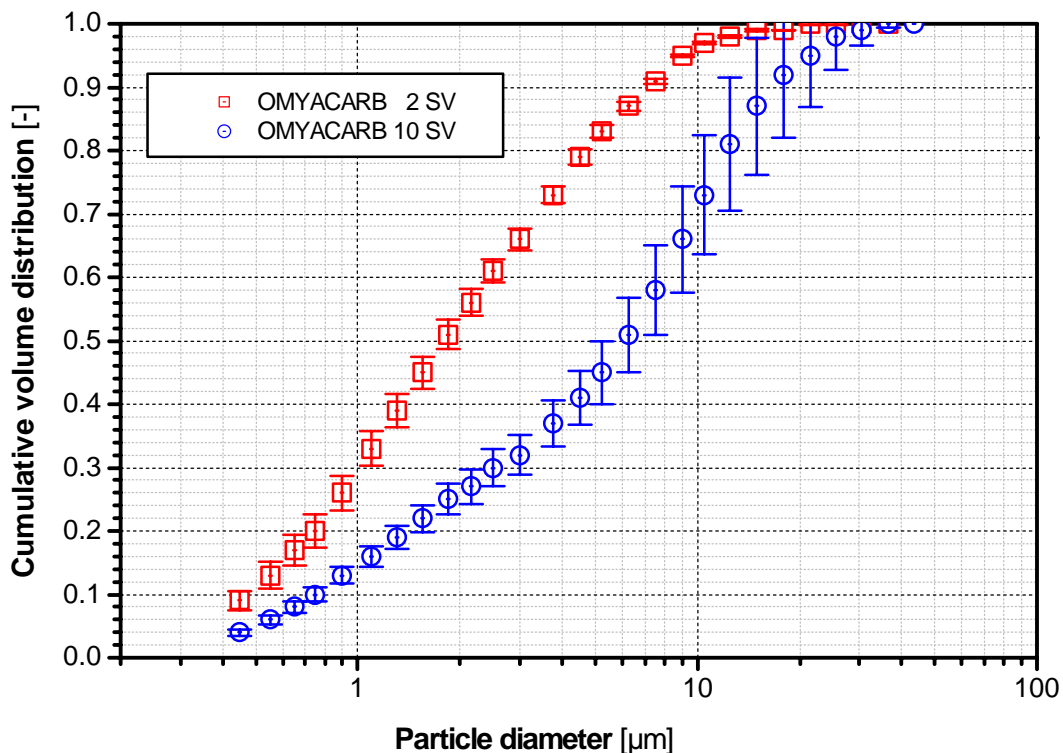


*Fig. 4-5: Particle size distributions of calcium carbonate OMYACARB 2 SV and OMYACARB 10 SV (Sympatec laser diffraction sensor HELOS in combination with the dispersion unit RODOS)*



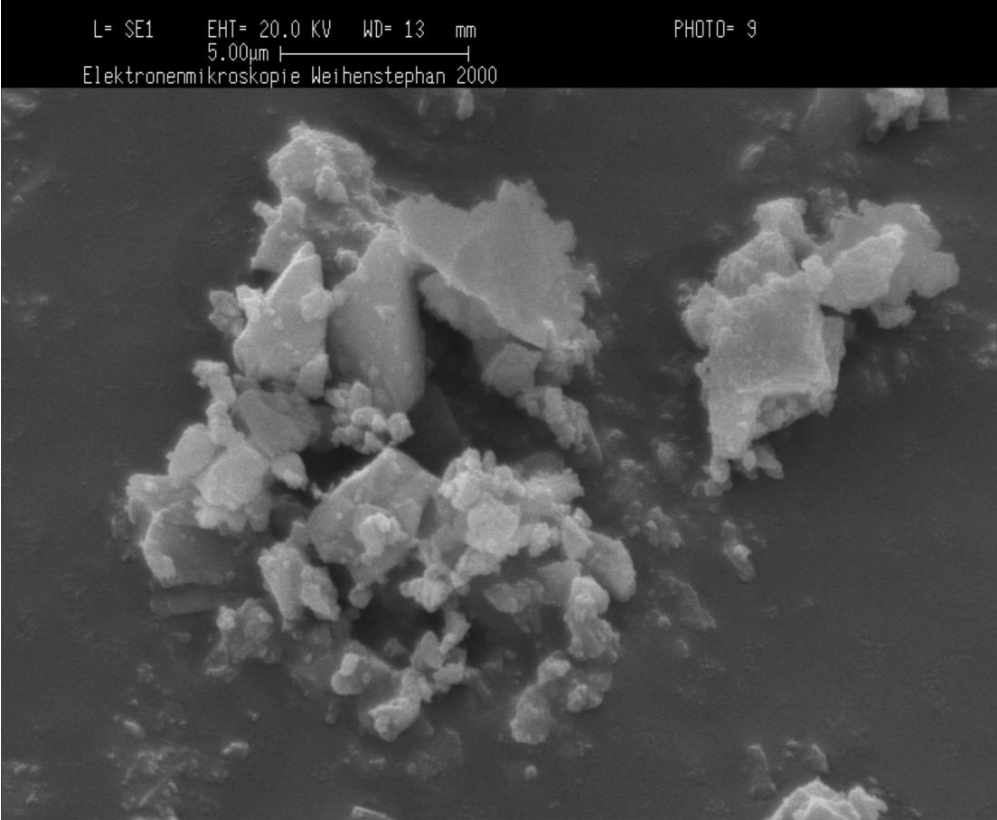


**Fig. 4-6:** Scanning electron microscope photo of calcium carbonate OMYACARB 2 SV

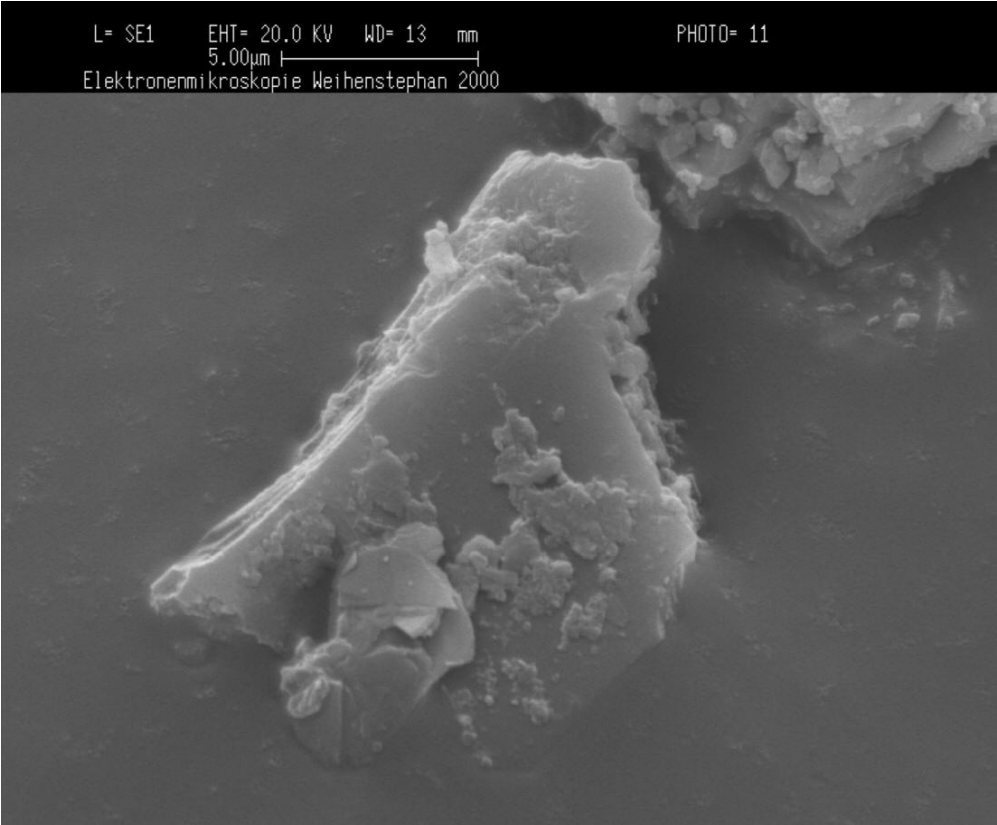


**Fig. 4-7:** Scanning electron microscope photo of calcium carbonate OMYACARB 2 SV

The true density of the powders was determined with the gas pycnometer *AccuPyc 1330* sponsored by the company *Micromeritics GmbH* (Mönchengladbach, Germany). The bulk density was determined by using a device, which was constructed at the *Lehrstuhl für Maschinen- und Apparatekunde* (see *Fig. 4-8*): A slide in the outlet of a funnel allows a defined falling of powdery material into a vessel with a defined volume. The Schulze ring shear tester *RST-01.pc* was used to determine the flowability of the powders. The main bulk characteristics are summarized in *Table 4-1* (see p. 67).



*Fig. 4-8: Device to determine the bulk density*

#### 4.2.2 Maize starch

Besides cellulose, starch belongs to the most important representatives of the polysaccharides. Starches consist of macromolecules, which are built up in an aliphatic way. Since the ancient history of man, starches have played an important role as technical adjuvant. One of the first uses of starches is the preparation of papyrus papers dated to the year 3500 before Christ. Today, starches are widely used in different industries. Examples for the industrial application of maize starch are

- the use as gelling and thickening agent for food products,
- the use as additive for the surface finishing of paper products,
- the use as additive for the production and the care of textiles,
- the use as basic material for a lot of adhesives,
- the use as basic material for cosmetic powders,
- the use as filler of tablets and
- the use as stabilizer for clay slurries, which are used as drilling mud for oil welling [84].

For the validation of the mixing model, the maize starch *Pharm 03406* with a median diameter of  $13 \mu\text{m}$  was used. The maize starch was made available by the company *Cerestar Deutschland GmbH* (Krefeld, Germany). The particle size distribution shows *Fig. 4-9*, the scanning electron microscope photos show *Fig. 4-10* and *Fig. 4-11*. The main bulk characteristics are summarized in *Table 4-1*(see p. 67).

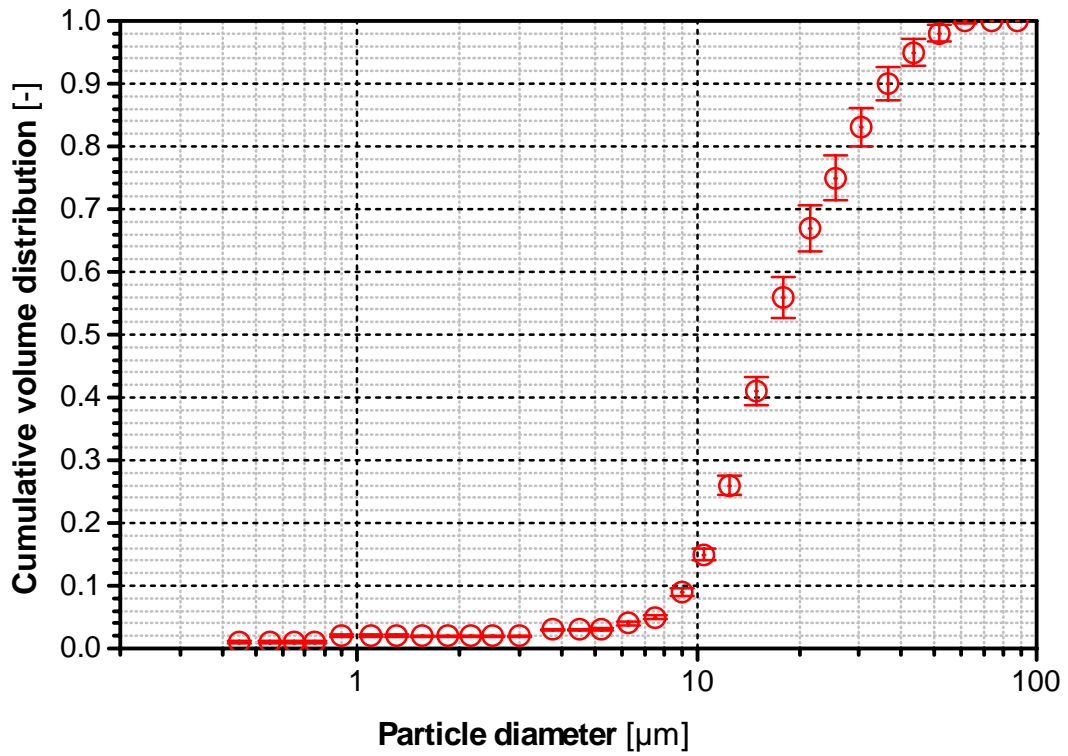


Fig. 4-9: Particle size distribution of maize starch Pharm 03406 (Sympatec laser diffraction sensor HELOS with a the dispersion unit RODOS)

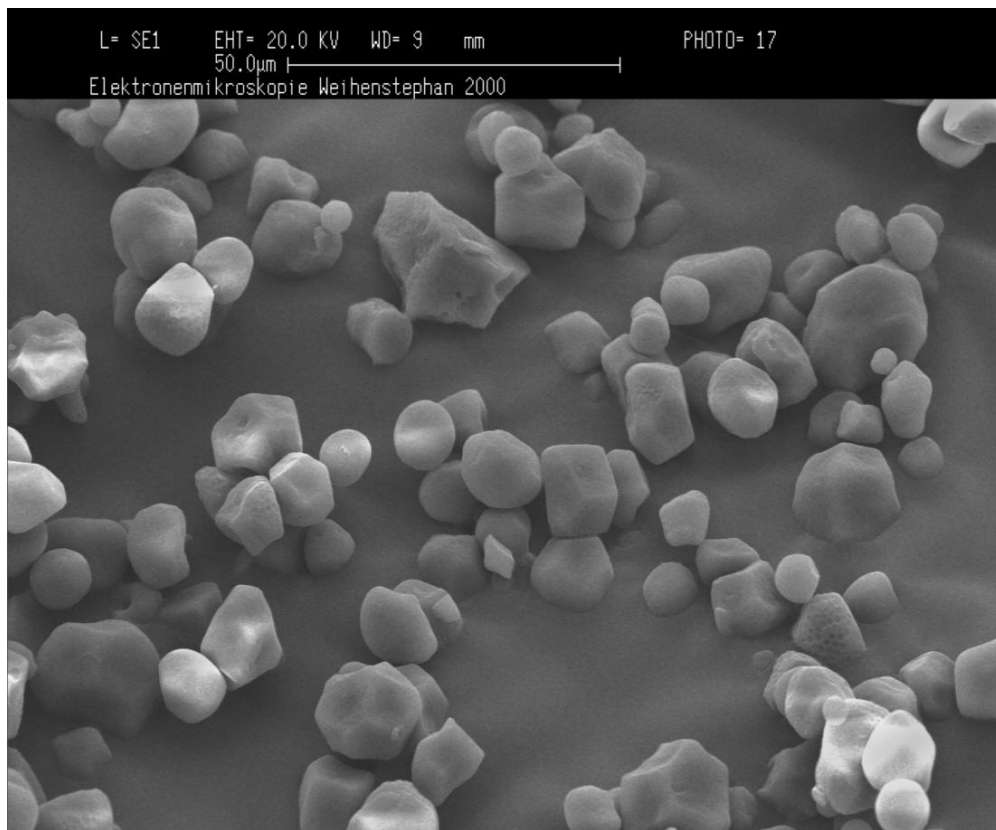
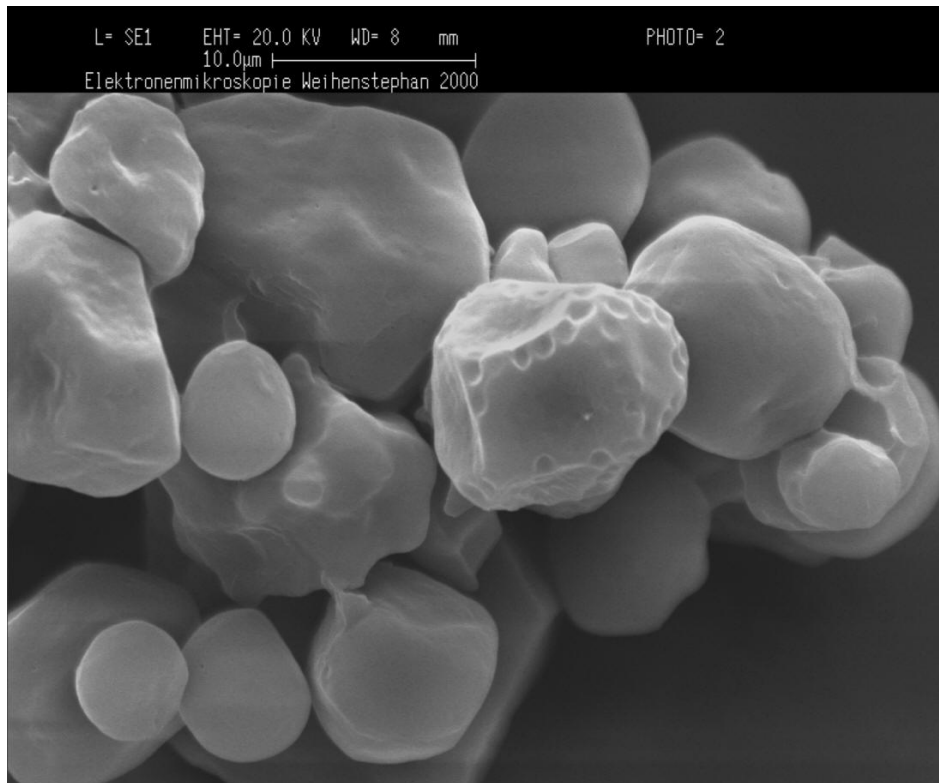


Fig. 4-10: Scanning electron microscope photo of maize starch Pharm 03406



**Fig. 4-11:** Scanning electron microscope photo of maize starch Pharm 03406

#### 4.2.3 Compilation of the main bulk characteristics

The main bulk characteristics (median diameter, true density, bulk density and flowability) of the powders used are summarized in **Table 4-1**.

**Table 4-1:** Compilation of the main bulk characteristics (confidence intervals based on a triple measurement and a probability of 95 %)

powder	median diameter $d_{p,50}$ [ $\mu\text{m}$ ]	true density $\rho_s$ [ $\text{kg}/\text{m}^3$ ]	bulk density $\rho_{\text{bulk}}$ [ $\text{kg}/\text{m}^3$ ]
calcium carbonate OMYACARB 2 SV	$2 \pm 0.21$	$2\,757 \pm 2.6$	$592 \pm 8.7$
calcium carbonate OMYACARB 10 SV	$6 \pm 1.02$	$2\,726 \pm 4.5$	$750 \pm 0.2$
maize starch Pharm 03406	$13 \pm 1.24$	$1\,503 \pm 3.9$	$600 \pm 14.7$

powder	flowability $ff_c$ (pre shear stress 5 000 Pa) [-]	consolidation stress $\sigma_I$ [Pa]
calcium carbonate OMYACARB 2 SV	$2.2 \pm 0.02$	$11\,452 \pm 234.5$
calcium carbonate OMYACARB 10 SV	$2.9 \pm 0.04$	$10\,588 \pm 150.5$
maize starch Pharm 03406	$5.7 \pm 0.43$	$10\,803 \pm 1\,187.2$

### 4.3 Generation of defined mass flow fluctuations

For the experimental validation of the mixing model, it is necessary to determine the reduction of concentration fluctuations by the continuous mixer. An in-line determination of concentration fluctuations, entering the continuous mixer, is not possible. Therefore, defined mass flow fluctuations coming out of the volumetric feeders used have to be generated. Defined mass flow fluctuations allow the calculation of the resulting concentration fluctuations.

To simplify the validation of the mixing model, the mass flow of one component fluctuated periodically and the mass flow of the other component was constant. Within the scope of a follow-up research project, it is planned that two mass flows fluctuating periodically without and with phase shifts will be examined.

The primary objective was the generation of sinusoidal mass flow fluctuations with a defined period length  $T$ , amplitude  $A$  and offset  $O$ . The optional generation of a square wave fluctuation with a defined period length, amplitude and offset should also be possible (compare *Fig. 4-12*).

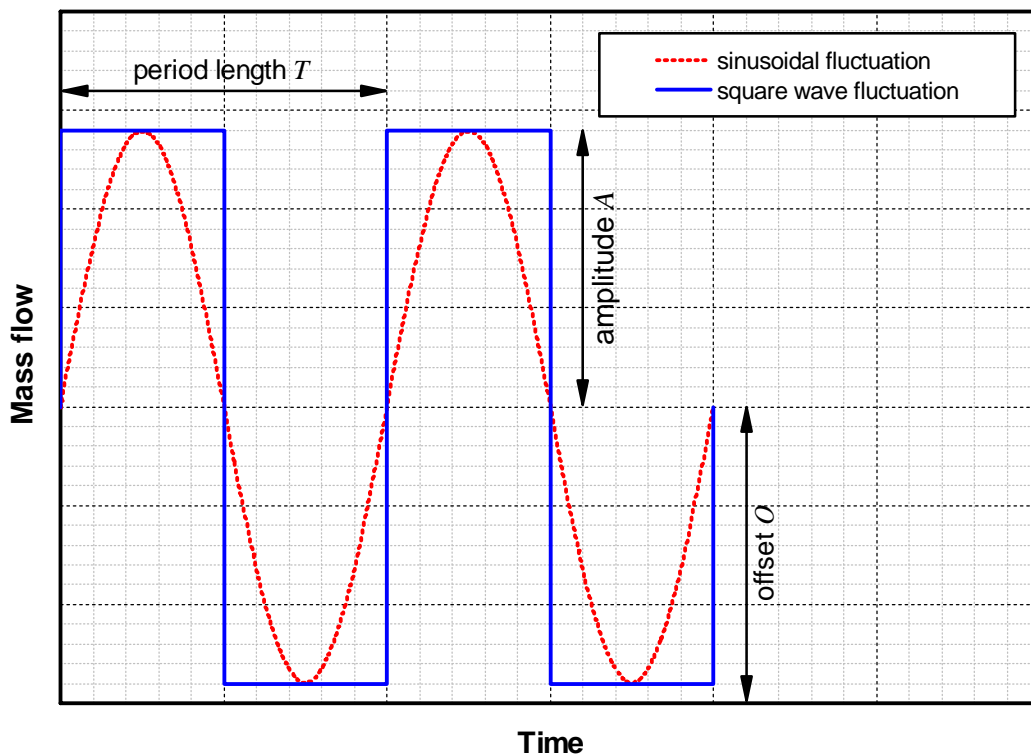


*Fig. 4-12: Illustration of sinusoidal and square wave fluctuations*

A general square wave mass flow fluctuation  $s(t)$  with the period length  $T$ , the amplitude  $A$  and the offset  $O$  can be described mathematically by *Eq. 4-1* and *Eq. 4-2*.

$$s(t) = O \quad \text{for } t = 0 \quad \text{Eq. 4-1}$$

$$s(t) = A \cdot \frac{\sin\left(\frac{2 \cdot \pi}{T} \cdot t\right)}{\left|\sin\left(\frac{2 \cdot \pi}{T} \cdot t\right)\right|} + O \quad \text{for } t > 0 \quad \text{Eq. 4-2}$$

The square wave fluctuation  $s(t)$  can also be described by a Fourier series. The Fourier series corresponds to a superposition of sine waves with different period lengths and amplitudes [81]:

$$s(t) = \frac{4 \cdot A}{\pi} \cdot \left( \sin\left(\frac{2 \cdot \pi}{T} \cdot t\right) + \frac{1}{3} \cdot \sin\left(\frac{2 \cdot \pi}{3 \cdot T} \cdot t\right) + \frac{1}{5} \cdot \sin\left(\frac{2 \cdot \pi}{5 \cdot T} \cdot t\right) + \frac{1}{7} \cdot \sin\left(\frac{2 \cdot \pi}{7 \cdot T} \cdot t\right) + \dots \right) + O \quad \text{Eq. 4-3}$$

$$s(t) = \left( \frac{4 \cdot A}{\pi} \cdot \sum_{i=1}^{\infty} \frac{1}{2 \cdot i - 1} \cdot \sin\left(\frac{2 \cdot \pi}{(2 \cdot i - 1) \cdot T} \cdot t\right) \right) + O \quad \text{Eq. 4-4}$$

For  $i = 0, 1, 2, 3$  and  $4$ , the Fourier series according to *Eq. 4-4* are shown in *Fig. 4-13*.

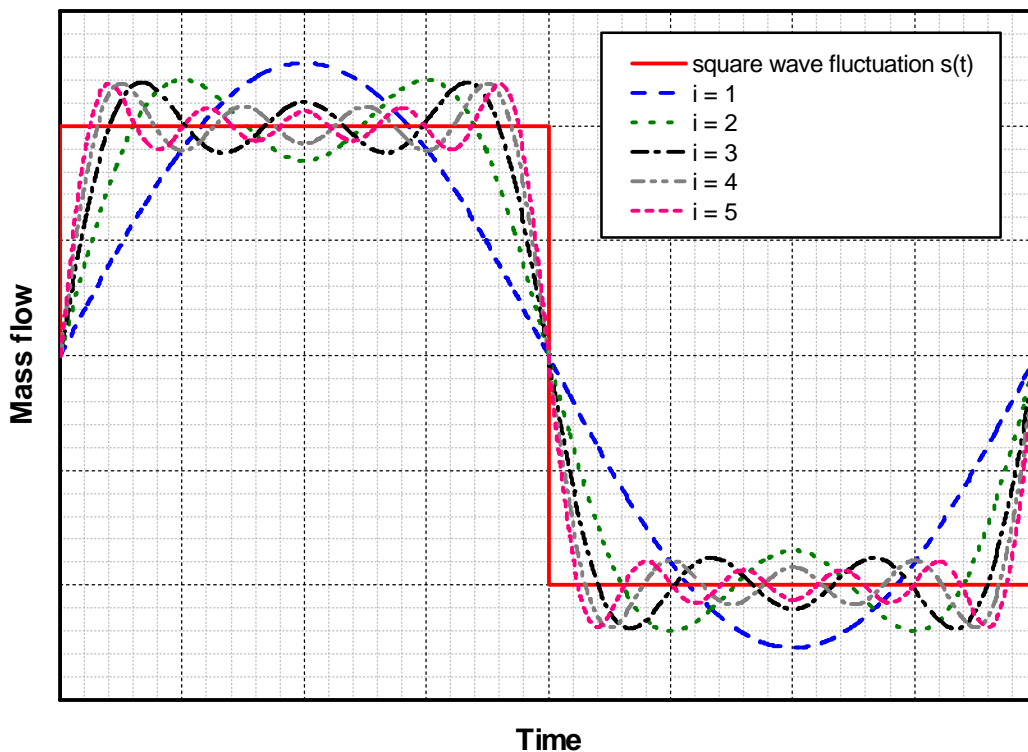


*Fig. 4-13: Fourier synthesis of a square wave fluctuation by the superposition of sine waves*

Any periodical fluctuation can be described by a Fourier series. For the case that the reduction of any square wave fluctuation determined experimentally can be described by the superposition of the reduction of sine waves determined experimentally, the reduction of any periodical fluctuation can be calculated.



Pilot tests with the volumetric feeder *GAC 132* from the company *Gericke GmbH* have shown that the generated mass flow, coming out of the standard dosing tube of the volumetric feeder, consists of the generated sinusoidal fluctuations and overlaid random fluctuations (see *Fig. 4-14*). The random fluctuations are in the same magnitude as the amplitude of the sinusoidal fluctuation.

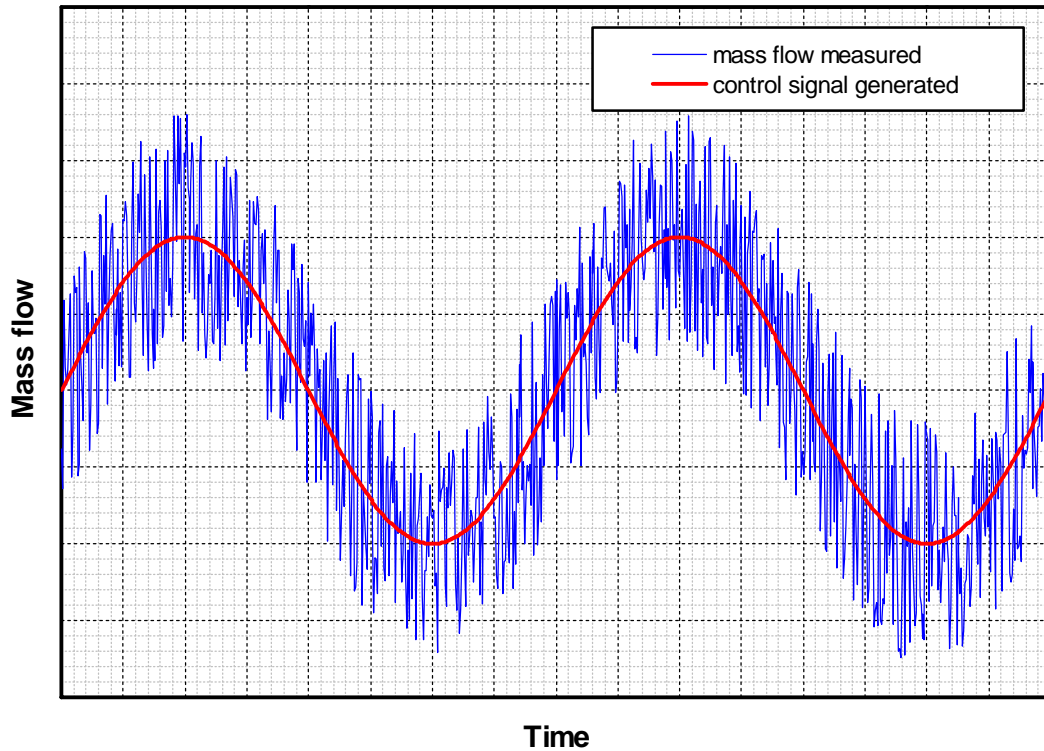


*Fig. 4-14: Illustration of a mass flow coming out of volumetric feeders and the corresponding generated control signal*

Much research work had to be performed to improve the short-term dosing constancy of the volumetric feeders used and to reduce the amount of unwanted random fluctuations respectively. Research results were already published in [29, 30, 64, 85, 86]. The improvement of the short-term dosing was not only important for the validation of the model developed but it is also very interesting for industrial continuous mixing processes. The higher the fluctuations entering a continuous dynamic mixer are, the higher the mixing performance in axial direction has to be.

#### 4.3.1 Possibilities to improve the short-term dosing constancy of volumetric feeders

Especially for cohesive powders, deviations of the mass flow from a given set point can occur. The reasons for the deviations depend on the considered space of time. Talking about deviations it has to be distinguished between:

- *long-term mass flow fluctuations*, which appear in an observation period of minutes, hours or days, and
- *short-term mass flow fluctuations*, which appear in an observation time of seconds.

Both deviations are shown in *Fig. 4-15*. On the left-hand side, the long-term mass flow fluctuations are shown. They can be caused by e.g.:

- the construction of the proportioning device, if the spiral or the screw rotates with a low number of revolutions, or
- a disturbed outflow, as a result of collapsing powder bridges or funnels [87, 88].

In both cases, fluctuations around the set point occur. A drift of the average mass flow  $\overline{\Delta \dot{m}}$  can occur, too [89]. A reduction of the filling degree or changes of the bulk density can be the reason. Changes of the bulk density can be caused by [87, 90, 91, 92, 93]:

- compaction as a result of storage or refilling,
- changing filling heights,
- using different batches with varying particle size distributions,
- changing environmental conditions (e.g. different temperature, humidity) or
- changes in the upstream production process (e.g. different settings of upstream machines).

For the case that a gravimetric feeder can be used, the mass flow is measured permanently and a detected deviation of the mass flow from a set point is adjusted by changing the rotational speed of the proportioning device [94, 95, 96].

In *Fig. 4-15*, a small area is encircled and enlarged on the right-hand side. In the enlargement, the short-term fluctuations are shown. They can be caused by e.g. a fast-rotating proportioning device and cohesion forces between the particles. The occurrence of a significant pulsation is known for talc, chopped strands, egg powder and flour [97].

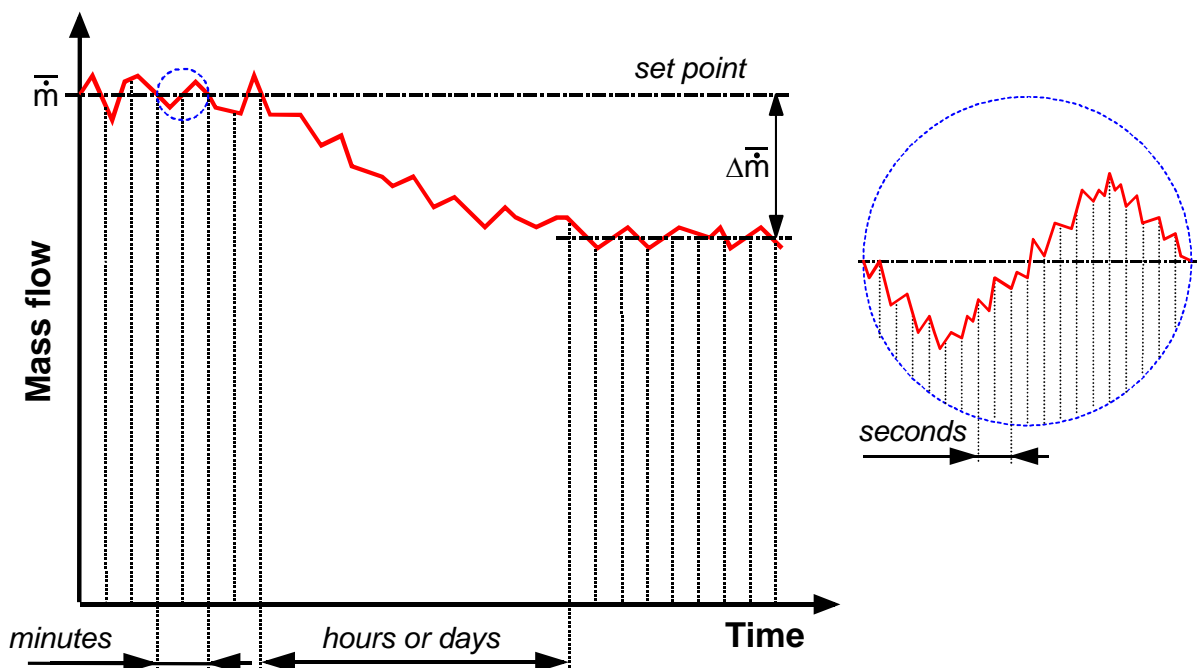


*Fig. 4-15: Illustration of long-term (left) and short-term mass flow fluctuations (right)*



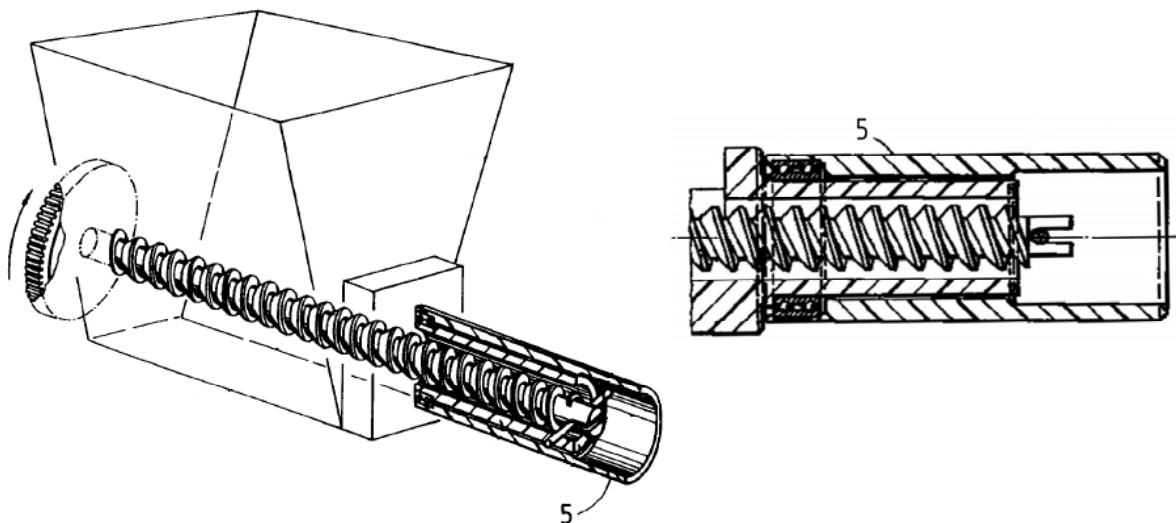
Different research groups have done a lot of experimental and theoretical work to improve the long-term dosing constancy of volumetric feeders. A compilation was published by VETTER [94]. Publications about possibilities to improve the short-term dosing constancy can hardly be found. A high short-term dosing constancy can improve the quality of the produced product for the case that:

- stoichiometric reactions run [89, 98, 99],
- absorber is fed into nappies,
- additives are fed into an extruder,
- powders are mixed in a static mixer [22] or a vertical dynamic mixer [27] or
- coal is fed into coal fired boilers, flash furnace smelters [100] or rotary cement kilns [101, 102].

Following, an overview about possibilities to improve the short-term dosing constancy of volumetric feeders is given. The focus is on feeders with a single spiral or screw but most of the presented devices can also be used for feeders with two proportioning devices.

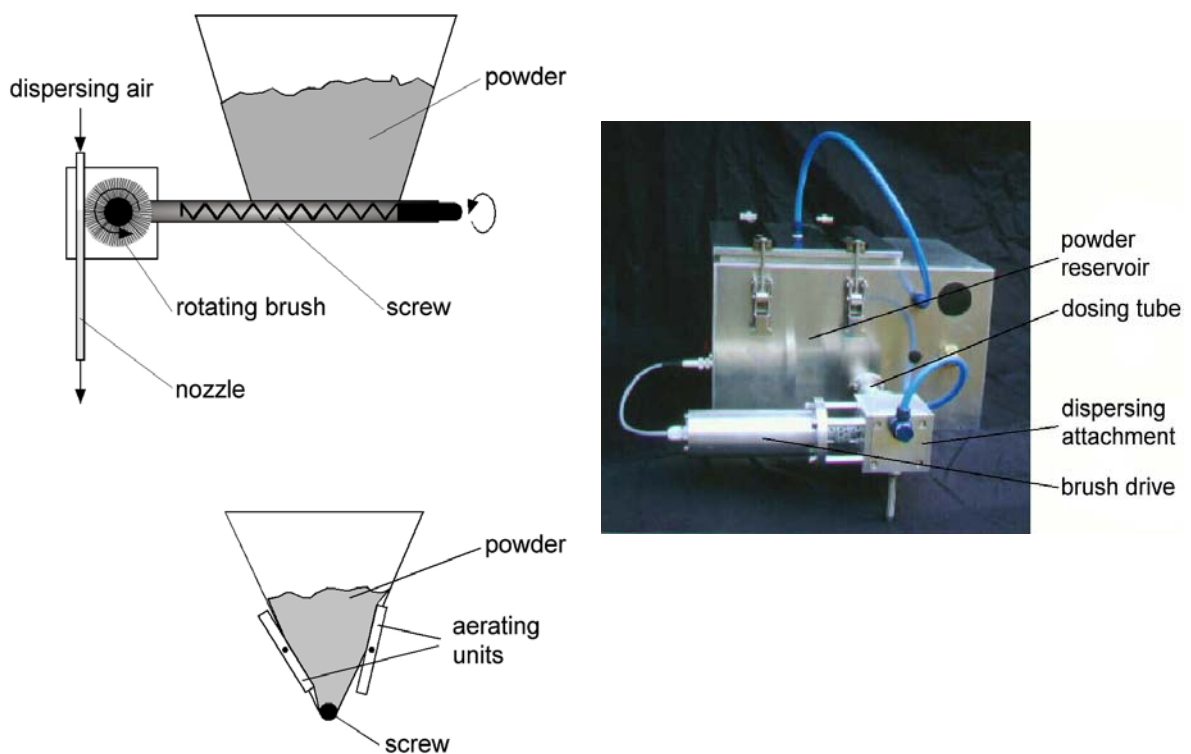
#### 4.3.1.1 State of the art

In 1992, *K-Tron Technologies* patented a rotating dosing tube end [103, 104], which is shown in *Fig. 4-16* (component 5). On the one hand the extension of the dosing tube should smooth the mass flow fluctuations and on the other hand the rotation of the tube end should support the transport of the powder and improve the drop off of the powder at the tube end. This feeder type is no longer sold.



*Fig. 4-16: Rotating dosing tube (component 5) of the company K-Tron Technologies [103, 104]*

In 1999, DITTLER and KASPER [105] reported about a volumetric feeder with a rotating brush in front of the dosing tube outlet (see *Fig. 4-17*). Compressed air was used to remove the powder from the brush. The feeder was developed for testing air filters. The dosing constancy of the feeder and the dispersion of the calcium carbonate powder used were assessed by means of in-line photometric concentration measurements and scanning electron microscope pictures of particles separated on filter media. For mass flows less than  $1 \text{ kg/h}$ , a constant dosing and a good dispersion is possible.

**Dispersing unit****Dosing unit**

**Fig. 4-17:** Volumetric feeder with a rotating brush in front of the outlet of the dosing tube [105]: Schematic drawing (left) and photo (right)<sup>1</sup>

<sup>1</sup> Reprinted with permission from Wiley-VCH Verlag GmbH & Co KG

In 2001, *K-Tron International* obtained a patent for modulating the rotational speed of the feeder's proportioning device. The functioning principle of the modulation is illustrated in *Fig. 4-18*. The left diagram shows the normal operation condition. The control variable is constant and periodic pulsations of the out flowing mass flow can be measured. The patented modulation algorithm is able to detect periodic fluctuations and to adjust the revolution speed of the proportioning device. For granulates, the dosing constancy could be increased up to a factor of two. [106, 107]

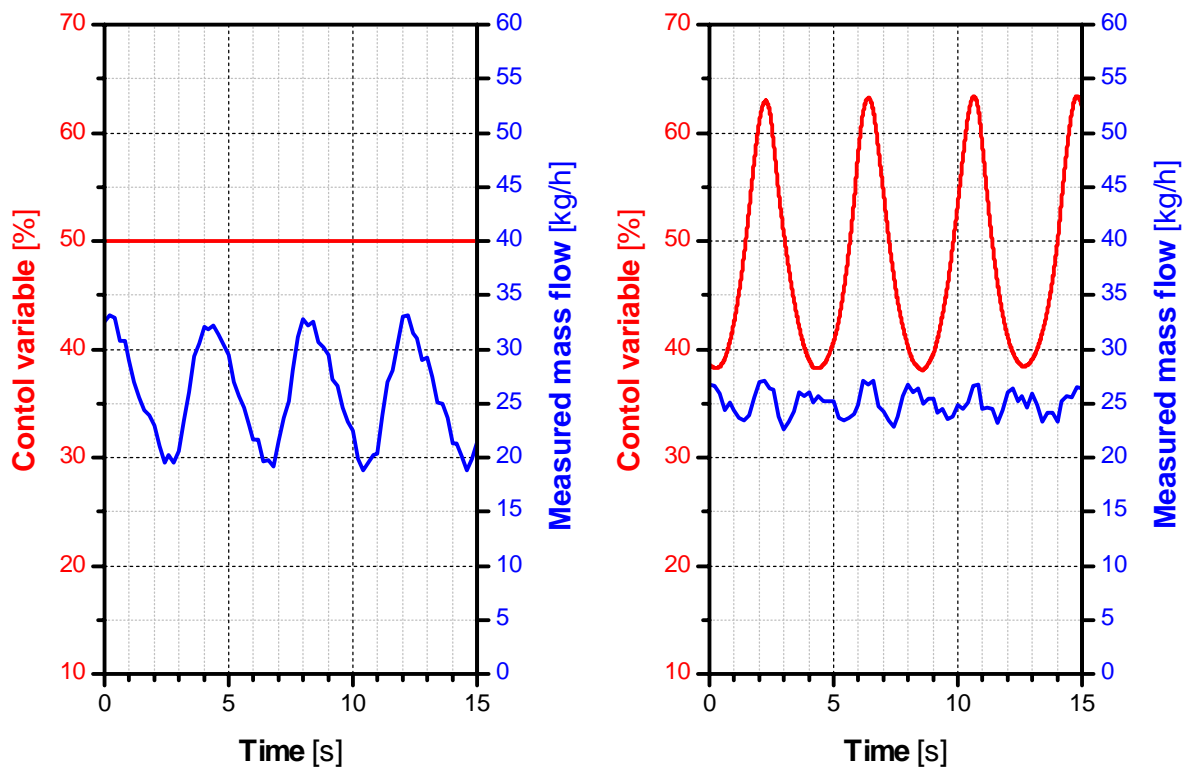


*Fig. 4-18: Screw modulation developed and patented by K-Tron International [107]*

The first scientific publication about examinations to improve the short-term dosing constancy is from WICHE and ROBERTS [100]. In 1998, they discussed the influence of

- different dosing tube outlet geometries (see *Fig. 4-19*),
- different scraper assemblies located one pitch beyond the end of the screw and
- an extension of the dosing tube one pitch beyond the screw end

on the dosing constancy. Graded silica sand and pulverized fuel coal were used for the experiments. The cohesion was changed from free-flowing to cohesive by moistening the silica sand with water.

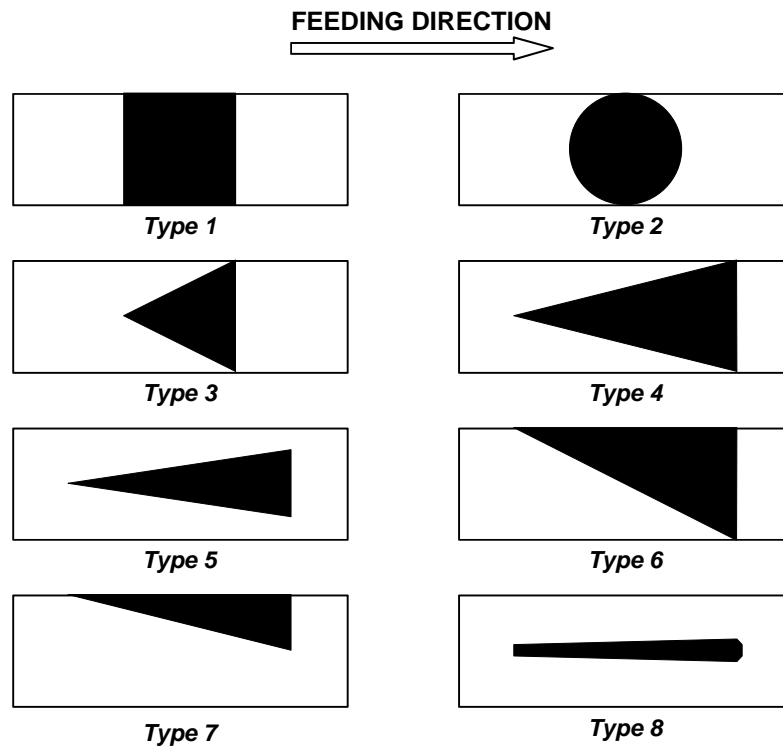


*Fig. 4-19: Different geometries of the dosing tube outlet examined by WICHE and ROBERTS (the powder falls through the black areas) [100]*

The fed particles were collected in a vessel standing on a weighing platform. The weighing platform was connected with a time base chart recorder, which plotted the mass increase with time. The experiments were evaluated qualitatively by comparing the smoothness of the plotted lines. Only a short period was considered and the drawn conclusions are based on single measurements. For dry sand, the outlet types 6, 7 and 8 were able to reduce the pulsations. For damp sand, no significant difference between the different outlet geometries (type 1 - 6) was observed. For dry sand, the pulsations were reduced if the screw ends one flight length before the outlet. For dry and damp sand as well as for pulverized fuel coal, a pulsation reduction was observed if a scraper blade assembly with angled blades is mounted before the outlet.

The use of multistart or double proportioning devices as well as the use of higher rotational speeds with smaller proportioning devices are other possibilities to reduce the pulsations of volumetric feeders [95, 108]. However, feeders with two proportioning devices are more expensive and the shaft sealing is more complicated.

#### 4.3.1.2 Own developments and examinations

In order to improve the short-term dosing constancy of the *Gericke* feeders *GAC 132* used (see *Fig. 4-20*), the effectiveness of different dosing tube ends and attachments for the standard dosing tube was investigated.

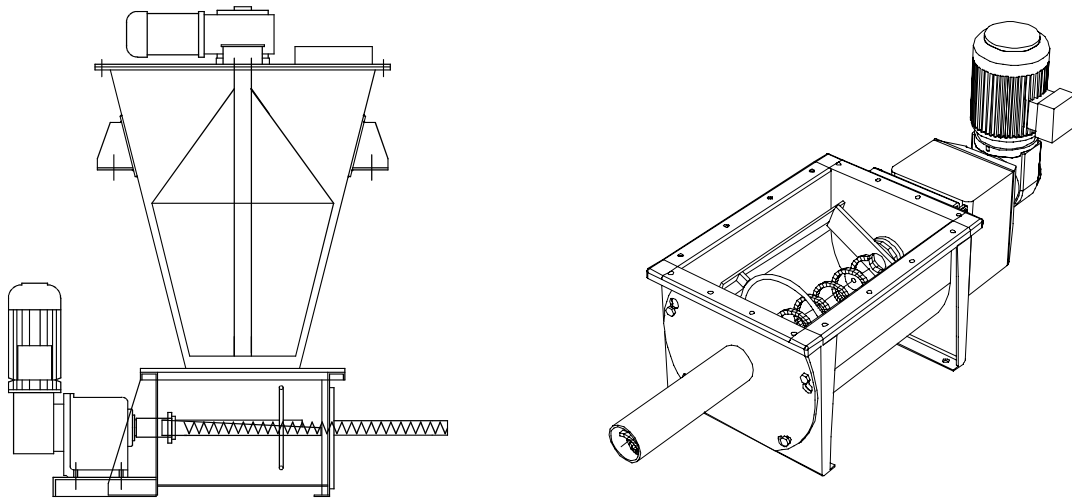


**Fig. 4-20:** Volumetric feeder GAC 132 [Courtesy of Gericke GmbH]

In **Fig. 4-21**, a selection of dosing tube ends and attachments for the standard dosing tube, which were tested within the scope of this thesis, is shown. The standard dosing tube has an inner diameter of  $35\text{ mm}$ . Underneath the standard dosing tube end, a dosing tube with a V-shaped dent and a dosing tube with an inner triangle are shown. The different dosing tube ends can easily be changed by using a bushing (see **Fig. 4-22**). On the right hand side of **Fig. 4-21**, a grid attachment and a commercially available star attachment from the company *Gericke GmbH* (Rielasingen, Germany) are shown.

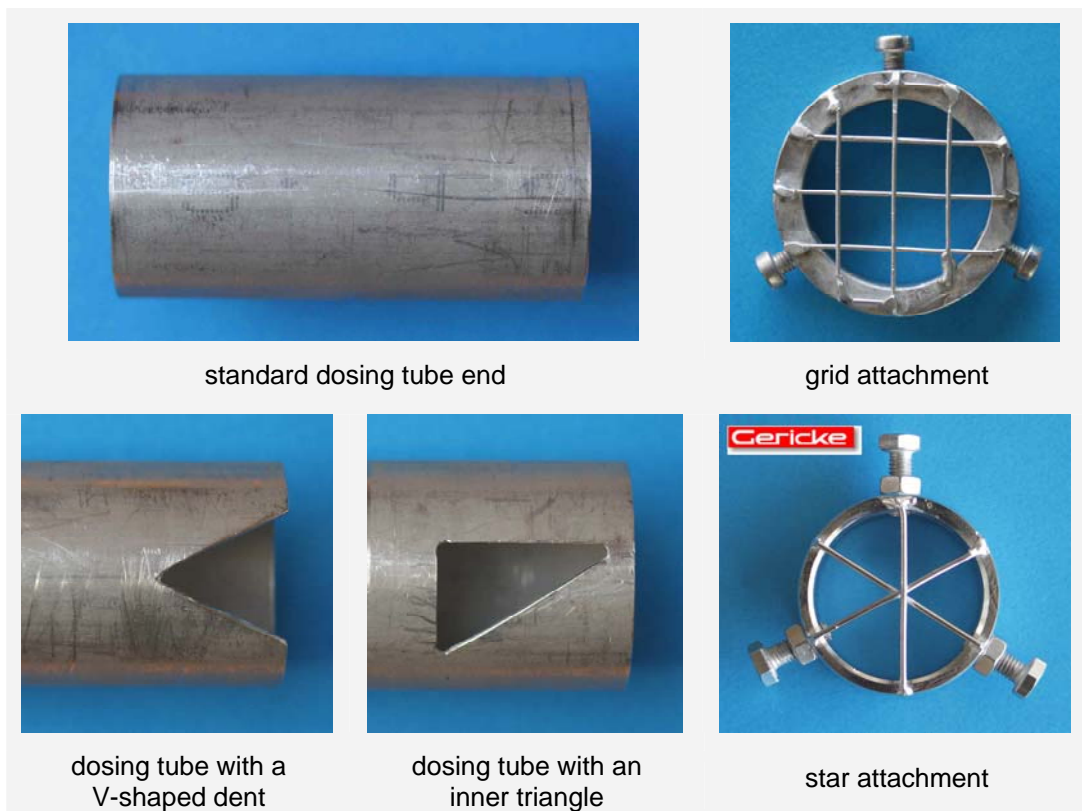


**Fig. 4-21:** Selection of tested dosing tube ends and attachments for the standard dosing tube with an inner diameter of  $35\text{ mm}$

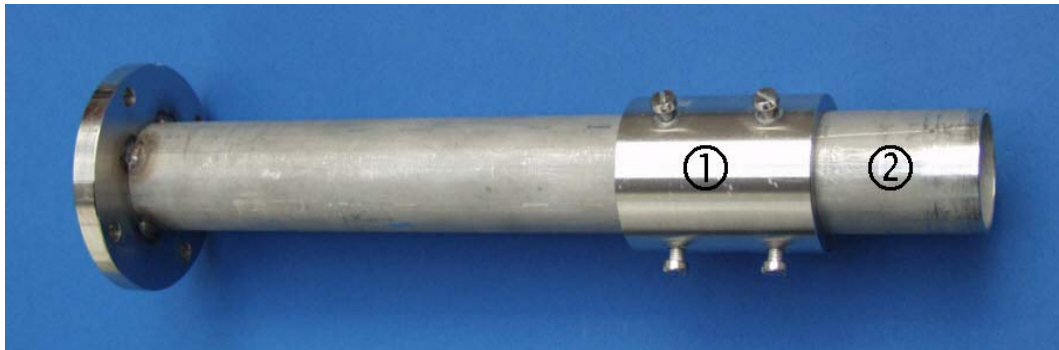


**Fig. 4-22:** Dosing tube with a bushing ① integrated for an easy changing of different dosing tube ends ②

A self-constructed rotating star attachment (see *Fig. 4-23*) was also tested. The attachment consists of a star, which is equipped with antifriction bearings and actuated by an electromotor with a reduction gear unit (4.5 : 1). To control the rotational speed, a voltage generator is attached to the electromotor.

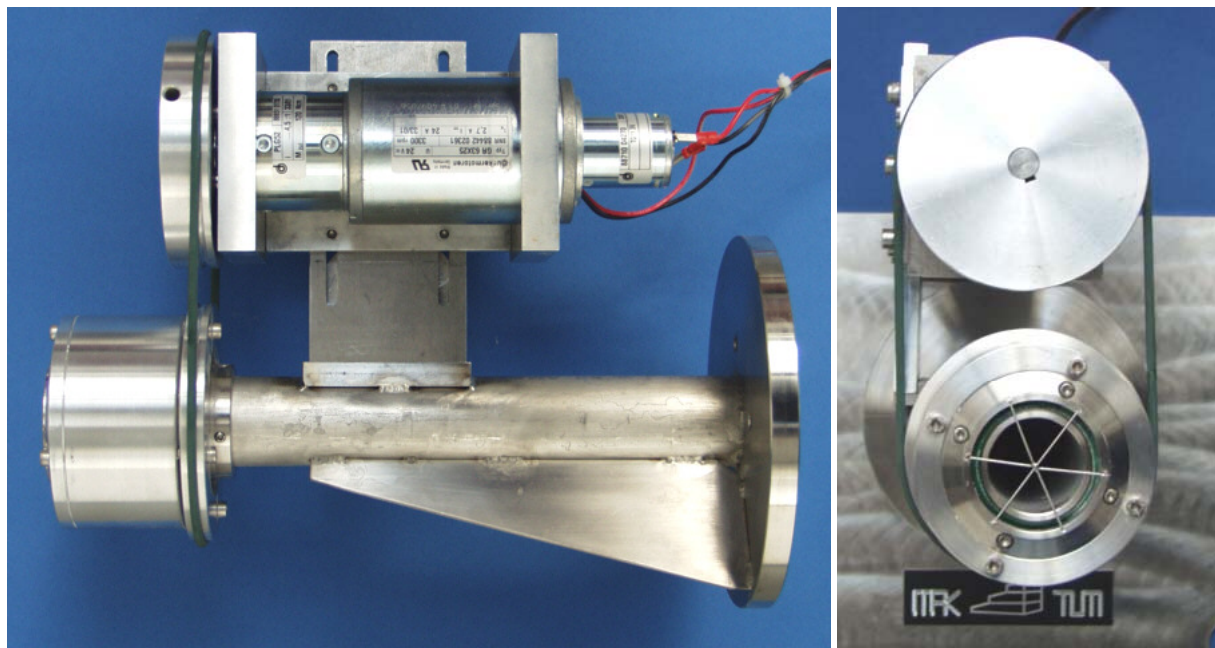


**Fig. 4-23:** Self-constructed rotating star attachment: Side view (left) and front view (right)

The trial equipment shown in *Fig. 4-24* and *Fig. 4-25* was built up for the quantitative comparison of the dosing tube ends and the dosing tube attachments. The experimental rig mainly consists of the volumetric feeder GAC 132 and the balance FB 34 EDE-P from the company Sartorius AG (Göttingen, Germany). The dosing tube and the balance are shielded with plastic plates to avoid an influence of airflow on the measuring result. The balance was connected to the serial interface RS 232 of a personal computer.





*Fig. 4-24: Trial equipment used for the dosing experiments: Volumetric feeder ①, balance ② and plastic housing ③*

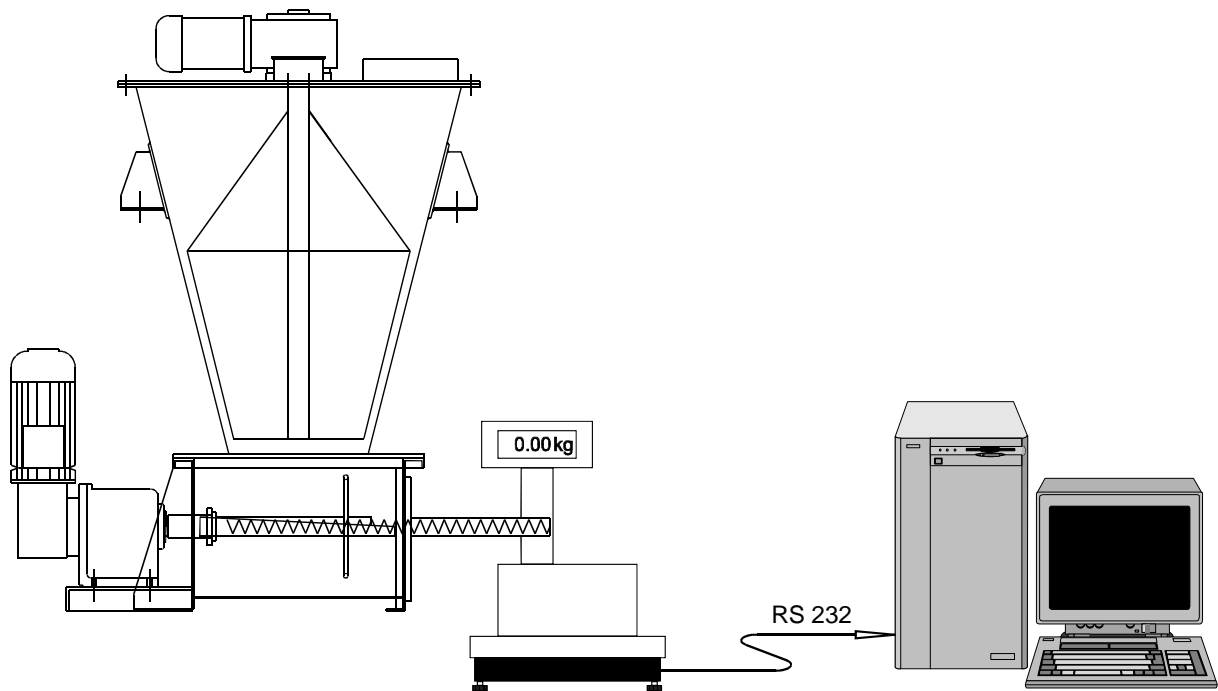


*Fig. 4-25: Illustration of the trial equipment used for the dosing experiments*

For the dosing experiments, cohesive calcium carbonate powder (*OMYACARB 2 SV*) with a median diameter of  $2 \mu\text{m}$  and maize starch powder (*Pharm 03406*) with a median diameter of  $13 \mu\text{m}$  were used. The powder was dosed in a vessel positioned on the balance. The actual mass of the dosed powder was measured every  $0.1 \text{ s}$  and 2 200 times. Every trial was repeated four times. The fed powder was put back in the volumetric feeder after every dosing trial. The mass flow and the standard deviation of the mass flow were calculated.

#### 4.3.1.2.1 Dosing examinations using calcium carbonate

The experimental results of the dosing experiments obtained by using calcium carbonate and a set average mass flow of  $14 \text{ g/s}$  are shown in *Fig. 4-26*. On the ordinate, the average standard deviation of the measured mass flow is plotted. The average standard deviation  $\bar{s}$  of the measured mass flow fluctuations was calculated out of five single standard deviations  $s_i$  ( $n = 5$ ). Each standard deviation  $s_i$  is based on 2 200 mass flow values. Because of the high amount of measuring values, it can be assumed that the values are normally distributed. Therefore, the average standard deviation  $\bar{s}$  can be calculated with *Eq. 4-5*.

$$\bar{s} = \frac{1}{n} \sum_{i=1}^n s_i \quad \text{Eq. 4-5}$$

For a probability of  $P = 95 \%$ , the confidence interval of every calculated average standard deviation is shown in *Fig. 4-26*, too. The confidence interval  $\pm \Delta s$  of each calculated average standard deviation  $\bar{s}$  was calculated with *Eq. 4-6*. The standard deviation of the single standard deviations  $s_i$  was multiplied with the student factor  $t$ , which has a value of 2.776 for  $n = 5$  and  $P = 95 \%$  [109].

$$\pm \Delta s = \frac{\sqrt{\frac{1}{n-1} \cdot \sum_{i=1}^n (s_i - \bar{s})^2} \cdot t}{\sqrt{n}} \quad \text{Eq. 4-6}$$

The meaning of the confidence interval is that for a given probability  $P$  the true value of the calculated average standard deviation lies within in the interval  $\bar{s} \pm \Delta s$ .



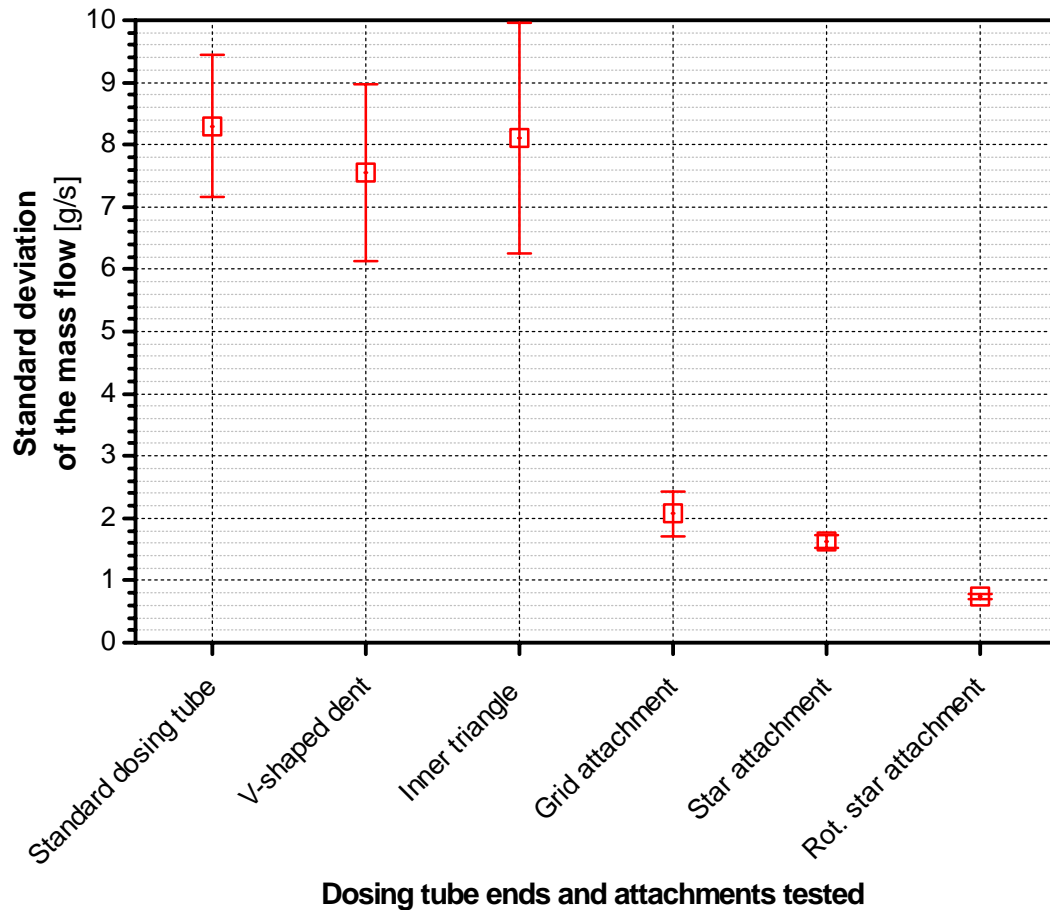


**Fig. 4-26:** Comparison of different tube ends and different attachments for the standard dosing tube with an inner diameter of 35 mm (calcium carbonate,  $\bar{m} = 14$  g/s, proportioning device: spiral)

The use of a tube with a V-shaped dent or an inner triangle caused no significant improvement of the dosing constancy. The slightly higher standard deviation of the grid attachment in comparison to the star attachment was caused by a higher compaction of the powder (see *Fig. 4-27*). By using the self-developed rotating star attachment, the highest reduction of the mass flow fluctuations was possible. The fluctuations were reduced to a tenth of the fluctuations determined for a standard dosing tube.



**Fig. 4-27:** Powder coming out of the grid attachment (left) and the star attachment (right)

To prove that the results shown in *Fig. 4-26* are independent of the operation time, the average standard deviation was determined after different operation times. The experimental results for a standard dosing tube, a star attachment and a rotating star attachment are shown in *Fig. 4-28*. Each shown measuring result is based on 3 runs. A mass of about 5 kg was dosed during each run and the actual mass of the dosed powder was measured every 0.1 s for 3 000 times. After each run, the volumetric feeder was stopped and the dosed powder was put back into the bin of the feeder. The set rotational speed of the spiral used was constant for all trials. The resulting average mass flow was about 15 g/s.

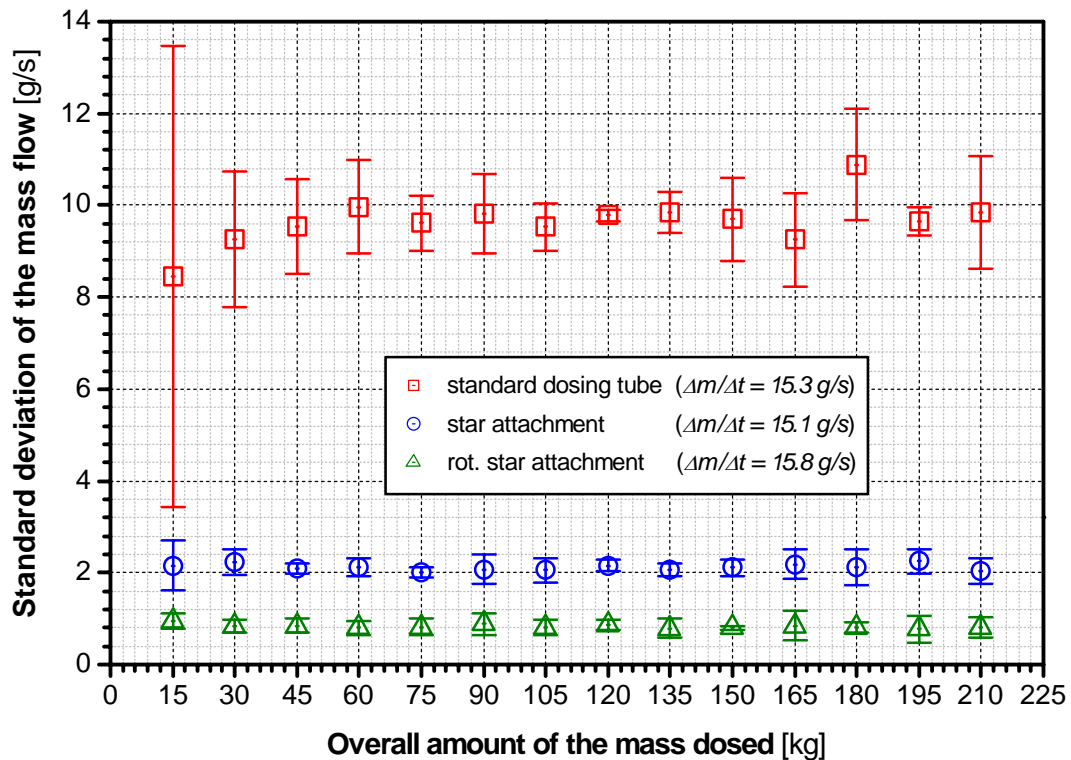


*Fig. 4-28: Influence of the overall amount of the mass dosed after a certain time on the standard deviation of the measured mass flow (constant rotational speed of the spiral used)*

**Fig. 4-29** reveals the reason for the large confidence interval for 15 kg of the mass dosed and using a standard dosing tube (compare **Fig. 4-28**): The experiments with the standard dosing tube were the first of the day. The fluctuations of the mass flow increased during the 1<sup>st</sup> run. The running-in time was too short. The measured negative mass flows result from an oscillation of the balance plate during the measurements.

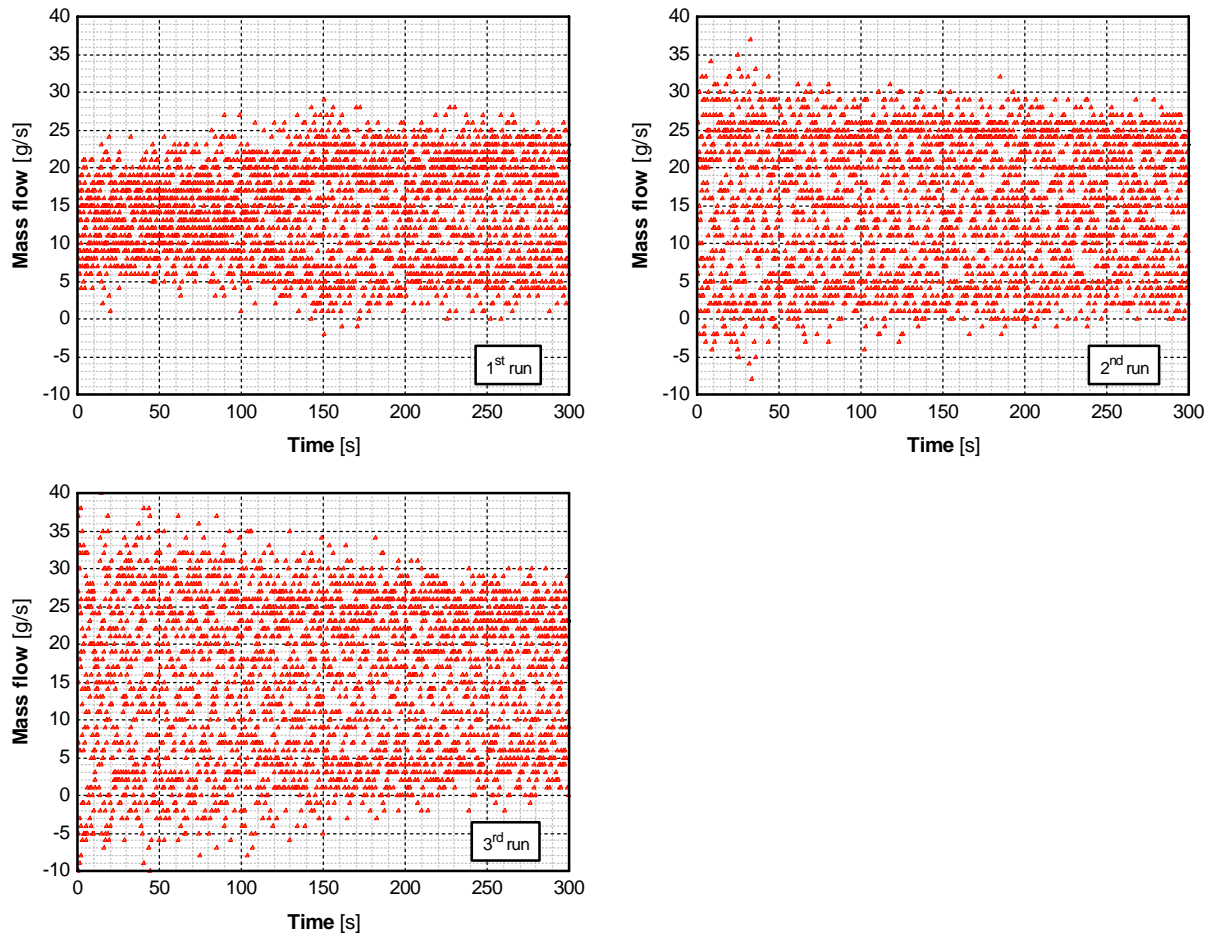


**Fig. 4-29:** Variation of the measured mass flow with time (basis for the calculation of the standard deviation after dosing 15 kg of powder and using a standard dosing tube; compare **Fig. 4-28**)

**Fig. 4-30** shows one reason for the higher short-term dosing constancy of the dosing tube equipped with an attachment. Without using an attachment, only a little amount of powder is fed when the end of the proportioning device (spiral or screw) is in the upper part of the dosing tube (left photo). The maximum amount is fed when the end of the proportioning device is at the bottom. The use of the attachments causes an accumulation of powder at the tube end. Thus, almost the same amount of powder is fed during the rotation of the proportioning device.

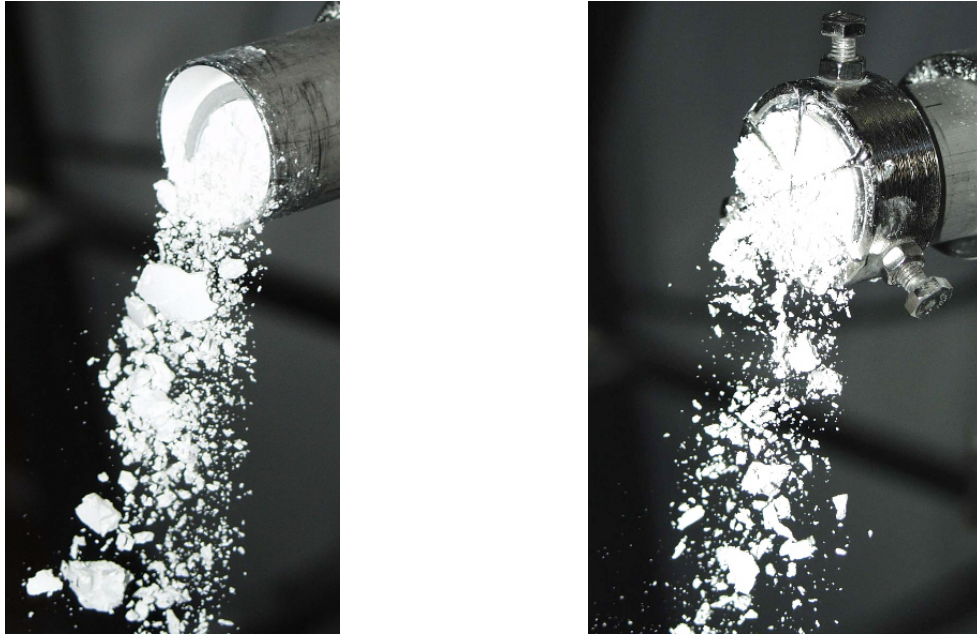


*Fig. 4-30: Dosing of calcium carbonate with a standard dosing tube (left) and a star attachment (right)*

In order to show that the mass flow fluctuations are mainly caused by the construction of the proportioning device (spiral or screw), the fast Fourier transformation is a very good tool. *Fig. 4-31*, *Fig. 4-32* and *Fig. 4-33* show the Fourier-transformed dosing results for the standard dosing tube with an inner diameter of 35 mm as well as the corresponding star attachment and rotating star attachment. The Fourier spectra of the mass flows are plotted against the frequency.

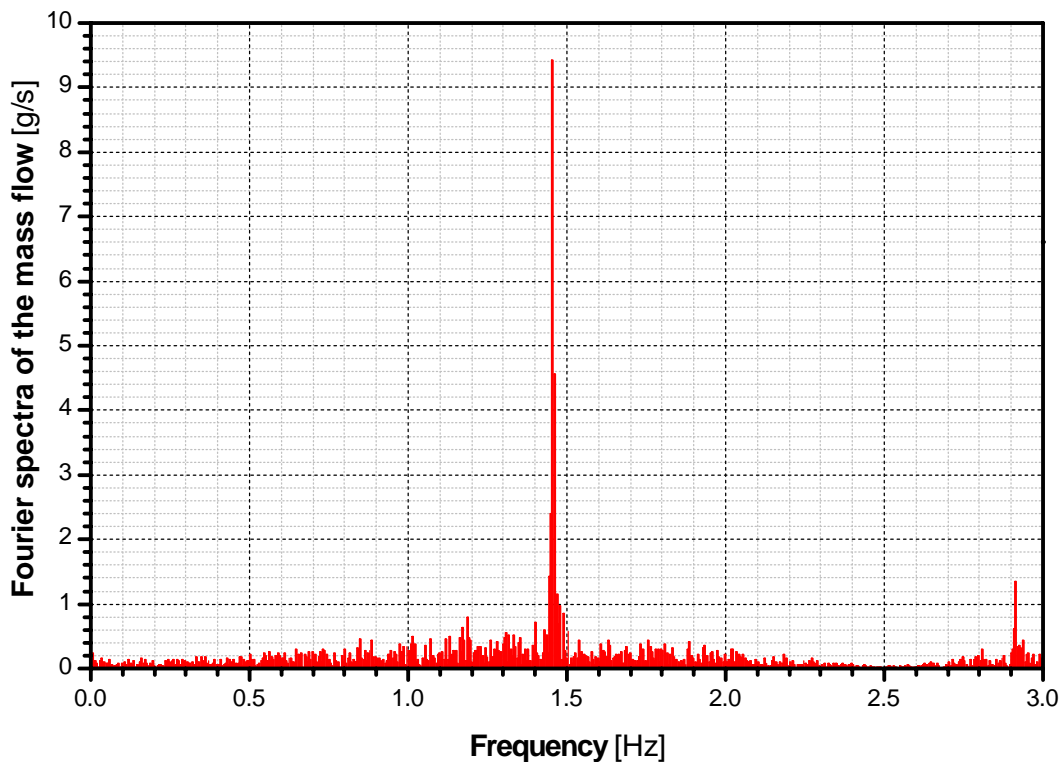


*Fig. 4-31: Fourier spectra of the dosing experiments using a standard dosing tube with an inner diameter of 35 mm (calcium carbonate,  $\bar{m} = 14$  g/s, proportioning device: spiral)*

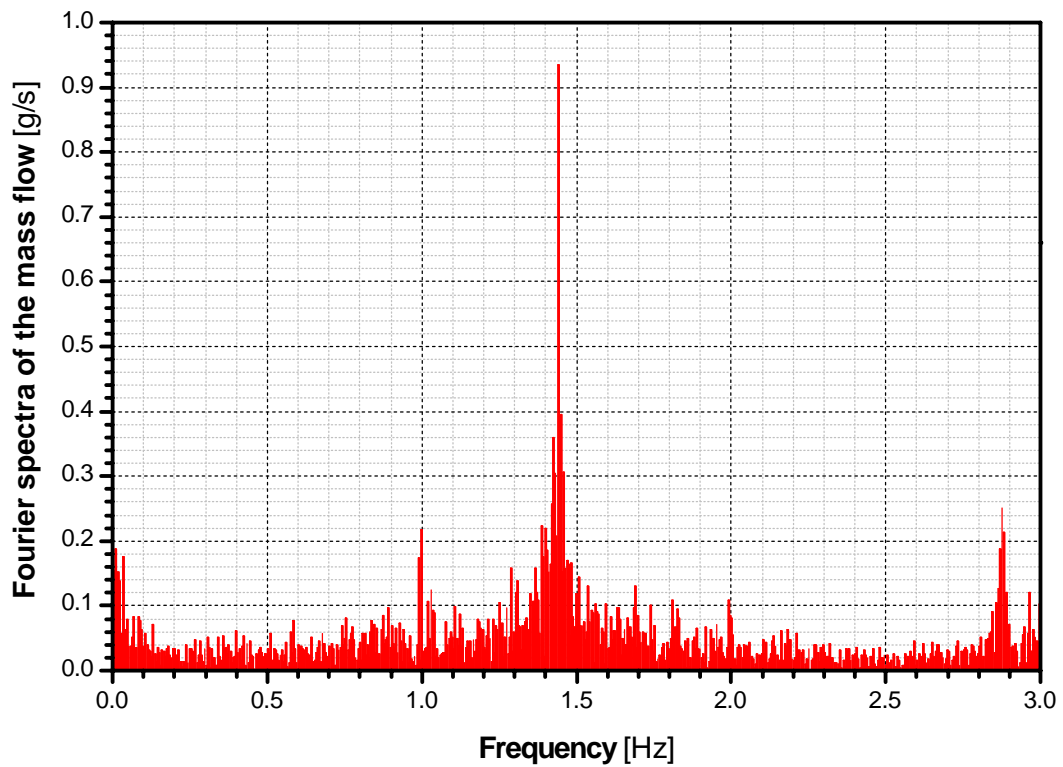


*Fig. 4-32: Fourier spectra of the dosing experiments using a star attachment mounted on the standard dosing tube with an inner diameter of 35 mm (calcium carbonate,  $\bar{m} = 14$  g/s, proportioning device: spiral)*

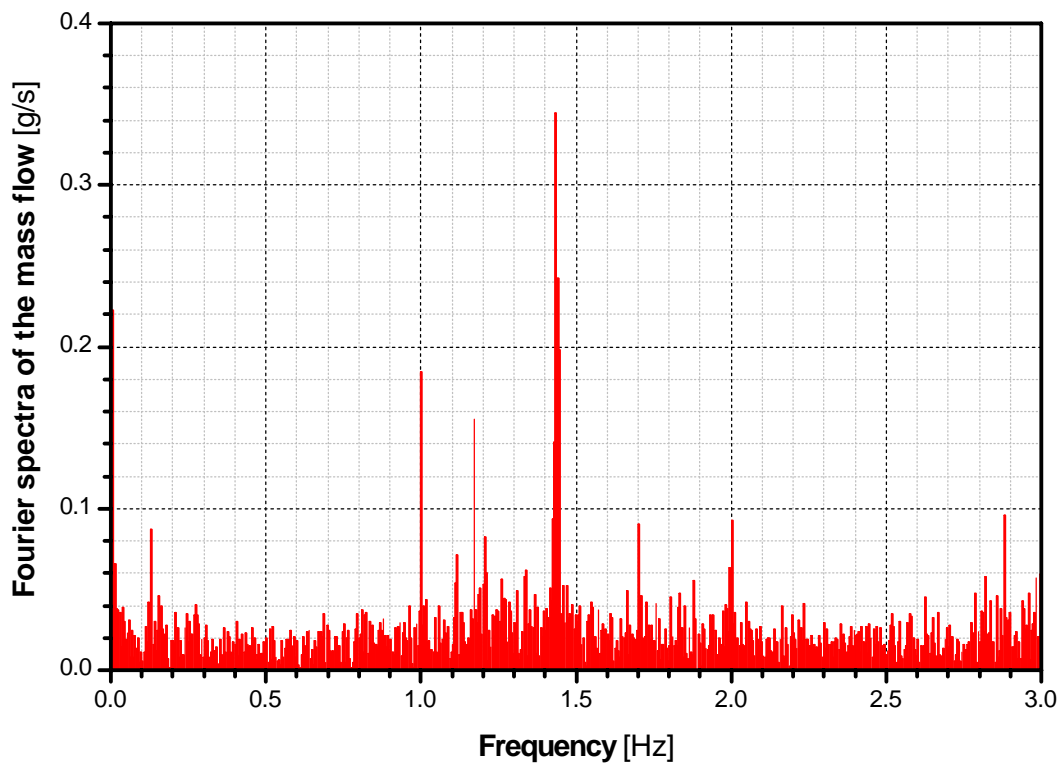


*Fig. 4-33: Fourier spectra of the dosing experiments using a rotating star attachment mounted on the standard dosing tube with an inner diameter of 35 mm (calcium carbonate,  $\bar{m} = 14$  g/s, proportioning device: spiral)*



A significant peak at a frequency of  $1.44\text{ Hz}$  is obvious in all figures. This frequency corresponds to the rotational speed of the spiral used, which was about  $86\text{ min}^{-1}$ . For the standard dosing tube, the amplitude of the mass flow determined at the frequency of  $1.44\text{ Hz}$  was about  $9.4\text{ g/s}$  (see *Fig. 4-31*). The amplitude was reduced from about  $0.9\text{ g/s}$  (see *Fig. 4-32*) for the star attachment to about  $0.3\text{ g/s}$  for the rotating star attachment (see *Fig. 4-33*). The single experimental results are listed in *Table 4-2*. Besides the amplitude reduction at a frequency of  $1.44\text{ Hz}$ , a reduction of the basic noise was observed.

*Table 4-2: Amplitudes determined at a frequency of  $1.44\text{ Hz}$  of the Fourier spectra (compare *Fig. 4-31*, *Fig. 4-32* and *Fig. 4-33*)*

standard dosing tube [g/s]	star attachment [g/s]	rotating star attachment [g/s]
9.7	0.9	0.3
9.9	0.7	0.3
9.0	0.8	0.1
9.4	0.7	0.1
10.6	0.7	0.1
$\varnothing 9.7 \pm 0.7$	$\varnothing 0.8 \pm 0.1$	$\varnothing 0.2 \pm 0.1$

During the dosing experiments, the star attachment caused sometimes a compaction of the calcium carbonate (see *Fig. 4-34*). After some minutes this phenomena disappeared and the powder was coming out again as shown in the right photo of *Fig. 4-30*. It was not possible to correlate this phenomenon with a changing of humidity, particle size distribution or bulk density. If the powder compacts, only the self-developed rotating star attachment will guarantee a very even outflow of the powder. High rotational speeds of the star attachment make it possible to partially overcome adhesion forces between the particles and to destroy agglomerates.



*Fig. 4-34: Calcium carbonate powder compacted due to the use of a star attachment*

### Influence of the rotational speed of the rotating star attachment

In order to find optimum working conditions for the rotating star attachment, the influence of the rotational speed of the attachment was examined. As shown in *Fig. 4-35*<sup>2</sup>, the influence of the speed and the direction of rotation is small (negative rotational speeds correspond to a rotation of the star attachment in the same direction as the proportioning device, both anticlockwise). Because the confidence intervals are smaller for positive rotational speeds and powder spreads out with increasing rotational speeds, a rotational speed of about  $160 \text{ min}^{-1}$  should be chosen.

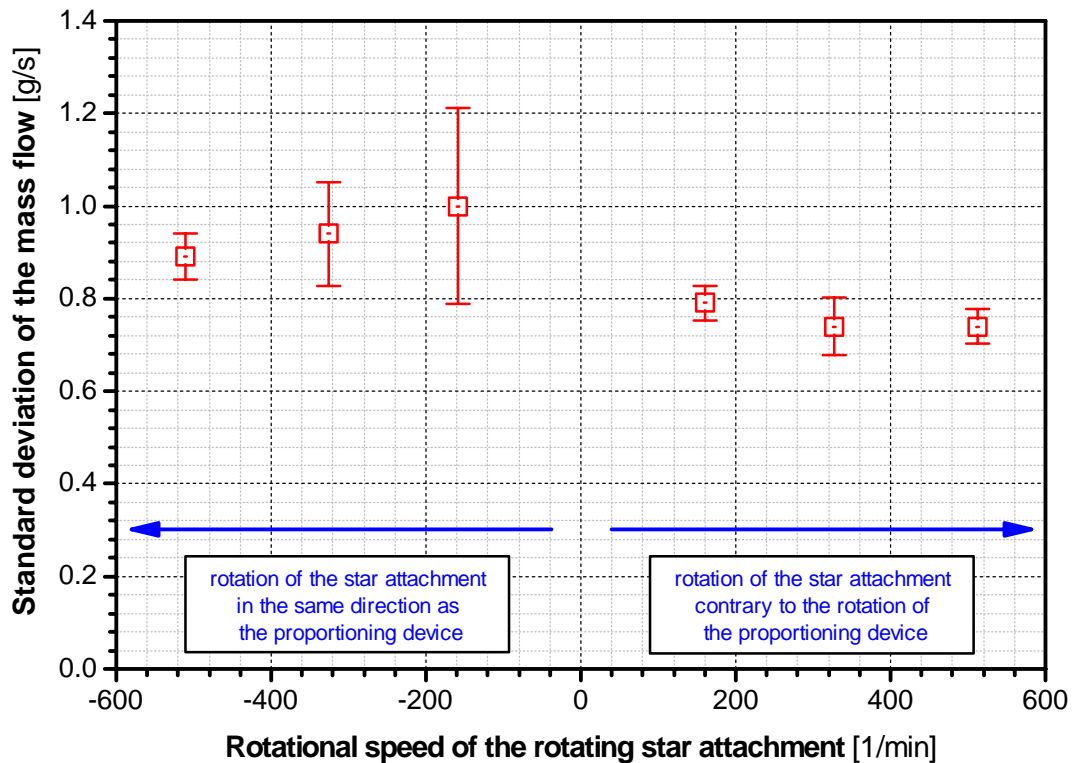


*Fig. 4-35: Influence of the rotational speed of the rotating star attachment on the standard deviation of the measured mass flow (calcium carbonate,  $\bar{m} = 14.3 \text{ g/s}$ , proportioning device: spiral)*

<sup>2</sup> The experimental results are based on the results already presented in [85]. Here the reduction of the gear (4.5 : 1) was not taken into account.

### Influence of the type of the proportioning device used

As shown in *Fig. 4-36*, the type of the proportioning device (spiral or screw) used influences the standard deviation of the measured mass flows. For almost the same set mass flow, the pulsation of the mass flow can be reduced from about 1.85 g/s for a spiral to 1.25 g/s for a screw.

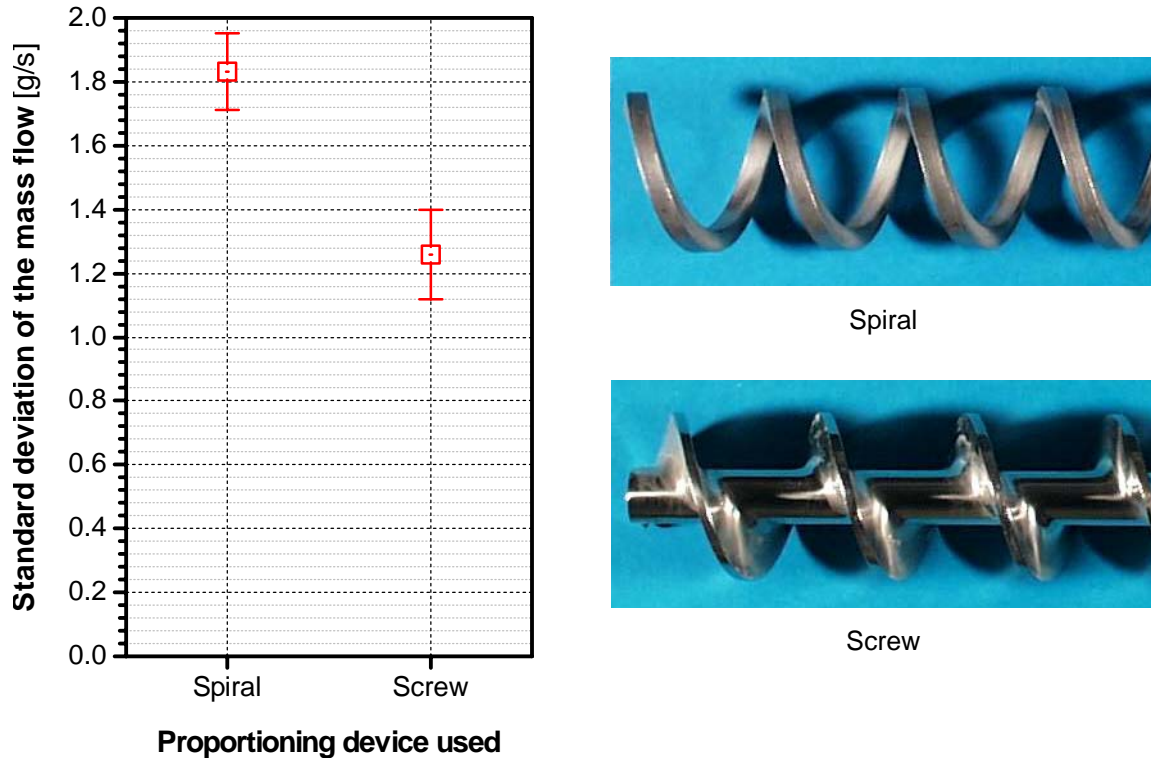


*Fig. 4-36: Influence of the proportioning device (spiral or screw) on the standard deviation of the measured mass flow (calcium carbonate, star attachment,  $\bar{m}_{spiral} = 15.2$  g/s,  $\bar{m}_{screw} = 15.1$  g/s)*

### Influence of the mass flow

The dependence of the mass flow fluctuations on the set mass flow is shown in *Fig. 4-37* for using a spiral as well as a screw. A standard dosing tube in combination with a star attachment was used. The results are based on 2 100 measured mass flow values and each trial was repeated four times.

For mass flows less than 20 g/s, the majority of the measured average standard deviations using a spiral are higher than the measured average standard deviations using a screw. For mass flows higher than 20 g/s, the type of the proportioning device used has no significant influence on the measured average standard deviations. A stepwise reduction of the measured average standard deviation was observed for mass flows higher than 19.5 g/s using a spiral and for mass flows higher than 21 g/s using a screw. The quantity of the stepwise change is higher for a spiral than for a screw.



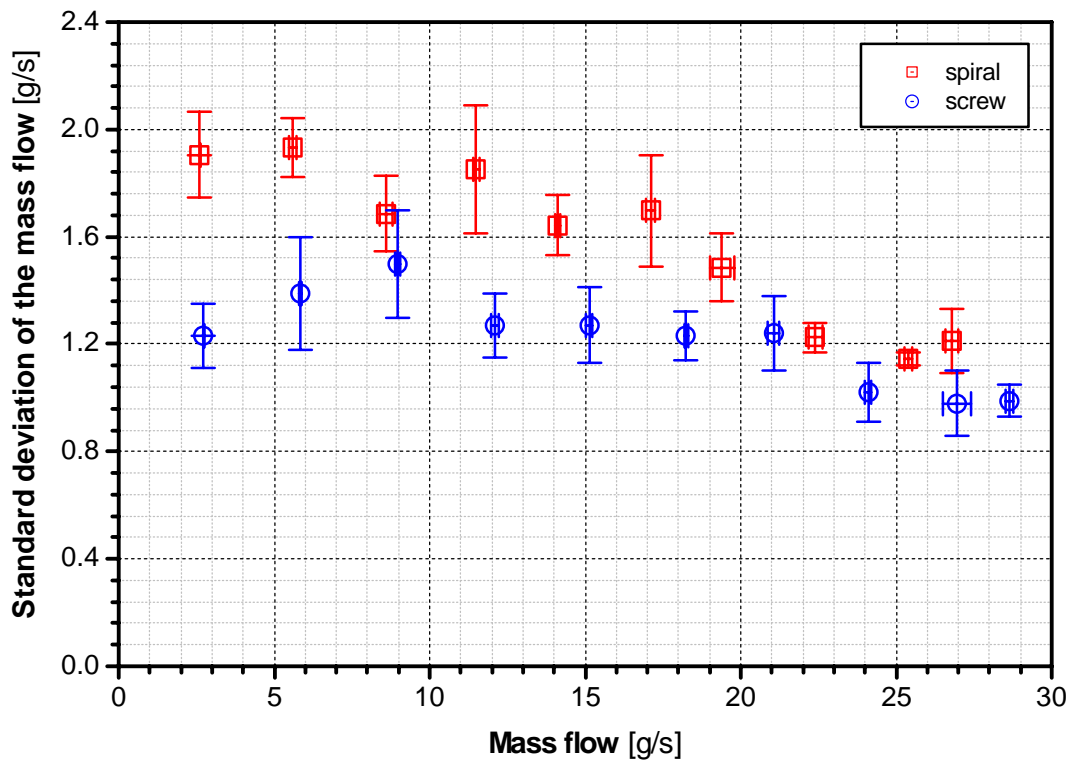


*Fig. 4-37: Influence of the mass flow on the standard deviation of the measured mass flow (calcium carbonate, star attachment)*

In literature, the mass flow fluctuations are often described by a coefficient of variation, the empirical relative standard deviation  $s_{rel.}$ , to discuss the influence of the mass flow on the mass flow fluctuations [94]. The empirical relative standard deviation is defined as the quotient of the empirical standard deviation  $s$  and the average mass flow  $\bar{\dot{m}}$  :

$$s_{rel.} = \frac{s}{\bar{\dot{m}}} \quad Eq. 4-7$$

The influence of the mass flow on the relative standard deviation is shown in *Fig. 4-38*. The mean value decreases with increasing mass flow.

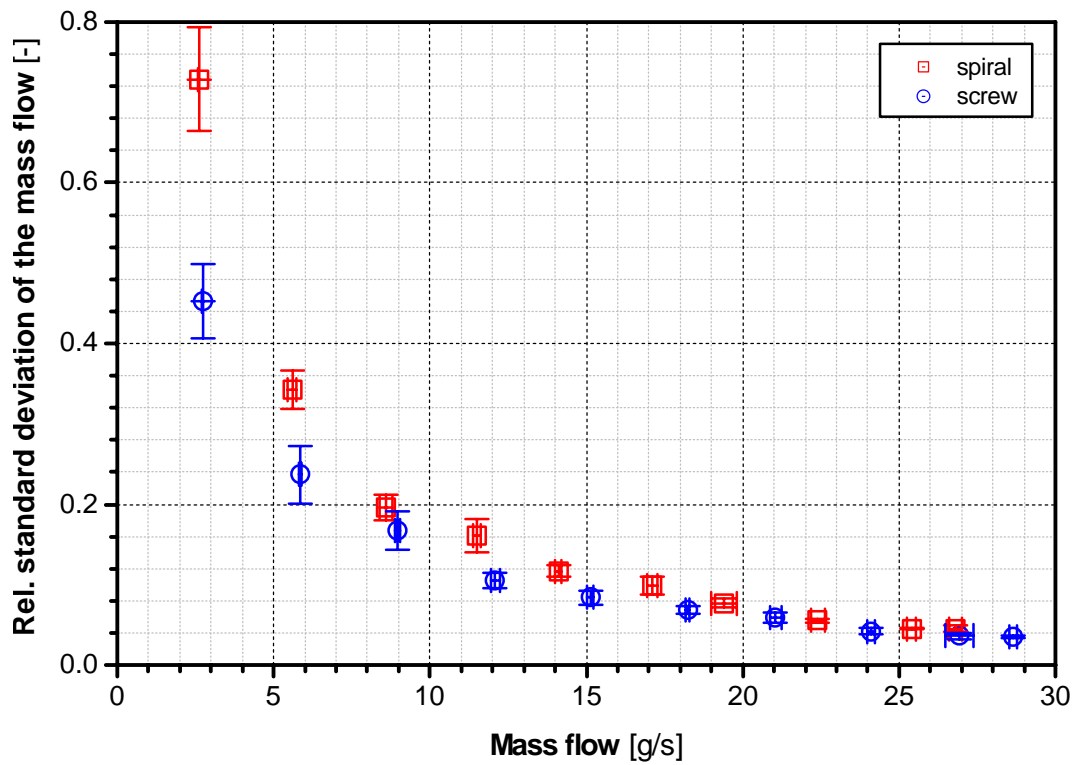


*Fig. 4-38: Influence of the mass flow on the relative standard deviation of the mass flow (calcium carbonate, star attachment)*

Using a screw as proportioning device in combination with a rotating star attachment, no significant influence of the set mass flow on the standard deviations of the measured mass flows was observed (see *Fig. 4-39*). The results are based on 2100 measured mass flow values. Two repetitions were run for each set mass flow. Dividing the standard deviation by the set average mass flow, the relative standard deviation decreases with increasing mass flows (see *Fig. 4-40*).

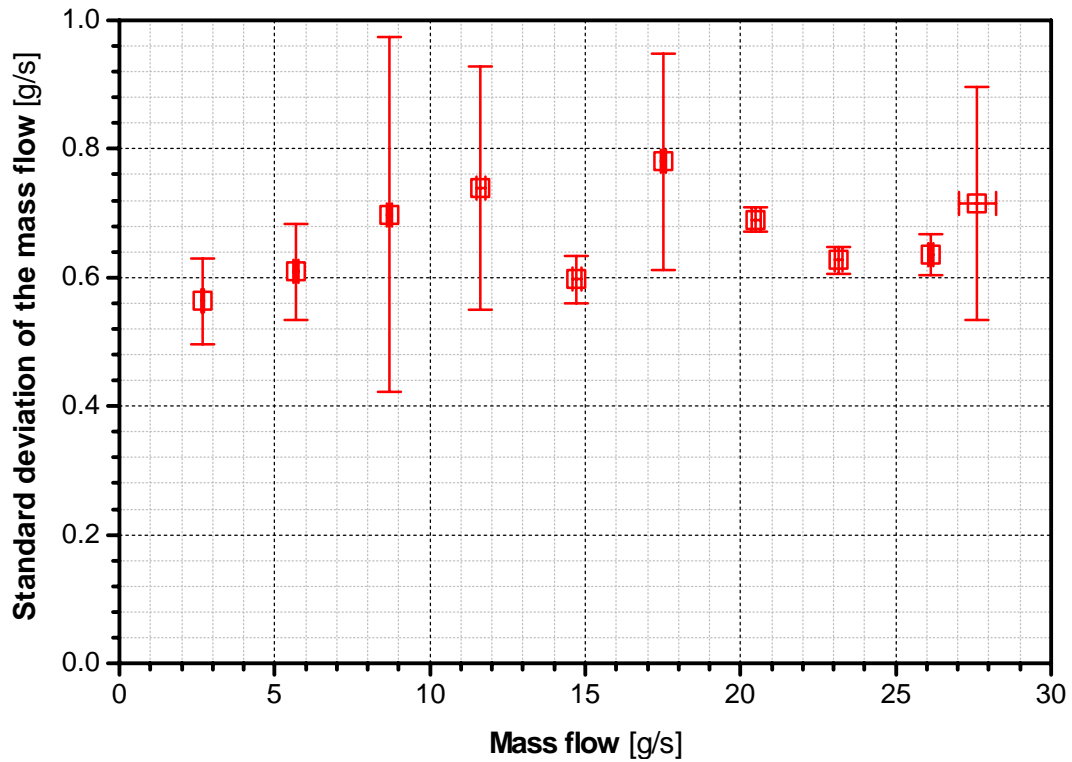


Fig. 4-39: Influence of the mass flow on the standard deviation of the measured mass flow (calcium carbonate, rotating star attachment with  $n = 330 \text{ min}^{-1}$ , proportioning device: screw)

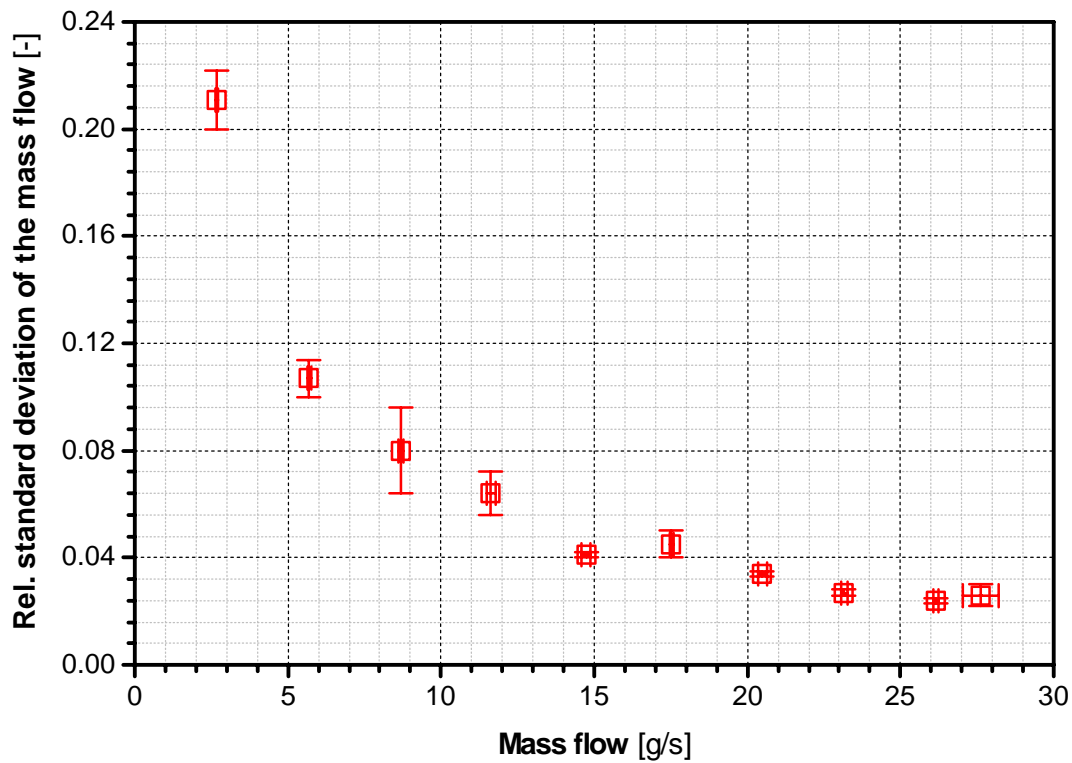
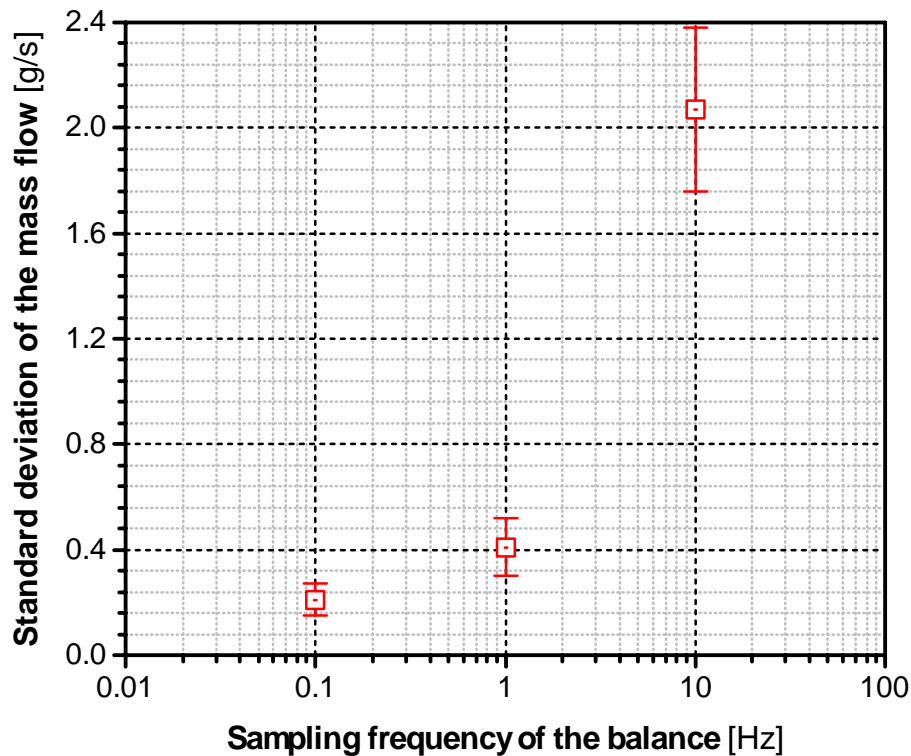


Fig. 4-40: Influence of the mass flow on the measured relative standard deviation of the mass flow (calcium carbonate, rotating star attachment with  $n = 330 \text{ min}^{-1}$ , proportioning device: screw)

### Influence of the sampling frequency of the balance

The dependence of the mass flow fluctuations on the sampling frequency of the balance is shown in *Fig. 4-41*. The measured standard deviation is about ten times higher for a sampling frequency of  $10\text{ Hz}$  than for a sampling frequency of  $0.1\text{ Hz}$ . A sampling frequency of  $0.1\text{ Hz}$  means that every  $10\text{ s}$  the increase of weight is measured whereas for a frequency of  $10\text{ Hz}$  every  $0.1\text{ s}$  the increase of weight is measured. For all sampling frequencies, the real mass flow fluctuations are the same! But for lower sampling frequencies, the period of time between each measured value becomes longer and fluctuations are averaged.



*Fig. 4-41: Influence of the sampling frequency of the balance on the standard deviation of the measured mass flow (calcium carbonate, star attachment,  $\bar{m} = 8.5\text{ g/s}$ , proportioning device: spiral)*

### Influence of the falling height

To examine the influence of the falling height on the standard deviation of the measured mass flow, a high plastic vessel was positioned on the balance. The distance between the dosing tube of the volumetric feeder and the bottom of the vessel was  $40\text{ cm}$ . For a set mass flow of  $15\text{ g/s}$ , it took  $405\text{ s}$  to fill the plastic vessel up to a height of  $36\text{ cm}$ . During this time, the mass flow was measured  $4\,050$  times. For the evaluation of the trial, the filling height of  $36\text{ cm}$  was divided in 9 intervals with a height of  $4\text{ cm}$ . For each interval, the mass flow and the resulting standard deviation was calculated out of 450 measured mass values. The trial was repeated four times. The results are shown in *Fig. 4-42*. Because of the reduced impulse of the falling particles, the standard deviation of the measured mass flow is more than  $50\%$  smaller for a falling height of  $6\text{ cm}$  than for a falling height of  $38\text{ cm}$ .

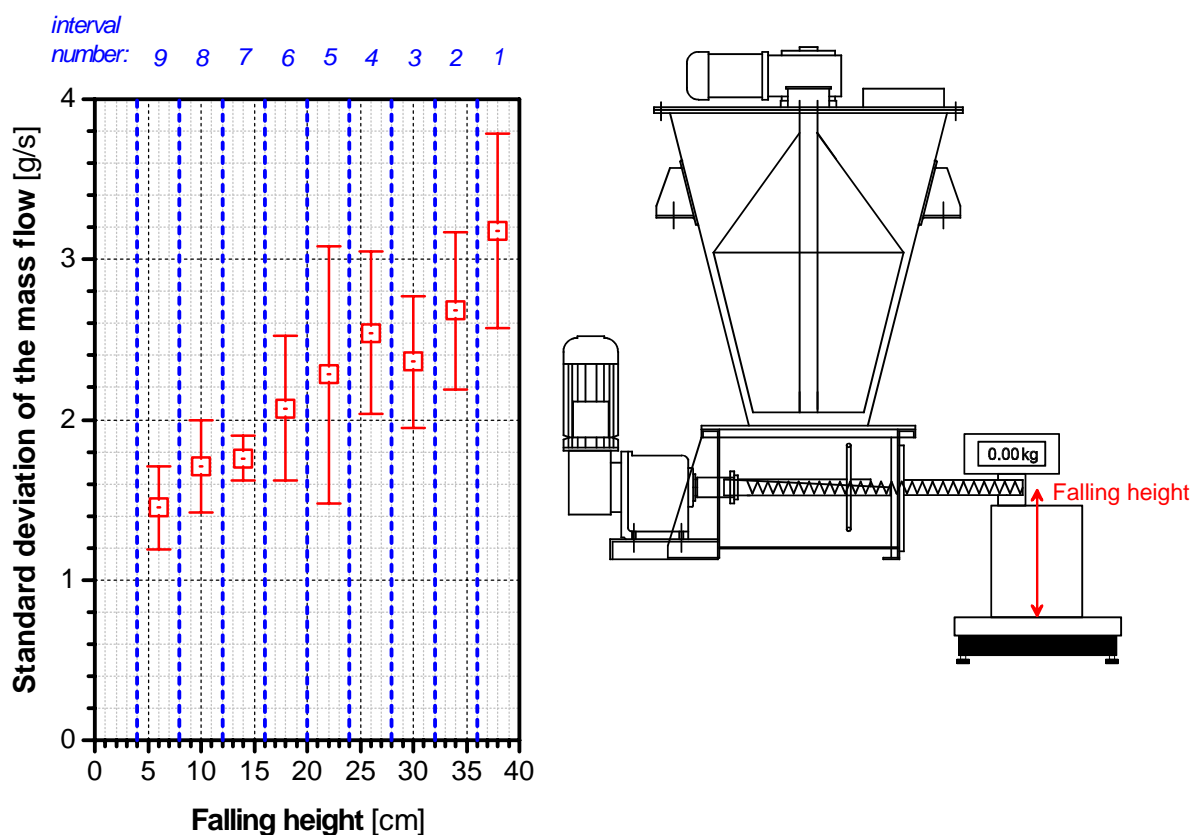


*Fig. 4-42: Influence of the falling height on the standard deviation of the measured mass flow (calcium carbonate, star attachment,  $\bar{m} = 15.1\text{ g/s}$ , proportioning device: spiral)*

### Influence of the filling height

To examine the influence of the filling height of the volumetric feeder on the measured mass flow, the mass in the feeder was reduced stepwise (120, 110, 100, 90, 70 and 50 kg). For each resulting filling level, the mass flow was determined 2 200 times. Each trial was repeated four times. The influence of the filling height on the mass flow is shown in *Fig. 4-43*. No significant influence was observed for filling heights between 45 and 55 cm. For filling heights smaller than 45 cm, the measured mass flow decreased with decreasing filling heights due to a decreasing bulk density.

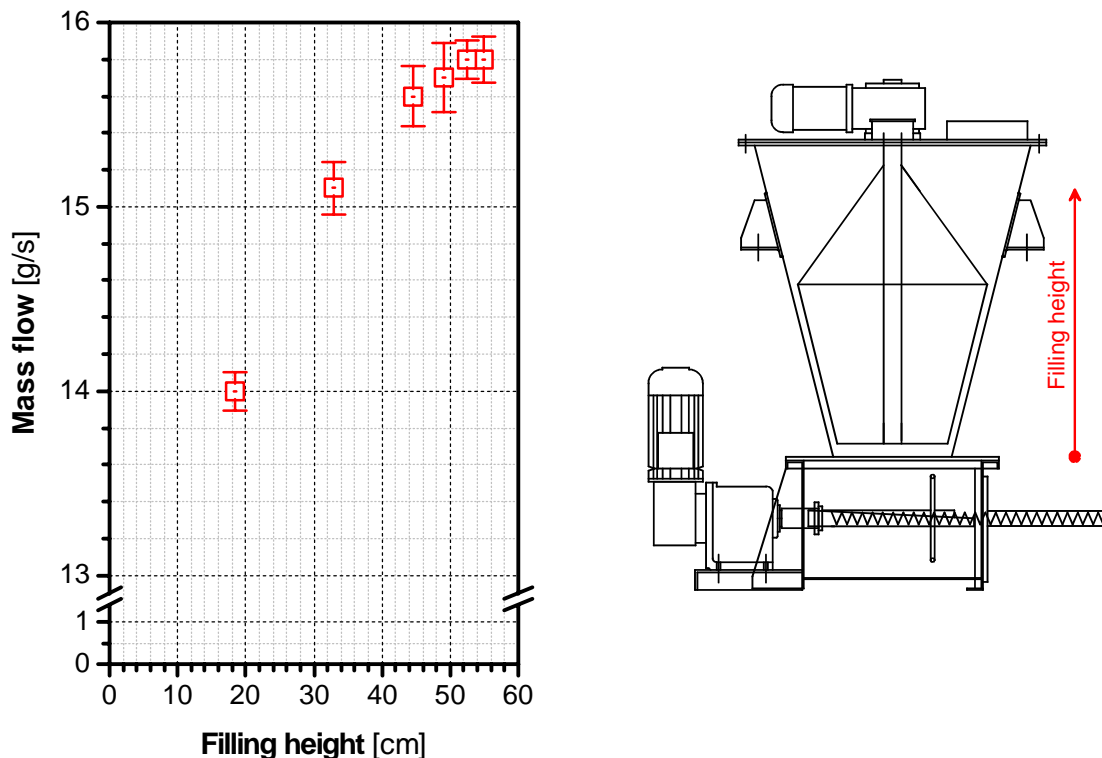


*Fig. 4-43: Influence of the filling height on the measured mass flow (calcium carbonate, rotating star attachment with  $n = 160 \text{ min}^{-1}$ , proportioning device: spiral with constant rotational speed)*

### Dosing tube with a bigger diameter

The volumetric feeder used can be equipped with dosing tubes of different diameter depending on the mass flow range needed. Following, the effectiveness of different attachments for the standard dosing tube with an inner diameter of 53 mm in combination with a spiral are presented. A grid attachment, a star attachment with 1 mm as well as 2 mm bars (*Fig. 4-44*) and a rotating star attachment (*Fig. 4-45*) were used.

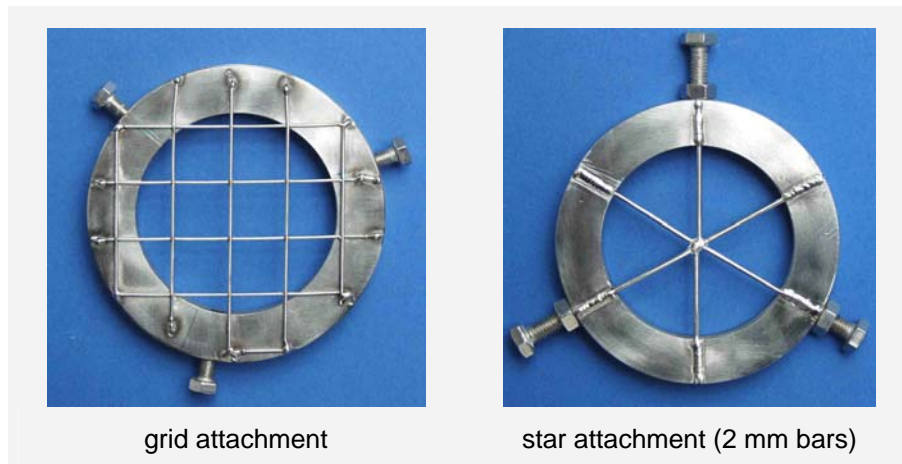


**Fig. 4-44:** Dosing tube attachments for a standard dosing tube with an inner diameter of 53 mm

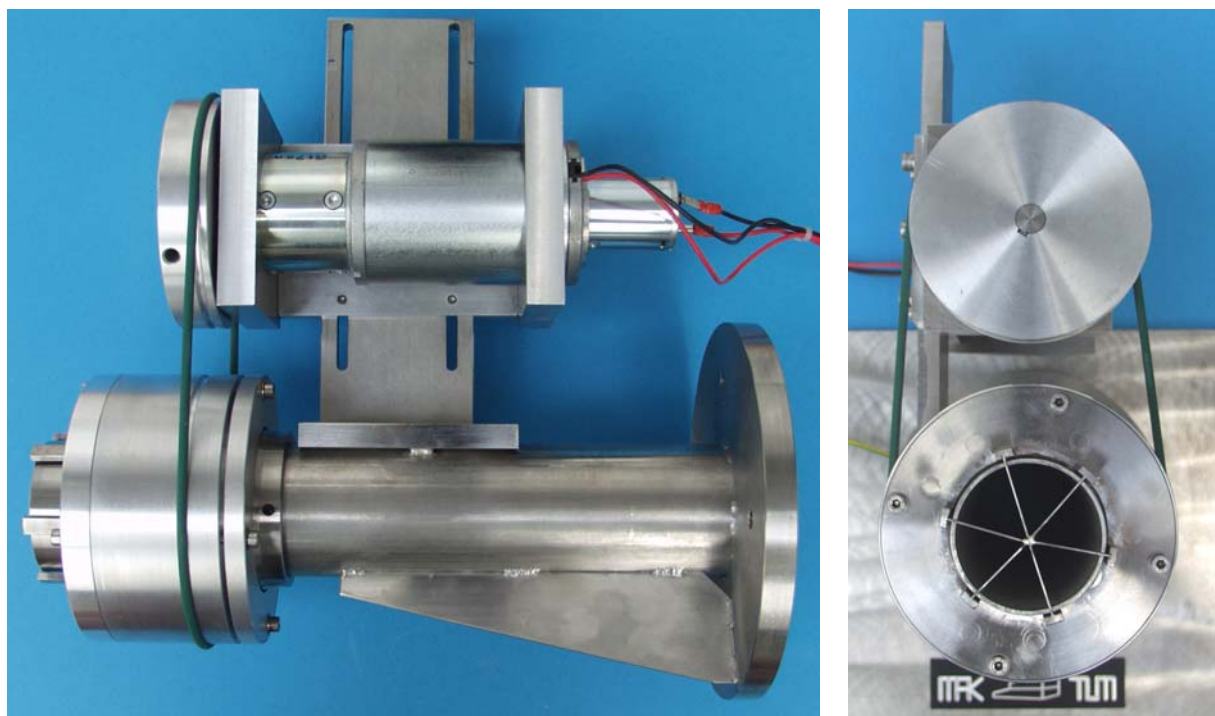


**Fig. 4-45:** New self-developed rotating star attachment for a dosing tube with an inner diameter of 53 mm: Side view (left) and front view (right)

During the dosing experiments using the rotating star attachment developed for the smaller dosing tube (inner diameter of 35 mm), powder accumulated in the gap between the rotating star attachment and the dosing tube (see arrow in *Fig. 4-46*, left). This does not correspond to hygienic design guidelines [110, 111]. During the development of the rotating star attachment for a dosing tube with a larger diameter, the hygienic aspect was taken into account. The right photo of *Fig. 4-46* shows the further developed rotating star attachment. The staggered body and the space between the holders of the bars allow an easy cleaning. Almost no powder accumulation was observed even after a long operating time.



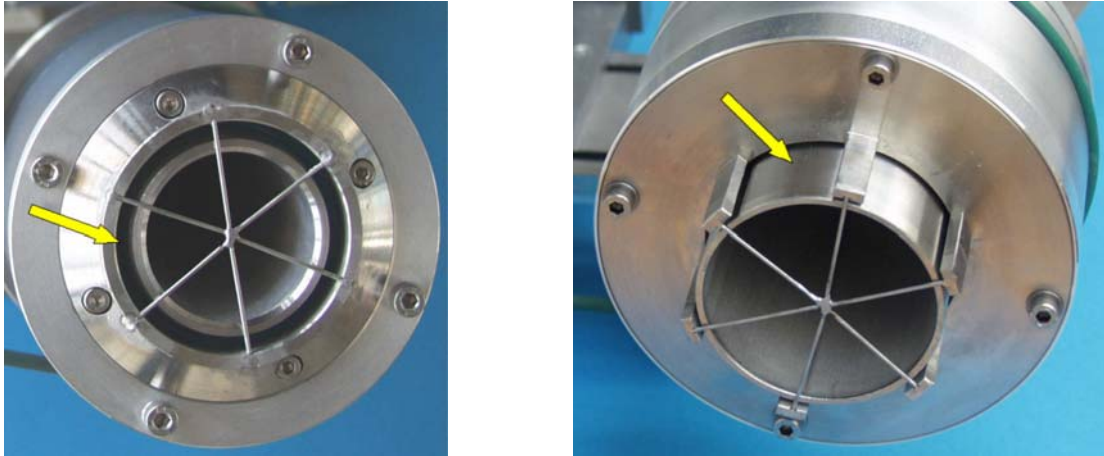


**Fig. 4-46:** Differences between the old rotating star attachment (left) and the new one (right)

For the assessment of the different attachments, the actual mass of the dosed powder was measured every  $0.1\text{ s}$  for 660 times. Every trial was repeated four times. The set average mass flow of  $68\text{ g/s}$  was about five times higher than the set mass flow used during the assessment of the attachments for the smaller dosing tube. The fed powder was put back in the volumetric feeder after each dosing trial. The mass flow and the standard deviation of the mass flow were calculated. The results of the experiments are shown in *Fig. 4-47* and *Fig. 4-48*.

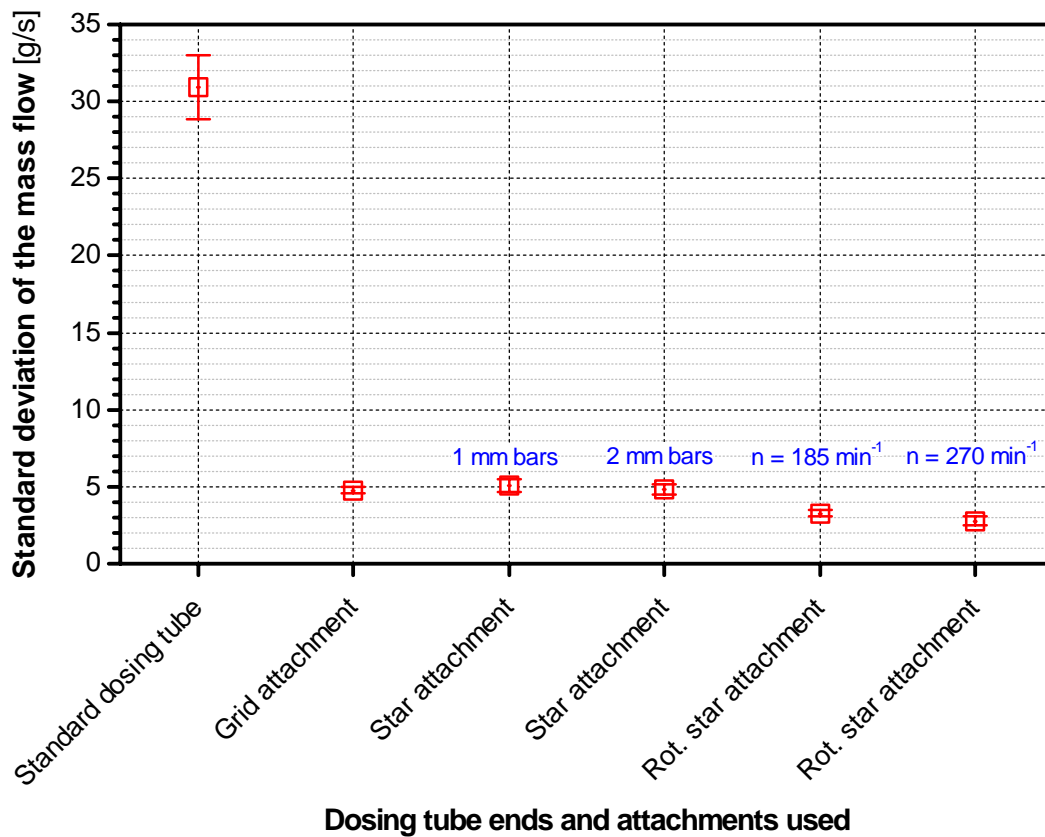


**Fig. 4-47:** Comparison of different tube ends and attachments for the dosing tube with an inner diameter of 53 mm (calcium carbonate,  $\dot{m} = 68\text{ g/s}$ , proportioning device: spiral)



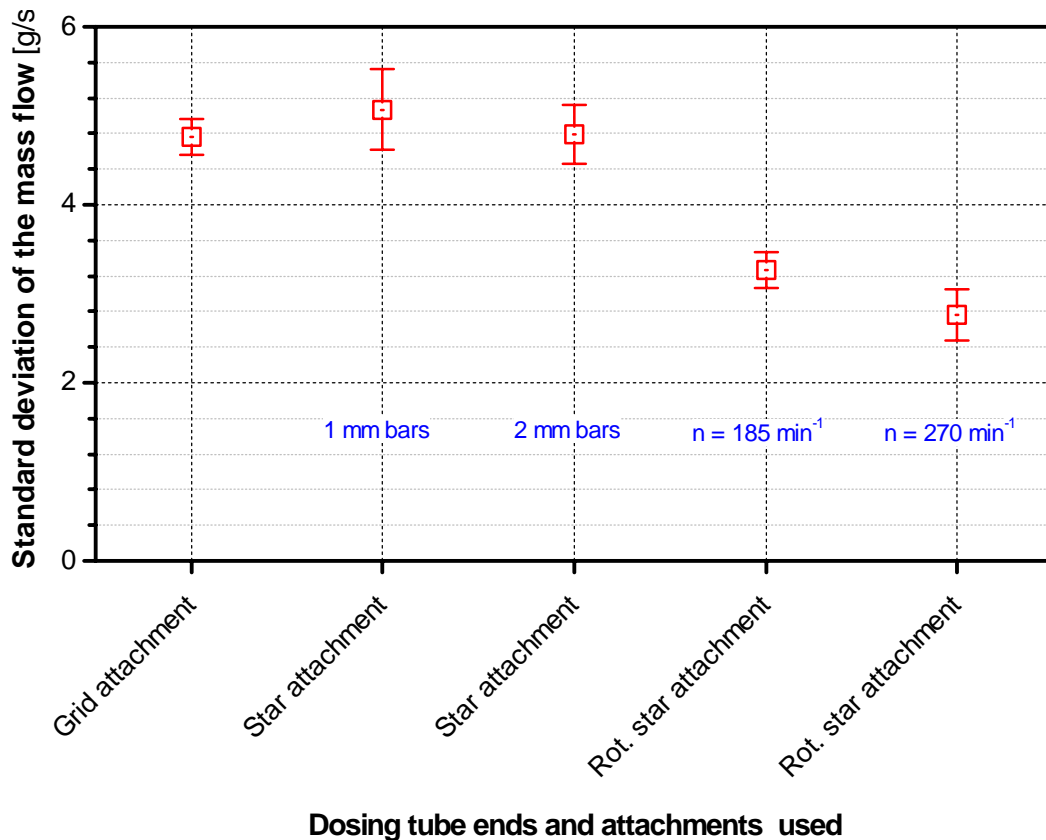


**Fig. 4-48:** Comparison of different tube ends and attachments for the dosing tube with an inner diameter of 53 mm (calcium carbonate,  $\dot{m} = 68$  g/s, proportioning device: spiral); in comparison to Fig. 4-47 the standard dosing tube is not considered

The standard deviation of the measured mass flows can be reduced significantly with each attachment. No significant difference was found between the grid attachment, the star attachment with 1 mm bars and the star attachment with 2 mm bars. The standard deviation obtained by using these three attachments is about a sixth of the standard deviation obtained by using the standard dosing tube. The standard deviation obtained by using the rotating star attachment is about a tenth of the standard deviation obtained by using the standard dosing tube and significantly smaller than the standard deviation obtained by using the three other attachments.

#### 4.3.1.2.2 Dosing examinations using maize starch

The results of the dosing experiments using maize starch are shown in *Fig. 4-49*. As for calcium carbonate, the dosed powder was measured every  $0.1\text{ s}$  for 2 200 times. Every trial was repeated four times. A dosing tube with an inner diameter of  $35\text{ mm}$  and a screw were used.

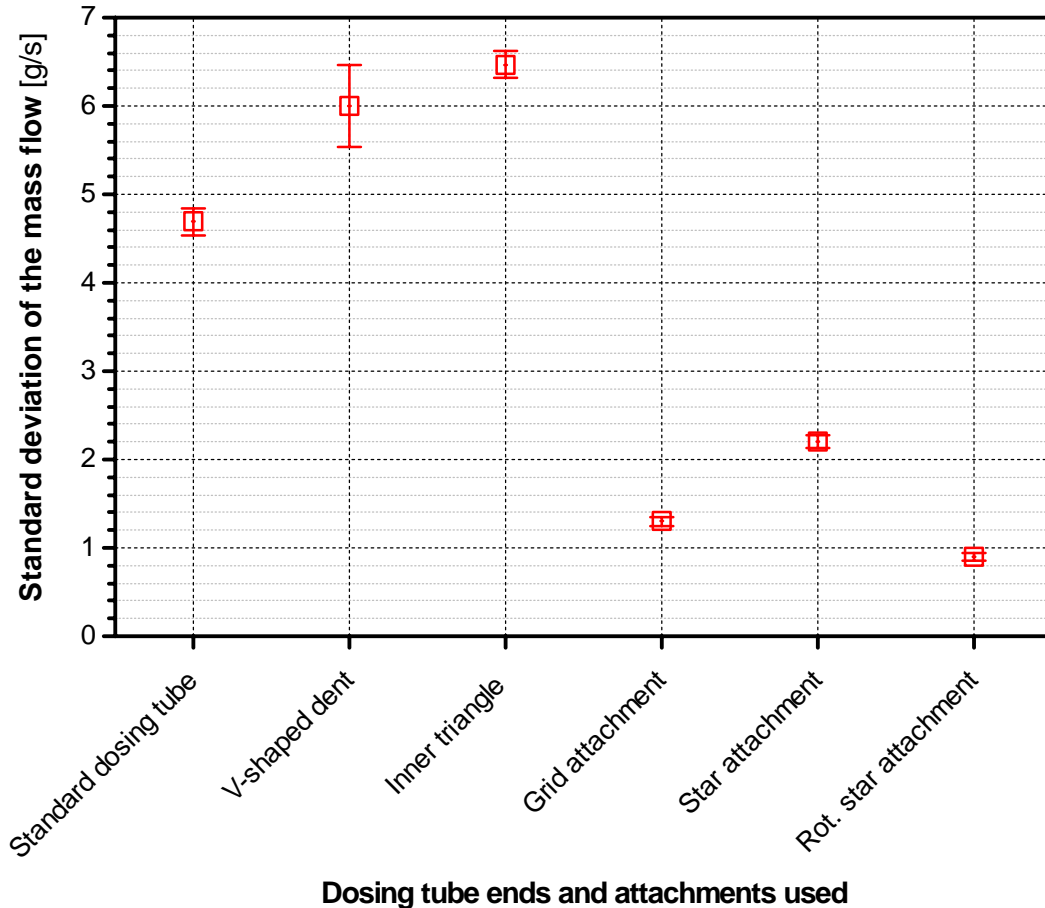


*Fig. 4-49:* Comparison of different tube ends and attachments for the standard dosing tube with an inner diameter of  $35\text{ mm}$  (maize starch,  $\bar{m} = 10.6\text{ g/s}$ , proportioning device: screw)

In contrast to the experiments performed with calcium carbonate, the use of a V-shaped dent and an inner triangle caused an increase of the mass flow fluctuations in comparison to the standard dosing tube. The mass flow fluctuations were reduced by the use of each attachment. The flow resistance of the grid attachment is higher than the flow resistance of the star attachment and caused a higher accumulation of the powder (without compaction). For maize starch, the highest dosing constancy was also obtained by using the rotating star attachment. The standard deviation is reduced to a fifth of the standard deviation obtained by using the standard dosing tube. The rotating star attachment has a higher flow resistance than the other attachments and causes a good dispersion of the powder particles.

A problem, which arose sometimes, is shown in *Fig. 4-50*. After a time of about  $130\text{ s}$ , the cone of the powder, dosed into the collecting bowl, collapsed. After further  $120\text{ s}$ , the cone collapsed again. High peaks of the mass flow in positive and negative direction were the result. For the assessment of the dosing tube ends and attachments, the peaks were eliminated. No significant peak was observed in the periods before the collapsing (see *Fig. 4-51*).

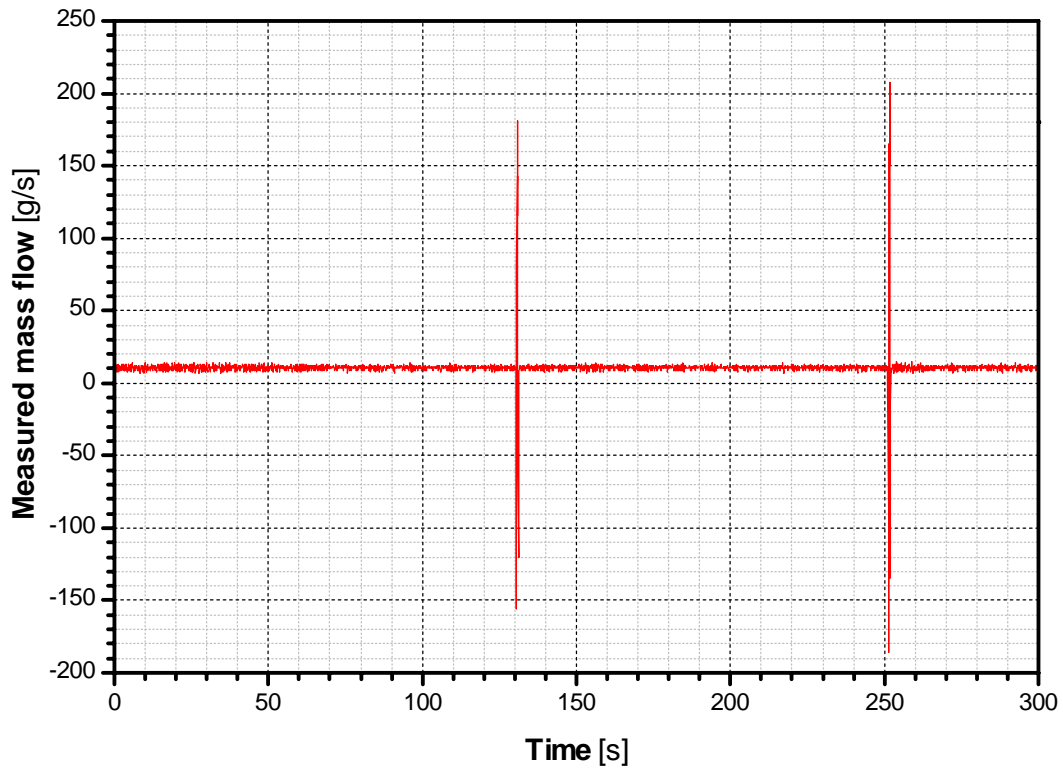


*Fig. 4-50: Mass flow fluctuations of maize starch for a set average mass flow of 10.6 g/s (maize starch, rotating star attachment with  $n = 330 \text{ min}^{-1}$ , proportioning device: screw)*

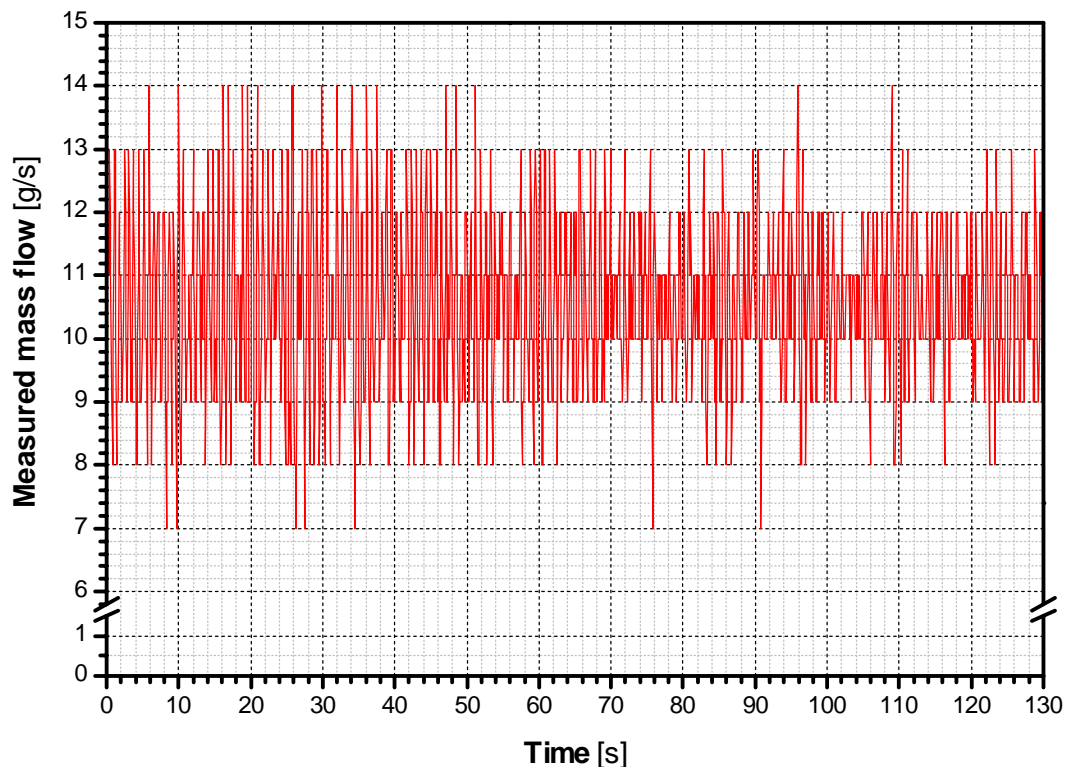


*Fig. 4-51: Mass flow fluctuations of maize starch for a set average mass flow of 10.6 g/s (maize starch, rotating star attachment with  $n = 330 \text{ min}^{-1}$ , proportioning device: screw)*

To find optimum working conditions for the rotating star attachment, the rotational speed was varied (see *Fig. 4-52*). In contrast to the experiments with calcium carbonate (compare *Fig. 4-35*, p. 86), the rotational speed and the direction of rotation had a significant influence on the standard deviation of the measured mass flows. Negative rotational speeds (rotation of the star attachment in the same direction as the proportioning device, both anticlockwise) caused significantly higher fluctuations than positive. A rotational speed of  $160 \text{ min}^{-1}$  caused the same result as a rotational speed of  $330 \text{ min}^{-1}$ .

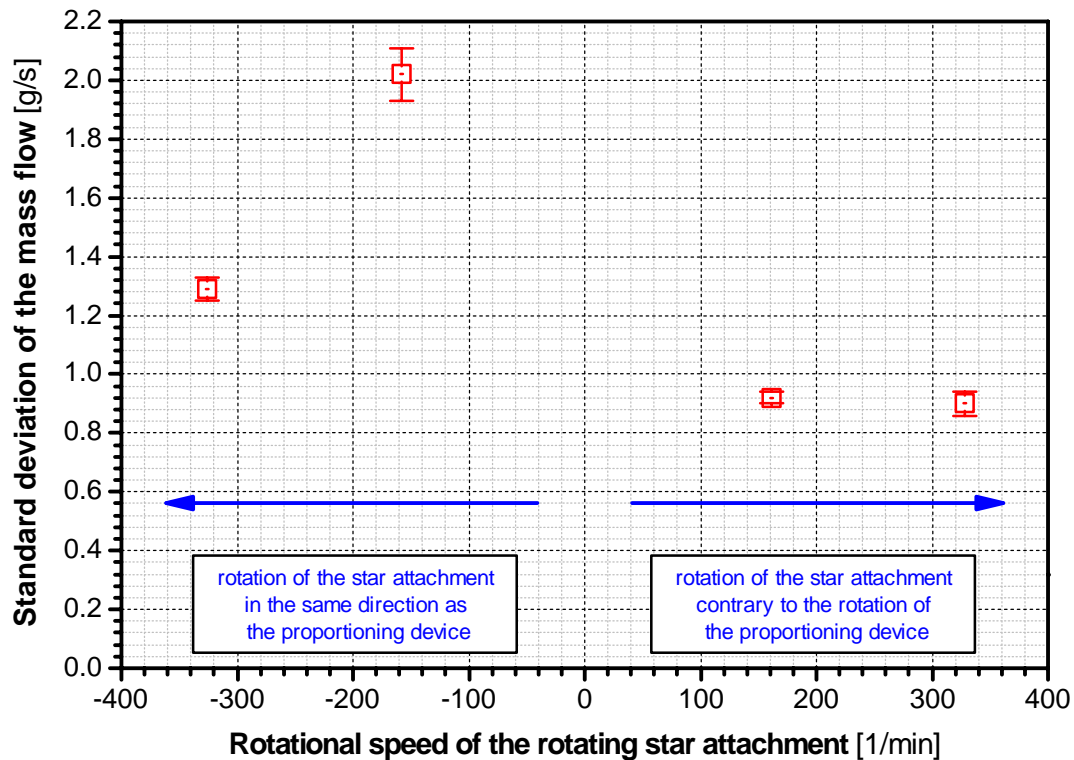


*Fig. 4-52: Influence of the rotational speed of the rotating star attachment on the standard deviation of the measured mass flow (maize starch,  $\bar{m} = 10.6 \text{ g/s}$ , proportioning device: screw)*

#### 4.3.2 Powder dosing in the continuous dynamic mixer

For the mixing experiments described later, the two volumetric feeders were equipped with a rotating star attachment. The dosing tubes were positioned opposite each other and orthogonal to the longitudinal axis of the mixer. *Fig. 4-53* shows the dosing tube for maize starch on the left-hand side and on the right-hand side the dosing tube for calcium carbonate. In order to avoid a formation of dust in the surrounding area, the inlet of the mixer and the two dosing tubes are caged with plastic plates.



*Fig. 4-53: Powder dosing in the continuous dynamic mixer: Maize starch (left) and calcium carbonate (right)*

#### 4.3.3 Hardware and software used for the generation of defined mass flow fluctuations

The generation of defined mass flow fluctuations should be achieved by a defined changing of the rotational speed of the proportioning device used. A prerequisite is a linear correlation between the rotational speed of the proportioning device and the mass flow coming out of the volumetric feeder.

In *Fig. 4-54*, the correlation between the measured average calcium carbonate mass flow and the rotational speed of the proportioning device is shown for a dosing tube with an inner diameter of  $35\text{ mm}$ . The experiments were performed with a spiral in combination with the use of a star attachment and with a screw in combination with the use of a star attachment as well as the use of a rotating star attachment (compare *Fig. 4-21* and *Fig. 4-23*). Every trial was repeated two times. The average mass flows were calculated out of 2 100 measuring values, which were measured every  $0.1\text{ s}$  with a balance. Up to a rotational speed of  $170\text{ min}^{-1}$ , a linear relation between the rotational speed and the mass flow was found for all proportioning devices. For rotational speeds higher than  $90\text{ min}^{-1}$ , the measured mass flows differ significantly. At the same rotational speed, the highest mass flows were obtained by using a screw in combination with a star attachment, followed by a screw in combination with a rotating star attachment ( $n = 330\text{ min}^{-1}$ ) and a spiral in combination with a star attachment.

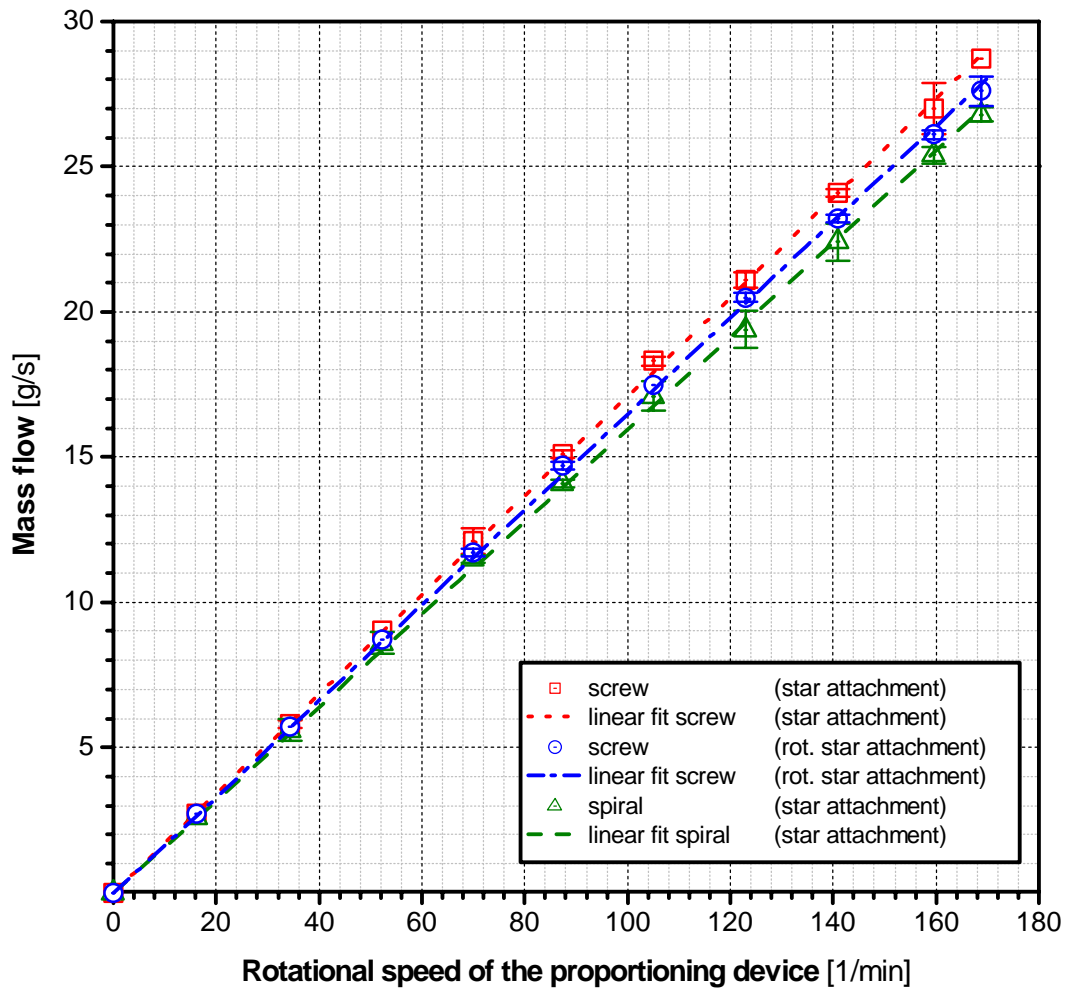


*Fig. 4-54: Correlation between the average mass flow of calcium carbonate OMYACARB 2 SV and the rotational speed of the proportioning device (dosing tube with an inner diameter of 35 mm)*

In *Fig. 4-55*, the correlation between the measured average calcium carbonate mass flow and the rotational speed of the proportioning device is shown for a dosing tube with an inner diameter of 53 mm. The experiments were performed with a spiral in combination with a star attachment (2 mm bars). Each trial was repeated four times. The average mass flows were calculated out of 600 mass flow values because of the higher set mass flow. The actual weight was measured every 0.1 s. Up to a rotational speed of 170  $\text{min}^{-1}$ , an almost linear correlation between the mass flow and the rotational speed was found.

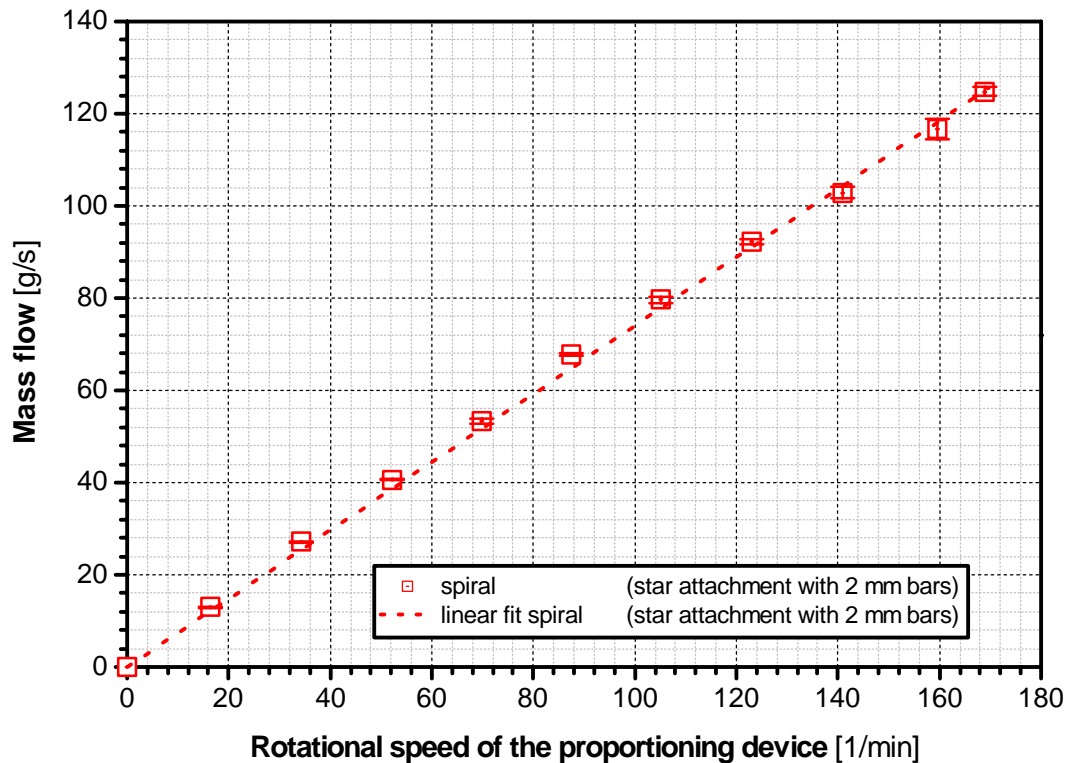


*Fig. 4-55: Correlation between the rotational speed of the proportioning device and the average mass flow of calcium carbonate OMYACARB 2 SV (dosing tube with an inner diameter of 53 mm)*

The generation of defined mass flow fluctuations is shown in detail in *Fig. 4-56*. The parameters of the fluctuation (period length, amplitude, offset and shape) of the mass flow fluctuation are set in the visualization and control surface (compare *Fig. 4-4*) programmed with *LabVIEW*. The set parameters are transferred via Direct Data Entry (DDE) to the recipe manager *PR 1740* from the company *GLOBAL Weighing Technologies GmbH*. Via the serial interface *RS 232*, the parameters set leave the control computer and are written into the programming system *PR 1750*. The programming system *PR 1750* from the company *GLOBAL Weighing Technologies GmbH* is the control software of the weighing controller *PR 1730*. The software is used to generate a sinusoidally fluctuating voltage signal coming out of the analog I/O-interface of the weighing controller. The I/O-interface of the weighing controller was connected with the control variable input of the frequency converter, which is connected with the drive motor of the proportioning device. The frequency converter generates a sinusoidal changing of the rotational speed of the proportioning device.



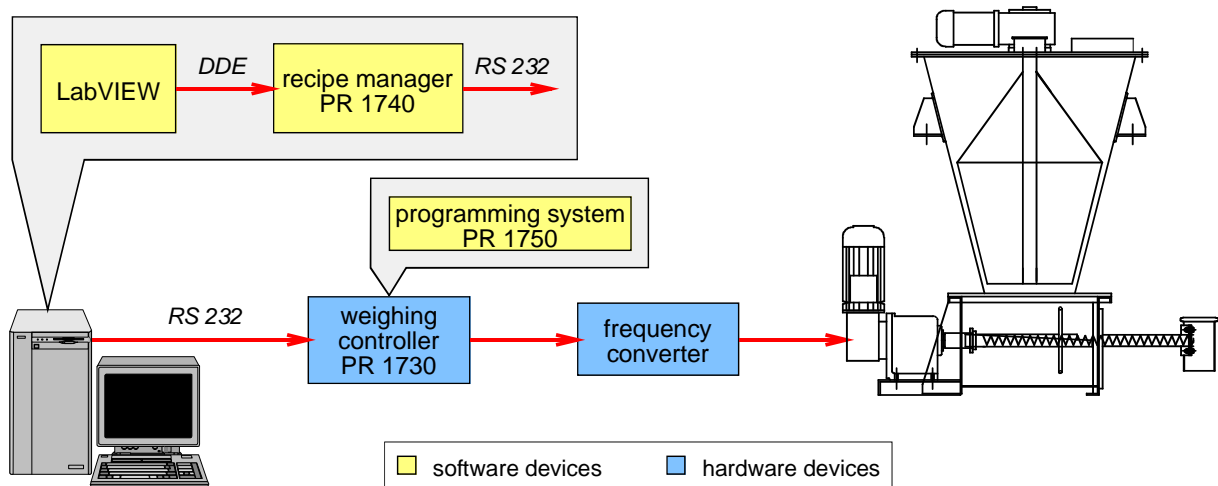


**Fig. 4-56:** Illustration of generating defined mass flow fluctuations

To validate the generation procedure, the generated functions can be measured directly and indirectly. The control signal from the weighing controller to the frequency converter is a voltage signal, which can be directly measured with an oscilloscope. A voltage generator was flanged on the driving gear of the volumetric feeder. The generated voltage signal is directly proportional to the rotational speed of the proportioning device. For a fluctuation generated with a period length of  $20\text{ s}$  both signals were overlaid and compared using an oscilloscope (see *Fig. 4-57*). No visual difference between the two signals was found.

During the start phase of the project, a generation of a sinusoidal control signal using *LabVIEW* was also taken into consideration. In this case, the weighing controller had only the function of an analog I/O-interface. This attempt was rejected because the generated signal was strongly influenced by other actions, e.g. the switching to another computer software or the movement of the computer mouse. The influence of the described actions can clearly be seen as steps in the control signal from the weighing controller to the frequency converter (see *Fig. 4-58*).

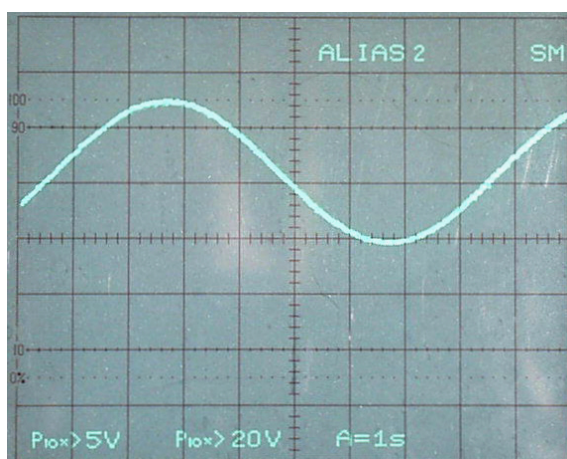


**Fig. 4-57:** Control signal from the weighing controller overlaid with the almost identical signal from the voltage generator (sinusoidal fluctuation)

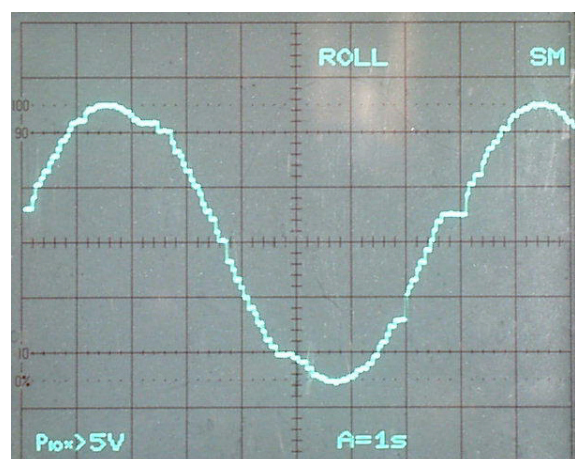


**Fig. 4-58:** Control signal from the weighing controller to the frequency converter generated with *LabVIEW* (sinusoidal fluctuation)



The generation of a rectangular fluctuation is also possible. For a rectangular fluctuation with a period length of  $20\text{ s}$ , the control signal from the weighing controller to the frequency converter overlaid with the signal from the voltage generator is shown in *Fig. 4-59*. The conformance of the two signals was excellent, too. Only a minor deviation between the two signals was observed for  $0.5\text{ s}$  when the rotational speed of the proportioning device was increased stepwise. The deviation is caused by the inertia of the feeding system.

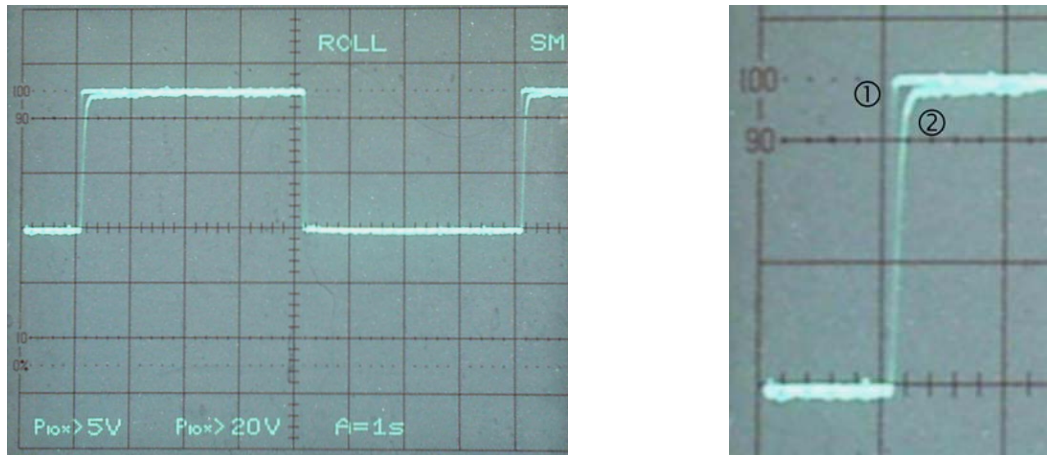


*Fig. 4-59: Control signal from the weighing controller to the frequency converter ① overlaid with the signal from the voltage generator ② (rectangular fluctuation)*

#### 4.3.4 Comparison between the generated mass flow fluctuations and the measured ones

In the last chapter, it was shown that generated sinusoidally fluctuating control signals can be transferred directly in a sinusoidal changing of the rotational speed of the proportioning device. *Fig. 4-60* shows an exemplary comparison between a generated sinusoidally fluctuating control signal generated and calcium carbonate mass flow fluctuations measured. The generated mass fluctuation had a period length of  $20\text{ s}$  and showed a very good conformance with the generated signal. A period length of  $20\text{ s}$  is the shortest period length used during the mixing experiments described later. Fluctuations with longer period lengths are easier to generate than shorter ones. Therefore, a good conformance between the generated mass flow fluctuations and the measured mass flow fluctuations was also expected for higher period lengths.

In addition to the graphical comparison, *Table 4-3*, *Table 4-4* and *Table 4-5* contain a tabular comparison. For varying period lengths, amplitudes and average mass flows the standard deviation of the generated mass flow fluctuation was compared with the standard deviation of the measured mass flows. Each standard deviation results from three measurements with 2 200 determined mass flow values each. In addition, the corresponding standard deviations for a constant feeding are listed in *Table 4-5*. Considering that the standard deviation for constant feeding was about  $0.7\text{ g/s}$  the standard deviations of the measured mass flow fluctuations correspond very well with the standard deviations of the generated fluctuations.

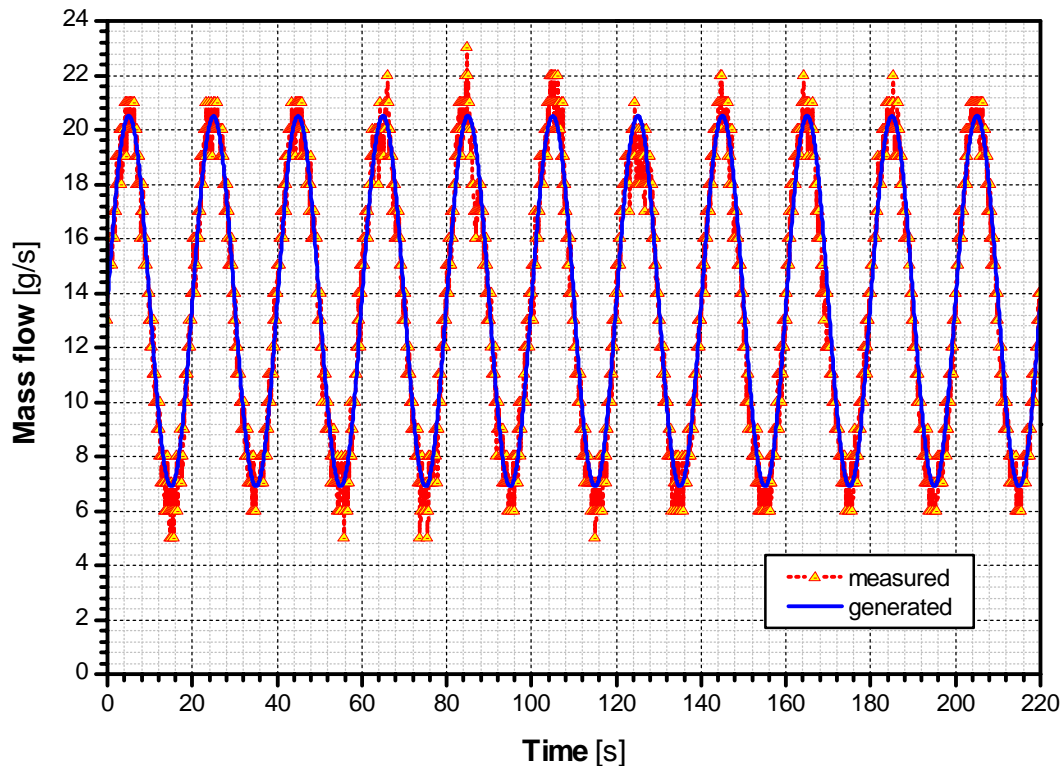


**Fig. 4-60:** Comparison between the generated mass flow fluctuations and the measured mass flow fluctuations (spiral, rotating star attachment ( $n \approx 330 \text{ min}^{-1}$ , clockwise), calcium carbonate,  $\bar{m}_{set} = 13.6 \text{ g/s}$ ,  $A = 6.8 \text{ g/s}$ ,  $T = 20 \text{ s}$ )

**Table 4-3:** Comparison between the ideal mass flow fluctuations and the generated mass flow fluctuations: Varying amplitude, constant average mass flow and period length, spiral, rotating star attachment ( $n \approx 330 \text{ min}^{-1}$ , clockwise), calcium carbonate

amplitude [g/s]	average mass flow [g/s]	period length [s]	standard deviation of the ideal mass flow [g/s]	standard deviation of the measured mass flow [g/s]
3.4	13.6	20	2.4	$2.5 \pm 0.06$
6.8	13.6	20	4.8	$5.0 \pm 0.30$
10.2	13.6	20	7.2	$7.3 \pm 0.06$

**Table 4-4:** Comparison between the ideal mass flow fluctuations and the generated mass flow fluctuations: Varying period length, constant average mass flow and amplitude, spiral, rotating star attachment ( $n \approx 330 \text{ min}^{-1}$ , clockwise), calcium carbonate

period length [s]	average mass flow [g/s]	amplitude [g/s]	standard deviation of the ideal mass flow [g/s]	standard deviation of the measured mass flow [g/s]
10	13.6	6.8	4.8	$4.8 \pm 0.24$
20	13.6	6.8	4.8	$5.0 \pm 0.30$
60	13.6	6.8	4.8	$4.9 \pm 0.08$

**Table 4-5:** Comparison between the ideal mass flow fluctuations and the generated mass flow fluctuations: Varying average mass flow and amplitude, constant period length, rotating star attachment ( $n \approx 330 \text{ min}^{-1}$ , clockwise), calcium carbonate

proportioning device	average mass flow [g/s]	amplitude [g/s]	period length [s]	standard deviation of the ideal mass flow [g/s]	standard deviation of the measured mass flow [g/s]
spiral	6.8	5.6	20	4.0	$4.2 \pm 0.12$
	20.4				$3.4 \pm 0.30$
spiral	6.8	0	-	0	$0.63 \pm 0.04$
	20.4				$0.73 \pm 0.08$
screw	6.8	5.6	20	4.0	$4.2 \pm 0.30$
	20.4				$3.9 \pm 0.08$
screw	6.8	0	-	0	$0.69 \pm 0.13$
	20.4				$0.65 \pm 0.07$

#### 4.4 In-line determination of the concentration in the outlet of the continuous mixer

For assessing the performance of powder mixing systems, the monitoring of the mixture and the determination of the mixing quality is necessary. The determination of the mixing quality requires the analysis of a huge number of samples. As the manual sampling and the preparation of samples is very time-consuming, an in-process measurement had to be found. In-process analysis techniques can be subdivided in on-line and in-line techniques. Because these two terms are used in different ways, a definition for the use in the context of this thesis and a demarcation to the terms off-line and at-line follows. These definitions are based on the definitions given by SIESLER [112].

- *Off-line analysis:* The samples are taken manually and transported to an analysis device located outside the production area.
- *At-line analysis:* The samples are taken manually and transported to an analysis device located inside the production area.
- *On-line analysis:* The samples are taken and transported automatically to the analysis device. An example is the in-line measurement in a bypass of the production line.
- *In-line analysis:* The probe of the analysis device is integrated in the production line.

Different off-line and in-line analyzing techniques to examine and assess the performance of powder mixers were published for example by SCHOFIELD [113], COOPER [114], CLEVETT [115], KAYE [16], SEGONNE et al. [116], BERNTSSON [117] as well as KEHLENBECK and SOMMER [118]. Following, analyzing techniques, which have already been used for the in-line determination of the mixing quality or the assessing of mixers, are shortly introduced and discussed. The examples are limited to techniques analyzing powdery or granular mass flows coming out of gravity mixers, continuous mixers or static mixers.

#### 4.4.1 Radiometric analysis techniques

MERZ and LÜCKE [26, 48], LETHOLA and KUOPPAMÄKI [119], THÝN [120] as well as HOLZMÜLLER [4] used radioactive tracers to study the residence time behavior of bulk material in different continuous dynamic and silo mixers as well as to determine the performance of these mixers. For the in-line concentration determination of radioactive tracers, scintillation detectors were installed along the longitudinal axis and/or in the outlet of the mixers. The radiation of the tracer penetrates through the bulk material as well as the mixer shell. Therefore, the measured radiation intensity characterizes a cross section of the mixer or the mixer outlet. Radiometric analysis techniques have the disadvantage that radioactive tracers are used, which require the compliance of very strict radiation protection regulations.

#### 4.4.2 Image analysis techniques

DAU et al. [121, 122], EICHLER [23], HABERMANN and PAHL [74] as well as MUERZA et al. [21] used a Charge-Coupled Device (CCD) camera to record and digitalize photos of bulk material flowing out of a silo mixer, a continuous dynamic mixer and a static mixer respectively. An image analysis programme allows the evaluation of the digital photos according to gray scale or colorimetric value differences. By means of a calibration, the color values can be associated to different concentrations of the tracer material. This analysis technique has the disadvantage that bulk materials of significantly different color (e.g. black and white) have to be used. Especially for the case that fine powders are examined, the concentration range of the dark tracer particles is limited to low concentrations. In addition, a lot of attention has to be paid to the illumination of the powder stream and the calibration of the image analysis system.

#### 4.4.3 Capacitance analysis techniques

EHRHARDT et al. [123] assessed the homogeneity of powder mixtures by using a capacitance method, which allows measuring permittivity changes of mixtures. The permittivity of the tracer has to differ significantly from the permittivity of the other bulk materials in the mixture. In addition, the mass flow of the bulk material has to be very constant.

#### 4.4.4 Photometric reflection analysis techniques

Different bulk materials have different reflection characteristics. The differences can be caused by different particle sizes or shapes as well as a different molecular composition. Illuminating the bulk material, the amount of the reflected light/radiation depends on the composition of the bulk material. This property can be used to assess powder mixtures. WEINEKÖTTER [50, 124] and STALDER [125] used the same laser device with a wavelength of  $514\text{ nm}$  for assessing the mixing quality of powder mixtures flowing out of a continuous dynamic powder mixer. EICHSTÄDT [126] developed a probe with Infrared Light Emitting Diodes (IR LED) to study the mixing process in a fluid mixer. The emitted light had an average wavelength of  $960\text{ nm}$ . Both techniques have the disadvantage that tracers of different color have to be used and that the concentration range of the tracer is limited.

#### 4.4.5 In-line concentration determination by Fourier Transformation Near-Infrared (FT-NIR) spectroscopy

The intention of this thesis is not only to contribute to the description and examination of the mixing mechanisms in continuous powder mixers, which is more an academic interest, but also to improve the design, the operation and the control of continuous powder mixers, which is more an industrial interest. Therefore, the selection of an analyzing technique for the validation of the developed mixing model was orientated on its applicability in a wide range of industrial mixing processes.

Different research groups have shown that radiometric, image analysis, capacitive and photometric reflection analysis techniques are suitable to study the continuous mixing process of powders. However, the techniques introduced have the disadvantage that radioactive tracers are used, powders of different colors are necessary, the tracer concentration range is limited or a constant mass flow is necessary. Therefore, the applicability of these techniques for the optimization or control of production processes is limited. An analyzing technique, which does not have the mentioned disadvantages, is the Near-Infrared (NIR) spectroscopy. Near-infrared spectroscopy is also a photometric analysis technique but it uses a wide range of different wavelengths in the NIR spectra and not merely a single wavelength as the mentioned photometric analysis techniques.

The potential of the NIR spectroscopy shows the so-called Process Analytical Technology (PAT) Initiative. This initiative was launched by the *U. S. Food and Drug Administration (FDA)* in 2001 to improve the manufacturing of pharmaceutical products. The initiative mainly concentrates on the use of NIR spectroscopy for the in-line analysis of critical quality parameters and performance attributes in pharmaceutical manufacturing processes. [127, 128]

Near-infrared spectroscopy is a comparatively new analyzing technique, which has its origin in the experimental work of the astronomer WILLIAM HERSCHEL. In the year 1800, HERSCHEL analyzed the spectrum of sunlight. Using a glass prism, he split the sun light in its spectral colors. With a thermometer, which bulb was wrapped in black paper, he measured the heating ability of each color. The determined temperature increase was astonishing small compared to the increase resulting from the pure sunlight. When HERSCHEL went for a meal, he put the thermometer on the table just outside the red band of the split spectrum. Coming back, he noticed a high increase of the temperature. He concluded that there is a different kind of light beyond (in Latin: infra) the red part of the spectrum, which is invisible to the human eye. This kind of light became known as “infrared” light. HERSCHEL’s work fell in the oblivion until the end of the 19<sup>th</sup> century when other researchers started with new experimental work. [129]

A classification of the infrared radiation in the electro-magnetic spectrum is shown in *Fig. 4-61*. Electro-magnetic radiation with a wavelength between  $0.75$  and  $500\ \mu\text{m}$  is called infrared radiation. This region is followed by micro waves (longer wavelengths) and the visible light (smaller wavelengths). The infrared region is subdivided in far-infrared, middle-infrared and near-infrared radiation. The NIR light has wavelengths between  $750$  and  $2\ 500\ \text{nm}$ .

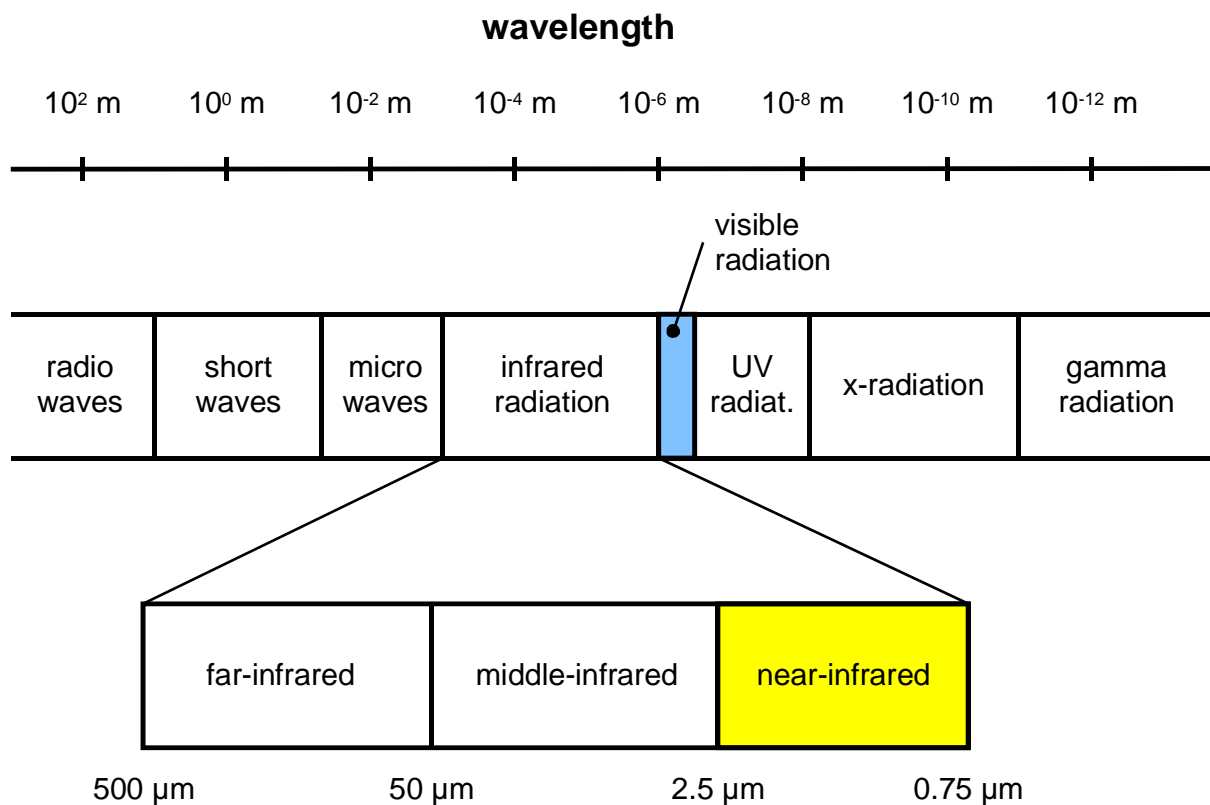


*Fig. 4-61: Classification of the near-infrared radiation in the electro-magnetic spectrum [130]*

FT-NIR Spectroscopy is based on the absorption of near-infrared light by substances to be measured. The absorbed light causes vibrations of covalent bonds between atoms. In *Fig. 4-62*, different vibration types are shown for a water molecule. A change of the bonding angle is called a deformation vibration. A deformation along the bond of two atoms is called a stretch vibration, which can be symmetrical or unsymmetrical [130, 131].

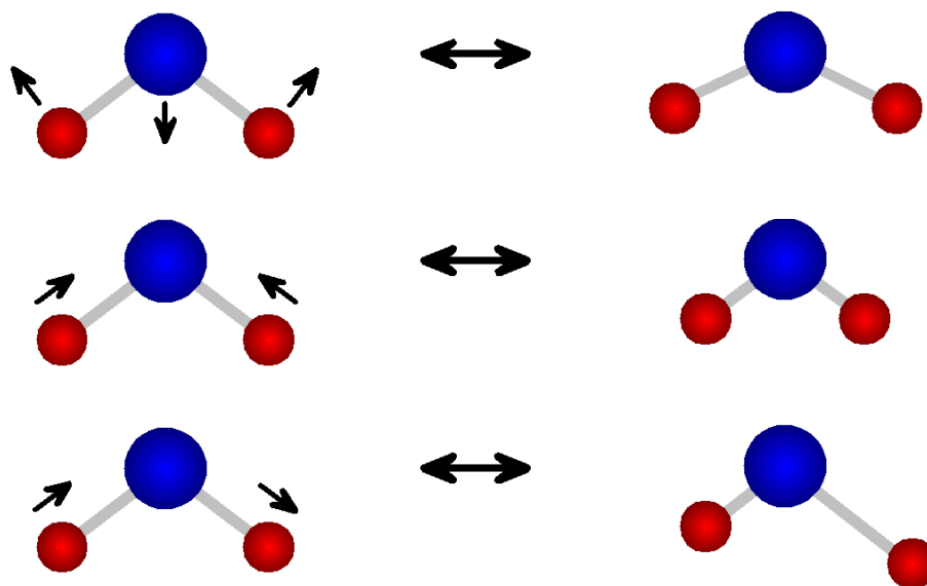


*Fig. 4-62: Illustration of possible vibrations of a three atomic molecule, e.g. water  $H_2O$  (top: deformation vibration, middle: symmetrical stretch vibration, bottom: unsymmetrical stretch vibration) [130]*

In order to use near-infrared spectroscopy for the qualitative or quantitative analysis of powder mixtures, the tracer component in the mixture has to contain C-H-, N-H- and O-H-groups. These molecule parts are found in all organic materials and absorb the NIR radiation. In this thesis, calcium carbonate and maize starch powder were used for the experimental validation of the developed mixing model. Calcium carbonate is an inorganic salt. Pure calcium carbonate does not absorb NIR light because of missing C-H-, N-H- and O-H-groups. Impurities and small amounts of water in the calcium carbonate can absorb small amounts of NIR light and thus effect the measurements. The organic maize starch is the active component (the tracer component) in the mixtures examined. Maize starch absorbs a high amount of NIR light. In *Table 4-6*, the absorption wavelengths as well as the corresponding bond vibration are listed for starch and water.



**Table 4-6:** Chemical assignments of some near-infrared absorption bands of starch and water [131]

wavelength [nm]	bond vibration	structure
760	O-H stretch vibration	water
970	O-H stretch vibration	water
990	O-H stretch vibration	starch
1 450	O-H stretch vibration	starch, water
1 528	O-H stretch vibration	starch
1 540	O-H stretch vibration	starch
1 580	O-H stretch vibration	starch
1 900	O-H stretch vibration, 2 · C-O stretch vibration	starch
1 940	O-H stretch vibration, O-H deformation vibration	water
2 000	2 · O-H deformation vibration, C-O deformation vibration	starch
2 100	2 · O-H deformation vibration, 2 · C-O stretch vibration	starch
2 252	O-H stretch vibration, O-H deformation vibration	starch
2 276	O-H stretch vibration, C-C stretch vibration	starch
2 461	C-H stretch vibration, C-C stretch vibration	starch
2 488	C-H stretch vibration, C-C stretch vibration	starch
2 500	C-H stretch vibration, C-C stretch vibration	starch

For this research project, the company *Bruker Optik GmbH* (Ettlingen, Germany) made the Fourier Transform Near-Infrared (FT-NIR) spectrometer *VECTOR 22/N* available (see *Fig. 4-63*). The system consists of the spectrometer itself and a probe. The probe is an extended fiber optic sampling probe of the type *IN 263E*. The probe has a diameter of *14 mm* and a length of *300 mm*. By means of a glass fiber bundle the probe is connected to the spectrometer. The main components of the spectrometer are a lamp for the generation of NIR light, a modified Michelson-Interferometer, which modulates the NIR light, and a detector for the reflected light.



**Fig. 4-63:** FT-NIR spectrometer VECTOR 22/N from the company Bruker Optik GmbH (① spectrometer, ② probe, ③ glass fiber cable)

The construction of the probe is illustrated in *Fig. 4-64*. The probe consists of fibers, which guide NIR light from the source to the sample. Each fiber has a diameter of  $0.2\text{ mm}$ . The NIR light interacts with the powder sample and a fraction is reflected diffusively. A certain amount of the reflected NIR light is collected by separate optical fibers, which guide the light to a detector in the spectrometer. The fibers for the light supply and for the reflected light end at the tip of the probe (see *Fig. 4-64*, right). The area of the optical fibers has a diameter of about  $3\text{ mm}$  and defines the analyzing area of the powder.

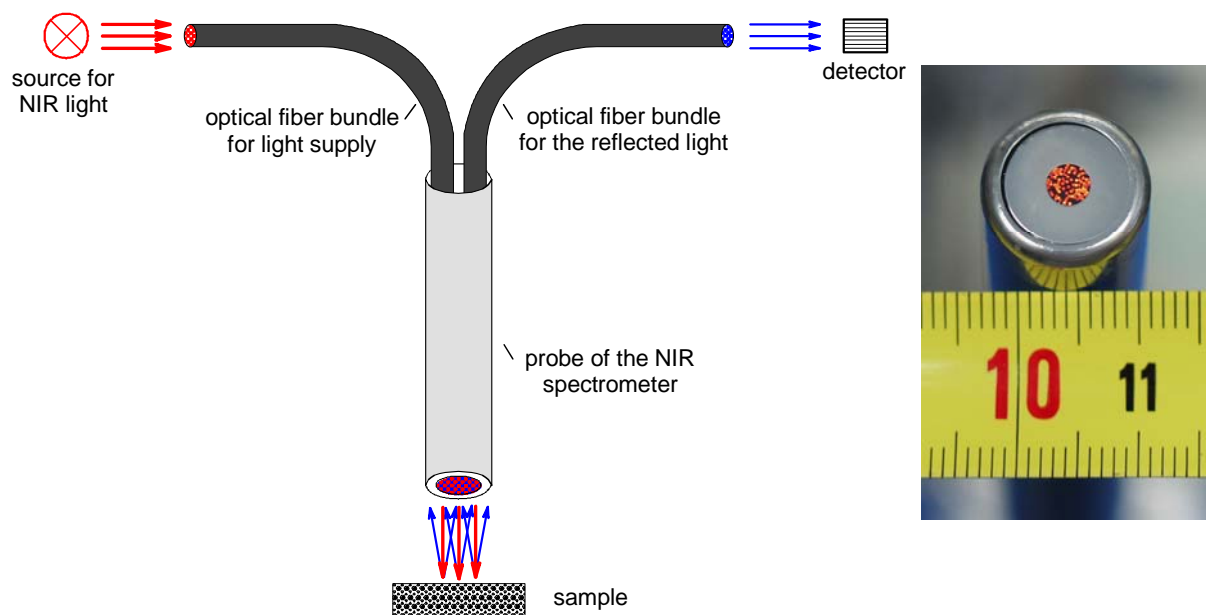


**Fig. 4-64:** Illustration of the probe assembly (left), probe tip of the FT-NIR spectrometer (right)

The main component of a FT-NIR spectrometer is a Michelson interferometer, which modulates the NIR light. The principle construction is shown in *Fig. 4-65*. NIR light with different wavelengths  $\lambda$  is emitted from a radiation source. The light hits a beam splitter after passing a lens. Ideally, 50 % of the light passes the beam splitter and hit a movable mirror. The other 50 % of the beam are reflected in the direction of a fixed mirror. The two partial beams are reflected at the mirrors, hit the beam splitter again, recombine and interfere in the direction of the sample. The partial beam, coming from the fixed mirror, has a total path length of  $2 \cdot l$ . The movable mirror changes its position in backward and forward direction. With the moving distance  $x$ , the total path length of the second partial beam is  $2 \cdot (l + x)$ . The two recombined partial beams have a phase difference of  $2 \cdot x$ . Considering the monochromatic components of the beam with the wavelength  $\lambda$ , a destructive interference will occur, if the phase difference  $2 \cdot x$  is an integer multiple  $i$  of the half wavelength:

$$2 \cdot x = i \cdot \frac{\lambda}{2} \quad \text{with } i = 0, 1, 2, 3, \dots \quad \text{Eq. 4-8}$$

The maximum intensity of the recombined beams occurs, if the phase difference is an integer multiple of the wavelength. The interfered beams and the modulated NIR light respectively hit the sample after passing a second lens. Interactions between the particles in the sample and the NIR light take place. A part of the light is absorbed and the rest is reflected diffusively. In dependence on the distance  $x$ , the intensity  $I(x)$  of the reflected light can be measured by a detector.  $I(x)$  is called the interferogram. For technical reasons, the interferogram is not measured continuously but pointwise. A helium/neon laser with a wavelength of  $633 \text{ nm}$  is used as trigger signal for data recording. The laser light is guided through the Michelson interferometer, too. A separate detector determines the interferogram of the laser. Only when the interferogram of the laser passes zero, data points from the NIR interferogram are recorded. This procedure is shown in *Fig. 4-66*. The interferogram of the NIR light is shown at the top and the laser interferogram at the bottom. [112, 130, 132, 133, 134]

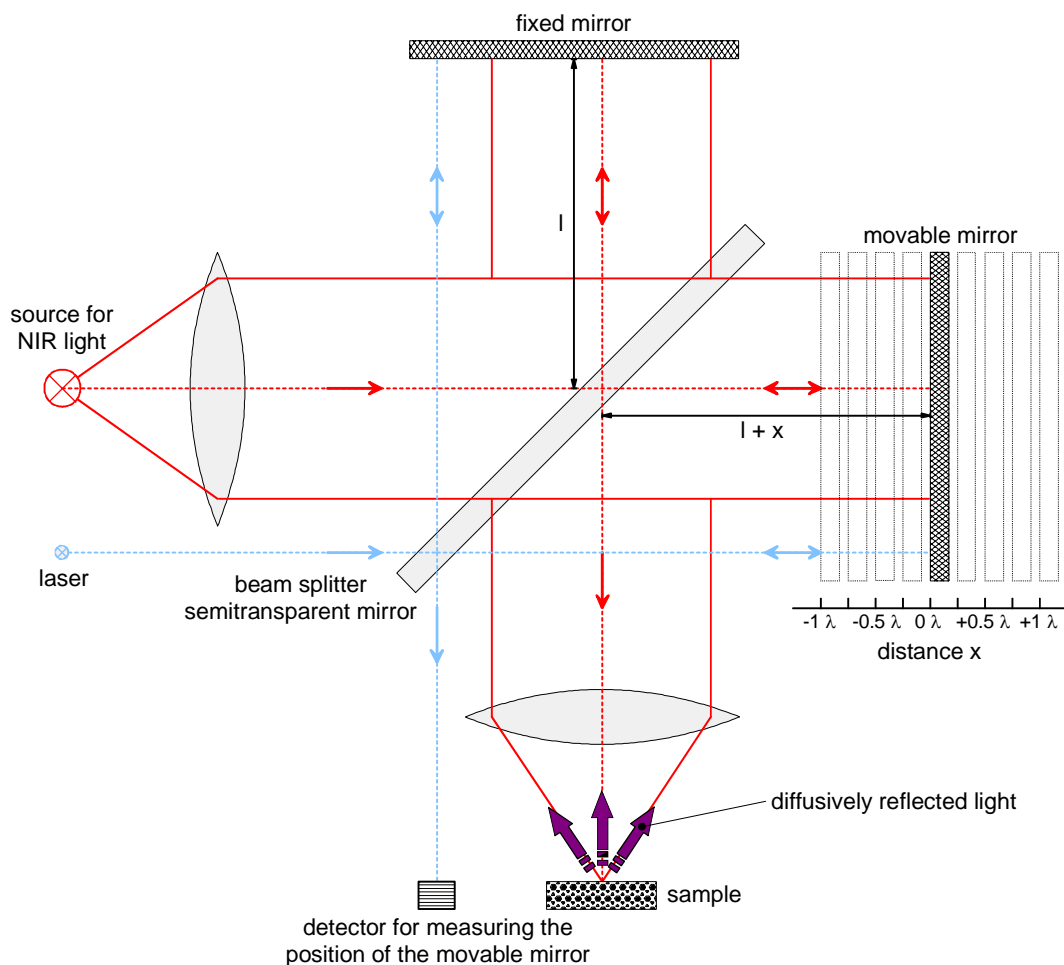


**Fig. 4-65:** Schematic illustration of the NIR light modulation by means of a Michelson interferometer [112, 132 133, 134]

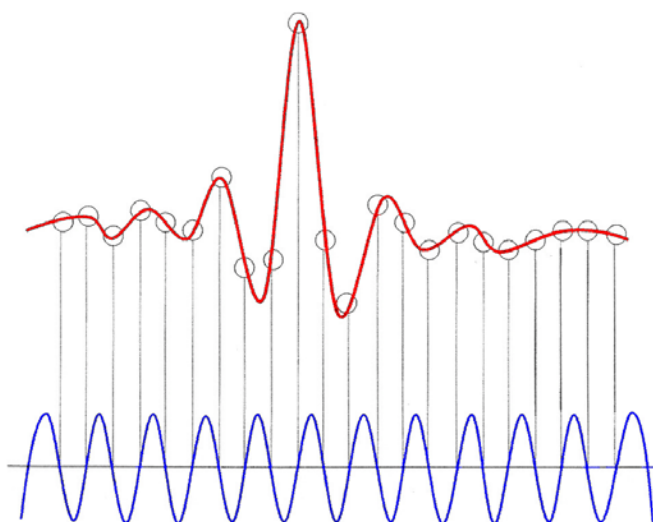


**Fig. 4-66:** Interferogram of a He/Ne laser (bottom) used to trigger the data recording of a NIR interferogram (top) [130]<sup>3</sup>

<sup>3</sup> Reprinted with permission from Wiley-VCH Verlag GmbH & Co KG

By means of Fourier transformation the NIR Spectra  $S(\nu)$  can be extracted from the interferogram.  $\nu$  is the wave number, which is the reciprocal value of the wavelength  $\lambda$ . **Fig. 4-67** shows some examples to illustrate the procedure. On the left-hand side, different interferograms are shown. On the right-hand side, the corresponding single-channel spectrum resulting from the Fourier transformation of the interferogram are shown. Interferogram a) is a periodical wave with one wavelength. In the corresponding spectra, only a single peak arises at the reciprocal value of the wavelength. The height of the peak corresponds to the amplitude of the periodical wave. Interferogram b) shows an interferogram of two overlaid periodical waves with slightly different wavelengths. The interferograms c) and d) consist of several overlaid periodical waves with different wavelengths.

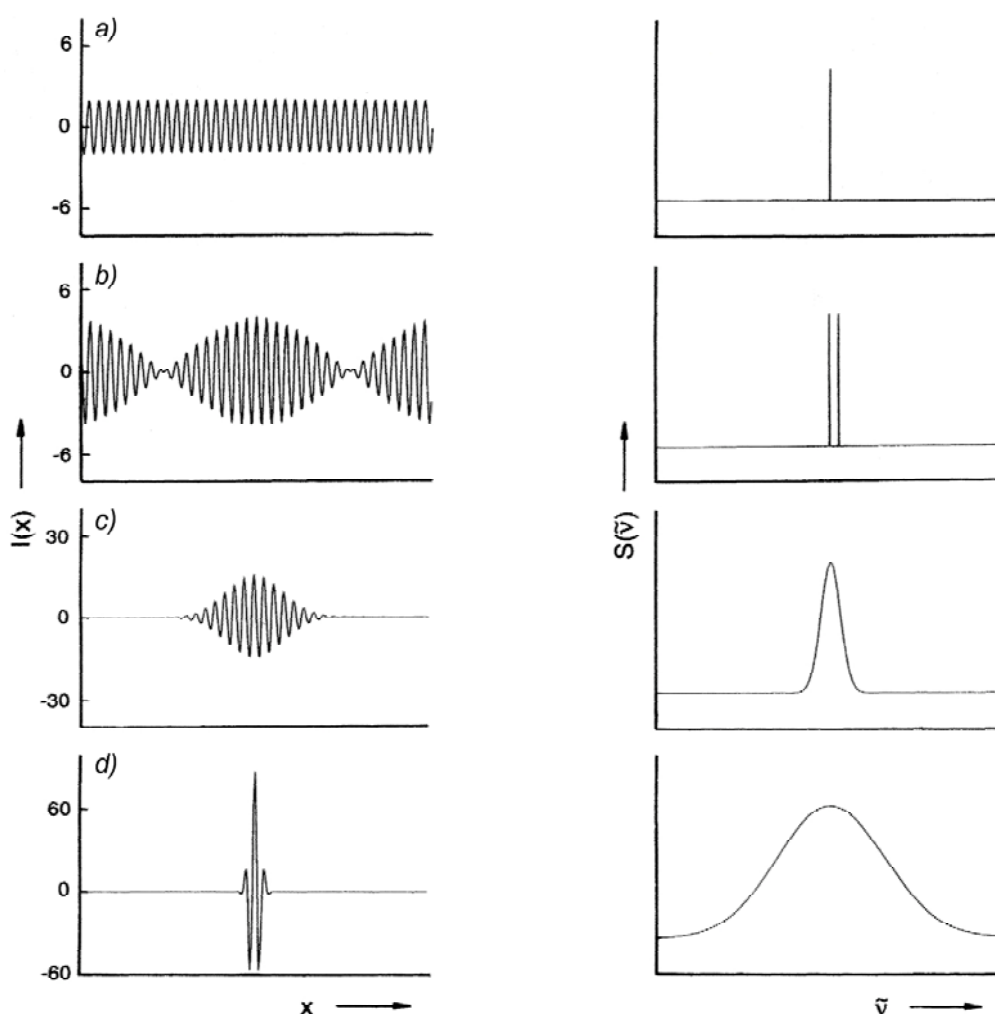


**Fig. 4-67:** Double-sided interferograms (left) and corresponding spectra obtained after a Fourier transformation (right): a) monochromatic radiation, b) two narrow-band emission lines, c) band-pass filtered thermal radiation and d) broadband thermal radiation [132]<sup>4</sup>

In **Fig. 4-68**, the measured interferograms using the powders calcium carbonate and maize starch as well as the reference material Spektralon are shown. In **Fig. 4-69**, the corresponding single-channel spectrum is shown. To reduce the influence of ambient conditions (temperature

<sup>4</sup> Reprinted with permission from Wiley-VCH Verlag GmbH & Co KG

and humidity) on the analysis result, an interferogram and a single-channel spectrum of the reference material are measured once a day, stored afterwards and taken into account during the following measurements.

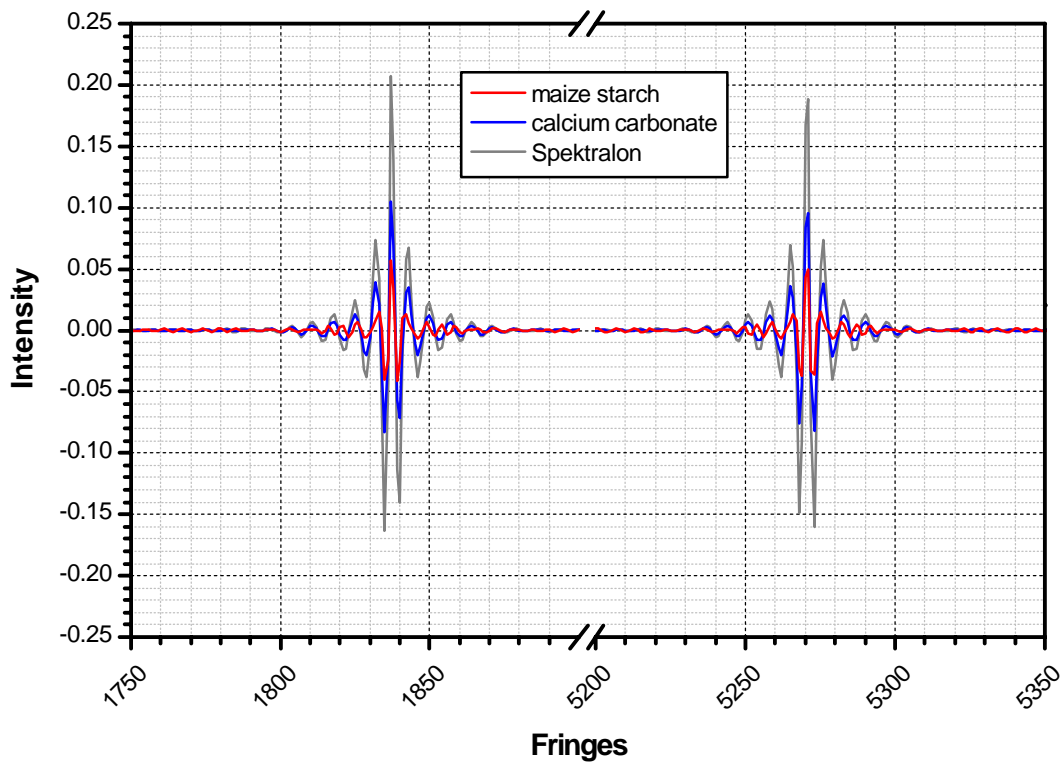


Fig. 4-68: Interferogram of maize starch, calcium carbonate and Spektralon

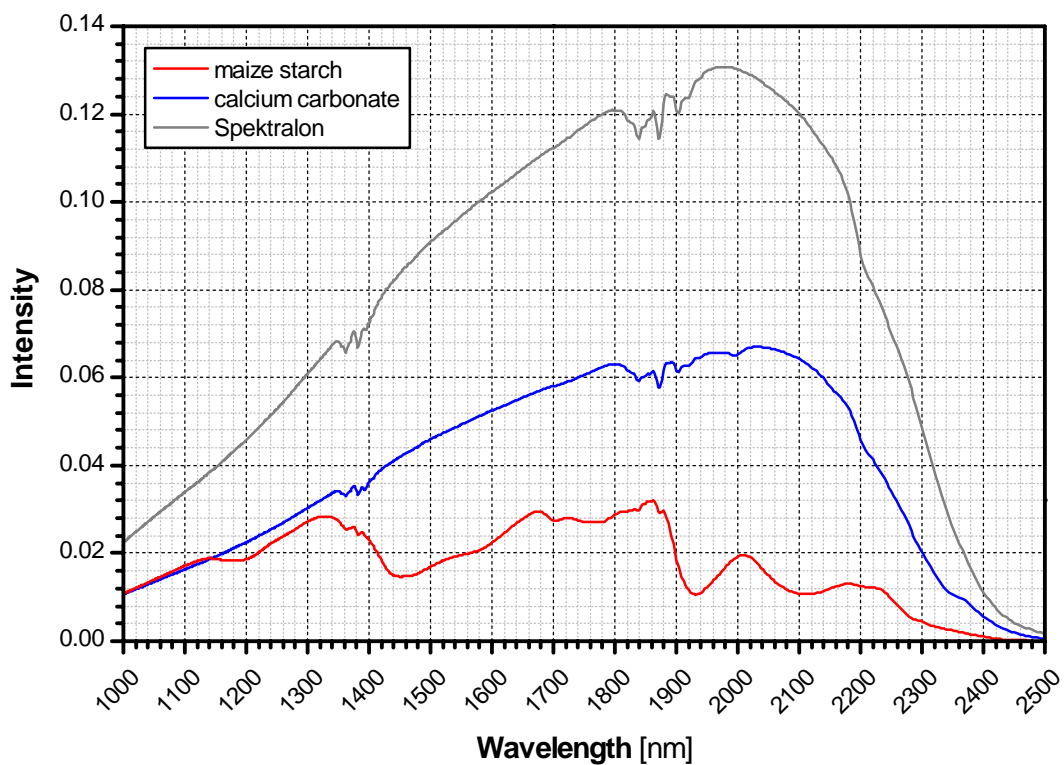


Fig. 4-69: Single-channel spectrum of maize starch, calcium carbonate and Spektralon

Working with reflection probes, FT-NIR spectroscopy spectra are typically presented in absorbance units  $AU$  plotted against the wavelength. The wavelength-dependent absorbance unit  $AU(\lambda)$  can be calculated with *Eq. 4-9*.

$$AU(\lambda) = -\log \frac{I_{sample}(\lambda)}{I_{reference}(\lambda)} \quad \text{Eq. 4-9}$$

$I_{sample}(\lambda)$  is the intensity of the NIR light reflected from the analyzed sample.  $I_{reference}(\lambda)$  is the intensity of the NIR light reflected from the reference material Spektralon.

For the single channel spectrum of calcium carbonate and maize starch (compare *Fig. 4-69*), the corresponding absorbance spectra are shown in *Fig. 4-70*.

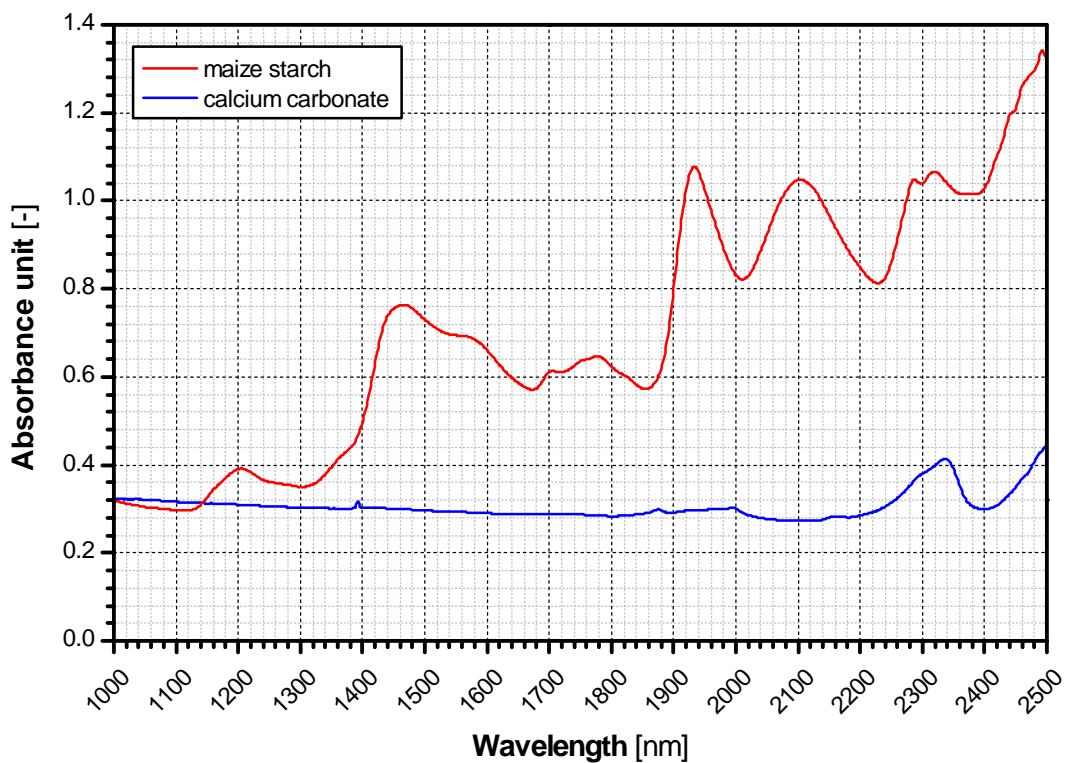


*Fig. 4-70: Absorbance spectra of calcium carbonate and maize starch*

In *Fig. 4-71*, the absorption spectra of different maize starch / calcium carbonate mixtures are shown. The maize starch concentration was varied in steps of 20 mass-%. The influence of the tracer concentration on the style of the spectra is often more obvious if the obtained spectra are manipulated (e.g. form the first or second derivative, eliminate a constant offset). In *Fig. 4-72*, the first derivative of the spectra shown in *Fig. 4-71* is presented.



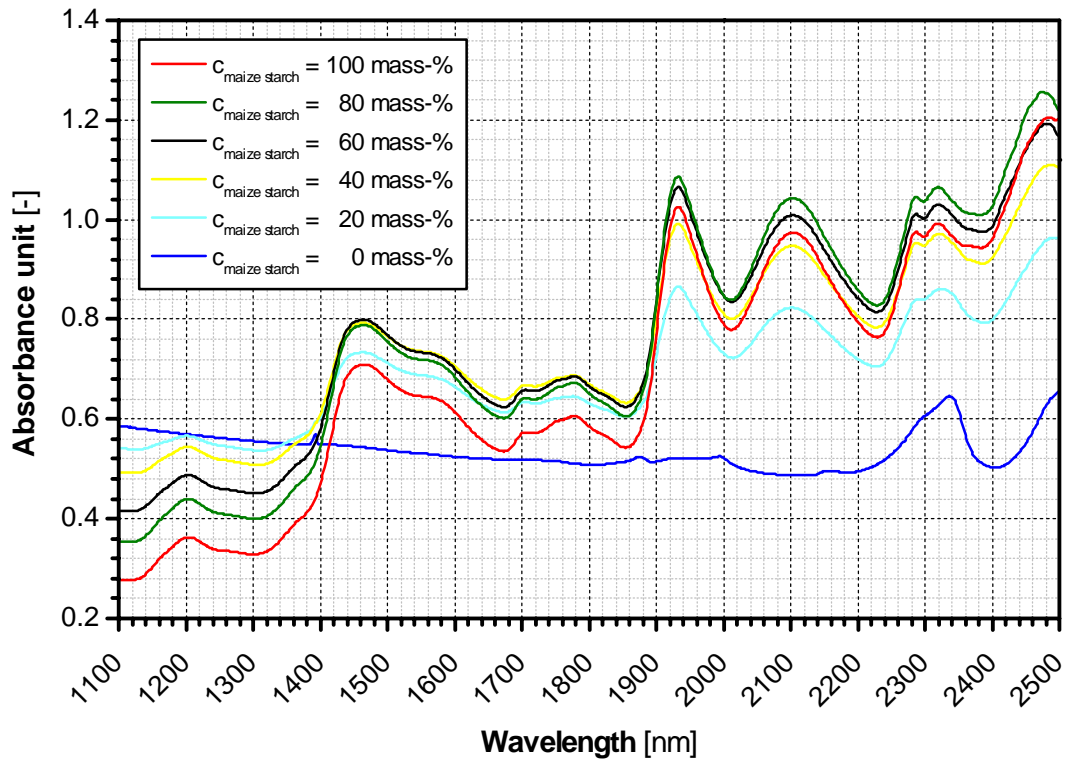


Fig. 4-71: NIR spectra of calcium carbonate / maize starch mixtures (variation of the maize starch concentration)

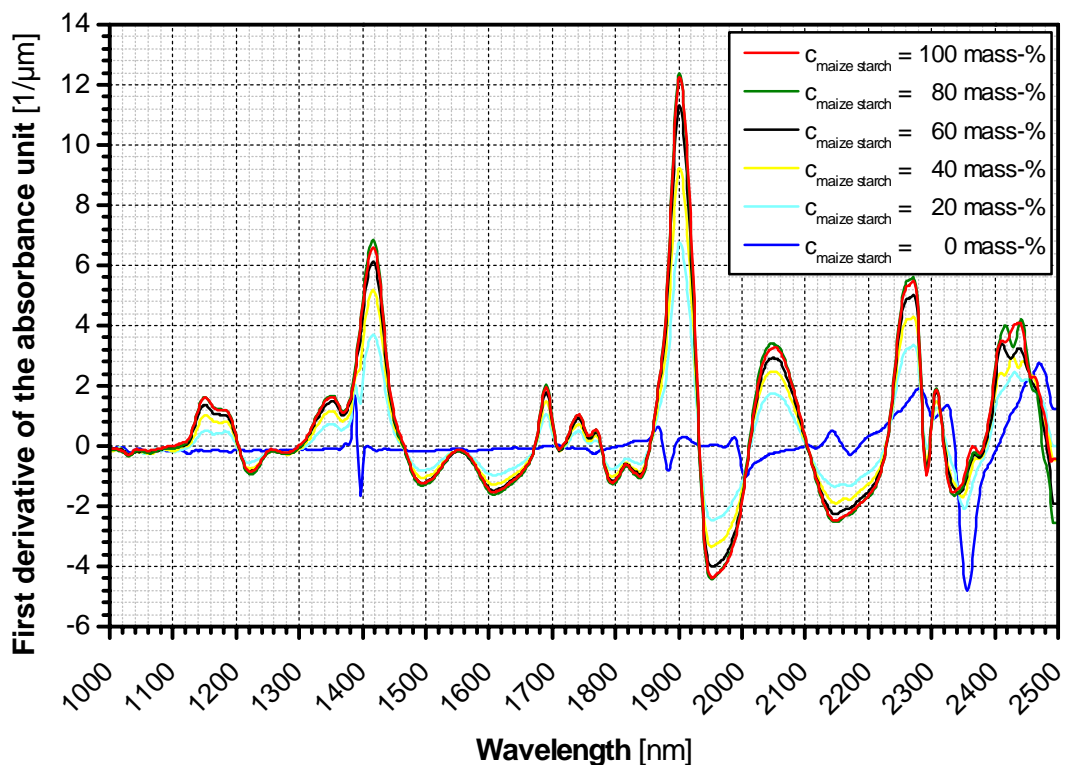
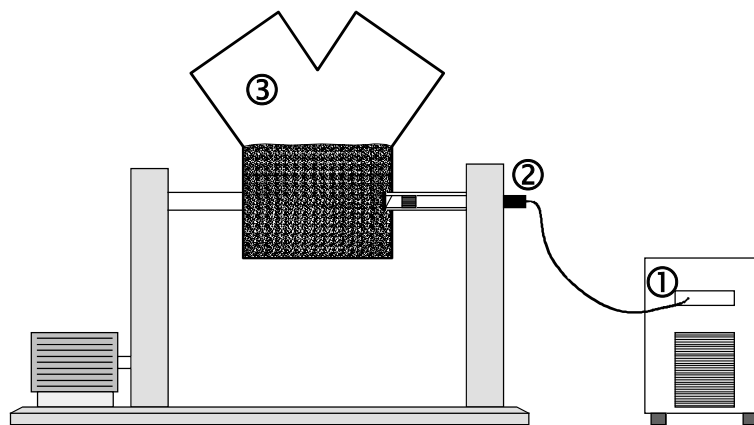


Fig. 4-72: NIR spectra of calcium carbonate / maize starch mixtures (first derivative of the spectra shown in Fig. 4-71)

#### 4.4.5.1 Existing applications for the in-line concentration determination of powder mixtures

FT-NIR spectroscopy has already been used in many industries for the qualitative and quantitative on-line and in-line analysis of gases, fluids, solids and suspensions. An overview about the wide application range of near-infrared spectroscopy is given by WORKMAN et al. [135]. Their review covers articles published in the period 1994 to 1998. The review gives an overview about applications in the fields of e.g. beverage production, biotechnology, chemical production, earth science, food production, medicine and pharmaceutical production. Only a few articles dealing with the quantitative in-line composition determination of powder mixtures in batch mixers or in pipes were published. A survey about different applications is presented below.

In 1994, ALDRIDGE applied for an European Patent protecting the in-line homogeneity detection in rotating tumbling batch mixers, e.g. V- and Y-mixer [136]. The probe of the NIR spectrometer is integrated in the axis of rotation (see *Fig. 4-73*). In the following years, the invention was used to control the mixing progress of pharmaceutical powders in V- and Y-mixers [137, 138, 139, 140, 141].



*Fig. 4-73: Determination of the mixing quality in a Y-mixer: ① NIR spectrometer, ② probe, ③ Y-mixer [138, 139, 140]*

BERNTSSON [117, 142] integrated the fiber optical probe of a NIR spectrometer in the shell of a Nauta mixer (see *Fig. 4-74*) and measured the temporal concentration changes in-line.

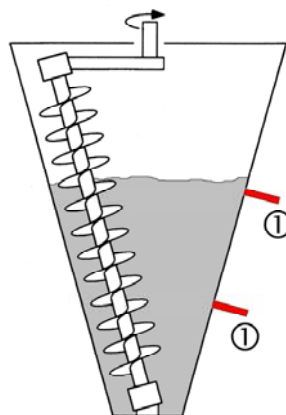


*Fig. 4-74: Determination of the mixing quality in a Nauta mixer using fiber optical probes ① [117, 142]*

Following ALDRIDGE's invention [136], the company *Carl Zeiss Jena GmbH* adapted their spectrometer to the in-line concentration determination in a Pharmatech Double Cone Blender (see *Fig. 4-75*) and in an Intermediate Bulk Container (see *Fig. 4-76*). For the measurements in the Intermediate Bulk Container, a data transfer from the NIR spectrometer to the computer was done by radio communication.

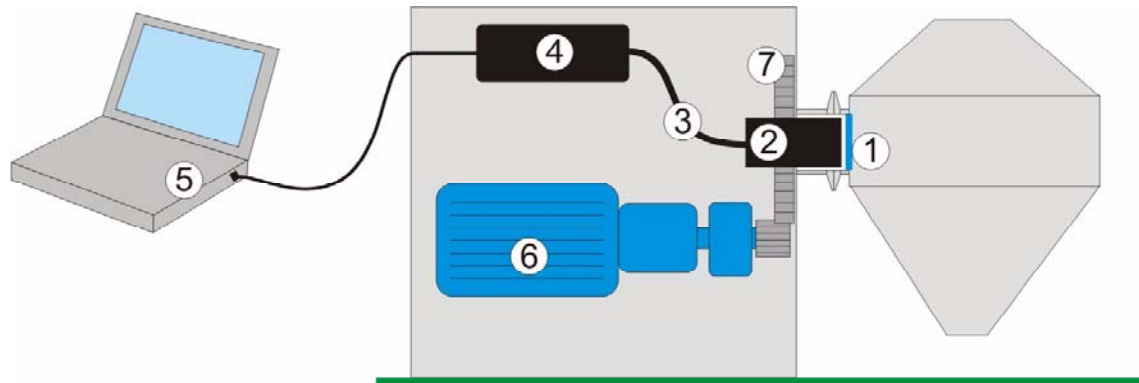


**Fig. 4-75:** Adaptation of a NIR spectrometer from the company *Carl Zeiss Jena GmbH* to the in-line determination of the mixing quality in a Pharmatech Double Cone Blender: ① sapphire window, ② diffuse reflectance measuring head OMK 500, ③ optical fiber cable, ④ spectrometer system CORONA [Courtesy of *Carl Zeiss Jena GmbH*]

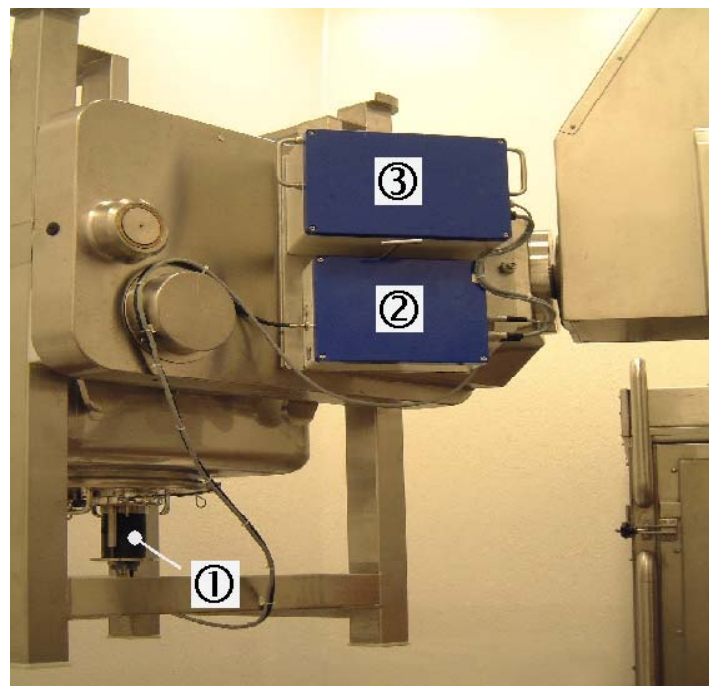


**Fig. 4-76:** Adaptation of a NIR spectrometer from the company *Carl Zeiss Jena GmbH* to the in-line determination of the mixing quality in an Intermediate Bulk Container, the data transfer from the NIR spectrometer to the computer is realized by radio communication: ① diffuse reflectance measuring head OMK 500, ② spectrometer system CORONA, ③ battery box [Courtesy of *Carl Zeiss Jena GmbH*]

SAATHOFF and HOYER invented a sample presentation unit for NIR spectrometers, which can be integrated in pipes and be used for the quantitative component determination of free-flowing bulk material [143, 144]. The sample presentation unit consists of a quadratic flow cell, which is inclined relatively to the pipe (see *Fig. 4-77*). The bulk material flows over the underside of the channel, where a sapphire window is integrated for the transmission of NIR light coming from the spectrometer mounted. A pneumatic vibrator can be switched on to clean the sapphire window.

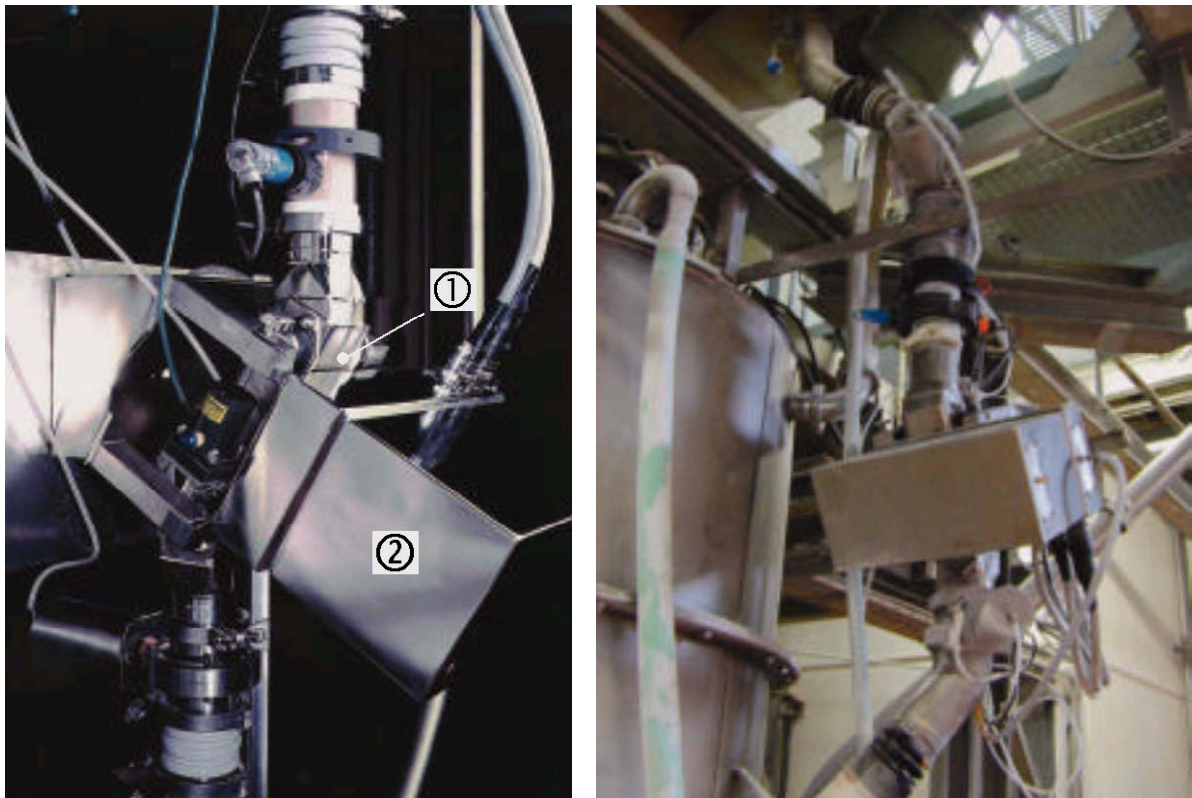


*Fig. 4-77: Analysis of free-flowing bulk material in a pipe with the InfraPowder system from the company Bran + Luebbe GmbH: ① sample presentation unit, ② NIR spectrometer [144]*

Especially for powders with a high fat content, the company *Bran + Luebbe* developed a special conveying unit [145]. The bulk material is fed below the analyzing unit (see *Fig. 4-78, Fig. 4-79*).

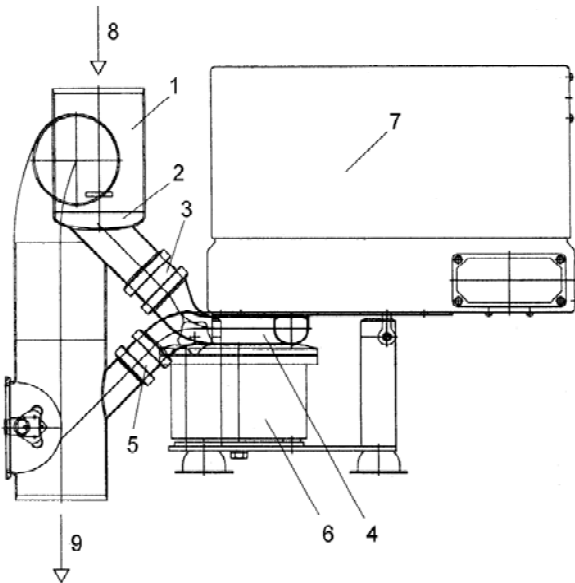


**Fig. 4-78:** Side view of the sample conveying unit from the company Bran + Luebbe GmbH [145]<sup>5</sup>: ① sample feed pipe, ② inlet funnel, ③ sample inlet, ④ sample conveyor pipe, ⑤ sample outlet, ⑥ vibrator motor, ⑦ optical module, ⑧ sample from main process stream, ⑨ bypass sample stream

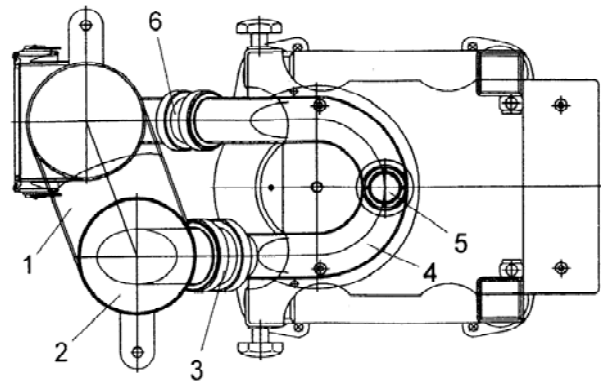


**Fig. 4-79:** Plan view of the sample conveying unit from the company Bran + Luebbe GmbH [145]<sup>5</sup>: ① sample feed pipe, ② inlet funnel, ③ sample inlet, ④ sample conveyor pipe, ⑤ sapphire window, ⑥ sample outlet

In all mentioned applications, a cleaning of the probe tip was insured by a powder movement induced by the rotation of the mixer itself, the rotation of a mixing device inside the mixer or gravity. However, the problem occurs that the powder movement can influence the analysis results [117, 146] because the porosity of the bulk material changes. Rotating mixing devices also influence the recorded spectra [117]. In front of the rotating mixing device there will be a smaller porosity than in the rear. To ensure an as good as possible calibration, the calibration should take place under the same flow regime as in the application. This would only be possible if the application mixer is used and high production costs for the calibration mixtures/samples are tolerated.

The scope of this thesis is the validation of the developed mixing model by using very cohesive powders. For this kind of powders, a layering on the NIR probe tip integrated in the mixer shell cannot be prevented by rotating mixing device. Because of production tolerances and a deformation of the rotating mixing device during the use, there has to be a gap between the rotating mixing devices and the probe tip. A powder layering at the bottom of the mixer shell up to the mixing device was observed during the mixing trials. Therefore, a different solution for the integration of the NIR probe in the mixer had to be found.

An opportunity could be a non-contact measurement, which was used for controlling the mixing of sticky bread dough [147, 148]. ALAVA et al. [147] fixed the probe of a *Perten* NIR/VIS

<sup>5</sup> Full credit acknowledgement will be given to VSP Publishers, an imprint of Brill Academic Publishers: (© VSP Publishers, an imprint of Brill Academic Publishers, Leiden, The Netherlands 1997)

spectrophotometer in the flap of a mixer (see *Fig. 4-80*). However, the surface of the dough and the distance between dough and probe change with time because of the dough movement.

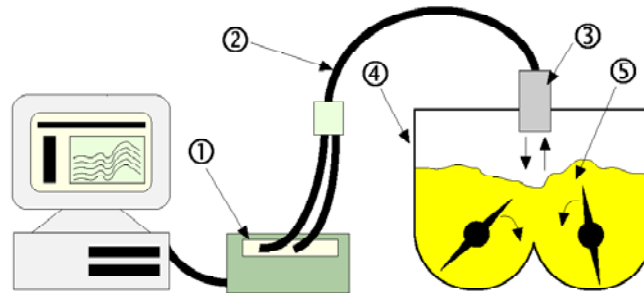


**Fig. 4-80:** Non-contact measuring method for determining the performance of wheat bread making:  
 ① Perten DA-7000 flexi-mode NIR/VIS spectrophotometer, ② fiber optic, ③ probe, ④ mixer bowl, ⑤ dough [147]<sup>6</sup>

Within the scope of this thesis, experiments for a non-contact concentration measurement with the FT-NIR spectrometer *VECTOR 22/N* were performed. The NIR probe was fixed above the conveyor belt located under the outlet of the continuous dynamic mixer (see *Fig. 4-81*). For a set mixture composition as well as different distances between the probe tip and the mixture, the concentration was measured. Because of the changing distance between the powder and the probe tip, high fluctuations of the determined concentration values were observed. To ensure a constant distance between the powder and the probe tip, a plow scraper was installed in front of the probe tip. However, the fluctuations of the determined concentration values could have been reduced only a bit. The use of a scraper has two disadvantages:

- The scraper causes a shearing of the powder, which has a mixing effect and influences the composition of the mixture [125].
- Cohesion forces cause the formation of lumps in the mixture. These lumps cause scratches in the scraped surface of the powder mixture.

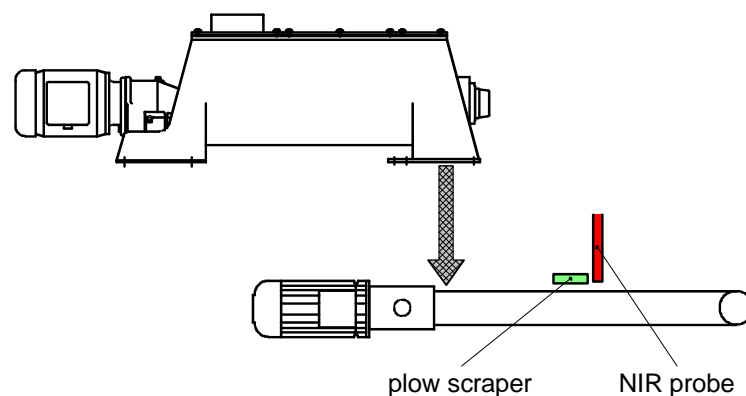


**Fig. 4-81:** Illustration of the non-contact concentration measurement within the scope of this thesis

ALAVA et al. [147] used a probe with a bigger analyzing area and a resulting bigger sample size. Therefore, the influence of a varying surface and distance is much less.

<sup>6</sup> Reprinted from [147] with permission from Elsevier Ltd



#### 4.4.5.2 Adaptation of the FT-NIR spectrometer VECTOR 22/N to the in-line concentration determination in the outlet of the continuous mixer GCM 500

In literature, no publication about the use of near-infrared spectrometers for the in-line concentration determination in the outlet of continuous mixers was found. Because of the disadvantages of already existing in-line concentration determination techniques for powder mixtures (compare the previous chapter), these techniques could not be adapted and a new one had to be developed within the scope of this thesis.

A weir is located at the end of the continuous mixer, which is used to change the filling degree of the mixer. The rotating mixing devices induce an outflow of the mixed powder over the weir. For the in-line concentration determination in the outlet of the continuous mixer, the probe of the FT-NIR spectrometer has to be positioned vertically behind the weir. A defined exchange of the powder in front of the probe tip is not ensured. Besides, the powder movement during the analysis influences the measurement. To overcome these problems LUNDSTROM's idea of a probe tip, which can be cleaned with compressed air, was refined. For sampling and measuring the characteristic of flowing granular material, LUNDSTROM developed the apparatus shown in *Fig. 4-82*. The apparatus was patented in 1979 for the United States of America [149] and in 1982 for Germany [150]. The main component of the apparatus is an air nozzle (42), which is formed in a semicircle around an analyzing window (32). A L-shaped bracket (49) is fixed under the window to accumulate bulk material in front of it.

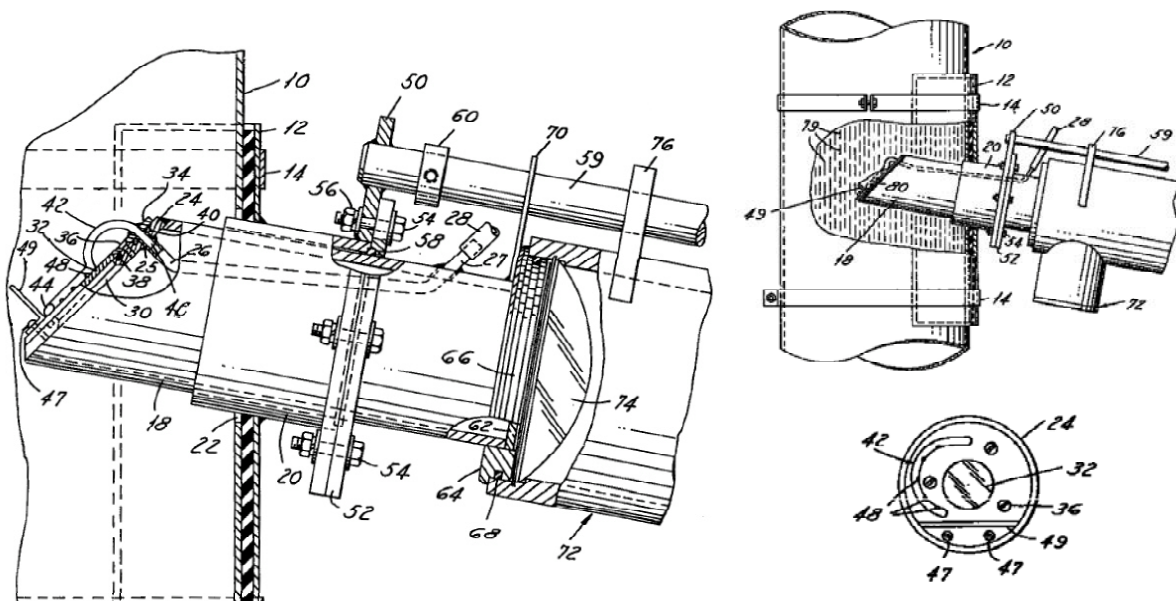


*Fig. 4-82: Apparatus for sampling and optical measuring the characteristic of flowing granular material, patented in 1979 by LUNDSTROM [149, 150]*

Following LUNDSTROM's idea, an attachment for cleaning the tip of the NIR probe with compressed air was designed (see *Fig. 4-83*). The drilled holes in the attachment allow a tangential air cleaning of the probe tip. The air inlet can be opened and closed by an electrically actuated valve, which is controlled by the spectrometer software. The attachment is fixed at the end of the NIR probe with a screw and is positioned behind the mixer weir (see *Fig. 4-84* and *Fig. 4-85*). The control software of the spectrometer is able to record NIR spectra automatically



and to clean the probe tip after each measurement. A concentration value of the mixture can be determined every 1.7 s.

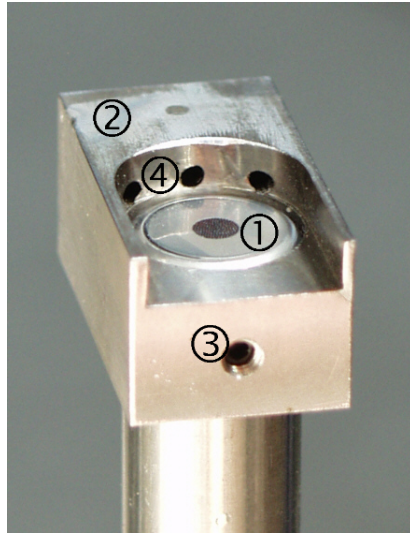


**Fig. 4-83:** Attachment for the probe of the FT-NIR spectrometer VECTOR 22/N: ① probe tip, ② attachment, ③ screw to fix the attachment on the probe, ④ drilled holes for horizontal air-cleaning

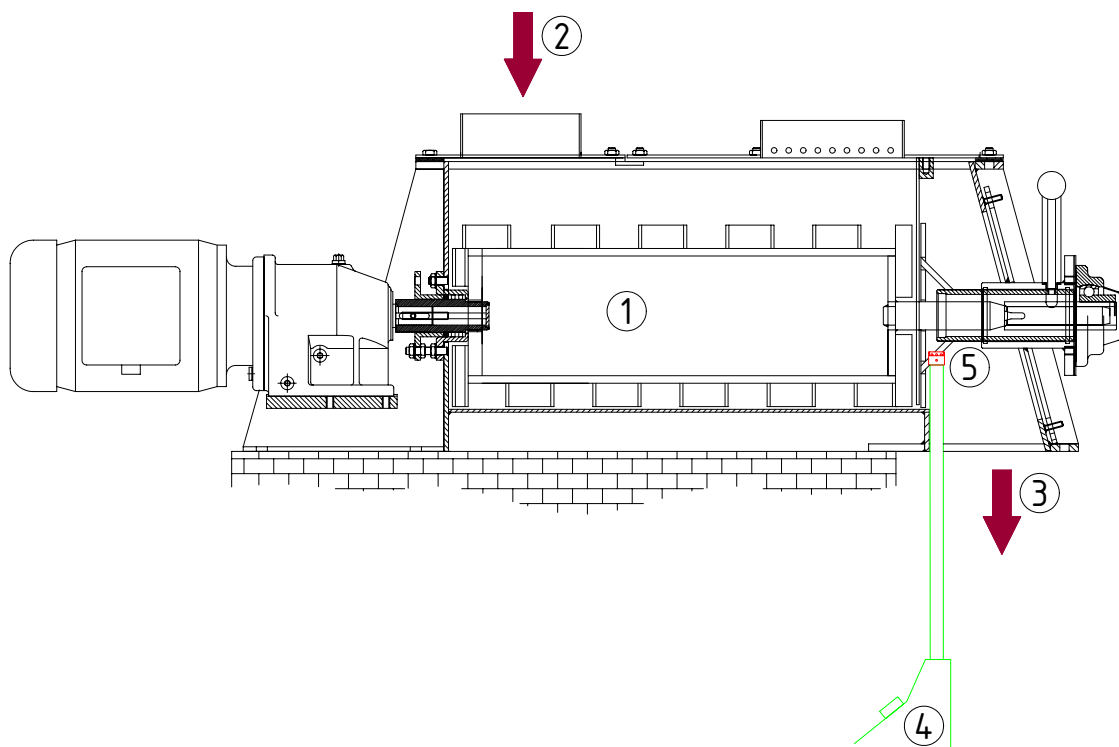


**Fig. 4-84:** In-line concentration determination in the outlet of the continuous dynamic mixer GCM 500 from the company Gericke: ① continuous mixer, ② powder inlet, ③ powder outlet, ④ probe of the FT-NIR spectrometer, ⑤ attachment for the probe of the FT-NIR spectrometer



**Fig. 4-85:** In-line concentration determination in the outlet of the continuous mixer GCM 500 from the company Gericke (left: empty mixer with ① mixing device, ② half-closed weir and ③ NIR probe with developed attachment for air-cleaning; middle: filled mixer and rotating mixing device; right: filled mixer and stopped mixing device)

After the development of the attachment shown in *Fig. 4-83*, the company *Precision Sensing Devices, Inc.* (Medfield, USA) put a NIR probe on the market that also uses compressed air for cleaning (see *Fig. 4-86*). The window, where the NIR light is transmitted, is moved back and the compressed air flows over a cone away from the window. It is assumed that a cleaning of cohesive powders is problematic because of the flow direction of the compressed air.



**Fig. 4-86:** NIR probe from the company *Precision Sensing Devices, Inc.* that uses compressed air for cleaning the probe tip (enlarged probe tip: ① window for NIR light, ② drilled holes for air-cleaning) [Courtesy of Bruker Optik GmbH]

#### 4.4.5.3 Calibration of the FT-NIR spectrometer VECTROR 22/N

The use of the FT-NIR spectrometer *VECTOR 22/N* for qualitative and quantitative analysis of powder mixtures is only possible after a calibration. In general, a calibration is carried out for making a correlation between a system characteristic  $Y$ , e.g. concentration, humidity, particle size or temperature, and a system variable  $X$ , e.g. conductivity, extinction or absorption. For the quantitative analysis of powder mixtures, a correlation between the known concentration of a tracer in the powder mixtures and the corresponding absorption spectra has to be found. The calibration of the FT-NIR spectrometer can be divided in five main steps:

1. Preparation of homogenous samples with different known tracer concentration each,
2. presentation of the samples,
3. NIR measurement of the samples,
4. finding the optimum functional correlation between the tracer concentration and the corresponding spectra,
5. validation of the developed calibration model.

Although it is known that the metering precision strongly depends on the precision of the calibration technique used [151], hardly any experimental work about the preparation and presentation of powdery samples for calibration can be found in literature. Within the scope of this thesis a lot of research work was carried out to improve the preparation and presentation of calibration samples because the analysis results can only be as exact as the previous calibration of the FT-NIR spectrometer used.

For the calibration of the FT-NIR spectrometer, a certain number of homogenous mixtures with known concentration have to be prepared. The concentration range of the calibration samples should be broader than the concentration range of the mixtures to be analyzed. The components in the mixtures should be homogenized as well as possible. Afterwards, NIR spectra of each mixture are collected and calibration models have to be developed. For the control of the FT-NIR spectrometer *VECTOR 22/N*, the development and the validation of calibration models as well as the analysis of the samples, the software *OPUS-NT* (version 3.1) from the company *Bruker Optik GmbH* was used.

#### 4.4.5.4 Analysis of calibration mixtures

For analyzing a powder sample, the probe of the FT-NIR spectrometer is commonly immersed in the powder mixture (see *Fig. 4-87*, left). Many false NIR spectra were obtained by using this method. *Fig. 4-88* shows five NIR spectra obtained by a five times measurement of a powder mixture with a known concentration. The shape of one spectrum differs significantly from the others – this is a false spectrum. Reasons for the occurrence of false spectra are:

- There will always be a certain movement of the probe tip during the measurement, which can cause an air gap between the probe tip and the powder.
- Although the powder was aerated after each measurement, different compactions of the powder cannot be avoided if the probe is immersed in the powder once again.

For the best possible calibration, false spectra have to be detected and replaced by correct ones. This is intensively time-consuming and the identification of bad spectra requires a great amount of experience of the person operating the spectrometer. False spectra are mostly not as obvious as the example shown in *Fig. 4-88*.

If the NIR probe is not immersed into the powder but the powder is put on the developed attachment for cleaning the probe with compressed air (see *Fig. 4-87*, right), better spectra and therefore better calibration results will be obtained. Examinations have shown that the use of the self-developed attachment allows a much easier, faster and more correct calibration of the FT-NIR spectrometer. Furthermore, the analysis of the calibration samples takes place under the same conditions as the sample analysis in the continuous mixer. Therefore, the bulk density is almost the same for both cases. A disadvantage of this method is the spreading of the powder during cleaning with compressed air. To avoid a dust pollution of the environment, the calibration apparatus shown in *Fig. 4-89* and *Fig. 4-91* was constructed. The NIR probe is integrated in a plastic housing. The powder to be analyzed is put into a circular opening on the topside. A cleaning cycle is started by a keystroke after the end of the analysis. A Stored Program Control (SPC) controls the cleaning of the probe and the aspiration of the powder by a vacuum cleaner. A dust-free calibration is possible.



**Fig. 4-87:** Possibilities to calibrate the FT-NIR spectrometer VECTOR 22/N: Immersing the probe into the powder mixture (left), putting powder on the tip of the NIR probe by using the developed attachment (right)



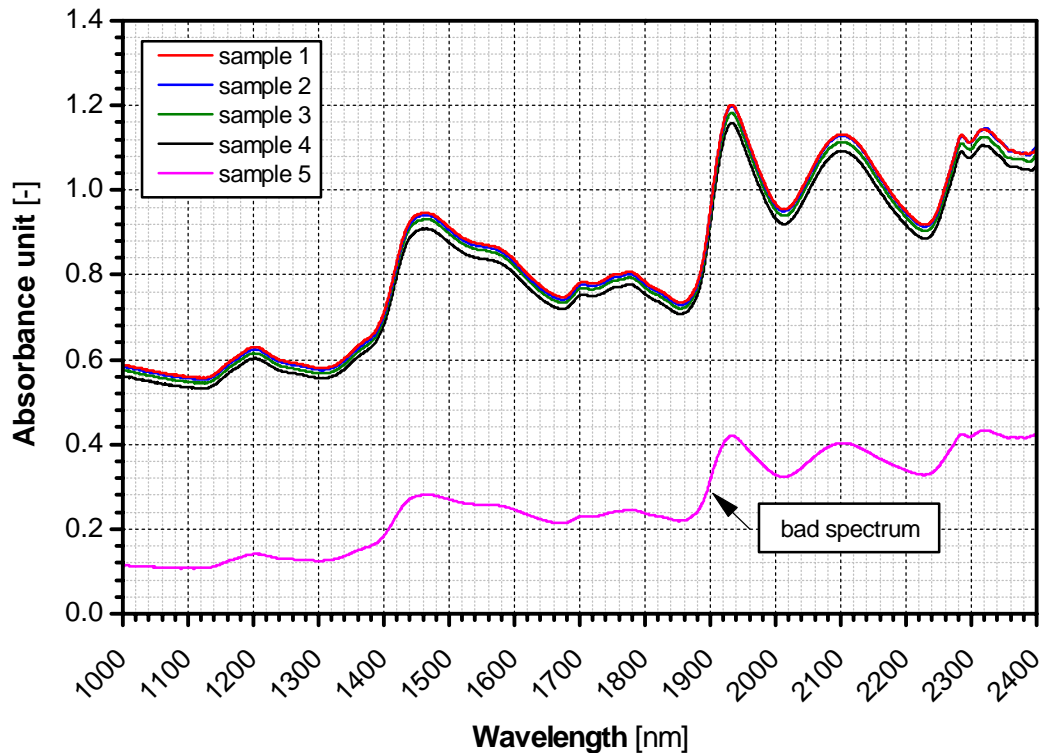


*Fig. 4-88: NIR spectra obtained by a five times measurement of a powder sample with defined concentration*

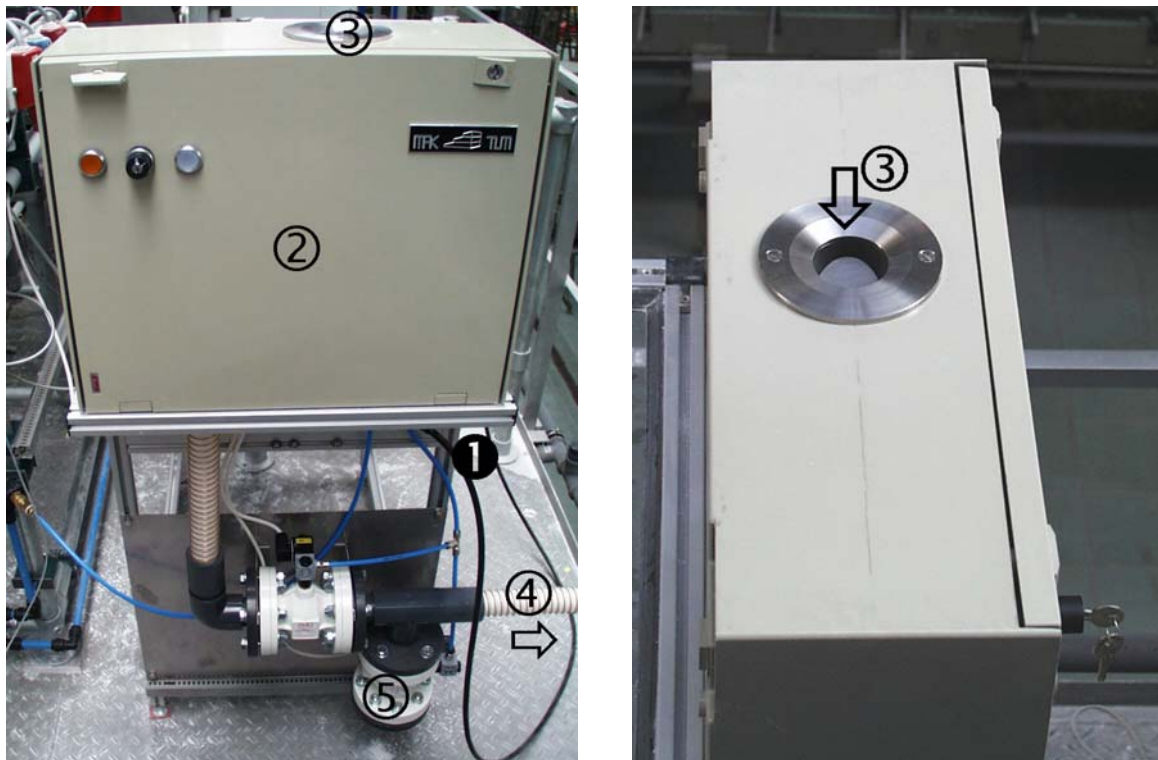


*Fig. 4-89: Self-constructed calibration apparatus: ① fiber optic cable of the probe, ② calibration apparatus, ③ inlet for samples to be examined, ④ flexible tube to the vacuum cleaner, ⑤ bypass*



**Fig. 4-90:** Self-constructed calibration apparatus: View in the inlet for the samples to be examined (compare ③ in Fig. 4-89)

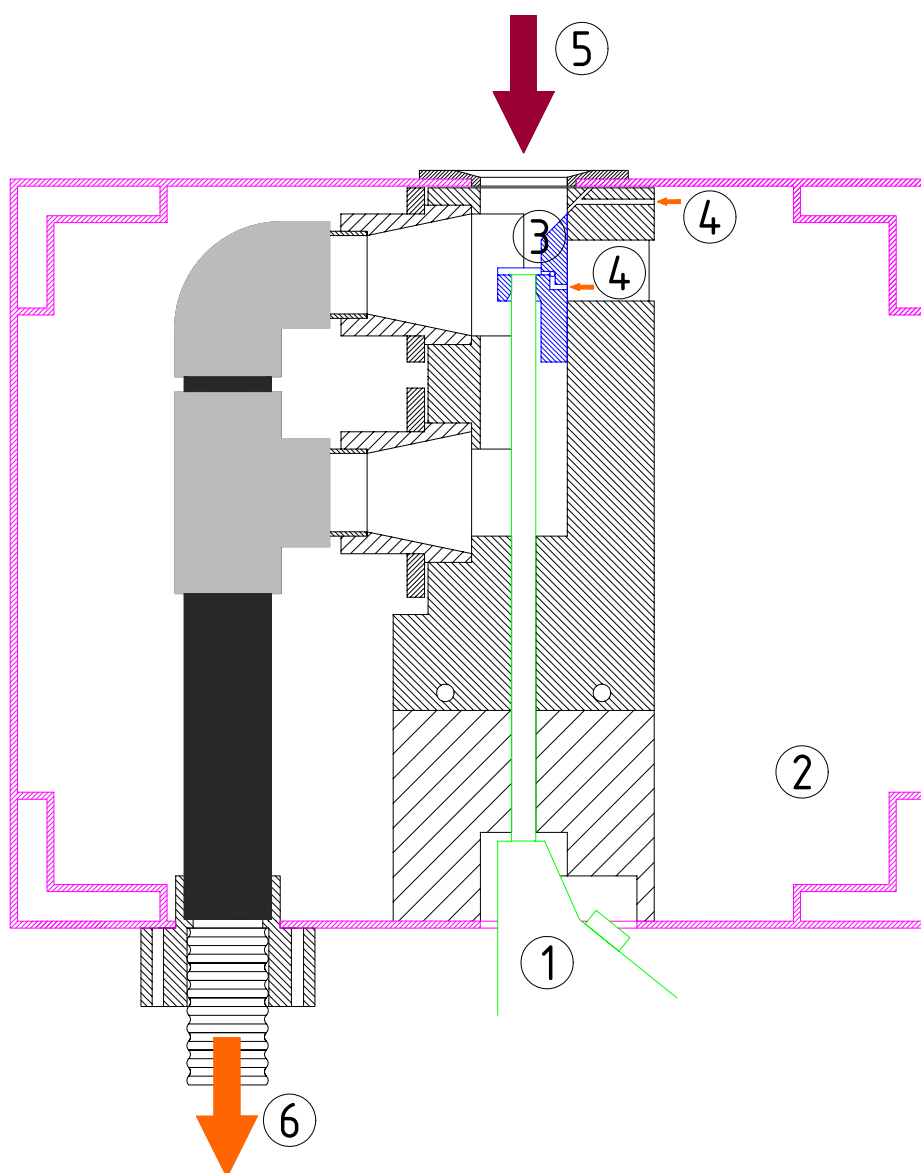


**Fig. 4-91:** Section drawing of the calibration apparatus: ① probe of the FT-NIR spectrometer, ② housing, ③ attachment for cleaning with compressed air, ④ inlet for compressed air, ⑤ inlet for the sample to be analyzed, ⑥ extraction

The calibration samples of cohesive powders often contain lumps (see *Fig. 4-92*) because of cohesion forces acting between the particles. A sieve attachment (see *Fig. 4-93*) can be put optionally on the opening of the calibration apparatus to make sure that the powder in front of the probe tip has an almost constant porosity. The powder has to be brushed through the sieve.



*Fig. 4-92: Calcium carbonate lumps*



*Fig. 4-93: Sieve attachment for the self-constructed calibration apparatus (to be put on the inlet for samples to be analyzed, compare © in Fig. 4-89)*

#### 4.4.5.5 Preparation of calibration mixtures

In the ideal case, the calibration should take place under the same conditions as the following analysis. The bulk density, the particle size distribution, the temperature and the humidity should be the same. Not only the calibration itself is very time-consuming but also the preparation of required calibration mixtures. As mentioned before, the calibration mixtures should be as homogenous as possible. In this context, the question of the optimum mixing procedure and the optimum mixing time arises.

The preparation of the calibration mixtures was carried out batchwise. For the preparation of calibration mixtures of defined concentration, the required amount of the two powders was weighed and mixed afterwards. Different mixing procedures were used:

1. The powder was mixed with a spatula in a beaker (see *Fig. 4-94*). This procedure was already used by WEINEKÖTTER [14, 53, 124] for the calibration of his photometer.
2. The mixtures were prepared with a self-constructed and hand-operated mixer (see *Fig. 4-95*). The hand-operated mixer consists of a lid, a sieve insert, an insert with baffle plates and an insert with metal pockets. The weighed powder was put inside the hand-operated mixer. Afterwards the mixer was turned over alternately ( $180^\circ$ ) for 100 times.
3. The powder was mixed in a batchwise working *Lödige* blade mixer.





Fig. 4-94: Sample preparation by mixing the powders in a beaker with a spatula

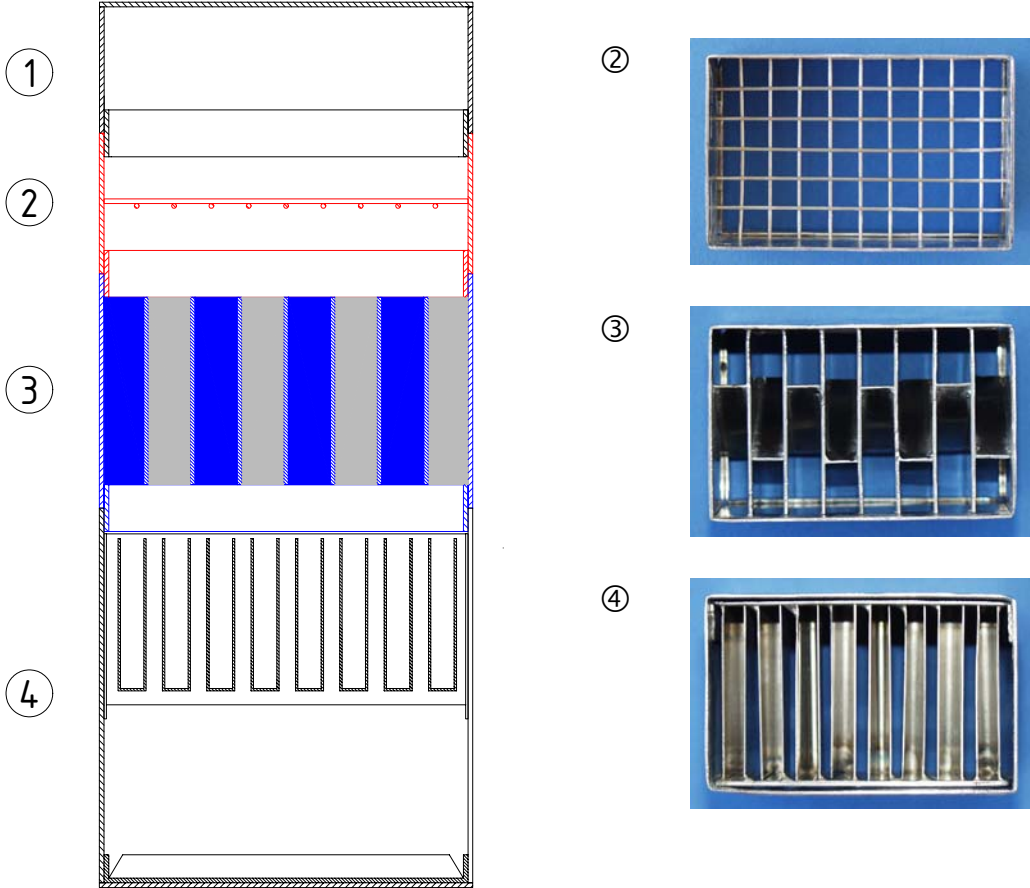
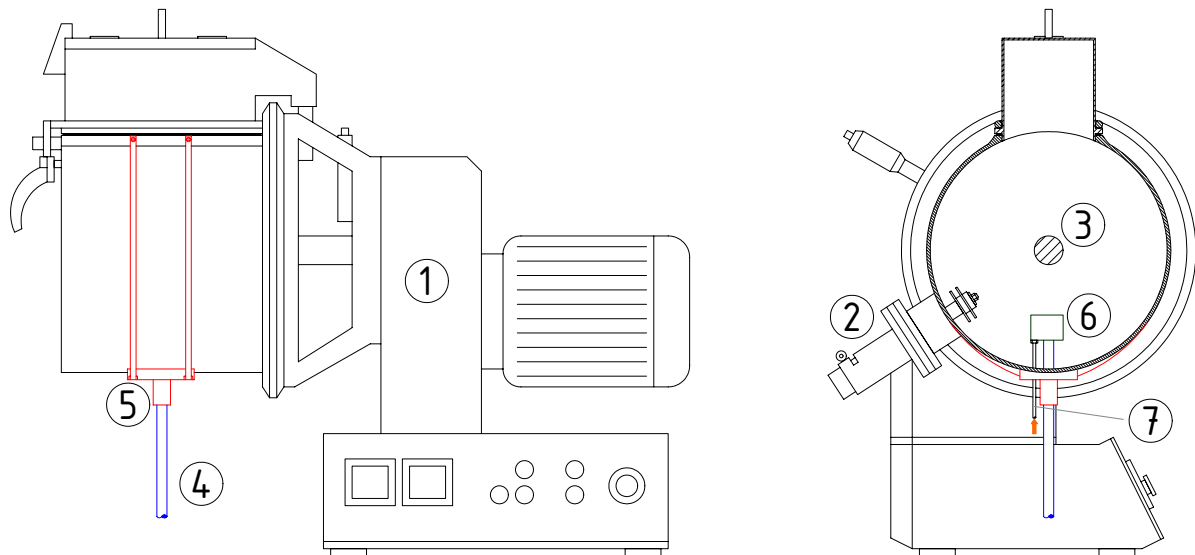


Fig. 4-95: Self-constructed and hand-operated mixer: ① lid, ② sieve insert, ③ insert with baffle plates, ④ insert with metal pockets (left: section drawing; right: top view photos of the inserts)

The positive experiences made with the in-line concentration determination in the outlet of the continuous dynamic mixer *GCM 500* caused to think about adapting the FT-NIR spectrometer to a batchwise working mixer, too. In the case of a positive result, the batch mixer could be used for an in-line calibration of the spectrometer. For the necessary tests, the company *Gebrüder Lödige Maschinenbau GmbH* (Paderborn, Germany) made the blade mixer *M 20 MK* (see *Fig. 4-96*) available. The mixing chamber has a capacity of *20 liters*.



**Fig. 4-96:** Modifications of the Lödige blade mixer *M 20 MK* necessary for the in-line control of the mixing process: ① blade mixer, ② chopper, ③ shaft with blades, ④ probe of the FT-NIR spectrometer, ⑤ flange for holding the probe, ⑥ probe attachment for cleaning with compressed air, ⑦ flexible tube for compressed air supply

The mixer is equipped with a chopper for dispersing lumps. The chopper is positioned axially in the middle of the mixer. The construction of the rotating blades (see *Fig. 4-97*) allows a positioning of the NIR probe only in the same plane as the chopper. Experiments with the attachment (compare *Fig. 4-83*), originally designed for the use in the continuous mixer *GCM 500*, showed significant fluctuations of the measured concentrations. Possible reasons for the fluctuations are the changing of the bulk density in front of the probe tip and/or a movement of the powder induced by the rotating blades. To improve the analysis results, a new attachment was constructed (see *Fig. 4-98*). As the previous one, the attachment is fixed with a screw on the NIR probe. The construction of the new attachment ensures that the powder in front of the probe tip does not move during the measurement and that the bulk density in the bored truncated cone is approximately constant. The truncated cone has a height of *20 mm*, a diameter of *38 mm* at the top and a diameter of *30 mm* at the bottom. In addition to the drilled holes for the horizontal cleaning of the probe tip, two drilled holes for a vertical fluidization and blowing out of the powder are integrated. The opening allows a horizontal outflow of blown away powder.



**Fig. 4-97:** *Blades of the Lödige mixer M 20 MK used*

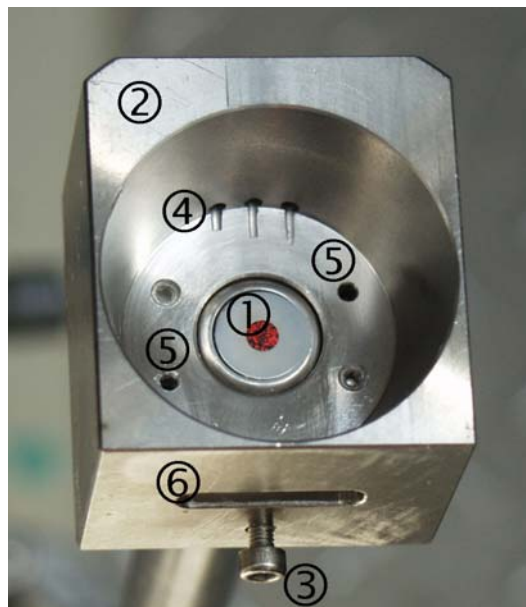


**Fig. 4-98:** *Attachment for the NIR probe used in the Lödige blade mixer M 20 MK: ① NIR probe, ② attachment, ③ screw to fix the attachment on the NIR probe, ④ drilled holes for horizontal cleaning with compressed air, ⑤ drilled holes for vertical cleaning with compressed air, ⑥ opening for horizontal outflow of blown away powder*

**Fig. 4-99** shows the result of in-line concentration measurements in the Lödige mixer M 20 MK. A mixture of 50 mass-% calcium carbonate and 50 mass-% maize starch was used for the experiment. The two powders were filled in the mixer one after the other. The mixing process was completed after a mixing time of about 30 s. A longer mixing will lead neither to an improvement nor to a worsening of the mixing result. The experimental result shows that an in-line concentration determination in the batchwise working Lödige blade mixer is possible.

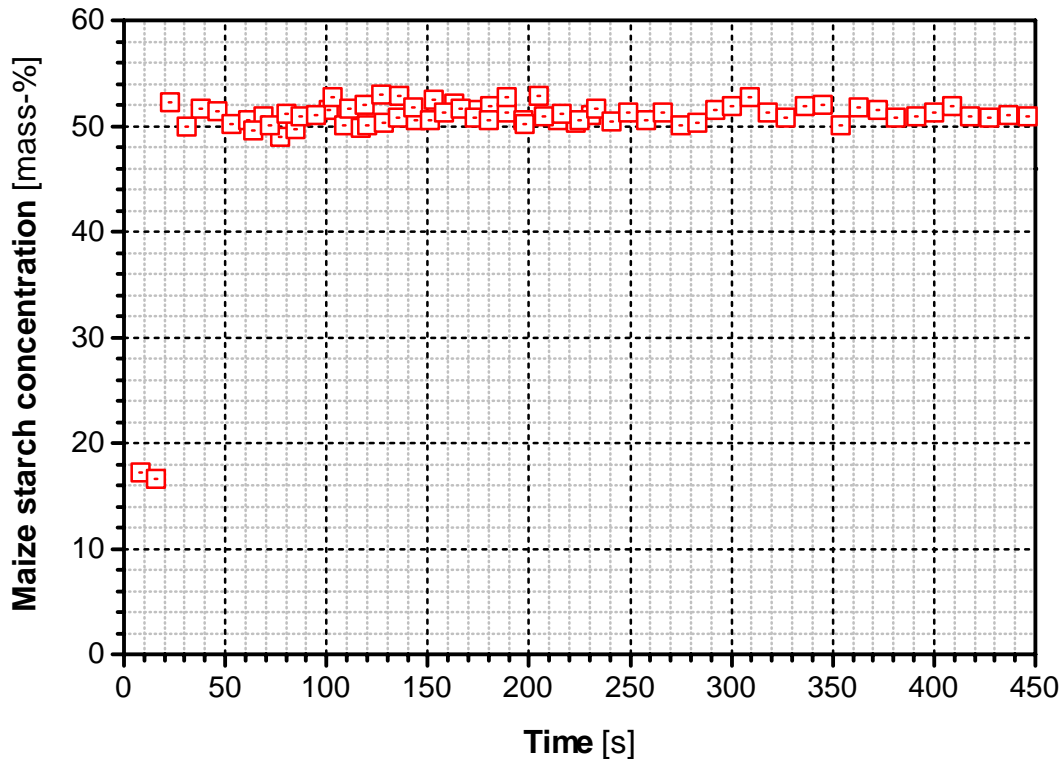


*Fig. 4-99: In-line concentration determination in the Lödige blade mixer M 20 MK (mixture of 50 mass-% calcium carbonate and 50 mass-% maize starch; pouring in the powder one after the other)*

### Theoretical basis for assessing the achieved mixing qualities using different mixing devices

To assess the mixing performance of the three different presented mixing devices (spatula mixing, hand-operated mixer and *Lödige* blade mixer) the mixing quality of the prepared mixtures has to be determined. The mixing quality is a measure for existing deviations of one product characteristic - often the concentration of the tracer. The smaller the alteration of the measured characteristic from a set point is, the better the mixing quality. Beginning from a demixed state (see *Fig. 4-100*), the goal of the mixing process is a uniform concentration in the whole mixture, which fulfills the demands. The ideal state of mixing can only be reached by ordered mixing, which is not possible in practice. At best a random mixture, after passing a transition state, can be reached [152].

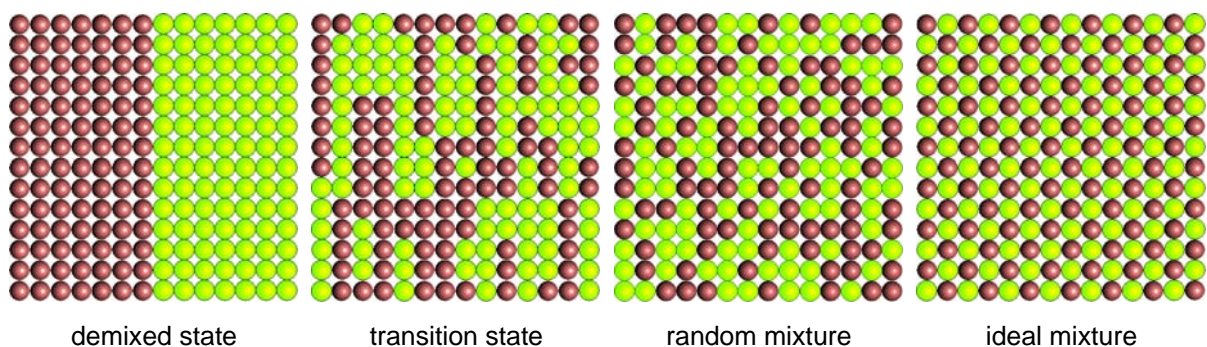


*Fig. 4-100: Different homogeneity states of a two-component mixture [152]*

For the determination of the mixing performance of the three different mixing devices, 20 samples were taken out of the mixing devices. Afterwards the concentration of the tracer in the samples was determined with the FT-NIR spectrometer. The concentration  $c_{1,i}$  of the samples taken from the mixer deviated from the set concentration  $p_1$ , which is the concentration of the tracer component 1 in the whole mixture (population). The quality of the mixture is highest when the average deviation of the concentration  $c_{1,i}$  from the set concentration  $p_1$  is smallest. For the mixing quality it does not matter if the deviation of the measured concentrations from the set concentration is negative or positive. For this reason, the average quadratic deviation, which is called the variance  $\sigma^2$ , is used to describe the mixing quality:

$$\sigma^2 = \lim_{n \rightarrow \infty} \frac{1}{n} \sum_{i=1}^n (c_{1,i} - p_1)^2 \quad \text{Eq. 4-10}$$

*Eq. 4-10* is only valid if an infinite number of samples is taken from the mixer and analyzed afterwards. This is not possible in practice and the variance has to be estimated with the empirical variance  $s^2$ .

$$s^2 = \frac{1}{n} \sum_{i=1}^n (c_{1,i} - p_1)^2 \quad \text{Eq. 4-11}$$

If the set concentration  $p_1$  is unknown,  $p_1$  has to be replaced by the average concentration  $\bar{c}_1$  of the taken samples:

$$\bar{c}_1 = \frac{1}{n} \sum_{i=1}^n c_{1,i} \quad \text{Eq. 4-12}$$

$$s^2 = \frac{1}{n-1} \sum_{i=1}^n (c_{1,i} - \bar{c}_1)^2 \quad \text{Eq. 4-13}$$

Because of bulk density changes in front of the probe tip, differences between the set concentration  $p_1$  and the average concentration  $\bar{c}_1$  can occur. Therefore, the average concentration  $\bar{c}_1$  was used to determine the empirical variance and the empirical standard deviation respectively although the concentration  $p_1$  was known. For the assessment of the mixing result it is more important to determine the average deviation of the measured concentrations  $c_{1,i}$  from the average concentration  $\bar{c}_1$  (characterized by *Eq. 4-13*) than to determine the average deviation of the measured concentrations  $c_{1,i}$  from the set concentration  $p_1$  (characterized by *Eq. 4-11*).

Based on  $n$  samples taken and analyzed the variance  $\sigma^2$  can be estimated with the calculated empirical variance  $s^2$ . If the samples are taken randomly, the measured concentrations are approximately normally distributed. In this case, the following value is "Chi-square-distributed":



$$\chi^2 = k \cdot \frac{s^2}{\sigma^2}$$

Eq. 4-14

$$k = n \quad \text{using Eq. 4-10}$$

$$k = n-1 \quad \text{using Eq. 4-13}$$

In Eq. 4-14,  $k$  is the degree of freedom. Using Eq. 4-15 and Eq. 4-16, the interval where the real variance  $\sigma^2$  lies can be calculated for a given probability  $P$ . The upper limit  $s_u^2$  and the lower limit  $s_l^2$  of the interval are calculated with the “Chi-square”-value  $\chi_u^2(k, P)$  for the upper and  $\chi_l^2(k, P)$  for the lower limit.  $\chi_u^2(k, P)$  and  $\chi_l^2(k, P)$  depend on the degree of freedom  $k$  and the probability  $P$ . For engineering applications, normally a probability of 95 % up to 99 % is chosen. For pharmaceutical applications, the probability is often set higher. [109]

$$\sigma^2 \leq k \cdot \frac{s^2}{\chi_u^2(k, P)} = s_u^2 \quad \text{Eq. 4-15}$$

$$s_l^2 = k \cdot \frac{s^2}{\chi_l^2(k, P)} \leq \sigma^2 \quad \text{Eq. 4-16}$$

$$s_l^2 \leq \sigma^2 \leq s_u^2 \quad \text{Eq. 4-17}$$

For a probability of  $P = 95\%$ , the dependence of  $k / \chi_u^2(k, P)$  and  $k / \chi_l^2(k, P)$  on the number of taken samples is shown in Fig. 4-101.

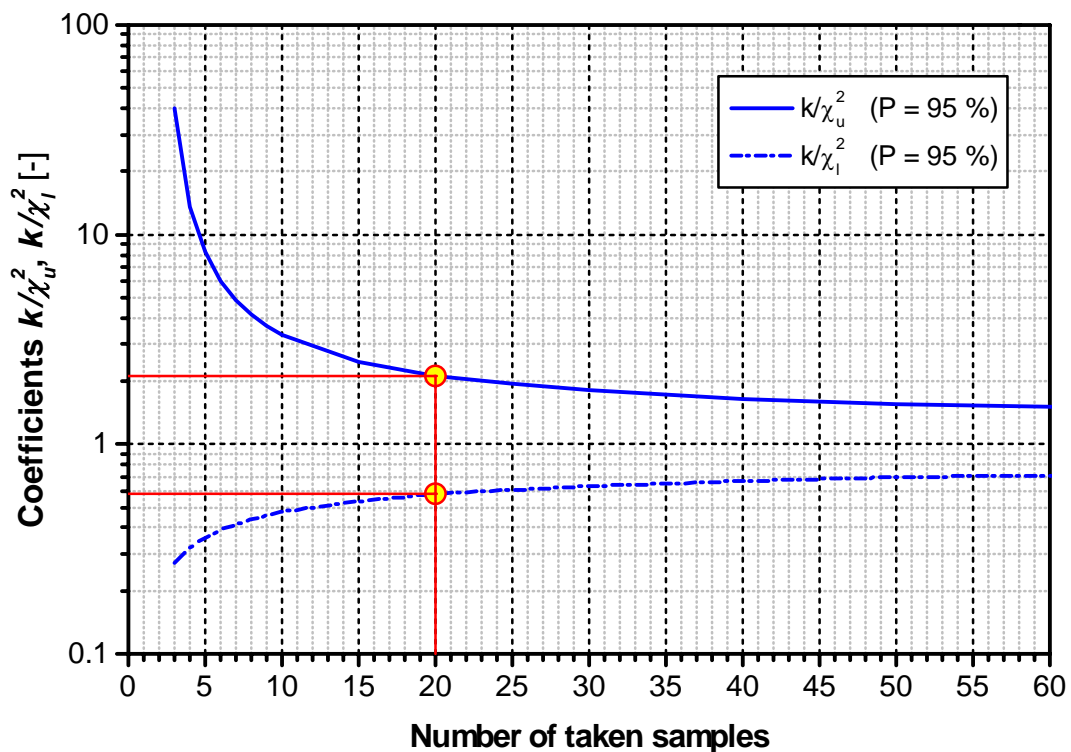


Fig. 4-101: Dependence of  $k / \chi_u^2(k, P)$  and  $k / \chi_l^2(k, P)$  on the number of taken samples (according to KREYSZIG [109])

### Assessing the mixing qualities achieved by using different mixing devices

The mixing qualities achieved by using different mixing devices are shown in *Fig. 4-102*. The mixing quality, characterized by the standard deviation of the measured tracer concentrations, is plotted versus the different mixing devices used. The samples taken from the mixtures prepared by spatula mixing and using the hand-operated mixer as well as the *Lödige* mixer were analyzed with the FT-NIR spectrometer. The probe of the spectrometer was fixed in the self-constructed calibration apparatus (compare *Fig. 4-89*, p. 129). The analyses were performed with and without using the sieve attachment (compare *Fig. 4-93*, p. 131). For the *Lödige* mixer, the mixing quality was also determined by means of the NIR probe positioned inside the mixer. The attachment (compare *Fig. 4-98*, p. 134) for cleaning the probe with compressed air was used. The spectra were detected in two ways:

1. Stopping the mixer before the measurement, taking a spectrum of the powder collected in the attachment, blowing the powder out of the attachment, starting the mixing process again, stopping the mixer after a certain time, taking a spectrum of the powder collected in the attachment, ...

This procedure is called “manual”.

2. Taking the spectra automatically without stopping the mixer before the measurement.

This procedure is called “macro” because the recording of the spectra is controlled by a programmed macro.

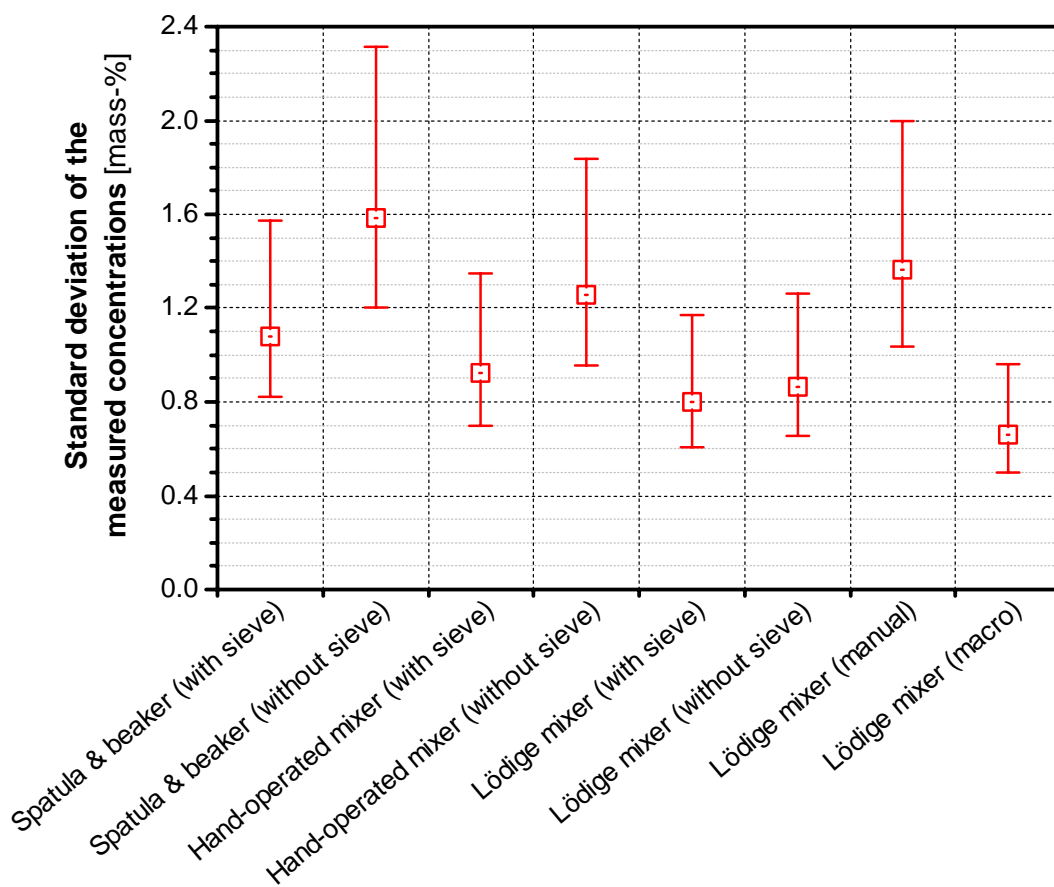


**Fig. 4-102:** Mixing qualities achieved by using different mixing devices (20 samples taken from each mixture, mixture with 50 mass-% calcium carbonate and 50 mass-% maize starch)



Most of the mixing qualities achieved by using different mixing devices are not significantly different. However, the influence of a sieve attachment in combination with the calibration apparatus and the operation procedure during the in-line concentration determination in the *Lödige* mixer are remarkable. The average standard deviation of the measured concentrations and the corresponding confidence intervals were smaller for the case that a sieve attachment was used. This is an indication that the prepared mixtures contained lumps, which were formed because of cohesion forces and destroyed when the mixtures were brushed through the sieve attachment. Recording the NIR spectra according to the “macro” procedure, a significantly better mixing quality with a much smaller confidence interval was obtained than using the “manual” procedure. This is an indication that the bulk density in front of the NIR probe was changing more for the “manual” procedure than for the “macro” procedure. During the mixing process, the bulk material in the *Lödige* mixer is fluidized above the attachment of the NIR probe. Particles fall into the attachment as long as the attachment is not completely filled:

- Using the “macro” procedure, the amount of particles in front of the attachment is almost constant. As a result, the bulk density in front of the probe tip is almost constant, too.
- Using the “manual” procedure, the rotation of the mixing devices is stopped before the measurement. The fluidized bed above the probe tip collapses and particles fall on the attachment. Depending on the position of the mixing devices, when the rotation is stopped, more or less particles fall on the probe tip. As a result, the bulk density in front of the probe tip will differ depending on the amount of particles falling down.

The influence of the measuring procedures “manual” and “macro” on the mixing quality was also examined for a set maize starch concentration of 20 and 80 *mass-%*. The results show the same tendency as already described for a concentration of 50 *mass-%* (see *Fig. 4-103*).

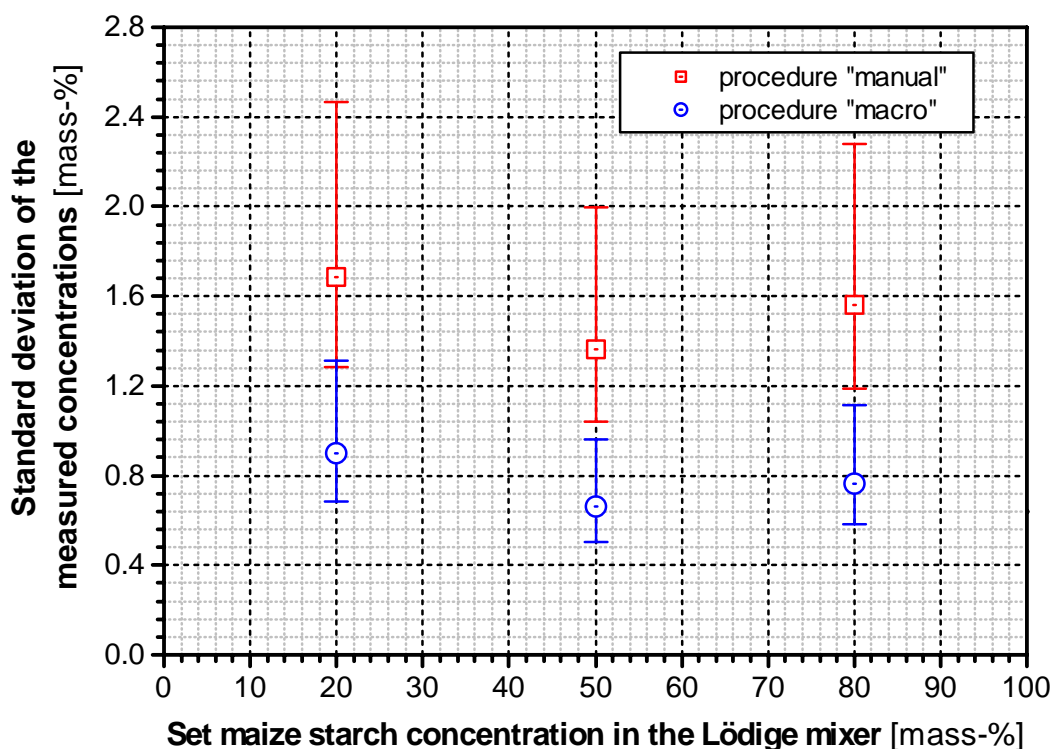


*Fig. 4-103: Influence of the analyzing procedures “manual” and “macro” on the analysis result*

### Determining the reproducibility of the analysis results

During the mixing experiments described, the spectrometer scanned the bulk material in front of the probe tip five times. The five spectra recorded were averaged and united to one spectrum by the spectrometer software. Afterwards the corresponding concentration value of the tracer was determined by the spectrometer software. To determine the reproducibility of the analysis results, the following procedure was used for different scan numbers:

1. 50 mass-% of calcium carbonate and 50 mass-% of maize starch were mixed in the *Lödige* mixer M 20 MK.
2. Afterwards the mixer was stopped and the concentration of the tracer in front of the probe tip was determined 20 times using a certain number of scans.
3. The powder in the probe attachment was blown away and the mixer was started again.
4. After a certain mixing time the mixer was stopped and the described procedure was repeated two times.

In *Fig. 4-104*, the standard deviation of the measured concentrations, which characterizes the reproducibility of the analysis results, is plotted against the number of scans. The influence of the scan number is comparatively small. Only between the standard deviations obtained for 2 scans and the standard variations obtained for scan numbers equal or higher than 32 a significant difference was observed. For a scan number of 5, the highest upper confidence interval limit was 0.87 mass-%. Comparing this result with the best obtained mixing quality shown in *Fig. 4-102*, no significant difference can be found. Even if there should be a possibility to increase the homogeneity of the calibration mixtures used, the improvement cannot be determined with the FT-NIR spectrometer *VECTOR 22/N* without changing the settings.

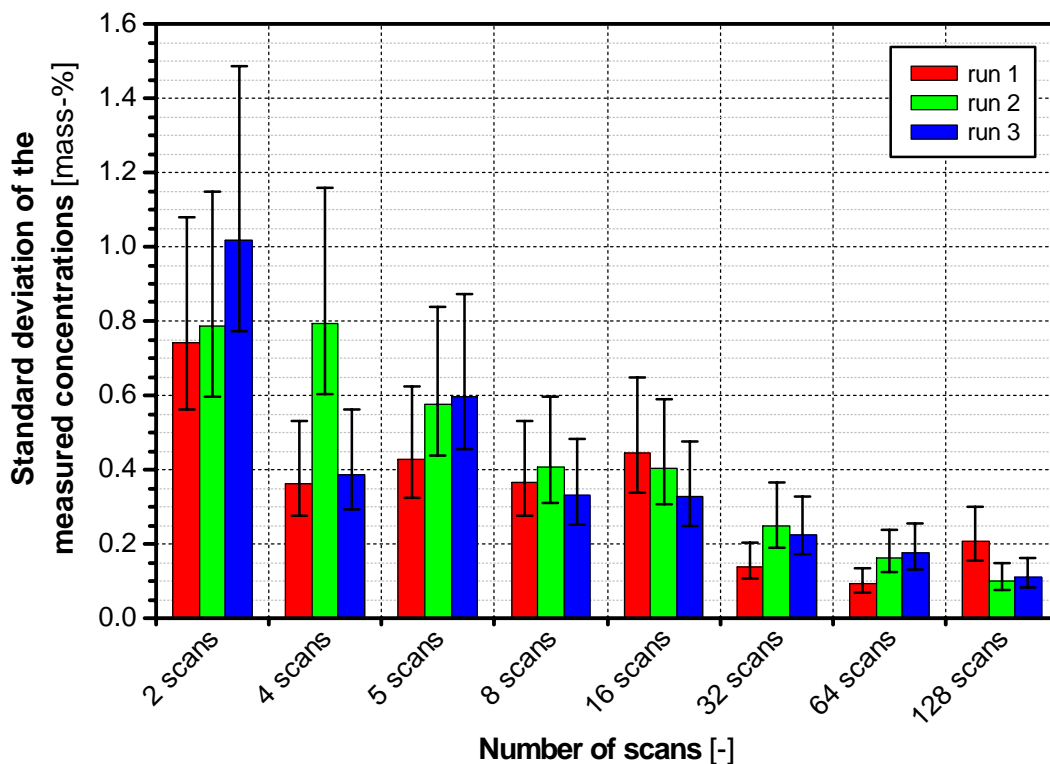


*Fig. 4-104: Influence of the scan number on the standard deviation of the measured concentrations (analysis of a static sample for twenty times in the *Lödige* mixer M 20 MK)*

The reproducibility was also determined by using the self-developed calibration apparatus. From each mixture, prepared with the *Lödige* mixer *M 20 MK*, a sample was taken and analyzed 20 times for different scan numbers. The analysis results presented in *Fig. 4-105* show the same tendency as the results obtained by analyzing the mixture inside the *Lödige* mixer. For a scan number of 64, the analysis result of run 1 is significantly higher than for run 2 and 3. The reason is shown in *Fig. 4-106*. The 20 measured maize starch concentrations are plotted for each run. For run 2 and 3, the measured concentration values fluctuate around an average value. For run 1, the measured average concentration drifted to a smaller average concentration between measurement 6 and 15. The drift could be the result of vibrations, which caused a changing of the bulk density in front of the probe tip.

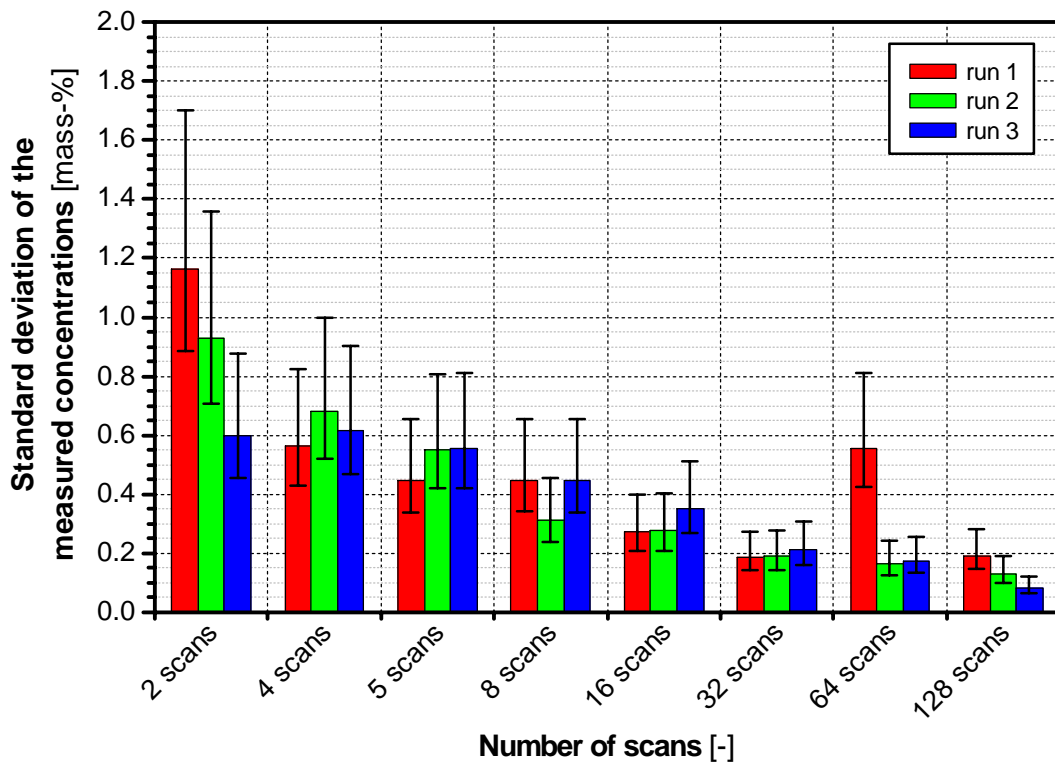


*Fig. 4-105: Influence of the scan number on the standard deviation of the measured concentrations (analysis of a static sample for 20 times in the calibration apparatus without using the sieve attachment)*

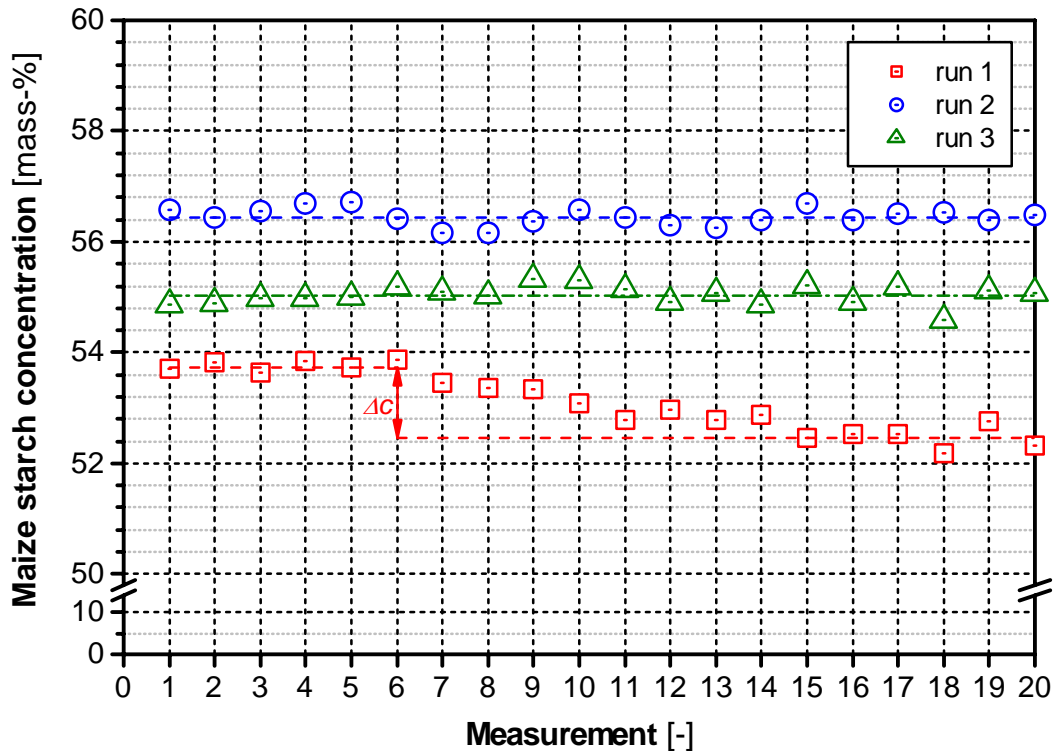


*Fig. 4-106: Measured maize starch concentrations corresponding to the standard deviations shown in Fig. 4-105 for 64 scans*

#### **Conclusion from the examinations for improving the calibration sample preparation**

The examinations for improving the calibration sample preparation have shown that the mixing quality obtained with the different mixing devices is in the same order as the reproducibility of a measurement. Therefore, almost no influence of the different tested mixing devices on the achieved mixing quality can be observed. For a constant scan number, the calibration cannot be improved by an improvement of the sample preparation. An improvement could only be possible if the number of the analyzed samples of each calibration mixture is increased. By an increase, the inhomogeneity of the calibration samples as well as the influence of a limited reproducibility can be better considered during the development of the calibration model.

The use of the *Lödige* mixer makes a much faster sample preparation possible. Especially the use of the programmed macro for spectra recording allows the consideration of a high spectra number resulting from a multiple analysis of calibration mixtures.

#### 4.4.5.6 Development and validation of a calibration model

Although many books and articles [e.g. 153, 154] describe the procedure for developing a calibration model, the basic steps are introduced to get an impression of the complexity of the procedure and the influencing parameters. The following results refer to the development of the calibration model used for

- the assessment of the mixtures obtained with different mixers (spatula mixing, hand-operated mixer, *Lödige* mixer) as well as
- the assessment of the different sample presentation procedures (calibration apparatus: with and without sieve attachment; *Lödige* mixer: “manual” and “macro” procedure).

For the later described mixing experiments with the continuous dynamic mixer *GCM 500* (⇒ validation of the developed mixing model), another calibration model was used because these mixing experiments were performed with *OMYACARB 2 SV* instead of *OMYACARB 10 SV*. *OMYACARB 10 SV* was used for the examinations to improve the sample preparation. The mixing experiments were finished half a year before the described examinations for the improvement of the sample preparation started, and the calcium carbonate *OMYACARB 2 SV* was used up.

For the development of the calibration model, a set of calibration mixtures of known concentration was prepared. The concentration range of the mixtures used for the calibration has to be broader than the concentration range of the samples, which are analyzed later with the developed calibration model. The calibration samples were prepared with the *Lödige* mixer *M 20 MK* and analyzed with the “macro” procedure (compare p. 138). Afterwards, the development of the calibration model was performed with the already mentioned control and analysis software *OPUS NT*. The software offers an input mask where the concentration values of the calibration mixtures analyzed can be assigned to the corresponding spectra. The software is able to determine a calibration function by using the “Partial Least Square” (PLS) regression. Detailed information about the PLS regression can be found in e.g. [153]. Following, the expression “calibration model” is used for the calibration function obtained for defined wavelength sections of the spectra, spectra manipulations and ranks. The meaning of spectra manipulation and rank will be explained later.

The so-called full cross validation is used for the validation of the calibration model obtained. Performing a full cross validation, the spectra corresponding to one calibration mixture are put aside. With the remaining spectra, a new calibration function using the same calibration model is determined. The corresponding concentration characterized by the spectra, which were put aside, is determined with the calibration function. Then the spectra put aside are integrated again and the spectra set of another calibration mixture is put aside. A new calibration function is determined with the remaining spectra and the corresponding concentration characterized by the spectra, which were put aside, is determined. This procedure is repeated until every spectra set was put aside and analyzed based on the remaining spectra by using the calibration function obtained. Afterwards the predicted concentrations were plotted against the reference values (see *Fig. 4-107*).

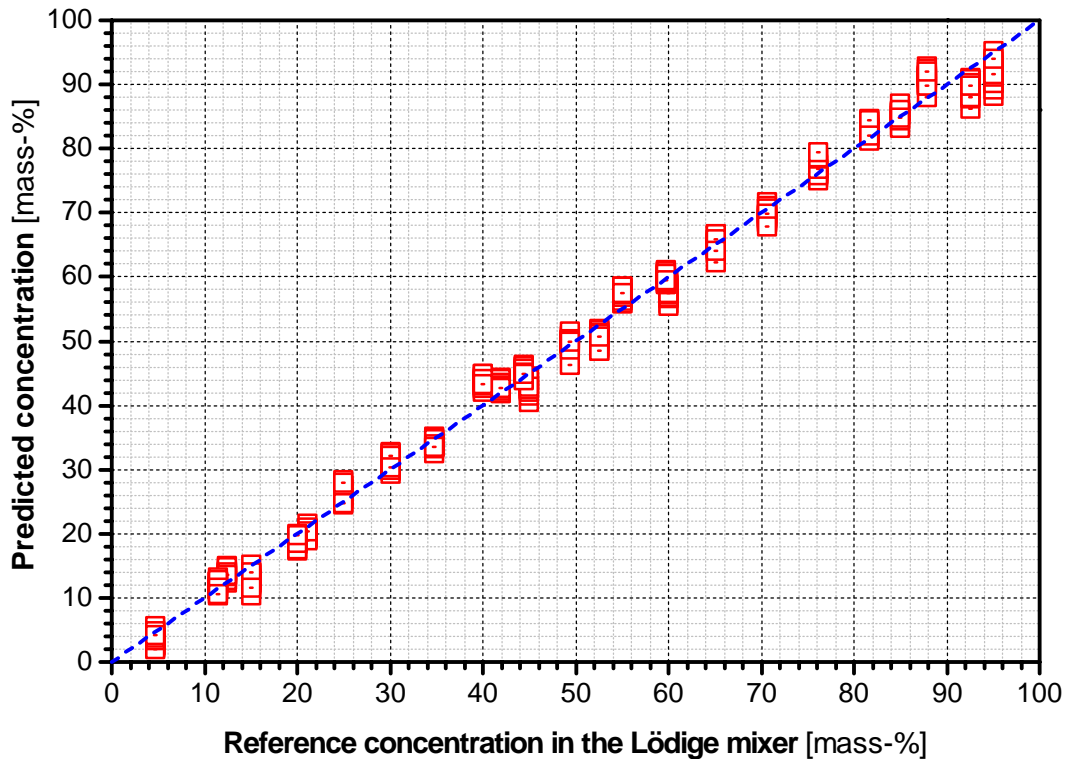


**Fig. 4-107:** Results of the full cross validation (For each reference concentration 20 spectra were recorded inside the Lödige mixer using the “macro” procedure.)

The calibration model is the better the smaller the deviations of the determined concentration values from the reference concentrations are. In the ideal case, every determined concentration value lays on the dashed line. The quality of the calibration model can be described quantitatively by the “**Root Mean Square Error of Cross Validation**” *RMSECV*. The *RMSECV* value is calculated with *Eq. 4-18*.  $c_{i,reference}$  is the reference concentration of the  $i^{th}$  calibration sample and  $c_{i,predicted}$  is the corresponding predicted concentration. The smaller the *RMSECV* value the smaller is the prediction error.

$$RMSECV = \sqrt{\frac{1}{n} \cdot \sum_{i=1}^n (c_{i,predicted} - c_{i,reference})^2} \quad Eq. 4-18$$

For finding the optimum calibration method, the spectrometer software *OPUS NT* offers an optimization procedure, which automatically changes the wavelength regions and the spectra manipulation procedures. After each changing, a cross validation is performed automatically and a *RMSECV* value is determined. Spectra manipulation procedures are for example the derivation of recorded spectra or the elimination of constant offsets. Before the PLS routine is started, the matrix *Y* (system characteristic), which contains the concentration values, as well as the matrix *X* (system variable), which contains the spectra, are factorized. For factorization, the eigenvectors and the corresponding eigenvalues of the matrix *Y* and the matrix *X* are determined. By factorization, the information of the matrix representing the concentration changes are extracted from the information representing the noise of the analysis results. The number of ranks is equivalent to the number of the eigenvectors.

The result of an optimization procedure is sorted according to increasing *RMSECV* values and presented as for example in *Fig. 4-108*. Besides the *RMSECV* value, the corresponding rank, the wavelength region used and the spectra manipulation procedure are also listed.

Number	RMSECV	Rank	Regions	Preprocessing
46	1.91	6	9002.1 - 4597.5	Constant Offset Elimination
38	1.95	5	9002.1 - 5446	Constant Offset Elimination
42	1.95	6	9002.1 - 6094 5453.7 - 4597.5	Constant Offset Elimination
58	2.07	7	9002.1 - 6094 5453.7 - 4242.6	Constant Offset Elimination
54	2.07	6	9002.1 - 5446 4605.2 - 4242.6	Constant Offset Elimination
62	2.08	9	9002.1 - 4242.6	Constant Offset Elimination
34	2.11	5	9002.1 - 6094	Constant Offset Elimination
50	2.11	6	9002.1 - 6094 4605.2 - 4242.6	Constant Offset Elimination
40	2.26	4	9002.1 - 7497.9 5453.7 - 4597.5	Constant Offset Elimination
56	2.33	4	9002.1 - 7497.9 5453.7 - 4242.6	Constant Offset Elimination
44	2.34	4	9002.1 - 7497.9 6101.7 - 4597.5	Constant Offset Elimination
60	2.36	4	9002.1 - 7497.9 6101.7 - 4242.6	Constant Offset Elimination
342	2.38	6	9002.1 - 6795.9	Constant Offset Elimination
11	2.4	8	9002.1 - 6094 5453.7 - 4597.5	No Spectral Data Preprocessing
193	2.42	9	9002.1 - 5446	First Derivative
15	2.42	7	9002.1 - 4597.5	No Spectral Data Preprocessing
27	2.46	9	9002.1 - 6094 5453.7 - 4242.6	No Spectral Data Preprocessing
209	2.5	9	9002.1 - 5446 4605.2 - 4242.6	First Derivative
31	2.5	9	9002.1 - 4242.6	No Spectral Data Preprocessing

**Fig. 4-108:** Tabular listing of calibration models obtained as a result of an automatic method optimization by using the software *OPUS QUANT* (version 3.1, Bruker Optik GmbH, Germany)

The calibration model with the smallest *RMSECV* value has not to be automatically the best calibration model. If the *RMSECV* value of a calibration model with a smaller rank is only slightly higher, this model should be used. Plotting the *RMSECV* value against the rank number, the low point of the curve corresponds to the optimum rank number (see *Fig. 4-109*).



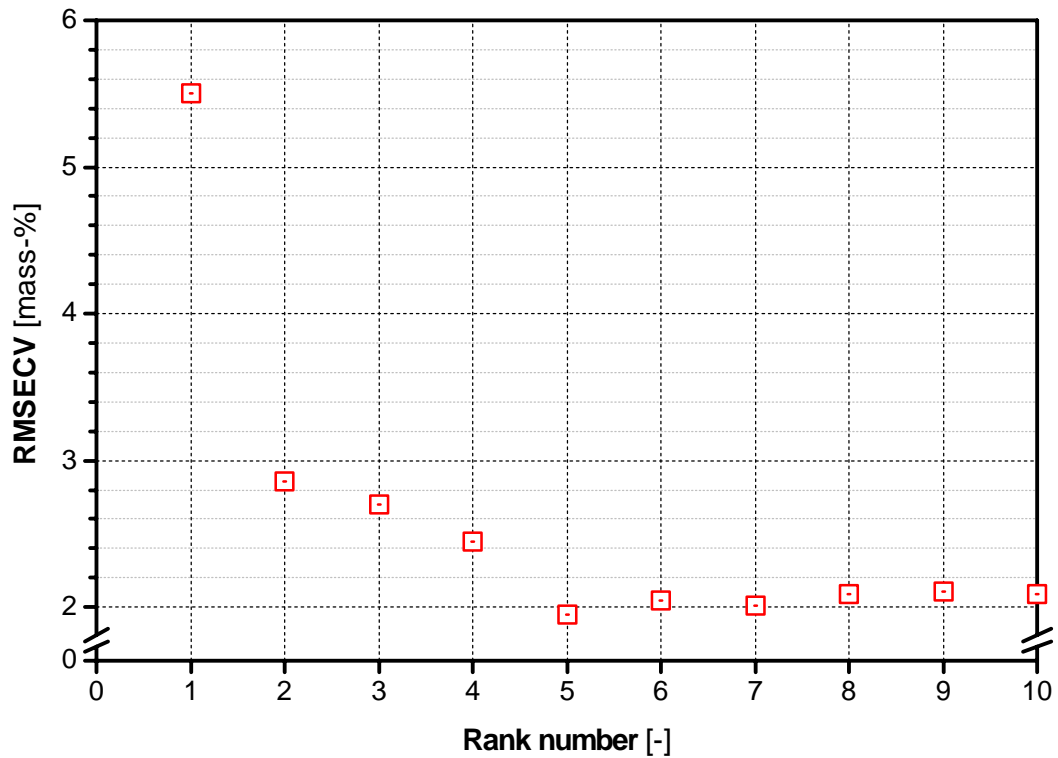


*Fig. 4-109: Influence of the rank number on the RMSECV value (spectra manipulation: elimination of a constant offset)*

After the cross validation, the developed calibration model should also be validated with mixtures of known concentration not used for developing the calibration model [153]. The validation of the developed calibration model is especially recommended if different calibration models based on the same rank but slightly different *RMSECV* values and different spectra manipulation procedures are available.

The validation result for the developed calibration model is shown in *Fig. 4-110*. The analysis was performed according to the “manual” and the “macro” procedure. 20 spectra were recorded for each concentration. Especially for the “macro” procedure, a very good prediction of the concentrations was possible.

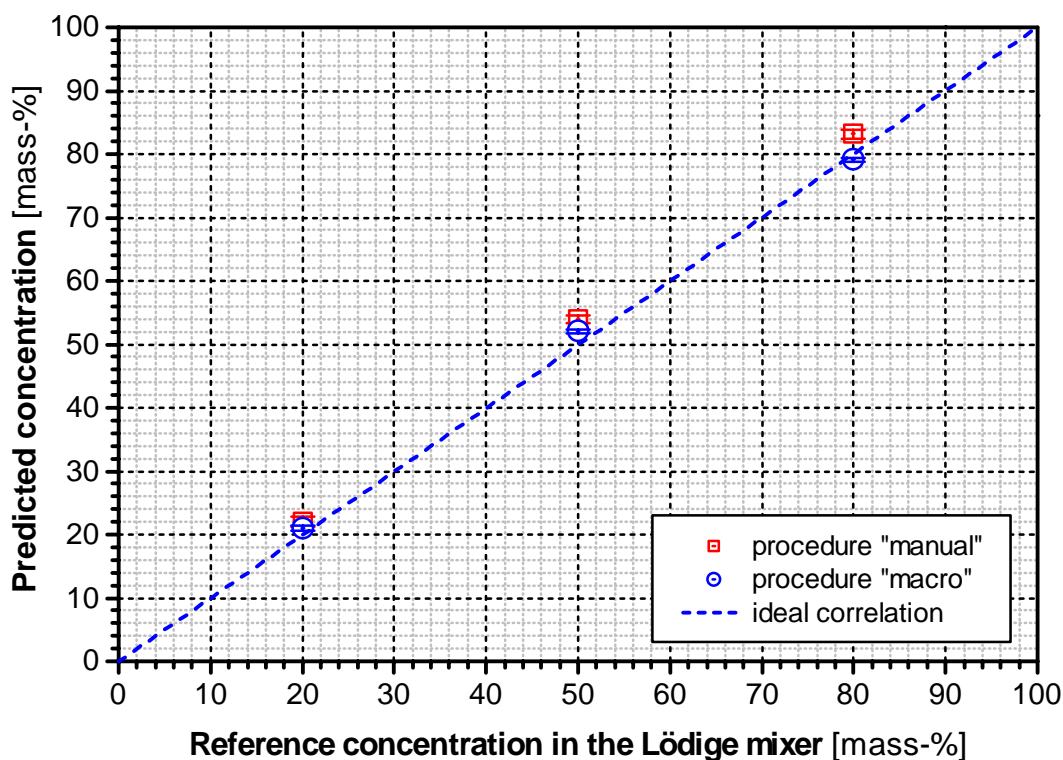


**Fig. 4-110:** Validation of the developed calibration model by using mixtures of known concentration prepared in the Lödige mixer M 20 MK and not used for the development of the calibration model (rank: 5, wave number region used:  $9\,002.1\text{ cm}^{-1}$  to  $5\,446\text{ cm}^{-1}$ , spectra manipulation: elimination of a constant offset)

#### 4.4.5.7 Estimation of the sample size

The determined mixing quality depends on the sample size [155, 156]. For the same mixture, the mixing quality will increase and the empirical variance will decrease respectively if the sample size is increased. An example to illustrate this is pointillism: Standing one meter in front of the canvas every single spot of paint can be seen, ten meters away the single spots of paint cannot be differentiated because the sample size is bigger (see *Fig. 4-111*).

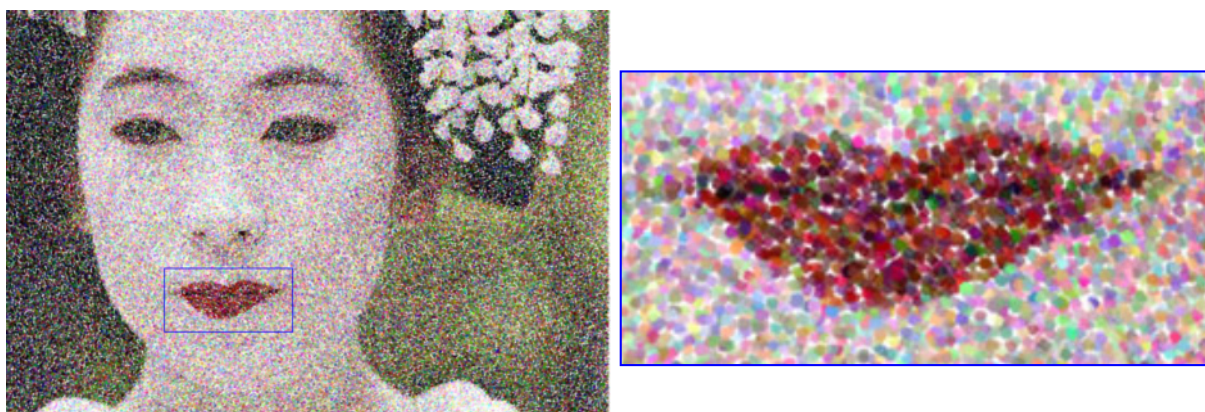


**Fig. 4-111:** Pointillism as an example for the influence of the sample size on the mixing quality: Original picture (left) [157], cut-out of the original picture and smaller sample size respectively (right)

The FT-NIR spectrometer *VECTOR 22/N* used in combination with the fiber optic sampling probe (type *IN 263E9*) analyzes a circular powder surface with a diameter of about  $3\text{ mm}$ . The penetration depth of the NIR light, which influences the effective sample mass, depends on the bulk properties (e.g. particle size, particle shape and porosity) and the analyzing parameters (e.g. wavelength and probe type) [50, 158, 159]. Therefore, it is difficult to determine the mass analyzed by the fiber optic probe. However, for some applications a determination, at least an estimation, of the effective sample size is necessary:

- The comparison of mixing qualities determined with different analyzing devices is only possible if the effective sample size is also considered.
- Some regulations, e.g. from the *FDA*, prescribe the limits for the mass of the samples used for assessing the mixture homogeneity [158].

In literature, two different procedures for estimating the effective sample size are presented. *BERNTSSON* [159] determined the penetration depth of NIR light by defined changes of powder layers put on a polyamide plate: The use of aluminum spacers allows a generation of defined powder layers ranging from  $0.25\text{ mm}$  to  $5.0\text{ mm}$  in  $0.25\text{ mm}$  increments. Using the polyamide plate without any powder coverage, almost all NIR light is absorbed. Putting defined powder layers on the polyamide plate, the absorption values recorded will decrease with increasing layer heights until the layer height is in the same magnitude as the penetration depth of the NIR light. For layer heights higher than the penetration depth, the absorbance values fluctuate randomly around an average value. *WEINEKÖTTER* [50] and *CHO* [158] used the dependence of the sampling variance on the sample mass to estimate the sample size.

The preparation of powder layers with defined height and porosity is quite complicated, especially using cohesive powders. Therefore, the estimation of the effective sample size was performed by comparing the variance of prepared powder mixtures with the calculated variance. A lot of literature describing the relation between variance and the mass of the sample, can be found. *SOMMER* [155, 156] derived equations for calculating the variance of a random two-component mixture on the pre-condition of a constant sample mass. He differentiated between two limiting cases:

1. The particle size distributions of the components to be mixed are the same.
2. The smallest particle of component 1 is larger than the largest particle of component 2.

For a similar particle size distribution of the two components, the variance  $\sigma_r^2$  of a random mixture can be calculated with *Eq. 4-19*.

$$\sigma_r^2 = \frac{p_1}{m_{sample}} \cdot \int_0^1 m_1(R_{3,1}) \cdot dR_{3,1} - \frac{2 \cdot p_1^2}{m_{sample}} \cdot \int_0^1 (1 - R_{3,1}) \cdot \int_0^R \frac{m_1(\xi)}{(1 - \xi)^2} \cdot d\xi \cdot dR_{3,1} \quad \text{Eq. 4-19}$$

$p_1$  is the mass concentration of component 1 in the whole mixture.  $m_{sample}$  is the mass of the taken samples.  $m_1(R_{3,1})$  is the mass of a single particle with the corresponding particle size of the residue distribution  $R_{3,1}$ .

$m_1(R_{3,1})$  is not a common expression and it is explained below. The mass of a single particle with the density  $\rho_1$  and the diameter  $d_1$  can be calculated with *Eq. 4-20*.

$$m_1(d_1) = \frac{\pi}{6} \cdot \rho_1 \cdot d_1^3 \quad \text{Eq. 4-20}$$

In *Fig. 4-112*, the cumulative residue distribution  $R_{3,1}$  is shown. For calculating  $m_1(R_{3,1})$ , the inverse function of  $R_{3,1}(d_1)$  has to be calculated. Incorporating the inverse function  $d_1(R_{3,1})$ , *Eq. 4-20* is transformed to *Eq. 4-21*.

$$m_1(d_1(R_{3,1})) = \frac{\pi}{6} \cdot \rho_1 \cdot (d_1(R_{3,1}))^3 \quad \text{Eq. 4-21}$$

In *Fig. 4-112*, the correlation between  $m_1$  and  $R_{3,1}$  is shown graphically. The cumulative residue distribution is based on a measured cumulative distribution of maize starch (compare *Fig. 4-9*, p. 66). The mass of a single particle was calculated with *Eq. 4-20*. Exemplary  $m_1(R_{3,1}(d_1))$  was determined for a particle diameter of  $23 \mu\text{m}$ . According to *Fig. 4-112*, the following relations arise:

$$\begin{aligned} R_{3,1}(d_1 = 23 \mu\text{m}) &= 0.05 \\ m_1(d_1 = 23 \mu\text{m}) &= 10^{-8} \text{ g} \\ \Rightarrow m_1(R_{3,1} = 0.05) &= 10^{-8} \text{ g} \end{aligned}$$

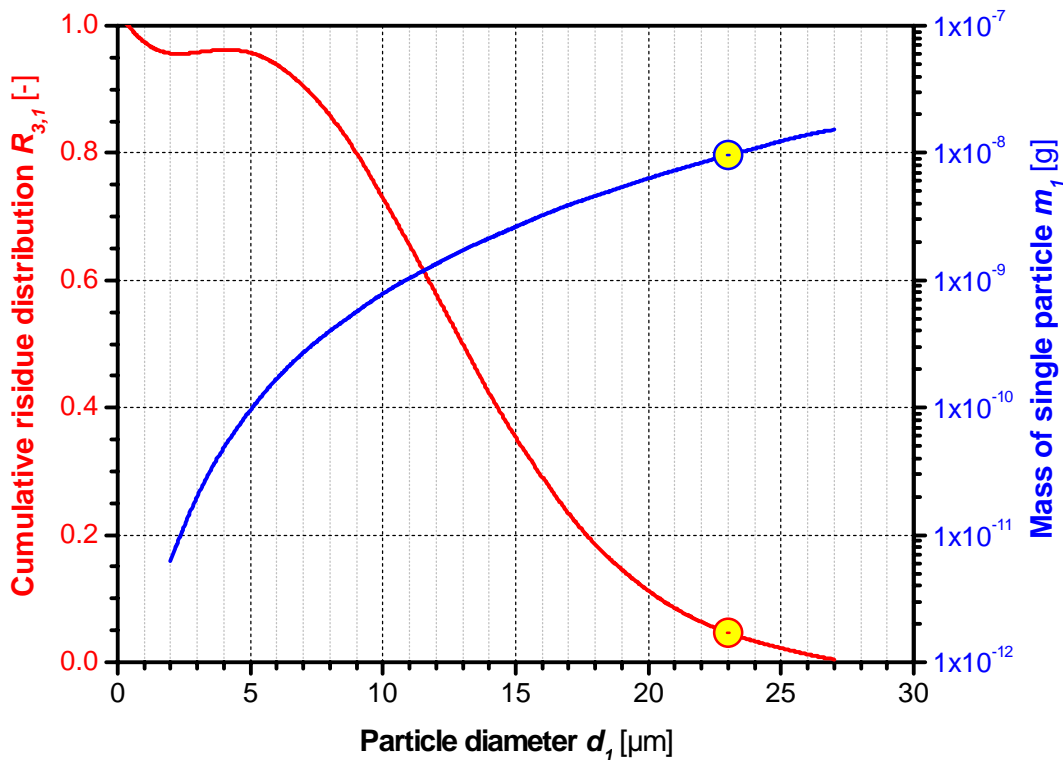


*Fig. 4-112: Graphical illustration of the meaning of the expression  $m_1(R_{3,1})$*

For the case that the smallest particle of component 1 is larger than the largest particle of component 2, the variance  $\sigma_r^2$  of a random mixture has to be calculated with *Eq. 4-22*<sup>\*)</sup>.

$$\sigma_r^2 = \frac{(1-p_1)^2 \cdot p_1}{m_{\text{sample}}} \cdot \int_0^1 \frac{m_1(Q_{3,1})}{(1-p_1 + p_1 \cdot Q_{3,1})^2} \cdot dQ_{3,1} \quad \text{Eq. 4-22}$$

In this equation,  $m_1(Q_{3,1})$  is the mass of a single particle corresponding to the value  $Q_{3,1}$  of the cumulative particle size distribution of component 1.

For mixtures of calcium carbonate (*OMYACARB 10 SV*) and maize starch (*Pharm 03406*), the effective mass of the sample analyzed by the FT-NIR spectrometer *VECTOR 22/N* in combination with the fiber optic sampling probe (type *IN 263E9*) was estimated. Detailed information about the powders can be found in *Chapter 4.2*. For maize starch concentrations of 10, 30, 50, 70 and 90 *mass-%*, mixtures were prepared in the *Lödige* mixer. After a mixing time of about 5 minutes, 50 spectra of each mixture were recorded using the “macro” procedure. The variance of the concentration values of each mixture was determined. The corresponding confidence intervals were calculated with *Eq. 4-15* and *Eq. 4-16*.

For the case that the mass of the taken samples is much higher than the mass of the single particles, the variance consists of the variance of the stochastic measuring mistakes  $\sigma_m^2$ , the variance of the random mixture  $\sigma_r^2$  and the variance of the systematical improvement of the mixing quality  $\sigma_{\text{sys}}^2(t)$ , which is the only time depending term [160, 161, 162]:

$$\sigma^2(t) = \sigma_m^2 + \sigma_r^2 + \sigma_{\text{sys}}^2(t) \quad \text{Eq. 4-23}$$

Because the number of the recorded spectra and the corresponding concentration values is not infinite, the variances in *Eq. 4-23*, except for the variance of the random mixture  $\sigma_r^2$ , have to be replaced by empirical variances.  $\sigma_{\text{sys}}^2(t)$  was set zero, assuming that a steady state was reached during the recording of the spectra. *Eq. 4-23* changes to *Eq. 4-24*.

$$s^2 = s_m^2 + \sigma_r^2 \quad \text{Eq. 4-24}$$

For the estimation of the effective mass of the sample, the variance of the random mixture  $\sigma_r^2$  has to be calculated according to *Eq. 4-24* by subtracting the empirical variance  $s_m^2$  of the stochastic measuring mistakes from the variance  $s^2$  of the determined concentrations.

For the determination of the empirical variance of the stochastic measuring mistakes, a sample with a maize starch concentration of about 44 *mass-%* was prepared and analysed 50 times without moving the sample. Afterwards the empirical variance  $s_m^2$  of the stochastic measuring mistakes and its confidence interval were calculated with *Eq. 4-15* and *Eq. 4-16*:

$$s_m^2 = 9.8 \cdot 10^{-2} \Rightarrow 6.9 \cdot 10^{-2} \leq \sigma_m^2 \leq 1.53 \cdot 10^{-1}$$

<sup>\*)</sup> Mistakenly, in the denominator of the original equation a minus was plotted instead of a plus! Compare: SOMMER, K.: Sampling of powders and bulk materials; Springer: Berlin, Heidelberg, New York, Tokyo, 1986, p. 155  
SOMMER, K.: Probenahme von Pulvern und körnigen Massengütern: Grundlagen, Verfahren, Geräte; Springer: Berlin, Heidelberg, New York, 1979, p. 158

The particle size distribution of calcium carbonate and maize starch overlap partially. Therefore, the requirement neither for using *Eq. 4-19* nor for using *Eq. 4-22* is fulfilled. In *Fig. 4-113*, the empirical variance of the measured maize starch concentrations and corrected with the empirical variance of the stochastic measuring mistakes is compared with the calculated variance of corresponding random mixtures. The variance of the random mixtures was calculated according to *Eq. 4-19* (method 1) as well as *Eq. 4-22* (method 2) for sample sizes of  $2\ \mu\text{g}$  and  $45\ \mu\text{g}$  as well as for varying maize starch concentrations.

The differences between the results obtained by using the two different methods are quite small. The curves for a sample size of  $2\ \mu\text{g}$  and  $45\ \mu\text{g}$  enclose the variances obtained experimentally. The approximated effective sample size is between  $2\ \mu\text{g}$  and  $45\ \mu\text{g}$ .

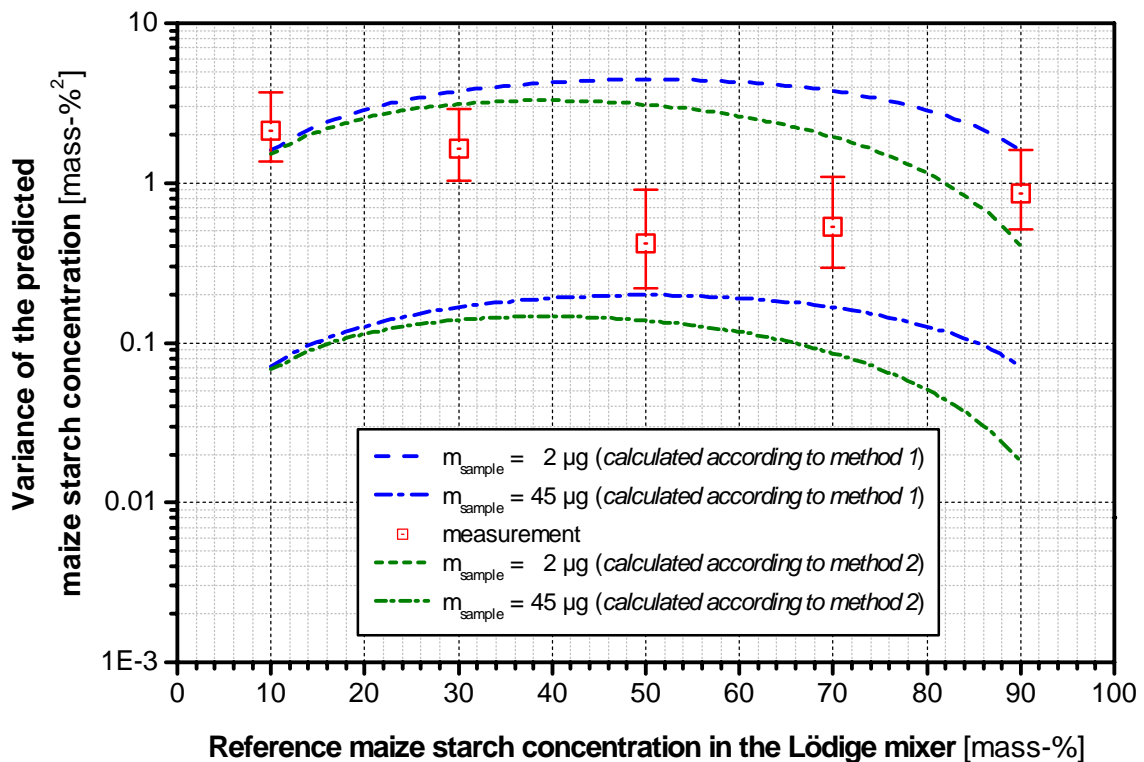


*Fig. 4-113: Comparison between the empirical variance of measured maize starch concentrations for mixtures of different composition and the variance of a random mixture calculated for different sample masses using method 1 (based on *Eq. 4-19*) and method 2 (based on *Eq. 4-22*)*

#### 4.5 Mixing experiments

The calculations with the developed mixing model have shown that the average residence time of the particles in the continuous mixer related to the period length of the entering concentration fluctuations is the main influencing parameter on the mixing quality (compare *Chapter 3.5*, p. 37). The mixing quality was defined as the quotient of the standard deviation  $\sigma_{out}$  of the concentration fluctuations in the outlet of the continuous mixer to the standard deviation  $\sigma_{in}$  of the concentration fluctuations in the inlet of the continuous mixer. For the validation of the developed model, it was necessary to compare the theoretically derived dependence of the



normalized average residence time on the mixing quality with the experimentally derived dependency.

*Fig. 4-114* shows the procedure applied during the mixing experiments. For simplification, only one mass flow (calcium carbonate) was fluctuating in a sinusoidal manner. The mass flow of the second component (maize starch) was constant. Dosing experiments have shown that a defined dosing of both powders is possible (compare *Chapter 4.3*, p. 68). Therefore, the concentration fluctuation in the mixer inlet is known and the standard deviation  $\sigma_{in}$  of the fluctuating concentration can be calculated. By the adaptation of the FT-NIR spectrometer *VECTOR 22/N*, it is possible to determine the remaining concentration fluctuations in the mixer outlet and to calculate the standard deviation  $\sigma_{out}$  of the determined concentrations. The influence of

- the rotational speed  $n$  of the mixing device,
- the mass flow  $\Delta m/\Delta t$ ,
- the period length  $T$  of the entering mass flow fluctuations and
- the filling degree  $\phi$

on the mixing quality, characterized as the fluctuation ratio  $\sigma_{out}/\sigma_{in}$ , was examined. Parallel to the determination of the mixing quality, the average residence time was determined. The determination of the average residence time is described in detail in *Chapter 4.5.1* (see p. 155).

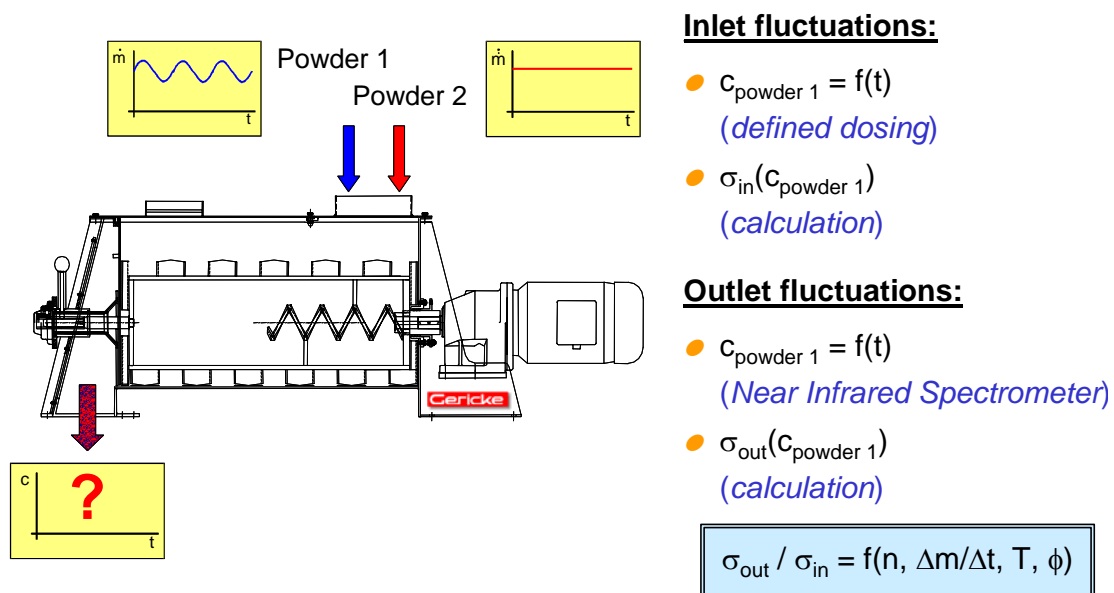


*Fig. 4-114: Illustration of the procedure for the experimental determination of the mixing quality*

The mass flow fluctuation  $\dot{m}_1(t)$  of the entering calcium carbonate (powder 1) can be described with *Eq. 4-25*. The constant mass flow  $\dot{m}_2(t)$  of the maize starch (powder 2) describes *Eq. 4-26*.

$$\dot{m}_1(t) = \dot{m}_{1,0} + \dot{m}_{1,A} \cdot \sin\left(2\pi \cdot \frac{1}{T} \cdot t\right) \quad \text{Eq. 4-25}$$

$$\dot{m}_2(t) = \dot{m}_{2,0} \quad \text{Eq. 4-26}$$



$\dot{m}_{1,0}$  is the offset of the calcium carbonate fluctuation,  $\dot{m}_{A,1}$  the amplitude and  $T$  the period length.  $\dot{m}_{2,0}$  is the offset of the maize starch fluctuation. The resulting concentration fluctuation  $c_1(t)$  of calcium carbonate in the inlet of the continuous mixer describes Eq. 4-27.

$$c_1(t) = \frac{\dot{m}_1(t)}{\dot{m}_1(t) + \dot{m}_2(t)} = \frac{\dot{m}_{1,0} + \dot{m}_{A,1} \cdot \sin\left(2\pi \cdot \frac{1}{T} \cdot t\right)}{\dot{m}_{1,0} + \dot{m}_{A,1} \cdot \sin\left(2\pi \cdot \frac{1}{T} \cdot t\right) + \dot{m}_{2,0}} \quad \text{Eq. 4-27}$$

The entering conditions for a constant maize starch mass flow of 20 g/s and a fluctuating calcium carbonate mass flow with an offset of 15 g/s, an amplitude of 14 g/s and a period length of 40 s is shown in Fig. 4-115.

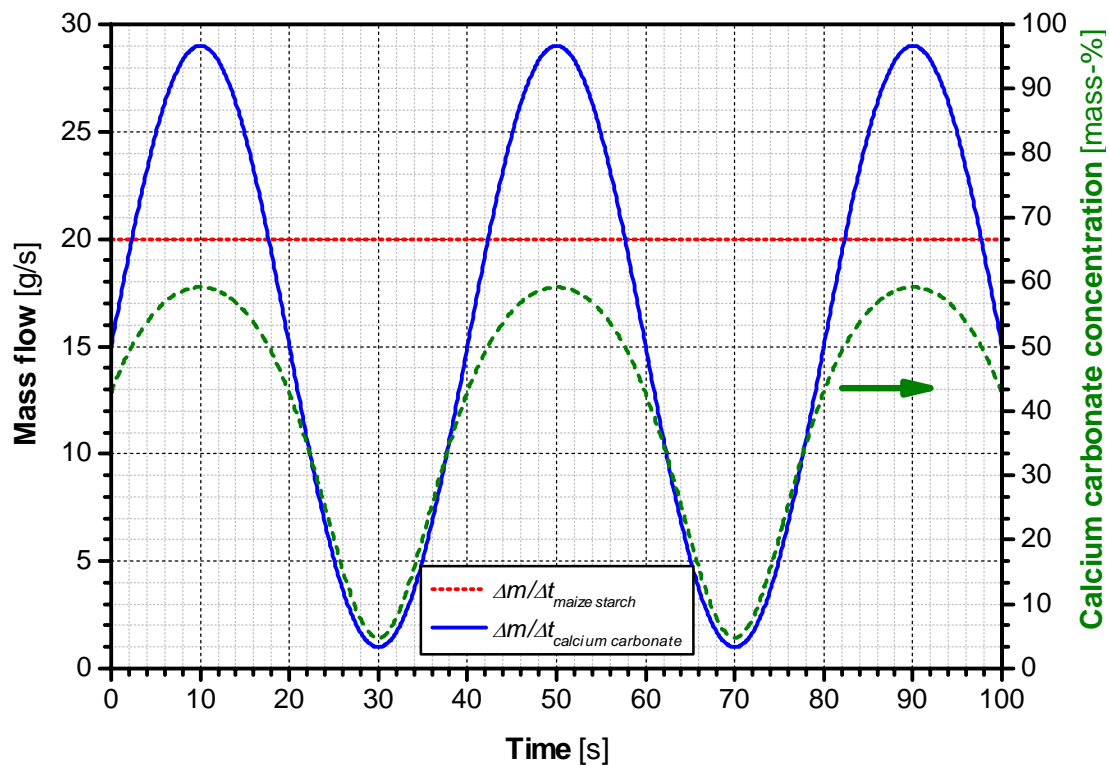


**Fig. 4-115:** Illustration of the inflow conditions (fluctuating calcium carbonate mass flow with  $\dot{m}_{O,1} = 15$  g/s,  $\dot{m}_{A,1} = 14$  g/s and  $T = 40$  s; constant maize starch mass flow with  $\dot{m}_{O,2} = 20$  g/s)

The calcium carbonate concentration fluctuations measured in the outlet of the continuous mixer are presented in Fig. 4-116. Besides the original data points, also filtered data points are shown. For filtering, three data points following each other were averaged to the new concentration  $c_i^*$  (algorithm see Eq. 4-28).

$$c_i^* = \frac{c_{i-1} + c_i + c_{i+1}}{3} \quad \text{Eq. 4-28}$$

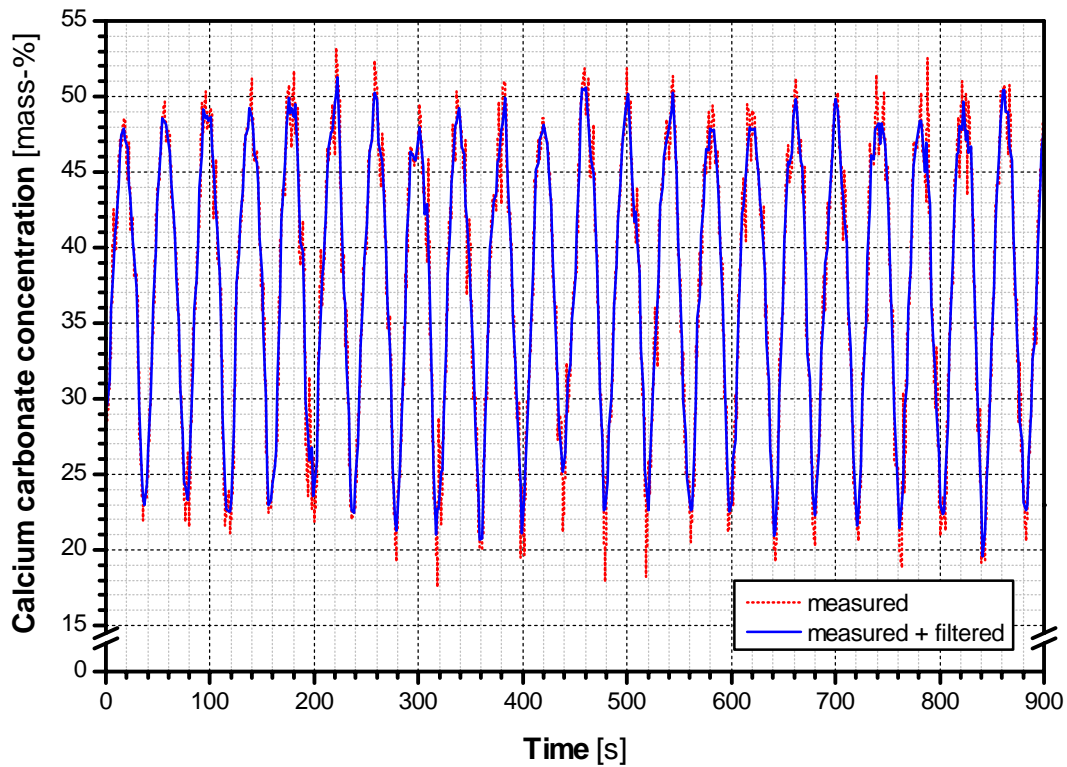


**Fig. 4-116:** Calcium carbonate concentration measured in the outlet of the continuous mixer for 196 revolutions of the mixing device per minute (inflow conditions: fluctuating calcium carbonate mass flow with  $\dot{m}_{O,1} = 15$  g/s,  $\dot{m}_{A,1} = 14$  g/s and  $T = 40$  s; constant maize starch mass flow with  $\dot{m}_{O,2} = 20$  g/s)

The reduction of the concentration fluctuations can also be illustrated very well in the frequency domain using the fast Fourier transformation. **Fig. 4-117** shows the Fourier spectra of the inlet concentration fluctuations and the Fourier spectra of the concentrations measured in the outlet of the continuous mixer, which were filtered afterwards. Significant peaks at  $0.025$ ,  $0.05$  and  $0.075$  Hz are obvious. The peak at the frequency of  $0.025$  Hz corresponds to the fundamental frequency of the generated concentration fluctuations with a period length of  $40$  s. The other frequencies are integer multiples of the fundamental frequency and correspond to the harmonics of the generated concentration fluctuations.

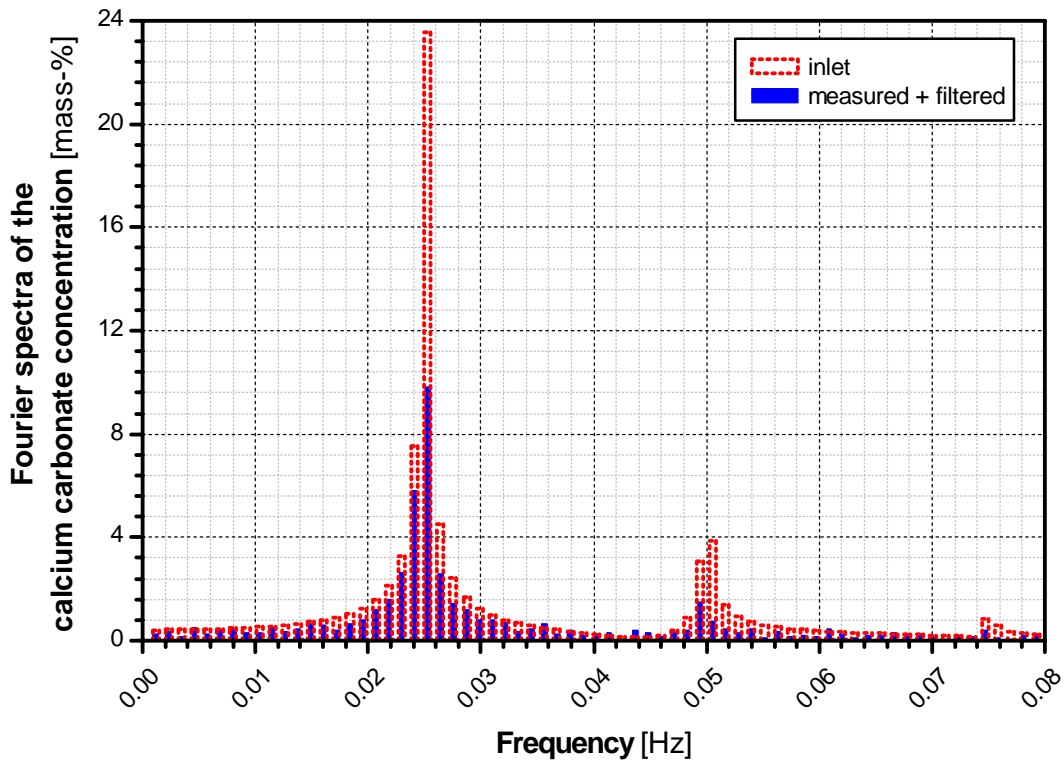


**Fig. 4-117:** Fourier spectra of the calcium carbonate concentrations measured in the outlet of the continuous mixer (inflow conditions: fluctuating calcium carbonate mass flow with  $\dot{m}_{O,1} = 15$  g/s,  $\dot{m}_{A,1} = 14$  g/s and  $T = 40$  s; constant maize starch mass flow with  $\dot{m}_{O,2} = 20$  g/s)

#### 4.5.1 Determination of the average residence time

The average residence time  $t_R^*$  of the two powders in the continuous dynamic mixer GCM 500 can be determined in two different ways:

- *Hold-up method:* The average residence time is determined by means of the average mass flow entering the continuous mixer and the mass hold-up in the mixer.
- *Step method:* The average residence time is determined by evaluating the influence of a stepwise concentration changing in the inlet of the mixer on the concentration in the outlet of the mixer.

##### 4.5.1.1 Determination of the average residence time using the “hold-up method”

The quotient of the accumulated mass (mass hold-up,  $m_{hold}$ ) in the mixer and the sum of the average mass flows entering the continuous mixer is called the average residence time  $t_{R,hold}^*$  of the powders in the mixer. For a two-component mixture, the following equation describes the calculation of the average residence time:

$$t_{R,hold}^* = \frac{m_{hold}}{\dot{m}_1(t) + \dot{m}_2(t)} \quad \text{Eq. 4-29}$$

$\dot{m}_1(t)$  and  $\dot{m}_2(t)$  are the average mass flows of the two powders (calcium carbonate and maize starch) fed in the continuous mixer. The feeders as well as the mixer were located on weighing cells. At the beginning of each experimental day, the maximum mass flow, which can be reached with the volumetric feeders, was determined. The decrease of the feeder weight as well as the increase of the mixer weight in a defined time was used to determine the mass flow. As shown in *Fig. 4-54* and *Fig. 4-55* (see p. 101), a linear dependency exists between the rotational speed of the proportioning device and the mass flow coming out of the volumetric feeders. Therefore, the average mass flows  $\dot{m}_1(t)$  and  $\dot{m}_2(t)$  result from the offset mass flows set in the control and visualization surface of the experimental rig (compare *Fig. 4-4*, p. 62). During the experimental day, the maximum mass flow coming out of the volumetric feeders was checked several times.

At the end of every mixing trial, the emergency bottom of the experimental rig was pushed, whereby the powder dosing and the rotation of the mixing device stopped immediately. The actual mass  $m_{hold}'$  in the mixer does not correspond to the mass hold-up  $m_{hold}$ , which has to be substituted in *Eq. 4-29*. An unknown amount of the powder accumulates on the mixer shell and does not take part in the mixing process. To determine the mass of the powder which takes part in the mixing process, the rotation of the mixing device is started again. As soon as no powder was falling out of the mixer, the rotation of the mixing device was stopped. The remaining mass in the mixer  $m_{hold}''$  corresponds to the mass which was accumulated on the mixer shell. The mass hold-up  $m_{hold}$  of the powder taking part in the mixing process can be calculated with *Eq. 4-30*:

$$m_{hold} = m_{hold}' - m_{hold}'' \quad \text{Eq. 4-30}$$

#### 4.5.1.2 Determination of the average residence time using of the “step method”

For the determination of the average residence time  $t_{R,step}^*$  by using the “step method”, the powders were fed with a constant mass flow in the continuous mixer. After reaching the steady state, the concentration of the mixture was changed in a stepwise manner. According to *Eq. 4-31*, the concentration response in the mixer outlet (e.g. maize starch concentration in dependence of time) was used to calculate the first moment of the cumulative residence time distribution  $F(t)$ . The resulting average residence time  $t_{R,step}^*$  was calculated with *Eq. 4-32*.  $c_2(t)$  is the change of the maize starch concentration with time.  $c_{2,0}$  is the maize starch concentration before the stepwise change of the concentration and  $c_{2,1}$  the maize starch concentration afterwards. [50]

$$F(t) = \frac{c_2(t) + c_{2,0}}{c_{2,1} - c_{2,0}} \quad \text{Eq. 4-31}$$

$$t_{R,step}^* = \sum_{i=1}^{\infty} F(t_i) \cdot t_i = \sum_{i=1}^{\infty} \frac{c_2(t_i) + c_{2,0}}{c_{2,1} - c_{2,0}} \cdot t_i \quad \text{Eq. 4-32}$$

A typical response in the mixer outlet to a stepwise changing of the maize starch concentration in the mixer inlet is shown in *Fig. 4-118*. For the experiment, the set mixture composition of 20 mass-% maize starch and 80 mass-% calcium carbonate was changed in a stepwise manner to

a maize starch concentration of 80 mass-%. After 425 s, the maize starch concentration was set back to the initial value. The corresponding cumulative residence time distribution resulting from the stepwise changing of the maize starch concentration from 20 to 80 mass-% is shown in Fig. 4-119.

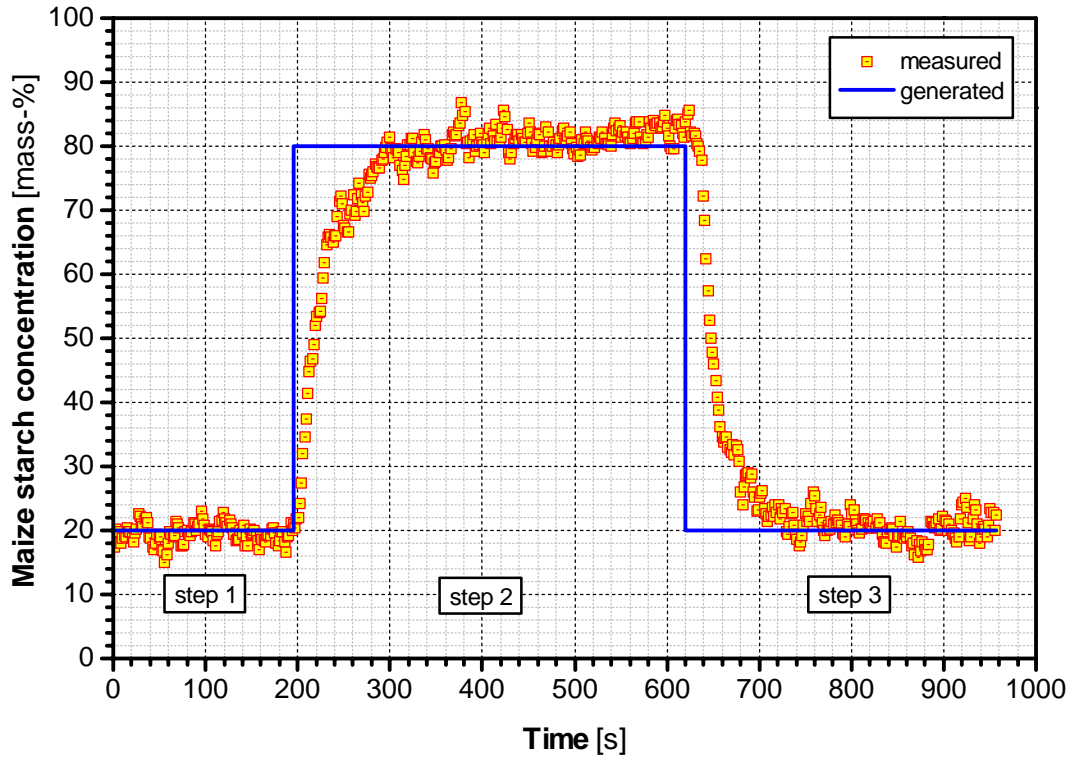


**Fig. 4-118:** In-line concentration determination in the mixer outlet to determine the average residence time (stepwise changing of the set maize starch concentration):

step 1:  $\dot{m}_{\text{maize starch}} \approx 5.5 \text{ g/s}$ ,  $\dot{m}_{\text{calcium carbonate}} \approx 21.1 \text{ g/s}$ ;

step 2:  $\dot{m}_{\text{maize starch}} \approx 21.1 \text{ g/s}$ ,  $\dot{m}_{\text{calcium carbonate}} \approx 5.1 \text{ g/s}$ ;

step 3:  $\dot{m}_{\text{maize starch}} \approx 5.3 \text{ g/s}$ ,  $\dot{m}_{\text{calcium carbonate}} \approx 21.4 \text{ g/s}$

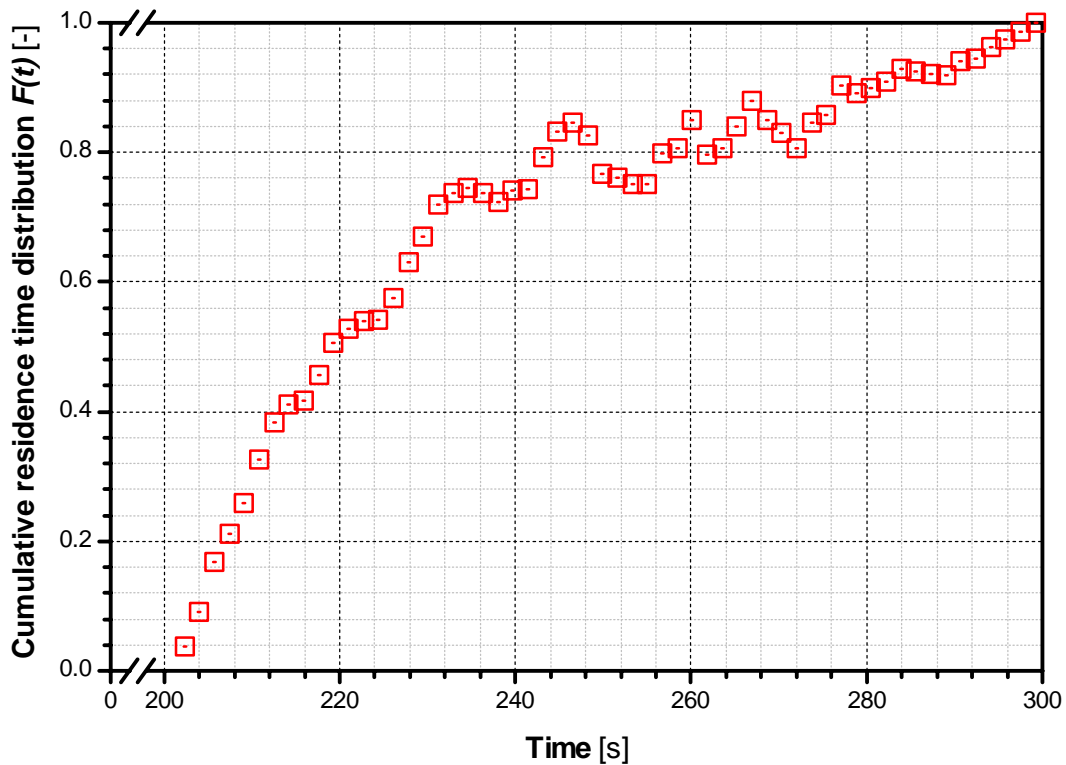


*Fig. 4-119: Cumulative residence time distribution resulting from a stepwise changing of the maize starch concentration from 20 to 80 mass-% (compare Fig. 4-118)*

#### 4.5.1.3 Comparison of the experimental results obtained by using the “hold-up method” and the “step method”

The determination of the average residence time applying the “hold-up method” is much easier than the determination of the average residence time applying the “step method”. To examine if there is a significant difference between the results obtained by using the two methods, the average residence time was determined at first by the “step method” and directly afterwards by the “hold-up method”. Each trial was repeated two times. For the conditions described in the previous chapter, the results are listed in *Table 4-7*.

*Table 4-7: Comparison between average residence times obtained by using the “hold-up method” and the “step method”*

“hold-up method”	“step method”
$t_{R,hold}^* = 23.4 \text{ s}$	$t_{R,step}^* = 26.9 \text{ s}$
$t_{R,hold}^* = 26.5 \text{ s}$	$t_{R,step}^* = 22.6 \text{ s}$
$t_{R,hold}^* = 26.6 \text{ s}$	$t_{R,step}^* = 26.2 \text{ s}$
$\overline{t_{R,hold}^*} = 25.5 \text{ s} \pm 4.6 \text{ s}$	$\overline{t_{R,step}^*} = 25.2 \text{ s} \pm 5.8 \text{ s}$

For a probability of 95 %, there was no significant difference between the two methods. Therefore, the determination of the average residence time by means of the “hold-up method” was used for the validation of the developed mixing model.

#### 4.5.2 Mixing experiments for the validation of the mixing model

Based on the publications of FAN, CHEN and WATSON [10], RUZBEHI [163, 164] as well as WEINEKÖTTER [50] the parameters influencing the mixing process in continuous dynamic powder mixers can be divided in four main groups:

1. *Machine parameters:* e.g. mixer size and type, style and number of the mixing devices, position of the mixing devices relative to the longitudinal axis
2. *Process parameters:* e.g. rotational speed of the mixing device, concentration composition, mass flow, weir position  $\Rightarrow$  filling degree of the mixer
3. *Product parameters:* e.g. direct particle parameters such as median diameter, size distribution, real density, shape, friability as well as indirect particle parameters such as bulk density, flowability and fluidization ability
4. *Environmental parameters:* e.g. humidity and temperature

During the mixing experiments for the validation of the mixing model the following parameters were varied:

- the mass flow of the maize starch  $\Delta m/\Delta t$ ,
- the rotational speed of the mixing device  $n$ ,
- the period length  $T$  of the sinusoidal mass flow fluctuations of the calcium carbonate and
- the weir position, which results in a changing of the filling degree  $\phi$  of the continuous mixer.

At the end of the continuous mixer, a weir is located. In *Fig. 4-120*, the two positions of the weir used during the mixing experiments are illustrated. The left drawing shows the half-closed weir and the right drawing the closed weir. The powder leaves the mixer through the white area.

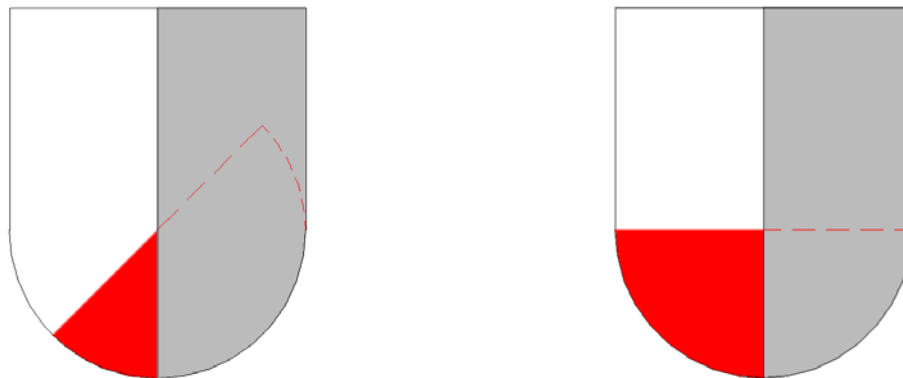


*Fig. 4-120: Different positions of the weir during the mixing experiments: Half-closed (left), closed (right); the powder flows through the white area*



During every mixing trial, the fluctuations of the calcium carbonate concentration in the outlet of the continuous mixer as well as the corresponding average residence time were determined. The fluctuations of the calcium carbonate concentration were characterized by the variance and the standard deviation respectively. The number of concentration values taken into account is limited. Therefore, some variances in *Eq. 4-23* (see p. 150) have to be replaced by empirical variances:

$$s^2(t) = s_m^2 + \sigma_r^2 + s_{sys}^2(t) \quad \text{Eq. 4-33}$$

$s_m^2$  is the empirical variance of the stochastic measuring mistakes,  $\sigma_r^2$  the variance of the random mixture and  $s_{sys}^2(t)$  the empirical variance of the systematical improvement of the mixing quality.

The evaluation of the mixing experiments started after the steady state was reached. Therefore, the empirical variance  $s_{sys}^2(t)$  of the systematical improvement of the mixing quality can be set equal to zero. The empirical variance  $s^2$  of a mixing trial is time-independent and consists of the empirical variance of the stochastic measuring mistakes  $s_m^2$  and the variance of the random mixture  $\sigma_r^2$ :

$$s^2 = s_m^2 + \sigma_r^2 \quad \text{Eq. 4-34}$$

The fluctuation ratio  $\sigma_{out} / \sigma_{in}$  calculated with the developed mixing model (compare chapter *3.5 Results of the performed simulation experiments*) only includes the standard deviation  $\sigma_r$  of the random mixture:

$$FR = \frac{\sigma_{out}}{\sigma_{in}} = \frac{\sigma_{r,out}}{\sigma_{r,in}} \quad \text{Eq. 4-35}$$

Regarding the later comparison of the calculated and the experimentally obtained fluctuation ratios, the empirical variance  $s^2$  and the empirical standard deviation  $s$  respectively determined by means of mixing trials have to be corrected by the empirical variance of the stochastic measuring mistakes  $s_m^2$  and the empirical standard deviation of the stochastic measuring mistakes  $s_m$  respectively.

$$FR_{experimental} = \frac{\sigma_{r,out}}{\sigma_{r,in}} = \frac{\sqrt{s_{out}^2 - s_m^2}}{\sigma_{r,in}} \quad \text{Eq. 4-36}$$

### **Determination of the empirical standard deviation of the stochastic measuring mistakes**

For the determination of the empirical standard deviation of the stochastic measuring mistakes, nine mixtures of different known concentration were prepared by mixing the powders in a beaker with a spatula. Only mixtures with maize starch concentrations between 10 and 90 mass-% were used because maize starch concentrations smaller than 5 mass-% and higher than 95 mass-% were not taken into account during the development of the calibration model.

The maize starch concentration of each mixture prepared was determined seven times. The results of the examinations are shown in *Fig. 4-121*.

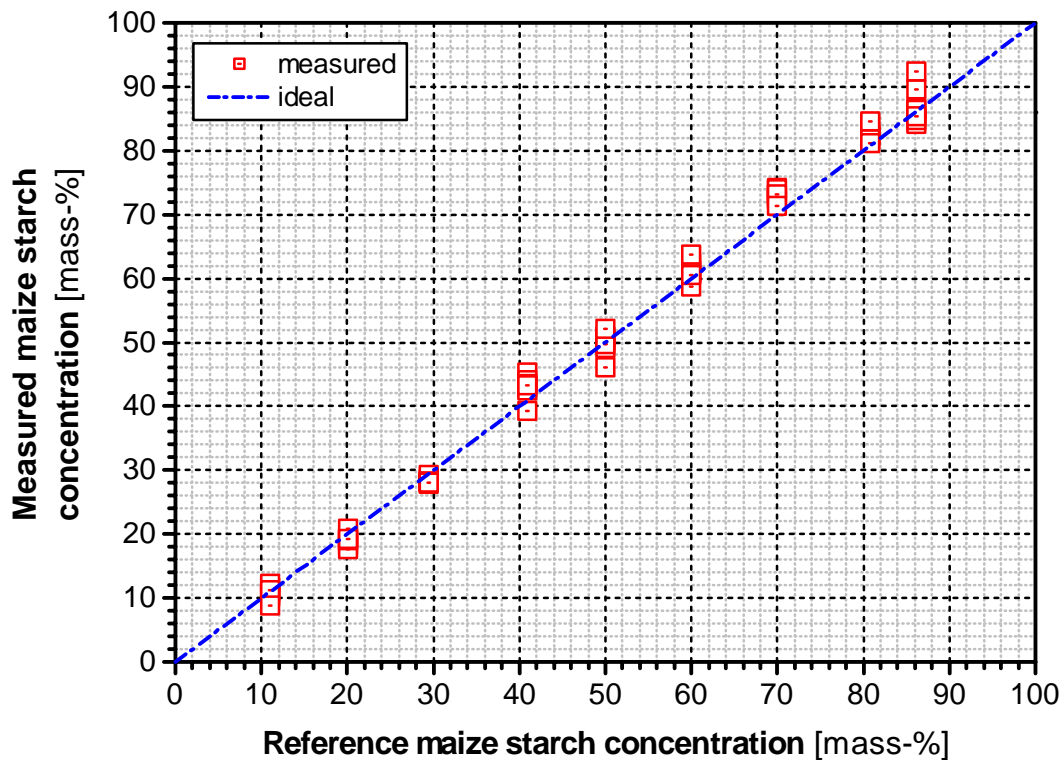


*Fig. 4-121: Maize starch concentrations determined for different set reference maize starch concentrations*

The average empirical standard deviation of the measured maize starch concentrations and the corresponding confidence interval were calculated for every set reference maize starch concentration. The results are shown in *Fig. 4-122*. For the whole concentration range, no significant difference exists.

The empirical standard deviation of the stochastic measuring mistakes  $s_m$  was determined with *Eq. 4-37* based on  $n = 63$  measuring points.

$$s_m = \sqrt{\frac{1}{n} \cdot \sum_{i=1}^9 \sum_{j=1}^7 (x_{i,j} - p_i)^2} \quad \text{with } n=63 \quad \text{Eq. 4-37}$$

The result for the average empirical standard deviation of the stochastic measuring mistakes  $\bar{s}_m$  and the limits of the confidence interval are:

$$s_m = 2.1 \text{ mass} - \% \Rightarrow 1.8 \text{ mass} - \% \leq \sigma_m \leq 2.6 \text{ mass} - \%$$

The confidence interval was calculated with *Eq. 4-15* and *Eq. 4-16*.

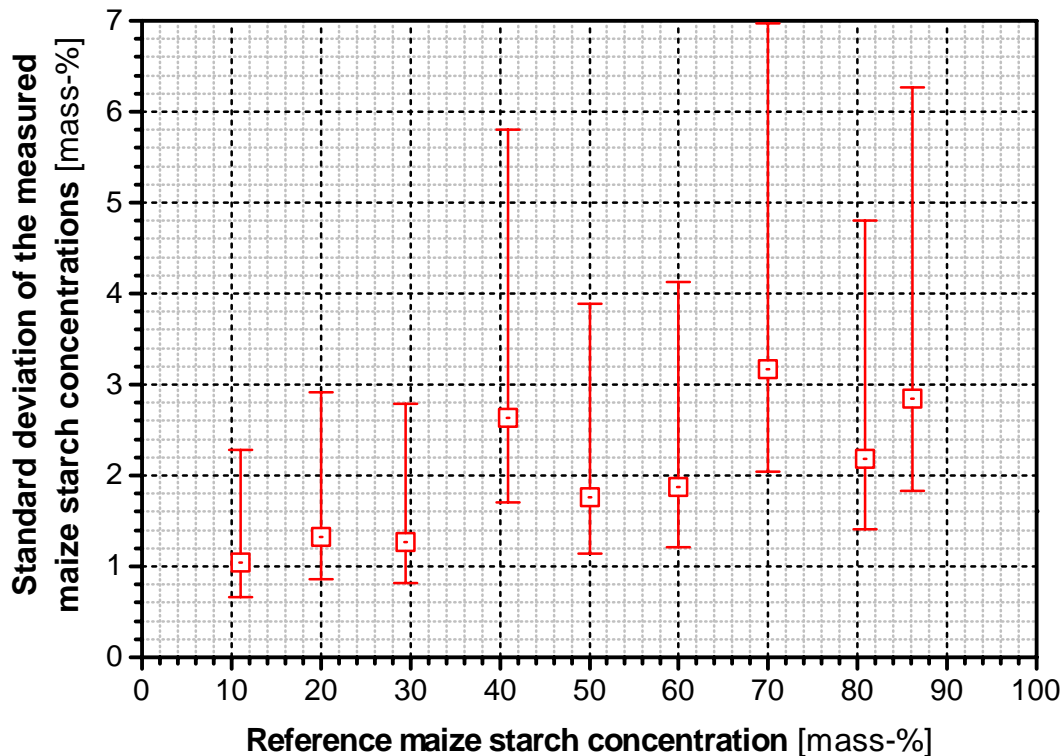


*Fig. 4-122: Standard deviation of maize starch concentrations measured for different set reference maize starch concentrations*

### Notes to the presentation of the results of the mixing performed experiments

The results of the performed mixing experiments are presented in the following order:

**Part I:** For a half-closed weir, the influence of

- the overall mass flow,
- the rotational speed of the mixing device and
- the period length of the entering calcium carbonate mass flow

on the fluctuation ratio (mixing quality) as well as the normalized average residence time are discussed.

**Part II:** For a closed weir, the influence of

- the overall mass flow,
- the rotational speed of the mixing device and
- the period length of the entering calcium carbonate mass flow

on the fluctuation ratio (mixing quality) as well as the normalized average residence time are discussed.

In the mixing results presented, the empirical standard deviation  $s$  was corrected with the empirical standard deviation of the measuring mistakes  $s_m$ . At the beginning of each chapter, the calcium carbonate concentration fluctuations in the inlet of the continuous mixer, which were calculated, are compared with one of three calcium carbonate concentration fluctuations measured in the outlet of the continuous mixer.

After the steady state was reached in the continuous mixer, 500 concentration values were recorded and used to calculate the empirical standard deviation of the concentration fluctuations in the outlet of the continuous mixer. Each mixing trial was repeated two times. The standard settings were:

*Powder 1 (fluctuating mass flow, calcium carbonate):*

- $\dot{m}_{0,1} = 15 \text{ g/s} = 54.0 \text{ kg/h}$  (offset),
- $\dot{m}_{A,1} = 14 \text{ g/s} = 50.4 \text{ kg/h}$  (amplitude),
- $T = 40 \text{ s}$  (period length)

*Powder 2 (constant mass flow, maize starch):*

- $\dot{m}_{0,2} = 10 \text{ g/s} = 36.0 \text{ kg/h}$  (offset),
- $\dot{m}_{A,2} = 0 \text{ g/s}$  (amplitude)

*Mixing device:*

- $n = 196 \text{ min}^{-1}$  (rotational speed)
- paddles on a rectangular steel frame (see *Fig. 4-123*)

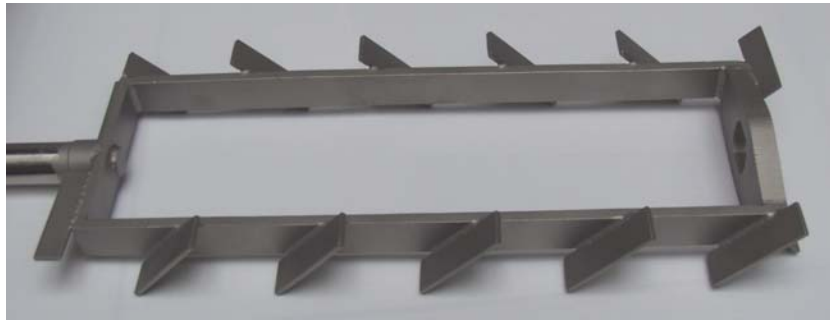


*Fig. 4-123: Mixing device used during the mixing trials*

#### 4.5.2.1 Influence of the average overall mass flow on the mixing result (half-closed weir)

The standard settings of the calcium carbonate mass flow ( $\dot{m}_{1,0} = 15 \text{ g/s}$ ,  $\dot{m}_{1,A} = 14 \text{ g/s}$ ,  $T = 40 \text{ s}$ ) and the standard rotational speed of the mixing device ( $n = 196 \text{ min}^{-1}$ ) were used to examine the influence of the average overall mass flow on the fluctuation ratio (mixing quality) and the normalized average residence time. The average maize starch mass flow was decreased from 20 to 5 g/s in steps of 5 g/s. For the resulting overall mass flows, the calcium carbonate concentration fluctuations in the inlet of the continuous mixer, which were calculated, were compared with the calcium carbonate concentration fluctuations in the outlet of the mixer, which were measured. The comparison was done in the time domain (see *Fig. 4-124*) and the frequency domain (see *Fig. 4-125*).

For the comparison in the frequency domain, the temporal changing of the calcium carbonate concentration was Fourier transformed. A higher reduction of the concentration fluctuations with a decrease of the average overall mass flow and the average maize starch mass flow respectively was observed. This tendency becomes more obvious if the fluctuation ratio  $\sigma_{out}/\sigma_{in}$  is plotted against the average overall mass flow (compare left diagram of *Fig. 4-126*).

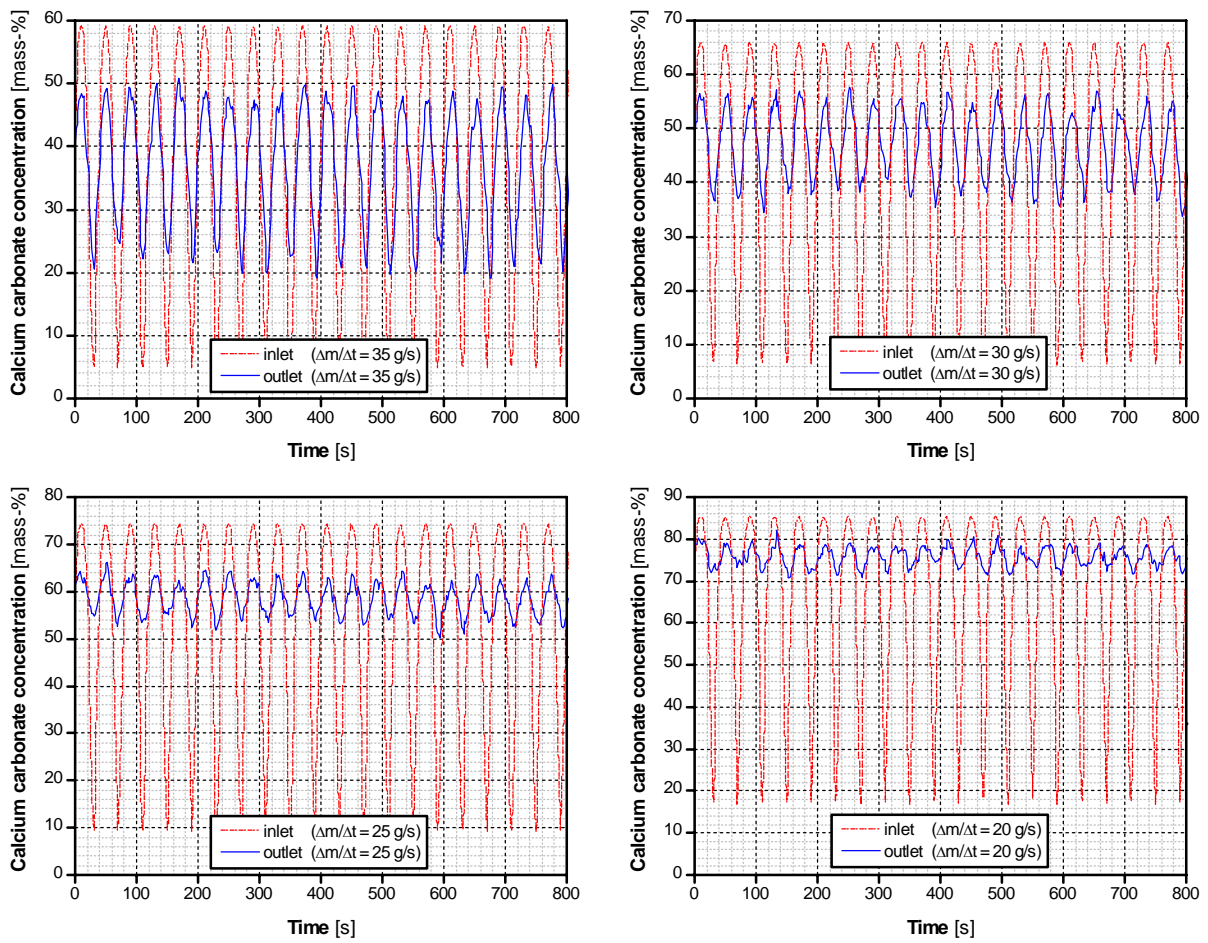


**Fig. 4-124:** Influence of the overall mass flow on the mixing result - The scale of the y-axis changes in each diagram! (time domain, half-closed weir)

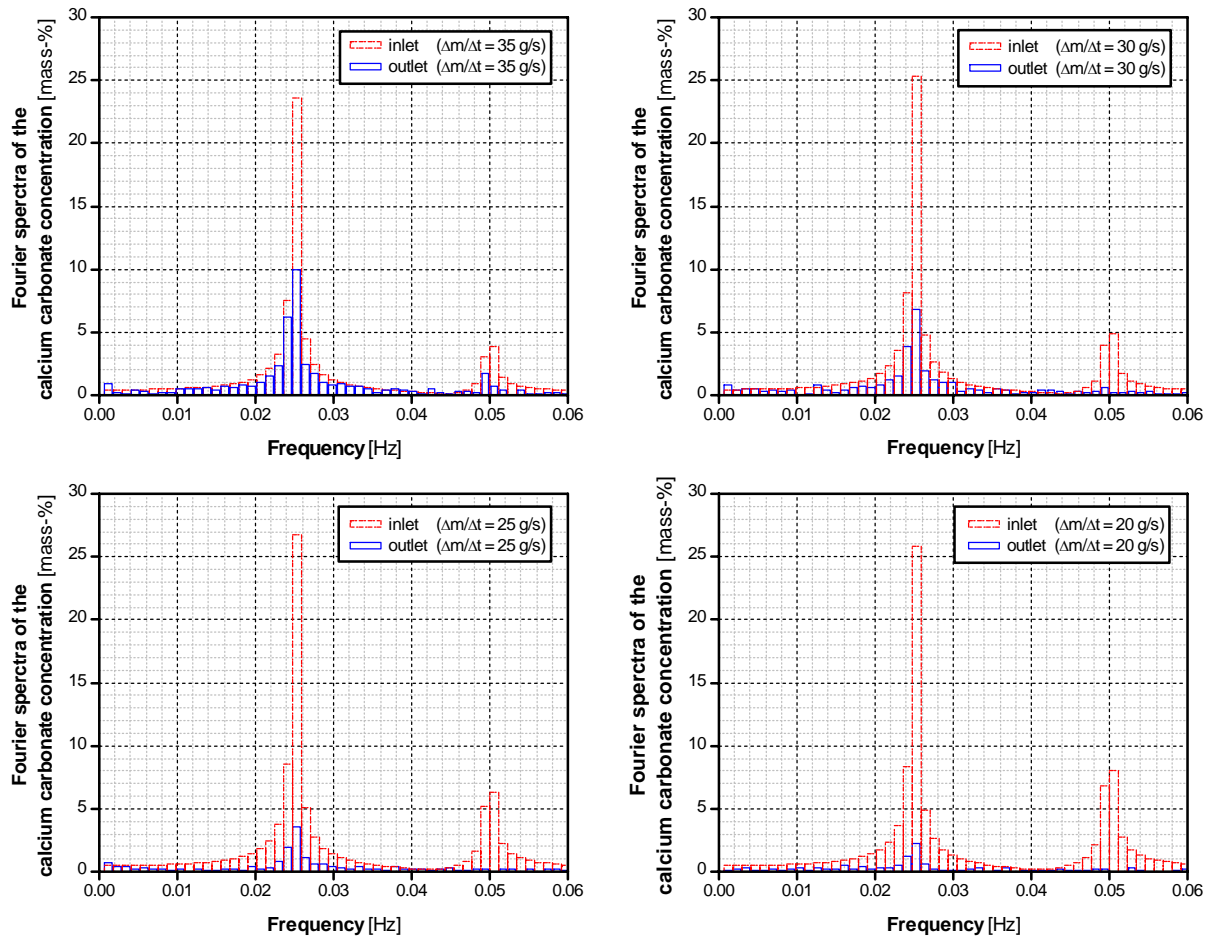


*Fig. 4-125: Influence of the average overall mass flow on the mixing result (frequency domain, half-closed weir)*

The right diagram of *Fig. 4-126* shows the influence of the average overall mass flow on the normalized average residence time  $t_R^*/T$ . The mixing experiments were performed with relatively small calcium carbonate and maize starch mass flows. As a result, the mass hold-up in the mixer is relatively small and the determined confidence intervals of the normalized average residence time are relatively big. Thus, no significant influence of the average overall mass flow on the normalized average residence time was observed.

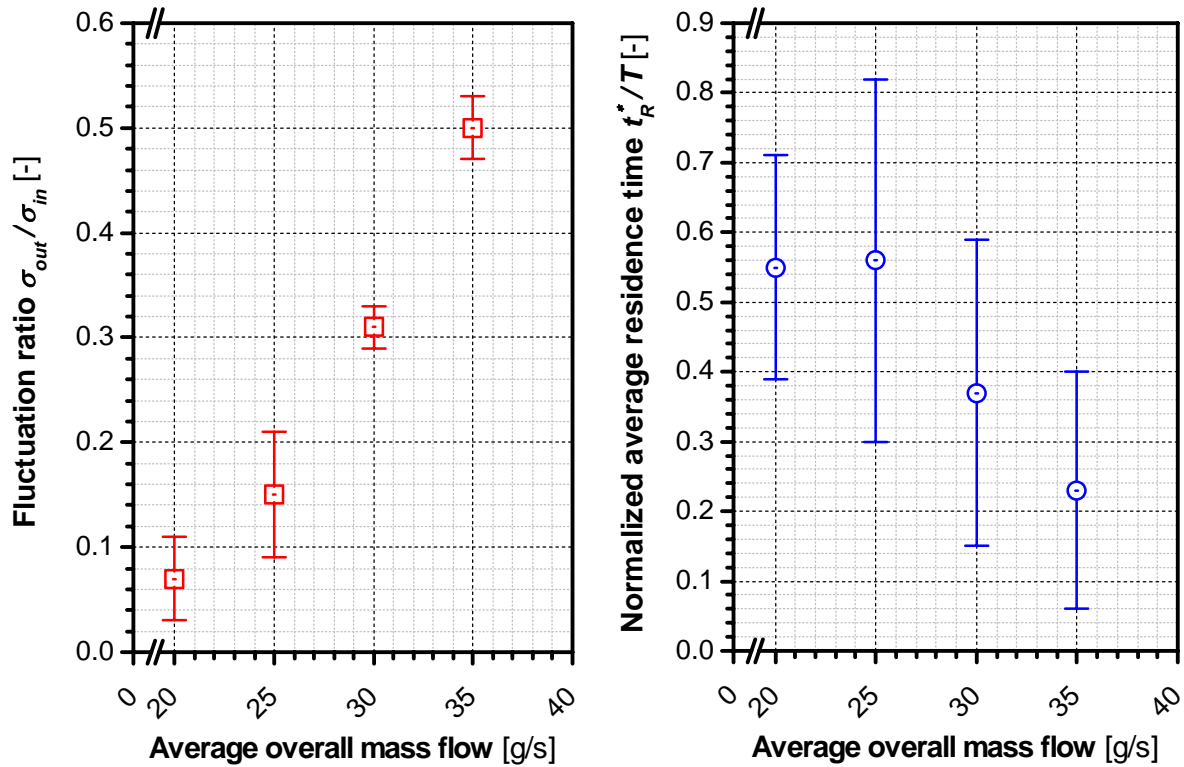


*Fig. 4-126: Influence of the average overall mass flow on the fluctuation ratio and the normalized average residence time (half-closed weir)*

To every fluctuation ratio, a corresponding normalized average residence time exists. These pairs are shown in *Fig. 4-127*. Resulting from the large confidence intervals of the normalized average residence time, no significant influence on the fluctuation ratio was found.



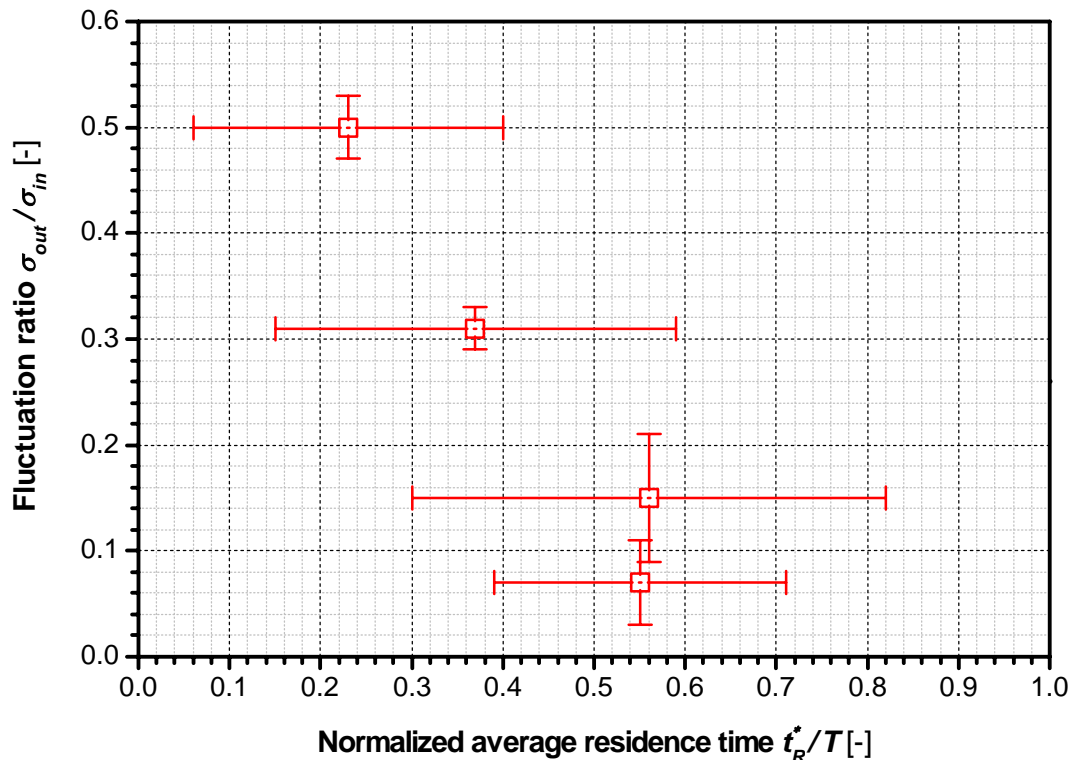


*Fig. 4-127: Influence of the normalized average residence time on the fluctuation ratio as a result of mass flow variations (half-closed weir)*

#### 4.5.2.2 Influence of the rotational speed of the mixing device on the mixing result (half-closed weir)

The standard settings of the calcium carbonate mass flow ( $\dot{m}_{1,O} = 15 \text{ g/s}$ ,  $\dot{m}_{1,A} = 14 \text{ g/s}$ ,  $T = 40 \text{ s}$ ) and the maize starch mass flow ( $\dot{m}_{2,O} = 10 \text{ g/s}$ ,  $\dot{m}_{2,A} = 0 \text{ g/s}$ ) were used to examine the influence of the rotational speed on the fluctuation ratio and the normalized average residence time. The rotational speed was decreased from the maximum of  $196 \text{ min}^{-1}$  to  $176$ ,  $118$ ,  $78$  and  $39 \text{ min}^{-1}$ . The calcium carbonate concentration fluctuations in the inlet of the continuous mixer, which were calculated, were compared with the calcium carbonate concentration fluctuations in the outlet of the mixer, which were measured. The comparison was done in the time domain (see *Fig. 4-128*) and in the frequency domain (see *Fig. 4-129*).

A reduction of the concentration fluctuations in the mixer was observed for decreasing rotational speeds. For rotational speeds smaller than  $118 \text{ min}^{-1}$ , the fluctuations in the mixer outlet were in the same magnitude. This tendency becomes more obvious if the fluctuation ratio  $\sigma_{out}/\sigma_{in}$  is plotted against the rotational speed (compare left diagram of *Fig. 4-130*). For rotational speeds smaller than  $118 \text{ min}^{-1}$ , the empirical standard deviations of the mixing experiments were small compared to the empirical standard deviation of the measuring mistakes. As a result, the fluctuation ratio becomes zero. The decrease of the fluctuation ratio with decreasing rotational speeds is caused by an increase of the average residence time. The right diagram of *Fig. 4-130* shows that the normalized average residence time  $t_R^*/T$  decreases with an increase of the rotational speed. For rotational speeds higher than  $118 \text{ min}^{-1}$ , the average residence time of the particles in the mixer was in the same magnitude or smaller than the period length of the entering concentration fluctuations.

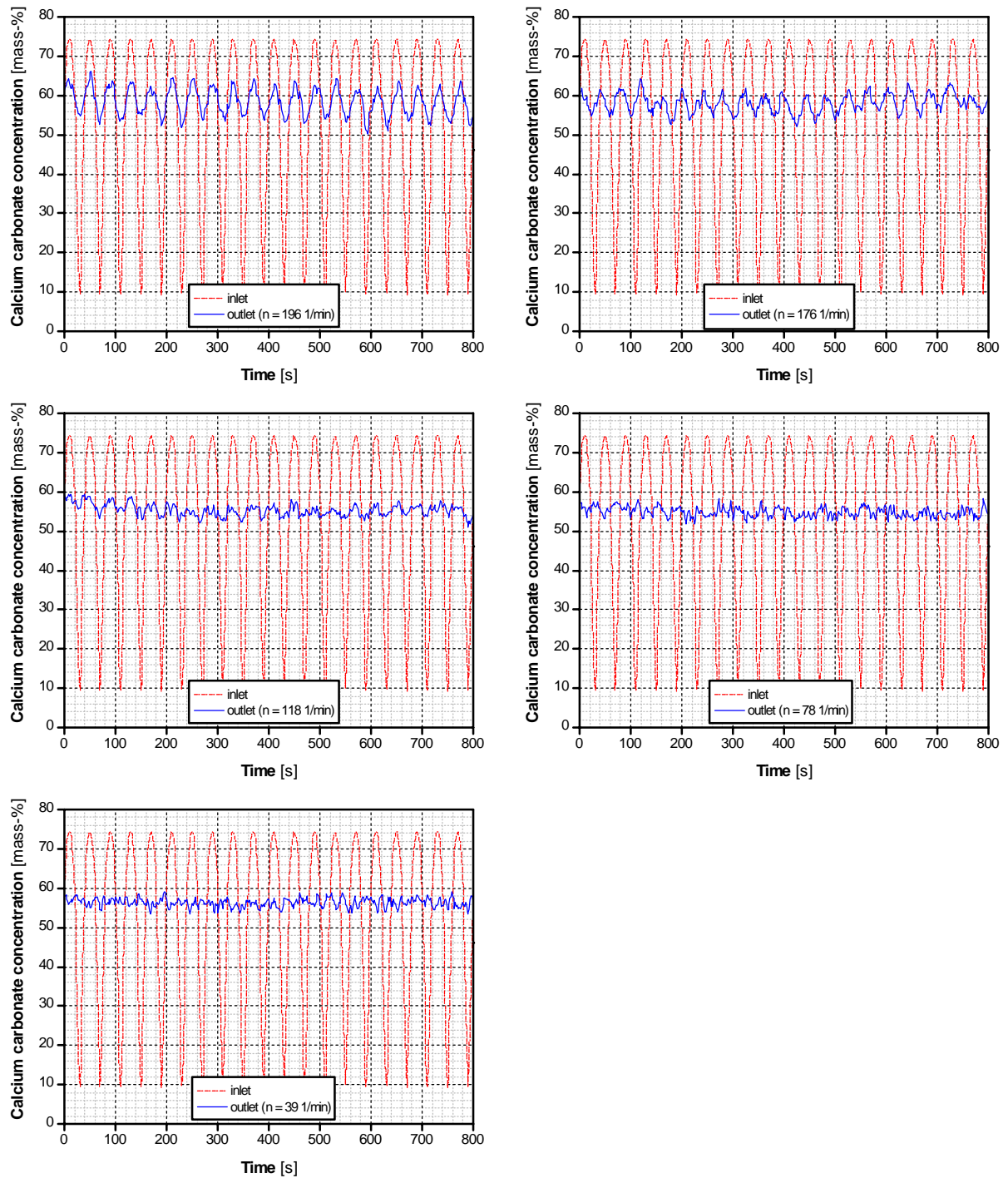


*Fig. 4-128: Influence of the rotational speed of the mixing device on the mixing result (time domain, half-closed weir)*

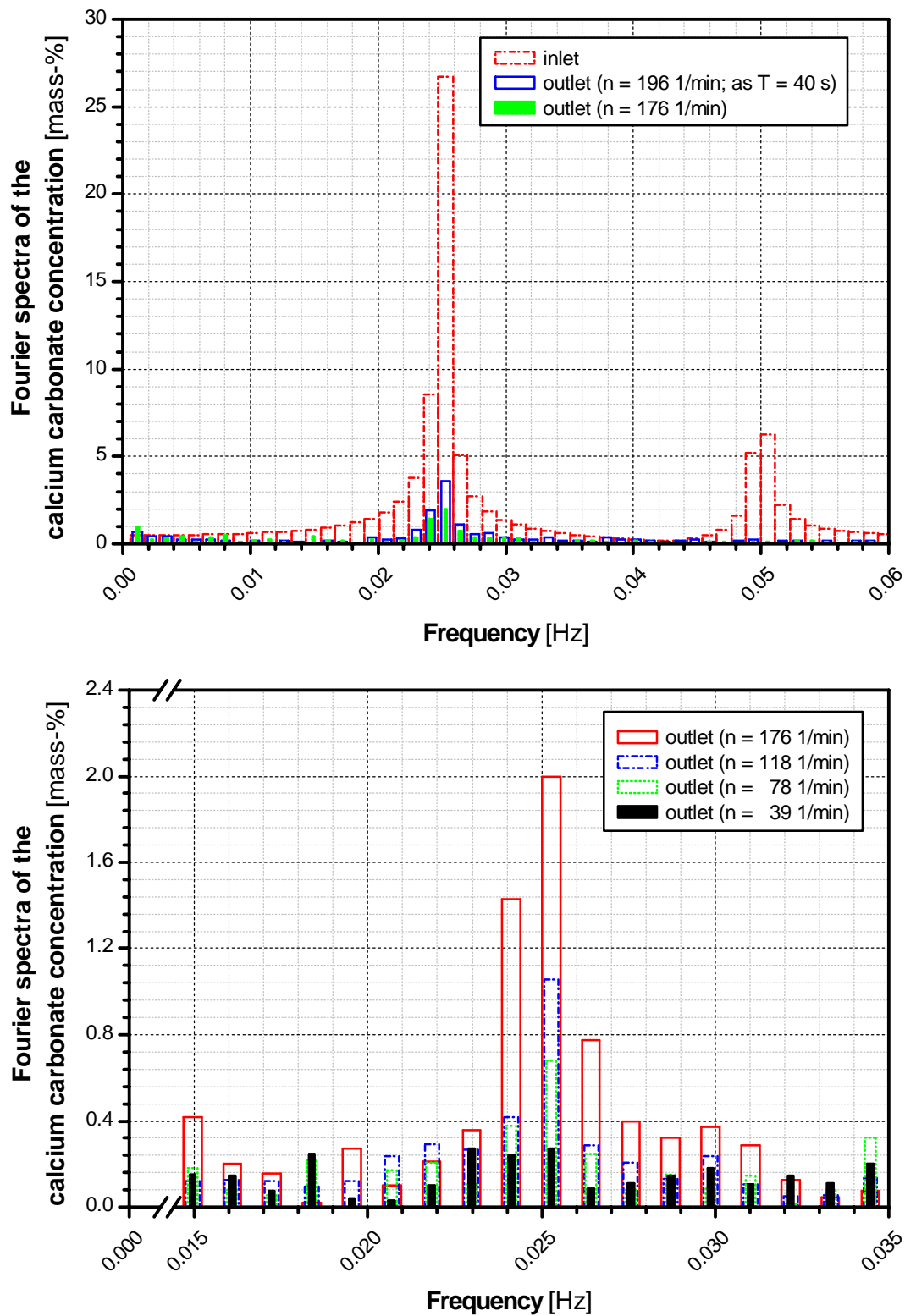
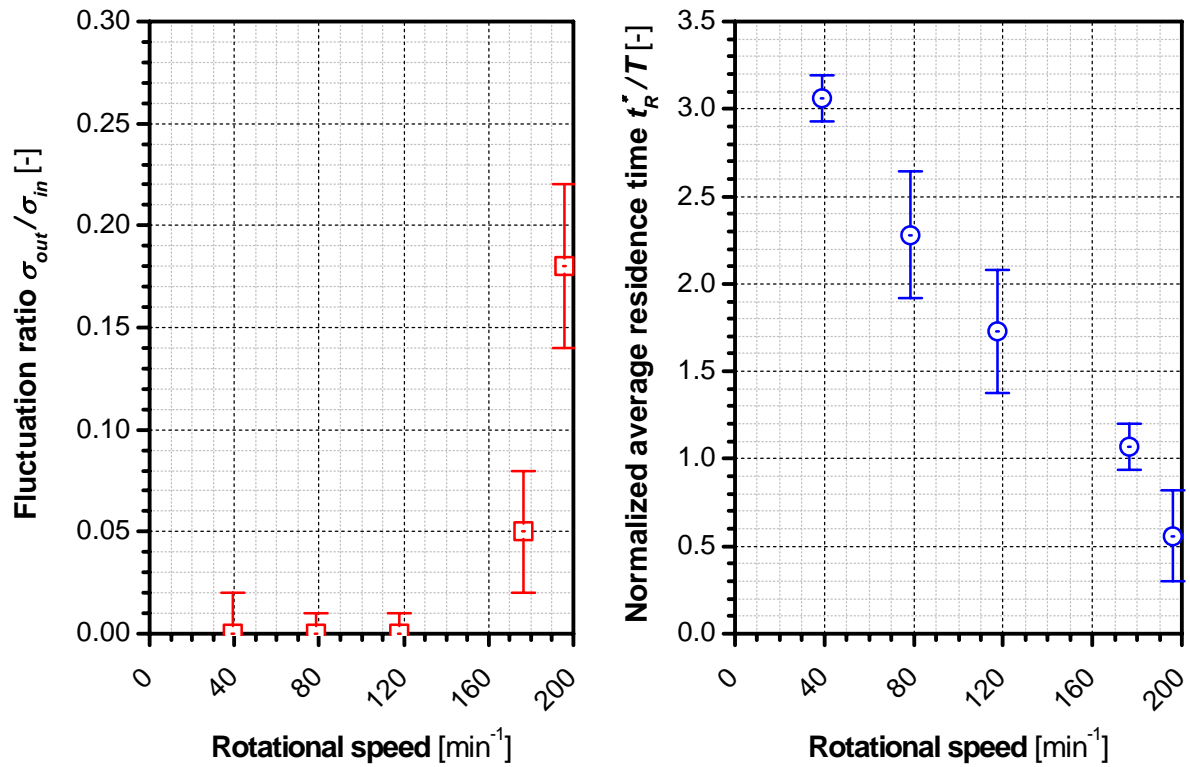
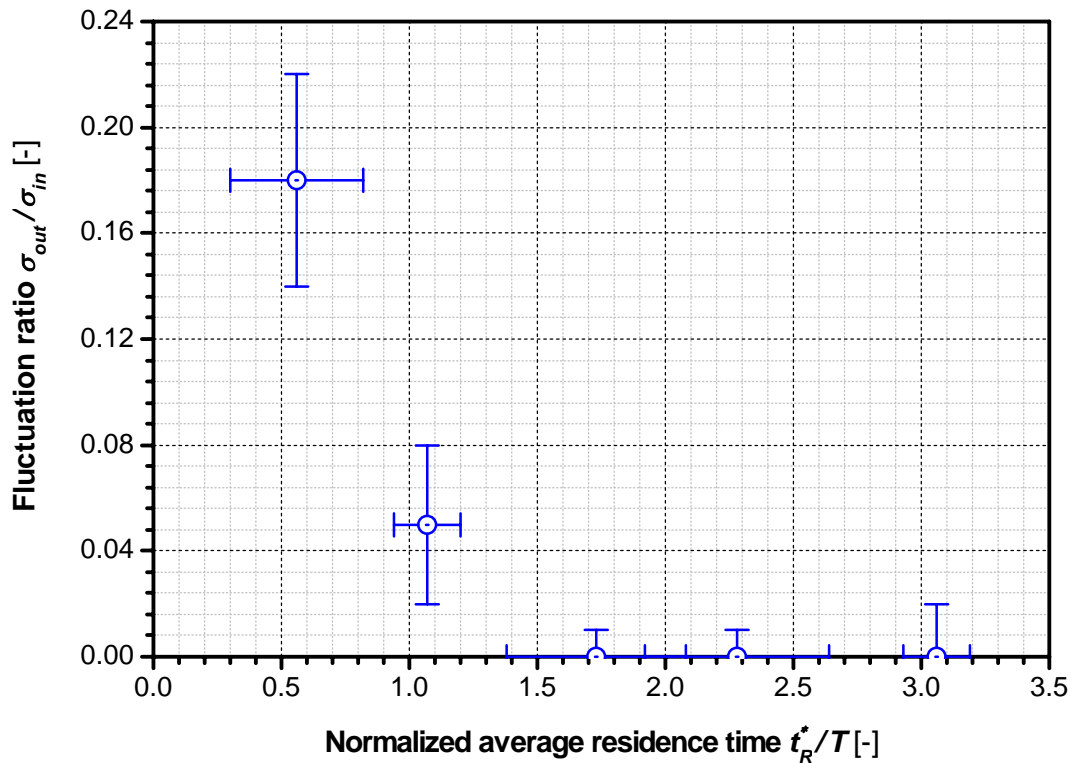


Fig. 4-129: Influence of the rotational speed of the mixing device on the mixing result (frequency domain, half-closed weir)



*Fig. 4-130: Influence of rotational speed of the mixing device on the fluctuation ratio and the normalized average residence time (half-closed weir)*

The two diagrams in *Fig. 4-130* were combined and the resulting pairs of the fluctuation ratio as well as the normalized average residence time are shown in *Fig. 4-131*. Up to a normalized average residence time of 1.7, the fluctuation ratio decreases with increasing normalized residence times. For a normalized average residence time of 1.7 or higher, the fluctuation ratio becomes zero because the empirical standard deviations of the mixing experiments were small compared to the empirical standard deviations of the measuring mistakes.



*Fig. 4-131: Influence of the normalized average residence time on the fluctuation ratio as a result of rotational speed variations (half-closed weir)*

#### 4.5.2.3 Influence of the period length on the mixing result (half-closed weir)

The standard settings of the calcium carbonate mass flow ( $\dot{m}_{1,O} = 15 \text{ g/s}$ ,  $\dot{m}_{1,A} = 14 \text{ g/s}$ ), the maize starch mass flow ( $\dot{m}_{2,O} = 10 \text{ g/s}$ ,  $\dot{m}_{2,A} = 0 \text{ g/s}$ ) and the rotational speed of the mixing device ( $n = 196 \text{ min}^{-1}$ ) were used to examine the influence of the period length on the fluctuation ratio and the normalized average residence time. The period length of the calcium carbonate mass flow fluctuations was decreased from  $T = 100 \text{ s}$  to  $20 \text{ s}$  in steps of  $20 \text{ s}$ . The calcium carbonate concentration fluctuations in the inlet of the continuous mixer, which were calculated, were compared with the calcium carbonate concentration fluctuations in the outlet of the mixer, which were measured. The comparison was done in the time domain (see *Fig. 4-132*) and in the frequency domain (see *Fig. 4-133*).

For decreasing period lengths, a higher reduction of the concentration fluctuations in the mixer outlet was observed. This tendency becomes more obvious if the fluctuation ratio  $\sigma_{out}/\sigma_{in}$  is plotted against the period length (compare left diagram of *Fig. 4-134*). The right diagram of *Fig. 4-134* shows that the normalized average residence time  $t_R^*/T$  decreases with an increase of the period length. Only the normalized average residence time corresponding to a period length of  $20 \text{ s}$  differs significantly from the others. The average values of the normalized average residence time decrease with increasing period lengths. The determined average residence times were independent of the period length (see *Fig. 4-135*).



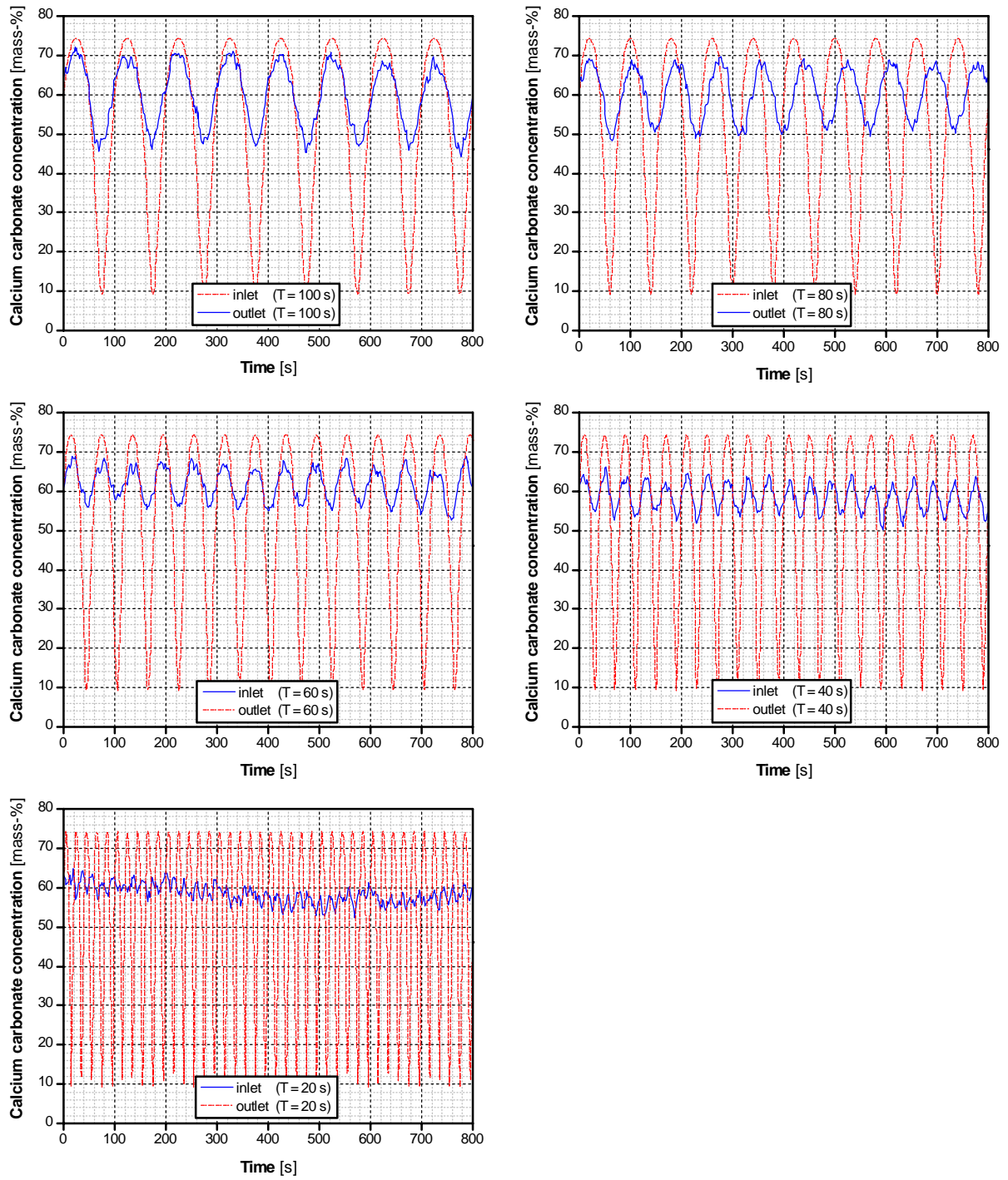


Fig. 4-132: Influence of the period length on the mixing result (time domain, half-closed weir)

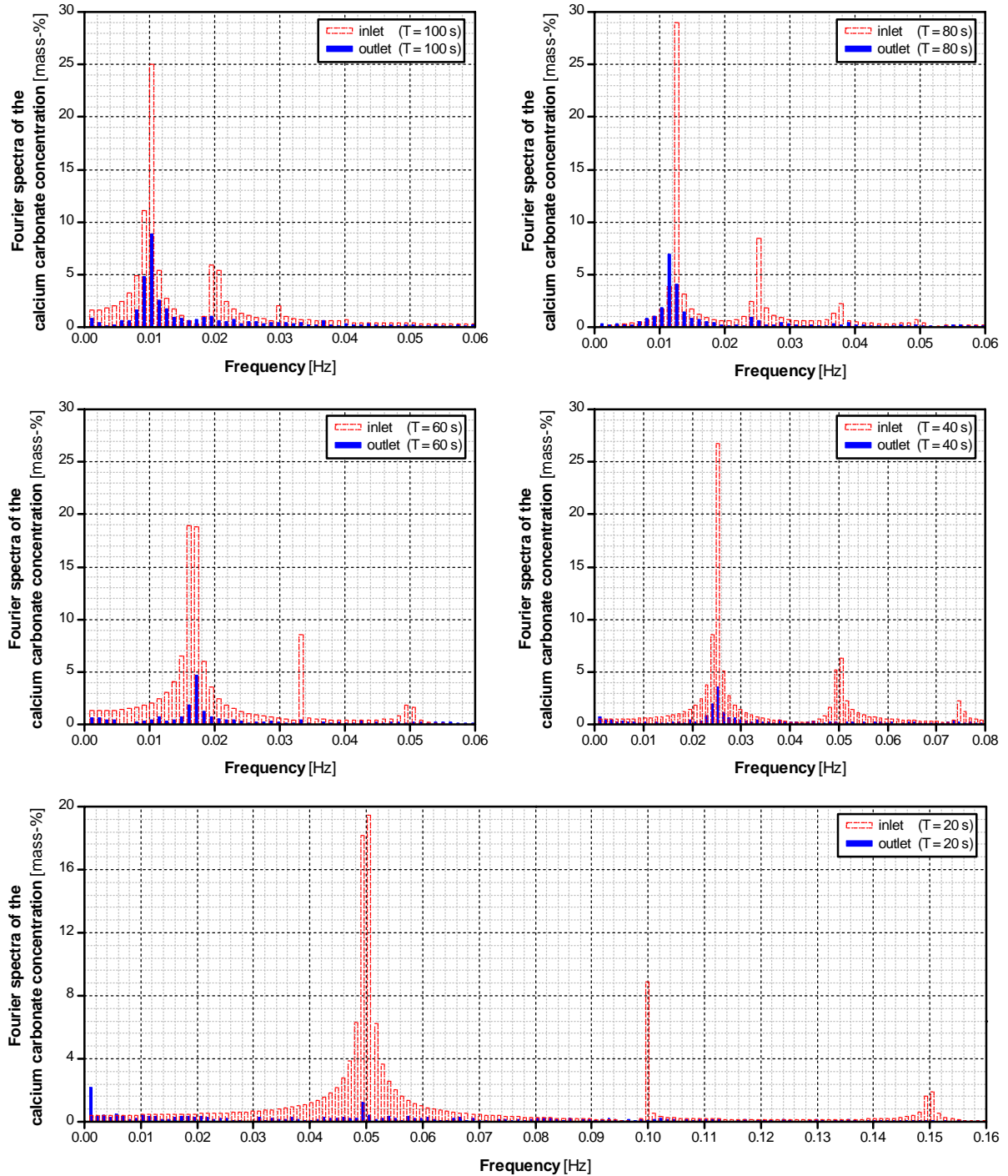


Fig. 4-133: Influence of the period length on the mixing result (frequency domain, half-closed weir)



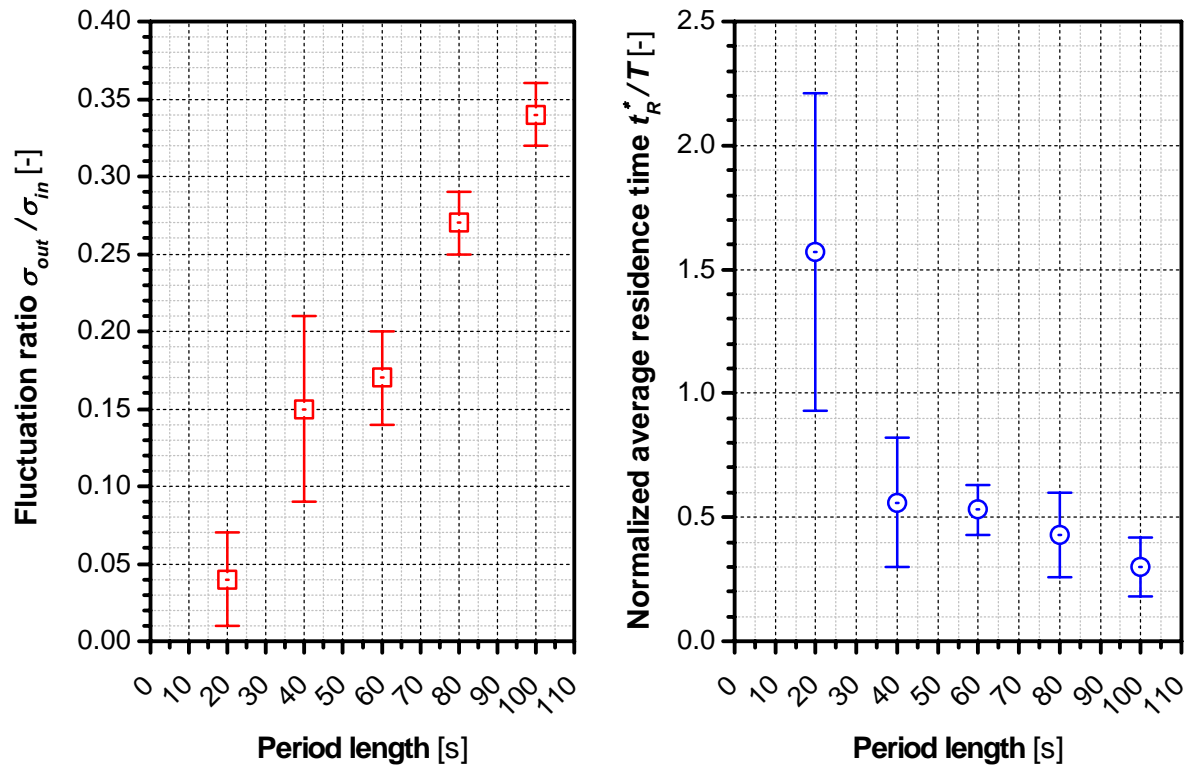


Fig. 4-134: Influence of the period length on the fluctuation ratio and the normalized average residence time (half-closed weir)

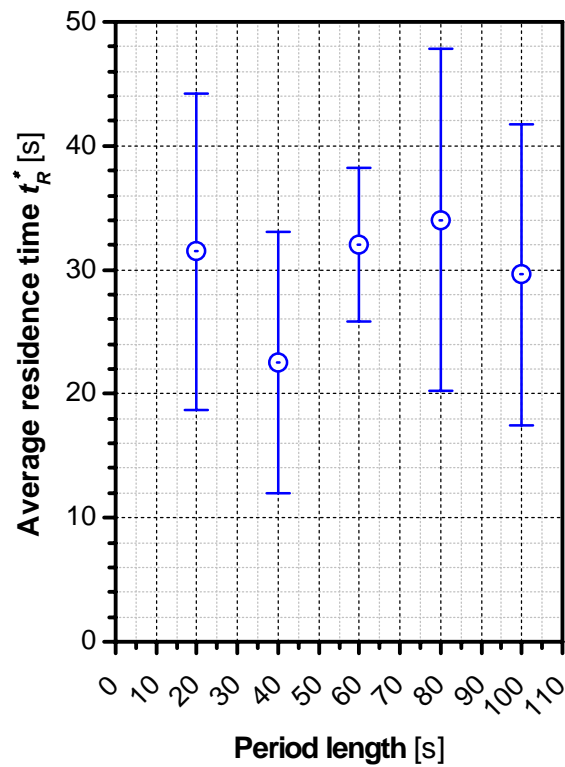
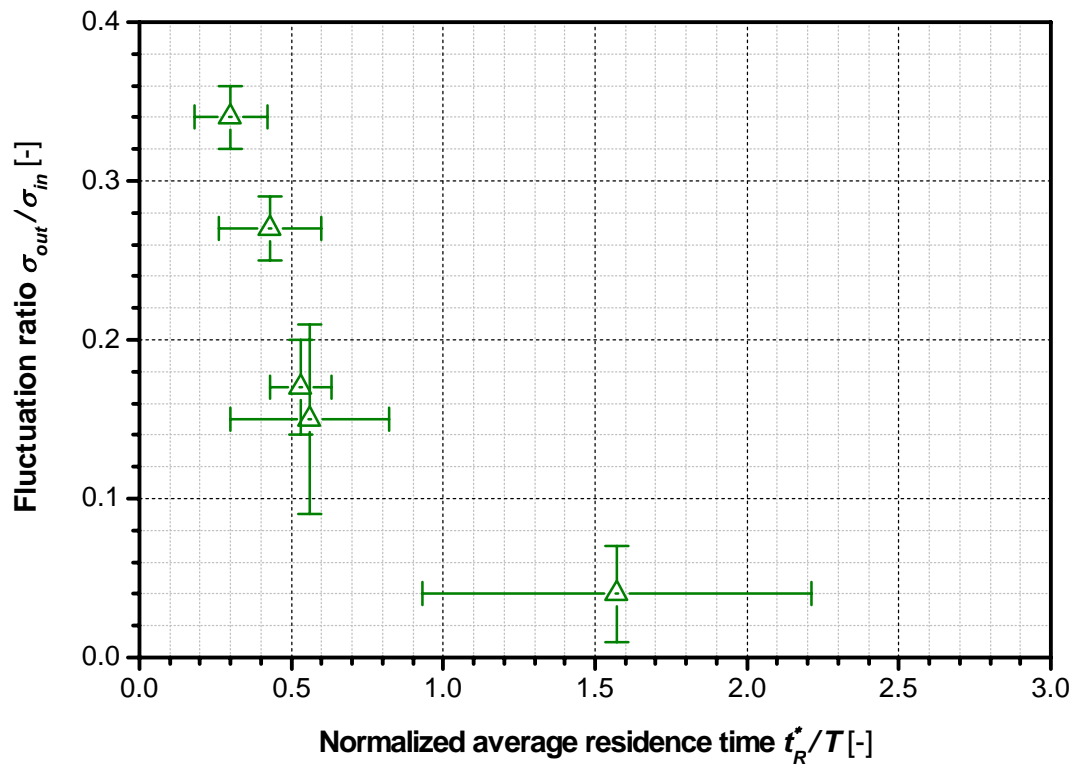


Fig. 4-135: Influence of the period length on the average residence time (half-closed weir)

The two diagrams in *Fig. 4-134* were combined and the resulting pairs of the fluctuation ratio as well as the normalized average residence time are shown in *Fig. 4-136*. The average values of the fluctuation ratio decrease with increasing normalized average residence times.



*Fig. 4-136: Influence of the normalized average residence time on the fluctuation ratio as a result of period length variations (half-closed weir)*

#### 4.5.2.4 Compilation of the mixing results (half-closed weir)

The results of the mixing experiments for a half-closed weir are shown in *Fig. 4-137*. The fluctuation ratio decreases with increasing normalized average residence time up to the point where it becomes zero. The experimental results are approximately lying on a master curve for all operation conditions.

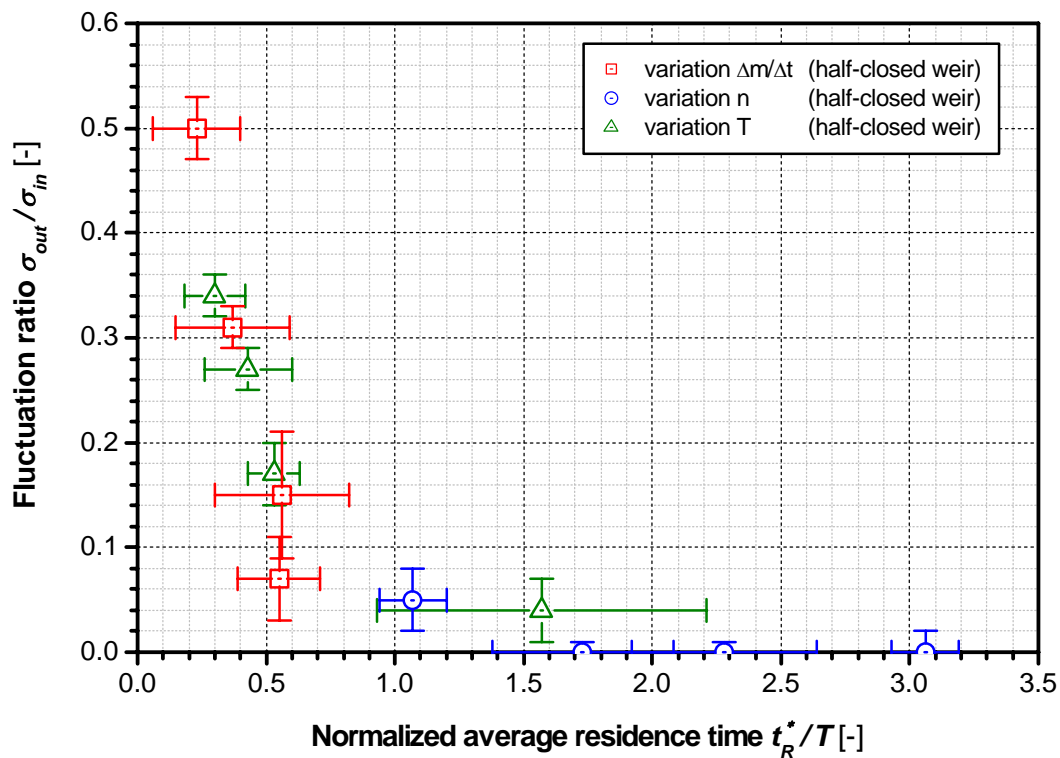


Fig. 4-137: Compilation of the mixing experiments (half-closed weir)

#### 4.5.2.5 Influence of the average overall mass flow on the mixing result (closed weir)

The standard settings of the calcium carbonate mass flow ( $\dot{m}_{1,O} = 15 \text{ g/s}$ ,  $\dot{m}_{1,A} = 14 \text{ g/s}$ ,  $T = 40 \text{ s}$ ) and the standard rotational speed of the mixing device ( $n = 196 \text{ min}^{-1}$ ) were also used to examine the influence of the average overall mass flow on the fluctuation ratio and the normalized average residence time for a closed weir. The average maize starch mass flow was decreased from 20 to 5 g/s in steps of 5 g/s. For the resulting average overall mass flows, the calcium carbonate concentration fluctuations in the inlet of the continuous mixer, which were calculated, were compared with the calcium carbonate concentration fluctuations in the outlet of the mixer, which were measured. The comparison was done in the time domain (see Fig. 4-138) and the frequency domain (see Fig. 4-139).

The experimental results show a higher reduction of the concentration fluctuations with decreasing average overall mass flows and decreasing average maize starch mass flows respectively. This tendency is more obvious than for a half-closed weir (compare Chapter 4.5.2.1, p. 163).

In the left diagram of Fig. 4-140, the fluctuation ratio  $\sigma_{out}/\sigma_{in}$  is plotted against the average overall mass flow. For average overall mass flows higher than 20 g/s, the fluctuation ratio decreases significantly for decreasing average overall mass flows. The right diagram of Fig. 4-140 shows the influence of the average overall mass flow on the normalized average residence time  $t_R^*/T$ . The closed weir caused a higher mass hold-up in the mixer than a half-closed weir. As a result, the fluctuations of the determined average residence time and the corresponding confidence interval are smaller than for a half-closed weir. A significant influence of the average overall mass flow on the normalized average residence time was only observed for the mass flow change from 25 to 30 g/s.

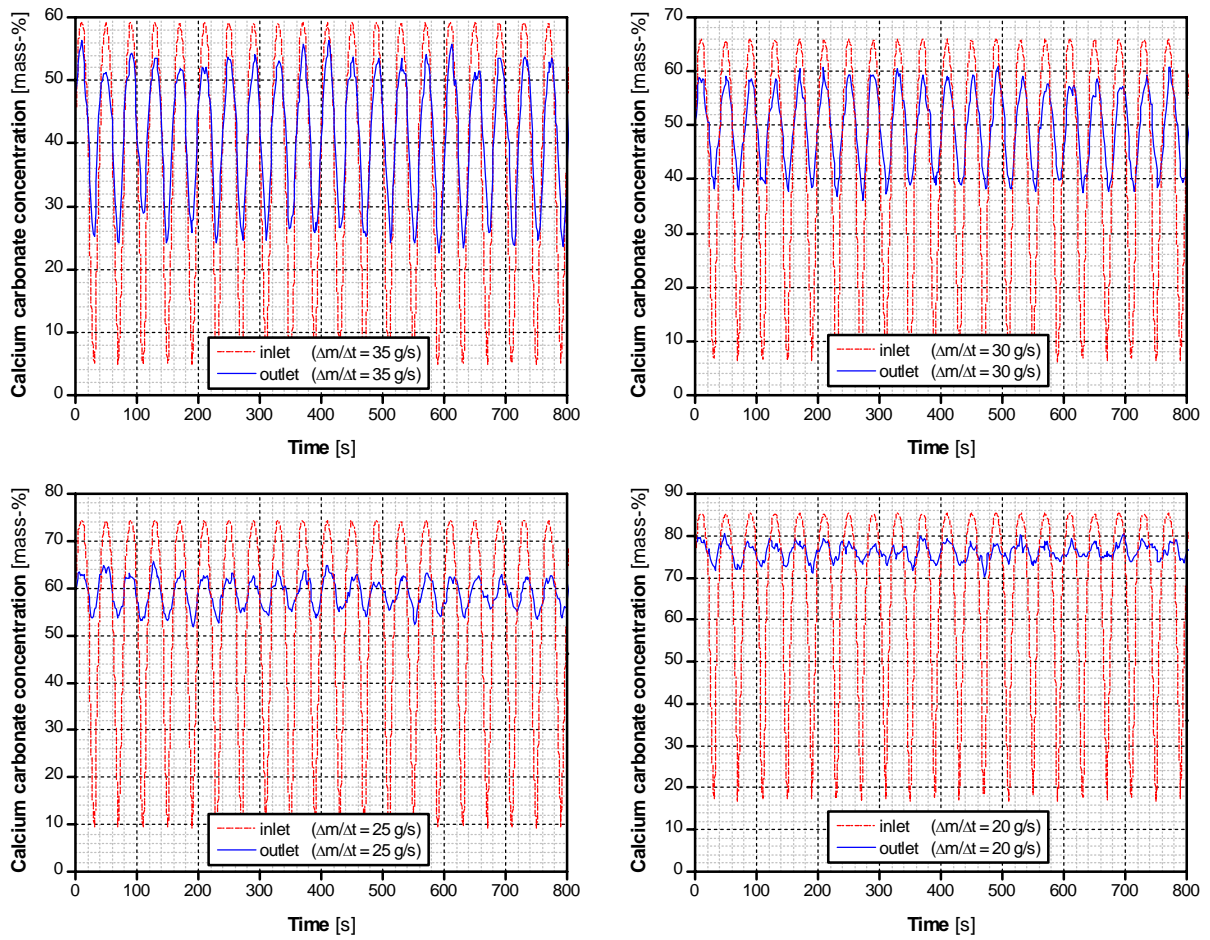


*Fig. 4-138: Influence of the overall mass flow on the mixing result - The scale of the y-axis changes in each diagram! (time domain, closed weir)*

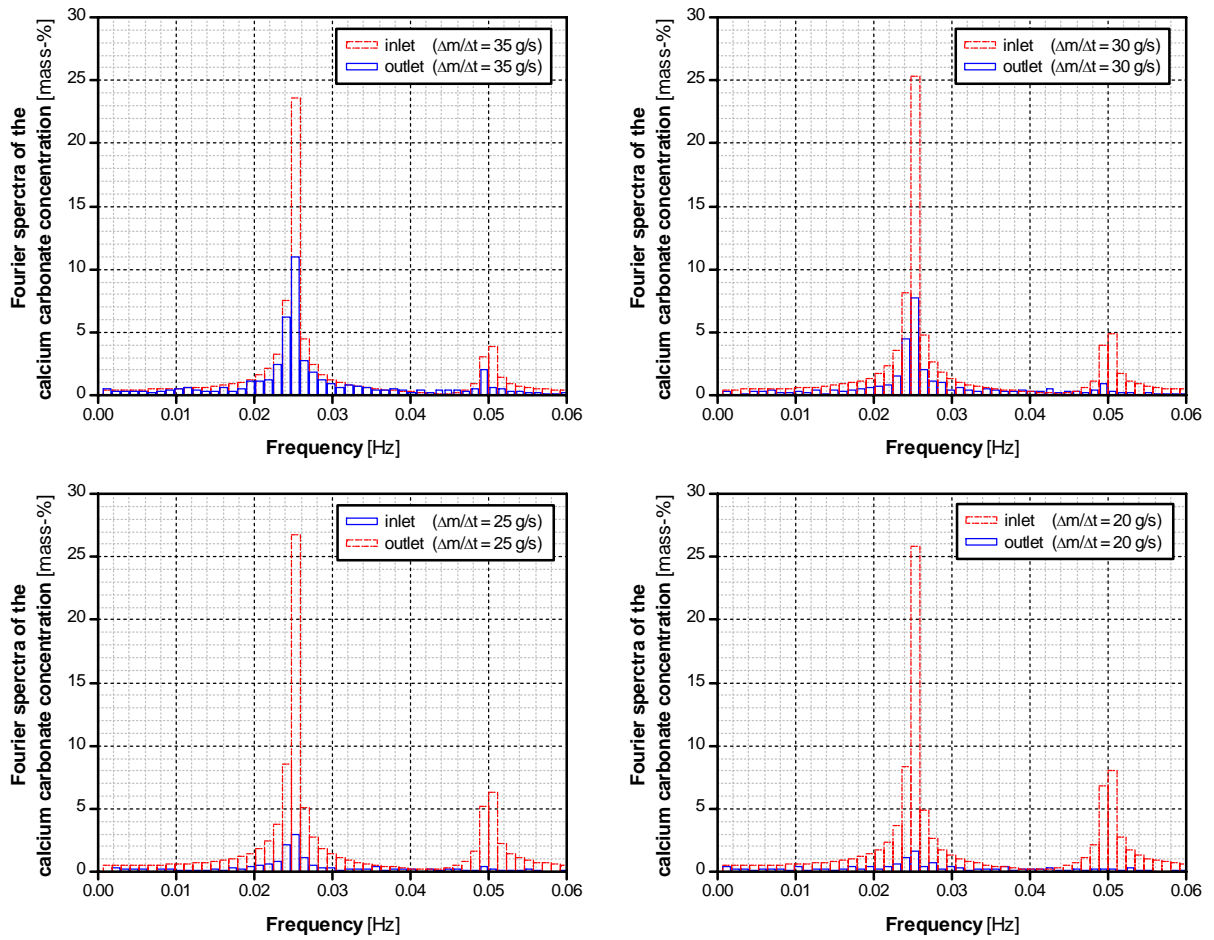
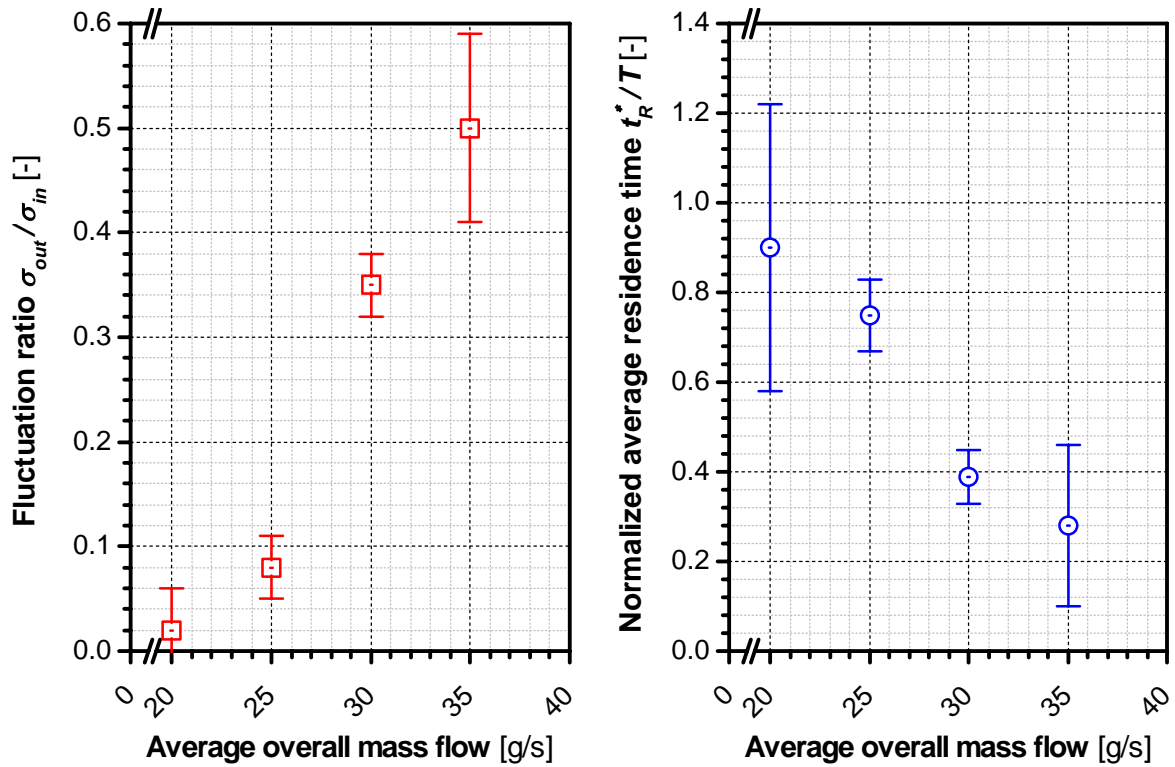
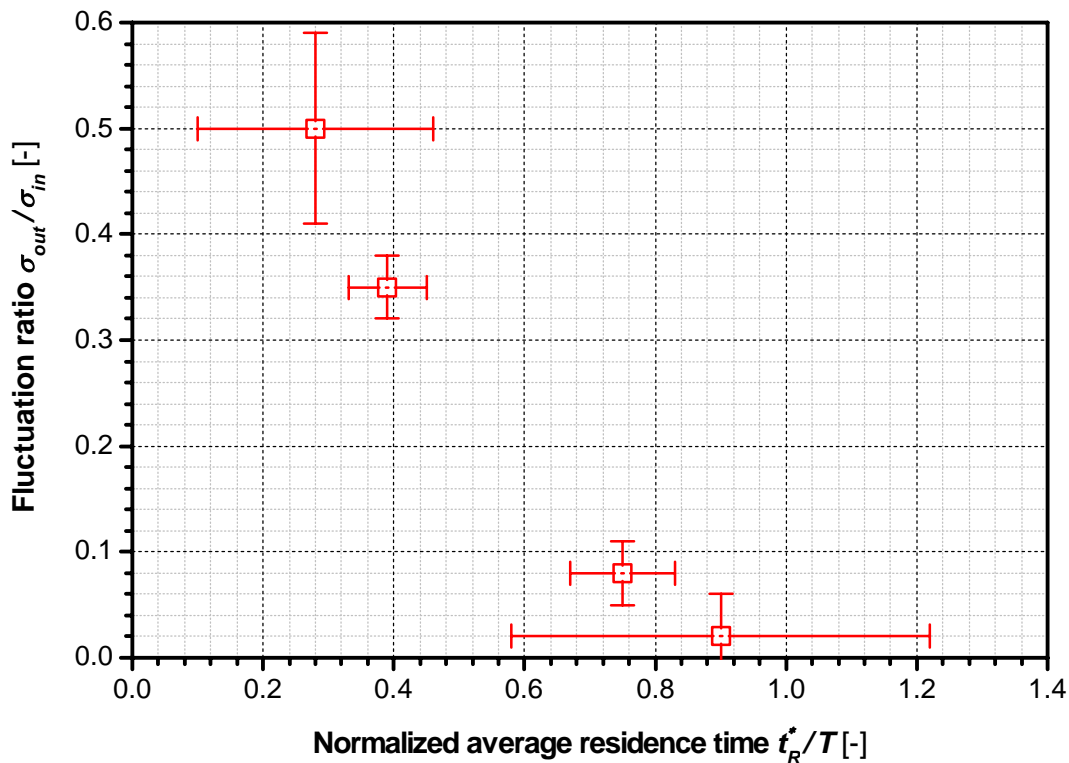


Fig. 4-139: Influence of the average overall mass flow on the mixing result (frequency domain, closed weir)



*Fig. 4-140: Influence of the average overall mass flow on the fluctuation ratio and the normalized average residence time (closed weir)*

The two diagrams in *Fig. 4-140* were combined and the resulting pairs of fluctuation ratio as well as the normalized average residence time are shown in *Fig. 4-141*. The average fluctuation ratios decrease with increasing normalized residence times.



*Fig. 4-141: Influence of the normalized average residence time on the fluctuation ratio as a result of mass flow variations (closed weir)*

#### 4.5.2.6 Influence of the rotational speed of the mixing device on the mixing result (closed weir)

The standard settings of the calcium carbonate mass flow ( $\dot{m}_{1,O} = 15 \text{ g/s}$ ,  $\dot{m}_{1,A} = 14 \text{ g/s}$ ,  $T = 40 \text{ s}$ ) and the maize starch mass flow ( $\dot{m}_{2,O} = 10 \text{ g/s}$ ,  $\dot{m}_{2,A} = 0 \text{ g/s}$ ) were also used to examine the influence of the rotational speed on the fluctuation ratio and the normalized average residence time for a closed weir. The rotational speed was decreased from the maximum value of  $196 \text{ min}^{-1}$  to  $176$ ,  $157$ ,  $118$ ,  $78$  and  $39 \text{ min}^{-1}$ . The calcium carbonate concentration fluctuations in the inlet of the continuous mixer which were calculated, were compared with the calcium carbonate concentration fluctuations in the outlet of the mixer that were measured. The comparison was done in the time domain (see *Fig. 4-142*) and in the frequency domain (see *Fig. 4-143*).

For all rotational speeds, a significant reduction of the entering concentration fluctuations was observed. For rotational speeds smaller than  $196 \text{ min}^{-1}$ , the remaining concentration fluctuations in the outlet of the continuous mixer are in the same magnitude. This tendency becomes more obvious if the fluctuation ratio  $\sigma_{out}/\sigma_{in}$  is plotted against the rotational speed (see left diagram of *Fig. 4-144*). For rotational speeds smaller than  $196 \text{ min}^{-1}$ , the empirical standard deviations of the mixing experiments were small compared to the empirical standard deviation of the measuring mistakes. As a result, the fluctuation ratio becomes zero. For rotational speeds of  $40$ ,  $80$ ,  $120$  and  $196 \text{ min}^{-1}$ , the normalized average residence time  $t_R^*/T$  decreases significantly with increasing rotational speeds (right diagram of *Fig. 4-144*).

The two diagrams in *Fig. 4-144* were combined and the resulting pairs of the fluctuation ratio as well as the normalized average residence time are shown in *Fig. 4-145*. Resulting from the



discussion of the influence of the rotational speed on the fluctuation ratio, the same tendency was found for the influence of the normalized average residence time.

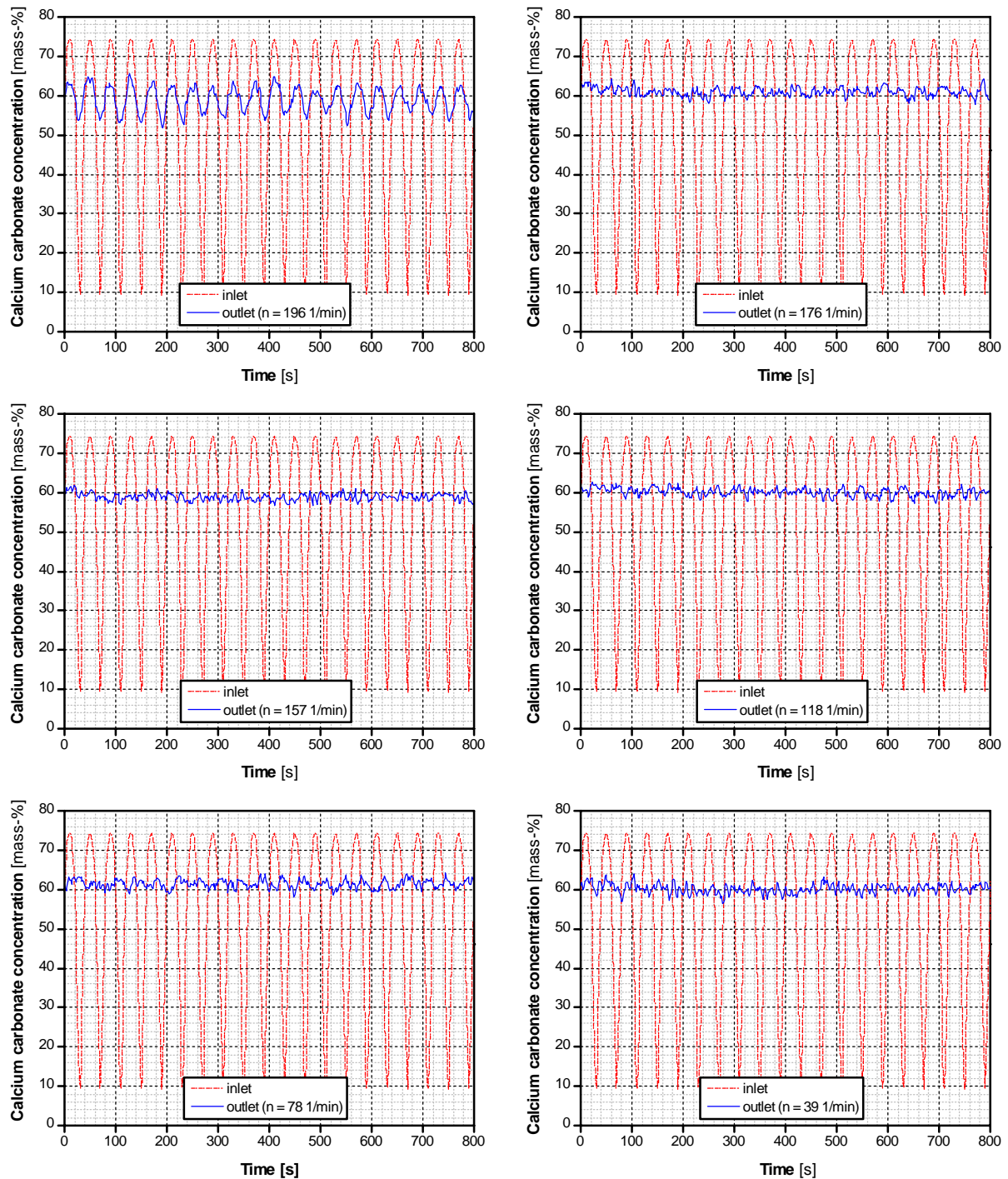


*Fig. 4-142: Influence of the rotational speed of the mixing device on the mixing result (time domain, closed weir)*

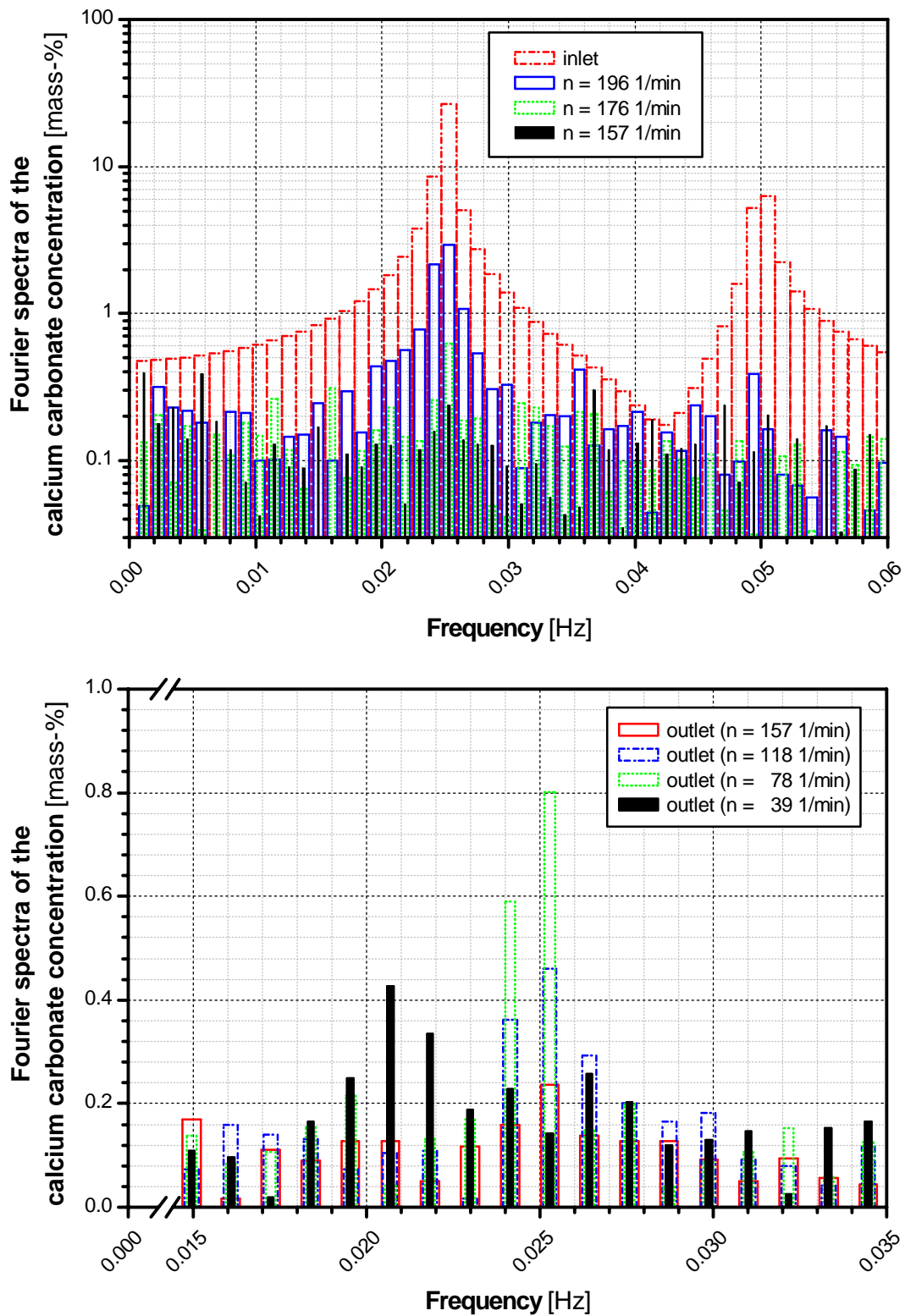


Fig. 4-143: Influence of the rotational speed of the mixing device on the mixing result (frequency domain, closed weir)

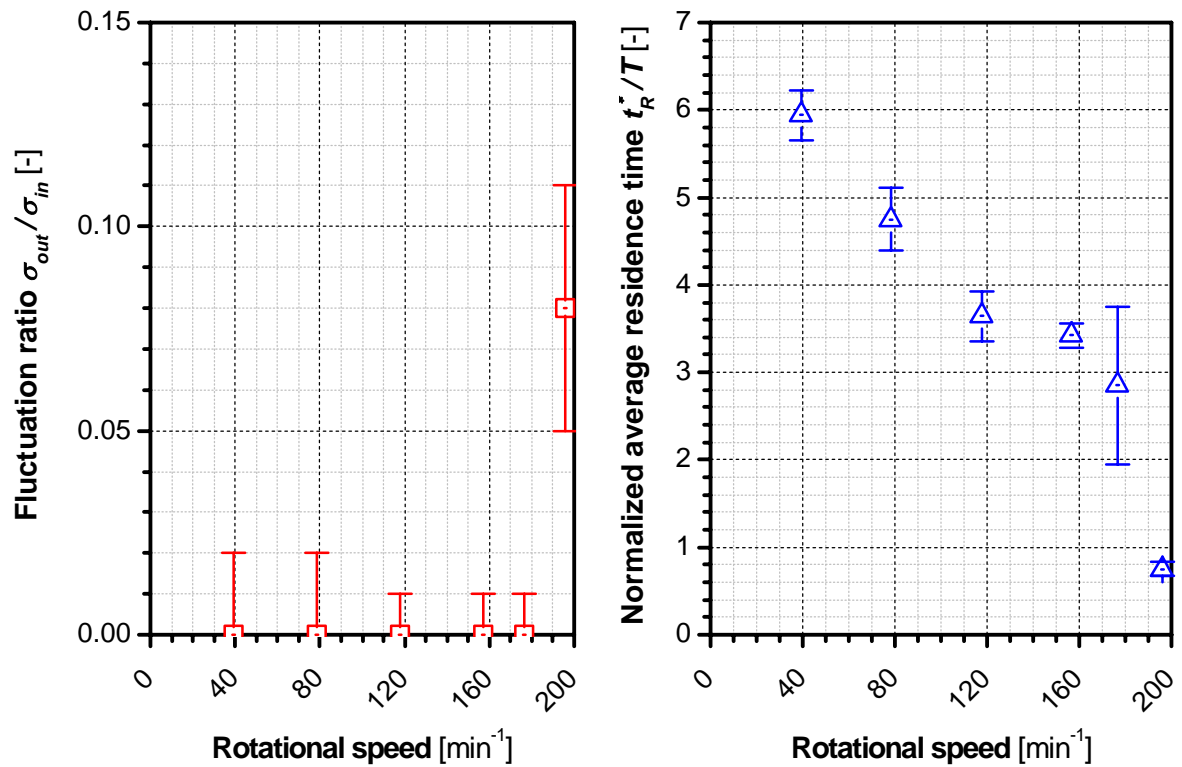


Fig. 4-144: Influence of the rotational speed of the mixing device on the fluctuation ratio and the normalized average residence time (closed weir)

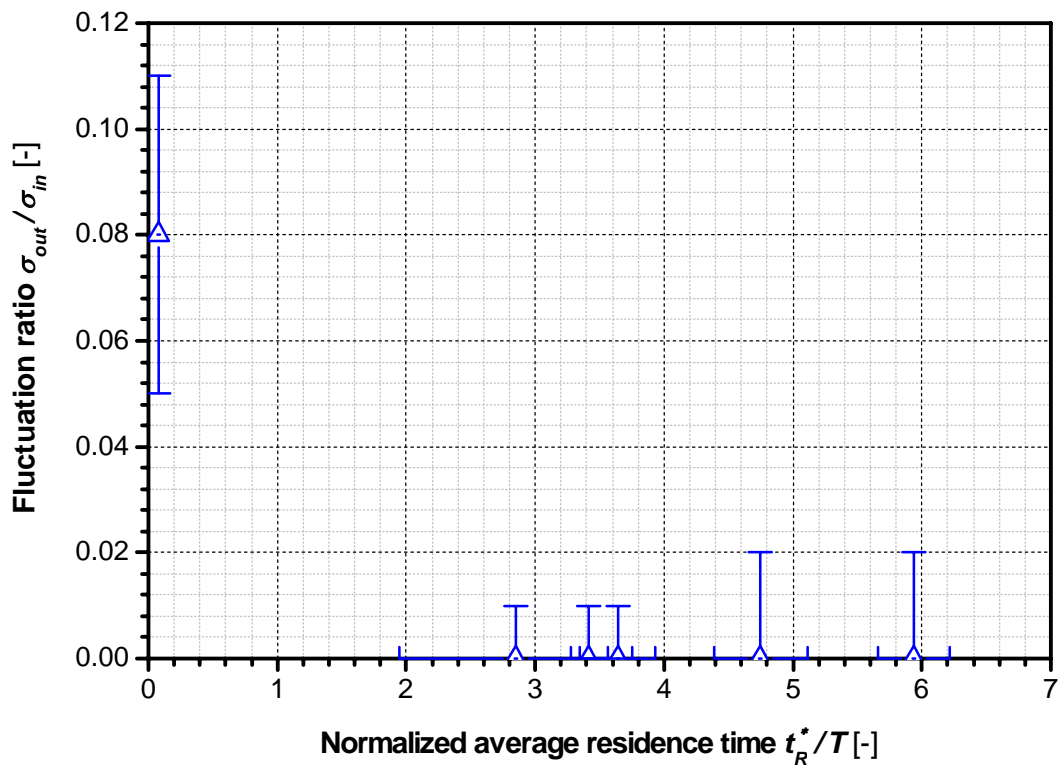


Fig. 4-145: Influence of the normalized average residence time on the fluctuation ratio as a result of rotational speed variations (closed weir)

#### 4.5.2.7 Influence of the period length on the mixing result (closed weir)

The standard settings of the calcium carbonate mass flow ( $\dot{m}_{1,O} = 15 \text{ g/s}$ ,  $\dot{m}_{1,A} = 14 \text{ g/s}$ ), the maize starch mass flow ( $\dot{m}_{2,O} = 10 \text{ g/s}$ ,  $\dot{m}_{2,A} = 0 \text{ g/s}$ ) and the rotational speed of the mixing device ( $n = 196 \text{ min}^{-1}$ ) were also used to examine the influence of the period length on the fluctuation ratio and the normalized average residence time for a closed weir. The period length of the calcium carbonate mass flow fluctuations was decreased from  $T = 100 \text{ s}$  to  $20 \text{ s}$  in steps of  $20 \text{ s}$ . The results for a period length of  $40 \text{ s}$  were taken over from the examination of the influence of the rotational speed. The calcium carbonate concentration fluctuations in the inlet of the continuous mixer, which were calculated, were compared with the calcium carbonate concentration fluctuations in the outlet of the mixer, which were measured. The comparison was done in the time domain (see *Fig. 4-146*) and in the frequency domain (see *Fig. 4-147*).

Except for a period length of  $40 \text{ s}$ , a reduction of the concentration fluctuations in the outlet was observed for decreasing period lengths. This tendency becomes more obvious if the fluctuation ratio  $\sigma_{out}/\sigma_{in}$  is plotted against the period length (see left diagram of *Fig. 4-148*). The right diagram of *Fig. 4-148* shows that the average values of the normalized residence time  $t_R^*/T$  decrease with increasing period lengths. Only the value for a period length of  $40 \text{ s}$  is an exception. The average residence time is independent of the period length (see *Fig. 4-149*). As already mentioned, the experimental values for a period length of  $40 \text{ s}$  result from another experimental series with comparable settings, but performed on another day.

The two diagrams in *Fig. 4-148* were combined and the resulting pairs of the fluctuation ratio and the normalized average residence time are shown in *Fig. 4-150*. The average fluctuation ratio decreases with increasing normalized average residence times.

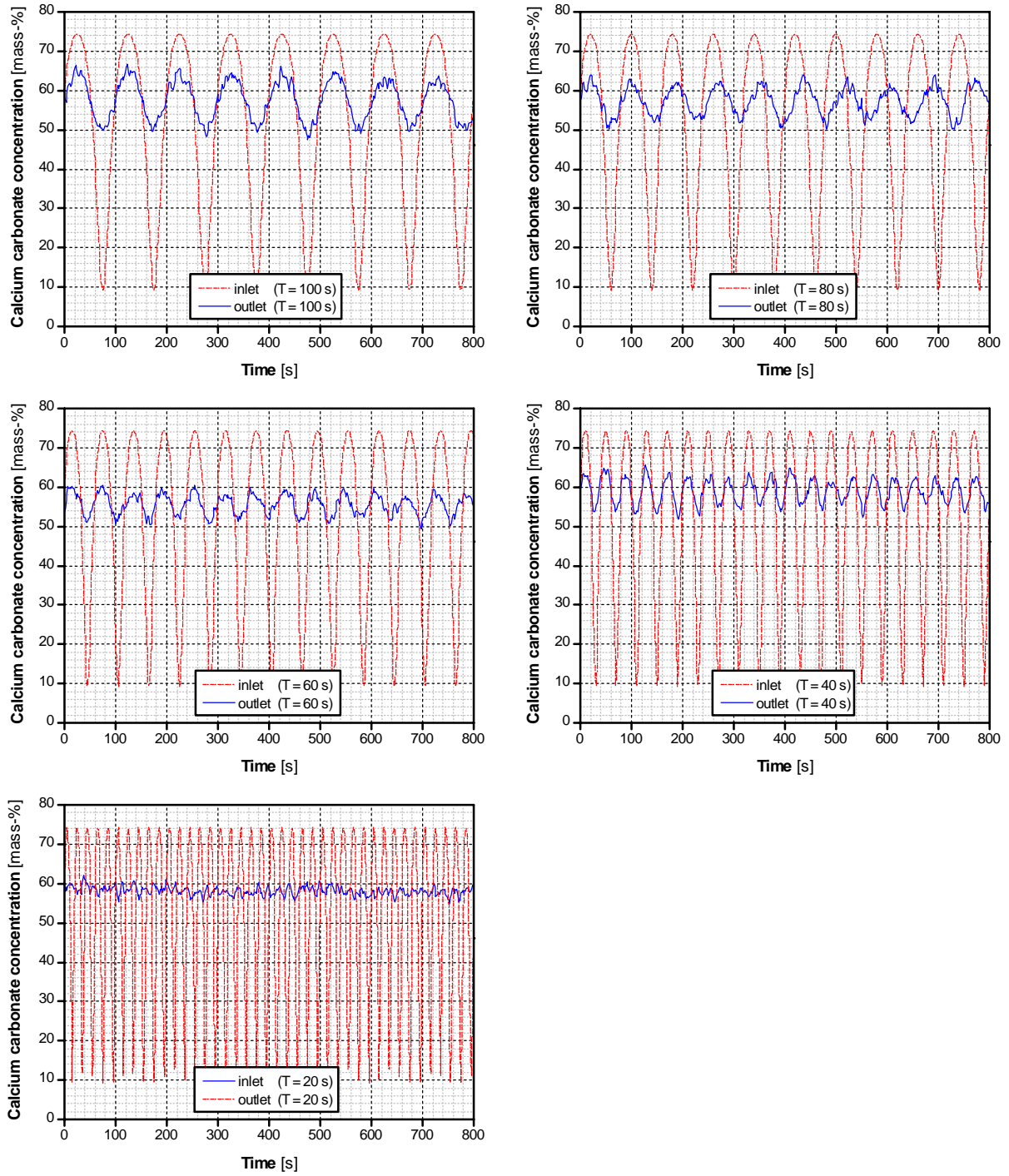


Fig. 4-146: Influence of the period length on the mixing result (time domain, closed weir)



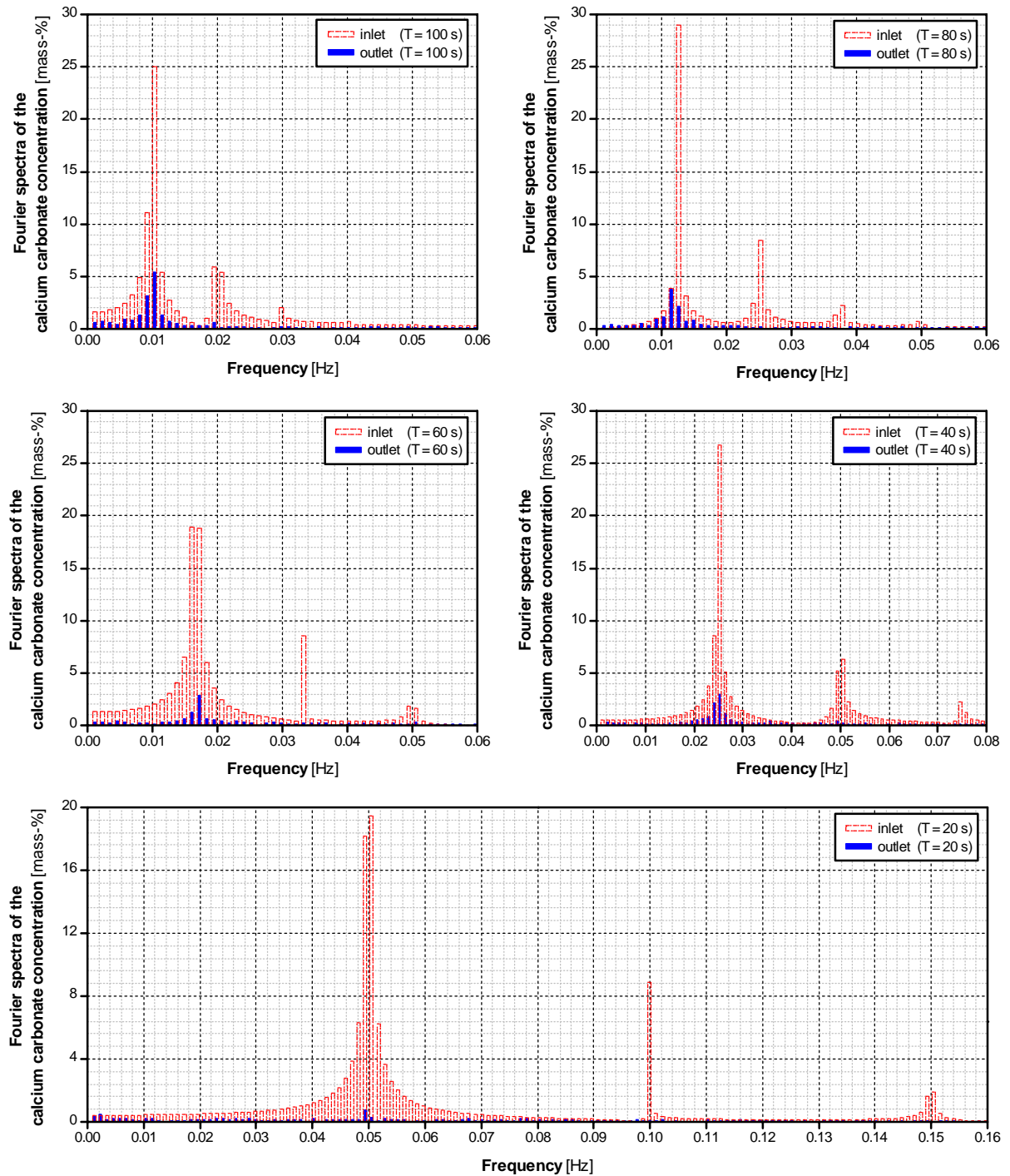


Fig. 4-147: Influence of the period length on the mixing result (frequency domain, closed weir)

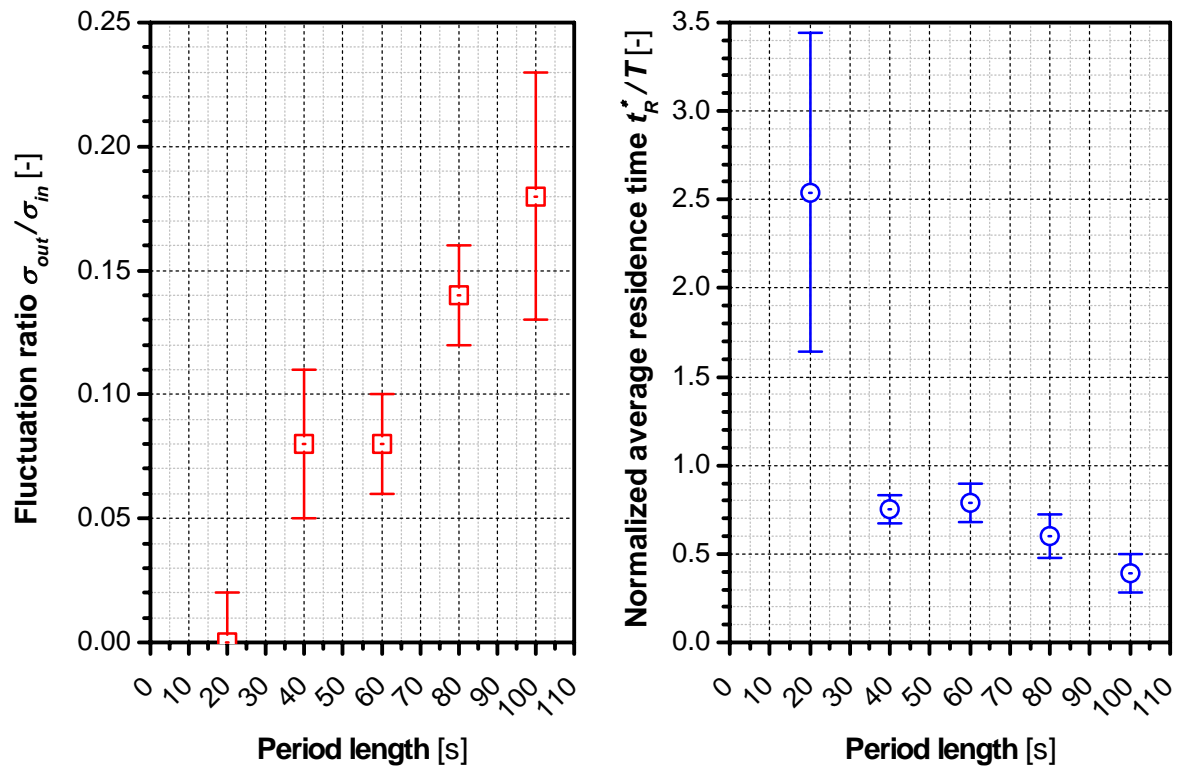


Fig. 4-148: Influence of the period length on the fluctuation ratio and the normalized average residence time (closed weir)

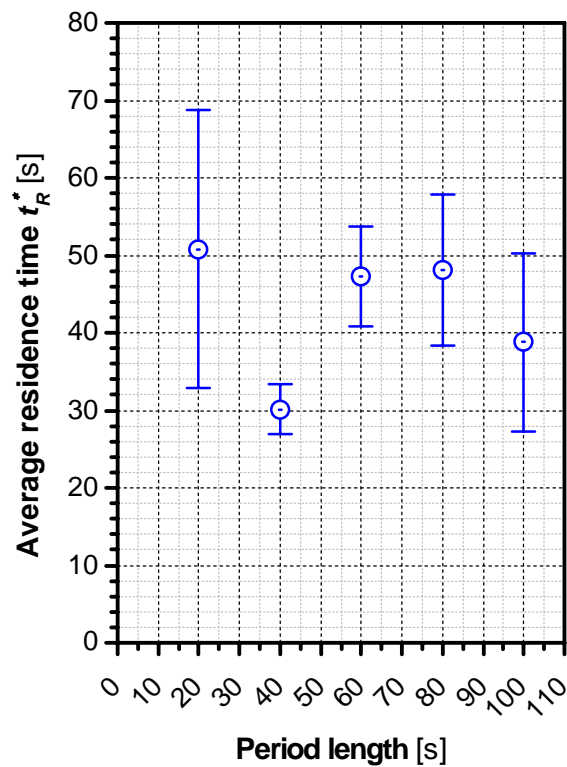
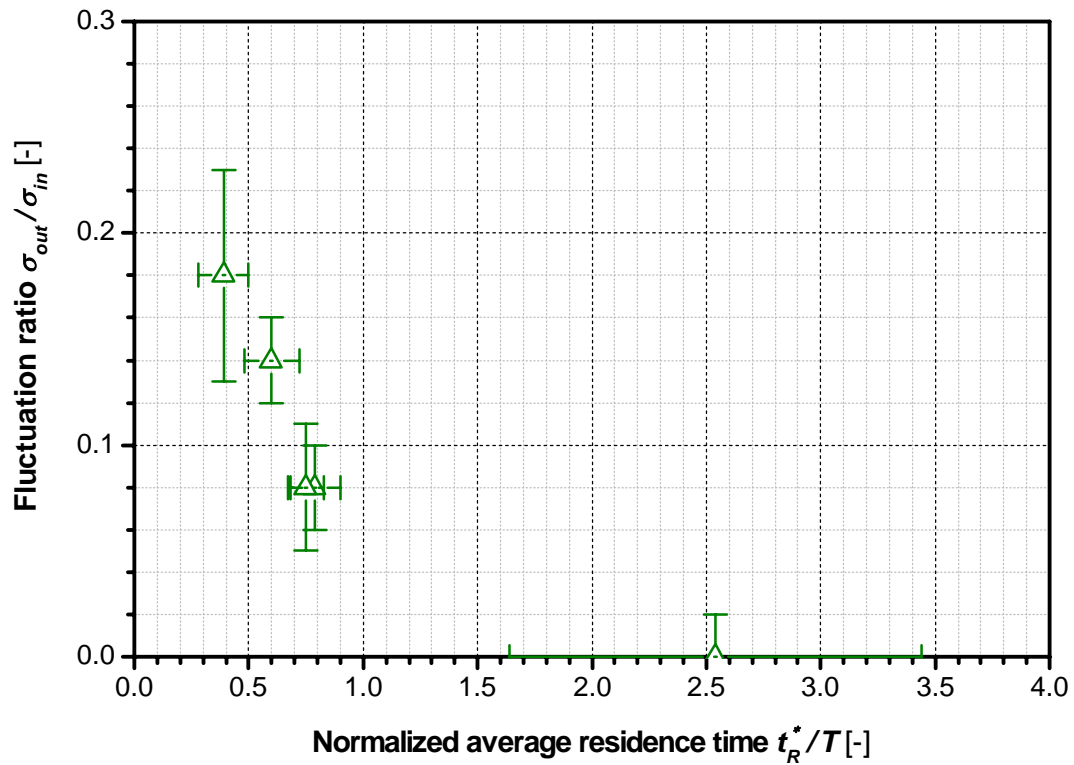


Fig. 4-149: Influence of the period length on the average residence time (closed weir)





*Fig. 4-150: Influence of the normalized average residence time on the fluctuation ratio as a result of period length variations (closed weir)*

#### 4.5.2.8 Compilation of the mixing results (closed weir)

The results of the mixing experiments for a closed weir are shown in *Fig. 4-151*. The fluctuation ratio decreases with increasing normalized average residence times down to the point where it becomes zero. The experimental results are lying approximately on a master curve for all operation modes.

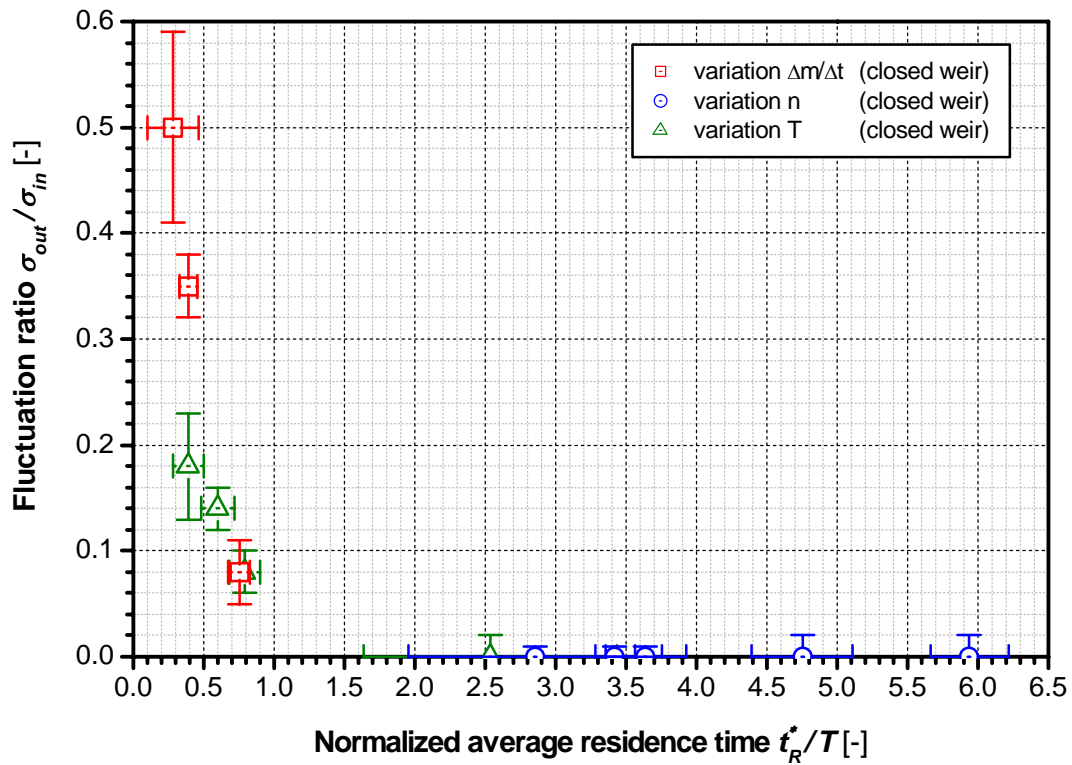


Fig. 4-151: Compilation of the mixing experiments (closed weir)

#### 4.5.3 Comparison of the mixing results calculated with the experimental mixing results

In Fig. 4-152 and Fig. 4-153, the mixing results obtained with a half-closed weir and a closed weir are compared with the mixing results calculated with the mixing model. For the three calculated curves, the dispersion coefficient  $D$  was set to 0.1, 0.2 or 0.3. For each curve the transport coefficient  $U$  was varied between 0.4 and 2.0 in steps of 0.2. In Fig. 4-154, the results are plotted in a log-log-scale.

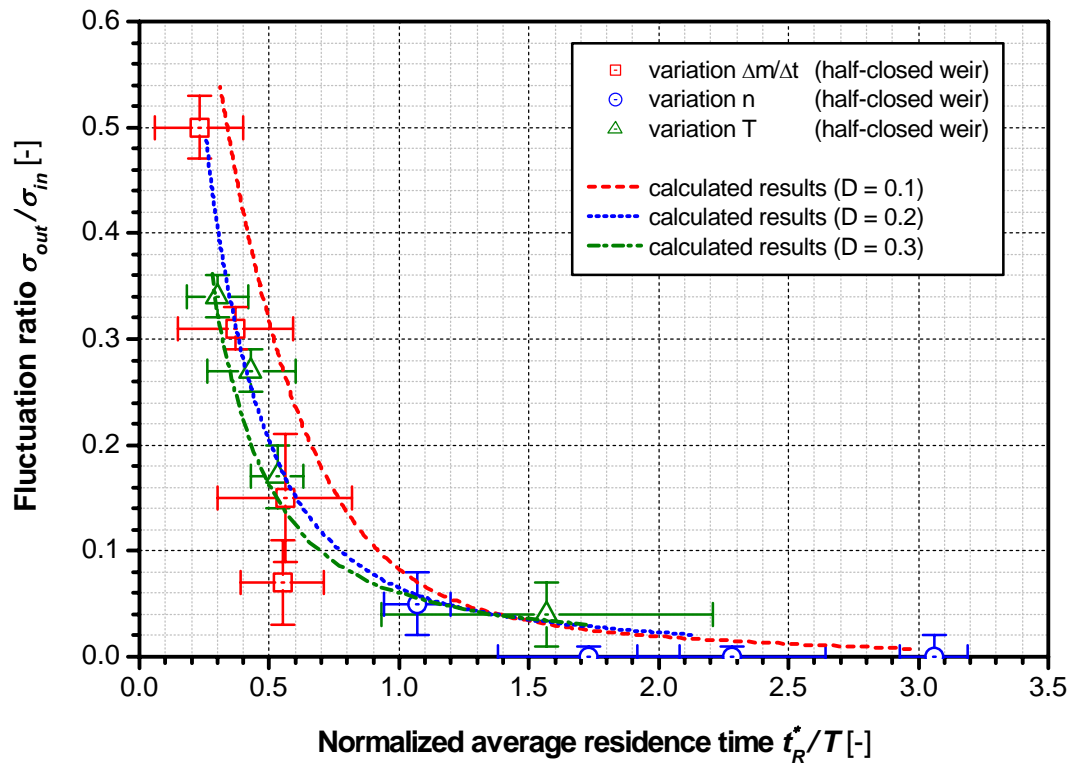


Fig. 4-152: Comparison of the calculated mixing qualities and the mixing qualities obtained experimentally (half-closed weir)

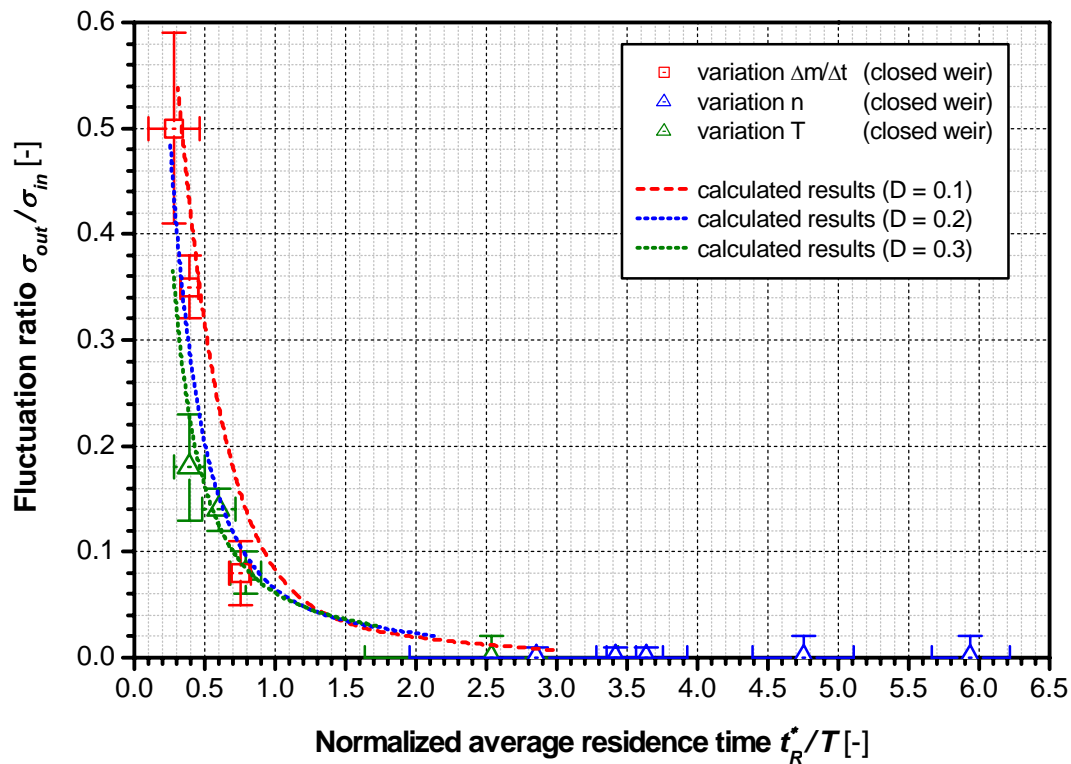
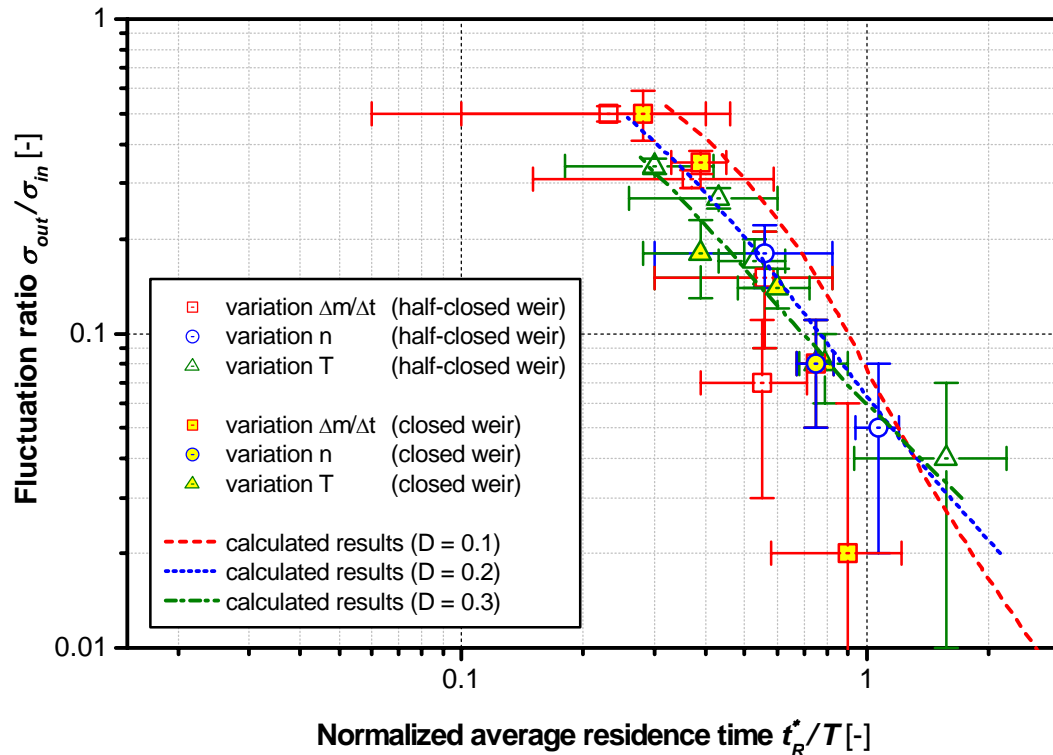


Fig. 4-153: Comparison of the calculated mixing qualities and the mixing qualities obtained experimentally (closed weir)



*Fig. 4-154: Comparison of the calculated mixing qualities and the mixing qualities obtained experimentally (half-closed and closed weir)*

The experimental and calculated results fit very well for both weir positions. The following inferences can be drawn:

- 1. For the mixer used as well as the calcium carbonate and maize starch powder used, the mixing mechanism in the continuous dynamic powder mixer from the company Gericke can be described very well with a system of two Fokker-Planck-Equations.**
- 2. The average residence time normalized with the period length of the entering mass flow fluctuations is the main influencing parameter of the mixing quality – independent of the mixer settings.**

#### 4.5.4 Comparison of the calculated mixing results and the experimental mixing results with literature data

Only a few experimental data resulting from mixing experiments using a continuous dynamic powder mixer are available in literature. WEINEKÖTTER [50] is the only author who published experimental results about the reduction of periodical concentration fluctuations and the corresponding average residence times. For his experiments, WEINEKÖTTER used different mixer types and mixer settings as well as different powders. Section drawings of the mixers used are shown in *Fig. 4-155* and *Fig. 4-156*. The first examined mixer is the continuous dynamic powder mixer *Multiflux* from the company *Gericke AG*. The mixer has two parallel shafts with nine paddle-like mixing devices each and a mixer chamber volume of about *16 l*. The powder can be fed optionally through four different inlets. By inserting a wall just behind the inlets, the mixing chamber can be reduced in size. No weir is located at the end of the mixer. The powder mixture leaves the mixer through two holes at its end. The shape of the mixing devices as well

as the number and the setting angle of the paddles can be changed. For the configuration *Multiflux I*, the setting angles relative to the transport direction were  $45^\circ$  and  $40^\circ$ . The paddles of the one shaft transported the powder in the direction of the mixer outlet and the paddles of the other shaft transported the powder in the direction of the mixer inlet. For the configuration *Multiflux II*, the mixing devices were arranged with a setting angle of  $10^\circ$  relative to the transport direction. Both mixing devices fed the powder in the direction of the mixer outlet. The second mixer examined was the continuous dynamic powder mixer GAC-307 from the company Gericke AG, which was primarily used for free-flowing powders. The mixing devices are two concentric spirals which rotate with different rotational speeds. The outer spiral rotated with  $60 \text{ min}^{-1}$  and the inner with  $120 \text{ min}^{-1}$ . The mixer chamber had a volume of about  $11 \text{ l}$ . A weir was located at the end of the mixer.

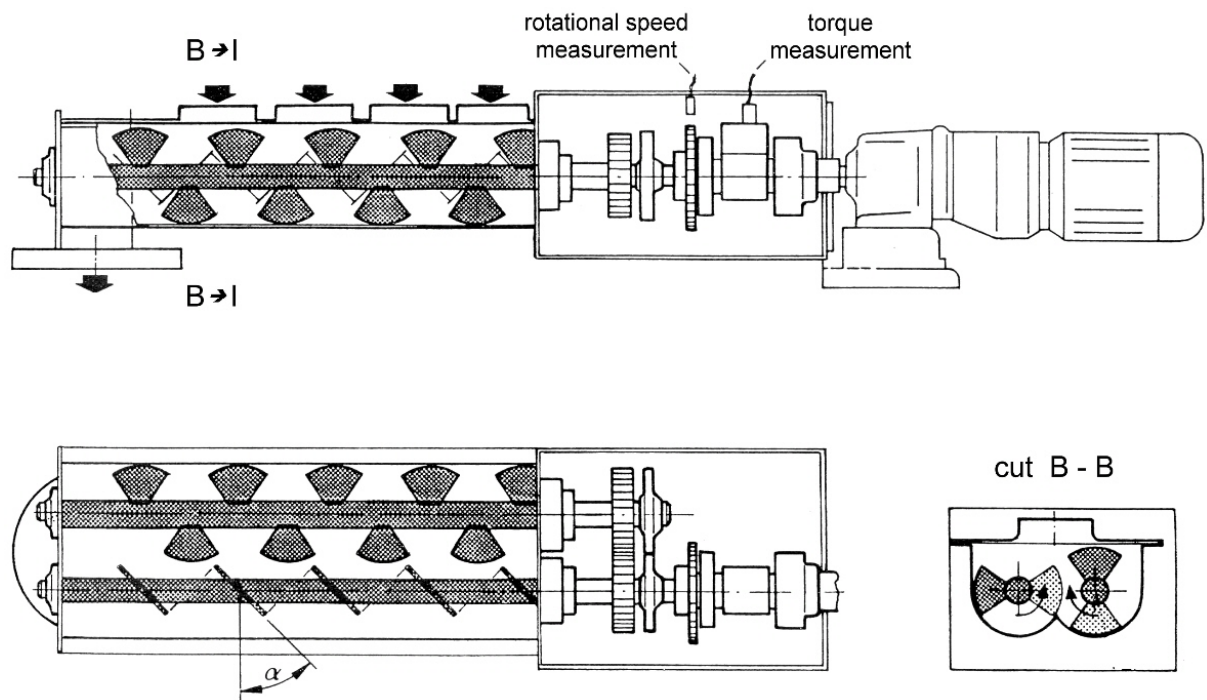


Fig. 4-155: Continuous dynamic powder mixer “Multiflux” used by WEINEKÖTTER [50]

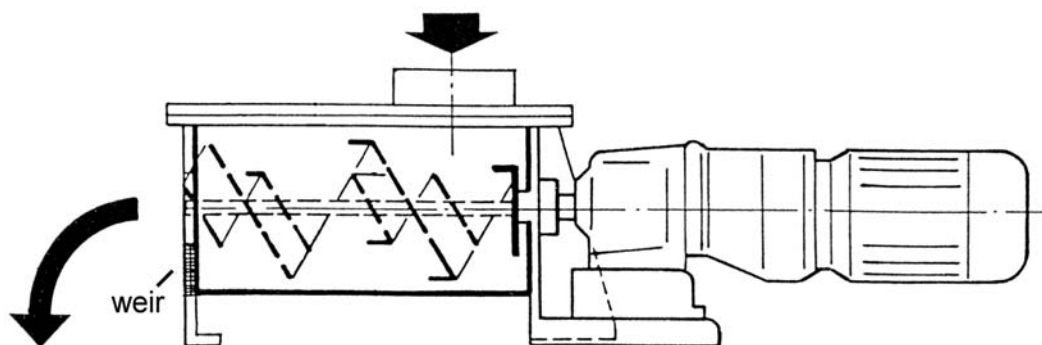
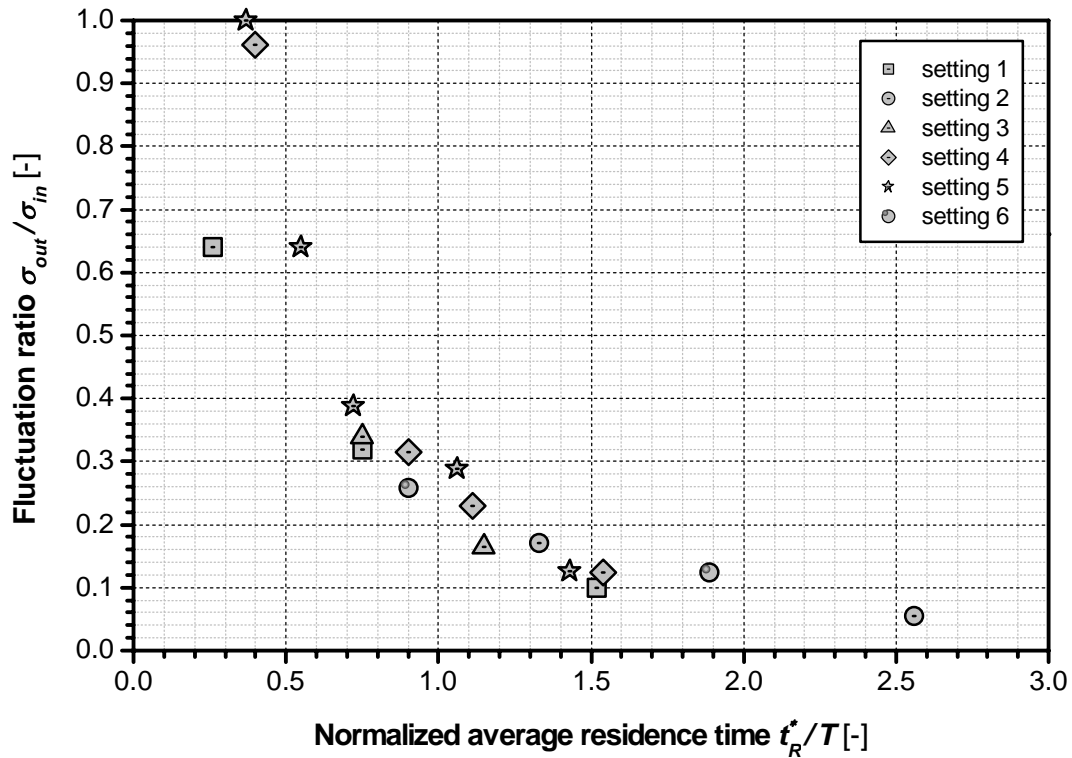


Fig. 4-156: Continuous dynamic powder mixer “GAC-307” used by WEINEKÖTTER [50]

WEINEKÖTTER [50] examined the mixing of the main component aluminum hydroxide ( $\text{Al}(\text{OH})_3$ ) with the tracer components silicon carbide (SiC) or Irgalite. The experimentally determined influence of the normalized average residence time on the fluctuation ratio is shown in *Fig. 4-157*. The median diameter of the powders used and the average concentration of the tracer are tabulated below the figure. The overall mass flow was about 20 g/s. The mass flow of the main component was constant and the tracer concentration was changed stepwise between 0 and the maximum mass flow. Only single measurements were performed. With the exception of one point, all other data points lay approximately on a master curve.

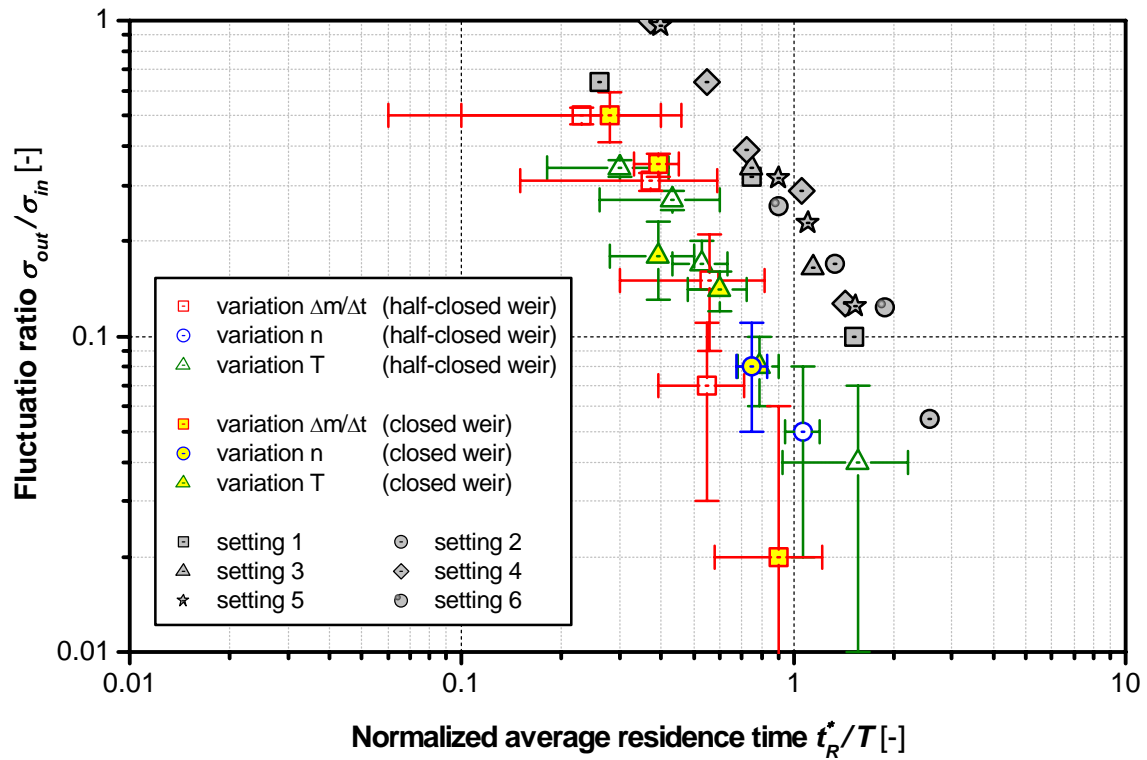


	mixer	particle size		concentration
		component 1	component 2	
setting 1	Multiflux I	$d_{50,\text{Al}(\text{OH})_3} = 28 \mu\text{m}$	$d_{50,\text{SiC}} = 26 \mu\text{m}$	$\bar{c}_{\text{SiC}} = 1 \text{ mass-\%}$
setting 2	Multiflux I	$d_{50,\text{Al}(\text{OH})_3} = 41 \mu\text{m}$	$d_{50,\text{SiC}} = 26 \mu\text{m}$	$\bar{c}_{\text{SiC}} = 1 \text{ mass-\%}$
setting 3	Multiflux I	$d_{50,\text{Al}(\text{OH})_3} = 49 \mu\text{m}$	$d_{50,\text{SiC}} = 26 \mu\text{m}$	$\bar{c}_{\text{SiC}} = 1 \text{ mass-\%}$
setting 4	Multiflux I	$d_{50,\text{Al}(\text{OH})_3} = 70 \mu\text{m}$	$d_{50,\text{Irgalite}} = 22 \mu\text{m}$	$\bar{c}_{\text{Irgalite}} = 0.12 \text{ mass-\%}$
setting 5	Multiflux II	$d_{50,\text{Al}(\text{OH})_3} = 70 \mu\text{m}$	$d_{50,\text{SiC}} = 26 \mu\text{m}$	$\bar{c}_{\text{SiC}} = 1 \text{ mass-\%}$
setting 6	GAC 307	$d_{50,\text{Al}(\text{OH})_3} = 70 \mu\text{m}$	$d_{50,\text{Irgalite}} = 22 \mu\text{m}$	$\bar{c}_{\text{Irgalite}} = 0.12 \text{ mass-\%}$

*Fig. 4-157: Mixing results extracted from WEINEKÖTTER [50]*

In *Fig. 4-158*, the mixing results extracted from WEINEKÖTTER [50] are compared with the mixing results presented in the previous chapters. A logarithmical scaling of the  $x$ - and  $y$ -axis was chosen. The data points of each series lay approximately on two parallel straight lines. The imaginary line, which fits the mixing results extracted from WEINEKÖTTER [50], intersects the  $x$ -axis at a higher value. Taking into account that no confidence intervals are available for

WEINEKÖTTER's mixing results and that the values are not corrected with the empirical variance of the measuring mistakes, the conformance of the two experimental series is very good. This fact underlines the hypothesis that the normalized average residence time is the main influencing parameter of the fluctuation ratio and the mixing quality respectively - independent of the mixer and the mixer settings.



	mixer	particle size		concentration
		component 1	component 2	
setting 1	Multiflux I	$d_{50,Al(OH)_3} = 28 \mu m$	$d_{50,SiC} = 26 \mu m$	$\bar{c}_{SiC} = 1 \text{ mass-\%}$
setting 2	Multiflux I	$d_{50,Al(OH)_3} = 41 \mu m$	$d_{50,SiC} = 26 \mu m$	$\bar{c}_{SiC} = 1 \text{ mass-\%}$
setting 3	Multiflux I	$d_{50,Al(OH)_3} = 49 \mu m$	$d_{50,SiC} = 26 \mu m$	$\bar{c}_{SiC} = 1 \text{ mass-\%}$
setting 4	Multiflux I	$d_{50,Al(OH)_3} = 70 \mu m$	$d_{50,Irgalite} = 22 \mu m$	$\bar{c}_{Irgalite} = 0.12 \text{ mass-\%}$
setting 5	Multiflux II	$d_{50,Al(OH)_3} = 70 \mu m$	$d_{50,SiC} = 26 \mu m$	$\bar{c}_{SiC} = 1 \text{ mass-\%}$
setting 6	GAC 307	$d_{50,Al(OH)_3} = 70 \mu m$	$d_{50,Irgalite} = 22 \mu m$	$\bar{c}_{Irgalite} = 0.12 \text{ mass-\%}$

Fig. 4-158: Comparison of the mixing results extracted from WEINEKÖTTER [50] and the mixing results obtained experimentally



## 5 Outlook

The primary objective of this thesis has been the experimental validation and improvement of the mixing model which was developed by SOMMER [7] to calculate the reduction of concentration fluctuations in a continuous dynamic powder mixer. It turned out that an experimental validation of the mixing model is only possible if the short-term feeding constancy of the volumetric feeders used as well as the in-line concentration determination in the outlet of the continuous mixer can be improved in advance.

After the necessary improvements in the field of dosing and near-infrared spectroscopy, the validation of the mixing model was performed for a two-component system of cohesive powders (calcium carbonate and maize starch). During the experimental and theoretical work, new questions and ideas for further research activities arose. Some ideas concerning the control of mixing processes by near-infrared spectroscopy, the continuous powder mixing as well as the modeling of the mixing process are presented below.

### 5.1 Ideas for future work in the field of in-line concentration determination by near-infrared spectroscopy

In this thesis, it was shown how the near-infrared spectrometer *VECTOR 22/N* can be adapted to the in-line concentration determination in the outlet of the continuous dynamic *Gericke* mixer *GCM 500* and a batchwise working *Lödige* mixer *M 20 MK*. Since the analysis results can only be as exact as the previous calibration, a great amount of research work was performed to improve the calibration procedure. The research activities were concentrated on the improvement of the sample presentation as well as the sample preparation. Following, some ideas are presented for future research work. These concern

- the improvement of the attachment for cleaning the probe of the NIR spectrometer with compressed air,
- the use of the NIR spectrometer for analyzing mixtures containing bigger particles and
- the in-line control of mixing processes without any calibration.

#### 5.1.1 Improvement of the attachment used for cleaning the probe of the NIR spectrometer with compressed air

For the in-line concentration determination in the outlet of the continuous dynamic mixer *GCM 500*, an attachment for cleaning the probe of the NIR spectrometer with compressed air was developed. During the in-line measurements, the mixing device throws powder on the attachment, which is fixed on the probe of the NIR spectrometer (compare *Fig. 4-85*, p. 126). A movement of the powder in front of the NIR probe during the measurement has a negative influence on the analysis result. For cohesive powders, it was assumed that the attachment used (see *Fig. 5-1*, left) ensures the formation of a static powder layer in front of the NIR probe. For better flowing powders, it might be necessary to extend the boundary walls on the left- and right-hand side as well as the area on the opposite side of the drilled holes (see *Fig. 5-1*, right).

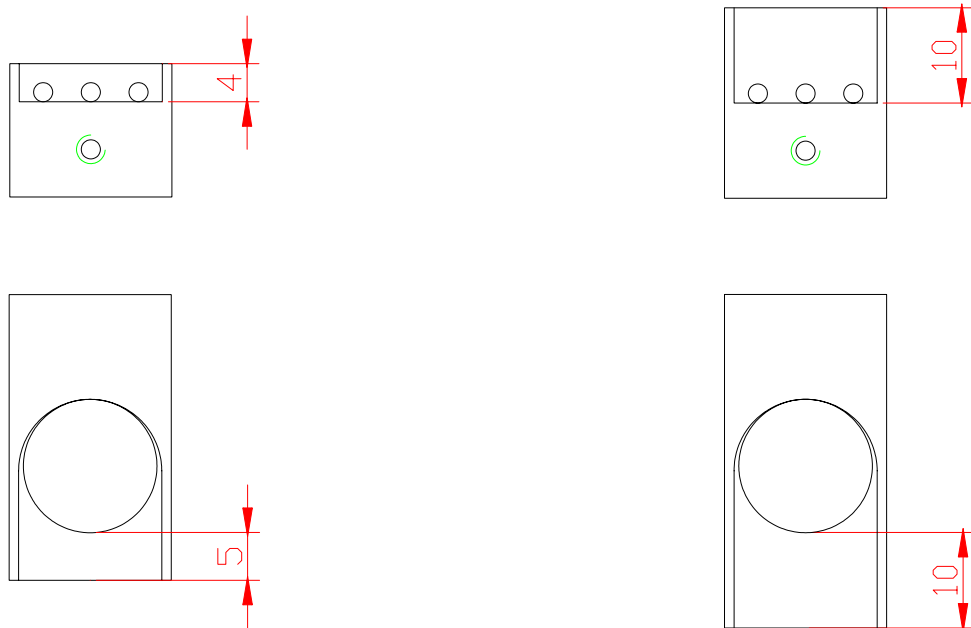


**Fig. 5-1:** Attachment for cleaning the probe of the NIR spectrometer with compressed air: Attachment used within the scope of this thesis (left) and modified attachment (right)

For the validation of the mixing model, the control of the cleaning cycle was programmed in the way that after recording two spectra of the sample (two scans), which takes about  $0.2\text{ s}$ , an electrically actuated valve opens the air supply for  $0.5\text{ s}$ . Afterwards the valve is closed again and powder can accumulate in front of the probe tip during a delay time of  $1\text{ s}$ . For a better resolution of the analyzed concentration fluctuations, the time interval between each measurement has to be decreased. A better resolution is necessary to examine mass flow fluctuations of a shorter period length.

A minor improvement of the analyzing resolution can be achieved by an optimization of the cleaning time and the following delay time. By using the multiplex unit of the NIR spectrometer *VECTOR 22/N*, a major improvement is possible. The multiplex unit offers the option to connect the spectrometer with up to four probes. Only one probe can be active during a measurement but it is possible to program the sequence of using each probe. The multiplexing capability of the NIR spectrometer can be used to control more than one probe in the outlet of the continuous mixer. A modified attachment for three probes is shown in *Fig. 5-2*. Three extended attachments for cleaning with compressed air are milled out of a stainless steel block. The three probes are fixed in the attachment with little screws. Every probe has a separate air supply.

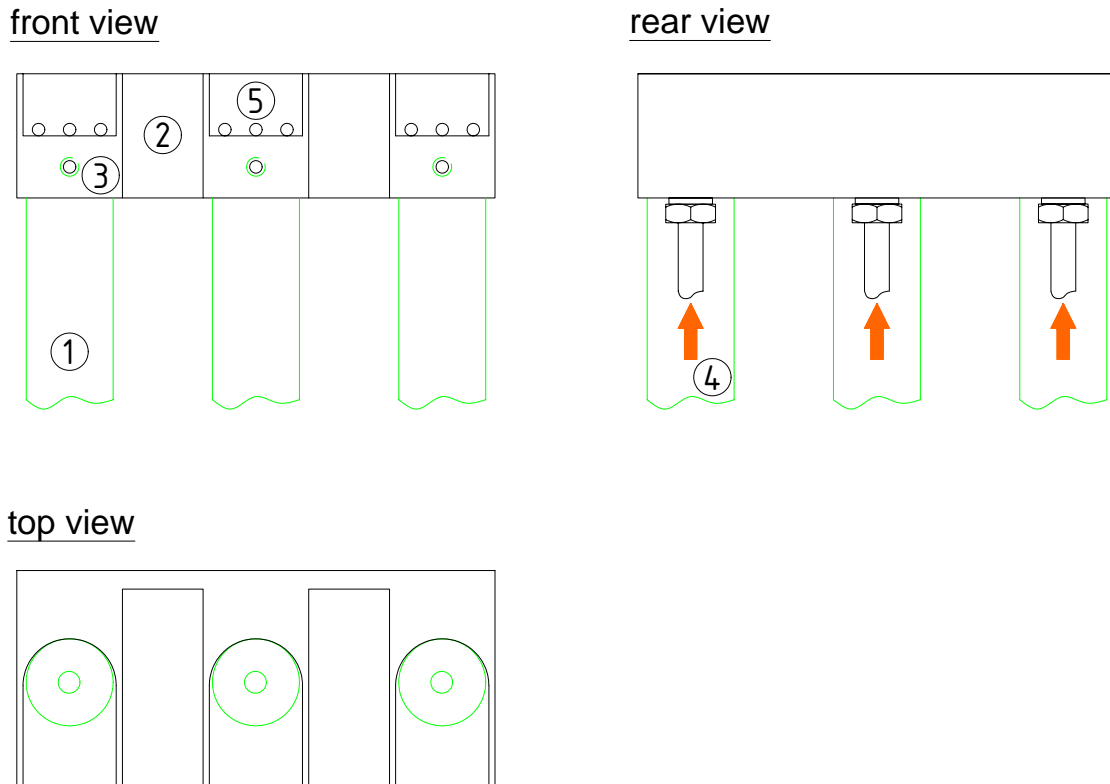


**Fig. 5-2:** Attachment to install three NIR probes in the outlet of the continuous mixer GCM 500: ① probe of the FT-NIR spectrometer, ② attachment for cleaning of the probe tip with compressed air, ③ screw to fix the probes, ④ air hose, ⑤ drilled holes for horizontal cleaning with compressed air

**Fig. 5-3** shows a possible control of the three separate units. Every square symbolizes a time interval of  $0.25\text{ s}$ . For simplification, the measuring time is set to  $0.25\text{ s}$ . Until the steady state is reached in the continuous mixer, air flows through every air hose. Afterwards the air supply of the first probe is stopped and a delay time of  $0.75\text{ s}$  is foreseen. Then the analysis of the powder lying above the first probe starts. After the analysis, the probe is cleaned for  $0.5\text{ s}$  with compressed air. The air supply of the second probe is stopped  $0.5\text{ s}$  after the first probe. For the third probe, the same is applied after  $1\text{ s}$ . Using the described cleaning procedure for the three NIR probes, the interval between each measurement can be decreased to  $0.25\text{ s}$ .

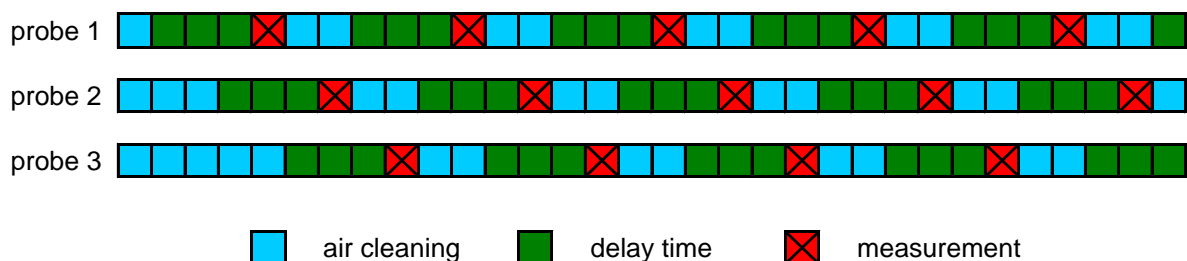


**Fig. 5-3:** Illustration of the cleaning procedure for the attachment shown in Fig. 5-2

### 5.1.2 Adaptation of the FT-NIR spectrometer to the examination of powder mixtures with larger particles

In this thesis, a fiber optic sampling unit probe of the type *IN 263E* (compare *Fig. 4-63* and *Fig. 4-64*, p. 112) was used. The analyzing area of the probe has a diameter of about *3 mm*. This type of probe can only be used if the diameter of the single particles is much smaller than the diameter of the analyzing area. In the follow-up work of this thesis, it is planned to validate the mixing model also for mixtures containing larger particles. This is only possible in the case that a NIR probe with a larger analyzing area is used. For the NIR spectrometer *MATRIX-F EMISSION*, the company Bruker Optik GmbH developed a new fiber optical sampling unit (see *Fig. 5-4*). The analyzing area has a diameter of *10 mm*. The functional principle of this analyzing unit differs from the unit used within the scope of this thesis. Four lamps generate NIR light, which is directed to the surface of the sample. The distance between the sampling unit and the sample is *17 cm*. Depending on the tracer concentration in the sample, a certain amount of the generated light is reflected by the sample. A collector guides the reflected light into optical fibers, which are connected to the NIR spectrometer *MATRIX-F EMISSION*.

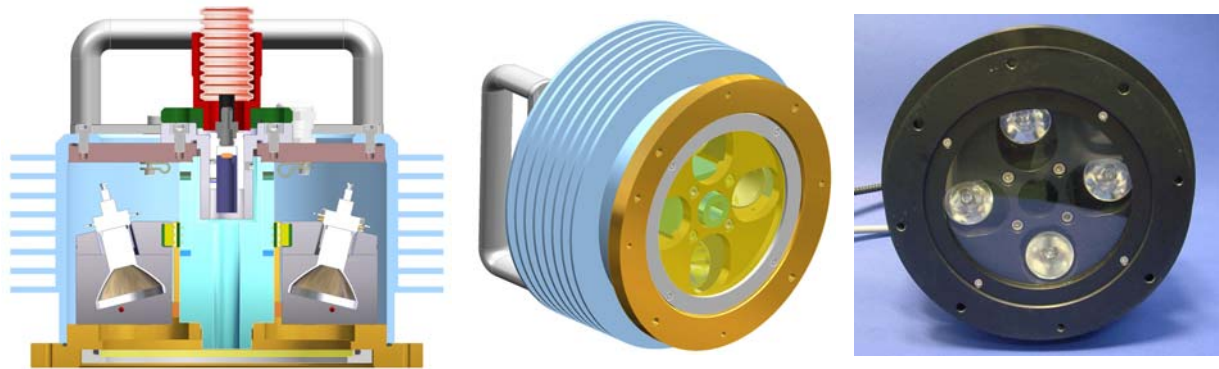


*Fig. 5-4: Fiber optical sampling unit for the NIR spectrometer MATRIX-F EMISSION from the company Bruker Optik GmbH [Courtesy of Bruker Optik GmbH]*

### 5.1.3 In-line control of the mixing process in continuous mixers without any calibration

Talking about the in-line control of the mixing process in continuous mixing processes, two different objectives can arise:

1. Detect the time when the steady state is reached in the continuous mixer.
2. Detect a deviation of the mixture composition from a given set point.

After starting the mixing process, it lasts a certain time until the steady state is reached in the continuous mixer. The product leaving the continuous mixer during the lead-time does not fulfill the specification. Because of the high throughput of continuous mixers, an immediate detection of the steady state as well as an immediate detection of a deviation from the set specification allows the reduction of scrap.

It must be differentiated between a quantitative and a qualitative in-line control. In both cases, NIR spectra of the product are recorded in the outlet of the continuous mixer. For a quantitative control, a time-consuming calibration of the NIR spectrometer used is necessary. The spectra

recorded are linked to concentration values and the temporal concentration fluctuations can be determined. For a qualitative control, the recorded spectra are compared and no calibration of the NIR spectrometer is necessary.

One possibility for the comparison of the spectra recorded is the Principal Component Analysis (PCA). The PCA is a mathematic algorithm, which determines correlations between samples and measurements using eigenvector analysis for data compression and information extraction [165].

To show the applicability of the Principal Component Analysis for the qualitative control of continuous mixing processes, the composition of a maize starch / calcium carbonate mixture was stepwise changed in the mixer inlet. Before and after the stepwise change of the set point, NIR spectra were recorded in the mixer outlet. These spectra were evaluated quantitatively and qualitatively. The temporal changing of the maize starch concentration in the mixer outlet (quantitative analysis) is shown in *Fig. 5-5*. The corresponding result of a Principal Component Analysis is shown in *Fig. 5-6*. The cluster on the left-hand side characterizes the steady state before the stepwise change of the maize starch concentration in the inlet. The cluster on the right-hand side characterizes the steady state after the stepwise changing of the set point. Some data points of the intermediate state are numbered to illustrate the change from one status to the other. Additional research work is necessary to examine the limits of the described method for the in-line control of mixing processes without a calibration.

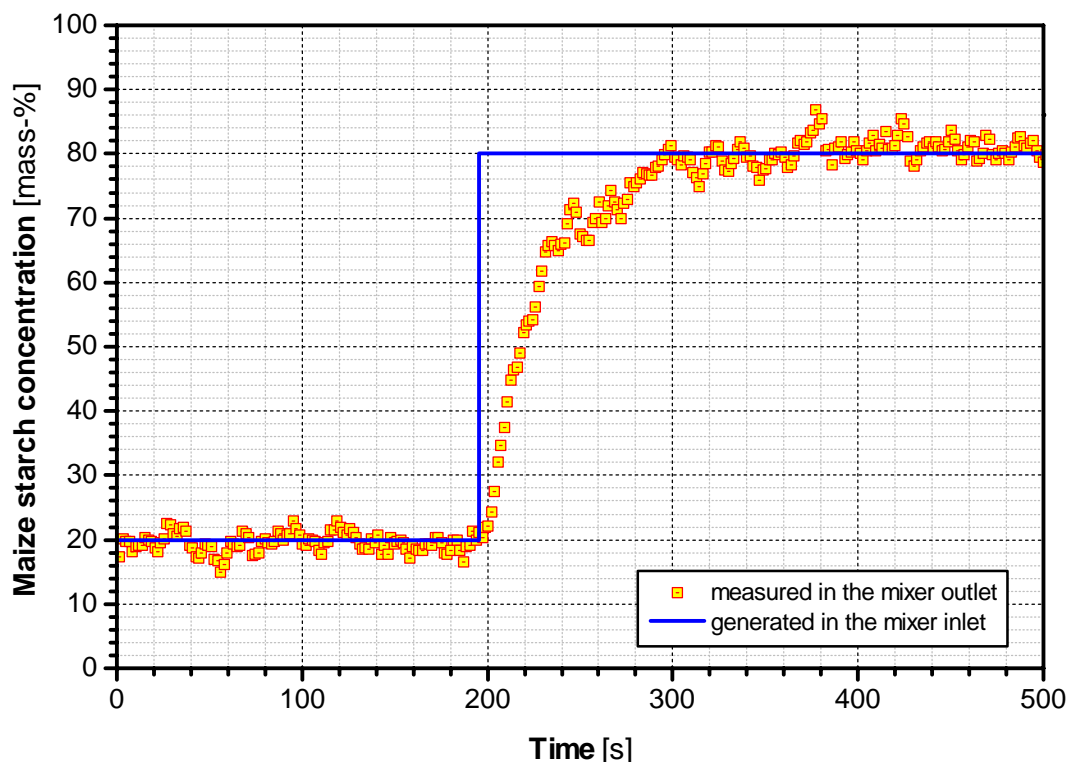


*Fig. 5-5: Change of the maize starch concentration in the outlet of a continuous mixer due to a stepwise change of the maize starch and calcium carbonate concentration in the mixer inlet*

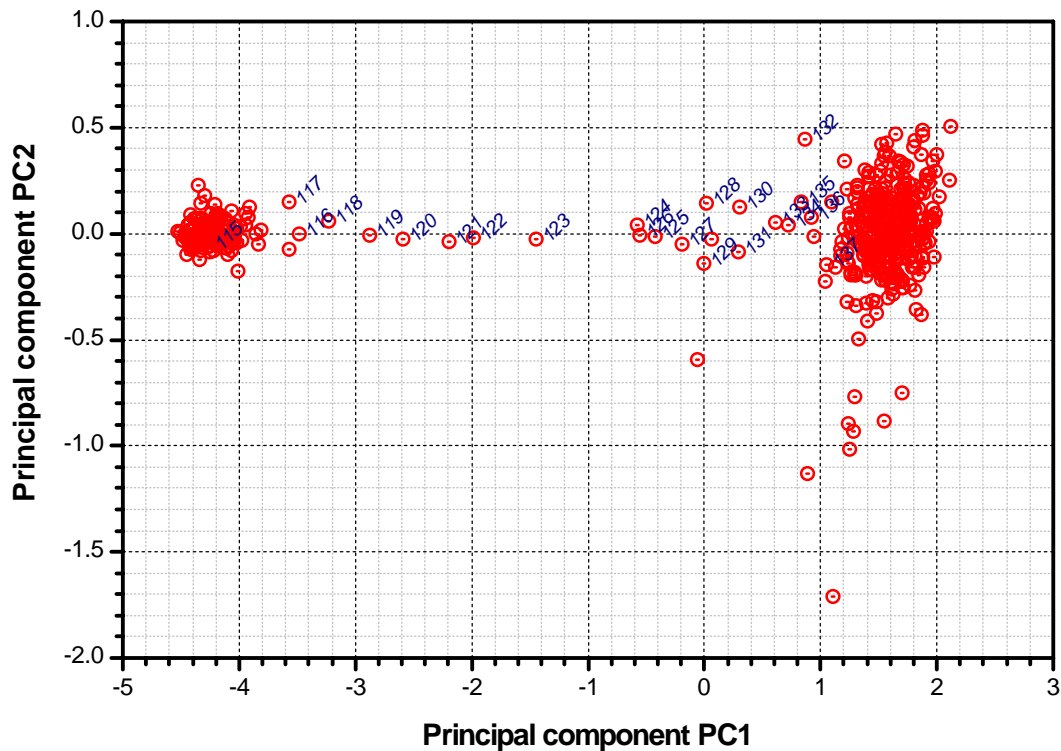


*Fig. 5-6: Principal Component Analysis of NIR spectra recorded before and after a stepwise change of the maize starch and the calcium carbonate concentration in the mixer inlet (compare Fig. 5-5)*

## 5.2 Ideas for future work in the field of continuous dynamic powder mixing

The ideas which have arisen in the field of continuous dynamic powder mixing concern the validation of the developed mixing model for

- higher mass flows,
- powders with different characteristics,
- different mixing devices and mixers,
- two sinusoidally fluctuating mass flows entering the continuous mixer as well as
- square wave like mass flow fluctuations.

The developed mixing model can be used to calculate residence time distributions and the inclination of the mixer filling degree. Both possibilities could be validated in the future.

### 5.2.1 Validation of the mixing model using higher mass flows

For the validation of the mixing model, the reduction of concentration fluctuations entering the continuous mixer and the average residence time of the powder in the mixer have to be determined experimentally. The average residence time is calculated by the mass hold-up in the mixer and the average overall mass flow entering the continuous mixer (compare *Chapter 4.5.1*, p. 155). Depending on the parameter settings, the determined mass hold-ups varied between 0.3 and 3.1 kg using a half-closed mixer weir and between 0.4 and 5.9 kg using a closed mixer

weir. For each parameter variation, the mass hold-up in the mixer was determined three times. The smaller the mass hold-up in the mixer the higher is the variation of the determined average residence times.

The volumetric feeders used can be equipped with proportioning devices (spiral or screw) and adequate dosing tubes of different diameters. For the improvement of the short-term dosing constancy, different attachments for a dosing tube with an inner diameter of  $35\text{ mm}$  were developed. Because of the dosing tubes used, the overall product mass flow was limited to  $140\text{ kg/h}$ . After the development of a rotating star attachment for dosing tubes with an inner diameter of  $53\text{ mm}$  (compare *Fig. 4-45*, p. 94) and the sponsoring of two suction conveyors for the refilling of the volumetric feeders (compare *Chapter 4.1*, p. 59), mixing experiments with higher overall mass flows are now possible. It is expected that the confidence intervals of the determined average residence times will decrease with higher overall mass flows.

The continuous mixer *GCM 500* from the company *Gericke* can handle flow rates of up to  $2.8\text{ m}^3/\text{h}$ . It has to be examined, if the performance of the mixer changes for the case that mixing experiments with much higher mass flows than the mass flows used in this thesis (maximum  $0.4\text{ m}^3/\text{h}$ ) are performed.

### 5.2.2 Validation of the mixing model using powders with different characteristics

Until now, the mixing experiments for the validation of the developed mixing model were only performed with calcium carbonate *OMYACARB 2 SV* and maize starch *Pharm 03406* (compare *Chapter 4.2*, p. 62). It would be interesting to repeat the mixing experiments using powders with different characteristics, e.g. particle size distribution and shape:

- Calcium carbonate is available with different particle size distributions.
- The spherical maize starch particles used (compare *Fig. 4-11*, p. 67) could be replaced by wheat or potato starch particles, which have an oblong shape (see *Fig. 5-7*).

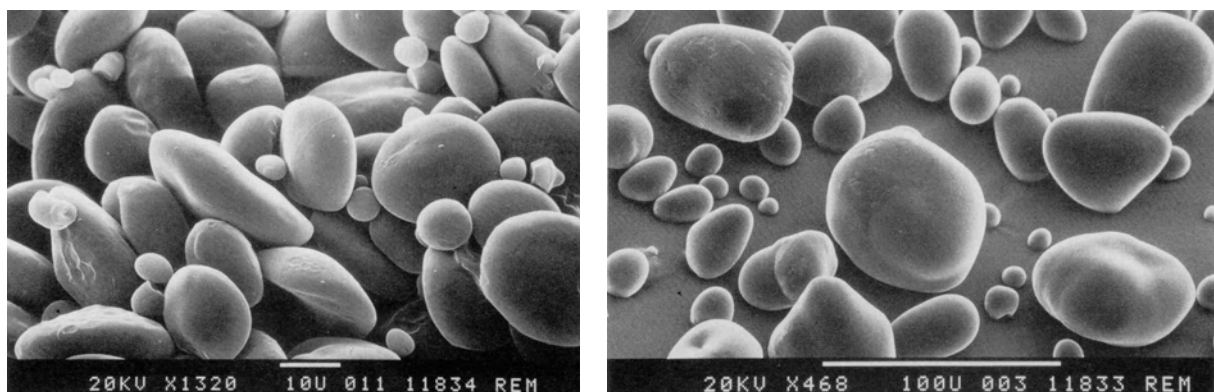


*Fig. 5-7: Examples of starch particles with a shape different to the shape of the maize starch particles used within the scope of this thesis: Wheat starch (left) and potato starch (right) [84]<sup>7</sup>*

<sup>7</sup> Reprinted from BEHR'S VERLAG GmbH & Co KG, Stärke und Stärkederivate, Günther Tegge



### 5.2.3 Validation of the mixing model using different mixing devices and mixers

The mixing experiments for the validation of the mixing model were all performed with a mixing device which feeds the powder in the direction of the mixer outlet (compare *Fig. 4-123*, p. 163). Three other mixing devices are available for the continuous mixer *GCM 500* from the company *Gericke*:

- A mixing device that feeds the powder in the direction of the mixer inlet (see *Fig. 5-8*, top): In comparison to the standard mixing device the paddles on the steel frame are inclined in the opposite direction. A feeding in the direction of the mixer inlet corresponds to a negative transport coefficient in the Fokker-Planck-Equation.
- A mixing device that neither feeds the powder in the direction of the mixer outlet nor the mixer inlet (see *Fig. 5-8*, bottom): The transport coefficient of the Fokker-Planck-Equation becomes zero and the mixing is only caused by dispersion.
- A mixing device with an increased number of paddles which are fixed on a shaft (see *Fig. 5-9*). Each paddle is staggered to the other: The feeding of the powder is in the direction of the mixer outlet.

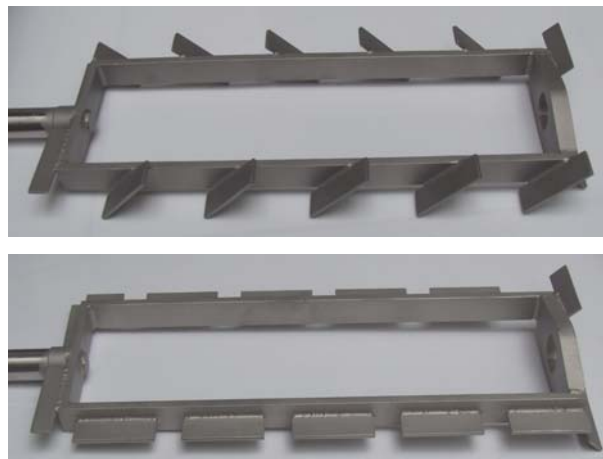


*Fig. 5-8: Mixing devices to be tested in the future: Feeding of the powder in the direction of the mixer inlet (top), feeding of the powder neither in the direction of the outlet nor in the direction of the inlet*



*Fig. 5-9: Mixing device to be tested in the future: Increased number of paddles fixed on a shaft*

Using the alternative mixing devices, it can be examined if

- the developed mixing model describes mixing processes with a negative transport coefficient,
- the developed mixing model describes mixing processes without a convective transport,
- the developed mixing model is independent of the type of the mixing device used.

In addition to the examination of different types of mixing devices, the influence of the mixer size can be examined. The company *Gericke* sells the continuous dynamic mixer *GCM 800* (see *Fig. 5-10*), which has the same style as the mixer *GCM 500* used but a larger mixing chamber. Depending on the product, the mixer can handle throughputs of up to  $12 \text{ m}^3/\text{h}$ .



*Fig. 5-10: Continuous dynamic mixer GCM 800 from the company Gericke [Courtesy of Gericke AG]*

Lager continuous powder mixers are also offered for sale by the company *Lödige* (see *Fig. 5-11*). The mixers can be equipped optionally with plowshares or blades (see *Fig. 5-12*).

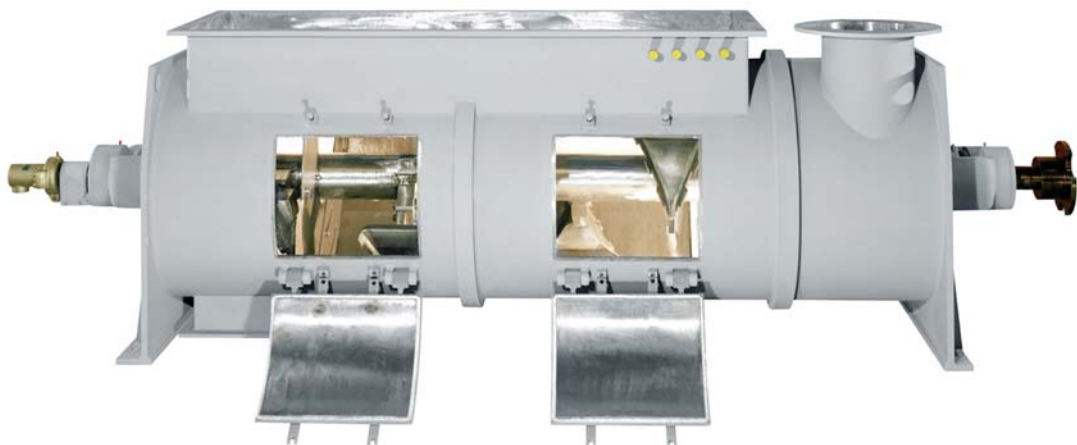


*Fig. 5-11: Continuous dynamic plowshare mixer from the company Lödige [Courtesy of Gebrüder Lödige Maschinenbau GmbH]*



**Fig. 5-12:** Different mixing devices available for the continuous dynamic mixers from the company Lödige: Plowshares (left) and blades (right) [Courtesy of Gebrüder Lödige Maschinenbau GmbH]

Not only mixers with a bigger mixing chamber than the mixer GCM 500 used within the context of the thesis could be examined in the future. In 2005, the Gericke AG complemented their product range by the continuous dynamic powder mixer GCM 250, which has a much smaller mixing chamber (see Fig. 5-13). The maximal mixing chamber volume which can be used is 1 l. The length of the mixing chamber is 250 mm. A patent application for the new horizontal mixer with one central inlet and outlet has been filed. The mixer is designed for high-priced and highest sanitary products in the pharmaceutical industry as well as laboratory processes with small throughputs.

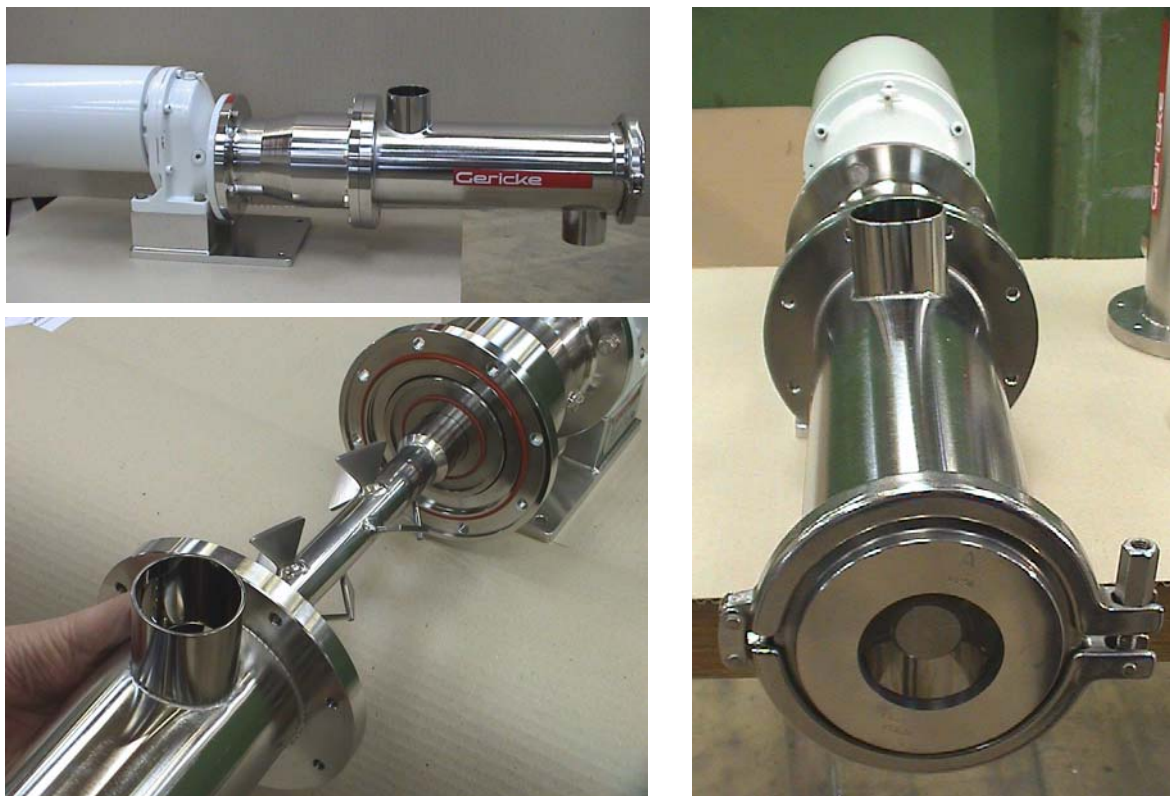
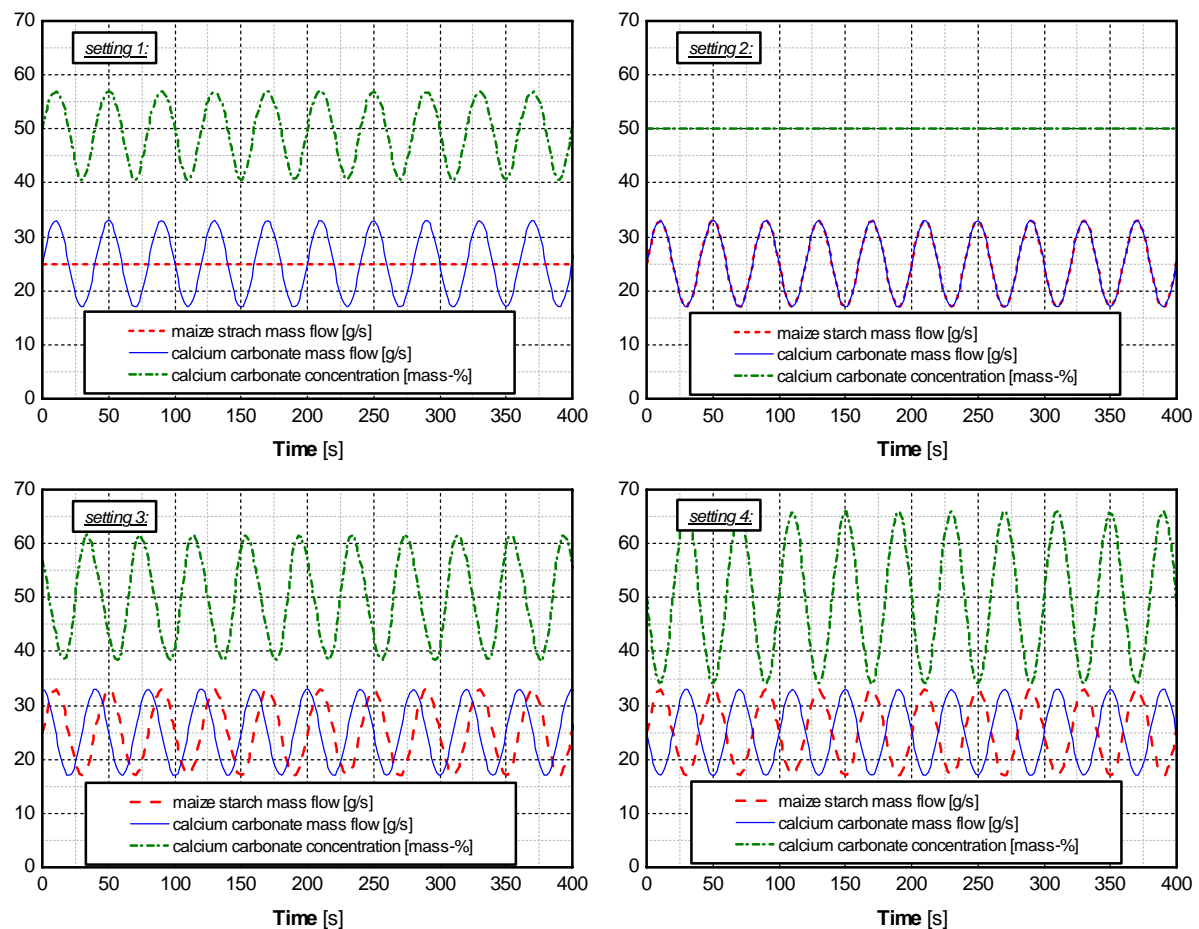


**Fig. 5-13:** Continuous dynamic mixer GCM 250 from the company Gericke [Courtesy of Gericke AG]

### 5.2.4 Validation of the mixing model using two sinusoidally fluctuating mass flows

For different periodic mass flow fluctuations of maize starch and calcium carbonate, the resulting calcium carbonate concentration fluctuations are shown in *Fig. 4-118*. Setting 1 illustrates the result for a constant maize starch mass flow and a sinusoidally fluctuating calcium carbonate mass flow (used for the validation of the developed mixing model). For the settings 2, 3 and 4, both mass flows are fluctuating in the same manner but with different phase shifts. Depending on the phase shift the amplitude of the concentration fluctuations varies. By an in-phase fluctuation of both components, no fluctuation of the resulting calcium carbonate fluctuation occurs. A phase shift of  $180^\circ$  causes the highest amplitude of the resulting calcium carbonate fluctuations.



	maize starch			calcium carbonate			
	average mass flow	amplitude	period length	average mass flow	amplitude	period length	phase shift
setting 1	25 g/s	-	-	25 g/s	8 g/s	40 s	$0^\circ$
setting 2	25 g/s	8 g/s	40 s	25 g/s	8 g/s	40 s	$0^\circ$
setting 3	25 g/s	8 g/s	40 s	25 g/s	8 g/s	40 s	$90^\circ$
setting 4	25 g/s	8 g/s	40 s	25 g/s	8 g/s	40 s	$180^\circ$

*Fig. 5-14: Calcium carbonate concentration fluctuations resulting from different fluctuations of the entering maize starch and calcium carbonate mass flows as well as different phase shifts between the two mass flows*



Until now, the mixing model was only validated for the case that one of the entering mass flows is constant and the other is fluctuating in a sinusoidal manner. The control software of the experimental rig offers also the possibility to generate two mass flows fluctuating in a sinusoidal manner. Additionally, the phase shift between the two mass flows can be varied.

It would be interesting, if the influence of the phase shift on the resulting concentration fluctuations can be used to improve the performance of a continuous mixer. It has been shown that a defined powder dosing and an in-line control of the concentration in the outlet of continuous mixer are possible. The calcium carbonate concentration fluctuation recorded in the mixer outlet can be analyzed by means of a fast Fourier transformation. The obtained information can be used to generate defined mass flow fluctuations in order to improve the mixing quality in the mixer outlet (see *Fig. 5-15*).

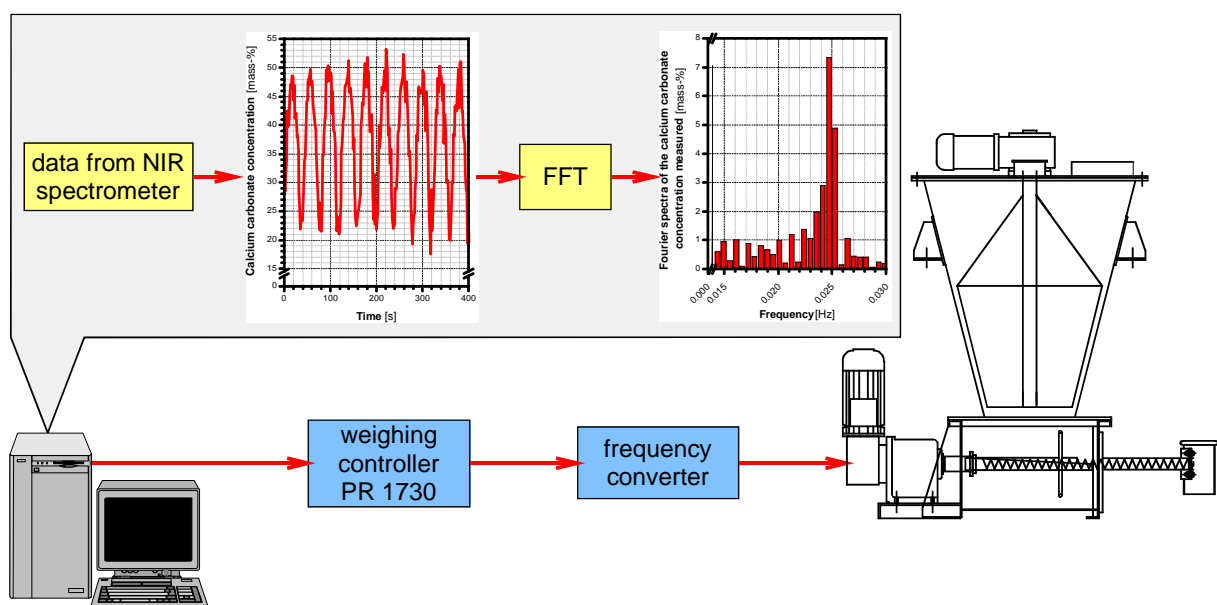


*Fig. 5-15: Generation of defined dosing fluctuations to improve the mixing performance*

### 5.2.5 Comparison between the mixing results obtained by using a square wave oscillation and the mixing results obtained by using a superposition of sinusoidal oscillations

Until now, one mass flow fluctuating in a sinusoidal manner and a second constant mass flow entering the continuous mixer were used for the validation of the mixing model. As mentioned in *Chapter 4.3.3* (see p. 100), the programmed control surface for the experimental rig allows also a generation of mass flows oscillating like a square wave. Square waves can be approximated by overlaying a sinus wave (same period length as the square wave) with its harmonics. It would be interesting to evaluate if the mixing results obtained by using a square wave oscillation of the mass flow could also be achieved by a superposition of mixing results gained by using mass flows oscillating in a sinusoidal manner.

### 5.2.6 Calculation of the residence time distribution

The presented mixing model was used to calculate the fluctuation ratio and the mixing quality respectively as well as the average residence time. After an adaptation, the developed *Mathcad* algorithm (compare *Chapter 9.3*, p. 235) could also be used to calculate residence time distributions resulting from stimulus response experiments.

The explicit determination of the transport coefficient and the dispersion coefficient of the Fokker-Planck-Equation is not possible because the solution of the differential equation system is ambiguous. An additional comparison between experimentally determined residence time distributions and the calculated residence time distributions could offer the opportunity to determine the transport coefficient and the dispersion coefficient of the Fokker-Planck-Equation for different parameter settings.

### 5.2.7 Validation of the calculated inclination of the filling degree in the continuous mixer

The presented mixing model can also be used to calculate the inclination of the filling degree in the continuous mixer (compare *Chapter 3.5.7*, p. 51). Until now, these results were not compared with experimental results. For the determination of the inclination, the continuous mixer has to be stopped immediately after the steady state is reached. Afterwards, the mixing device has to be removed carefully. Immersing thin metal sheets rectangular to the longitudinal axis of the mixer, the powder in the mixer can be segmented and volumes of defined width can be pushed out of the mixer exit one after each other. Dividing the powder mass of each segment by the powder mass of the last segment before the mixer outlet, the normalized filling degree can be calculated and compared with the calculated results.

As said previously, an explicit determination of the transport coefficient and the dispersion coefficient of the Fokker-Planck-Equation is not possible because the solution of the differential equation system is ambiguous. The inclination of the filling degree depends on the transport and dispersion coefficients. With the knowledge of the mixing results and the inclination of the filling degree, a determination of the coefficients could be possible.

## 6 Summary

Continuous powder mixers are mainly used to mix entering components radially and to smooth fluctuations of entering mass flows in axial direction. The radial mixing exceeds the axial mixing by several orders and normally causes no problems. The reduction of concentration fluctuations, which result from the mass flow fluctuations entering the continuous mixer, is much more challenging.

In 1994, SOMMER published a new mixing model to calculate the reduction of periodic concentration fluctuations entering a continuous dynamic powder mixer as well as the corresponding average residence time of the particles in the mixer. Within the scope of this thesis, the model was validated experimentally and improved. For simplification, the model was limited to a two-component system. However, it can be extended to as many components as wanted – only the experimental validation becomes more complicated.

A system of two Fokker-Planck-Equations, one for component 1 and one for component 2, is the basis for the mixing model:

$$\frac{\partial c_1(x,t)}{\partial t} = -U_1^* \cdot \frac{\partial c_1(x,t)}{\partial x} + D_1^* \cdot \frac{\partial^2 c_1(x,t)}{\partial x^2}$$

$$\frac{\partial c_2(x,t)}{\partial t} = -U_2^* \cdot \frac{\partial c_2(x,t)}{\partial x} + D_2^* \cdot \frac{\partial^2 c_2(x,t)}{\partial x^2}$$

The Fokker-Planck-Equations describe the temporal concentration alterations of the two components at a specific position  $x$  in axial direction of the continuous dynamic mixer. The concentration is defined as mass per chamber volume. As the radial mixing exceeds the axial mixing by several orders, the assumption of an ideal mixing in radial direction was made. Therefore, only concentration changes in  $x$ - and not in  $y$ - as well as  $z$ -direction have to be calculated. The mixing model used is not a linear model but the limit of a three-dimensional model!

Parameters of the two Fokker-Planck-Equations are the transport coefficient  $U^*$  and the dispersion coefficient  $D^*$ . The dispersion coefficient describes the random movement of the particles inside the mixer and depends on the mobility of the single particles. The transport coefficient corresponds to an existing convection stream inside the mixer and is generated by the rotating mixing device. For simplification the transport coefficients  $U_1^*$  and  $U_2^*$  as well as the dispersion coefficients  $D_1^*$  and  $D_2^*$  are set equal. This can be done because powders with similar median particle diameters, densities and shapes were used for the experimental validation.

The coupling of the two Fokker-Planck-Equations is done by the transactions at the weir, which is located at the end of the mixer. As soon as the truncation chamber next to the weir is filled up to the height of the weir, the sum of the filling degree of component 1 and the filling degree of component 2 is constant for all following time steps. The transport by dispersion and/or convection causes the filling degree at the end of the mixer. A rising above the given height of the weir causes an immediate discharging of the overflow over the weir. Based on the conservation of mass, the sum of the mass flows entering the last chamber from the previous



one is the same as the sum of the mass flows discharged over the weir. The quantity of the discharged single mass flows is calculated by using the composition of the mass in the truncation chamber next to the weir. The coupling conditions used allow an extension of the model to as many components as wanted.

For the experimental validation of the mixing model used, it was necessary to

- generate defined concentration fluctuations entering the continuous mixer,
- determine the remaining concentration fluctuations in the outlet of the mixer,
- determine the average residence time of the particles in the mixer and
- compare the experimentally obtained reductions of concentration fluctuations as well as the corresponding average residence times with the calculated ones for different machine, process and product parameters.

Hardware and software solutions were developed to be able to generate defined mass flow fluctuations. Without any modification of the volumetric feeders used, a high pulsation of the mass flow coming out of the dosing tube can occur. In some cases, the average deviations of the mass flow were more than 50 % higher than the set average mass flow. The generation of defined mass flow fluctuations was only possible after improving the short-term dosing constancy of the volumetric feeders used. It was shown that unwanted pulsations can be reduced tremendously by using attachments for the standard dosing tube. The best results were obtained with a self-developed rotating star attachment, which reduces the pulsations to a tenth of the pulsations of a standard dosing tube.

The determination of remaining concentration fluctuations in the mixer outlet requires the analysis of a large number of samples. As the manual sampling and the preparation of the taken samples is very time-consuming, a suitable in-process analysis had to be found and adapted. The in-line concentration determination in the outlet of the continuous mixer was done by using a Near-Infrared (NIR) spectrometer. By the development of an attachment for cleaning the probe tip of the spectrometer with compressed air, concentration values can be determined in-line every 1.7 s. For calcium carbonate and maize starch mixtures, it was shown that near-infrared spectroscopy can be used for the in-line concentration determination of the tracer component in continuous and batch mixers. To use NIR Spectroscopy, the tracer must contain C-H-, N-H- and O-H-groups. These groups will be found in all organic powders. Therefore, NIR spectroscopy can be used for a wide variety of different powders and it is not limited to two-component mixtures.

The analysis results can only be as exact as the previous calibration of the FT-NIR spectrometer. Therefore, a great amount of research work was done to improve the calibration procedure. The work was concentrated on the sample preparation as well as the sample presentation. Three different techniques for the preparation of the calibration samples were examined:

- Mixing the powders in a beaker with a spatula
- Mixing the powders with a self-constructed and hand-operated mixer
- Mixing the powder with a batchwise working *Lödige* mixer

No significant difference in the mixing performance of the three preparation techniques was observed because the standard deviation of the determined concentrations was in the same

range as the stochastic measuring mistake. For the sample presentation, an apparatus for a much easier, faster, better as well as dust free calibration was developed. The apparatus mainly consists of the NIR probe and an attachment to clean the probe tip with compressed air. The NIR probe and the attachment are placed in a plastic housing. A Stored Program Control regulates the cleaning of the probe tip and the aspiration of the powder by a vacuum cleaner. Alternatively, the calibration sample presentation in the batchwise working *Lödige* mixer was successfully tested. The NIR probe and a modified attachment for cleaning the probe tip were placed inside the *Lödige* mixer. This approach has the big advantage that an unlimited number of NIR spectra, corresponding to an unlimited number of calibration samples, can be recorded automatically. The more samples are used for a calibration the better sample inhomogeneities can be taken into consideration during the development of the calibration model.

Until now, the validation of the developed model was performed with the inorganic powder calcium carbonate (median particle diameter of about  $2\ \mu\text{m}$ ) and the organic powder maize starch (median diameter of about  $15\ \mu\text{m}$ ). During the mixing experiments, the mass flow, the rotational speed of the mixing device, the period length of the entering mass flow fluctuation and the filling degree were varied. The results obtained experimentally correspond very well with the calculated results (see *Fig. 6-1*).

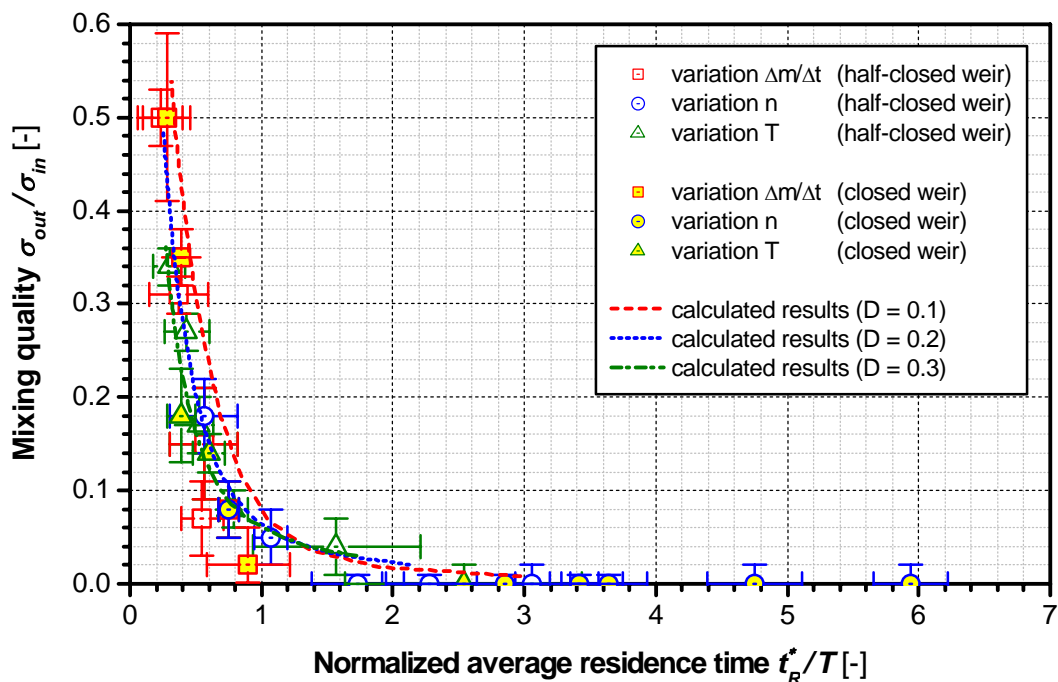


*Fig. 6-1: Comparison of the calculated mixing qualities and the mixing qualities obtained experimentally (half-closed and closed weir)*

The main results of the simulations and the experiments are:

- 1. The mixing mechanisms in a continuous dynamic powder mixer can be described very well with a system of Fokker-Planck-Equations.**
- 2. The average residence time normalized with the period length of the entering mass flow fluctuations is the main influencing parameter of the mixing quality – independent of the mixer settings.**

## 7 Zusammenfassung

Kontinuierliche Pulvermischer werden hauptsächlich dazu verwendet, um eintretende Massenströme radial miteinander zu vermischen und um Konzentrationsschwankungen, die aus Massenstromschwankungen resultieren, zu reduzieren. Das Vermischen in axialer Richtung verläuft um Größenordnungen langsamer als das Vermischen in radialer Richtung und stellt somit die größere Herausforderung dar.

Im Jahre 1994 stellte SOMMER ein neues Modell für kontinuierliche Feststoffmischer vor, mit dem die Reduktion von eintretenden periodischen Konzentrationsschwankungen sowie die dazugehörige mittlere Verweilzeit der Partikel im Mischer berechnet werden können. Im Rahmen dieser Dissertation wurde das von SOMMER vorgestellte Modell experimentell validiert und weiterentwickelt. Zur Vereinfachung wurde das Modell auf ein Zweikomponentensystem begrenzt. Es kann allerdings auf beliebig viele Komponenten erweitert werden – wodurch sich lediglich die experimentelle Validierung erschwert.

Ein System von zwei Fokker-Planck-Gleichungen, eine für Komponente 1 und eine für Komponente 2, bildet die Grundlage für das Modell:

$$\frac{\partial c_1(x,t)}{\partial t} = -U_1^* \cdot \frac{\partial c_1(x,t)}{\partial x} + D_1^* \cdot \frac{\partial^2 c_1(x,t)}{\partial x^2}$$

$$\frac{\partial c_2(x,t)}{\partial t} = -U_2^* \cdot \frac{\partial c_2(x,t)}{\partial x} + D_2^* \cdot \frac{\partial^2 c_2(x,t)}{\partial x^2}$$

Die Fokker-Planck-Gleichungen beschreiben die zeitlichen Konzentrationsänderungen des betrachteten Zweikomponentensystems an einem bestimmten Ort  $x$  in axialer Richtung des kontinuierlichen Feststoffmischers. Die Konzentration ist definiert als Masse pro betrachtetes Kammervolumen. Weil der radiale Mischvorgang den axialen um Größenordnungen übersteigt, wird eine ideale Durchmischung in radialer Richtung angenommen. Daher werden nur Konzentrationsveränderungen in  $x$ - und nicht in  $y$ - sowie  $z$ -Richtung betrachtet. Das entwickelte Modell ist somit kein lineares Modell, sondern ein Sonderfall eines dreidimensionalen Modells.

Parameter der Fokker-Planck-Gleichungen sind der Transportkoeffizient  $U^*$  und der Dispersionskoeffizient  $D^*$ . Der Dispersionskoeffizient beschreibt die Zufallsbewegung der Partikel im Mischer. Er hängt von der Beweglichkeit der Einzelpartikel ab. Der Transportkoeffizient entspricht einem im Mischer vorhandenen Konvektionsstrom, der durch das rotierende Mischwerkzeug hervorgerufen wird. Zur Vereinfachung wurden die beiden Transportkoeffizienten  $U_1^*$  und  $U_2^*$  sowie die Dispersionskoeffizienten  $D_1^*$  und  $D_2^*$  gleichgesetzt. Diese Vereinfachung ist möglich, weil für die experimentelle Validierung des Modells nur Pulverpartikel mit annähernd gleicher Größe, Dichte und Form verwendet wurden.

Die Kopplung der beiden Fokker-Planck-Gleichungen wurde unter Zuhilfenahme der Vorgänge am Wehr, das sich am Ende des Mixers befindet, durchgeführt. Sobald die letzte Diskretisierungskammer des Mixers bis zur Höhe des Wehrs gefüllt ist, ist die Summe der Füllgrade der Komponente 1 und der Komponente 2 für alle nachfolgenden Zeitschritte konstant. Der dispersive und/oder konvektive Transport bestimmt den Füllgrad am Ende des Mixers. Ein Ansteigen des Füllgrades der letzten Diskretisierungskammer über die Höhe des

Wehrs führt zu einem augenblicklichen Austritt des überschüssigen Pulvers. Aufgrund des Massenerhaltungssatzes ist die Summe der Massenströme, die in die letzte Diskretisierungskammer eintreten, gleich der Summe der Massenströme, die über das Wehr aus der letzten Diskretisierungskammer austreten. Die Massenströme der einzelnen Komponenten werden unter Berücksichtigung der Zusammensetzung des Gemisches in der letzten Diskretisierungskammer berechnet. Durch die verwendete Kopplungsbedingung lässt sich das Modell auf das Vermischen von beliebig vielen Komponenten erweitern.

Für die experimentelle Validierung des Mischermodells ist es notwendig,

- definierte Konzentrationsschwankungen zu generieren und in den kontinuierlichen Mischer einzubringen,
- die im Mischeraustritt verbliebenen Konzentrationsschwankungen zu bestimmen,
- die mittlere Verweilzeit der Partikel im Mischer zu bestimmen und
- die experimentell bestimmte Reduktion der Konzentrationsschwankungen sowie die dazugehörige mittlere Verweilzeit im Mischer mit den berechneten Größen für verschiedene Maschinen-, Prozess- und Produktparameter zu vergleichen.

Definierte Konzentrationsschwankungen können nur mittels definierter Massenstromschwankungen generiert werden. Hierzu wurden softwaretechnische und hardwaretechnische Lösungen entwickelt. Ohne eine Modifikation der verwendeten volumetrischen Dosierer können, bei festgelegten konstanten Dosierströmen, hohe Schwankungen der aus den Dosierrohren austretenden Massenströme auftreten. In einigen Fällen waren die gemessenen Massenstromschwankungen mehr als 50 % höher als der festgelegte Massenstrom. Das Generieren von definierten Massenstromschwankungen war erst möglich, nachdem die Kurzzeitdosierkonstanz der volumetrischen Dosierer erhöht werden konnte. Es wurde gezeigt, dass sich die ungewollten Massenstromschwankungen erheblich reduzieren lassen, wenn Vorsätze für die Standarddosierrohre verwendet werden. Die besten Ergebnisse wurden mit einem selbstentwickelten rotierenden Sternvorsatz erzielt, mit dem sich die Massenstromschwankungen auf ein Zehntel der Schwankungen bei Verwendung eines Standarddosierrohres reduzieren lassen.

Das Bestimmen der im Mischeraustritt verbliebenen Konzentrationsschwankungen erfordert die Analyse einer hohen Anzahl von Proben. Da die manuelle Probennahme und das anschließende Präparieren der entnommenen Proben sehr zeitintensiv ist, musste eine In-line-Analysetechnik gefunden und an den Anwendungsfall adaptiert werden. Die In-line-Konzentrationsbestimmung im Mischeraustritt wurde mit einem Nah-Infrarot (NIR) Spektrometer realisiert. Durch die Entwicklung eines Reinigungsaufsatzes für die Sonde des NIR Spektrometers ist es möglich, alle 1,7 Sekunden einen Konzentrationswert zu ermitteln. Für Mischungen aus Calciumcarbonat und Maisstärke konnte gezeigt werden, dass sich die NIR Spektroskopie zur In-line Konzentrationsbestimmung in kontinuierlich und absatzweise arbeitenden Mischern eignet. Voraussetzung für die Anwendung der NIR Spektroskopie ist, dass die zu detektierenden Pulverkomponenten C-H-, N-H- and O-H-Gruppen enthalten. Da dies bei allen organischen Pulvern der Fall ist, kann die NIR Spektroskopie für die Analyse verschiedenster Pulvermischungen verwendet werden. Der Einsatz ist dabei nicht auf Zweikomponentenmischungen beschränkt.

Die mit dem NIR Spektrometer erhaltenen Analyseergebnisse können nur so gut sein wie die vorangegangene Kalibration. Daher war sehr viel Forschungsarbeit nötig, um die Kalibrationsprozedur zu vereinfachen und das Kalibrationsergebnis zu verbessern. Die Forschungstätigkeit konzentrierte sich auf das Herstellen der für die Kalibration nötigen Proben sowie deren Präsentation. Drei unterschiedliche Verfahren zur Herstellung der für die Kalibration benötigten Proben wurden untersucht:

- Das Vermischen der Pulver mittels eines Spatels in einem Becher
- Das Vermischen der Pulver in einem selbstentwickelten Handmischer
- Das Vermischen der Pulver mit einem absatzweise arbeitenden *Lödige* Mischer

Es konnte kein signifikanter Unterschied zwischen den Mischergebnissen der drei Verfahren festgestellt werden, weil die Standardabweichung der ermittelten Konzentrationswerte in der gleichen Größenordnung wie der stochastische Messfehler des NIR Spektrometers lag. Für die Präsentation der Kalibrationsproben wurde eine Apparatur entwickelt, die eine sehr viel einfachere, schnellere, genauere und zudem staubfreie Kalibration ermöglicht. Die Apparatur besteht hauptsächlich aus einem Plastikgehäuse, in dem die NIR Sonde und ein Sondenaufsatz zur Reinigung der Sondenspitze mittels Druckluft integriert sind. Eine speicherprogrammierbare Steuerung (SPS) steuert die Reinigung der Sondenspitze und das Absaugen des weggeblasenen Pulvers. Alternativ wurde die Präsentation der Kalibrationsproben in einem absatzweise arbeitenden *Lödige* Mischer erfolgreich getestet. Die NIR Sonde und ein modifizierter Sondenaufsatz zur Reinigung der Sondenspitze wurden in einen *Lödige* Mischer integriert. Dieser Kalibrationsansatz hat den großen Vorteil, dass eine unbegrenzte Anzahl von NIR Spektren automatisch aufgenommen werden kann. Dies entspricht einer unbegrenzten Anzahl von berücksichtigten Kalibrationsproben. Je mehr Proben bei der Kalibration berücksichtigt werden, desto besser können Inhomogenitäten der Kalibrationsproben bei der Entwicklung des Kalibrationsmodells berücksichtigt werden.

Bisher erfolgte die Validierung des Mischmodells mit anorganischem Calciumcarbonat (medianer Partikeldurchmesser ca.  $2\ \mu\text{m}$ ) und organischer Maisstärke (medianer Partikeldurchmesser ca.  $15\ \mu\text{m}$ ). Bei den durchgeführten Mischversuchen wurde der Massenstrom, die Drehzahl des Mischwerkzeuges, die Periodenlänge der in den Mischer eintretenden Massenstromschwankungen und der Füllgrad des Mixers variiert. Die experimentell erhaltenen Ergebnisse stimmen sehr gut mit den Simulationsergebnissen überein (siehe *Abb. 7-1*).

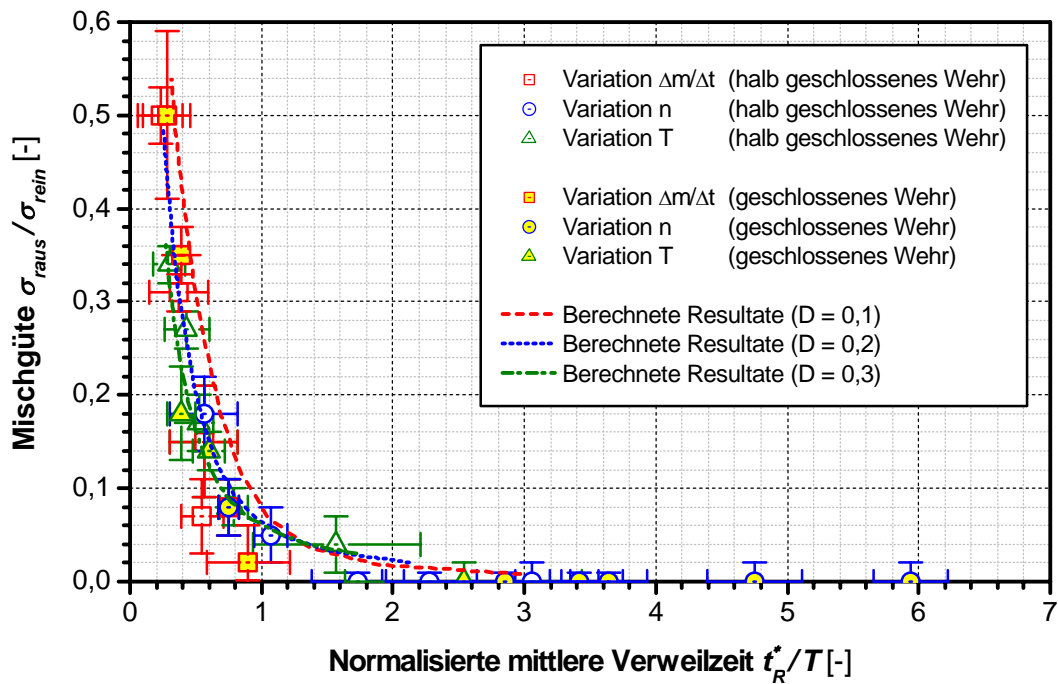


*Abb. 7-1: Vergleich der berechneten Mischgüten mit den experimentell ermittelten Mischgüten (halb geschlossenes und geschlossenes Wehr)*

Die Hauptergebnisse der durchgeführten Simulationen und Mischversuche sind:

- 1. Die Mischmechanismen in einem kontinuierlichen dynamischen Pulvermischer können sehr gut mit einem System von Fokker-Planck-Gleichungen beschrieben werden.**
- 2. Die mit der Periodenlänge der in den Mischer eintretenden Konzentrationsschwankungen normierte mittlere Verweilzeit ist die Haupteinflussgröße auf die Mischgüte. Dies gilt unabhängig von den Betriebsparametern des Mixers.**

## 8 References

- [1] Sommer, K.: Powder mixing mechanisms; *Journal of Powder & Bulk Solids Technology* Vol. 3 (1979) No. 4, pp. 2-9
- [2] Sommer, K.: Mechanismen des Pulvermischens; *Chemie-Ingenieur-Technik* Vol. 49 (1977) No. 4, pp. 305-311
- [3] Weinekötter, R.: Zusammenspiel von Mechatronik und Mischtechnik; *CIT plus* Vol. 6 (2003) No. 5, pp. 76-78
- [4] Holzmüller, R.: Untersuchungen zur Schüttgutbewegung beim kontinuierlichen Feststoffmischen; PhD thesis Universität Stuttgart (Germany), 1984
- [5] Keuter, H.; Pahl, M.: Kontinuierliches Feststoffmischen: Ein Überblick; *Schüttgut* Vol. 1 (1995) No. 3, pp. 487-495
- [6] Keuter, H.; Nothelle, R.; Seyffert, I.: Simulation und Auslegung kontinuierlicher Feststoffmischer; *Chemie-Ingenieur-Technik* Vol. 67 (1995) No. 7, pp. 879-883
- [7] Sommer, K.: Continuous powder mixing; in: *First International Particle Technology Forum Part III* (1994) No. 4, pp. 343-349
- [8] Müller, E.; Oestreich, C. (Eds.): *Handling of highly dispersed powder*; *Berichte aus der Verfahrenstechnik*, Shaker: Aachen, 2004
- [9] Weidenbaum, S. S.: *Mixing of solids*; in: *Drew, T. B.; Hoopes, J. W.: Advances in chemical engineering*; 2<sup>nd</sup> edition, Academic Press: New York, pp. 211-333, 1958
- [10] Fan, L. T.; Chen, S. J.; Watson, C. A.: *Solids mixing*; *Industrial and Engineering Chemistry* Vol. 62 (1970) No. 7, pp. 53-69
- [11] Cooke, M. H.; Stephens, D. J.; Bridgwater, J.: *Powder mixing - A literature survey*; *Powder Technology* Vol. 15 (1976) No. 1, pp. 1-20
- [12] Poux, M.; Fayolle, P.; Bertrand, J.; Bridoux, D.; Bousquet, J.: *Powder mixing: Some practical rules applied to agitated systems*; *Powder Technology* Vol. 68 (1991) No. 3, pp. 213-234
- [13] Sommer, K.: *Mixing of solids*; in: *Ullmann's Encyclopedia of Industrial Chemistry*; 5<sup>th</sup> edition, Vol. B2, VCH: Weinheim, pp. 27-1 - 27-16, 1988
- [14] Weinekötter, R.; Gericke, H.: *Mixing of solids*; *Kluwer Academic Publishers*: Dordrecht, Boston, London, 2000
- [15] Weinekötter, R.; Gericke, H.: *Mischen von Feststoffen: Prinzipien, Verfahren, Mischer*; *Springer*: Berlin, Heidelberg, New York, London, Paris, Tokyo, Hong Kong, Barcelona, Budapest, 1995
- [16] Kaye, B. H.: *Powder mixing*; *Chapman & Hall*: London, Weinheim, New York, Tokyo, Melbourne, Madras, 1997
- [17] Paulsen, H.: *Leistungsaufnahme und Axialdispersion des Mahlgutes in der Ein-Kammer-Kugelmühle*; PhD thesis Technische Hochschule Karlsruhe (Germany), 1969



- [18] Molerus, O.; Paulsen, H.: Axialdispersion des Mahlgutes und Energieausnutzung bei Durchlaufmahlung in der Kugelmühle; *Chemie-Ingenieur-Technik* Vol. 42 (1970) No. 5, pp. 270-270
- [19] Schönert, K.: Mathematische Simulation von Zerkleinerungsprozessen in kontinuierlich betriebenen Mühlen; Postdoctoral lecture qualification thesis Technische Hochschule Karlsruhe (Germany), 1971
- [20] Fan, L. T.; Chen, S. J.; Eckhoff, N. D.; Watson, C. A.: Evaluation of a motionless mixer using a radioactive tracer technique; *Powder Technology* Vol. 4 (1970/1971) No. 6, pp. 345-350
- [21] Muerza, S.; Berthiaux, H.; Massol-Chaudeur, S.; Thomas, G.: A dynamic study of static mixing using on-line image analysis; *Powder Technology* Vol. 128 (2002) No. 2-3, pp. 195–204
- [22] Gyenis, J.: Motionless mixers in bulk solids treatments – A review; *KONA* Vol. 20 (2002), pp. 9-23
- [23] Eichler, P.: Analyse, Modellierung und Optimierung von Schwerkraftmischern; *Fortschritt-Berichte, VDI Reihe 3, Nr. 568*, VDI: Düsseldorf, 1998
- [24] Dauth, H.: Einfluß der Verweilzeitverteilung auf den Mischeffekt in Schwerkraft-Mischsilos – Experiment und rechnergestützte Simulation; PhD thesis Technische Universität München (Germany), 1999
- [25] Williams, J. C.; Rahman, M. A.: The continuous mixing of particulate solids; *Journal of Cosmetic Science* Vol. 21 (1970) No. 1, pp. 3-36
- [26] Merz, A.: Untersuchungen zur Axialvermischung in einem kontinuierlich betriebenen Drehrohr mit Isotopenmarkierung; PhD thesis Technische Hochschule Karlsruhe (Germany), 1973
- [27] Miyanami, K.; Sato, M.; Ynao, T.: Continuous mixing of fine particles; *Journal of Powder and Bulk Solids Technology* Vol. 2 (1979) No. 3, pp. 47-52
- [28] Polman, A.: Effektiv mischen und agglomerieren: Weiterentwicklungen bei Intensivmischern; *Chemie-Anlagen + Verfahren* Vol. 35 (2002) No. 10, pp. 50-52
- [29] Kehlenbeck, V.; Weinzierl, B.; Sommer, K.: Erhöhen der Kurzzeitdosierkonstanz von volumetrischen Einwellendosierern; *wägen, dosieren + mischen* (2002) No. 4, pp. 6-10
- [30] Kehlenbeck, V.; Sommer, K.: Volumetric feeding of cohesive powders with a high short-term constancy; *powder handling & processing* Vol. 15 (2003) No. 2, pp. 86-92
- [31] Kehlenbeck, V.; Sommer, K.: Possibilities to improve the short-term dosing constancy of volumetric feeders; *Powder Technology* Vol. 138 (2003) No. 1, pp. 51-56
- [32] Holzmüller, R.: Verweilzeitverhalten von Schüttgütern in kontinuierlichen Feststoffmischern; *Technische Mitteilungen* Vol. 77 (1984) No. 12, pp. 603-608
- [33] Danckwerts, P. V.; Sellers, E. S.: The effect of hold-up and mixing on a stream of fluctuating composition; *The Industrial Chemist* (1951) No. 9, pp. 395–398

- [34] Danckwerts, P. V.: Continuous flow systems: Distribution of residence times; *Chemical Engineering Science* Vol. 2 (1953) No. 1, pp. 1–13
- [35] Raouf, M. S.: Continuous mixing of solids; PhD thesis Agricultural University Wageningen (Netherlands), 1963
- [36] Poole, K. R.; Taylor, R. F.; Wall, G. P.: Mixing powders to fine-scale homogeneity: Studies of continuous mixing; *Transactions of the Institute of Chemical Engineers* Vol. 43 (1965), pp. T261–T270
- [37] Molerus, O.: Über die Axialvermischung bei Transportprozessen in kontinuierlich betriebenen Apparaten; *Chemie-Ingenieur-Technik* Vol. 38 (1966) No. 2, pp. 137-145
- [38] Williams, J. C.; Rahman, M. A.: Prediction of the performance of continuous mixers for particulate solids using residence time distributions: Part II. Experimental; *Powder Technology* Vol. 5 (1971/1972) No. 5, pp. 307-316
- [39] Williams, J. C.; Rahman, M. A.: Prediction of the performance of continuous mixers for particulate solids using residence time distributions: Part I. Theoretical; *Powder Technology* Vol. 5 (1971/1972) No. 2, pp. 87-92
- [40] Enns, J.: Ermittlung eines Systemcharakteristikums für kontinuierliche Mischer; *Powder Technology* Vol. 7 (1973) No. 4, pp. 247-248
- [41] Harwood, C. F.; Walanski, K.; Luebcke, E.; Swanstrom, C.: The performance of continuous mixers for dry powders; *Powder Technology* Vol. 11 (1975) No. 3, pp. 289-296
- [42] Schofield, C.: The continuous mixing of particulate solids; PhD thesis Loughborough University of Technology (Great Britain), 1975
- [43] Williams, J. C.: Continuous mixing of solids. A review; *Powder Technology* Vol. 15 (1976) No. 2, pp. 237-243
- [44] Williams, J. C.: Mixing of particulate solids; in: Uhl, V. W.; Gray, J. B: *Mixing. Theory and practice*; Vol. 3, Academic Press: Orlando et al., pp. 265-305, 1986
- [45] Lücke, R.; Merz, A.: Radionuklidtechnische Mischgüteuntersuchungen an kontinuierlich und chargenweise betriebenen Pflugscharmischern; *VDI-Berichte* (1977) No. 290, pp. 513-518
- [46] Lücke, R.; Merz, A.: Radionuklidtechnische Mischgüteuntersuchungen an kontinuierlich und chargenweise betriebenen Pflugscharmischern; *Chemie-Ingenieur-Technik* Vol. 49 (1977) No. 3, p. 275
- [47] Lücke, R.: Kontinuierliches Mischen von Feststoffen in Lödige-Pflugscharmischern; *Chemie-Technik* Vol. 7 (1978) No. 6, pp. 247-250
- [48] Merz, A.; Lücke, R.: Einfluß der Schaufelgeometrie auf Axialdispersion und konvektiven Transport beim kontinuierlichen Feststoffmischen; *Chemie-Technik* Vol. 7 (1978) No. 8, pp. 313–318
- [49] Wang, R. H.: Residence time distribution models for continuous solids mixers; *Proceedings of the "11<sup>th</sup> Annual Powder and Bulk Solids Conference"*, Rosemont (USA), May 1986, pp. 8–17

- [50] Weinekötter, R.: Kontinuierliches Mischen feiner Feststoffe; PhD thesis Eidgenössische Technische Hochschule Zürich (Switzerland), 1993
- [51] Weinekötter, R.: Kontinuierliches Mischen feiner Feststoffe; Chemie Ingenieur Technik Vol. 67 (1995) No. 11, pp. 1507-1511
- [52] Weinekötter, R.; Reh, L.: Continuous mixing of fine particles; Particle & Particle Systems Characterization Vol. 12 (1995), pp. 46-53
- [53] Weinekötter, R.: Kontinuierliche Mischprozesse für Feststoffe; wägen + dosieren (1997) No. 1, pp. 6-11
- [54] Sommer, K.: Mixing of particulate solids; KONA (1996) No. 14, pp. 73-78
- [55] Laurent, B.; Bridgwater, J.: Kontinuierliches Feststoffmischen; Chemie Ingenieur Technik Vol. 71 (1999) No. 6, pp. 583-558
- [56] Laurent, B. F. C.; Bridgwater, J.; Parker, D. J.: Convection and segregation in a horizontal mixer; Powder Technology Vol. 123 (2002) No. 1, pp. 9-18
- [57] Laurent, B. F. C.: Powder flow patterns in a horizontal mixer using positron emission particle tracking; PhD thesis University of Cambridge (United Kingdom), 1998
- [58] Jones, J. R.; Bridgwater, J.: A case study of particle mixing in a ploughshare mixer using positron emission particle tracking; International Journal of Mineral Processing Vol. 53 (1998) No. 1-2, pp. 29-38
- [59] Laurent, B. F. C.; Bridgwater, J.; Parker, D. J.: Motion in a particle bed agitated by a single blade; AIChE Journal Vol. 46 (2000) No. 9, pp. 1723-1734
- [60] Laurent, B. F. C.; Bridgwater, J.: Performance of single and six-bladed powder mixers; Chemical Engineering Science Vol. 57 (2002) No. 10, pp. 1695-1709
- [61] Laurent, B. F. C.; Bridgwater, J.: Dispersive granular flow in a horizontal drum stirred by a single blade; AIChE Journal Vol. 48 (2002) No. 1, pp. 50-58
- [62] Laurent, B. F. C.; Bridgwater, J.: Influence of agitator design on powder flow; Chemical Engineering Science Vol. 57 (2002) No. 18, pp. 3781-3793
- [63] Walch, K.: Transportmechanismen von Schüttgütern und Pasten in einem Paddelreaktor; Fortschritt-Berichte, VDI Reihe 3, Nr. 638, VDI: Düsseldorf, 2000
- [64] Kehlenbeck, V.; Sommer, K.: Possibilities to even the product discharge of a screw feeder and presentation of our research project on continuous dynamic mixing; Proceedings of the PARTEC 2001 (published on CD), Nuremberg (Germany), 2001
- [65] Kehlenbeck, V.; Sommer, K.: A new model for continuous dynamic mixing of powders as well as in-line determination of the mixing quality by NIR spectroscopy; Proceedings of the "World Congress on Particle Technology 4" (published on CD), Sydney (Australia), 2002
- [66] Kehlenbeck, V.; Sommer, K.: Modeling of the mixing process of very fine powders in a continuous dynamic mixer; Proceedings of "The 4<sup>th</sup> International Conference for Conveying and Handling of Particulate Solids", Budapest (Hungary), 2003, pp. 9.38-9.43

- [67] Kehlenbeck, V.; Sommer, K.: Modelling of the mixing process of cohesive powders in a continuous dynamic powder blender; Proceedings of the "4<sup>th</sup> European Congress in Chemical Engineering", Granada (Spain), 2003, BOOK 7, TOPIC 8.1. - Solids Handling
- [68] Kehlenbeck, V.; Sommer, K.: Modeling the reduction of periodic concentration fluctuations entering a continuous dynamic powder mixer; Proceedings of the AIChE (American Institute of Chemical Engineers) Annual Meeting, San Francisco (USA), 2003
- [69] Ghaderi, A.: Continuous mixing of particulate materials; Proceedings of "The 4<sup>th</sup> International Conference for Conveying and Handling of Particulate Solids", Budapest (Hungary), May 2003, pp. 9.43–9.47
- [70] Ghaderi, A.: On characterization of continuous mixing of particulate materials; Particulate Science and Technology Vol. 21 (2003) No. 3, pp. 271-282
- [71] Marikh, K.: Mélange des poudres en continu: Dynamique et modélisation; PhD thesis Ecole des Mines d'Albi-Carmaux (France), 2004
- [72] Marikh, K.; Barantzeva, E.; Ponomarev, D.; Berthiaux, H.; Mizonov, V.: Modelling continuous powder mixing by means of the theory of markov chains; Proceedings of "The 4<sup>th</sup> International Conference for Conveying and Handling of Particulate Solids", Budapest (Hungary), May 2003, pp. 12.27-12.32
- [73] Habermann, R.: Untersuchungen zur Verknüpfung von Verweilzeit-Verteilung und Mischgüte in einem kontinuierlichen Pflugscharmischer; PhD thesis Universität Paderborn (Germany), 2005
- [74] Habermann, R.; Pahl, M. H.: Modellansätze für Verweilzeitanalysen an kontinuierlichen Feststoffmischern; Schüttgut Vol. 7 (2001) No. 2, pp. 297-304
- [75] Kaneko, Y.; Shiojima, T.; Horio, M.: Numerical analysis of particle mixing characteristics in a single helical ribbon agitator using DEM simulation; Powder Technology Vol. 108 (2000) No. 1, pp. 55-64
- [76] Stewart, R. L.; Bridgwater, J.; Zhou, Y. C.; Yu, A. B.: Simulated and measured flow of granules in a bladed mixer - A detailed comparison; Chemical Engineering Science Vol. 56 (2001) No. 19, pp. 5457-5471
- [77] Cleary, P. W.; Laurent, B.; Bridgwater, J.: DEM prediction of flow patterns and mixing rates in a ploughshare mixer; Proceedings of the "World Congress on Particle Technology 4" (published on CD), Sydney (Australia), 2002
- [78] Bertrand, F.; Leclaire, L.-A.; Levecque, G.: DEM-based models for the mixing of granular materials; Chemical Engineering Science Vol. 60 (2005) No. 8-9, pp. 2517-2531
- [79] Gardiner, C. W.: Handbook of stochastic methods for physics, chemistry and the natural sciences; 2<sup>nd</sup> edition, Springer: Berlin, Heidelberg, New York, 1997
- [80] Honerkamp, J.: Stochastische dynamische Systeme: Konzepte, numerische Methoden, Datenanalysen; VCH: Weinheim, 1990
- [81] Bronstein, I. N.; Semendjajew, K. A.; Taschenbuch der Mathematik; 25<sup>th</sup> edition, Nauka: Moskau, B. G. Teubner: Stuttgart, Leipzig, Harri Deutsch: Thun, Frankfurt am Main, 1991

- [82] Oates, J. A. H.: Lime and limestone: Chemistry and technology, production and uses; Wiley-VCH: Weinheim, 1998
- [83] Tegethoff, W. F.; Rohleder, J.; Kroker, E.: Calciumcarbonat: Von der Kreidezeit ins 21. Jahrhundert; Birkhäuser: Basel, Boston, Berlin, 2001
- [84] Tegge, G.: Stärke und Stärkederivate; Behr: Hamburg, 1984
- [85] Kehlenbeck, V.; Sommer, K.: Possibilities to improve the short-term dosing constancy of a volumetric feeder; Proceedings of the "World Congress on Particle Technology 4" (published on CD), Sydney (Australia), 2002
- [86] Kehlenbeck, V.; Sommer, K.: Possibilities to smooth the mass flow pulsations of volumetric feeders; Proceedings of "The 4<sup>th</sup> International Conference for Conveying and Handling of Particulate Solids", Budapest (Hungary), 2003, pp. 14.13-14.18
- [87] Fritsch, D.: Zum Verhalten volumetrischer Schneckendosiergeräte für Schüttgüter; PhD thesis Universität Erlangen-Nürnberg (Germany), 1988
- [88] Vetter, G.; Wolfschaffner, H.: Rührreinrichtungen in Schneckendosiergeräten – Wirkung und Auslegungsstrategie; Chemie-Ingenieur-Technik Vol. 66 (1994) No. 2, pp. 163-171
- [89] Vetter, G.: Systematik und Dosiergenauigkeit der Dosierverfahren für Stoffkomponenten; wägen + dosieren (1991) No. 1, pp. 2-13
- [90] Gericke, H. R.: Dosieren von Schüttgütern; Aufbereitungs-Technik Vol. 12 (1971) No. 1, pp. 19-25
- [91] Hüppmeier, B.: Volumetrische Dosierung und Genauigkeit – ein Widerspruch?; Chemie-Anlagen + Verfahren Vol. 20 (1987) No. 12, p. 25
- [92] Kruse, M.: Eine harte Nuss – Zuführ-, Dosier- und Mischsysteme bei der Herstellung von Müsliriegeln; LEBENSMITTELTECHNIK (2003) No. 1-2, pp. 16-19
- [93] Reiser, B.: Eingespieltes Team – Maximale Dosiergenauigkeit durch optimale Abstimmung von Förderung und Dosierung; Verfahrenstechnik Vol. 37 (2003) No. 10, pp. 16-17
- [94] Vetter, G.: Handbuch Dosieren; 2<sup>nd</sup> edition, Vulkan: Essen, 2001
- [95] Gericke, H.: Dosieren von Feststoffen (Schüttgütern); Gericke AG: Regensburg, 1989
- [96] Vetter, G.: Dosiertechnik auf der Achema 2000; wägen, dosieren + mischen (2000) No. 4, pp. 22-34
- [97] Becker, H.: Pulsationsschwankungen beim Dosieren; Neue Verpackung Vol. 38 (1985) No. 1, pp. 38-44
- [98] Tesch, M.; Reh, L.: Zeitkonstantes Dosieren feiner Feststoffe; Chemie-Ingenieur-Technik Vol. 64 (1992) No. 11, pp. 1034-1036
- [99] Göb, R.: Messen der Kurzzeitgenauigkeit beim Dosieren; Automatisierungstechnische Praxis Vol. 28 (1986) No. 11, pp. 530-533

- [100] Wiche, S. J.; Roberts, A.: Investigations into obtaining constant feed rates from screw feeders; Proceedings of the "World Congress on Particle Technology 3", Brighton (Great Britain), 1998
- [101] Häfner, H. W.: Gravimetric dosing of pulverized materials into pneumatic transport lines; Bulk solids handling Vol. 14 (1994) No. 3, pp. 551-558
- [102] Heinrici, H.: Economical and reliable feeding of coal dust – The coriolis measuring principle; Bulk solids handling Vol. 14 (1994) No. 3, pp. 559-561
- [103] K-Tron Technologies: Schneckenförderer; European Patent EP 0 475 909 A1, 1991
- [104] K-Tron Technologies: Screw conveyor; United States Patent US 5,143,202, 1992
- [105] Dittler, A.; Kasper, G.: Kontinuierliche Dosierung und Dispergierung feindisperser, kohäsiver Feststoffe mit einem neuartigen Staubdosierer; Chemie Ingenieur Technik Vol. 71 (1999) No. 7, pp. 685-688
- [106] K-Tron International: K-Tron's news at the powder and bulk show; powder handling & processing Vol. 14 (2002) No. 1, p. 56
- [107] K-Tron Technologies: Dosing device for a worm dosing device; International Patent, international publication number WO 01/48444 A1, 2001
- [108] Breuker, T.: Volumetrische Dosiergeräte; Technische Mitteilungen Vol. 77 (1984) No. 12, pp. 615-619
- [109] Kreyszig, E.: Statistische Methoden und ihre Anwendungen; 7<sup>th</sup> edition, Vandenhoeck & Ruprecht: Göttingen, 1998
- [110] EHEDG: General hygienic design criteria for the safe processing of dry particulate materials; Trends in Food Science & Technology Vol. 12 (2001) No. 8, pp. 296-301
- [111] EHEDG: Hygienic design of equipment for open processing; Trends in Food Science & Technology Vol. 6 (1995) No. 9, pp. 305-310
- [112] Siesler, H. W.; Ozaki, Y.; Kawata, S.; Heise, H. M.: Near-infrared spectroscopy; WILEY-VCH: Weinheim, 2002
- [113] Schofield, C.: The definition and assessment of mixture quality in mixtures of particulate solids; Powder Technology Vol. 15 (1976) No. 2, pp. 169-180
- [114] Cooper, H. R.: Advances in on-line particulate composition analysis; Powder Technology Vol. 69 (1992) No. 1, pp. 93-99
- [115] Clevett, K. J.: Process analytical chemistry – industry perspectives. Trends in applications and technology; Process Control and Quality Vol. 6 (1994) No. 2-3, pp. 81-90
- [116] Segonne, Y. P.; Briens, C. L.; Chabagno, J. M.; Bousquet, J.: Assessment of agitation and detection of deposits in mechanical solids mixers; Powder Technology Vol. 116 (2001) No. 1, pp. 69-75
- [117] Berntsson, O.; Danielsson, L.-G.; Lagerholm, B.; Folestad, S.: Quantitative in-line monitoring of powder blending by near infrared reflection spectroscopy; Powder Technology Vol. 123 (2002) No. 2/3, pp 185-193

- [118] Kehlenbeck, V.; Sommer, K.: Different methods to determine the mixing performance of a batchwise working screw mixer; Powder handling & processing Vol. 15 (2003) No. 5, pp. 318-327
- [119] Lehtola, S.; Kuoppamäki, R.: The measurement of mixing efficiency of continuous mixers; Chemical Engineering Science Vol. 37 (1982) No. 2, pp. 185-191
- [120] Thýn, J.: Evaluation of mixing of particulate solids by radiotracer method; Isotopenpraxis Vol. 19 (1983) No. 12, pp. 411-418
- [121] Dau, G.; Ebert, F.; Hähner, F.: On-line-Analyse der Austrittskonzentration von Feststoffmischern / On-line analysis of discharge concentration in solids mixers (bilingual); Aufbereitungs-Technik Vol. 35 (1994) No. 6, pp. 281-289
- [122] Dau, G.; Ebert, H.; Hähner, F.: Mischgüte on-line messen; Kunststoffe Vol. 84 (1994) No. 11, pp. 1553-1557
- [123] Ehrhardt, N.; Montange, M.; Berthiaux, H.; Dalloz-Dubrujeaud, B.; Gatumel, C.: Assessing the homogeneity of binary and ternary powder mixtures by on-line electrical capacitance; Proceedings of "The 4<sup>th</sup> International Conference for Conveying and Handling of Particulate Solids", Budapest (Hungary), May 2003, pp. 9.32–9.37
- [124] Weinekötter, R.; Reh, L.: Characterization of particulate mixtures by in-line measurement; Particle & Particle Systems Characterization Vol. 11 (1994) No. 4, pp. 284–290
- [125] Stalder, B.: Ermittlung der Mischgüte beim Pulvermischen; PhD thesis Eidgenössische Technische Hochschule Zürich (Switzerland), 1993
- [126] Eichstädt, O.: Kontinuierliches Mischen feiner Feststoffe in fluid-dynamischen Fallrohrmischern; PhD thesis Eidgenössische Technische Hochschule Zürich (Switzerland), 1998
- [127] Wechsler, J.: Modernizing pharmaceutical manufacturing; Pharmaceutical Technology (2002) No. 2, pp. 16-24
- [128] Conzen, J.-P.: Einblick in Echtzeit; PROCESS · PharmaTEC (2003) No. 3, pp. 40-41
- [129] Ciurczak, E. W.; Drennen III, J. K.: Pharmaceutical and medical applications of near-infrared spectroscopy; Marcel Dekker: New York, Basel, 2002
- [130] Gottwald, W.; Wachter, G.: IR-Spektroskopie für Anwender: Die Praxis der instrumentellen Analytik; WILEY-VCH: Weinheim, New York, Chichester, Brisbane, Singapore, Toronto, 1997
- [131] Osborne, B. G.; Fearn, T.; Hindle, P. H.: Practical NIR spectroscopy with applications in food and beverage analysis; 2<sup>nd</sup> revised edition, Longman Scientific & Technical: Harlow, 1993
- [132] Günzler, H.; Gremlich, H.-U.: IR spectroscopy: An introduction; WILEY-VCH: Weinheim, 2002
- [133] Günzler, H.; Heise, H. M.: IR-Spektroskopie: Eine Einführung; 3<sup>rd</sup> revised edition, VCH: Weinheim, New York, Basel, Cambridge, Tokyo, 1996



- [134] Skoog, D. A.; Leary, J. L.: *Instrumentelle Analytik: Grundlagen – Geräte – Anwendungen*; translated by Brendel, D. and Hofstetter-Kuhn, S., Springer: Berlin, Heidelberg, 1996
- [135] Workman, J.; Veltkamp, D. J.; Doherty, S.; Anderson, B. B.; Creasy, K. E.; Koch, M., Tatera, J. F.; Robinson, A. L.; Bond, L.; Burgess, L. W.; Bokerman, G. N.; Ullmann, A. H.; Darsey, G. P.; Mozayeni, F.; Bamberger, J. A.; Stautberg Greenwood, M.: *Process analytical chemistry*; *Analytical Chemistry* Vol. 71 (1999) No. 12, pp. 121R–180R
- [136] Aldridge, P. K.: *Apparatus for mixing and detecting on-line homogeneity*; European patent EP 0 631 810 B1, 1997
- [137] Sekulic, S. S.; Ward, H. W.; Brannegan, D. R.; Stanley, E. D.; Evans, C. L.; Sciavolino, S. T.; Hailey, P. A.; Aldridge, P. K.: *On-line monitoring of powder blend homogeneity by near-infrared spectroscopy*; *Analytical Chemistry* Vol. 68 (1996) No. 3, pp. 509–513
- [138] Hailey, P. A.: *The role of NIR spectroscopy in the measurement of pharmaceutical manufacture*; *European Pharmaceutical Review* Vol. 1 (1996) No. 2
- [139] Hailey, P. A.; Doherty, P.; Tapsell, P.; Oliver, T.; Aldridge, P. K.: *Automated system for the on-line monitoring of powder blending processes using near-infrared spectroscopy: Part I. System development and control*; *Journal of Pharmaceutical and Biomedical Analysis* Vol. 14 (1996) No. 5., pp. 551-559
- [140] Sekulic, S. S.; Wakeman, J.; Doherty, P.; Hailey, P. A.: *Automated system for the on-line monitoring of powder blending processes using near-infrared spectroscopy: Part II. Qualitative approaches to blend evaluation*; *Journal of Pharmaceutical and Biomedical Analysis* Vol. 17 (1998) No. 8, pp. 1285-1309
- [141] de Maesschalck, R.; Cuesta Sánchez, F.; Massart, D. L.; Doherty, P.; Hailey, P.: *On-line monitoring of powder blending with near-infrared spectroscopy*; *Applied Spectroscopy* Vol. 52 (1998) No. 5, pp. 725–731
- [142] Berntsson, O.: *Characterization and application of near infrared reflection spectroscopy for quantitative process analysis of powder mixtures*; PhD thesis Kungl Tekniska Högskolan (Sweden), 2001
- [143] Saathoff, J.; Nehring, E.; Hoyer, H.: *Vorrichtung zur optischen Bestimmung von Inhaltsstoffen eines rieselfähigen Gutes*; Patentschrift Bundesrepublik Deutschland DE 197 14 115 C2, 1999
- [144] Jochimsen, J.: *Im nahen Infrarot: Möglichkeiten der Online-Prozesskontrolle von Schüttgütern*; *chemie-anlagen + verfahren* (2001) No. 8, pp. 24–25
- [145] Hoyer, H.: *NIR on-line analysis in the food industry*; *Process Control and Quality* Vol. 9 (1997) No. 4, pp. 143–152
- [146] Berntsson, O.; Danielsson, L.-G.; Folestad, S.: *Characterization of diffuse reflectance fiber probe sampling on moving solids using a Fourier transform near-infrared spectrometer*; *Analytica Chimica Acta* Vol. 431 (2001) No. 1, pp. 125-131

- [147] Alava, J. M.; Millar, S. J.; Salmon, S. E.: The determination of wheat breadmaking performance and bread dough mixing time by NIR spectroscopy for high speed mixers; *Journal of Cereal Science* Vol. 33 (2001) No. 1, pp. 71–81
- [148] Wesley, I. J.; Larsen, N.; Osborne, B. G.; Skerritt, J. H.: No-invasive monitoring of dough mixing by near infrared spectroscopy; *Journal of Cereal Science* Vol. 27 (1998) No. 1, pp. 61–69
- [149] Lundstrom, J. W.: Meßeinrichtung zur optischen Messung einer vorbestimmten Eigenschaft von strömenden Granulat; Patentschrift Bundesrepublik Deutschland DE 2717064 C2, 1982
- [150] Lundstrom, J. W.: Method and apparatus for sampling and measuring a characteristic of flowing granular material; United States Patent 4,180,331, 1979
- [151] Zhang, H.; Johnston, P. M.; Zhu, J.-X.; de Lasa, H. I.; Bergougnou, M. A.: A novel calibration procedure for a fiber optic solids concentration probe; *Powder Technology* Vol. 100 (1998) No. 2-3, pp. 260-272
- [152] Pahl, M. H.; Sommer, K.; Streiff, F.: Mischen beim Herstellen und Verarbeiten von Kunststoffen; VDI: Brugg-Windisch, 1985
- [153] Conzen, J.-P.: Multivariate Kalibration: Ein praktischer Leitfaden zur Methodenentwicklung in der quantitativen Analytik; 3<sup>rd</sup> revised edition, Bruker Optik GmbH: Ettlingen, 2001
- [154] Conzen, J.-P.: Methodvalidierung in der quantitativen NIR-Spektroskopie; *GIT Labor-Fachzeitschrift* Vol. 42 (1998), pp. 97-102
- [155] Sommer, K.: Probenahme von Pulvern und körnigen Massengütern: Grundlagen, Verfahren, Geräte; Springer: Berlin, Heidelberg, New York, 1979
- [156] Sommer, K.: Sampling of powders and bulk materials; Springer: Berlin, Heidelberg, New York, Tokyo, 1986
- [157] Haye, J.; Essa, I.: Image and video-based painterly animation [online, cited 6<sup>th</sup> May 2005]; available at: <http://www.cc.gatech.edu/cpl/projects/artstyling/index.htm>
- [158] Cho, J. H.; Gemperline, P. J.; Aldridge, P. K.; Sekulic, S. S.: Effective mass sampled by NIR fiber-optic reflectance probes in blending processes; *Analytica Chimica Acta* Vol. 348 (1997) No. 1-3, pp. 303–310
- [159] Berntsson, O.; Danielsson, L.-G.; Folestad, S.: Estimation of effective sample size when analysing powders with diffuse reflectance near-infrared spectrometry; *Analytica Chimica Acta* Vol. 364 (1998) No. 1-3, pp. 243-251
- [160] Sommer, K.: Praktische Ermittlung der Mischgüte nach der Mischzeit; *Technische Mitteilungen* Vol. 77 (1984) No. 12, pp. 551-562
- [161] Hauser, G.; Koch, T.; Sommer, K.: Bestimmung der Mischzeit eines Schaufelmischers mit Schnellentleerung für die Herstellung von Trockenmörtel und Putzen / Determination of mixing times of a paddle mixer with rapid discharge for production of dry mortar and plaster (bilingual); *Aufbereitungs-Technik* Vol. 30 (1989) No. 6, pp. 367-374

- 
- [162] Koch, T.; Hauser, G.; Zettl, T.; Sommer, K.: Mischzeitbestimmung an einem horizontalen Einwellenmischer; Schüttgut Vol. 2 (1996) No. 1, pp. 67-71
- [163] Ruzbehi, M.; Alt, C.; Lücke, R.: Untersuchungen über den Einfluß von Schüttgutgrößen im Mischprozeß; Aufbereitungs-Technik Vol. 23 (1982) No. 6, pp. 316–326
- [164] Ruzbehi, M.: Untersuchungen über den Einfluß von Schüttgutgrößen im Mischprozeß; PhD thesis Universität Stuttgart (Germany), 1982
- [165] Booksh, K. S.: Chemometric methods in process analysis; in: Meyers, R. A.: Encyclopedia of analytical chemistry; Wiley: Chichester, pp. 8145-8169, 2000

## 9 Appendix

In the following four subchapters, a tabular survey of the literature mentioned in chapter 2 *State of the art* (see p. 5), a survey of published transport and dispersion coefficients, the *Mathcad* routine to model the mixing processes in continuous dynamic mixers as well as a tabular compilation of the experimental mixing results are presented.

### 9.1 Tabular literature survey

In *Table 9-1*, a chronological survey of scientific publications dealing with the experimental examination and modeling of mixing processes in continuous dynamic powder mixers is given.

**Table 9-1:** Survey of scientific publications dealing with the experimental examination and the modeling of continuous dynamic mixing processes

Year of publication	Name	Topic
1953	DANCKWERTS, P. V.	Continuous flow systems: Distribution of residence times [34]
1963	RAOUF, M. S.	Continuous mixing of solids [35]
1965	POOLE, K. R.; TAYLOR, R. F.; WALL, G. P.	Mixing powders to fine-scale homogeneity: Studies of continuous mixing [36]
1966	MOLERUS, O.	Über die Axialvermischung bei Transportprozessen in kontinuierlich betriebenen Apparaten [37]
1971/1972	WILLIAMS, J. C.; RAHMAN, M. A.	Prediction of the performance of continuous mixers for particulate solids using residence time distributions: Part I. Theoretical [39]
1971/1972	WILLIAMS, J. C.; RAHMAN, M. A.	Prediction of the performance of continuous mixers for particulate solids using residence time distributions: Part II. Experimental [38]
1973	MERZ, A.	Untersuchungen zur Axialvermischung in einem kontinuierlich betriebenen Drehrohr mit Isotopenmarkierung [26]
1973	ENNS, J.	Ermittlung eines Systemcharakteristikums für kontinuierliche Mischer [40]
1975	HARWOOD, C. F.; WALANSKI, K.; LUEBCKE, E.; SWANSTROM, C.	The performance of continuous mixers for dry powders [41]
1975	SCHOFIELD, C.	The continuous mixing of particulate solids [42]
1976	COOKE, M. H.; STEPHENS, D. J.; BRIDGWATER, J.	Powder mixing – A literature survey [11]
1976	WILLIAMS, J. C.	Continuous mixing of solids [43]

Year of publication	Name	Topic
1977	LÜCKE, R.; MERZ, A.:	Radionuklidtechnische Mischgüteuntersuchungen an kontinuierlich und chargenweise betriebenen Pflugscharmischern [45]
		Radionuklidtechnische Mischgüteuntersuchungen an kontinuierlich und chargenweise betriebenen Pflugscharmischern [46]
1977	SOMMER, K.	Mechanismen des Pulvermischens [2]
1978	LÜCKE, R.	Kontinuierliches Mischen von Feststoffen in Lödige-Pflugscharmischern [47]
1978	MERZ, A.; LÜCKE, R.:	Einfluß der Schaufelgeometrie auf Axialdispersion und konvektiven Transport beim kontinuierlichen Feststoffmischen [48]
1979	SOMMER, K.	Powder mixing mechanisms [1]
1983	HOLZMÜLLER, R.	Untersuchungen zur Schüttgutbewegung beim kontinuierlichen Feststoffmischen [4]
1984	HOLZMÜLLER, R.	Verweilzeitverhalten von Schüttgütern in kontinuierlichen Feststoffmischern [32]
1986	WILLIAMS, J. C.	Mixing of particulate solids [44]
1986	WANG, R. H.	Residence time distribution models for continuous solids mixers [49]
1993	WEINEKÖTTER, R.	Kontinuierliches Mischen feiner Feststoffe [50]
1994	SOMMER, K.	Continuous powder mixing [7]
1995	KEUTER, H.; PAHL, M.	Kontinuierliches Feststoffmischen: Ein Überblick [5]
1995	KEUTER, H.; NOTHELLE, R.; SEYFFERT, I.	Simulation und Auslegung kontinuierlicher Feststoffmischer [6]
1995	WEINEKÖTTER, R.; REH, L.	Kontinuierliches Mischen feiner Feststoffe [51]
1995	WEINEKÖTTER, R.; REH, L.	Continuous mixing of fine particles [52]
1996	SOMMER, K.	Mixing of particulate solids [54]
1997	WEINEKÖTTER, R.	Kontinuierliche Mischprozesse für Feststoffe [53]
1999	LAURENT, B.; BRIDGWATER, J.; REISEMANN, M.	Kontinuierliches Feststoffmischen [55]
2000	WALCH, K.	Transportmechanismen von Schüttgütern und Pasten in einem Paddelreaktor [63]
2001	HABERMANN, R.; PAHL, M. H.	Modellansätze für Verweilzeitanalysen an kontinuierlichen Feststoffmischern [74]
2001	KEHLENBECK, V.; SOMMER, K.	Possibilities to even the product discharge of a screw feeder and presentation of our research project on continuous dynamic mixing [64]
2002	KEHLENBECK, V.; SOMMER, K.	A new model for continuous dynamic mixing of powders as well as in-line determination of the mixing quality by NIR spectroscopy [65]

Year of publication	Name	Topic
2003	KEHLENBECK, V.; SOMMER, K.	Modelling of the mixing process of very fine powders in a continuous dynamic mixer [66]
2003	GHADERI, A.	Continuous mixing of particulate materials [69]
2003	MARIKH, K.; BARANTZEVA, E.; PONOMAREV, D.; BERTHIAUX, H.; MIZONOV, V.	Modelling continuous powder mixing by means of the theory of markov chains [72]
2003	KEHLENBECK, V.; SOMMER, K.	Modelling of the mixing process of cohesive powders in a continuous dynamic powder blender [67]
2003	KEHLENBECK, V.; SOMMER, K.	Modeling the reduction of periodic concentration fluctuations entering a continuous dynamic powder mixer [68]
2003	GHADERI, A.	On characterization of continuous mixing of particulate solids [70]
2004	MARIKH, K.	Mélange des poudres en continu: Dynamique et modélisation [71]
2005	HABERMANN, R.	Untersuchungen zur Verknüpfung von Verweilzeit-Verteilung und Mischgüte in einem kontinuierlichen Pflugscharmischer [73]

## 9.2 Published transport and dispersion coefficients

In his PhD thesis, MERZ [26] published transport and dispersion coefficients, which were determined experimentally with a continuous drum mixer. Transport and dispersion coefficients, determined experimentally with a continuous dynamic mixer, were published by MERZ and LÜCKE [48] as well as HOLZMÜLLER [4]. As mentioned in *Chapter 2*, continuous dynamic mixers are defined as continuous mixers with a horizontal rotating mixing device.

The figures presented in the following subchapters contain the original experimental results of the authors on the left-hand side and the corresponding normalized results (according to the mixing model used in this thesis) on the right-hand side. For the normalization, a mixer length of  $L = 500 \text{ mm}$  and a period length  $T = 40 \text{ s}$  were used. The presented experimental results are based on single measurements. Therefore, the results are more suitable to get a reference value for the order of magnitude of the transport and dispersion coefficients than to derive a significant influence of the varied parameters on the transport and dispersion coefficients.

The authors applied the momentum method, introduced by MOLERUS [37], to determine the transport and dispersion coefficients by means of stimulus response experiments.

### 9.2.1 Experiments by Merz

For his mixing experiments, MERZ [26] used a continuous drum mixer with an inner diameter of  $200 \text{ mm}$  and a length of  $200 \text{ mm}$ . Different sieve fractions between  $150$  and  $1000 \mu\text{m}$  of quartz sand were used. For every sieve fraction, the median diameter was determined by sedimentation analysis (see *Table 9-2*).

*Table 9-2: Sieve fractions and corresponding median diameter used by MERZ for his mixing experiments [26]*

sieve fraction [ $\mu\text{m}$ ]	150 - 250	250 - 300	430 - 500	750
median diameter [ $\mu\text{m}$ ] (resulting from a sedimentation analysis)	257	334	518	858

In *Fig. 9-1*, the influence of the median particle diameter as well as the filling degree on the transport coefficient and the normalized transport coefficient respectively is shown. The transport coefficient increased with increasing median diameter. A significant influence of the filling degree could not be derived.

In *Fig. 9-2*, the influence of the median particle diameter as well as the filling degree on the dispersion coefficient and the normalized dispersion coefficient respectively is shown. A significant influence of the median diameter on the dispersion coefficient could not be derived. For a filling degree of  $0.34$ , higher dispersion coefficients were obtained than for a filling degree of  $0.23$  and  $0.48$ . The dispersion coefficient obtained for a filling degree of  $0.23$  and a filling degree of  $0.48$  were in the same order.



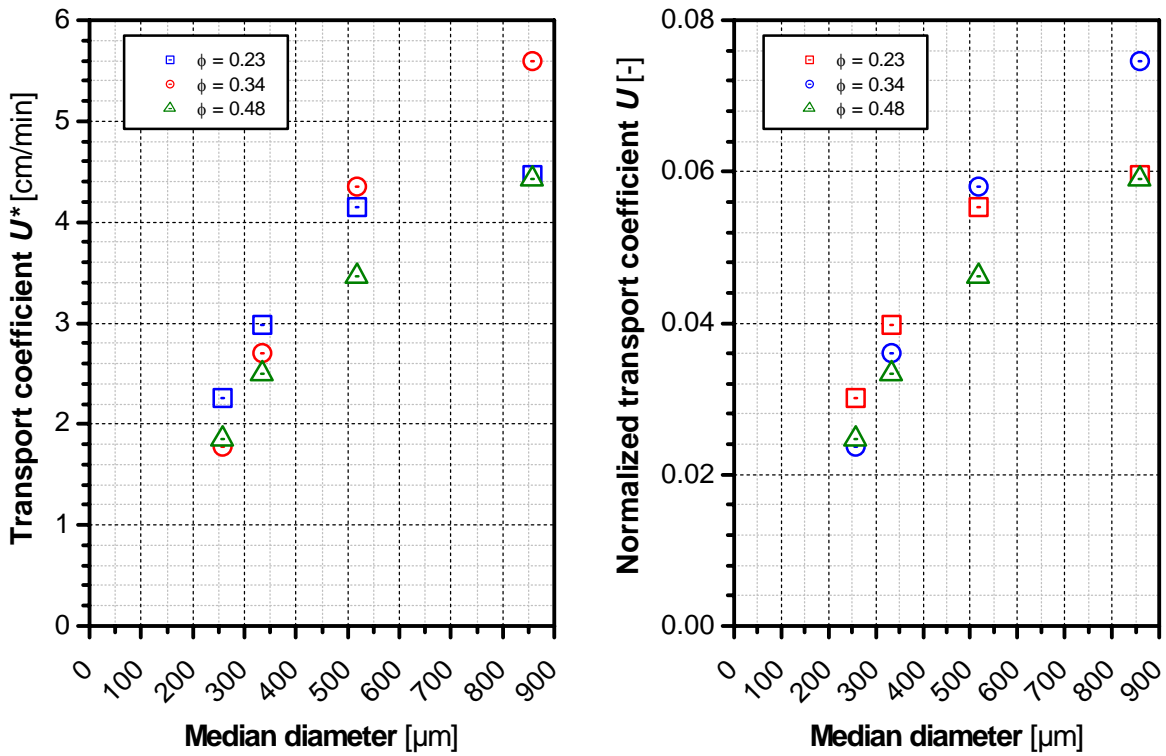


Fig. 9-1: Transport coefficients published by MERZ: Origin (left) [26], normalized according to the mixing model used in this thesis (right)

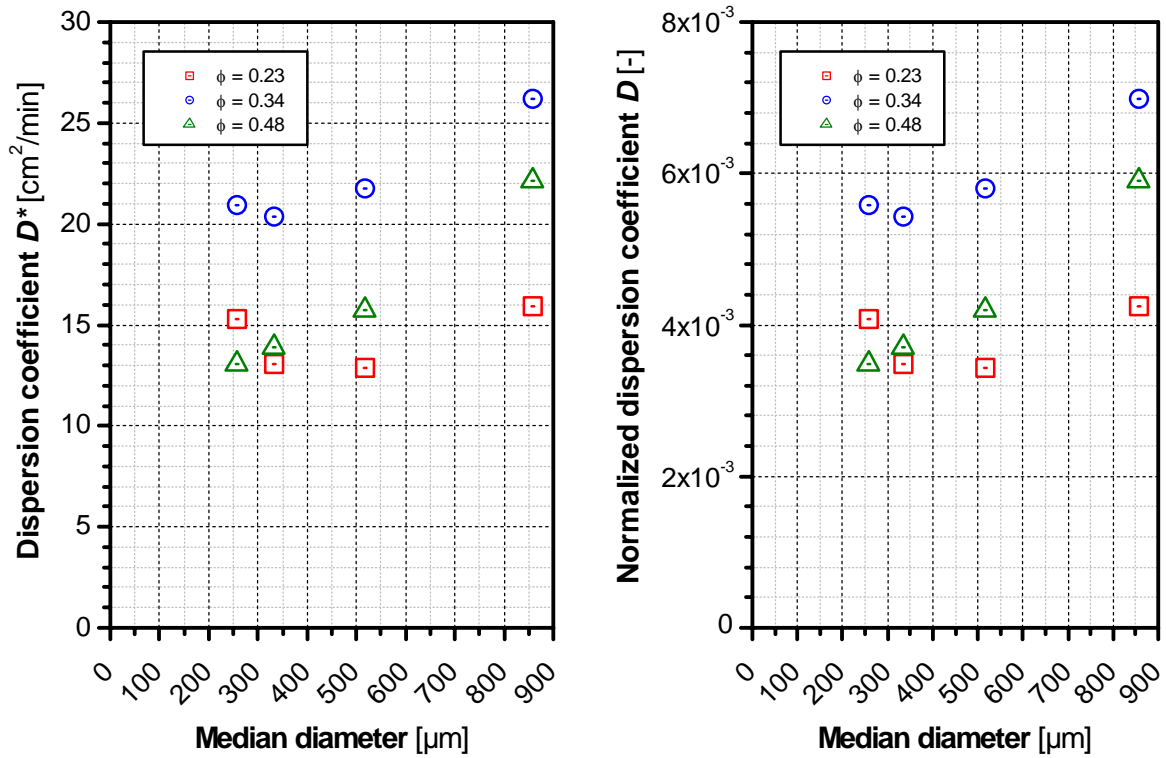
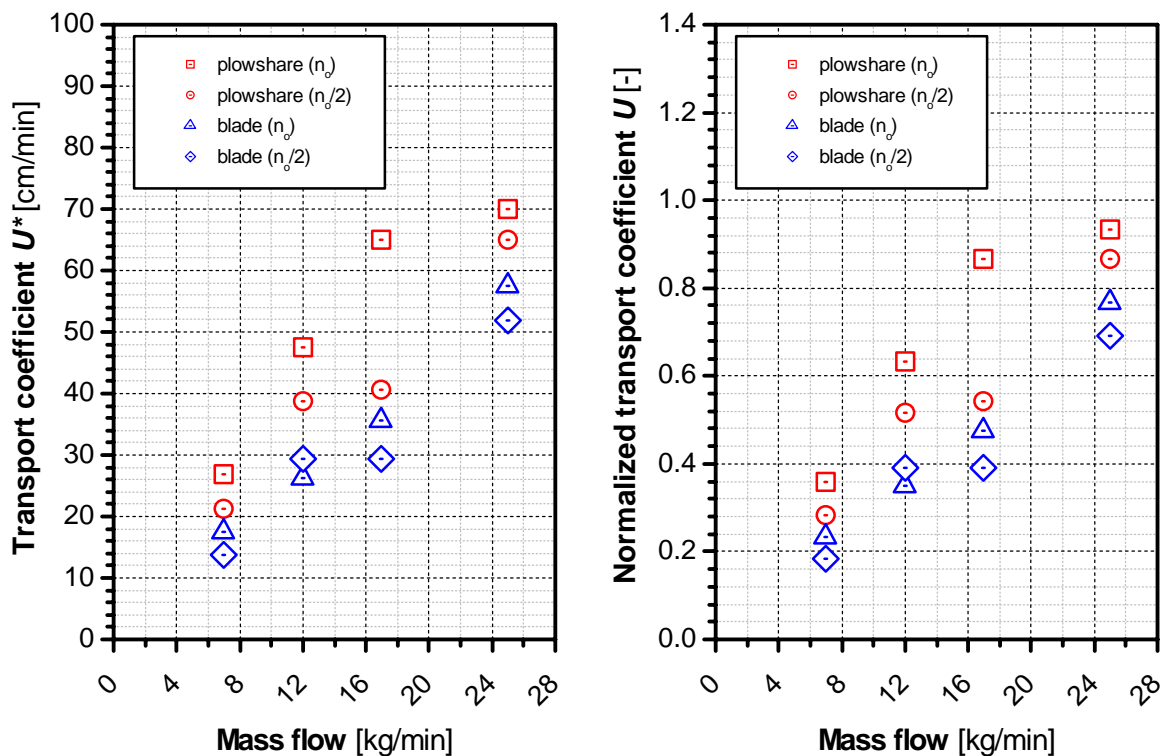


Fig. 9-2: Dispersion coefficients published by MERZ: Origin (left) [26], normalized according to the mixing model used in this thesis (right)

### 9.2.2 Experiments by Merz and Lücke

For their mixing experiments, MERZ and LÜCKE [48] used a continuous *Lödige* mixer with a mixing chamber of 150 l, which was optionally equipped with plowshares or blades. Bruised maize grain with an average particle diameter of 370  $\mu\text{m}$  was used.

In *Fig. 9-3*, the influence of the mass flow, the type of the mixing device used as well as the rotational speed of the mixing device on the transport coefficient and the normalized transport coefficient respectively is shown. MERZ and LÜCKE found out that the transport coefficient increases with increasing mass flows. Higher transport coefficients were reached with plowshares than with blades. For plowshares, a doubling of the rotational speed caused higher transport coefficients. For blades, no significant influence of the rotational speed was found.



*Fig. 9-3: Transport coefficients published by MERZ and LÜCKE: Origin (left) [48], normalized according to the mixing model used in this thesis (right)*

In *Fig. 9-4*, the influence of the mass flow, the type of the mixing device used as well as the rotational speed of the mixing device on the dispersion coefficient and the normalized dispersion coefficient is shown. MERZ and LÜCKE found out that higher rotational speeds cause higher dispersion coefficients. The influence of the mass flow and the mixing device is not significant.

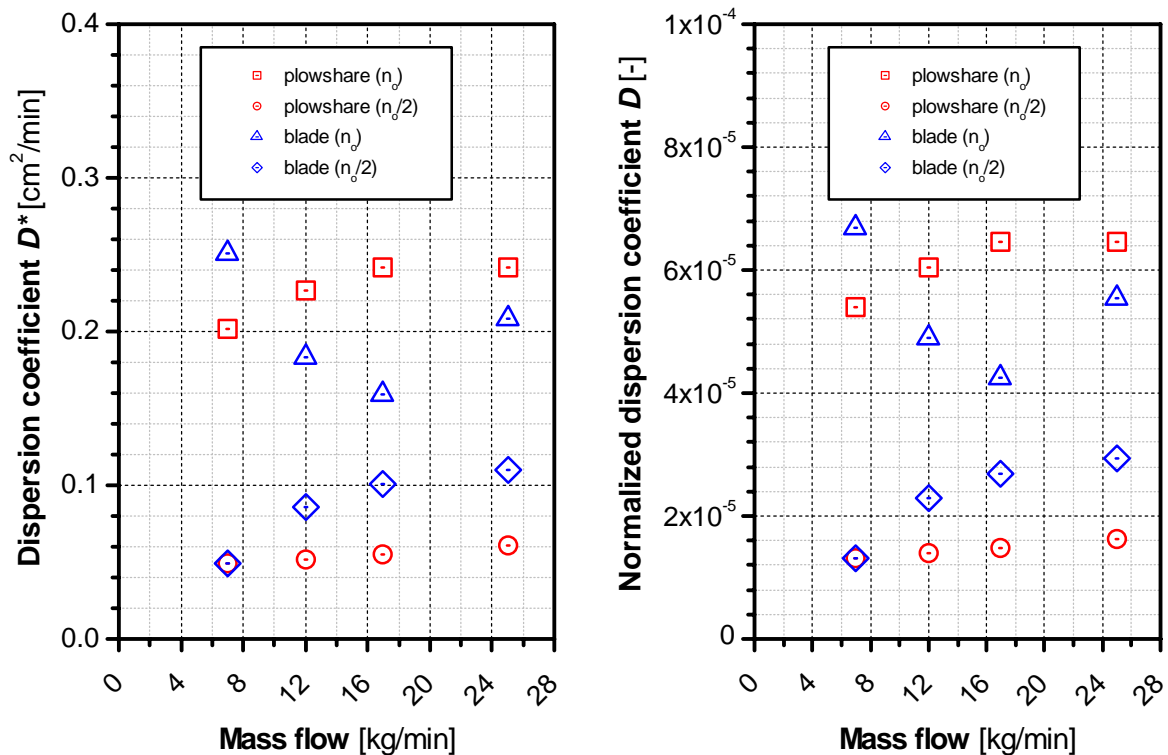


*Fig. 9-4: Dispersion coefficients published by MERZ and LÜCKE: Origin (left) [48], normalized according to the mixing model used in this thesis (right)*

### 9.2.3 Experiments by Holzmüller

For his mixing experiments, HOLZMÜLLER [4] used a continuous *Lödige* plowshare mixer with a mixing chamber of 150 l. Free-flowing bruised maize grain (BMG) with particle diameters between 60 and 2000  $\mu\text{m}$  (median diameter of 340  $\mu\text{m}$ ) as well as free-flowing plastic granulates (PG) with particle diameters between 1400 and 3150  $\mu\text{m}$  (median diameter of 2700  $\mu\text{m}$ ) were examined. Two different radial arrangements of the plowshares (variant A and B) were used. Variant A supports the transport to the mixer outlet, variant B works against the mass flow.

In *Fig. 9-5* and *Fig. 9-6*, the influence of the Froude number, the mass flow and the bulk material on the transport coefficient and the normalized transport coefficient respectively is shown for the two plowshare arrangements A and B. HOLZMÜLLER found out that the transport coefficient increases with increasing Froude numbers. The increase was higher for variant A than for variant B. No significant influence of the bulk material and the mass flow was found.

In *Fig. 9-7* and *Fig. 9-8*, the influence of the Froude number, the mass flow and the bulk material on the dispersion coefficient and the normalized dispersion coefficient respectively is shown for the two plowshare arrangements A and B. The dispersion coefficient increased with increasing Froude numbers. The increase was higher for variant A than for variant B. For higher Froude numbers, the dispersion coefficients obtained by using bruised maize grain was higher than the dispersion coefficients obtained by using plastic granulates. No significant influence of the mass flow was found.

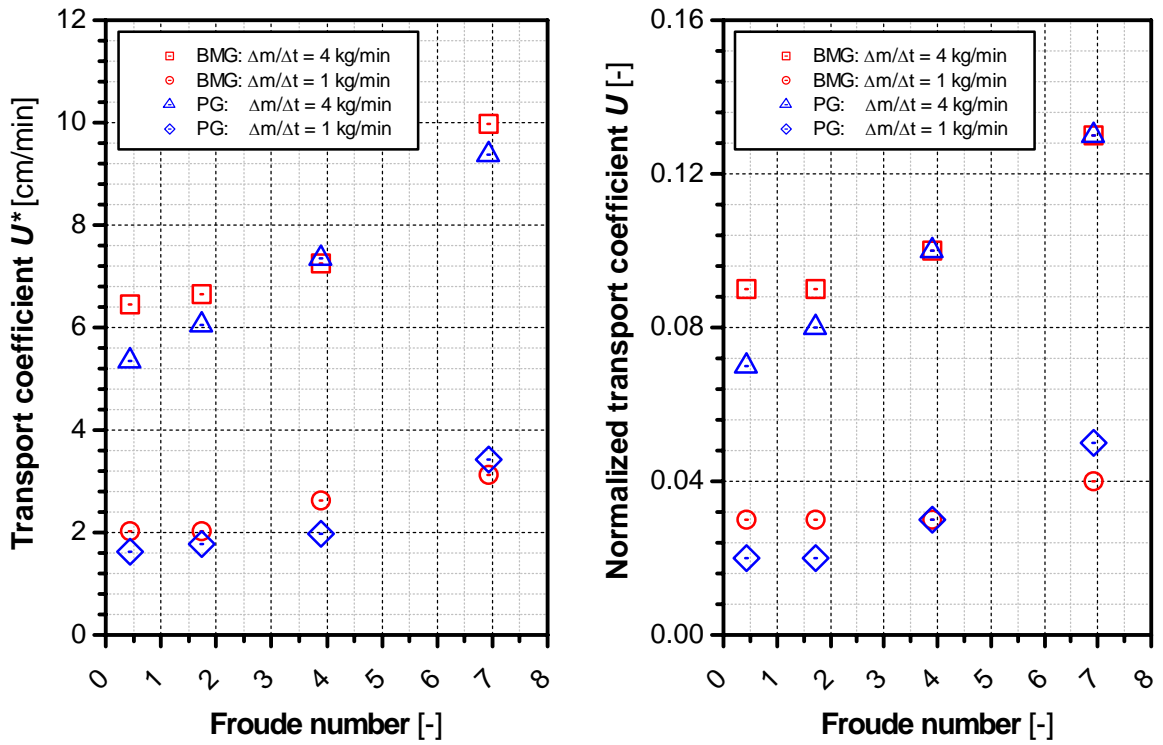


Fig. 9-5: Transport coefficients published by HOLZMÜLLER (variant A): Origin (left) [4], normalized according to the mixing model used in this thesis (right)

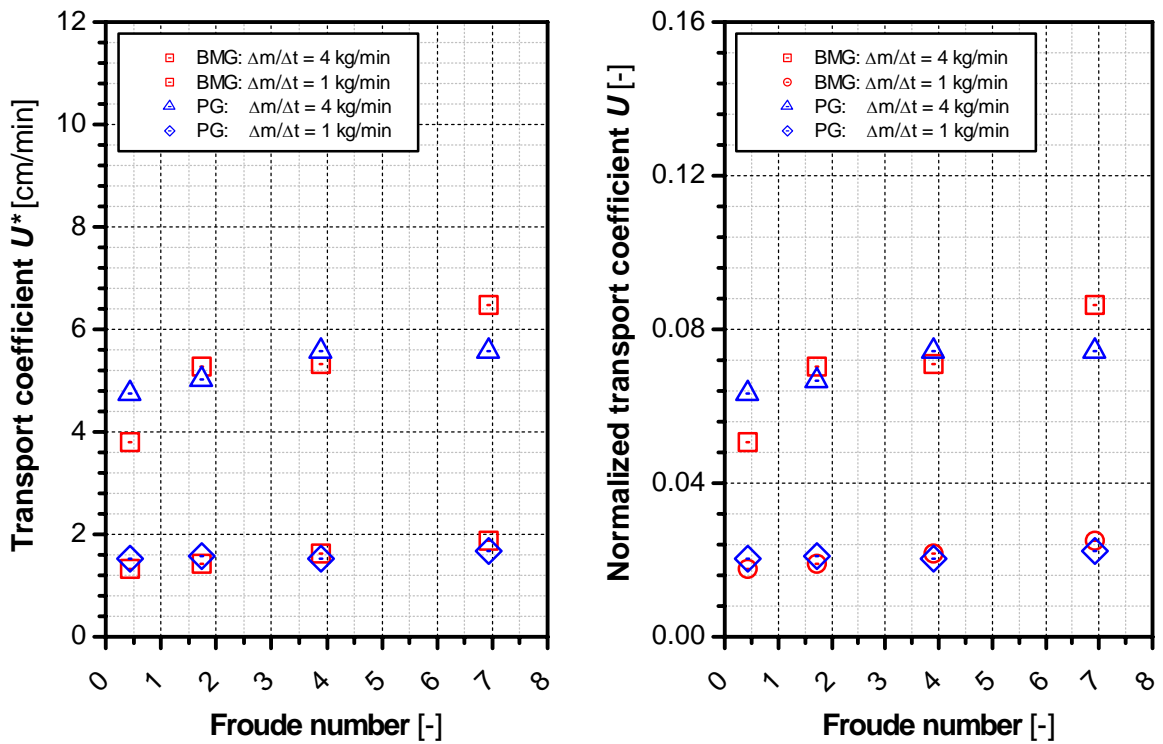


Fig. 9-6: Transport coefficients published by HOLZMÜLLER (variant B): Origin (left) [4], normalized according to the mixing model used in this thesis (right)

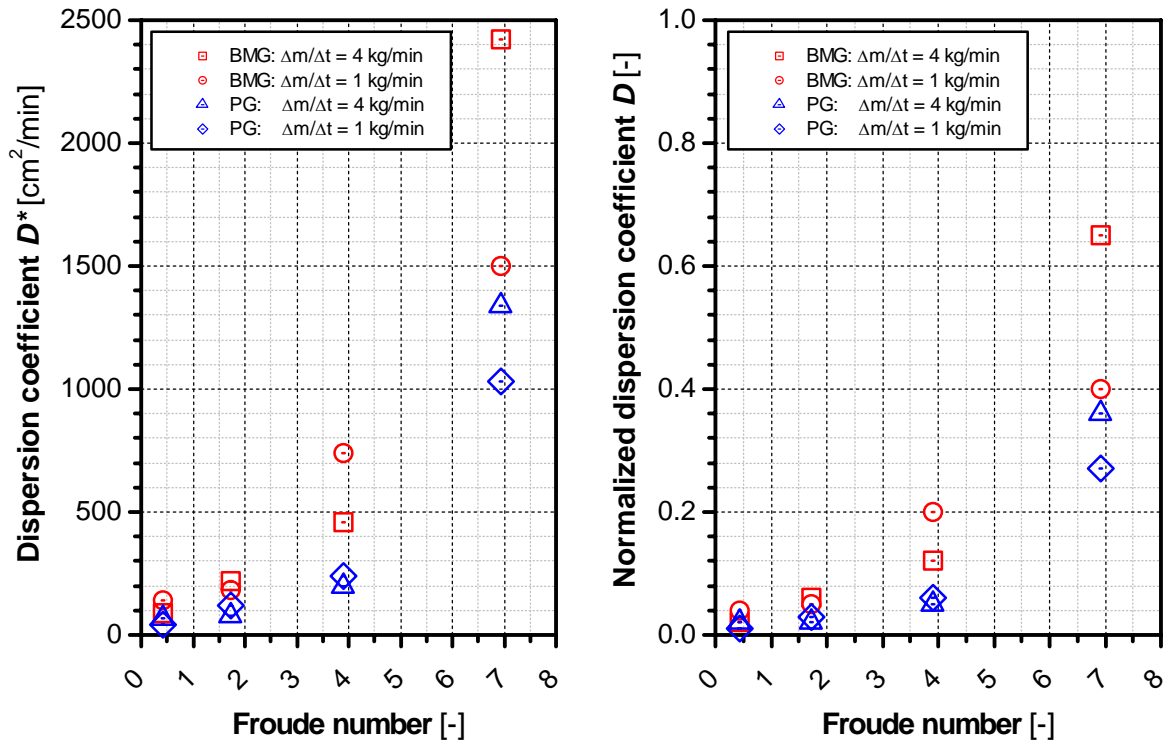


Fig. 9-7: Dispersion coefficients published by HOLZMÜLLER (variant A): Origin (left) [4], normalized according to the mixing model used in this thesis (right)

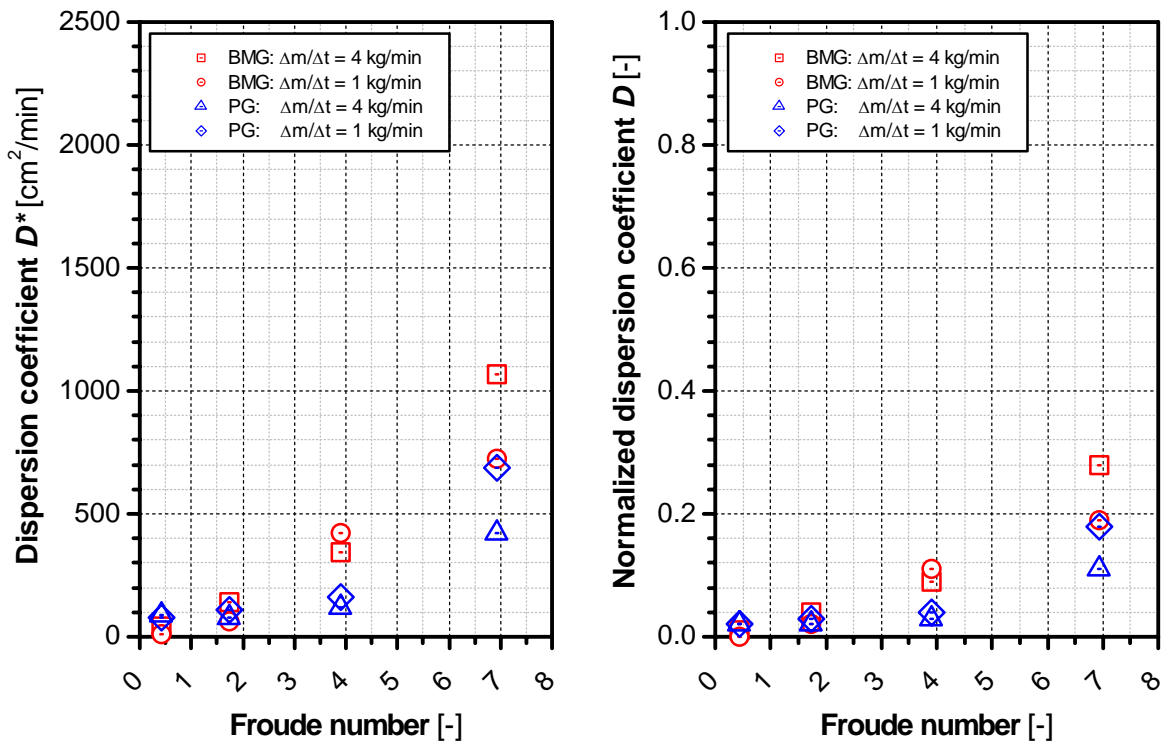


Fig. 9-8: Dispersion coefficients published by HOLZMÜLLER (variant B): Origin (left) [4], normalized according to the mixing model used in this thesis (right)

### 9.3 Mathcad algorithm for the calculation of the fluctuation ratio and the normalized average residence time

The numerical solution of the differential equation system derived for the calculation of the fluctuation ratio and the corresponding average residence time was programmed with *Mathcad 2000 Professional* from the company *MathSoft Inc.* In *Fig. 9-9* to *Fig. 9-15*, the different parts of the routine programmed are presented.

```

ORIGIN = 1
R := "filling degree up to the height of the weir (experiment):"
 $\phi_w \leftarrow 0.1$ 
"normalized angular velocity of component 1:"
 $\Omega_1 \leftarrow 2 \cdot \pi$ 
"normalized angular velocity of component 2:"
 $\Omega_2 \leftarrow 0$ 
"counting variable:"
 $v \leftarrow 1$ 
"running time (multiple of the period length):"
for  $Rt \in 20$ 
  "active mass hold-up [g] (mixing experiment):"
  for  $m\_hold \in 560$ 
    "offset of the mass flow fluctuations of component 1 [g/s] (mixing experiment):"
     $mO1 \leftarrow 15$ 
    "amplitude of the mass flow fluctuations of component 1 [g/s] (mixing experiment):"
     $mA1 \leftarrow 14$ 
    "offset of the mass flow fluctuations of component 2 [g/s] (mixing experiment):"
     $mO2 \leftarrow 10$ 
    "amplitude of the mass flow fluctuations of component 2 [g/s] (mixing experiment):"
     $mA2 \leftarrow 0$ 
    "period length of the concentration fluctuations [s] (mixing experiment):"
    for  $T \in 40$ 
      "normalized offset of the mass flow fluctuations of component 1:"
      for  $\mu O1 \in \frac{mO1 \cdot T}{m\_hold}$ 
        "normalized amplitude of the mass flow fluctuations of component 1:"
        for  $\mu A1 \in \frac{mA1 \cdot T}{m\_hold}$ 
          "normalized offset of the mass flow fluctuations of component 2:"
          for  $\mu O2 \in \frac{mO2 \cdot T}{m\_hold}$ 
            "normalized amplitude of the mass flow fluctuations of component 2:"
            for  $\mu A2 \in \frac{mA2 \cdot T}{m\_hold}$ 
              "number of truncation chambers:"
              for  $n \in 50$ 
                "number of time steps:"
                for  $nt \in 100000$ 
                  "number of truncation chambers, over which the entering powders are spread:"

```

*Fig. 9-9: Mathcad algorithm for the calculation of the fluctuation ratio and the normalized average residence time (part I)*

```

"number of truncation chambers, over which the entering powders are spread:"
n_s ← 1
"spreading factor:"
for SF ∈  $\frac{n_s}{n}$ 
  "normalized dispersion coefficient of component 1:"
  for D1 ∈ 0.1, 0.2.. 0.9
    "normalized dispersion coefficient of component 2:"
    D2 ← D1
    "normalized transport coefficient of component 1:"
    for U1 ∈ 0.2, 0.4.. 2.0
      "normalized transport coefficient of component 2:"
      U2 ← U1
      "width of the truncation chambers:"
       $\Delta\lambda \leftarrow \frac{1}{n}$ 
      "width of the time steps:"
       $\Delta\tau \leftarrow \frac{Rt}{nt}$ 
      "definition of new coefficients for simplification:"
       $CU1 \leftarrow U1 \cdot \frac{\Delta\tau}{\Delta\lambda}$ 
       $CD1 \leftarrow D1 \cdot \frac{\Delta\tau}{\Delta\lambda^2}$ 
       $CU2 \leftarrow U2 \cdot \frac{\Delta\tau}{\Delta\lambda}$ 
       $CD2 \leftarrow D2 \cdot \frac{\Delta\tau}{\Delta\lambda^2}$ 
      "definition of the starting normalized filling degree in each chamber:"
      for i1 ∈ 1..n
         $\phi_{1,1} \leftarrow 0$ 
         $\phi_{2,1} \leftarrow 0$ 
         $\begin{pmatrix} \phi_1 \\ \phi_2 \end{pmatrix}$ 
      "definition of the starting conditions:"
       $si\phi_1 \leftarrow 0$ 
       $si\phi_2 \leftarrow 0$ 
       $so\phi_1 \leftarrow 0$ 
       $so\phi_2 \leftarrow 0$ 
      counter ← 0
      status ← 10
      F ←  $\begin{pmatrix} \phi_1 \leftarrow \phi_1 \\ \phi_2 \leftarrow \phi_2 \end{pmatrix}$ 
      for t ∈ 1..nt - 1
        "column number of the result matrix:"
        t_jump ← 10000
         $r \leftarrow \text{floor}\left(\frac{t}{t\_jump}\right)$ 
        z ← t if t ≤ t_jump - 1
        z ← t_jump if t = r·t_jump
        z ← t - r·t_jump if t > r·t_jump
        a ← z
        "calculation of the filling degree changes for the time steps z = 1 .. t_jump-1:"

```

**Fig. 9-10:** Mathcad algorithm for the calculation of the fluctuation ratio and the normalized average residence time (part II)



```

"calculation of the filling degree changes for the time steps z = 1 .. t_jump-1."
if a ≤ t_jump - 1
  φ1, z+1 ← (1 - CU1 - CD1) · φ1, z + CD1 · φ1, z + [μO1 + μA1 · sin[Ω1 · (t · Δτ)]] ·  $\frac{1}{n \cdot SF} \cdot \frac{\Delta \tau}{\Delta \lambda}$ 
  φ2, z+1 ← (1 - CU2 - CD2) · φ2, z + CD2 · φ2, z + [μO2 + μA2 · sin[Ω2 · (t · Δτ)]] ·  $\frac{1}{n \cdot SF} \cdot \frac{\Delta \tau}{\Delta \lambda}$ 
  for s ∈ 2..n-1
    φ1, z+1 ← (CU1 + CD1) · φ1, s-1, z + (1 - CU1 - 2 · CD1) · φ1, s, z + CD1 · φ1, s+1, z
    φ2, z+1 ← (CU2 + CD2) · φ2, s-1, z + (1 - CU2 - 2 · CD2) · φ2, s, z + CD2 · φ2, s+1, z
  if n-SF ≥ 2
    for s ∈ 2..n-SF
      φ1, z+1 ← (CU1 + CD1) · φ1, s-1, z + (1 - CU1 - 2 · CD1) · φ1, s, z + CD1 · φ1, s+1, z ...
      + [μO1 + μA1 · sin[Ω1 · (t · Δτ)]] ·  $\frac{1}{n \cdot SF} \cdot \frac{\Delta \tau}{\Delta \lambda}$ 
      φ2, z+1 ← (CU2 + CD2) · φ2, s-1, z + (1 - CU2 - 2 · CD2) · φ2, s, z + CD2 · φ2, s+1, z ...
      + [μO2 + μA2 · sin[Ω2 · (t · Δτ)]] ·  $\frac{1}{n \cdot SF} \cdot \frac{\Delta \tau}{\Delta \lambda}$ 
    for s ∈ n-SF + 1..n-1
      φ1, z+1 ← (CU1 + CD1) · φ1, s-1, z + (1 - CU1 - 2 · CD1) · φ1, s, z + CD1 · φ1, s+1, z
      φ2, z+1 ← (CU2 + CD2) · φ2, s-1, z + (1 - CU2 - 2 · CD2) · φ2, s, z + CD2 · φ2, s+1, z
  siφ1, z+1 ← (CU1 + CD1) · φ1, n-1, z - CD1 · φ1, n, z
  siφ2, z+1 ← (CU2 + CD2) · φ2, n-1, z - CD2 · φ2, n, z
  φ1, n, z+1 ← wenn  $\left[ \begin{array}{l} (\phi_{1, n, z} + \phi_{2, n, z}) > 1, \phi_{1, n, z} + \text{si}\phi_{1, z} - \phi_{1, n, z} + \phi_{2, n, z} \cdot (\text{si}\phi_{1, z} + \text{si}\phi_{2, z}) \cdot \phi_{1, n, z} + \text{si}\phi_{1, z} \end{array} \right]$ 
  φ2, n, z+1 ← wenn  $\left[ \begin{array}{l} (\phi_{1, n, z} + \phi_{2, n, z}) > 1, \phi_{2, n, z} + \text{si}\phi_{2, z} - \phi_{1, n, z} + \phi_{2, n, z} \cdot (\text{si}\phi_{1, z} + \text{si}\phi_{2, z}) \cdot \phi_{2, n, z} + \text{si}\phi_{2, z} \end{array} \right]$ 
  soφ1, z+1 ← wenn  $\left[ \begin{array}{l} (\phi_{1, n, z} + \phi_{2, n, z}) > 1, \phi_{1, n, z} + \phi_{2, n, z} \cdot (\text{si}\phi_{1, z} + \text{si}\phi_{2, z}) \cdot 0 \end{array} \right]$ 
  soφ2, z+1 ← wenn  $\left[ \begin{array}{l} (\phi_{1, n, z} + \phi_{2, n, z}) > 1, \phi_{1, n, z} + \phi_{2, n, z} \cdot (\text{si}\phi_{1, z} + \text{si}\phi_{2, z}) \cdot 0 \end{array} \right]$ 
  "control that the filling degree does not exceed its limit:"
  for s ∈ 1..n
    φs, z+1 ← φ1, s, z+1 + φ2, s, z+1
    status ← 0 if φs, z+1 ≥  $\frac{1}{\phi_w}$ 
"calculation of the filling degree changes for the time step z = t_jump."

```

Fig. 9-11: Mathcad algorithm for the calculation of the fluctuation ratio and the normalized average residence time (part III)

```

"calculation of the filling degree changes for the time step z = t_jump:"
if a = t_jump
   $\phi_{1,1} \leftarrow (1 - CU1 - CD1) \cdot \phi_{1,z} + CD1 \cdot \phi_{2,z} + [\mu O1 + \mu A1 \cdot \sin[\Omega 1 \cdot (t \cdot \Delta\tau)]] \cdot \frac{1}{n \cdot SF} \cdot \frac{\Delta\tau}{\Delta\lambda}$ 
   $\phi_{2,1} \leftarrow (1 - CU2 - CD2) \cdot \phi_{2,z} + CD2 \cdot \phi_{1,z} + [\mu O2 + \mu A2 \cdot \sin[\Omega 2 \cdot (t \cdot \Delta\tau)]] \cdot \frac{1}{n \cdot SF} \cdot \frac{\Delta\tau}{\Delta\lambda}$ 
  for s ∈ 2..n-1
    if n-SF < 2
       $\phi_{1,s,1} \leftarrow (CU1 + CD1) \cdot \phi_{1,s-1,z} + (1 - CU1 - 2 \cdot CD1) \cdot \phi_{1,s,z} + CD1 \cdot \phi_{1,s+1,z}$ 
       $\phi_{2,s,1} \leftarrow (CU2 + CD2) \cdot \phi_{2,s-1,z} + (1 - CU2 - 2 \cdot CD2) \cdot \phi_{2,s,z} + CD2 \cdot \phi_{2,s+1,z}$ 
    if n-SF ≥ 2
      for s ∈ 2..n-SF
         $\phi_{1,s,1} \leftarrow (CU1 + CD1) \cdot \phi_{1,s-1,z} + (1 - CU1 - 2 \cdot CD1) \cdot \phi_{1,s,z} + CD1 \cdot \phi_{1,s+1,z} \dots$ 
         $\quad + [\mu O1 + \mu A1 \cdot \sin[\Omega 1 \cdot (t \cdot \Delta\tau)]] \cdot \frac{1}{n \cdot SF} \cdot \frac{\Delta\tau}{\Delta\lambda}$ 
         $\phi_{2,s,1} \leftarrow (CU2 + CD2) \cdot \phi_{2,s-1,z} + (1 - CU2 - 2 \cdot CD2) \cdot \phi_{2,s,z} + CD2 \cdot \phi_{2,s+1,z} \dots$ 
         $\quad + [\mu O2 + \mu A2 \cdot \sin[\Omega 2 \cdot (t \cdot \Delta\tau)]] \cdot \frac{1}{n \cdot SF} \cdot \frac{\Delta\tau}{\Delta\lambda}$ 
      for s ∈ n-SF+1..n-1
         $\phi_{1,s,1} \leftarrow (CU1 + CD1) \cdot \phi_{1,s-1,z} + (1 - CU1 - 2 \cdot CD1) \cdot \phi_{1,s,z} + CD1 \cdot \phi_{1,s+1,z}$ 
         $\phi_{2,s,1} \leftarrow (CU2 + CD2) \cdot \phi_{2,s-1,z} + (1 - CU2 - 2 \cdot CD2) \cdot \phi_{2,s,z} + CD2 \cdot \phi_{2,s+1,z}$ 
       $si\phi_1 \leftarrow (CU1 + CD1) \cdot \phi_{1,n-1,z} - (CD1) \cdot \phi_{1,n,z}$ 
       $si\phi_2 \leftarrow (CU2 + CD2) \cdot \phi_{2,n-1,z} - (CD2) \cdot \phi_{2,n,z}$ 
       $\phi_{1,n,1} \leftarrow \text{wenn} \left[ \left( \phi_{1,n,z} + \phi_{2,n,z} \right) > 1, \phi_{1,n,z} + si\phi_1 - \frac{\phi_{1,n,z}}{\phi_{1,n,z} + \phi_{2,n,z}} \cdot \left( si\phi_1 + si\phi_2 \right), \phi_{1,n,z} + si\phi_1 \right]$ 
       $\phi_{2,n,1} \leftarrow \text{wenn} \left[ \left( \phi_{1,n,z} + \phi_{2,n,z} \right) > 1, \phi_{2,n,z} + si\phi_2 - \frac{\phi_{2,n,z}}{\phi_{1,n,z} + \phi_{2,n,z}} \cdot \left( si\phi_1 + si\phi_2 \right), \phi_{2,n,z} + si\phi_2 \right]$ 
       $so\phi_1 \leftarrow \text{wenn} \left[ \left( \phi_{1,n,z} + \phi_{2,n,z} \right) > 1, \frac{\phi_{1,n,z}}{\phi_{1,n,z} + \phi_{2,n,z}} \cdot \left( si\phi_1 + si\phi_2 \right), 0 \right]$ 
       $so\phi_2 \leftarrow \text{wenn} \left[ \left( \phi_{1,n,z} + \phi_{2,n,z} \right) > 1, \frac{\phi_{2,n,z}}{\phi_{1,n,z} + \phi_{2,n,z}} \cdot \left( si\phi_1 + si\phi_2 \right), 0 \right]$ 
      "control that the filling degree does not exceed its limit:"
      for s ∈ 1..n
         $\phi_{s,1} \leftarrow \phi_{s,1} + \phi_{2,s,1}$ 
        status ← 0 if  $\phi_{s,1} \geq \frac{1}{\phi_w}$ 
      counter ← counter + 1
      TIME_STEPS1,1 ← counter
      STATUS1,1 ← status
      (
         $\phi_1$ 
         $\phi_2$ 
         $so\phi_1$ 
         $so\phi_2$ 
        TIME_STEPS
        STATUS
      )
"transfer of the calculated results:"

```

Fig. 9-12: Mathcad algorithm for the calculation of the fluctuation ratio and the normalized average residence time (part IV)

```

"transfer of the calculated results:"
 $\phi_1 \leftarrow F_1$ 
 $\phi_2 \leftarrow F_2$ 
 $so\phi_1 \leftarrow F_3$ 
 $so\phi_2 \leftarrow F_4$ 
TIME_STEPS  $\leftarrow F_5$ 
STATUS  $\leftarrow F_6$ 

"calculation of the concentrations at the inlet and the outlet of the mixer:"
CONCENTRATION  $\leftarrow$  for t  $\in$  1..t_jump
     $\mu_{1t} \leftarrow \mu_{O1} + \mu_{A1} \cdot \sin[\Omega_1 \cdot (t \cdot \Delta\tau)]$ 
     $\mu_{2t} \leftarrow \mu_{O2} + \mu_{A2} \cdot \sin[\Omega_2 \cdot (t \cdot \Delta\tau)]$ 
     $C1in_t \leftarrow \frac{\mu_{1t}}{\mu_{1t} + \mu_{2t}}$ 
     $C1out_t \leftarrow \frac{so\phi_1 t}{so\phi_1 t + so\phi_2 t}$ 
     $\begin{pmatrix} C1in \\ C1out \end{pmatrix}$ 
C1in  $\leftarrow$  CONCENTRATION1
C1out  $\leftarrow$  CONCENTRATION2

"calculation of the mass hold-up in the mixer:"
for i1  $\in$  1..n
     $\phi_{1M_{i1}} \leftarrow \phi_{1i1, t\_jump}$ 
     $\phi_{2M_{i1}} \leftarrow \phi_{2i1, t\_jump}$ 
M1  $\leftarrow \sum \phi_{1M} \cdot \frac{1}{n}$ 
M2  $\leftarrow \sum \phi_{2M} \cdot \frac{1}{n}$ 

"calculation of the normalized residence time:"
tR  $\leftarrow \frac{M1 + M2}{\mu_{O1} + \mu_{O2}}$ 

"read out of the inlet and outlet concentrations for the last period:"
N1  $\leftarrow \frac{1}{\Delta\tau}$ 
N2  $\leftarrow t\_jump - N1 - 1$ 
for t1  $\in$  1..N1
     $c1in_{t1} \leftarrow C1in_{\text{floor}(N2+t1)}$ 
     $c1out_{t1} \leftarrow C1out_{\text{floor}(N2+t1)}$ 

"calculation of the variance of the concentration fluctuations:"
 $\sigma_{in} \leftarrow \text{stdev}(c1in)$ 
 $\sigma_{out} \leftarrow \text{stdev}(c1out)$ 

"transfer of the main results calculated and the set parameters:"

```

**Fig. 9-13:** Mathcad algorithm for the calculation of the fluctuation ratio and the normalized average residence time (part V)

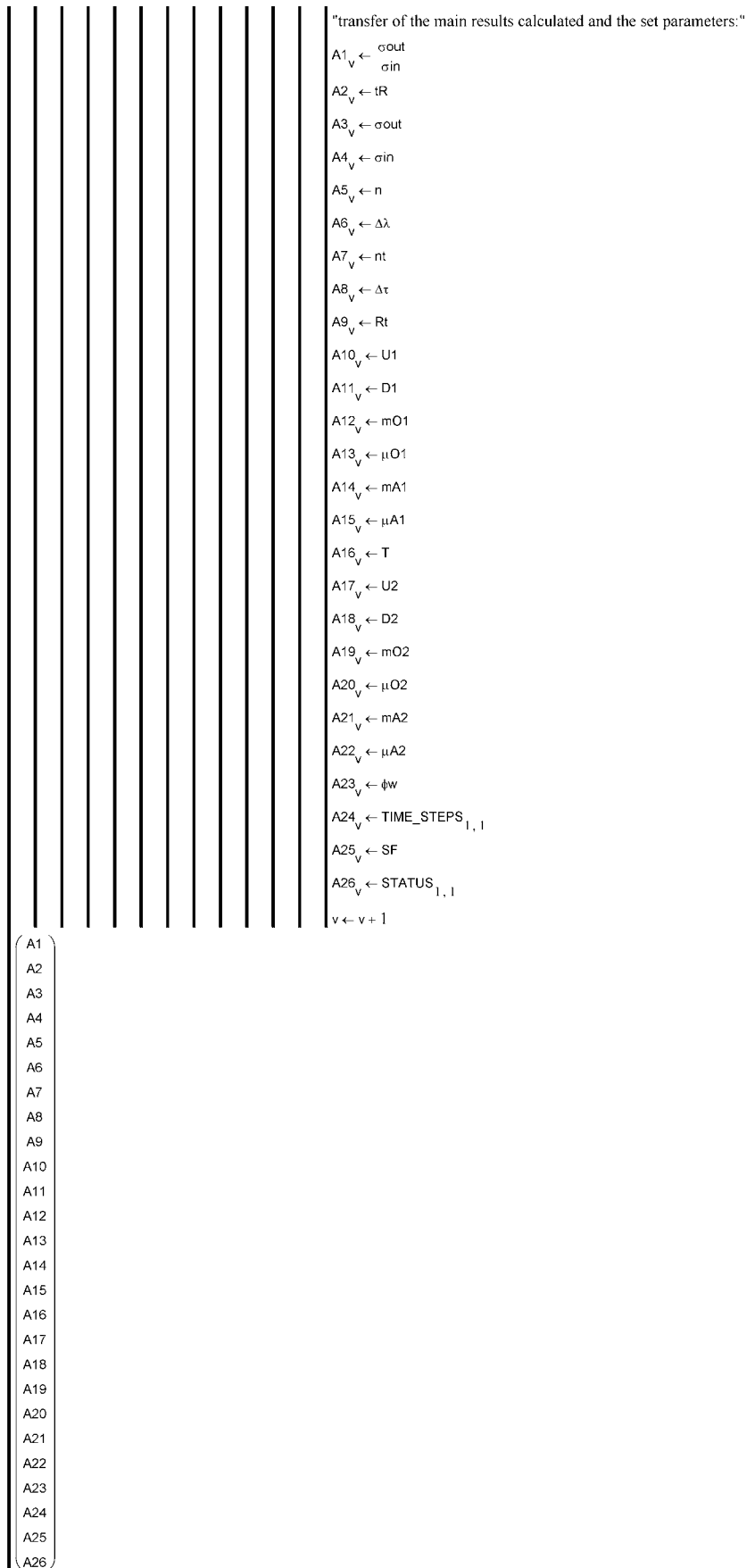


**Fig. 9-14:** Mathcad algorithm for the calculation of the fluctuation ratio and the normalized average residence time (part VI)

"matrix with the calculation results:"

```
Z := stapeln(R1^T, R2^T, R3^T, R4^T, R5^T, R6^T, R7^T, R8^T, R9^T, R10^T, R11^T, R12^T, R13^T, R14^T, R15^T, R16^T, R17^T, R18^T, R19^T, R20^T, R21^T, R22^T, R23^T, R24^T, R25^T, R26^T)
```

"matrix with the calculation results:"

"meaning of the different rows of the matrix with the calculation results:"

Z = ■	explanation_vector :=	<p style="text-align: center;">"fluctuation ratio"</p> <p style="text-align: center;">"normalized average residence "</p> <p style="text-align: center;">"standard deviation at the mixer outlet"</p> <p style="text-align: center;">"standard deviation at the mixer inlet"</p> <p style="text-align: center;">"number of truncation chambers"</p> <p style="text-align: center;">"number of time steps"</p> <p style="text-align: center;">"width of a truncation chamber"</p> <p style="text-align: center;">"multiple of the period length"</p> <p style="text-align: center;">"width of a time step"</p> <p style="text-align: center;">"normalized transport coefficient of component 1"</p> <p style="text-align: center;">"normalized dispersion coefficient of component 1"</p> <p style="text-align: center;">"offset of component 1 (experiment)"</p> <p style="text-align: center;">"normalized offset of component 1"</p> <p style="text-align: center;">"amplitude of component 1 (experiment)"</p> <p style="text-align: center;">"normalized amplitude of component 1"</p> <p style="text-align: center;">"period length (experiment)"</p> <p style="text-align: center;">"normalized transport coefficient of component 2"</p> <p style="text-align: center;">"normalized dispersion coefficient of component 2"</p> <p style="text-align: center;">"offset of component 2 (experiment)"</p> <p style="text-align: center;">"normalized offset of component 2"</p> <p style="text-align: center;">"amplitude of component 2 (experiment)"</p> <p style="text-align: center;">"normalized amplitude of component 2"</p> <p style="text-align: center;">"filling degree up to the height of the weir (experiment)"</p> <p style="text-align: center;">"control of the time steps"</p> <p style="text-align: center;">"spreading factor"</p> <p style="text-align: center;">"status of the filling degree control: 10 = o. k., 0 = not o. k."</p>
-------	-----------------------	---

"saving the calculation results:"

```
PRNSCHREIBEN("J:\Diss U=0.001..6, D=0.1..0.9, Nx=50, Nt=100.000.dat, TL=20") := Z
```

**Fig. 9-15:** Mathcad algorithm for the calculation of the fluctuation ratio and the normalized average residence time (part VII)

## 9.4 Tabular compilation of the experimental mixing results

An enormous effort is necessary to generate defined concentration fluctuations entering the continuous mixer and to determine the remaining concentration fluctuations in the outlet of the mixer. To offer other researchers the possibility to validate their developed mixing models, the experimental mixing results presented in *Chapter 4.5.2* (see p. 159) are shown in the following tables. Until now, such a data set was not published. The standard deviations of the concentration fluctuations in the outlet of the continuous mixer, which were determined experimentally, are presented for the different operation conditions examined (The variance of the stochastic measuring mistakes was not considered!). The values of the mass hold-ups measured for the corresponding operation conditions are also listed.

### 9.4.1 Mass hold-ups as well as standard deviations of the concentration fluctuations in the inlet and the outlet of the mixer (half-closed weir)

**Table 9-3:** Influence of the average overall mass flow on the mixing result (half-closed weir; calcium carbonate:  $\dot{m}_{1,O} = 15$  g/s,  $\dot{m}_{1,A} = 14$  g/s,  $T = 40$  s; maize starch:  $\dot{m}_{2,O} = 5, 10, 15, 20$  g/s; mixing device:  $n = 196$  min<sup>-1</sup>)

$\dot{m}_{overall}$	$m_{hold}''$	$m_{hold}'$	$m_{hold}$	$\bar{m}_{hold}$	$s_{in}$	$s_{out}$	$\frac{s_{out}}{s_{in}}$	$\left(\frac{s_{out}}{s_{in}}\right)_{ave.}$
[g/s]	[kg]	[kg]	[kg]	[kg]	[mass-%]	[mass-%]	[-]	[-]
35	2.03	1.60	0.43	0.32	18.8	9.14	0.49	0.49
	1.81	1.55	0.26		18.8	9.14	0.49	
	1.73	1.47	0.26		18.8	9.40	0.50	
30	2.22	1.69	0.53	0.45	20.4	6.44	0.32	0.32
	2.14	1.66	0.48		20.4	6.62	0.32	
	1.99	1.66	0.33		20.4	6.47	0.32	
25	2.04	1.59	0.45	0.56	21.8	4.23	0.19	0.17
	2.29	1.71	0.58		21.8	3.66	0.17	
	2.34	1.68	0.66		21.8	3.23	0.15	
20	1.88	1.39	0.49	0.44	22.1	2.37	0.11	0.11
	1.88	1.49	0.39		22.1	2.22	0.10	
	1.99	1.54	0.45		22.1	2.82	0.13	

**Table 9-4:** Influence of the rotational speed of the mixing device on the mixing result (half-closed weir; calcium carbonate:  $\dot{m}_{1,O} = 15$  g/s,  $\dot{m}_{1,A} = 14$  g/s,  $T = 40$  s; maize starch:  $\dot{m}_{2,O} = 10$  g/s)

$n$	$m_{hold}''$	$m_{hold}'$	$m_{hold}$	$\bar{m}_{hold}$	$s_{in}$	$s_{out}$	$\frac{s_{out}}{s_{in}}$	$\left(\frac{s_{out}}{s_{in}}\right)_{ave.}$
[ $min^{-1}$ ]	[kg]	[kg]	[kg]	[kg]	[mass-%]	[mass-%]	[-]	[-]
196	2.04	1.59	0.45	0.56	21.9	4.32	0.20	0.20
	2.29	1.71	0.58		21.9	4.72	0.22	
	2.34	1.68	0.66		21.9	4.10	0.19	
176	2.88	1.80	1.08	1.07	21.9	2.36	0.11	0.11
	2.88	1.86	1.02		21.9	2.52	0.12	
	2.96	1.84	1.12		21.9	2.11	0.10	
118	3.25	1.66	1.59	1.73	21.9	1.32	0.06	0.06
	3.56	1.69	1.87		21.9	1.38	0.06	
	3.47	1.73	1.74		21.9	1.32	0.06	
78	3.86	1.70	2.16	2.28	21.9	1.26	0.06	0.06
	3.89	1.68	2.21		21.9	1.34	0.06	
	4.21	1.73	2.48		21.9	1.25	0.06	
39	5.31	2.20	3.11	3.06	21.9	1.03	0.05	0.05
	5.26	2.25	3.01		21.9	1.14	0.05	
	5.51	2.44	3.07		21.9	1.20	0.05	

**Table 9-5:** Influence of the period length on the mixing result (half-closed weir; calcium carbonate:  $\dot{m}_{1,O} = 15$  g/s,  $\dot{m}_{1,A} = 14$  g/s; maize starch:  $\dot{m}_{2,O} = 10$  g/s; mixing device:  $n = 196$   $min^{-1}$ )

$T$	$m_{hold}''$	$m_{hold}'$	$m_{hold}$	$\bar{m}_{hold}$	$s_{in}$	$s_{out}$	$\frac{s_{out}}{s_{in}}$	$\left(\frac{s_{out}}{s_{in}}\right)_{ave.}$
[s]	[kg]	[kg]	[kg]	[kg]	[mass-%]	[mass-%]	[-]	[-]
100	2.15	1.55	0.60	0.74	22.0	7.90	0.36	0.35
	2.41	1.61	0.80		22.0	7.57	0.34	
	2.51	1.69	0.82		22.0	7.84	0.36	
80	2.59	1.65	0.94	0.85	21.9	6.10	0.28	0.29
	2.35	1.66	0.69		21.9	5.82	0.27	
	2.60	1.68	0.92		21.9	6.13	0.28	
60	2.52	1.67	0.85	0.80	21.9	3.73	0.17	0.18
	2.55	1.73	0.82		21.9	4.04	0.18	
	2.43	1.70	0.73		21.9	4.02	0.18	
40	2.04	1.59	0.45	0.56	21.9	4.23	0.19	0.17
	2.29	1.71	0.58		21.9	3.66	0.17	
	2.34	1.68	0.66		21.9	3.23	0.15	
20	2.39	1.55	0.84	0.79	22.0	2.47	0.11	0.10
	2.46	1.58	0.88		22.0	2.15	0.10	
	2.22	1.58	0.64		22.0	2.11	0.10	



### 9.4.2 Mass hold-ups as well as standard deviations of the concentration fluctuations in the inlet and the outlet of the mixer (closed weir)

**Table 9-6:** Influence of the average overall mass flow on the mixing result (closed weir; calcium carbonate:  $\dot{m}_{1,0} = 15$  g/s,  $\dot{m}_{1,A} = 14$  g/s,  $T = 40$  s; maize starch:  $\dot{m}_{2,0} = 5, 10, 15, 20$  g/s; mixing device:  $n = 196$  min<sup>-1</sup>)

$\dot{m}_{overall}$	$m_{hold}''$	$m_{hold}'$	$m_{hold}$	$\bar{m}_{hold}$	$s_{in}$	$s_{out}$	$\frac{s_{out}}{s_{in}}$	$\left(\frac{s_{out}}{s_{in}}\right)_{ave.}$
[g/s]	[kg]	[kg]	[kg]	[kg]	[mass-%]	[mass-%]	[-]	[-]
35	1.81	1.32	0.49	0.39	18.8	8.60	0.46	0.49
	1.54	1.25	0.29		18.8	9.95	0.53	
	1.64	1.25	0.39		18.8	9.25	0.49	
30	1.82	1.33	0.49	0.46	20.4	7.42	0.36	0.36
	1.80	1.33	0.47		20.4	7.28	0.36	
	1.75	1.32	0.43		20.4	7.06	0.35	
25	2.24	1.50	0.74	0.75	21.8	2.46	0.11	0.12
	2.23	1.50	0.73		21.8	2.98	0.14	
	2.32	1.53	0.79		21.8	2.67	0.12	
20	2.33	1.57	0.76	0.72	22.1	1.79	0.08	0.09
	2.38	1.59	0.79		22.1	1.94	0.09	
	2.24	1.64	0.60		22.1	2.32	0.10	

**Table 9-7:** Influence of the rotational speed of the mixing device (weir closed; calcium carbonate:  $\dot{m}_{1,0} = 15$  g/s,  $\dot{m}_{1,A} = 14$  g/s,  $T = 40$  s; maize starch:  $\dot{m}_{2,0} = 10$  g/s)

$n$	$m_{hold}''$	$m_{hold}'$	$m_{hold}$	$\bar{m}_{hold}$	$s_{in}$	$s_{out}$	$\frac{s_{out}}{s_{in}}$	$\left(\frac{s_{out}}{s_{in}}\right)_{ave.}$
[min <sup>-1</sup> ]	[kg]	[kg]	[kg]	[kg]	[mass-%]	[mass-%]	[-]	[-]
196	2.24	1.50	0.74	0.75	21.9	2.46	0.11	0.12
	2.23	1.50	0.73		21.9	2.98	0.14	
	2.32	1.53	0.79		21.9	2.67	0.12	
176	4.60	1.60	3.00	2.85	21.9	1.05	0.05	0.05
	4.15	1.71	2.44		21.9	1.03	0.05	
	4.85	1.73	3.12		21.9	0.97	0.04	
157	4.68	1.35	3.33	3.42	21.9	1.00	0.05	0.04
	4.52	1.39	3.13		21.9	0.96	0.04	
	5.38	1.59	3.79		21.9	0.91	0.04	
118	5.36	1.69	3.67	3.64	21.9	1.02	0.05	0.05
	5.49	1.75	3.74		21.9	1.09	0.05	
	5.21	1.70	3.51		21.9	1.11	0.05	
78	6.18	1.57	4.61	4.75	21.9	1.25	0.06	0.06
	6.21	1.55	4.66		21.9	1.31	0.06	
	6.53	1.54	4.99		21.9	1.16	0.05	
39	7.33	1.52	5.81	5.94	21.9	1.30	0.06	0.05
	7.65	1.62	6.03		21.9	1.15	0.05	
	7.57	1.60	5.97		21.9	1.05	0.05	

**Table 9-8:** Influence of the period length on the mixing result (closed weir; calcium carbonate:  $\dot{m}_{1,0} = 15$  g/s,  $\dot{m}_{1,A} = 14$  g/s; maize starch:  $\dot{m}_{2,0} = 10$  g/s; mixing device:  $n = 196$  min<sup>-1</sup>)

$T$	$m_{hold}''$	$m_{hold}'$	$m_{hold}$	$\bar{m}_{hold}$	$s_{in}$	$s_{out}$	$\frac{s_{out}}{s_{in}}$	$\left(\frac{s_{out}}{s_{in}}\right)_{ave.}$
[s]	[kg]	[kg]	[kg]	[kg]	[mass-%]	[mass-%]	[-]	[-]
100	2.90	1.89	1.01	0.97	22.0	4.12	0.19	0.21
	2.75	1.91	0.84		22.0	4.51	0.21	
	2.88	1.82	1.06		22.0	4.92	0.22	
80	3.03	1.76	1.27	1.20	21.9	3.51	0.16	0.16
	2.96	1.71	1.25		21.9	3.60	0.16	
	2.89	1.80	1.09		21.9	3.66	0.17	
60	3.02	1.84	1.18	1.18	21.9	2.51	0.11	0.12
	3.06	1.81	1.25		21.9	2.70	0.12	
	2.97	1.85	1.12		21.9	2.55	0.12	
40	2.24	1.50	0.74	0.75	21.9	2.46	0.11	0.12
	2.23	1.50	0.73		21.9	2.98	0.14	
	2.32	1.53	0.79		21.9	2.67	0.12	
20	2.92	1.84	1.08	1.27	22.0	1.16	0.05	0.05
	3.19	1.75	1.44		22.0	1.21	0.06	
	2.98	1.69	1.29		22.0	1.06	0.05	

# Curriculum vitae

of

Volker Kehlenbeck

born on October 21<sup>st</sup>, 1970, in Bremen (Germany)



- 1990                      Abitur at the Gymnasium of the *Kooperativen Gesamtschule Weyhe*
- 1990                      2<sup>nd</sup> place at the Landeswettbewerb *jugend forscht* with a work on:  
„Photochemischer Abbau von CKW-verschmutzten Abwässern“  
„Photochemical degradation of waste water containing chlorinated hydrocarbon“
- 07/1990 - 06/1991      Military service in the German air force
- 1991                      1<sup>st</sup> place at the Landeswettbewerb *jugend forscht* with a work on:  
„Photochemische Reinigung von PER-haltigen Abwässern“  
„Photochemical deflection of waste water containing perchloroethylene“  
⇒ participation at the 26<sup>th</sup> Bundeswettbewerb *jugend forscht*
- 10/1991 - 09/1997      Studies of mechanical engineering with specialization in the field of process engineering at the *Technische Universität Braunschweig* (Germany)
- 04/1996 - 10/1996      Scientific work at the *Langnese-Iglo GmbH* in Reken (Germany) with the topic:  
„Untersuchungen zur Bilanzierung und zur Reduzierung des Endwasser-gehaltes bei der Spinatproduktion“  
„Examinations of the water balance and the reduction of the final water content during the production of spinach“
- 03/1997 - 10/1997      Diploma thesis at the *BOKELA Ingenieurgesellschaft für Mechanische Verfahrenstechnik mbH* in Karlsruhe (Germany) with the topic:  
„Erarbeitung eines Optimierungskonzeptes für ein Scherspaltfilter“  
„Development of an optimization plan for a dynamic cross flow filter“
- 02/1998 - 11/2003      Scientific co-worker of Prof. Dr.-Ing. Karl Sommer at the *Lehrstuhl für Maschinen- und Apparatekunde* of the *Technische Universität München - Weihenstephan*
- 05/2002 - 06/2002      Scientific work at the *Particle Engineering Research Center* at the *University of Florida* in Gainesville (USA) supervised by Prof. Brian Scarlett
- since 12/2003              Project manager for dehydrated culinary products at the *Nestlé Product Technology Centre Lebensmittelforschung GmbH* in Singen (Germany)